CA-125

CA-125, a glycoprotein antigen, is currently the most commonly used tumor marker for ovarian cancer. Its value lies in the assessment and monitoring of recurrent ovarian cancer. In primary ovarian cancer it is less specific, particularly in premenopausal women and in early-stage disease.

►Carcinoma, Ovarium

Cacchi-Ricci disease

►Medullary Sponge Kidney

Caffey Disease

Alan E. Oestreich
Cincinnati Children's Hospital Medical Center, Cincinnati, Ohio, USA
Alan.Oestreich@cchmc.org

Synonym

Infantile cortical hyperostosis

Definitions

A skeletal condition in infants and fetuses manifest by periosteal reaction, involving only a few bones, especially tubular bones and the mandible and scapula, associated with warmth and tenderness, and not due to a known specific cause. The condition is generally self-limited and heals. Because of its close simulation of the skeletal effect of long-term use of high dose prostaglandin E, it may well be metabolic in nature; however, others (including, at one time, Caffey) have postulated a viral cause, and sometimes it occurs in several members of a family, raising the question of genetic susceptibility. As a periosteal process, it manifests only at sites of membranous bone growth.

Pathology/Histopathology

The hyperostosis (periosteal reaction) of Caffey disease eventually heals into a somewhat thick cortex, which slowly returns to normal over time. The role of biopsy would be principally to exclude competing diagnoses, such as osteomyelitis or metastases from neuroblastoma, in the unusual circumstance that the diagnosis is in question. The periosteal reaction of Caffey disease will stop short of the short, straight ►metaphyseal collar at the metaphysis, since such reaction only occurs where periosteum is present, and it cannot occur on exclusively enchondral bones (*viz*, tarsal or carpal bones) that do not have a periosteum.

Clinical Presentation

The earliest presentation of Caffey disease is intrauterine polyhydramnios, presumably as a consequence of mandible involvement making swallowing painful for the fetus. After a baby is born, the findings are warmth, tenderness, possible swelling, and reduction in motion of the affected bones.

Similar signs may be found in high dose prostaglandin E use leading to periosteal reaction (1); additionally vomiting may occur from antral narrowing in babies so treated. The Scotch terrier puppies that get a Caffey-like hyperostosis of the mandible refuse food or drink because of pain, but survive nicely if tube fed during the active disease.

If periosteal reaction simulating Caffey disease is due to neuroblastoma, metastases, redness, warmth, and even tenderness may be absent (unless there is a pathological fracture).

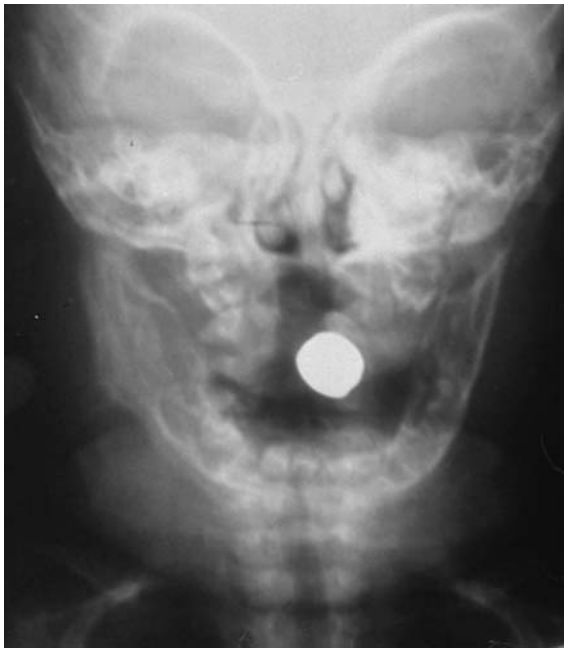

Caffey Disease. Figure 1 Right-sided mandibular periosteal reaction in Caffey disease. From Oestreich AE, Crawford AH (1985) Atlas of Pediatric Orthopedic Radiology. Thieme Verlag, Stuttgart p 104.

Imaging

Careful analysis of long bones, mandible (Fig. 1), scapula, clavicle, and ribs for periosteal reaction on plain radiographs, using magnification of the images in symptomatic areas, is the method to document Caffey disease. In high dose prostaglandin E disease, we have seen similar involvement of small tubular bones of the hand (Fig. 2); perhaps that may also occur in Caffey disease. Periosteal reaction can be shown with ultrasound or CT, but plain images suffice, especially if careful attention is directed to symptomatic sites and 10 days have elapsed since the onset of the disease. On prenatal ultrasound, evaluation for polyhydramnios is pertinent.

Nuclear Medicine

Since it takes about 10 days for periosteal reaction of any etiology to appear on conventional radiographs, nuclear imaging is capable of demonstrating abnormal activity earlier, as early as the first day of the process, in Caffey disease, as well as earlier than 10 days in simulating conditions, including prostaglandin E high dose, hypervitaminosis A, trauma (such as abuse), and tumor (such

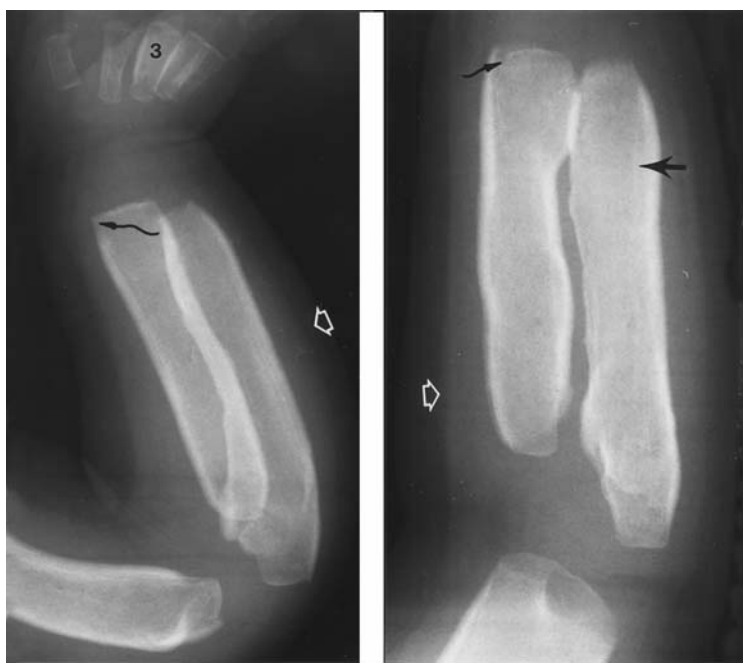

Caffey Disease. Figure 2 Painful swollen forearm following 3 months of prostaglandin E therapy. The deep soft tissues are swollen (white arrows). Note periosteal reaction at metacarpal 3 (3). The metaphyseal collars (curved arrows) are spared from the periosteal reaction. The earlier cortex of the ulna (black arrow) is barely discernable. From Oestreich AE, Shownkeen H (1993) Massive prostaglandin-E periosteal reaction in an infant. Lessons to be learned. Year Book of Pediatr Radiol (Miskolc) 5:49.

as neuroblastoma metastases; once neuroblastoma is suspected, I131MIBG is the nuclear method of choice). Caffey disease is particularly supported by increased mandible activity on bone scan.

Diagnosis

Periosteal reaction along long bones in Caffey disease stops short of the 1–3 mm metaphyseal collar (Fig. 2). For the mandible, clavicle and scapula, it may merely present as enlarged dense bone. Rib disease is best seen if the most lateral portions are involved.

Other causes of diffuse periosteal reaction in infancy or later in childhood include neuroblastoma metastasis, Weismann–Netter Stuhl disease, Erdheim-Chester disease, ▶Melhem hyperostosis and hyperphosphatemia (2), as well as physiologic periosteal reaction found in a significant percentage of normal (and even abnormal) infants 1–6 months of age (3).

Bibliography

1. Benz-Bohm G, Emons D et al (1984) Cortical hyperostoses after long-term prostaglandin E2 therapy [in German]. Radiologe 24:72–78
2. Melhem RE, Najjar SS, Khachadurian AK (1970) Cortical hyperostosis with hyperphosphatemia: a new syndrome? J Pediatr 77:986–990
3. Shopfner CE (1966) Periosteal bone growth in normal infants. A preliminary report. Am J Roentgenol Radium Ther Nucl Med 97:154–163

Calcific Periarthritis

Calcifications within periarticular soft tissues frequently with a history of pain.
▶HADD

Calcific Tendinosis or Calcific Tendinotis

Calcifications within tendons frequently with a history of pain.
▶HADD

Calcification, Intracranial, Neonatal

Veronica Donoghue
Radiology Department, Children's University Hospital, Dublin, Ireland
veronica.donoghue@cuh.ie

C

Synonym

TORCH infections

Definition

Pathological calcification of the newborn brain is detected on plain radiography or CT examination. The numerous causes include perinatal toxoplasmosis, others i.e. HIV, rubella, cytomegalovirus, herpes (TORCH) infections, metabolic abnormalities, vascular disease, brain infarction, tumours and ▶neurophakomatoses.

Pathology/Histopathology

The pathology in neonatal intracranial calcification varies with the underlying cause.

Each one is discussed in more detail elsewhere in this section.

Clinical Presentation

Some infants with *congenital infection*, in particular *cytomegalovirus* present with a small head circumference and infants with toxoplasmosis may have hydrocephalus (1) All these infections are generalised infections and the infants may have skin rashes and haemorrhages, hepatosplenomegaly, chorioretinitis and pneumonitis.

The diagnosis of *tuberous sclerosis* depends on detecting the characteristic cutaneous lesions and the presence of cardiac tumours such as rhabdomyomas which can be diagnosed using antenatal sonography. They can also present with renal cysts and hamartomas.

In *Sturge–Weber disease* a facial haemangioma causing a port-wine stain in the distribution of the trigeminal nerve is characteristic.

In *Von–Hippel–Lindau disease* there are cerebellar and retinal haemangiomas and the patients may also present with polycystic kidney disease and cysts in other organs.

Many of these patients including those with inherited metabolic diseases and brain infarction may also present with seizures.

A ►pseudo-TORCH syndrome has been described such that patients who are microcephalic at birth have delayed motor and cognitive development, long tract signs and their work-up for congenital infections is normal. Many have affected siblings and parental consanguinity has been reported in approximately one-third of patients suggesting an autosomal recessive inheritance (3).

Imaging

Intracranial calcification maybe curvilinear, linear, punctuate or clumpy. If dense it may be seen on plain radiographs but it is more easily identified with CT (Fig. 1). Ultrasonography can identify calcification particularly if it is in the periventricular regions (Fig. 2). MR imaging is a poor tool to detect calcification but it may be seen using gradient-echo sequences and also as reduced signal on T2 and increased signal on T1 sequences.

In cytomegalovirus and less commonly rubella and toxoplasmosis infections, the calcification tends to be periventricular in location (Figs. 1 and 2). It may also involve the basal ganglia. In the other infections the location is non-specific and can occur almost anywhere in the brain. Increased echogenicity of the lenticulostriate regions on sonography, sometimes referred to as *non-calcifying vasculopathy*, has been reported in infants with congenital infection. This however is a non-specific finding and can also be seen in some trisomy syndromes, ischaemia and storage disorders (2).

MR and CT imaging may also detect various brain developmental anomalies such as delayed myelination, lissencephaly, polymicrogyria, cerebellar hypoplasia and schizencephaly, depending on the gestational age at the time of infection.

Infants with pseudo-TORCH syndrome also demonstrate calcification which is mainly periventricular in location but may also involve the basal ganglia. They also have ventricular dilatation secondary to white matter volume loss and the cerebellum and brainstem may be small.

Intracranial tubers of tuberous sclerosis are seldom calcified in the newborn period.

In Sturge–Weber syndrome, the calcification characteristically occurs in the cerebral cortex underlying the angiomatosis and typically has a gyriform pattern. The calcification however is seldom seen in the newborn period.

In tumours and areas of infarction the calcification is non-specific.

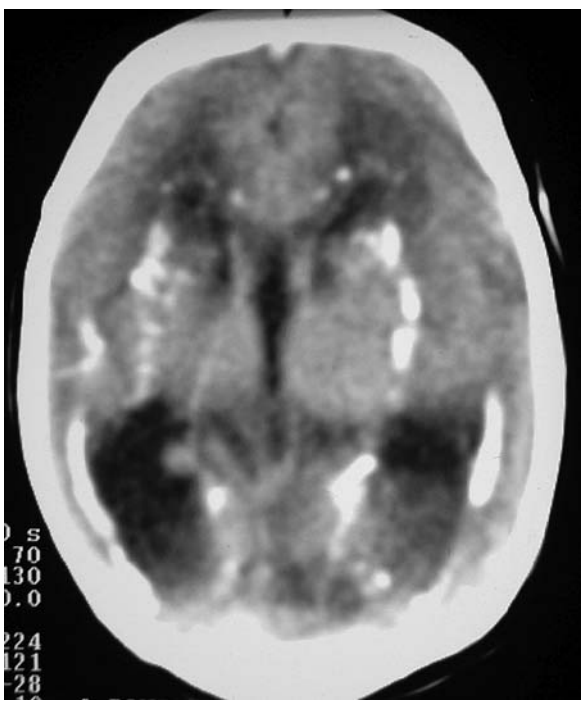

Calcification, Intracranial, Neonatal. Figure 1 CT brain on newborn infant with congenital cytomegalovirus infection. There is extensive intracranial calcification of a punctuate, clumpy and curvilinear nature.

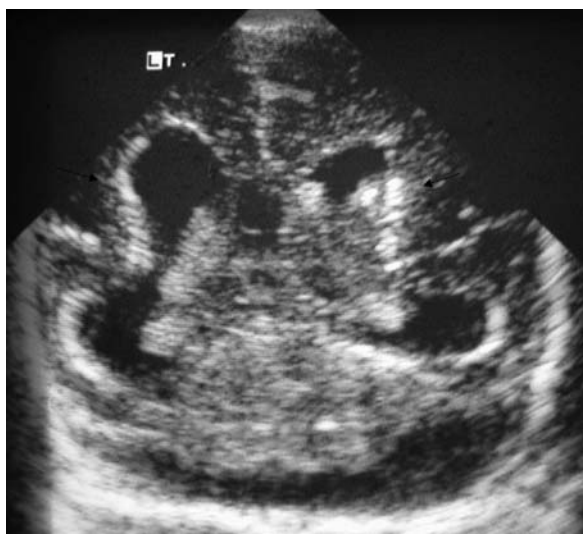

Calcification, Intracranial, Neonatal. Figure 2 Ultrasound image in infant with congenital cytomegalovirus infection. There is extensive increased periventricular echogenicity in keeping with calcification (arrows).

Diagnosis

If dense, intracranial calcification can be seen on plain radiography. It may also be identified on sonography particularly when periventricular in location.

CT is the most sensitive imaging modality.

MR imaging is poor at detecting calcification but it maybe suggested on gradient-echo sequences and also as reduced signal on T2 and increased signal on T1 sequences.

Bibliography

1. Barkovich JA (ed) (2005) Pediatric Neuroimaging. 4th edn. Lippincott Williams and Wilkins, Baltimore
2. El Ayoubi M, de Bethmann O, Monset-Couchard M (2003) Lenticulostriate echogenic vessels: clinical and sonographic study of 70 neonatal cases. Pediatr Radiol 33:697–703
3. Reardon W, Hockey A, Silberstein P et al (1994) Autosomal recessive congenital intrauterine infection-like syndrome of microcephaly, intracranial calcification and CNS disease. Am J Med Genet 52:58–65

Calcifications, Breast

Arne Fischmann
University of Tübingen Department of Diagnostic Radiology, Tübingen, Germany
arne.fischmann@med.uni-tuebingen.de

Synonym

Microcalcifications

Definition

Crystals of calcium phosphate, calcium carbonate, calcium oxalate, and magnesium phosphate developing in different benign or malignant transformations of breast tissue.

Pathology/Histopathology

Calcifications are usually localized in the terminal ductulolobular unit (1). In general, the various calcifications are deposited in areas where compound lipids are present. Calcifications may be psammous, granular, laminar, or amorphous. Sometimes they form circular structures referred to as Liesegang rings within cysts (2).

While most calcifications are easily detectable in H&E-stained sections, calcium oxalate is obscure to standard work-up and only visible in polarized light. As calcium oxalate is mainly associated to benign disease, detection is important to avoid unnecessary follow-up biopsies.

Radiologic–pathologic correlation of calcifications is difficult, as up to 25% of calcifications are lost during embedding and fixation of specimens. Moreover, microcalcifications smaller than 100 are undetectable at mammography. Therefore all specimens taken for microcalcifications should undergo specimen radiography and the pathologist should thoroughly search for calcifications marked radiologically.

Clinical Presentation

Due to their size and distribution, calcifications are impalpable and clinically invisible, therefore only lesions with mass effect and associated calcifications are clinically detectable.

Approximately 40–50% of mammary carcinomas have calcifications that are mammographically detectable. Intraductal comedocarcinoma and infiltrative carcinoma, in particular, are frequently associated with calcifications, whereas lobular carcinomas are rarely calcified. Among the benign lesions, sclerosing adenosis is associated with calcifications with a frequency of 50%.

With 58% positive predictive value in patients treated with breast-conserving therapy, calcifications are a valuable tool in the detection of recurrence.

Imaging

Mammography is the primary imaging modality in the detection and description of calcifications. The widespread use of screening mammography since the 1970s has caused a substantial increase in the incidence of calcifications.

In general, detection of clustered calcifications in mammography should advocate the performance of magnification views, preferably in craniocaudal and mediolateral positioning to localize precisely the calcifications and to detect milk of calcium.

Sonography is useful in showing cystic changes in fibrocystic disease. In some cases microcalcifications can be viewed directly on sonographs.

Despite the characteristic appearance of calcium on magnetic resonance imaging (MRI) with low signal on T1-weighted and T2-weighted images, MRI has no practical use in the detection or classification of calcifications. This is mainly due to the small size of single

calcifications, which is far below the voxel size. MRI is therefore only able to detect the underlying disease. As sensitivity for *in-situ* carcinoma is about 80%, a normal MRI in cases of suspicious microcalcifications cannot rule out malignant disease. In fibroglandular or dense breast tissue, preoperative magnetic resonance tomography can be useful in detecting multifocal disease. This is also true for new calcifications after breast-conserving therapy, where it is difficult to distinguish liponecrotic calcifications *in statu nascendi* from recurrent breast cancer.

Nuclear Medicine

Currently there is no known tracer for classifying calcifications. Nuclear medicine is therefore confined to cases where calcifications lead to a diagnosis of breast cancer and require further work-up.

Diagnosis

Mammography is currently the only imaging modality that can detect and classify microcalcifications with sufficient diagnostic accuracy.

Morphology and distribution are the most important parameters when differentiating benign from malignant calcifications, whereas the number of calcifications is of little importance.

All calcifications should be classified according to the categories described in the Breast Imaging Reporting and Data System (BI-RADS) lexicon by the American College of Radiology (ACR). A summary of these descriptions is given below.

Typically, benign calcifications can rule out malignancy with a high probability and are usually pathognomonic. These include: skin calcifications, vascular (Fig. 1), round, popcorn-like (fibroadenoma), large rod-like (plasma cell mastitis), lucent centered, egg-shell or rim calcifications (lipid necrosis), milk of calcium (Fig. 1), suture, and dystrophic calcifications.

Coarse, heterogeneous calcifications are of intermediate concern and often represent fibroadenoma, fibrosis, or trauma.

Amorphous or punctuate calcifications have a diameter of less than 0.5 mm, and are usually indistinct (Fig. 2). Pathologically they often represent psammoma-like structures (1).

Fine pleomorphic calcifications are of similar shape but vary in size without casting parts, which are more suspicious (3).

Fine-linear or fine-linear branching calcifications are usually associated with comedocarcinoma (Fig. 3).

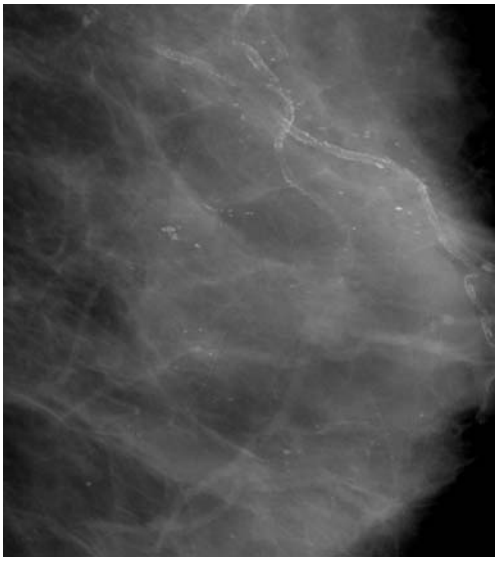

Calcifications, Breast. Figure 1 Multiple crescent shaped calcifications in this lateral view represent milk of calcium. These are typically benign as well as the vascular calcifications in this image.

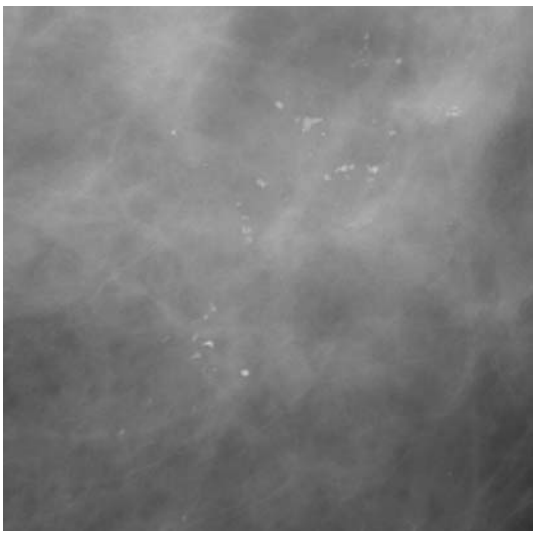

Calcifications, Breast. Figure 2 A small group of amorphous calcifications in a segmental distribution representing ductal carcinoma *in situ*.

Groups can be classified into segmental, linear, multilocular, regional (>2cm^2 in an area that does not suggest a ductal distribution), grouped or clustered (<2cm^2), and diffuse/scattered. In particular, segmental and linear distributions are strongly associated to malignant disease. However, the diagnostic accuracy for calcifications is lower than for solid lesions. Sensitivity is reported to be as low

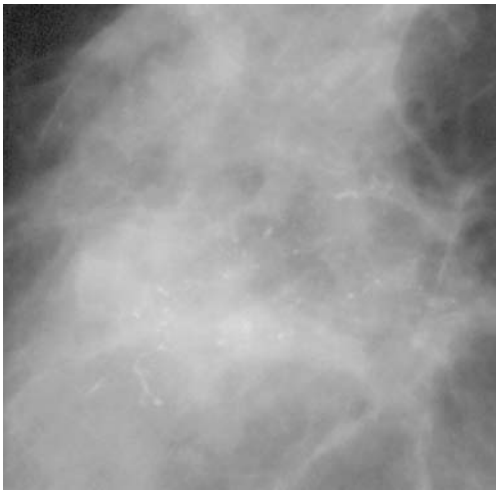

Calcifications, Breast. Figure 3 Polymorphous, casting calcifications in a regional distributions representing typical DCIS.

as 67%. As the specificity is lower, biopsy should be performed more often: the definite diagnosis of the underlying disease in the case of suspicious calcifications can only be obtained by histology.

In addition to this, calcifications tend to either underestimate tumor extent due to uncalcified parts of the lesion, or to overestimate the extent, because benign calcifications are included in the suspicious group.

Interventional Radiology

Biopsy with stereotactic guidance is the preferred diagnostic method for biopsy work-up of suspicious calcifications. Especially in BI-RADS 4 calcifications, vacuum biopsy is superior to core biopsy because underdiagnosis is lower and additional excision biopsies can be avoided. Ultrasound-guided biopsy of calcifications should only be performed if the mammographic and ultrasound-detected lesion can be correlated with certainty. In this case a specimen radiograph and a postbiopsy mammograph are obligatory to verify the correct biopsy.

If open biopsy is necessary, preoperative localization with a guidewire should be performed. Specimen radiography is advocated to verify complete biopsy. The exact localization of the calcifications should be described and communicated to the pathologist to assure correct work-up.

Bibliography

1. Tabar L, Dean PB, Tot T (2001) Teaching Atlas of Mammography. 3rd edn. Thieme Medical Publishers, Stuttgart
2. Tavassoli FA (1999) Microcalcifications. In: Tavassoli FA (ed) Pathology of the Breast. McGraw-Hill, New York, pp 174–186
3. American College of Radiology (2004) Breast Imaging Reporting and Data System (BI-RADS). 4th edn. American College of Radiology, Reston, VA

C

Calcifications, Coronary, Plaque, Calcium Scoring

Christoph R. Becker
Ludwig-Maximilians-Universität, Munich, Germany
christoph.becker@med.uni-muenchen.de

Development of Coronary Atherosclerosis

Coronary atherosclerosis begins as early as in the first decade of life with endothelial dysfunction, proliferation of smooth muscle cells, and deposition of fatty streaks in the coronary artery wall. At the later stage of the still clinically silent disease, which may have already occurred in the first decade of life, these lesions may further accumulate cholesterol within the intima and media coronary artery wall layer, with a fibrous cap separating the lipid pool from the coronary artery lumen. Inflammatory processes with invasion of macrophages and activation of matrix-metallo proteases may cause consecutive weakening of the fibrous cap. Such vulnerable plaques may rupture when exposed to shear stress, and the thrombogenic lipid material may enter the bloodstream. In the most unfortunate event, thrombus progression may turn the vulnerable plaques into culprit lesions that occlude the coronary vessels, leading to myocardial ischemia, ventricular fibrillation, and even death.

In the initial stadium of atherosclerosis, the coronary vessel widens at the location of the atherosclerotic plaques. The phenomenon is called "positive remodeling" and explains why such plaques may not be seen by cardiac catheterization. Nonfatal plaque rupture or erosion at the end stage may heal, organize, and subsequently calcify. Fibrocalcified lesions may reduce vessel lumen diameter by scarring (negative remodeling) with consecutive reduction of blood flow, resulting in myocardial ischemia.

Estimation of Cardiac Event Risk

In many patients, unheralded myocardial infarction associated with a mortality of approximately 20% is the

first sign of coronary artery disease (CAD). Approximately 40% of the general population is considered to have a moderate (10–20%) midterm risk (within the next 10 years) of developing a myocardial infarction. Taking the conventional cardiovascular risk factors (diabetes, hypertension, hypercholesteremia, smoking, family history) into account currently provides the base for myocardial infarction risk assessment according to established risk stratification schemes. All of the currently available risk stratification schemes, however, suffer from lack of accuracy to correctly determine risk, and in particular, uncertainty exists regarding how to treat those who have been identified to be at intermediate risk. Further tools providing information about the necessity to either reassure or treat these individuals are warranted. Computed tomography (CT) is currently the only reliable and practical tool that allows noninvasive investigation of the entire coronary artery tree and quantification of coronary calcium as a surrogate marker of atherosclerotic plaque burden.

Coronary Calcium Screening

As a fundamental requirement for screening for coronary atherosclerosis by CT, the radiation exposure should be reduced to a minimum (about 1 mSv). Any MDCT scanner can perform coronary calcium screening without contrast media by acquiring 3-mm consecutive or better overlapping slices. Even the tiniest calcification will become visible by reconstruction with a no-edge enhancing soft-tissue kernel. After the reconstruction, the image data need to be analyzed and postprocessed by a dedicated workstation. After identification of the specific lesions, the workstation may automatically display the amount of coronary calcium in quantities such as the Agatston score, volume equivalent, and absolute mass.

Coronary calcium is a specific marker for coronary atherosclerosis. In large cohorts of 10,000 asymptomatic persons, it was demonstrated that the amount of calcium depends on gender and increases with age. It was also found that 70% of unheralded myocardial infarction occurred in those patients with a calcium score above the 75th percentile compared with an age- and gender-related asymptomatic cohort. Furthermore, it had been proposed that the amount of calcium detected in an individual asymptomatic person should be seen in conjunction with his or her conventional cardiovascular risk factors. In particular, in persons with an intermediate cardiovascular risk, lower age and lower gender-related calcium in the coronary arteries (<25th percentile) may allow the person to be reassured, whereas any higher amounts of coronary calcium (>75th percentile) may act as a guide to risk factor modification and probably intensive medical therapeutic strategies.

The progression of coronary calcium in subjects with hypercholesteremia may depend on the intensity and efficacy of statin therapy. In asymptomatic hypercholesteremic persons without therapy, ineffective (high-density lipoprotein >120 mg/dL) and effective statin therapy (high-density lipoprotein <120 mg/dL), the annual progression rate was reported to be 52 ± 36%, 25 ± 22%, and −7 ± 23%, respectively. However, it remains unclear how the change in the amount of coronary calcium is related to event risk.

Assessment of Patients with Acute Coronary Syndrome and Acute Chest Pain

The diagnosis, risk stratification, and management of patients with suspected acute coronary syndrome entering the emergency department remains a clinical challenge. Acute coronary syndrome constitutes a broad spectrum of clinical status including ST-elevation myocardial infarction, non-ST-elevation myocardial infarction, and unstable angina. Clinical management with percutaneous intervention, thrombolysis, or medical therapy is clearly established only in a small fraction of patients with acute coronary syndrome. The larger group of patients may present with ambiguous electrocardiogram (ECG) signs or laboratory markers for myocardial ischemia. It has been shown that patients with angina-like chest pain, normal cardiac enzymes, normal or indeterminate ECG, and negative coronary calcium scans as detected by CT may be safely discharged from the emergency department without further testing or observation.

In rare cases, myocardial infarction may occur in patients with no coronary calcium as detected by CT. The entire extent of coronary atherosclerosis with calcified and noncalcified plaques may become visible by the administration of contrast media. The current gold standard for detecting coronary atherosclerosis *in vivo* is intracoronary ultrasound (ICUS). Studies comparing ICUS with MDCT have shown a good correlation between the echogeneity and CT density of coronary atherosclerotic lesions. Plaques with low, intermediate, and high echogeneity may correspond to plaques in MDCT with a density of 14 ± 26 HU, 91 ± 21 HU, and 419 ± 194 HU, respectively. The sensitivity and specificity of CT to detect calcified and noncalcified coronary atherosclerosis is between 78 and 94%, respectively. However, the sensitivity to detect noncalcified plaques in a lesion-by-lesion comparison between CTA and ICUS is only 53%. In heart specimens, the low-density (40 HU) and high-density (90 HU) components of plaques as detected by CT may correspond to lipid and fibrous tissue, respectively. Micro-CT with ultrahigh

spatial resolution is able to distinguish between different plaque components such as lipid, fibrin, and calcium by the different Hounsfield units. In the early stage of atherosclerosis, the proliferation of smooth muscle cells increases the Hounsfield units of atherosclerotic plaques.

In patients with myocardial infarction, noncalcified lesions in the culprit coronary artery may likely correspond to an intracoronary thrombus. Although the entire extent of atherosclerosis is similar in patients with myocardial infarction and stable angina, patients with acute myocardial infarction may present with significantly more noncalcified lesions. On the other side, the extent of calcified lesions was found to be significantly higher in patients with chronic stable angina.

Patients with unstable angina may present with noncalcified low-density plaques in their coronary arteries that may correspond to vulnerable plaques. The vulnerable plaque that had been detected before its rupture may present with a low-density center surrounded by a high-density rim, most likely corresponding to a lipid pool and a fibrous cap, respectively. In due course these plaques may rupture, resulting in a culprit lesion with subsequent myocardial infarction.

As mentioned earlier, large lipid components may be found predominantly in vulnerable plaques that are prone to rupture, with subsequent thrombosis and occlusion of the coronary artery. Currently, however, it appears unlikely that coronary CTA may be used as a screening tool for vulnerable plaques in asymptomatic subjects because of the necessity of administering contrast media and the comparably high radiation exposure for this application. Furthermore, the prospective value for the detection of noncalcified lesions has not been demonstrated so far and needs to be further investigated in clinical studies. If the ability of coronary CTA to detect vulnerable plaques in patients with acute coronary syndrome holds true, new strategies need to be considered for appropriate management of these patients. The noninvasive detection of vulnerable plaques may probably justify intensive medical treatment and follow-up or, alternatively, may lead to invasive approaches, such as plaque sealing. Moreover, in patients with atypical chest pain, CTA may soon serve as a tool for comprehensive diagnostic work-up. A single CTA investigation will allow differential diagnosis for a variety of diseases that need to be taken into account for acute chest pain, including ruling in or out pulmonary embolism, aortic dissection, and CAD.

In the near future, coronary CTA may become a valid pretest before cardiac catheterization for patient triage for conservative, interventional, or surgical therapy, and may reduce the use of invasive diagnostic procedures to preselected patients in whom coronary interventions are essentially required.

Calcinosis Cutis

Calcinosis cutis is a feature of scleroderma, and especially of its subset CREST syndrome. Grouped and speckled calcium deposits are found subcutaneously mainly at pressure-exposed locations like the fingertips. Calcification in hydroxylapatite deposition disease or in polymyositis/dermatomyositis must be considered as the differential diagnosis and can be distinguished by location and morphology as well as additional features (clinical, radiologic).

▶Connective Tissue Disorders, Musculoskeletal System

Calcium Hydroxyapatite Deposition Disease

▶HADD

Calcium pyrophosphate Deposition Disease

▶CPPD

Calcium Pyrophosphate Dihydrate Crystals Deposition Disease (CPPD)

Calcium pyrophosphate dihydrate crystals deposition disease or pseudogout is a joint disease caused by calcium pyrophosphate dihydrate crystal deposits with intermittent attacks of acute arthritis and degenerative arthropathy. A radiographic feature is a linear calcification of articular cartilage, especially fibrocartilage. CPPD is an important differential diagnosis to hemochromatosis.

▶Hemochromatosis, Skeletal

Cane-of-Bamboo Fragment

Cane-of-bamboo fragment describes the complete syndesmophytic bridging of only a few segments, contrasting

with the otherwise normal radiologic appearance of the vertebral spine; it is relatively typical in SAPHO.
▶Spondyloarthropathies, Seronegative

Cane of Bamboo

Cane of bamboo is a typical late-stage radiographic appearance of the lumbar vertebral spine in patients suffering from ankylosing spondylitis. Multisegmentally, the discs are completely bridged by circular ossification of the annulus fibrosus.
▶Spondyloarthropathies, Seronegative

Capillary Telangiectasia

Small nests of dilated capillaries with normal intervening brain tissue. Also known as capillary angioma.
▶Congenital Malformations, Vascular, Brain

Capsule of Ultrasound Contrast Media

▶Contrast Media, Ultrasound, Shell of, Influence on Pharmacology and Acoustic Properties

Caput Medusae Sign

A classic sign of developmental venous anomaly on digital subtraction angiography and magnetic resonance imaging. It is characterized by a nest of small vessels converging toward a bigger enlarged transcortical vein.
▶Congenital Malformations, Vascular, Brain

Carbon Monoxide

Carbon monoxide (CO) is a colorless, odorless gas produced from incomplete fuel combustion. It has a high affinity for hemoglobin and other heme-containing molecules, and severe or prolonged exposure can result in hypoxic brain injury, most commonly affecting the globi pallidi.
▶Toxic Disorders, Brain

Carcinoid Tumor

The term carcinoid covers a broad spectrum of neoplasms that originate from a variety of neuroendocrine cells. The most common carcinoid tumors of the small intestine secrete serotonin or serotonin precursors.
▶Neoplasms Small Bowel

Carcinoid Tumor, Pancreatic

A rare neuroendocrine tumor of the pancreas that originates from the enterochromaffin cells that produce serotonin. It causes a syndrome caused by the increased secretion of serotonin, called carcinoid syndrome. Carcinoid syndrome includes flushing, diarrhea, bronchoconstriction, and cardiac disease. Most patients with carcinoid tumors do not develop carcinoid syndrome.
▶Islet Cells Tumors, Pancreatic

Carcinoma, Breast, Imaging Mammography, Primary Signs

Sue Barter
Cambridge Breast Unit,
Addenbrookes Hospital,
Cambridge, UK
sue.barter@addenbrookes.nhs.uk

Definition

The primary signs of malignancy on mammography are defined as follows:

- Dominant mass
- Microcalcification
- Asymmetric density
- Architectural distortion
- Carcinoma usually appears on a mammogram as a mass, cluster of microcalcification or architectural distortion.

Characteristics

Dominant Mass

A mass as defined by the BIRADS Breast Imaging Lexicon (1) is a space-occupying lesion seen on two different projections. Masses may be irregular, ill-defined, dense or have a spiculated margin, where the lesion is characterised by lines radiating from the margin of the mass. A dense irregular mass with a spiculated margin that is not related to previous surgery is virtually diagnostic of malignancy.

The spicules may radiate out from an ill-defined mass for several centimetres or appear as a 'brush border'. They may be readily visualised when the breast tissue is fatty, but difficult to detect in dense breast tissue (Fig. 1a).

Magnification/paddle mammographic views of ill-defined masses are invaluable for demonstrating spiculation that may be partially obscured by overlying glandular breast tissue.

Pathologically, the spicules represent strands of fibro-malignant tissue that is related to the generalised desmoplastic response produced by cancer in the surrounding tissue.

A mass with spiculated margins should be considered malignant even if it remains stable over time, and biopsied.

Poor definition of the margin of a mass is a common feature of malignancy, though not as specific as a spiculated margin. Cancer should always be considered when a mass has poorly defined margins. Many cancers do not elicit the desmoplastic reaction in the surrounding tissue that produces spiculation, but the lack of definition of the borders raises concern that there is invasion of the surrounding tissue by the malignant process (Fig. 1b).

A mass with microlobulated margins where the lobulations are multiple and measure a few millimetres in diameter is suspicious of malignancy (Fig. 1c).

Some malignant masses contain irregular malignant-type microcalcification (see later). This is usually due to necrosis within the tumour mass, or an associated intraductal component. It is important to identify calcification associated with a malignant mass, especially if it extends beyond the margins of the mass, since there is a high risk of recurrence if the intraduct component is not also excised.

Microcalcifications

Certain shapes and patterns of microcalcification are strongly associated with breast cancer (Fig. 2).

BIRADS defines microcalcification associated with malignancy into the following categories:

- Amorphous or indistinct calcifications. These are often round- or flake-shaped calcifications that have a sufficiently small or indistinct appearance that a more specific morphological classification cannot be determined. They do not layer on horizontal beam magnification lateral images, and are therefore not microcystic. They are of intermediate suspicion and may be associated with malignancy (Fig. 2a).
- Pleomorphic or heterogeneous calcifications. These are usually more conspicuous than the amorphic forms and are neither typically benign, nor malignant in appearance, being irregular in shape with varying sizes and density. They are usually less than 0.5 mm in diameter. They should be regarded as suspicious of malignancy (Fig. 2b).
- Fine, linear or fine, linear and branching (casting) calcifications. These are thin irregular calcifications that appear linear, but are discontinuous and under 0.5 mm in width. Their distribution follows the course of the duct system involved, and the casting appearance is due to filling of the lumen of the duct involved irregularly with necrotic carcinoma cells. This pattern of microcalcification is most often seen with comedo-type ductal carcinoma *in situ* (DCIS), and is virtually diagnostic (Fig. 2c).

Distribution of suspicious microcalcification

The ACR BIRADS defines four patterns of distribution:

1. Clustered
2. Segmental
3. Regional
4. Diffusely scattered

Clustered microcalcification is suspicious, especially if the cluster has a triangular shape. A cluster of five or more particles of pleomorphic microcalcification, which is demonstrated in a volume of 1 cc has a 20–25% risk of malignancy.

Microcalcification that falls into any of the above categories should be investigated further with core biopsy or wide-bore needle (mammotome) biopsy.

Asymmetric Density

This is a density that cannot be accurately described by shape. It is visible as asymmetry of tissue density with similar shape on two views, but completely lacks borders or the definition of a true mass.

It may represent an island of normal breast tissue but its lack of specific benign characteristics warrants further investigation by magnification/paddle views and ultrasound.

Additional imaging may reveal an underlying true mass or significant architectural distortion (Fig. 3).

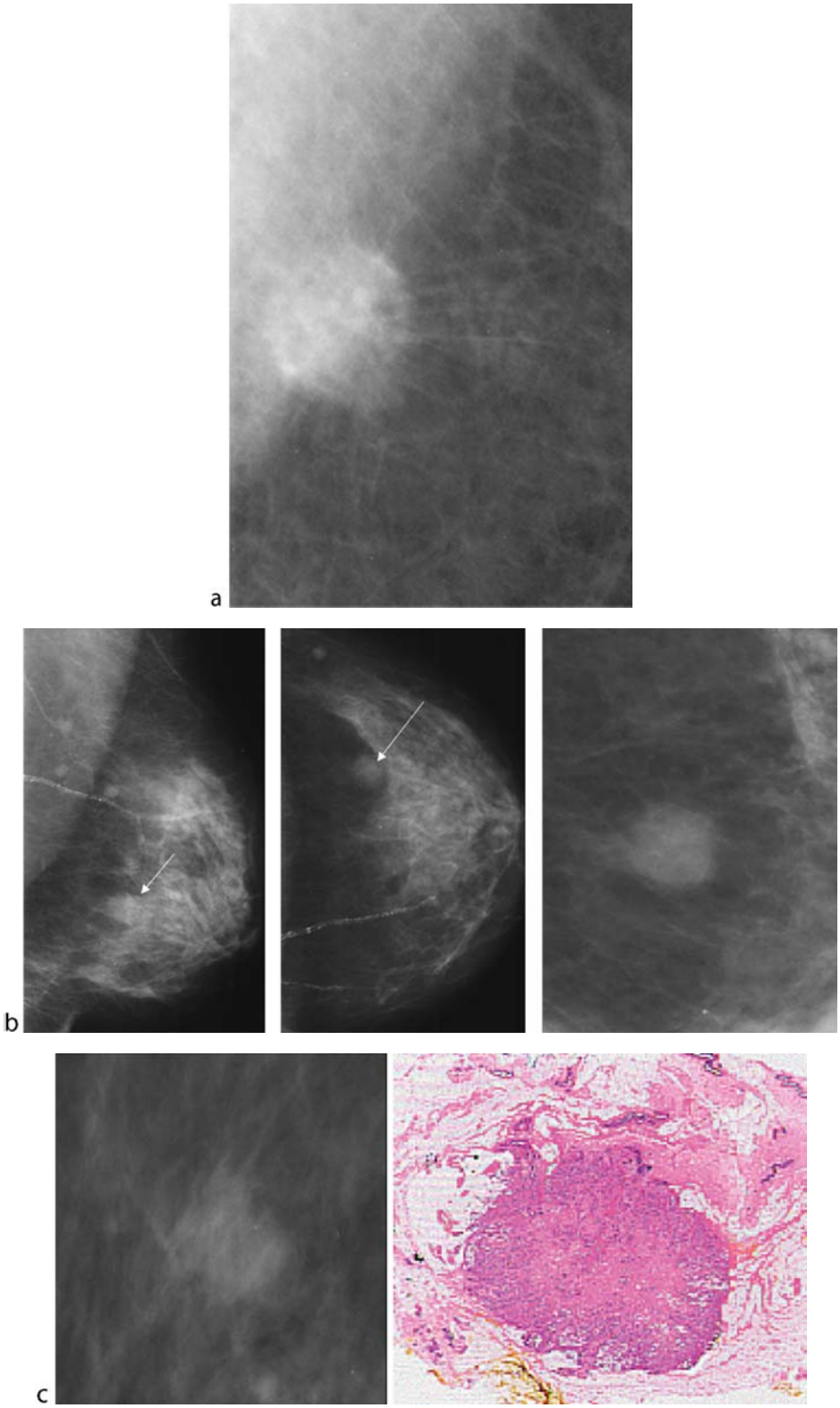

Carcinoma, Breast, Imaging Mammography, Primary Signs. Figure 1 (a) Spiculate mass due to 11 mm invasive ductal carcinoma. (b) Poorly defined mass due to invasive ductal carcinoma Grade 3. (c) Lobulated mass due to Grade 3 infiltrating ductal carcinoma.

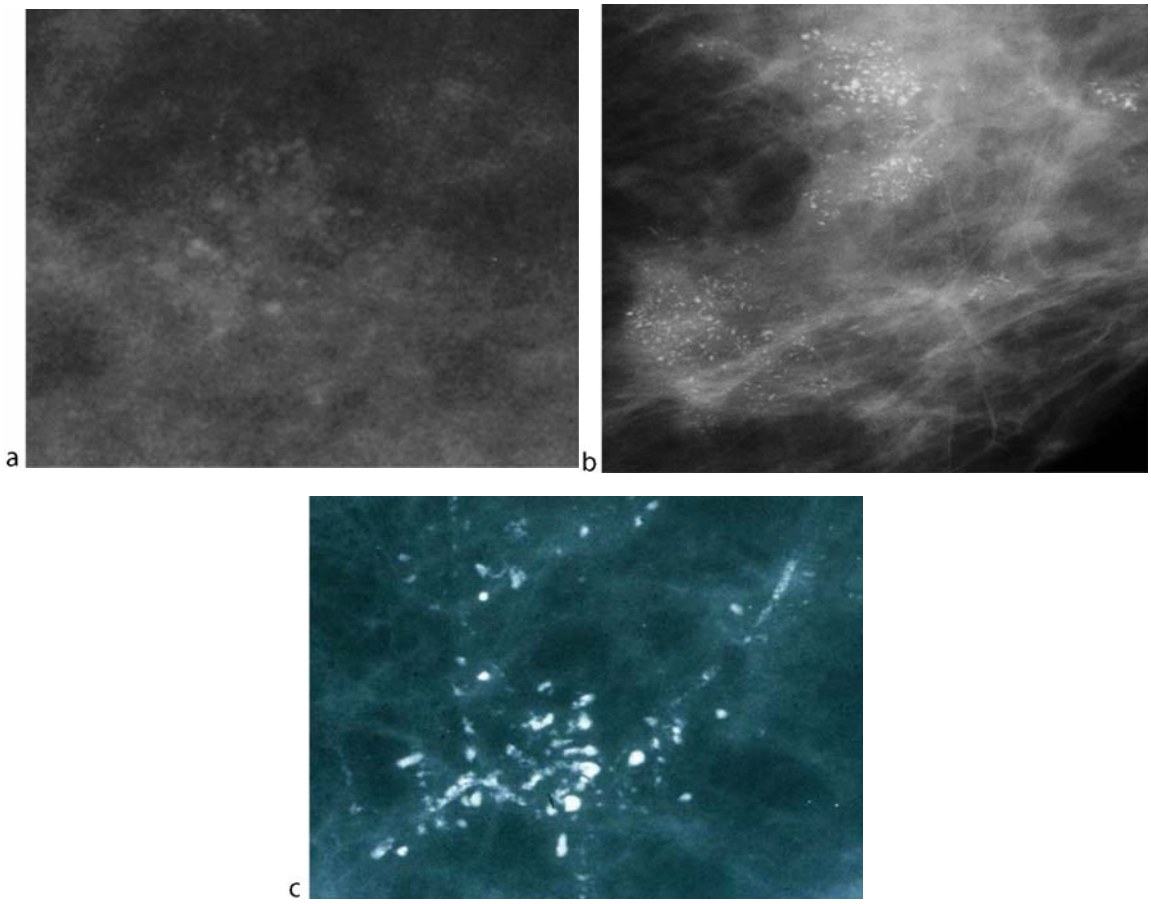

Carcinoma, Breast, Imaging Mammography, Primary Signs. Figure 2 (a) DCIS: Amorphous microcalcification. (b) DCIS: Pleomorphic-type microcalcification. (c) DCIS: Casting-type microcalcification.

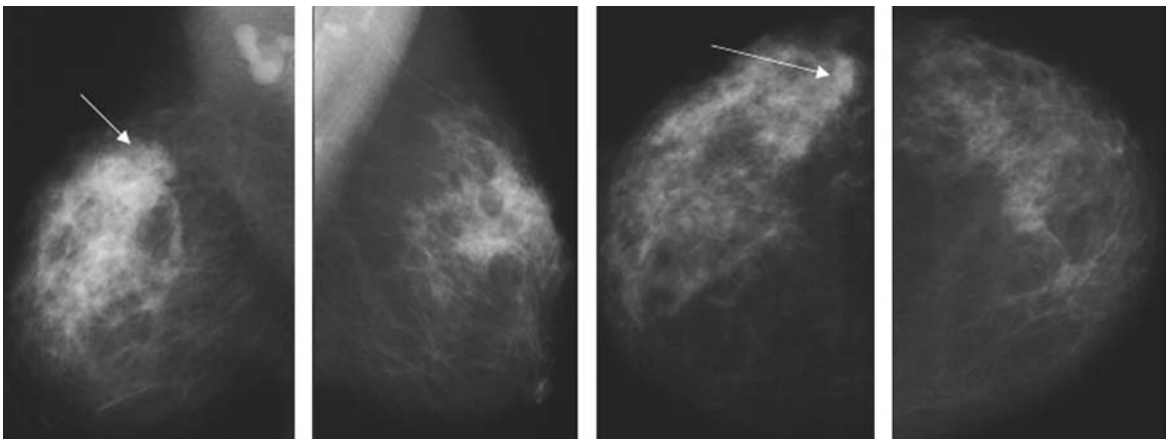

Carcinoma, Breast, Imaging Mammography, Primary Signs. Figure 3 Asymmetric density, Grade 2 38 mm IDC and ILC.

Architectural Distortion

Normal breast architecture is distorted with no definite mass visible. This includes spiculation radiating from a point. Architectural distortion is often visible at the parenchyma/subcutaneous fat interface as a flattening or retraction of the parenchyma.

The posterior margin of the parenchyma is the other site that should be carefully examined for signs of

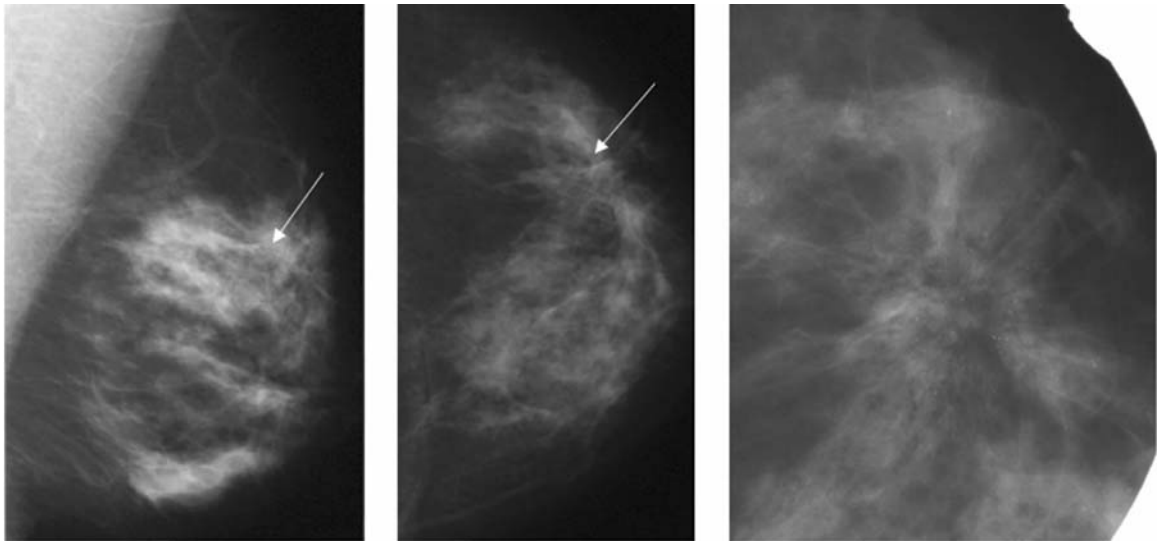

Carcinoma, Breast, Imaging Mammography, Primary Signs. Figure 4 Parenchymal distortion, Grade 1 tubular carcinoma.

architectural distortion. Focal retraction or distortion of the parenchymal edge should be investigated further with magnification/paddle views and high-resolution ultrasound (Fig. 4).

Breast cancer does not always produce a mammographically visible mass but frequently disrupts the normal surrounding tissue. This is an important but often subtle sign of malignancy.

Post-surgical scarring and fat necrosis are the most common non-malignant causes of architectural distortion. Radial scars may also produce architectural distortion.

If any of the primary signs of malignancy are detected on mammography, full breast assessment should be carried out, including needle biopsy.

Bibliography

1. American College of Radiology (ACR) (2003) Breast Imaging Reporting and Data System Atlas (BI-RADS Atlas). Reston, Virginia

Carcinoma, Breast, Imaging Mammography, Secondary Signs

Sue Barter
Cambridge Breast Unit,
Addenbrookes Hospital,
Cambridge, UK
sue.barter@addenbrookes.nhs.uk

Definition

The secondary signs of malignancy on mammography are defined as

- Enlarged axillary lymph nodes
- Asymmetric ducts or duct dilatation
- Skin and nipple changes
- Oedema of all or part of the breast
- Asymmetric breast tissue
- Increased vascularity with vascular engorgement
- Distortion of parenchymal edge, obliteration of the subcutaneous or retromammary space.

Enlarged Axillary Lymph Nodes

Enlarged axillary lymph nodes as the sole indicator of underlying malignancy in the breast are uncommon. Mammography only gives a limited view of the axilla, with the lower level 1 lymph nodes visible on the MLO view (Fig. 1).

Normal axillary nodes are less than 2 cm in size and have a hilar notch or lucent centre due to fat in the hilum. They may be almost replaced by fat so that only a thin rim of lymphoid tissue is visible around a lucent centre. When fatty replacement of a node occurs, the node may be enlarged, reaching up to 3–4 cm in size.

Lymph nodes that are 1.5–2 cm in size without a fatty hilum or lucent centre should be considered suspicious and investigated. Such findings are however non-specific, and may be secondary to reactive hyperplasia, lymphoma, collagen/vascular disease or metastases from other sites. It is not possible mammographically to differentiate benign lymphadenopathy from secondary involvement with breast cancer on mammography, and ultrasound and core biopsy or fine needle aspiration cytology of abnormal nodes is indicated (1, 2).

When malignancy suspicious for a breast primary is detected in axillary nodes, without any evidence of a

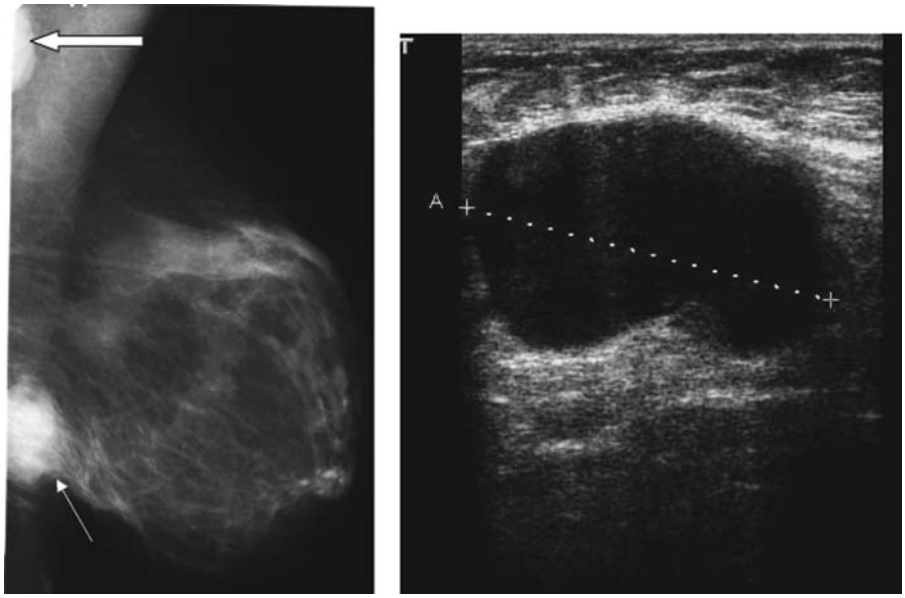

Carcinoma, Breast, Imaging Mammography, Secondary Signs. Figure 1 Diffuse breast oedema: note skin and trabecular thickening. Inflammatory carcinoma with axillary lymph node involvement.

primary lesion on mammography, MRI has become the investigation of choice for demonstrating occult breast malignancy (3).

Asymmetric Ducts or Duct Dilatation

Breast tissue may contain serpentine or nodular structures on mammography, and these represent asymmetric ducts or duct dilatation. Wolfe suggested that the presence of such findings was an indicator of malignancy, but other authors have found that asymmetric ducts are fairly common and part of the spectrum of benign breast change. Unless asymmetric or dilated ducts are associated with a palpable abnormality or mammographic sign of malignancy such as a mass or microcalcification, they should be considered a normal variant (4, 5).

A group of ducts converging on the nipple, and asymmetric compared to the contralateral breast is striking mammographically, but usually represents benign duct ectasia (5).

Skin and Nipple Changes

Skin changes associated with breast cancer are generally late changes due either to direct invasion by tumour, or obstruction of draining veins or lymphatics. Generally skin and nipple changes are best evaluated clinically.

Nipple retraction or inversion is usually long standing and due to benign changes such as involution or duct ectasia. When associated with malignancy it occurs over a short period of time, and is usually associated with a cancer lying close beneath the nipple, readily visible on the mammogram. It is very rarely the only mammographic sign of malignancy and scrutiny of the retroareolar region in such cases, augmented by magnification/paddle views will invariably demonstrate the underlying tumour.

When skin retraction is visible clinically, the tumour mass is usually readily seen on the mammogram. Sometimes a deep cicatrizing tumour deeper within the breast can cause skin retraction through involvement with Cooper's ligaments.

Diffuse skin thickening associated with cancer indicates advanced disease. There is usually associated diffuse thickening of the trabecular pattern. (Fig. 2). These appearances are non-specific and may represent oedema due to lymphatic or venous obstruction.

Thickened skin is often demonstrated in inflammatory carcinoma, usually due to diffuse permeation of the dermal lymphatics by tumour. The diagnosis is usually evident clinically with the classic triad of skin oedema, erythema and inflammation, in the absence of infection.

Oedema of All or Part of the Breast

The mammographic features of oedema of the breast are non-specific. There is a diffuse thickening of the trabecular pattern, often associated with skin thickening. If due to malignancy it is usually a late change indicating advanced disease, and is either due to diffuse infiltration, or lymphatic or venous obstruction (Fig. 2).

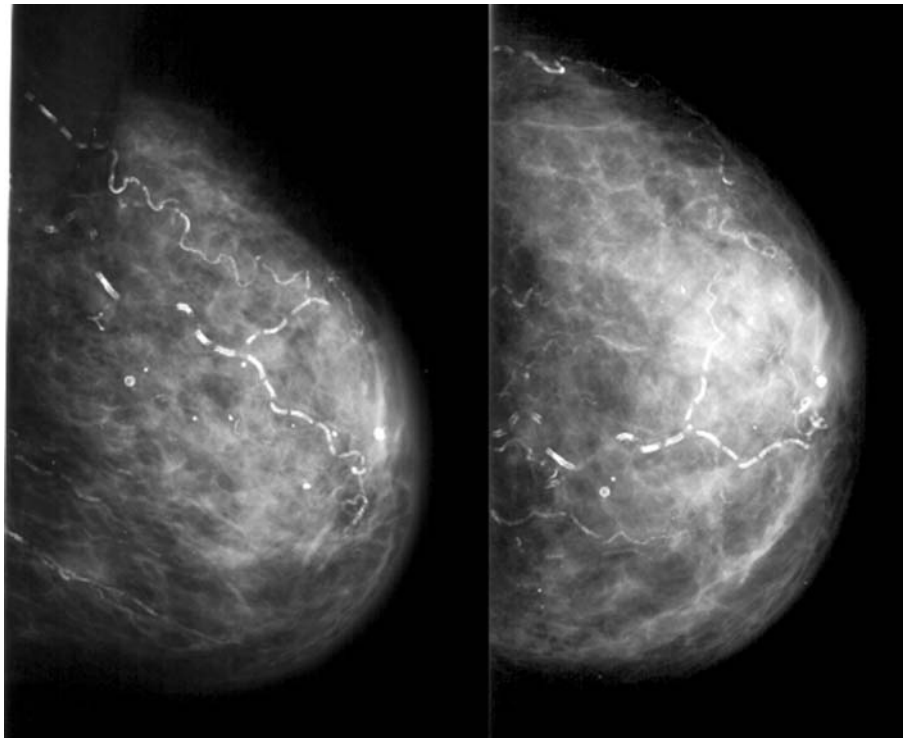

Carcinoma, Breast, Imaging Mammography, Secondary Signs. Figure 2 Mammogram and ultrasound of enlarged axillary node (block arrow) The cancer is readily visible inferiorly (small arrow).

Radiotherapy may also be a cause of diffuse breast oedema in the treated breast and should not be mistaken for recurrence. Oedema may be evident on the baseline post-treatment mammogram, but usually improves over time.

Asymmetric Breast Tissue

This should not be confused with focal asymmetric density (see primary signs of malignancy). Asymmetric breast tissue is a variant of normal, where there is a greater volume of glandular breast tissue in either the whole breast or part of the breast when compared to the other side. It is rarely due to an underlying breast cancer, usually a diffuse invasive lobular cancer.

Some palpable cancers do not produce a mammographically discreet lesion, or microcalcification, and the only visible finding may be an increase in density usually in part and rarely in all of the mammogram.

A progressive increase occurs in asymmetric density, particularly when focal should be investigated further; but it should be borne in mind that hormone replacement therapy (HRT) can often cause a diffuse or focal increase in breast density.

If the breast architecture is preserved, and there is no underlying mass or microcalcification, and the patient is clinically normal, then the asymmetry is almost always a normal variation (5).

Increased Vascularity with Vascular Engorgement

Increased vascularity as the only sign of breast carcinoma is extremely uncommon. Asymmetric prominence of veins in the breast is usually caused by under-compression during acquisition of the mammogram. Advanced breast cancer causing venous obstruction in the axilla may cause venous engorgement of the affected breast.

Distortion of Parenchymal Edge, Obliteration of the Subcutaneous or Retromammary Space

In the normal breast, the interface between the subcutaneous fat and the breast parenchyma shows a

scalloped pattern due to Cooper's ligaments attaching to the skin. Breast cancer, which develops near the edge of the breast parenchyma, can cause distortion of this pattern, either by causing flattening or retraction of the parenchymal edge, or a bulge into the subcutaneous fat. Similarly, the fat/parenchymal interface posteriorly may be distorted or shows a focal bulge due to a carcinoma.

Bibliography

1. Murray GM, Given-Wilson RM (1997) The clinical importance of axillary lymphadenopathy detected on screening mammography. *Clin Radiol* 52(6):458–461
2. Patel T, Given-Wilson RM, Thomas V (2005) The clinical importance of axillary lymphadenopathy detected on screening mammography: revisited. *Clin Radiol* 60(1):64–71
3. Buchanan CL, Morris EA, Dorn PL et al (2005) Utility of breast magnetic resonance imaging in patients with occult primary breast cancer. *Ann Surg Oncol* 12(12):1045–1053
4. Wolfe JN (1967) Mammography: ducts as a sole indicator of breast carcinoma. *Radiology* 89:206
5. Kopans DB, Swann CA, White G et al (1989) Asymmetric breast tissue. *Radiology* 171:639–643

Carcinoma, Breast, Demography

Sue Barter
Cambridge Breast Unit,
Addenbrookes Hospital,
Cambridge, UK
sue.barter@addenbrookes.nhs.uk

Definition

Breast cancer is the third most common cancer in the world, creating a burden of disease comparable with that of colorectal cancer. With over half a million new cases in the world each year, only cancer of the lung and stomach occurs with greater frequency, and breast cancer, overall, accounts for about 9% of cancer cases in the world, and over 18% of cancers occurring in women. It is most common in North America and Western Europe, accounting for about one in four female cancers in these regions, whereas in the Far East (China and Japan) it is very much rarer. It is also common in southern South America. The highest incidence rates of all are found in Hawaii, where a rate of 93.9 per 100,000 female population has been reported, and in US white women. The incidence rises with age from about 30 years, but more slowly after the menopause than before. There are ethnic variations such as a high incidence in Israeli Jews compared with non-Jews in Israel. It is more common in single women, in higher social classes, and in urban rather than in rural areas. About 1% of cases occur in males.

Risk Factors

Breast cancer is a multifactorial disease that may involve life style, environmental and reproductive factors, as well as genetic factors. As with many other cancers, it may also involve as yet unknown factors. One in ten women will develop breast cancer by the age of 80. For most women, as they get older, their risk of breast cancer increases.

Risk Associated with Family History

- The risk of breast cancer in women with an affected first-degree relative (mother, sister, or daughter) is approximately twice the risk to other women.
- The risk of breast cancer is related to the strength of the family history. The risk increases with the number of affected relatives, and increases as the age of the affected relatives decrease.
- Only a minority of this increase risk is due to the known high risk genes BRCA1 and BRCA2.
- The chance of carrying a BRCA1 or BRCA2 mutation is related to the strength of the family history not only of breast cancer but also of ovarian cancer and male breast cancer.
- The risks of breast cancer in carriers of BRCA1 or BRCA2 mutations have been estimated as between 60% and 80% and between 40% and 80%, respectively.

Hormonal Factors

Factors that influence the amount of estrogen produced by a woman's body over her lifetime (such as the ages at the onset of menstruation, pregnancy, and age at menopause) are known to influence breast cancer risk. During the reproductive years, a woman's body produces high levels of estrogen.

- Earlier menarche (aged 12 or younger) and late menopause (aged 55 or older) is associated with an increase in risk of breast cancer Women who start to menstruate at an early age and reach menopause at a late age are exposed to high levels of estrogen for more years than are women who have a late menarche or early menopause.

- Nulliparity and late age at first birth are associated with significant increases in breast cancer risk.
- Women who have their first full-term pregnancy at a relatively early age have a lower risk of breast cancer than those who never have children or those who have their first child relatively late in life.
- Pregnancy may lead to lasting changes in the sensitivity of breast tissue to cancer-causing agents, as well as in the maturation of breast tissue. In addition, several hormonal changes occur after a full-term pregnancy and may persist for years.
- Increased parity has been found to be associated with a decrease in breast cancer risk (38% decrease in risk in women who reported five or more live births, 32% decrease in risk in women who reported three or more births compared to women who reported one birth).

Hormone Replacement Therapy

Evidence suggests that hormone replacement therapy (HRT) is associated with an increase in breast cancer risk.

- The Million Women Study found that the relative risk of breast cancer in current users increased with increasing total duration of use of HRT (1). The risk associated with HRT is small for short duration use (up to 2 years) but is in the region of a two-fold risk for women taking combined HRT for 10 years or more.
- The Million Women Study found that the associated risk was substantially greater for estrogen–progestagen than for other types of HRT, and suggests that there is little or no overall increase in the relative risk of breast cancer in past users of HRT.
- The Collaborative Group (2) has shown that there is 2.3% increase in relative risk for every year used. The risk appears to be confined to current users and women who have used HRT in the last 5 years and that the risk of HRT use disappears 5 years after stopping.

Hormonal Contraceptives

Numerous scientific studies have investigated the relationship between the use of oral contraceptives (birth control pills) and the risk of breast cancer.

- Use of oral contraceptives slightly increases the risk of breast cancer.
- This increase in risk appears to be confined to current and recent use (within 5–10 years, relative risk 1.24 for current users).

Breastfeeding

Breastfeeding confers a protective effect on breast cancer risk.

- The Collaborative Group (3) found that each 12 months of breastfeeding confers a reduction of about 4%.
- The protective effect of breastfeeding is in addition to the protective effect of pregnancy alone.
- The reduction in breast cancer risk is related to total duration of breastfeeding.
- If breastfeeding does protect against breast cancer, it may do so by delaying the resumption of ovulation (with its accompanying high estrogen levels) after pregnancy.

Alcohol Consumption

The risk of breast cancer increases with alcohol consumption.

- The Collaborative Group (4) reported an increase of 7.1% in relative risk for each additional 10 g/day intake of alcohol.
- Women who drink moderate amounts of alcohol have been found to have a slightly higher risk of breast cancer than do those who abstain. It is uncertain, however, whether this association reflects a cause-and-effect relationship.
- The use of alcohol may vary among women who differ with regard to other factors that are known to influence breast cancer risk—such as age, obesity, and reproductive history.

Weight

A high body mass index (BMI) is associated with a significant increase in post-menopausal breast cancer risk in the general population.

- A recent IARC report (5) suggested that more than 100 studies over nearly 30 years in populations in many countries have established that increased body weight increases breast cancer risk among post-menopausal women.
- Almost all of these studies have shown that this association is largely independent of a wide variety of reproductive and life style risk factors.
- The association between being overweight and breast cancer appears to increase in a stepwise fashion with advancing age after the menopause (5).
- This relationship is probably mediated by estrogen production. Fat cells produce some and obese

post-menopausal women, therefore, tend to have higher blood estrogen levels than non-obese women do.

- Obesity does not seem to be a risk factor for breast cancer in pre-menopausal women. In younger women, the ovaries are the main producers of estrogen. The much smaller amount of estrogen produced by the fat cells does not appear to have any significant impact on breast cancer risk.

Physical Activity

Scientific studies have consistently shown that the risk of breast cancer is lower among physically active pre-menopausal women than among sedentary women.

- Moderate physical exercise is associated with a decreased risk in breast cancer. The effect of physical activity on breast cancer risk may be due at least in part to effects of exercise on the female hormones.
- Although the effects of obesity and physical inactivity on breast cancer risk are not as strong as the effects of previous breast disease or family history of breast cancer, they are important risk factors because they are modifiable.
- Exercise and weight control currently represent the most effective life style changes that a woman can make to reduce her risk of breast cancer.
- Lack of physical activity is an established risk factor for pre-menopausal breast cancer and represents part of a complete approach to weight management.

Radiation

Exposure to ionizing radiation, particularly in the young breast, is associated with an increased risk of developing breast cancer.

There is now substantial evidence that women who received radiotherapy at or below the age of 35, which included part of their breast tissue (upper body mantle radiotherapy), have a higher risk of developing breast cancer.

Bibliography

1. Million Women Study Collaborators (2003) Breast cancer and hormone-replacement therapy in the Million Women Study. Lancet 362:419–427
2. Collaborative Group on Hormonal Factors in Breast Cancer (1997) Breast cancer and hormone replacement therapy: collaborative reanalysis of data from 51 epidemiological studies of 52,705 women with breast cancer and 108,411 women without breast cancer. Lancet 350:1047–1059
3. Collaborative Group on Hormonal Factors in Breast Cancer (2002) Breast cancer and breastfeeding: collaborative reanalysis of individual data from 47 epidemiological studies in 30 countries, including 50,302 women with breast cancer and 96,973 women without the disease. Lancet 360:187–195
4. Collaborative Group on Hormonal Factors in Breast Cancer (2002) Alcohol, tobacco and breast cancer—collaborative reanalysis of individual data from 53 epidemiological studies, including 58,515 women with breast cancer and 95,067 women without the disease. Lancet 87:1234–1245
5. International Agency for Research on Cancer (IARC) (2002) IARC Handbooks of Cancer Prevention. Volume 6: Weight Control and Physical Activity. IARC Press, Lyon

Carcinoma, Breast, Inflammatory

Common features of inflammatory carcinomas are skin thickening and diffuse increased breast density. Other findings such as trabecular thickening, axillary lymphadenopathy, architectural distortion, focal asymmetric density, and nipple retraction may be found. Less often, calcifications or masses are present. This tumor entity may be misdiagnosed as benign inflammatory process.

▶Carcinoma, Other, Invasive

Carcinoma, Cervix Uteri

Martin Unterweger
Diagnostic Radiology, Cantonal Hospital Baden, Baden, Switzerland
Martin.Unterweger@ksb.ch

Synonyms

Cervical carcinoma

Definition

Carcinoma of the cervix uteri is 3rd most common tumor of the female pelvis. After the age of 20 years the incidence increases with two incidence peaks around 30 years for *in situ* carcinoma and around 60 years for invasive cancer. Risk factors for the development of cervical carcinoma include early age intercourse, multiple sexual partners, and perhaps the most important exposure to specific subtypes of the human papillomavirus (HPV). Screening is possible with the Papanicolau smear.

Pathology/Histopathology

Approximately 80–90% of cervical malignancies are squamous cell carcinomas. The remaining 10% of cervical cancers consist of adenocarcinomas and rarely sarcomas. The majority of cervical carcinomas occur at the squamocolumnar junction. Cervical carcinoma normally arises from a preexisting dysplastic lesion. Carcinoma *in situ* represents extension of malignant cells to the basal membrane of the epithelium. The metastatic spread is generally lymphatic, first in the iliac lymph nodes and further in the retroperitoneal lymph nodes. Hematogenic metastases are rarely seen. The most common sites of metastasis are the lungs, bones, and liver.

Clinical Presentation

The major symptoms of cervical carcinoma are vaginal discharge and bleeding, but over 20% of patients with invasive cervical carcinoma are asymptomatic. Pelvic or abdominal pain and urinary problems are less common symptoms and occurs normally in advanced cases.

The International Federation of Gynecology and Obstetrics (FIGO) classification is used for staging in most institutions (Fig. 1). This classification is based on clinical findings of the primary tumor as well as on lymphatic spread. Because of good soft tissue contrast MRI was shown to be superior to CT in staging cervical carcinomas, e.g., for diagnosis of parametrial invasions (1, 2). It was shown to be a helpful addition to transvaginal ultrasound especially in tumors exceeding 2 cm *in situ* (3).

Surgery is usually performed in FIGO I-IIA. In FIGO IIB or more adjuvant radiotherapy is regarded as therapy of choice. Therefore, pretherapeutic staging is important for decision-making.

Imaging

MRI with his high soft tissue contrast is an ideal imaging modality for evaluation of cervical carcinoma. Cervical carcinoma will be identified as a high signal intensity mass on T2-weighted images. Cervical carcinomas are lesser conspicuous on T1-weighted images, because of similar signal intensity to the normal cervical tissue. MR contrast medias cause variable tumor enhancement and are rarely indicated. They could be helpful for depiction of bladder or rectal wall infiltration.

TNM	FIGO	MRI findings
Tis	0	Carcinoma in situ (before invasion), no indication for MRI
T1	I	Cervical carcinoma confined to the cervix
T1a	IA	Microscopic diagnosis, no tumor on MRI
T1b	IB	Carcinoma only in cervix uteri, tumor hyperintense compared to cervical stroma
T2	II	Tumor invades beyond uterus, no expansion in the pelvic sidewall
T2a	IIA	Invasion of vagina excluding lower 1/3, parametrium without tumor
T2b	IIB	Infiltration of parametria, disruption of low-signal-intensity stromal ring (T2w)
T3	III	Tumor in the lower vagina, pelvic wall infiltration or hydronephrosis
T3a	IIIA	Tumor infiltrating the lower vagina, best seen on sagittal plane
T3b	IIIB	Tumor infiltrating the pelvis wall or hydronephrosis, dilated ureter (MR urography)
T4	IV	Tumor outside the pelvis, distant metastasis
T4a	IVA	Invasion of the bladder and rectal mucosa, obliteration of fat planes between cervix and bladder or rectum, retrospectively
T4b	IVB	Distant metastasis

Carcinoma, Cervix Uteri. Figure 1 Staging of carcinoma cervix uteri according to TNM and FIGO. (From Pakkal MV, Rudralinbgam V, McCluggage WG et al MR staging in carcinoma of the endometrium and carcinoma of the cervix)

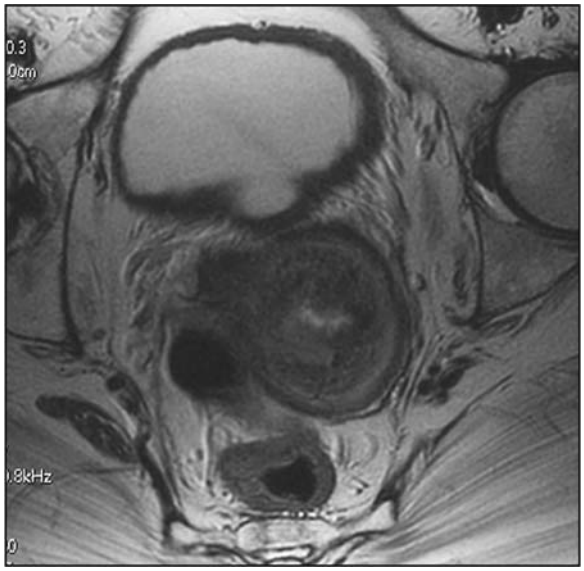

Carcinoma, Cervix Uteri. Figure 2 Axial oblique (perpendicular to the cervical cancel) T2-weighted MRI with a cervical carcinoma in stage IB. The tumor is restricted to the cervix uteri, the hypointense stroma is not disrupted.

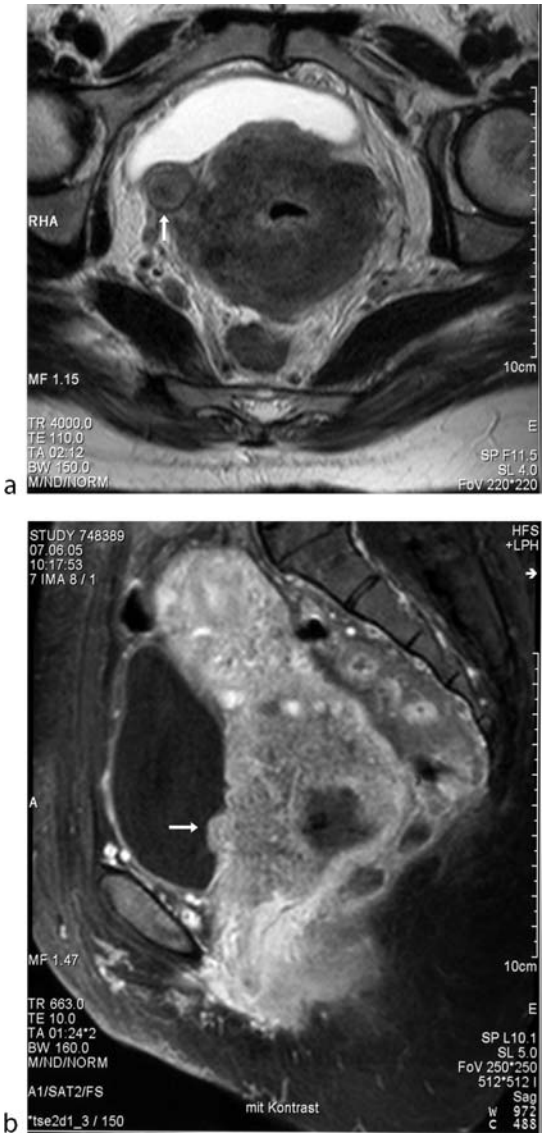

Carcinoma, Cervix Uteri. Figure 3 (a) Cervical carcinoma stage IVA with infiltration of the bladder and rectal wall on a T2-weighted transversal MR image. Enlarged lymph node (arrow). (b) Sagittal contrast-enhanced T1-weighted MR image shows the cervical carcinoma with urinary bladder wall infiltration (arrow) in stage IVA.

The staging of cervical carcinoma with MRI is based on the FIGO criteria. In stage IA there is no MR correlation of the cervical carcinoma because it is a preclinical diagnosis, which can only be demonstrated microscopically. In stage IB the tumor is restricted to the cervix without infiltration of the vagina (Fig. 2) and the stroma surrounding the tumor is intact. In stage IIB the parametria are infiltrated, where the tumor extend over the cervix border into the parametria. The low-signal-stromal ring is disrupted on MRI. In FIGO IIIA tumor infiltrates the lower vagina best seen on sagittal images and in IIIB extend to obturator internal, piriformis or levator ani muscle. Hydronephrosis also is a sign for this stage. In such cases, additional MR urography will be helpful. In stage IVA the tumor infiltrates the bladder or rectal wall, which can be well demonstrated on T2-weighted MRI without fat saturation because of the fat plane obliteration between cervix and bladder or rectal wall (Fig. 3). Distant metastases are seen in stage IVB. In the literature the overall accuracy of MRI staging is reported to be 76–92%.

The most important prognostic criteria are the parametrial infiltration and lymphatic spread. MRI, as CT, has a limited sensitivity for lymph node metastases. CT has become increasingly popular in the staging of cervical carcinomas. CT is able to demonstrate the primary tumor in cases of extensive disease as well as hydronephrosis. Furthermore encasements of the iliac vessels, enlargements of the obturator or piriformis muscles are all signs of stage III disease. But the most important use of CT in cervical carcinoma is the evaluation of lymphatic nodes. However, lymph node size is the only morphological criterion used to determine the presence of metastases. CT has a fairly high specificity (93%) when utilizing criteria of nodal enlargement greater than 1 cm in the short axis as pathologic. However, the overall accuracy of detecting lymph node metastasis varies in the literature between 70% and 75%. In the evaluation of parametrial infiltration, CT has an overall accuracy of 76%, a positive predictive value of 58%, and a negative predictive value of 85%.

Endovaginal sonography is normal directly applied by the gynecologist. Large necrotic tumors can appear as hypoechogenic masses. Sonography can demonstrate urinary obstruction with high degree of accuracy. Invasion of the bladder and parametrium infiltration can sometimes be seen. However, sonography is limited in differentiating between tumor and normal cervical tissue. Furthermore, accuracy for the evaluation of pelvic and retroperitoneal lymph nodes is limited with sonography.

Recurrence of cervical carcinoma occurs normally within 2 years. The difference of fibrosis and recurrence is seldom possible with MRI within 12 month after the end of treatment, since reparative tissue change after radiotherapy will also show contrast enhancement.

Bibliography

1. Durfee SM, Zou KH, Muto MG et al (1996) The role of magnetic imaging in treatment planning of cervical carcinoma. J Woman Imaging :63-68 vol 12(2)
2. Hamm B, Kubik- Huch RA, Fleige B (2001) MR and CT of the female pelvis. Radiological–Pathological Correlation Europ Radiol 11:233–245
3. Akata D, Kerimoglu U, T Hazirolan et al (2005) Efficacy of transvaginal contrast-enhanced MRI in the early staging of cervical carcinoma. Eur Radiol 15:1727–1733
4. Pakkal MV, Rudralinbgam V, McCluggage WG et al MR staging in carcinoma of the endometrium and carcinoma of the cervix (2004) The Ulster medical journal, 73(1), 20–24
5. Tavassoli FA and P Deville (2003) Tumor of the Breast and Female Genital Organs. WHO classification of tumors. Pathology and Genetics Tumor of the Breast and female Genital organs. Lyon: IARC Press

Carcinoma, Ductal, *In Situ*, Breast

Fischmann Arne
Department of Diagnostic Radiology, University of Tübingen, Tübingen, Germany
arne.fischmann@med.uni-tuebingen.de

Synonyms

Ductal intra-epithelial neoplasia (►DIN) type 1c to 3

Definition

DCIS is an epithelial neoplasia originating in the terminal ductulo-lobular unit and progressing into the ductal system that is confined to its natural basement membrane boundaries. The differentiation of the DCIS from premalignant lesions with identical origin (ductal hyperplasia or DIN 1a, atypical ductal hyperplasia or DIN 1b) may often be difficult. DCIS is a precursor of invasive ductal carcinoma but does not invariably lead to invasion and is therefore omitted in the pathologic classification by the concept of ductal intra-epithelial neoplasia. The different patterns are risk factors for invasive growth of different magnitude.

Pathology/Histopathology

DCIS poses an increasing problem to pathology as more lesions are detected with modern imaging methods and mammography screening. Gradual changes with increasing likelihood of malignancy often lead to inter-individual variation of classification.

According to the pathologic pattern in HE-stains DCIS is divided into five groups: comedo type with necrosis, cribriform, papillary, micropapillary and solid mosaic. The comedo subtype is the most common form of DCIS having the highest risk of infiltrative growth. In more than 50% these patterns coexist in the same specimen or sometimes even in the same duct especially in large tumours. The former concept of 'non-invasive' carcinoma is nowadays replaced by cellular and structural changes representing increasing probability of malignant transformation and infiltrating growth.

The following grading system of ductal intra-epithelial neoplasia (DIN) was advocated by the world health organization (WHO). It represents the view that transformation from ductal hyperplasia to intra-epithelial neoplasia is a gradual process and no clear-cut margin of malignant disease can be established

- DIN 1a represents intraductal hyperplasia without atypia
- DIN 1b represents atypical intraductal hyperplasia (►AIDH)
- DIN 1c is a low-grade DCIS or G1 lesion often of the micropapillary or cribriform subtype
- DIN 2 represents an intermediate grade (or grade 2) DCIS
- DIN 3 is a high-grade (or grade 3) DCIS usually of the comedo subtype displaying cellular atypia and necrosis

Microinvasion is described as extension of cancer cells beyond the basement membrane with no single focus larger than 1mm in greatest diameter (T1mic) and is seen in approximately 14% of cancer cases increasing with size (1).

Although this system has many advantages over previous classifications the precise grading of a single

lesion, especially the differentiation of AIDH and DCIS remains difficult and inter-observer variability remains high, e.g. mitotic activity may vary according to age and is of little use in the classification of DCIS and AIDH. Therefore exact grading does not only include histologic changes but also extent of disease: a lesion with the cytologic and architectural features of low-grade DCIS not exceeding 2 mm qualifies to be AIDH (2).

As histologic grading (especially presence of comedonecrosis) and tumour-free margin of less than 1mm are known to be associated with increased risk of recurrence, the so-called Van Nuys Prognostic index was developed that shows a good correlation to the risk of recurrence.

Van Nuys prognostic index

Value	1 Point	2 Points	3 Points
Tumour size	≤15 mm	16–40 mm	>40 mm
Tumour-free margin	≥10 mm	1–9 mm	<1 mm

Values are added and the result correlates to prognosis: An index of 3–4 has a risk of recurrence of about 2%, 5–7 about 19%, 8–9 of more than 50%.

Molecular markers are of increasing importance in the grading of DCIS, as these changes seem to persist in consecutive invasive disease: low-grade DCIS will usually lead to low grade IDC while high-grade DCIS will cause high-grade IDC. Oestrogen receptor is negatively correlated to histologic grading and therefore more likely to be expressed in low grade DCIS, while p53 is mainly expressed in DIN 3. HER2 is negatively correlated with prognosis. Cellular alterations (like loss of oestrogen receptor or actin in the myoepithelium) are often present before morphological changes can be detected by ►H&E-staining, this being true especially in hyperplastic areas adjacent to comedocarcinoma. ►VEGF, Ki-S1 and ►PDGF as well as c-erb are expressed but clinical significance remains obscure.

Clinical Presentation

Most patients with DCIS present without clinical symptoms and are detected during screening mammography, only about 10% of patients with DCIS present with irregularities or lumps in the breast and in rare cases with Paget's disease or nipple discharge.

With the increasing use of mammography, incidence of DIN in breast biopsies increased from 25% to 28%. The overall age-adjusted incidence of DCIS ranges from 10 to 31/100.000. In autopsy series the prevalence of DCIS ranged from 4.3% to 18.2% for women above 60 years. DCIS constitutes about 10–15% of newly diagnosed breast cancers, of which at least 90% are detected by mammography. About 20% (10–77%) of breast cancers detected with mammography screening represent DCIS.

DCIS is a precursor of invasive disease. Unfortunately the natural history of DCIS is not known in an individual lesion, therefore the risk-benefit ratio should be considered carefully in each individual lesion. The rate of progression of untreated DCIS to invasive cancer ranged from 14% to 43%. The relative risk of AIDH to develop into invasive cancer ranged from 1 to 13 (2). DCIS increases the risk to develop breast cancer 8 to 10-fold. Interestingly the risk is increased in the contralateral breast as well, indicating that DCIS is not an unequivocal precursor of IDC but also an important risk factor.

Usually the pathologic extent of DCIS is larger than the clinically and mammographically estimated size. This is not only true for the macroscopic but also for the microscopic extent of disease: 1–2% of patients with DCIS have LN-metastases at the time of diagnosis indicating undetected invasive disease (2). Incidence of bilaterality either as DCIS or as IDC is reported to range from 2.2% to 22% (2). DCIS is also known to be multifocal in about 30%.

Risk factors for the development of DCIS and IDC are similar, hormonal replacement therapy seems to be of minor importance in DCIS, contrary to IDC. Up to now no hormonal or other stimulus for DIN is known and changes seem to be irreversible.

Treatment

Complete excision with or without radiotherapy is currently the treatment of choice for locally confined DCIS. Without radiation, 10–60% of the patients develop recurrences. Several studies showed that radiation reduced the risk of recurrence after breast conservation therapy by about 50%, causing 3.5–23% recurrences. Lumpectomy without radiation should not be considered until several ongoing studies present their data. About 75–100% of patients can be salvaged after recurrence.

Although mastectomy has a lower risk of recurrence than lumpectomy and radiation (1.4% vs. 8.9%) there is no significant difference in survival, making lumpectomy the preferable therapy option. In high-risk patients mastectomy with axillary lymph node resection can be considered as it only shows a recurrence rate of 0.75%. In all other patients axillary resection and sentinel lymph-node is presently investigational and should only be performed in case of a suspected invasion.

Tamoxifen reduced the risk of ipsilateral local failure in patients treated with excision and radiotherapy,

although it seems to be profitable only in ER-positive breast cancers and should not be used in patients with low risk of recurrence.

Imaging

Currently mammography is the only modality able to identify calcifications that are associated with DCIS in 70–90%. Especially linear branching, casting calcifications (Fig. 1) or multiple clusters of fine granular calcifications or calcifications in segmental distribution (Fig. 2) are regularly consistent with DCIS. Still diagnostic accuracy in the classification of MC remains lower than for solid masses. The latter are usually associated with invasive disease. Ductal distribution of calcifications has a positive predictive value of 30–63%, Although mammography can detect up to 83% of DCIS lesions, it is know to underestimate the extent of disease by up to several centimetres (3).

Sonography does usually not show any specific result hence positive predictive value for sonography is only about 50%. About 80–90% of DCIS show enhancement on MRI, which is in 50% unspecific. Contrast enhancement is correlated to the size and density packing of involved ducts and to neoangiogenesis, which is low in most DCIS. The differentiation of high- and low-grade DCIS as well as to IDC is not possible.

Typical signs of DCIS in MRI are irregular ductal enhancement and stippled regional enhancement while spiculated mass and washout seem to be signs of IDC. Ring enhancement is not detectable in DCIS. Ductal enhancement can be assigned to DCIS in about 20% but also to IDC, LCIS and to benign lesion in 55%. Although ductal enhancement is detected in 38–60% of DCIS on MR, specificity remains low with 45% (4). Especially small lesions below 5 mm are easy to be missed by MRI, while it is particularly useful in evaluating residual disease, and multi-centricity.

Nuclear Medicine

^{99m}Tc-sestamibi scintimammography shows areas of diffuse heterogeneous uptake. To improve diagnostic accuracy images should always be evaluated together with the mammograms. It is especially useful in evaluating areas of extensive intraductal carcinoma around IDC and to evaluate palpable masses in dense breasts. Still it is less specific for DCIS than for IDS.

^{18}FDG-PET is especially useful in the detection of invasive and metastatic breast cancer. Up to the present time there was no published study evaluating the role of ^{18}FDG-PET in the detection and classification of DCIS. It should therefore only be used in an experimental setting.

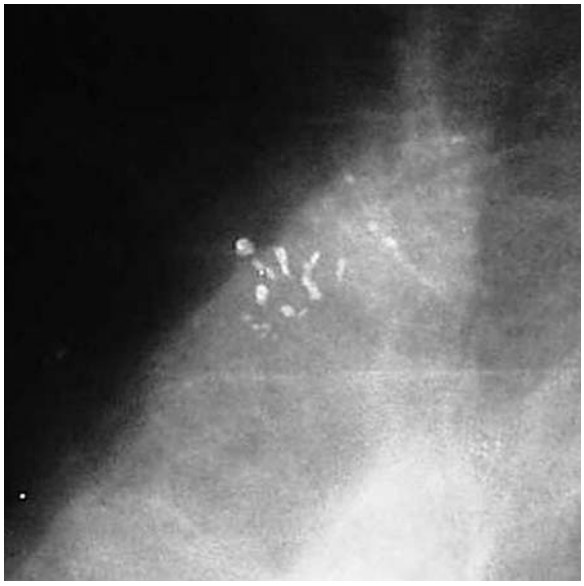

Carcinoma, Ductal, *In Situ*, Breast. Figure 1 Casting calcifications typical for a small DCIS, which was proven by ▶VB.

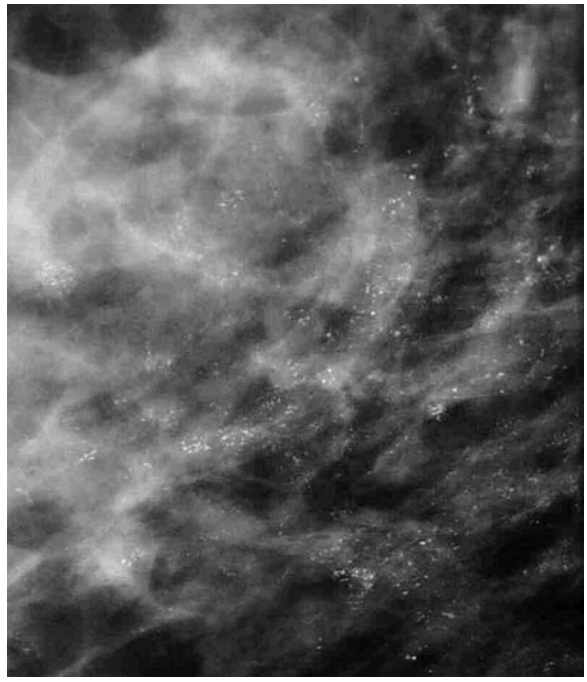

Carcinoma, Ductal, *In Situ*, Breast. Figure 2 Granular calcifications in a ductal distribution including more than one quadrant of a breast.

Diagnosis

Most DCIS are first detected by screening mammography. Screening intervals correlate strongly with histological grading and extent of disease. As most lesions should be confirmed histologically before treatment, core needle biopsy with stereotactic or sonographic guidance is the usual means to diagnose DCIS.

Interventional Radiology

DCIS is usually diagnosed by stereotactic core needle biopsy or VB, although the former has a higher tendency to underestimate disease: 10% of patients with DCIS in core-biopsy are found to have IDC. Nipple aspirate fluid, ductal lavage and fine needle aspiration are of limited value in the diagnosis.

Several techniques for minimal invasive breast therapy have been described: laser-induced thermotherapy, radiofrequency ablation, high-intensive focused ultrasound, cryotherapy and thermal ablation using magnetic nanoparticles. Especially in the case of pure DCIS these methods remain experimental as imaging modalities tend to underestimate tumour extension and as margins cannot be evaluated.

Bibliography

1. Leonard GD, Swain SM (2004) Ductal carcinoma *in situ*, complexities and challenges. J Natl Cancer Inst 96:906–920
2. Tavassoli FA (ed) (1999) Ductal intraepithelial neoplasia: risk factors for subsequent development of invasive carcinoma. In: Pathology of the Breast. McGraw-Hill, New York, pp 205–312
3. Holland R, Hendriks JH, Vebeek AL et al (1990) Extent, distribution, and mammographic/histological correlations of breast ductal carcinoma *in situ*. Lancet 335:519–522
4. Liberman L, Morris EA, Dershaw DD et al (2003) Ductal enhancement on MR imaging of the breast. Am J Roentgenol 181 (2):519–525

Carcinoma, Ductal, Invasive

Silvia Obenauer
Department of Radiology, Georg-August-University of Goettingen, Goettingen, Germany
obenauerheuser@yahoo.de

Synonyms

IDC; Infiltrating ductal carcinoma; Not otherwise specified (NOS); Scirrhous carcinoma

Definition

An invasive carcinoma is a tumor with extension of tumor cells through the ductal basement membrane. About 65% of breast carcinomas are invasive ductal carcinomas. Invasive ductal carcinomas are classified as 75% NOS, 10% medullary, 10% mucinous, 5% tubular, 5% papillary, under 1% adenoid cystic carcinomas, and others. An ▶interval cancer is a malignant tumor which presents clinically during the interval between routine screenings. This type must be distinguished from missed cancers that were overlooked on prospective initial studies, but were visible on review.

Pathology

Gross pathology often shows a hard mass.

Staging of the tumor depends on the tumor size (TNM of UICC):

Tx tumor not judgeable
T0 no tumor
Tis intraductal carcinoma, carcinoma lobulare *in situ*, M. Paget without tumor
T1 tumor ≤2 cm
T1mic: <1 mm (microinvasion)
T1a: >1mm – ≤5mm
T1b: >5 mm – ≤10 mm
T1c: >10 mm – ≤20 mm
T2 tumor >2 cm – ≤5 cm
T3 tumor ≥5 cm
T4 metastatic disease
T4a infiltration of thoracic wall
T4b infiltration of skin
T4c infiltration of both structures
T4d inflammatory carcinoma
N regional lymph nodes
Nx lymph node not judgeable
N0 no regional lymph nodes
N1 metastases in ipsilateral axillary lymph nodes, moveable
N2 metastases in ipsilateral axillary lymph nodes, not moveable
N3 metastases in ipsilateral lymph nodes of mammaria interna.

Furthermore, peritumoral intraductal tumor components must be distinguished:

PIC predominant intraductal component
More than 80% intraductal component and 20% invasive component
EIC extensive intraductal component
Between 25 and 80% intraductal component
Less than 75% invasive component

SIC small intraductal component
Less than 25% intraductal component
More than 75% invasive component.

Multifocality and multicentricity are discussed in the chapter about multiple carcinomas of the breast.

Clinical Presentation

The patient may present with a hard, palpable mass and/or skin, and/or nipple retraction. More details are described in the section on primary and secondary signs. However, sometimes the tumor is occult.

Imaging

All descriptions of the imaging characteristics of invasive tumors should be made according to the BI-RADS classifications. Furthermore, the localization and size of the tumor must be reported with precision. The differential diagnosis includes invasive lobular carcinoma, radial scar, or scars after surgery. Some fat necrosis or abscesses could mimic an ▶invasive ductal carcinoma. Changes from a previous mammogram should be considered, such as a new density, mass, or microcalcifications.

Mammography

A spiculated mass with irregular margins is a typical sign of invasive ductal carcinomas. The density of the tumor is often higher than that of the parenchyma. In some cases, the tumors also present with amorphous or pleomorphic microcalcifications. Other imaging features may be focal asymmetry or architectural distortion, and therefore changes from a previous mammogram must be interpreted carefully (Figs. 1 and 2).

Ultrasound

The tumor is often characterized by an irregular, hypoechoic mass, typically more tall than wide, with a thick echogenic rim and posterior acoustic enhancement. The tumor is not comprisable.

MR Mammography

Typical findings on magnetic resonance (MR) images are rim-enhancing masses, which are irregular or spiculated with heterogeneous enhancement. Signal intensity curves show a high initial contrast media uptake and a postinitial

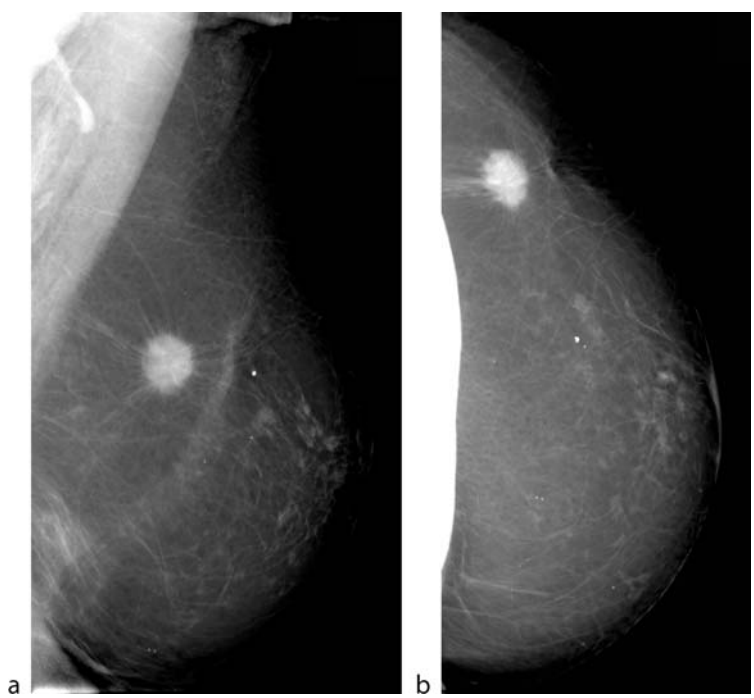

Carcinoma, Ductal, Invasive. Figure 1 Patient with a new, palpable mass in the upper, outer quadrant of the left side. On mammography, an irregular and spiculated mass of 1.5 cm with skin retraction is seen on mediolateral oblique (a) and craniocaudal views (b). Histology revealed an invasive ductal carcinoma, IDC pT1c N0 G2.

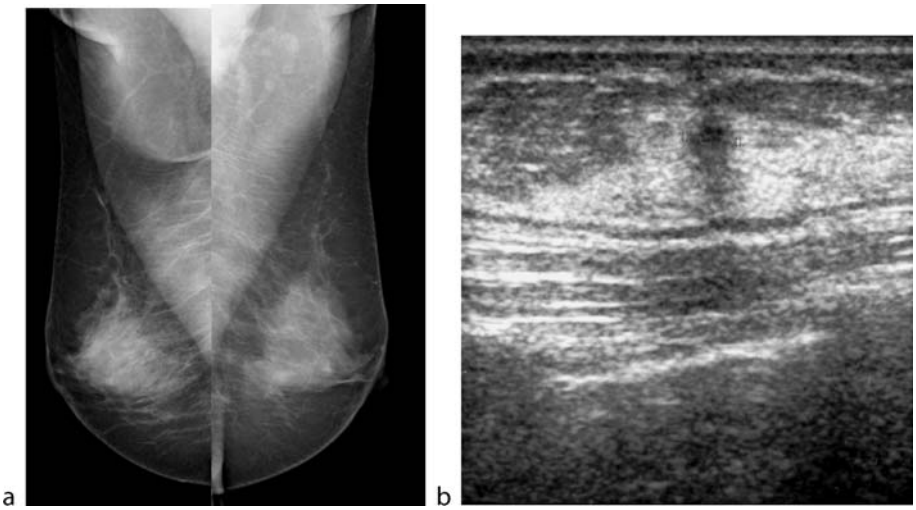

Carcinoma, Ductal, Invasive. Figure 2 Patient with a new, palpable mass on the right side. The tumor is difficult to see on the mammography due to the density of the parenchyma (a). On ultrasound, the tumor is characterized by an irregular, hypoechoic, 1-cm mass, more tall than wide with a thick echogenic rim and posterior acoustic enhancement (b). The tumor is not comprisable. Histology revealed an invasive ductal carcinoma.

plateau or wash-out. On water-sensitive sequences, the tumor has an intermediary signal and on T1-weighted images the tumor is hypointense (Fig. 3).

Bibliography

1. Newstead GM, Baute PB, Toth HK (1992) Invasive lobular and ductal carcinoma: mammographic findings and stage at diagnosis. Radiology 184:623–627
2. Boetes C, Mus RD, Holland R et al (1995) Breast tumors: comparative accuracy of MR imaging relative to mammography and US for demonstrating extent. Radiology 197:743–747

Carcinoma, Endometrium Uteri

Martin Unterweger
Diagnostic Radiology, Cantonal Hospital Baden, Baden, Switzerland
Martin.Unterweger@ksb.ch

Synonyms

Endometrial carcinoma

Definition

Endometrial carcinomas are the most common malignancies of the female pelvis. The mortality of this disease has decreased in the last few years because of earlier detection and advances in tumor treatment. The peak incidence of endometrial carcinoma is around 60 years. The disease is uncommon before the age of 40 years. Risk factors include nulliparity, infertility, obesity, diabetes, and Stein–Leventhal syndrome. One important variable is prolonged stimulation of the endometrium with high-dose estrogen treatment, that is, postmenopausal hormonal replacement or oral contraception. On the other hand, endometrial carcinoma is rarely seen in patients with ovarian agenesis.

Pathology/Histopathology

Endometrial carcinoma arises from the glandular component of the endometrium in the upper uterus. It may grow in a circumscribed pattern, presenting as a focal mass protruding into the uterine cavity and occasionally within an endometrial polyp. However, endometrial carcinomas can also grow diffusely, involving multiple parts of the endometrium. Approximately 90–95% of endometrium carcinomas are adenocarcinomas (Fig. 3). The remaining 10% of nonepithelial uterine cancers comprise sarcomas, mixed tumors, and secondary malignancies. Some less common epithelial varieties include mucinous, secretory, clear cell, and papillary serous carcinomas. The clear cell tumor is highly malignant and has a bad prognosis. Endometrial carcinoma typically arises from the endometrial mucosa. The depth of

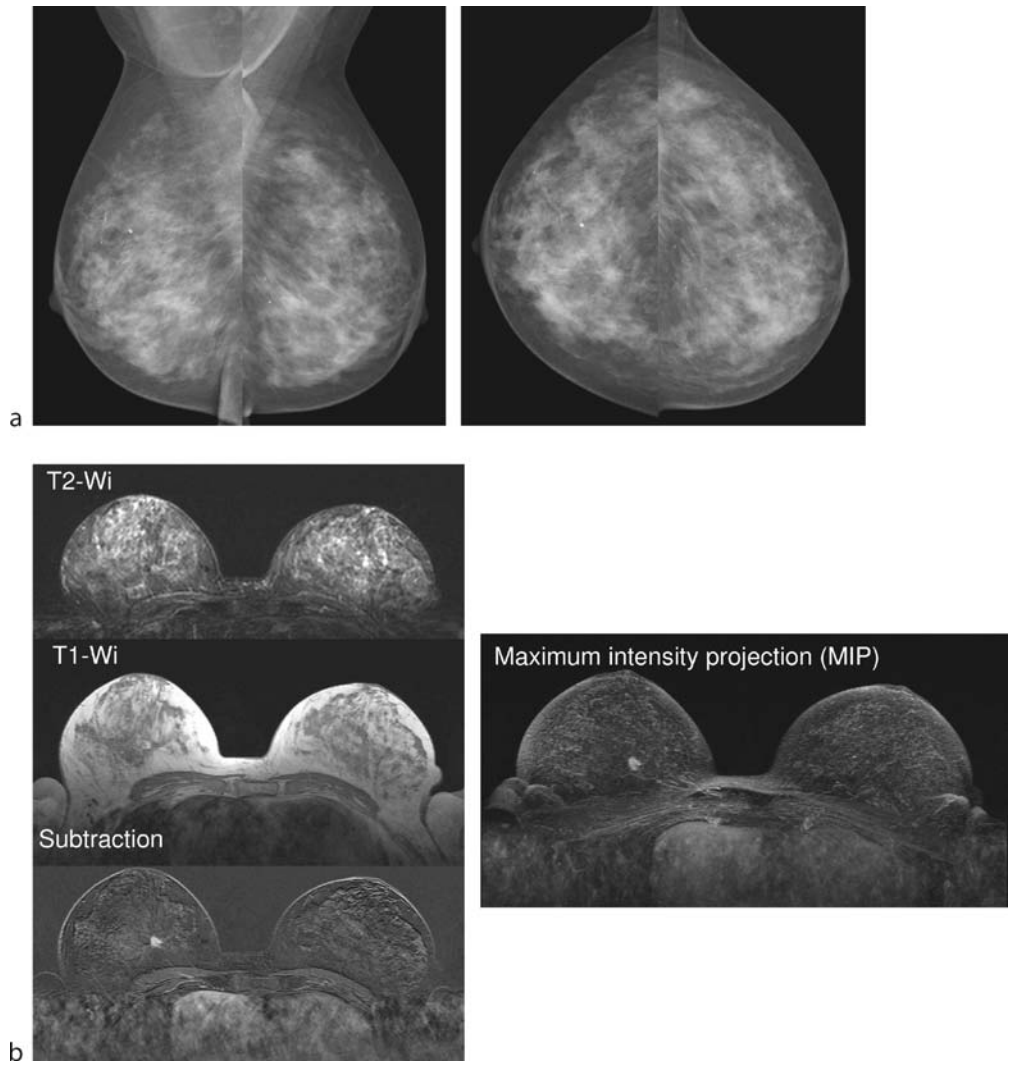

Carcinoma, Ductal, Invasive. Figure 3 Mammography of extremely dense breast tissue (ACR type 4). Tumor is difficult to see on the right side in the inner quadrant (a). MR mammography shows an irregular and spiculated rim-enhancing mass in the right breast (b). The size of the suspected tumor is about 1 cm and it is localized in the inner upper quadrant of the right breast. On T2-weighted imaging, the tumor has intermediary signal. Signal intensity curve shows a rapid initial increase with a plateau in the delayed phase.

myometrial invasion is a very important prognostic factor and correlates with frequency of lymphatic metastasis. The most common sites of distant metastases are the lung, liver, brain, and bone.

Clinical Presentation

Postmenopausal bleeding is the most important presenting symptom of endometrial carcinoma. Because there are multiple benign causes of postmenopausal bleeding, including estrogen therapy, endometrial hypertrophy, atrophic vaginitis, and endometrial and cervical polyps, only 15% of patients with this symptom and endometrial carcinoma will be diagnosed. Less than 5% of patients with carcinoma of the endometrium are asymptomatic at the time of diagnosis. Endometrial carcinoma in premenopausal women usually presents as abnormal uterine bleeding, oligomenorrhea, or menometrorrhagia. The diagnosis of endometrial carcinoma is made histologically with fractional endocervical curettage.

In most institutions, the International Federation of Gynecology and Obstetrics (FIGO) classification is applied for staging of endometrial carcinomas (Fig. 1).

TNM	FIGO	Remarks
T is	0	Carcinoma *in situ*
T1	I	Disease confined to the corpus uteri
T1a	-	Tumor limited to the endometrium
T1b	-	<50% of the myometrium involved
T1c	-	>50% of the myometrium involved
T2	II	Invasion of the uterine cervix, but not extending into the uterus fundus
T2a	IIA	Invasion of the endocervix
T2b	IIB	Cervical stroma invasion
T3	III	Vaginal extension, with spread into the adnexa or parametrium
T3a	IIIA	Invasion into serosa or adnexa or positive peritoneal cytologic finding
T3b	IIIB	Invasion in the vagina
T4	IV	Tumor extention outside the true pelvis, invading the bladder or rectal mucosa
T4a	IVA	Carcinoma involving the rectal mucosa or bladder
T4b	IVB	Distant metastases

Carcinoma, Endometrium Uteri. Figure 1 Staging of endometrial carcinoma according to TNM and the International Federation of Gynecology and Obstetrics (FIGO).

Around 70% of patients are diagnosed with stage I disease. The 5-year survival in this subpopulation is 76%. This survival rate decreases to 59% for stage II and 29% for stage III. Tumor grade also shows a correlation with 5-year survival.

Imaging

On sonography, stage I endometrial carcinoma typically appears as widening of the hyperechogenic endometrium. The postmenopausal endometrium is atrophic and generally measures less than 3 mm. A thickness of greater than 5 mm should always be considered abnormal in women not receiving estrogen therapy. Endovaginal sonography can be useful for screening women with postmenopausal bleeding.

The value of computed tomography (CT) in local staging of endometrial carcinoma is limited, since the spread of endometrial carcinomas is normally small or microscopic to the cervix, parametrium, and lymph nodes.

On magnetic resonance imaging (MRI), the signal intensity of endometrial carcinomas is typically similar to that of normal endometrium on nonenhanced MR images. Tumors are generally hyperintense on T2-weighted images compared to the endometrium and isointense on T1-weighted images. The lesions can be heterogeneous because of necrosis or contents of blood products in the tumor. Large carcinomas are often seen as polypoid masses expanding the endometrial cavity. Secondary signs of small tumors include an increased thickness or lobulation of the endometrium. Endometrial carcinoma enhances variably on dynamic gadolinium-enhanced images. The enhancement is typically different from that of normal myometrium or endometrium. With contrast-enhanced images, the detection of small tumors and differentiation between lesions and fluid or necrosis can be improved. Thus, contrast agents should be routinely applied for staging of endometrial carcinoma. Myometrial invasion is best evaluated on T2-weighted images (Fig. 2) and gadolinium-enhanced scans (Fig. 3). An intact junctional zone is present in stage IA without myometrial invasion. In stage IB, lesions infiltrate the junctional zone and the inner part of the myometrium. Invasion of more than 50% of the myometrium indicates stage IC disease. Cervical invasion (stage II) is best seen on T2-weighted or contrast-enhanced images in the sagittal plane.

In stage III, the local extrauterine disease is demonstrated as extension of tumor outside the myometrium, adnexal masses, vaginal metastases, or pelvic lymphadenopathy. Rectal or bladder wall invasion of tumor (stage IVA) is suspected if the normal fat planes between these organs are interrupted. The overall accuracy of gadolinium-enhanced MRI in the staging of endometrial carcinoma is between 84 and 94%.

Tumor recurrence usually depends on the type of therapy. Patients treated with radiation and surgery typically present with distant metastases. Patients treated only with surgery more often present with pelvic wall, parametrial, or vaginal apex recurrences. Most recurrent tumors will occur within 3 years after initiation of treatment. Early-stage and low-grade tumors often recur late, more than 5 years after initiation of treatment.

Diagnosis

Endocervical and endometrial biopsy is the only reliable option for diagnosis.

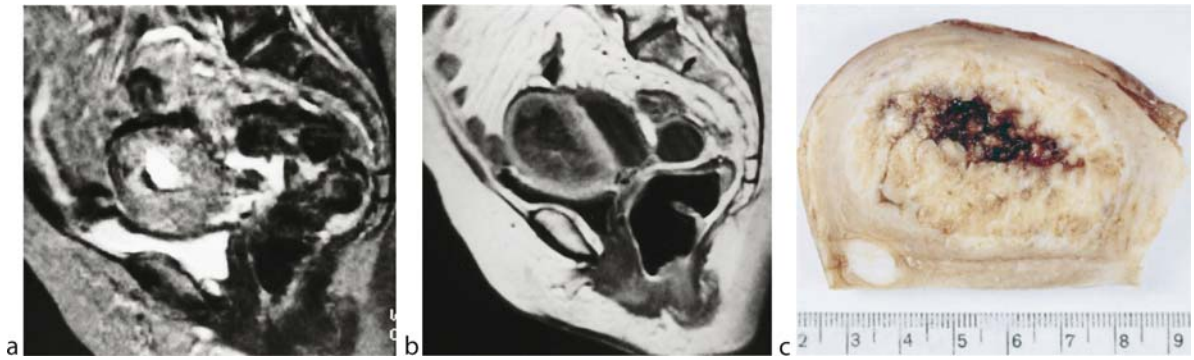

Carcinoma, Endometrium Uteri. Figure 2 (a–c) Pictorial review using MR imaging and CT of the female pelvis. Endometrial carcinoma in stage IC. (a) Sagittal T2-weighted magnetic resonance (MR) image. The T2-weighted image demonstrates only an increased amount of fluid in the uterine cavity. Demarcation of the histologically proven endometrial carcinoma is missing. (b) Sagittal T1-weighted MR image immediately after intravenous contrast administration. Significantly better demarcation of the carcinoma relative to the myometrium is noted. The hypovascularized endometrial carcinoma extends to the outer layers of the myometrium. (c) Gross specimen. Note the good morphologic correlation with the contrast-enhanced MR image. (Figure 9a–c: Reprinted from Hamm, B., Kubik-Huch, R.A., Fleige, B., *Eur. Radiol,*. 9, 3–15, 1999).

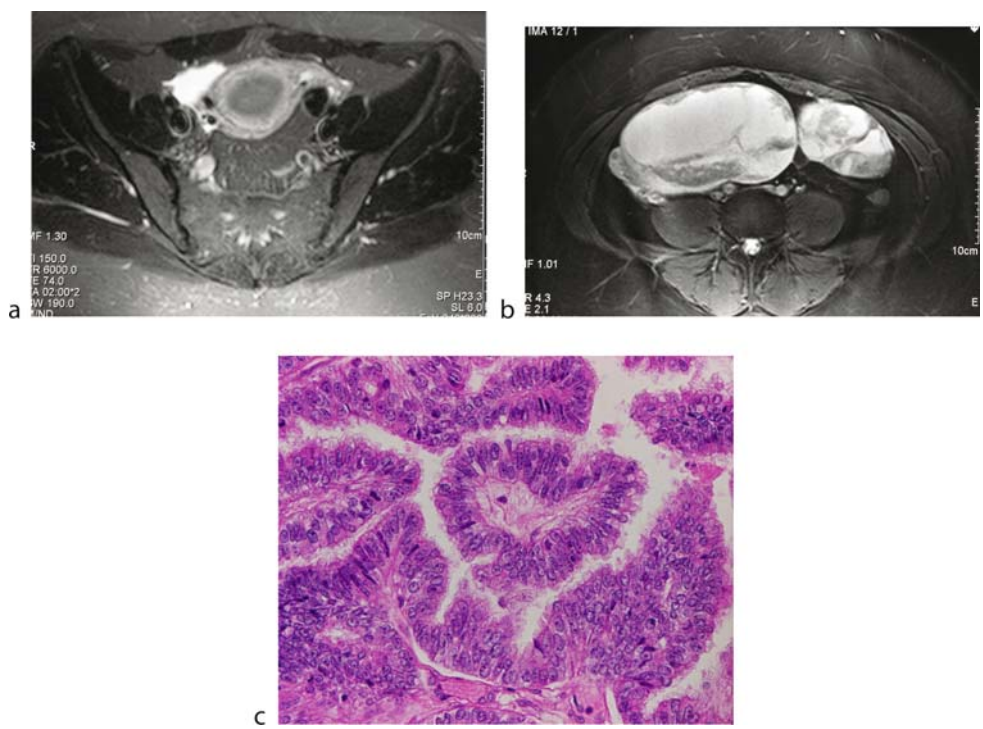

Carcinoma, Endometrium Uteri. Figure 3 (a–c) (a) Axial T2-weighted magnetic resonance imaging (MRI) demonstrates an enlarged nonhomogenous hyperintense uterus, which was histologically proven as an endometrial carcinoma, stage III. (b) Axial T2-weighted MRI shows huge ovaries on both sides, which shows the invasion. (c) Histology of an endometrial adenocarcinoma of the uterus.

Bibliography

1. Frei KA, Kinkel K, Bonel HM et al (2000) Prediction of deep myometrial invasion in patients with endometrial cancer: clinical utility of contrast-enhanced MR imaging a meta analysis and Bayesian analysis. Radiology 216:444–449
2. Seki H, Takan T, Sakai K (1999) Value of dynamic MR imaging in assessing endometrial carcinoma involvement of the cervix. Am J Roentgenol., Jul 2000; 175:171–176
3. Kinkel K, Kaja Y, Yu KK et al (2000) Radiological staging in patients with endometrial cancer: a Meta-analysis. Radiology 1999; 212:711–718
4. Tavassoli FA, and Deville P (2003) Tumor of the breast and female genital organs. WHO classification of tumors
5. Hamm B, Kubik-Huch RA, Fleige B (1999) Eur Radiol 9:3–15

Carcinoma, Gallbladder

Malignant tumor arising from the gallbladder epithelium.
►Neoplasms, Gallbladder

Carcinoma, Hypopharynx

Stefano Cirillo
Institute for Cancer Research and Treatment, Turin, Italy
stefano.cirillo@ircc.it

Definition

Hypopharyngeal carcinoma is a malignant neoplasm originating from the mucosal surface of the hypopharynx.

The ►hypopharynx is a musculomembranous conduit; it lies behind the larynx and extends from its junction with the oropharynx at the tip of the epiglottis (at the level of the hyoid bone) superiorly to the lower border of the cricoid cartilage inferiorly. The muscular-supporting structure is formed by the middle and inferior pharyngeal constrictor muscles. It extends inferiorly down to the cricopharyngeus muscle, where the pharynx joins with the cervical esophagus.

The hypopharynx can be divided into three segments: the *pyriform sinus*, the *postcricoid area*, and the *posterior pharyngeal wall*.

Pathology/Histopathology

The most frequent macroscopic presentation of hypopharyngeal carcinoma is an ulcerative infiltrative lesion (90% of the cases), often associated with a necrotic evolution and erosion of the adjacent cartilaginous, membranous and muscular anatomic structures. The latter represent a form of barrier which hinders further diffusion to the contiguous areas.

Over 95% of malignancies of the hypopharynx are squamous cell carcinomas (well differentiated or undifferentiated); the remaining 5% are squamous cell carcinoma with sarcomatous component, undifferentiated carcinomas, and verrucous and basaloid carcinoma. The hypopharyngeal carcinomas can arise in the pyriform fossa (60%), in the posterior hypopharyngeal wall (25%), and in the postcricoid area (15%).

The cancer spread depends on the site of origin: when the diagnosis is made at a late stage the site of origin is often unrecognizable.

Carcinomas of the *pyriform sinus* are rarely confined. They can extend to the supraglottis larynx involving the aryepiglottic folds, the fatty tissue of the superior paralaryngeal space, and the preepiglottic space; or they can involve the glottic plane anteriorly.

Pyriform sinus tumors originating from the apex and the lateral walls often invade the thyroid cartilage and they may extend directly to the thyroid.

Carcinomas of the *posterior hypopharyngeal wall* can spread in a craniocaudal direction (to the oropharynx or esophagus), in a circumferential direction, or deeply and posteriorly to the prevertebral muscles.

Carcinomas of the *postcricoid area* show a submucosal spread, anteriorly to the posterior cricothyroid muscle and the cricoid cartilage, circumferentially or caudally to the esophagus (1).

Clinical Presentation

Its incidence varies widely. In males, it ranges from 0.3 per 100.000 inhabitants in Iceland to 17 per 100 in France. Among women, the variability is less pronounced. Hypopharynx carcinoma represents approximately 8 and 5% of head and neck epithelial cancers in males and females, respectively, excluding tumors of the skin and the thyroid gland.

Most patients who develop cancer of the hypopharynx have a history of heavy smoking and drinking. Males are about eight times more susceptible to cancer of the hypopharynx than females, In females of Irish and Scandinavian descent who present with Plummer–Vinson syndrome—characterized by esophageal webs, iron deficiency anemia, glossitis, and increased incidence of esophageal cancer—there is also an increased incidence of carcinoma of the postcricoid region.

Hypopharynx carcinoma may remain asymptomatic for a long period; at presentation, the disease is often

advanced. The characteristic symptoms are sore throat, otalgia due to involvement of the Arnolds nerve, a branch of the tenth pair of the cranial nerves, and dysphagia. A "hot potato" voice or hoarseness due to vocal cord paralysis may be present.

Among patients with ►head and neck cancers, hypopharyngeal carcinomas carry a lower survival rate than cancers of other sites. There are several reasons for this poor prognosis: the hypopharynx is a "silent" area and at the time of presentation patients are often at an advanced stage of disease. Seventy-five percent of patients have lymph nodal metastases at the time of diagnosis, 36% have clinically evident adenopathies, 20–40% have distant metastases, and 4–15% show a second synchronous or metachronous tumor.

Tumor size is also associated with metastases to the neck, as they occur in 50% of cases when the tumor is bigger than 4 cm, but in 85% of the cases when it is smaller than 4 cm.

The overall survival of patients with hypopharyngeal carcinoma is about 40% at 5 years. The site, size, and presence or absence of neck metastases have a significant effect on the outcome; in patients with cervical metastases, there is a 20–25% risk of distant metastases within 2 years of treatment. Stage I and II posterior hypopharyngeal wall carcinomas have an excellent prognosis. In contrast, even small pyriform sinus carcinomas are notorious for metastasizing early and carry a poor prognosis. Postcricoid lesions usually present as advanced lesions with extensive paratracheal and mediastinal metastases, and have a poor prognosis (Table 1) (2).

Carcinoma, Hypopharynx. Table 1 T staging for hypopharynx carcinoma

T1	Tumor limited to one subsite of the hypopharynx and ≤2 cm in greatest dimension
T2	Tumor invading more than one subsite of the hypopharynx or an adjacent site, or measuring >2 cm but ≤4 cm in the largest diameter without fixation of the hemilarynx
T3	Tumor measuring >4 cm in largest dimension or fixation of the hemilarynx
T4	Tumor invading the thyroid/cricoid cartilage, hyoid bone, thyroid gland, esophagus, or central compartment soft tissue, which includes prelaryngeal strap muscles and subcutaneous fat
T5	Tumor invading the prevertebral fascia, encasing the carotid artery, or involving the mediastinal structures

Diagnosis

The physical examination should include a thorough head and neck assessment with particular attention given to the oral cavity and the patient's general appearance for signs of severe nutritional deficiencies. The physical examination must be associated with indirect mirror examination and direct endoscopy. The tumor must be confirmed histologically, and any other pathologic data obtained from a biopsy should be included.

The most important goal of the staging endoscopy is to determine the lowermost extent of the tumor and its relation with the pyriform apex and the cervical esophagus.

Esophagoscopy and biopsies should be performed after mapping of the tumor, and complete evaluation of the esophagus down to the gastroesophageal junction is mandatory, as the esophagus is the most frequent site of asymptomatic synchronous primary tumors.

Hypopharyngeal carcinomas arise from the mucosa, thus they are usually visible at the surface, but their submucosal extension cannot be evaluated by endoscopic examination alone. Indeed, clinical and endoscopic examination may underestimate tumor extension. Integration between clinical, endoscopic, and imaging (CT/MR) data is necessary for the correct staging.

Imaging

The disease extent is often endoscopically underestimated because of submucosal tumor spread that can be well visualized with computed tomography (CT) or ►magnetic resonance imaging (MRI). CT and MRI scans are often valuable to further delineate disease extent at the primary site and in the neck. Imaging techniques may, however, underestimate the mucosal growth and overestimate its extension due to difficulty in differentiating cancer tissue from perilesional edematous reaction.

Thus, integration between clinical–endoscopic examination and imaging is necessary.

The role of imaging in hypopharynx carcinoma is as follows:

- Identifying the cancer
- Measuring its volume and dimension
- Evaluating deep tissue diffusion
- Identifying and characterizing of adenopathies
- Follow-up.

Conventional radiography with barium swallow has a limited role for staging, despite a reported sensitivity of 96, 87, 44% in detection of cancer of the pyriform fossa, posterior hypopharyngeal wall, and postcricoid area, respectively.

►Multidetector CT (MDCT) is the first-choice exam for staging hypopharyngeal carcinoma: because of its rapidity, motion artifacts can be erased and scans

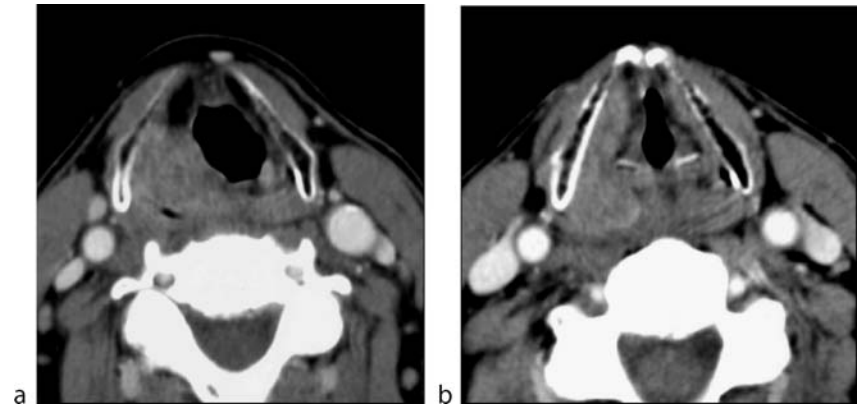

Carcinoma, Hypopharynx. Figure 1 Squamocellular cancer of right pyriform sinus—MDCT: extension anteriorly to paraglottic space, associated with enlargement of thyroarytenoid space.

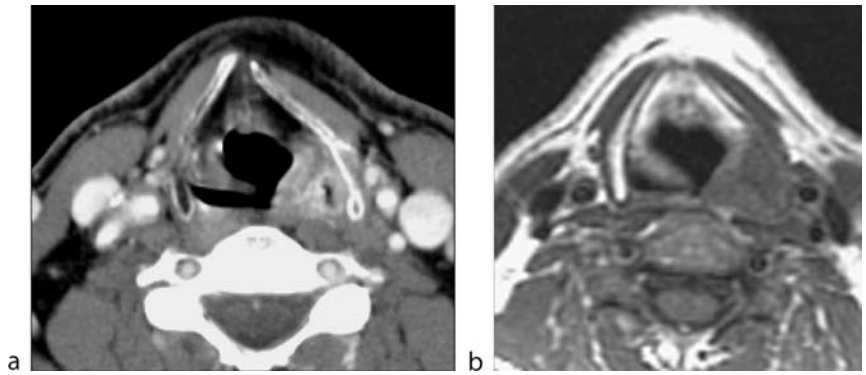

Carcinoma, Hypopharynx. Figure 2 Squamocellular cancer of left pyriform sinus—MDCT (a) shows cancer in contiguity with the left thyroid cartilage, sclerotic. MRI (b) T1-weighted image shows low intensity of left thyroid cartilage for infiltration.

can be performed during functional and dynamic maneuvers, such as phonation or Valsalva, sometimes needed for better visualization of the apex of the pyriform sinus.

MDCT allows the radiologists to make multiplanar reconstruction of excellent quality, obtaining imaging on different planes with optimal tumor visualization and delimitation of tumor volume and of the size of any associated adenopathy.

Identification is possible by evaluation of a space-occupying mass, an area with anomalous enhancement, an obliteration of the adipose space, an asymmetric enlargement of soft tissue, and an asymmetry of the pyriform sinus.

For identification, the sensitivity of MDCT (95%) is higher than that of MRI (87%).

A critical point for hypopharynx carcinoma is the infiltration of the pharyngeal constrictor muscle, the laryngeal cartilages, the paraglottic space, and the prevertebral space (Fig. 1).

The accuracy of MDCT in staging hypopharynx carcinomas is 84–86.4% versus 70–87% of MRI.

Although MRI permits an accurate contrast resolution of the anatomic structure, it can be biased by motion artifacts, due to the long acquisition time, especially in elderly patients with dyspnea, cough, and large expiratory excursions. MRI is necessary when MDCT cannot exclude infiltration of the laryngeal cartilages, the prevertebral muscle, and the cervical esophagus.

MRI has a better sensitivity than MDCT (97 vs. 68% respectively) for assessing cartilage infiltration. Thyroid cartilage infiltration is present in most cancers arising from the apex and in 55% of those arising from the lateral walls (Fig. 2).

For infiltration of the prevertebral muscles, MRI has a sensitivity of 88%, a specificity of 14–29%, and a diagnostic accuracy of 53–60% (Fig. 3).

The MRI criteria useful for determining infiltration of the cervical esophagus show variable accuracy, ranging from 67 to 86%.

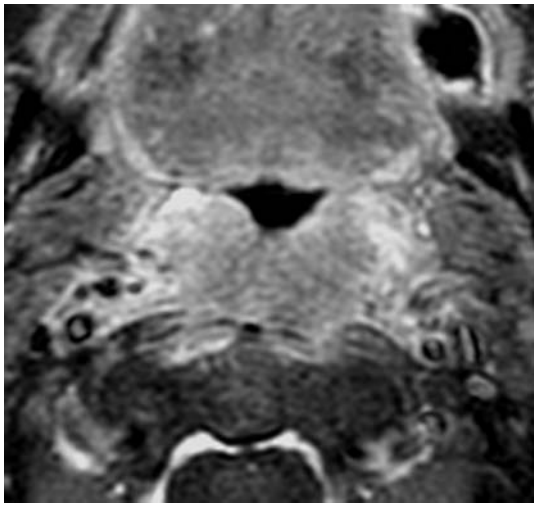

Carcinoma, Hypopharynx. Figure 3 Squamocellular cancer of posterior wall—MRI: T1-weighted image after i. v. gadolinium administration: thickening of posterior wall, associated with involvement of the prevertebral muscles.

The role of imaging is also to identify adenopathies that cannot be assessed by physical examination, by characterizing them and detecting possible capsular rupture.

Ultrasonography is the most useful examination for assessing superficial laterocervical adenopathies, by providing an accurate morphologic and dimensional evaluation. MDCT and MRI evaluation is indicated for deep adenopathies (i.e., retrolateral pharyngeal, which represent an important prognostic factor for local recurrence and distant metastases).

Another imaging objective is to identify lymph node capsular rupture, present in 23% of lymph nodes greater than 10 mm, 40% of those smaller than 20 mm, 50% of those greater 20 mm, and 70% of those greater than 30 mm. Capsular rupture is present in 25% of lymph nodes presenting with normal dimensional criteria (3, 4).

Nuclear Medicine

Nuclear medicine tests are useful in the follow-up of patients who underwent surgery or radiotherapy, for whom there is a clinical suspicion of local recurrence. In this setting, FDG-positron emission tomography (PET) provides a high sensitivity (86–100%) and specificity (69–87%) (5).

PET has some limitations due to its low spatial resolution and the absence of anatomic reference points, which is of particular relevance considering the complexity of the head and neck region. Moreover, uptake is at times present in physiological conditions generating possible false-positive findings. Anatomic limitations can be partially overcome by the combination of CT–PET, which permits simultaneous acquisitions of morphological and metabolic data.

Bibliography

1. American Cancer Society (2006) Cancer Facts and Figures 2006. American Cancer Society, Atlanta, GA
2. Sturgis EM, Wei Q, Spitz MR (2004) Descriptive epidemiology and risk factors for head and neck cancer. Semin Oncol December 31(6):726–733
3. Keberle M, Kenn W, Hahn D (2002) Current concepts in imaging of laryngeal and hypopharyngeal cancer. Eur Radiol July 12(7):1672–1683. Epub 2002 Feb 9
4. Becker M, Hasso AN (1996) Imaging of malignant neoplasms of the pharynx and larynx. In: Taveras JM, Ferruci JT (eds), Radiology: Diagnosis—Imaging—Intervention Lippincott, Philadelphia, PA, pp 1–16
5. Sharon F. Hain (2005) Positron emission tomography in cancer of the head and neck. Brit J Oral Maxillofac Surg 43:1–6

Carcinoma, Lobular, *In situ*, Breast

Arne Fischmann
Department of Diagnostic Radiology, University of Tübingen, Tübingen, Germany
arne.fischmann@med.uni-tuebingen.de

Synonyms

Lobular intraepithelial neoplasia (LIN); Lobular neoplasia (LN)

Definition

Lobular carcinoma *in situ* (LCIS) is carcinoma filling and dilating the intralobular ductuli with loosely aggregated monomorphous cells without stromal invasion. Contrary to prior beliefs describing LCIS as a premalignant lesion, it is nowadays regarded as a risk factor for invasive cancer.

Atypical lobular hyperplasia (ALH) is defined as a lesion that either has some, but not all, of the features of LCIS or has all the features of LCIS but involves up to only 50–75% of a lobule.

Pathology/Histopathology

The cells are uniform, bland, and homogenous without mitosis and are often arranged in a linear file or planar

growth pattern. Pathology is confined to the terminal ductulolobular unit, although a pagetoid involvement of the ducts can sometimes be observed. Necrosis and microcalcifications may occur in LCIS but are rare.

If less than half of one terminal ductulolobular unit is involved, the lesion is called ALH. It remains unclear whether the separation of LCIS and ALH is of clinical relevance because several features used to distinguish ALH and LCIS have no influence on prognosis (1).

Similar to the classification of ductal intraepithelial neoplasia (DIN), ALH, and LCIS are classified as ►lobular intraepithelial neoplasia (LIN) 1–3 depending on the extent of lobular involvement:

1. LIN 1 represents partial or complete filled acini without distention.
2. In LIN 2, multiple or all acini are filled and distended but to a lower degree than in LIN 3. Undermining growth into the terminal ductuli may occur.
3. LIN 3 represents extensive distention of the acini or confluent acini. If goblet cells are detected or the polymorphous form of LCIS is present, the lesion is classified as LIN 3 irrespective of extent.

Coexistence of ductal and lobular neoplasia in one specimen occurs in up to 16% of cases.

Cells are estrogen-receptor positive in up to 60%, a higher rate by far than in invasive carcinoma. A loss of E-cadherin enables the cells to move relatively freely in the ductulolobular system.

LCIS is multicentric in 47–93% and bilateral in 30–67%. Generally, a diffuse involvement of the breast is detected. Therefore, some authors advocate assuming bilateral involvement if LCIS is detected in a specimen.

A finding of lobular hyperplasia, especially with atypia, should mandate further sectioning to exclude invasive lobular carcinoma (ILC), with which it is associated in 5–16% of cases (2).

Clinical Presentation

LCIS does not lead to a palpable mass and is almost always an incidental finding in a specimen retrieved for another reason. Hence, the true incidence of LCIS in the general population is unknown, as it has no clinical or mammographic manifestation. LCIS is found in about 1.1–3% of breast biopsies and in 5.7% of all breast malignancies.

Although ILC is associated with contralateral carcinoma, contralateral malignancy is lower in LCIS (2%) than in DCIS (6%). Generally, LCIS is multifocal (47–93%) and bilateral (30–67%).

The average age of women with LCIS is between 44 and 46, which is 10 years younger than for DCIS. A high proportion (90%) are premenopausal.

LCIS is today considered to be a risk indicator for invasive breast neoplasia rather than being a true precursor lesion: 2.2–7% of patients with LCIS develop invasive carcinoma in 5 years, and 35% develop ipsilateral and 25% contralateral ILC in 20 years, which indicates a fivefold risk of breast carcinoma. A positive family history of breast carcinoma increases this risk to about 11-fold. More than 50% of these malignancies occur more than 15 years after LCIS is diagnosed, in contrast to DCIS, in which more than 90% of recurrences occur within 5 years, indicating the slow growth pattern of LCIS. Most malignancies that follow LCIS are of ductal origin, supporting the view, that LCIS is a risk factor rather than a precursor of malignant disease. One explanation of this fact would be that coexisting DCIS grows faster and becomes invasive sooner than LCIS.

Mortality for LICS is low—less than 7.2% in long-term follow-up, and newer studies even report absent mortality in LCIS.

Risk factors associated with LCIS are comparable to those associated with DCIS or invasive carcinoma: family history or previous history of cancer, late age of pregnancy, or nulliparity. Increasing age actually reduces the risk of subsequent carcinoma in women with LCIS.

Therapy

Because of the wide dissemination of disease, early studies suggested mastectomy for DCIS: after open biopsy, up to 60% of patients were found to have residual LCIS and 6% to have residual ILC in a consecutive mastectomy, in 80% involving a different quadrant. Hence, clear margins cannot resolve the risk of recurrence.

Some groups have suggested bilateral mastectomy on prophylactic grounds. Because initial mastectomy has never been shown to reduce mortality over observation alone, conservative treatment—usually close long-term follow-up—is more advisable, especially considering the relatively young age of the patients.

Ample biopsy in the contralateral breast has been proposed to examine bilateral disease but is nowadays no longer acceptable in the absence of clinical or imaging criteria for biopsy.

LCIS is to be viewed as a risk factor, like a family history of breast cancer, rather than as a premalignant lesion.

There is no evidence that radiation therapy, chemotherapy, or axillary lymph node sampling or dissection have any therapeutic role in LCIS.

Tamoxifen has reduced the risk of invasive breast carcinoma by 56% in women with LCIS and by 86% in women with ALH.

Imaging

Due to the slow growth and infiltrative pattern, neither calcifications nor a solid mass is visible in LCIS. The only mammographic sign is sometimes a parenchyma-like aggregation of breast tissue. Calcifications—usually of the powderish type—are sometimes found in adjacent breast tissue, referred to as "neighborhood calcifications." In rare cases, LIN 3 can present with necrosis and associated microcalcifications, usually of the fine granular type (3). Because these are often associated with ILC, more aggressive treatment should be considered.

Sonography does not show any specific sign.

Although 30% of patients with LCIS show an unsharp region of enhancement on magnetic resonance imaging (MRI), the lesion is not distinguishable from breast parenchyma or mastopathic changes. No prospective signs of malignancy can be detected.

Nuclear Medicine

At the present time, nuclear medicine has no role in the evaluation of LCIS. Diffuse heterogeneous uptake of ^{99m}Tc-sestamibi and ^{99m}Tc-(V)DMSA has been reported. Still, the number of cases was too low to render this method more than experimental.

Because of its slow growth, LCIS does not show increased uptake of ^{18}FDG.

Diagnosis

LCIS is usually a chance finding, detected in specimens taken for evaluation of a neighboring finding. If LCIS is found in a specimen, it must be questioned whether the clinical symptoms can be explained by the LCIS. If not, a further biopsy should be considered to rule out neighboring ILC or DCIS, especially because a rate of underestimation in ►core needle biopsy of 31% has been reported (4).

MRI can be performed to rule out invasive disease associated with LCIS.

Bibliography

1. Tavassoli FA (1999) Lobular neoplasia. In: Tavassoli FA (ed) Pathology of the Breast. McGraw-Hill, New York, pp 373–397
2. Frykberg ER (1999) Lobular carcinoma in situ of the breast. Breast J 5(5):296–303
3. Sapino A, Frigerio A, Peterse JL et al (2000) Mammographically detected in situ lobular carcinomas of the breast. Virchows Archiv 436(5):421–430
4. Elsheikh TM, Silverman JF (2005) Follow-up surgical excision is indicated when breast core needle biopsies show atypical lobular hyperplasia or lobular carcinoma in situ: a correlative study of 33 patients with review of the literature. Am J Surg Pathol 29(4):534–543

Carcinoma, Lobular, Invasive

Silvia Obenauer
Department of Radiology, Georg-August-University of Goettingen,
Goettingen, Germany
obenauerheuser@yahoo.de

Synonyms

Infiltrating lobular carcinoma (ILC)

Definition

About 10% of all breast cancers are invasive lobular carcinomas (ILCs). The cytologic features of the cells suggest that they arise from the lobules.

Pathology

The tumor is more often multifocal or multicentric or controversial (bilaterality). The tumor metastasizes frequently to bone, the peritoneum, adrenals, gastrointestinal tract, ovary, and leptomeninges.

Clinical

The patient may present with a palpable mass and with negative mammography and ultrasound. Sometimes the patient reports a decrease in size of the affected breast ("►shrinking").

Imaging

All descriptions of the imaging of the invasive tumors should be done according to the BI-RADS classifications. Furthermore, localization and size of the tumor must be reported exactly. There are large crossovers with other tumor entities in appearance (Figs. 1, 2).

Mammography

ILCs are often difficult to detect mammographically due to an insidious growth pattern. Therefore, the tumors are often larger at diagnosis than other cancers and may present as palpable masses. ILC is the tumor entity with

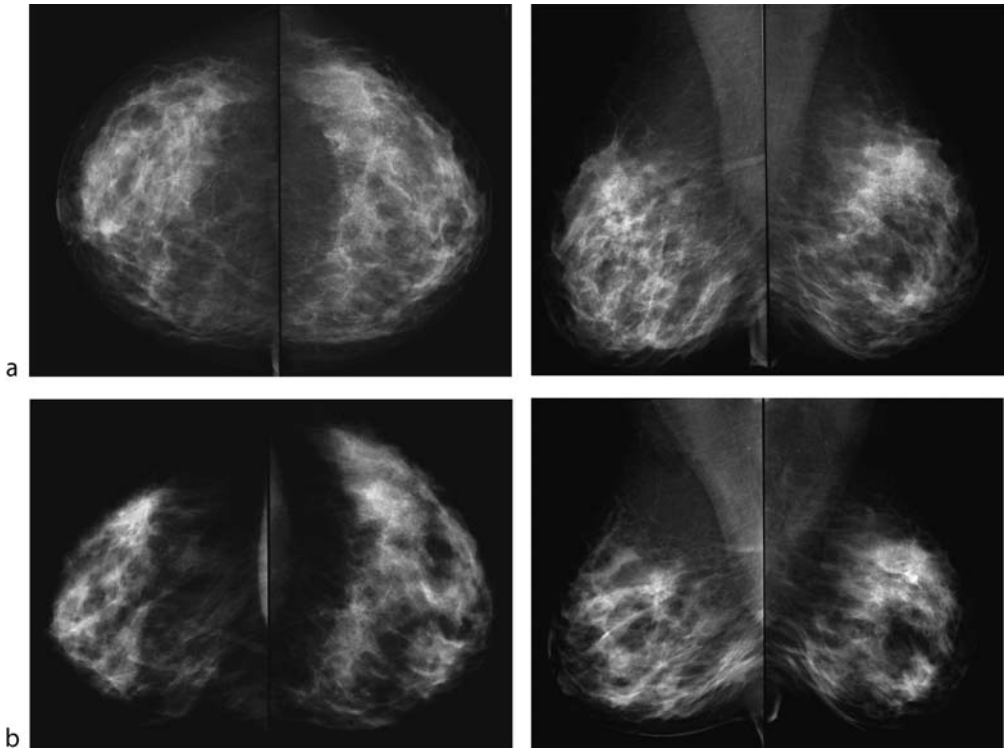

Carcinoma, Lobular, Invasive. Figure 1 (a) Normal mammography. (b) Mammography follow-up after nine months due to a new palpable mass on the right side. Mammography shows only a "shrinking sign" of the right breast in the follow-up. Histology: invasive lobular carcinoma.

the most diagnostic failures, especially in mammography. Most commonly, the tumor presents as a spiculated mass or mass of asymmetric density without definable margins.

Architectural distortion is also possible, whereas calcifications are rare. Sometimes the tumor is seen only in one view. In addition, even when mammography shows the tumor, its extent is often underestimated.

Ultrasound

The tumor is often characterized as a vague area of shadowing without defined borders. But the tumor is often not easily recognized on ultrasound because it grows diffusely.

Magnetic Resonance Mammography

Typical findings in magnetic resonance imaging are rim-enhancing masses that are irregular or spiculated with heterogeneous enhancement. Signal-intensity curves show a high initial contrast media uptake and a postinitial plateau or wash-out. The tumor is presented in water-sensitive sequences by an intermediary signal.

References

1. Boetes C, Veltman J, van Die L et al (2004) The role of MRI in invasive lobular carcinoma. Breast Cancer Res Treat 2773:1–7
2. Hilleren DJ, Andersson IT, Lindholm K et al (1991) Invasive lobular carcinoma: mammographic findings in a 10-year experience. Radiology 178:149–154
3. Newstead GM, Baute PB, Toth HK (1992) Invasive lobular and ductal carcinoma: mammographic findings and stage at diagnosis. Radiology 184:623–627

Carcinoma, Male Breast

Karin Bock
University of Marburg, Marburg, Germany
bock@med.uni-marburg.de

Synonyms

Breast cancer, male; Breast neoplasm, male; Breast tumors, male; Tumors, male breast

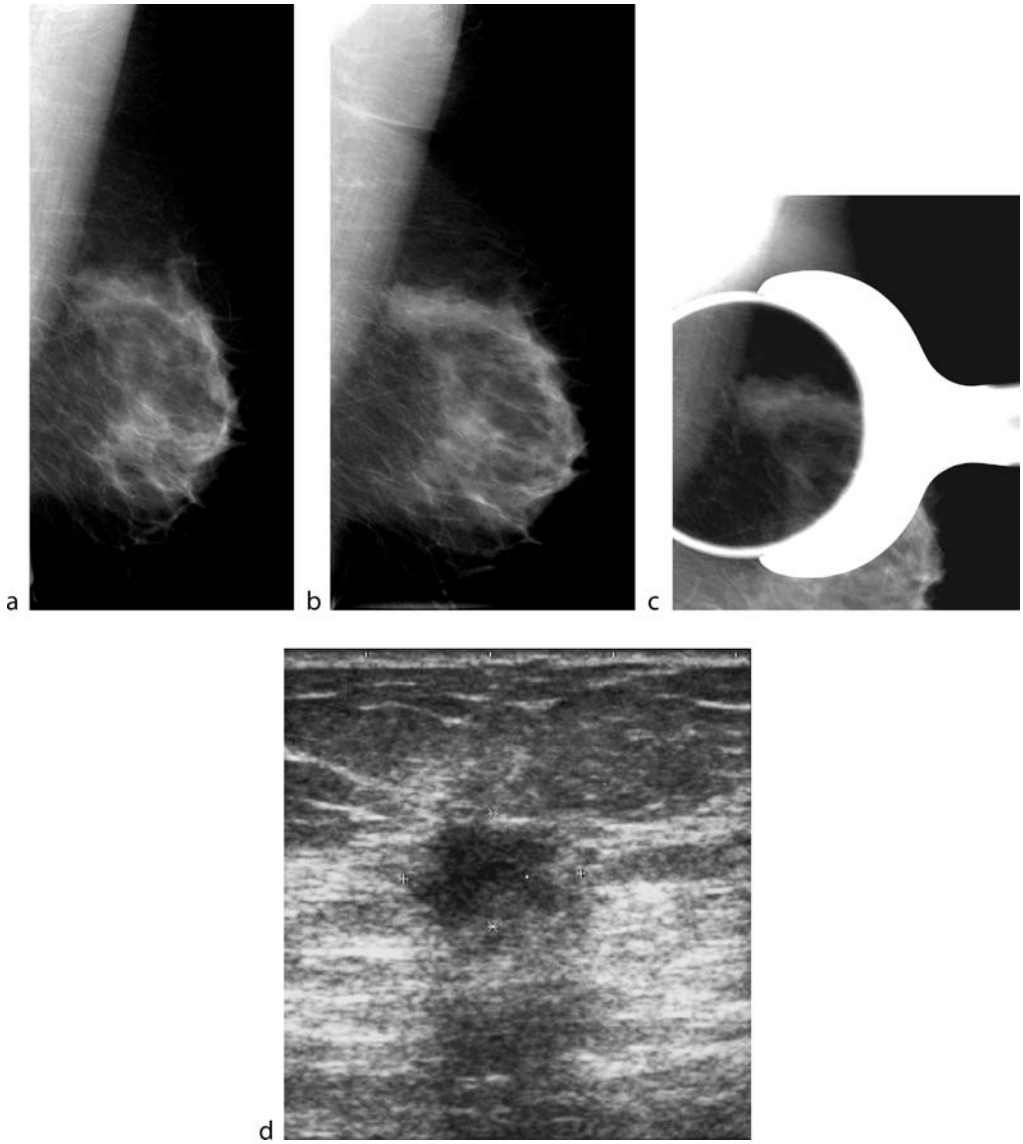

Carcinoma, Lobular, Invasive. Figure 2 (a–d): a Mammography in mlo view without pathology (a). At the six-month follow-up, a new mass in the left upper quadrant is seen, (b) which is most visible in the spot view (c). Ultrasound shows a hypoechoic mass with irregular borders (d).

Definitions

Malignant neoplasms of the male breast that account for approximately 0.7% of all breast cancer diagnoses and less than 1% of all malignant neoplasms in males.

The mean age at diagnosis for men is 67 years, which is 5 years older than the average age at diagnosis for women.

Primary malignant neoplasms with an overall incidence of 0.5–3% must be distinguished from metastases to the breast of extramammary carcinomas (e.g., melanoma, lymphoma, prostate cancer).

Pathology/Histopathology

Physiologically, the male breast consists of fat and a few strands of fibrous and connective tissue behind a small nipple with rudimentary ducts only.

The range of histologic subtypes for male and female breast cancers is similar, but relative distributions differ significantly.

Thus, ductal carcinoma *in situ* compromises approximately 10% of breast cancers in men, while the majority of cases are invasive cancers. Data obtained from more

than 2,000 male patients from the SEER cancer registry demonstrated 93.7% of male breast cancers as ductal or unclassified carcinomas, the others being papillary (2.6%), mucinous (1.8%), or lobular (1.5%).

In comparison to female breast cancers, male breast cancers show higher rates of estrogen receptor expression and equal rates of progesterone receptor expression. Moreover, in contrast to women, the c-erbB2 proto-oncogene is less likely to be overexpressed (approximately 5% only).

Clinical Presentation

As male breast cancer is still considered a rare disease, there is no screening for it and diagnosis is usually made clinically and in an advanced stage of disease.

The most common clinical presenting symptoms in male breast cancer patients are

1. Painless subareolar lumps
2. Nipple retraction
3. Bloody nipple discharge.

Imaging

The most appropriate work-up of suspicious breast findings is diagnostic *mammography*. As for women, the examination should consist of craniocaudal and mediolateral oblique views of each breast (see Fig. 1a, b). A small metal marker can be placed on the skin over the mass to help identify its location on mammographs. In contrast to females, supplementary mammographic views (e.g., spot compression, magnification, exaggerated craniocaudal, cleavage) are rarely needed to clarify lesions. The value of digital mammography has not been evaluated yet.

For evaluation of male mammograms, the breast imaging reporting and data system (BI-RADS) can be used successfully (1, 2).

The sensitivity, specificity, and overall accuracy of mammography in the diagnosis of male breast cancer have been reported by some investigators to be 92%, 89–90%, and 90%, respectively (3,4).

However, although there are characteristic mammographic features that allow breast cancer in men to be recognized, overlap between these features and the mammographic appearance of benign nodular lesions cannot be neglected (5).

Malignant breast tumors are more often eccentric, displacing ill-defined, spiculated, or macrolobulated margins (see Figs 1a, b and 2a, b), but even well-defined margins have been described (4–6). On the other hand, benign breast tumors, such as cysts or fibroadenoma, are seldom found, due to normally rudimentary ducts and glandular tissue.

Calcifications are fewer, coarser, and less frequently rod-shaped than in female breast cancer (5). Secondary features can include skin thickening as well as nipple retraction and axillary lymphadenopathy.

Computer-assisted diagnosis (*CAD*)—Systems do not play a role in the diagnosis of male breast disease, as mammography in men is only performed when clinical findings are present.

Breast ultrasound (7.5–13 MHz, linear arrays) is considered a useful adjunct without radiation hazards,

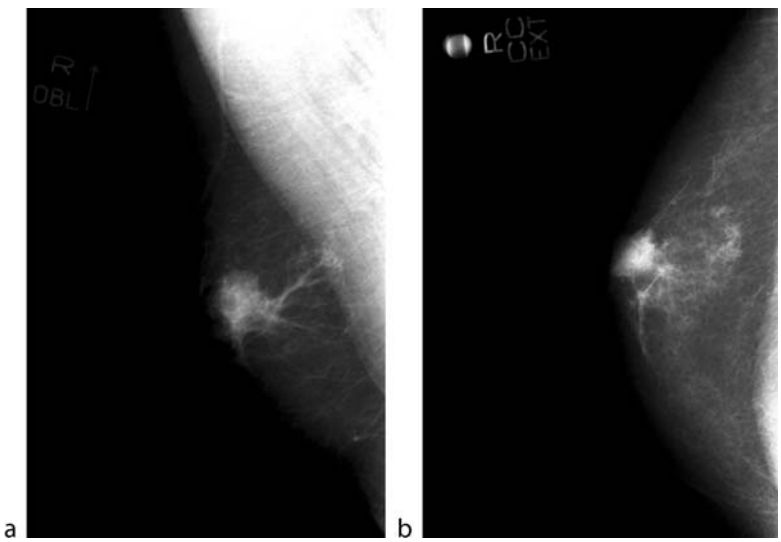

Carcinoma, Male Breast. Figure 1 (a, b) Two standard view mammographs of a man's left breast displaying pseudogynecomastia with retroareolar breast cancer.

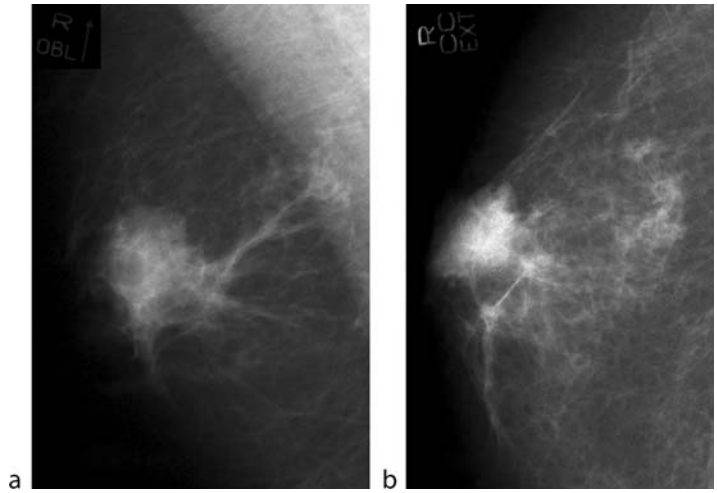

Carcinoma, Male Breast. Figure 2 (a, b) Magnification views (compare Figure 1a, b) displaying male breast cancer. Retroareolar irregular hyperdense lesion with convex borders, satellites toward the chest wall.

increasing the diagnostic specificity and providing additional information regarding nodal involvement, and is an image guide of choice for percutaneous procedures.

The BI-RADS—Ultrasound atlas (6) improves effective use of ultrasound by defining a lexicon of terms and characterizing typical features in the sonographic assessment of lesions.

Sonographic features of malignant tumors of the male breast do not differ substantially from those in female breast cancer (7). The most important features for malignant lesions being irregular shape, architectural distortion, and posterior shadowing (see Fig. 3).

Other imaging techniques such as *MRI* are still investigational in the diagnosis of female breast cancer. Moreover, to date, there are no published data on MRI in male breast cancer.

Studies on molecular imaging such as positron emission tomography (*PET*) or single photon emission computed tomography (*SPECT*) are of distinct diagnostic value in female breast cancer, but have not been tested for male breast cancer. So far, it does not seem feasible to use any of these techniques in the evaluation of clinically apparent breast findings.

Nevertheless, a normal imaging evaluation should never overrule a strongly suspicious finding on physical examination.

Nuclear Medicine

Not applicable in male breast disease, except for sentinel node biopsy in cases of proven breast cancer.

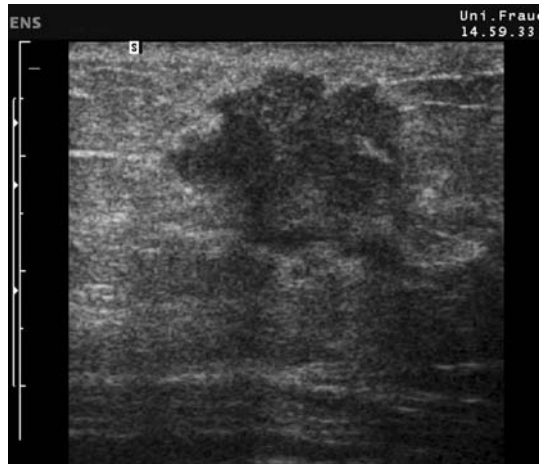

Carcinoma, Male Breast. Figure 3 Male breast cancer (compare Figure 1a, b and 2a, b). B-mode ultrasound (10 MHz, Siemens Sonoline Elegra 10 MHz, linear array) displaying an irregular-shaped, infiltrating mass with disturbed sound transmission as the most reliable characteristic features of malignancy.

Diagnosis

After appropriate local imaging, a suspicious mass requires biopsy to confirm the diagnosis. As in the diagnosis of breast lumps in women, the method of choice should be a minimally invasive procedure, that is, core needle biopsy (≤14G) (8).

Despite limited data, sentinel node biopsy seems feasible in male patients too.

Bibliography

1. ACR BI-RADS (2003) Mammography. 4th edn. Reston, VA
2. Bock K, Iwinska-Zelder J, Duda VF et al (2001) Validity of the Breast Imaging—Reporting and Data System (BI-RADS) for clinical mammography in men. Fortschr Röntgenstr 173:1019–1023
3. Evans GF, Anthony T, Turnage RH et al (2001) The diagnostic accuracy of mammography in the evaluation of male breast disease. Am J Surg 181:96–100
4. Partik B, Mallek R, Rudas M et al (2001) Malignant and benign diseases of the breast in 41 male patients: mammography, sonography and pathohistological correlations. Fortschr Röntgenstr 173:1012–1018
5. Appelbaum AH, Evans GFF, Levy KR et al (1999) Mammographic appearances of male breast disease. Radiographics 19:559–568
6. ACR BI-RADS (2003) Ultrasound. 1st edn. Reston, VA
7. Günhan-Bilgen I, Bozkaya H, Üstün EE et al (2002) Male breast disease: clinical, mammographic, and ultrasonographic features. Eur J Radiol 43:246–255
8. Janes SE, Lengyel JA, Singh S (2005) Needle core biopsy for the assessment of unilateral breast masses in men. Breast July 15 (Epub ahead of print)

Carcinoma, Multiple, Breast

Silvia Obenauer
Department of Radiology, Georg-August-University of Goettingen, Goettingen, Germany
obenauerheuser@yahoo.de

Definition

An invasive carcinoma is a tumor with extension of tumor cells through the ductal basement membrane. About 65% of carcinomas are invasive ductal carcinomas. Multifocal tumors must be distinguished from multicentric tumors.

Pathology

The tumors are classified as already described in the chapter on ductal invasive carcinomas.

Clinical Presentation

The patient could present with many hard, palpable masses and/or skin, and/or nipple retraction.

Imaging

All descriptions of the imaging of invasive tumors should be made according to the BI-RADS classification. Furthermore, the localization and size of the tumor must be reported with precision (Figs. 1 and 2).

Multifocality

One or more masses are found in one quadrant, at a maximum of 2 cm away from the main tumor. The therapy of choice is quadrantectomy.

Multicentricity

One or more tumors are more than 2 cm away from the main tumor, often in different quadrants. Mastectomy is usually performed.

Often a tumor is seen on mammography. Because mutifocal, multicentric, or contralateral tumors have a big influence on the therapy and prognosis, we perform MR mammography preoperatively.

Mammography

A spiculated mass with irregular margins is a typical sign of invasive ductal carcinomas. The density of the tumor is often higher than that of the parenchyma. In some cases the tumors also present with amorphous or pleomorphic microcalcifications. Other imaging features may be asymmetry or architectural distortion, and therefore changes from a previous mammogram must be interpreted carefully.

Ultrasound

The tumor is often characterized by an irregular, hypoechoic mass, typically more tall than wide with a thick echogenic rim and posterior acoustic enhancement. The tumor is not comprisable.

MR mammography

Typical findings on magnetic resonance mammography (MRM) are rim-enhancing masses that are irregular or spiculated with heterogeneous enhancement. Signal intensity curves show a high initial contrast media uptake and a postinitial plateau or wash-out. On water-sensitive sequences the tumor has an intermediary signal.

MRM reveals additional tumors not previously seen on mammography or ultrasound. Therefore, MRM could be performed before therapy to exclude ▶multifocality or ▶multicentricity. Studies have found that MRM reveals about 14% additional findings that were not previously seen.

Bibliography

1. Fischer U (2000) Lehratlas der MR-Mammographie. Thieme Verlag, Stuttgart-New York
2. Heywang SH, Wolf A, Pruss E et al (1989) MR imaging of the breast with Gd-DTPA: use and limitations. Radiology 171:95–103

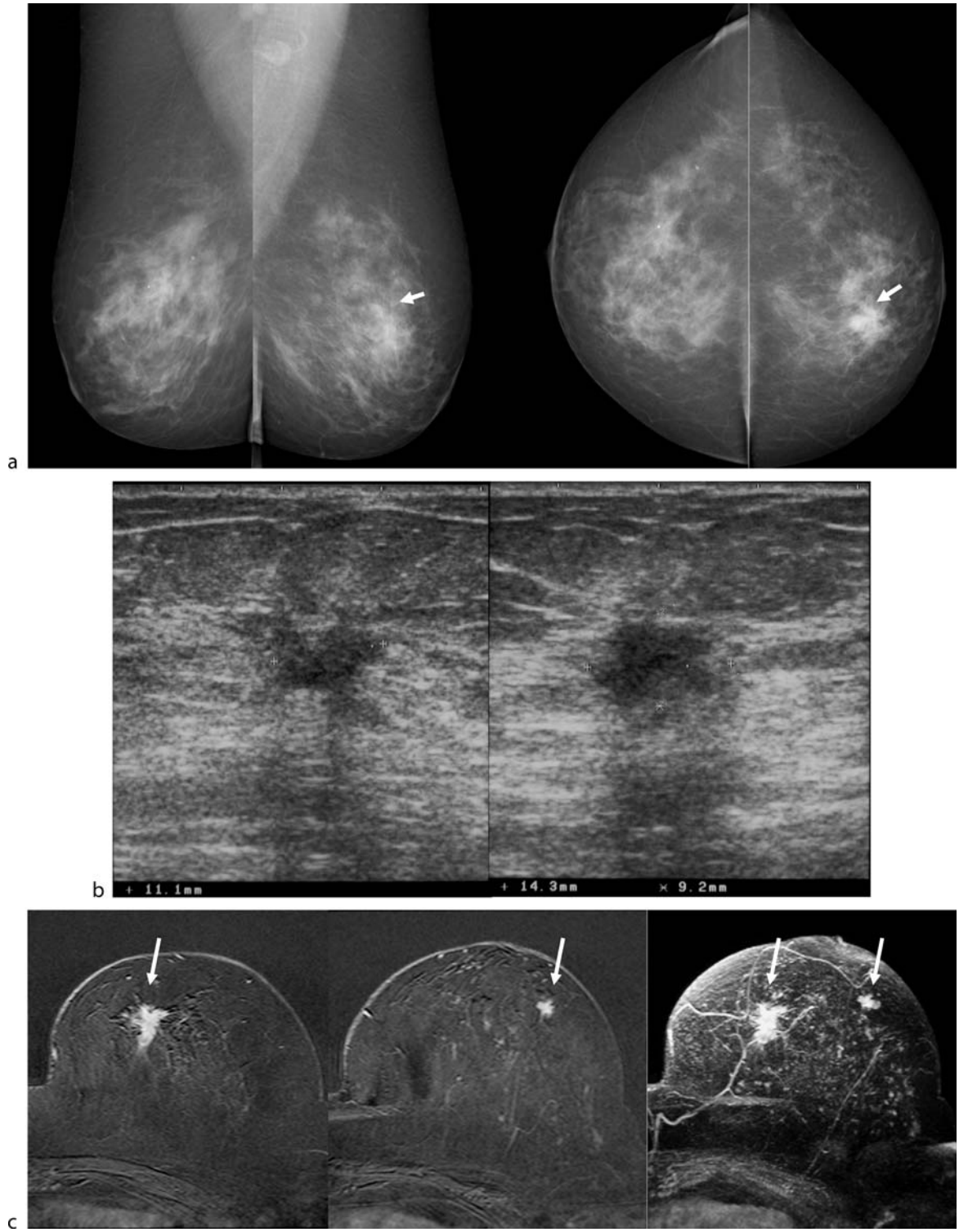

Carcinoma, Multiple, Breast. Figure 1 Mammography of a patient with a palpable mass on the left side. Typical spiculated mass on the left side in mediolateral oblique and craniocaudal views (a). Ultrasound revealing a second mass on the left side (b) which was confirmed by MRM on a subtraction image and maximum intensity projection (c). Histology determined bifocal invasive ductal carcinoma.

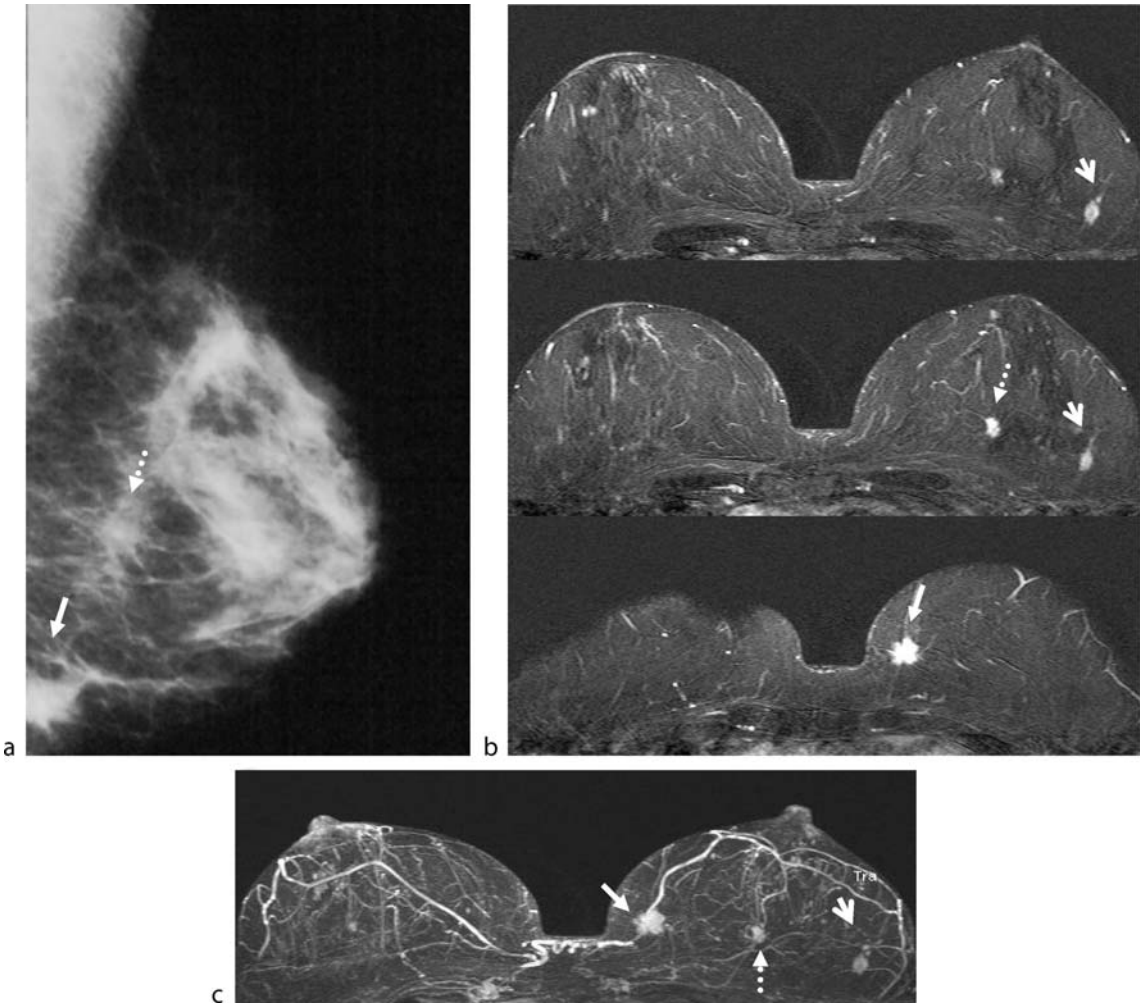

Carcinoma, Multiple, Breast. Figure 2 Mammography of a patient with a palpable mass in the left breast (caudal quadrant). Additional suspicious lesion in the middle of the breast (a). MRM of a multicentric carcinoma in the left breast, on subtraction image (b) and on maximum intensity projection (c).

Carcinoma, Other, Invasive, Breast

Silvia Obenauer
Department of Radiology, Georg-August-University of Goettingen, Goettingen, Germany
obenauerheuser@yahoo.de

Synonyms

Circumscribed carcinoma; Colloid carcinoma; Gallert carcinoma; Gelatinous carcinoma; Infiltrating papillary carcinoma; Inflammatory carcinoma; Intracystic papillary carcinoma with invasion; Medullary carcinoma; Mucinous carcinoma; Papillary carcinoma; Tubular carcinoma

Definition

Invasive carcinomas comprise medullary carcinoma, mucinous carcinoma, tubular carcinoma, papillary carcinoma, and ►inflammatory carcinoma.

Papillary carcinoma is a rare form of specified invasive ductal carcinoma (about 1–2% of all breast cancers). Medullary and mucinous carcinomas are also rare tumors (<5% of all breast cancers). Medullary carcinoma presents with a rapid growth and local aggressiveness. Mucinous

carcinoma is a well-differentiated, invasive adenocarcinoma. Tubular carcinoma is a well-differentiated form of infiltrating ductal carcinoma, which is slow growing. Inflammatory carcinoma typically presents with a rapid onset of diffuse breast changes and aggressive tumor invasion of the dermal lymphatics.

Pathology/Histopathology

Medullary Carcinoma

Medullary carcinoma is often a well-defined expansive mass, which is softer than most breast carcinomas. The cut edge reveals a nodular architecture with hemorrhage and necrosis.

The typical type contains no glandular elements and has an intense lymphoplasmacytic reaction, poorly differentiated nuclear grades with a high mitotic rate, and minimal desmoplastic stromal reaction.

Mucinous Carcinoma

Pathological pure and mixed types are distinguished. The pure type consists of more than 75% mucinous cells and the mixed type of mucinous and invasive, not otherwise specified elements. The pure type is usually smaller than the mixed type. The tumor cells are often found in lakes of mucin.

Tubular Carcinoma

On gross pathology, the tumor shows a tan-to-gray cut surface with ill-defined or spiculated margins. Microscopic features show well-formed tubular elements with often uniform nuclei and a low mitotic rate.

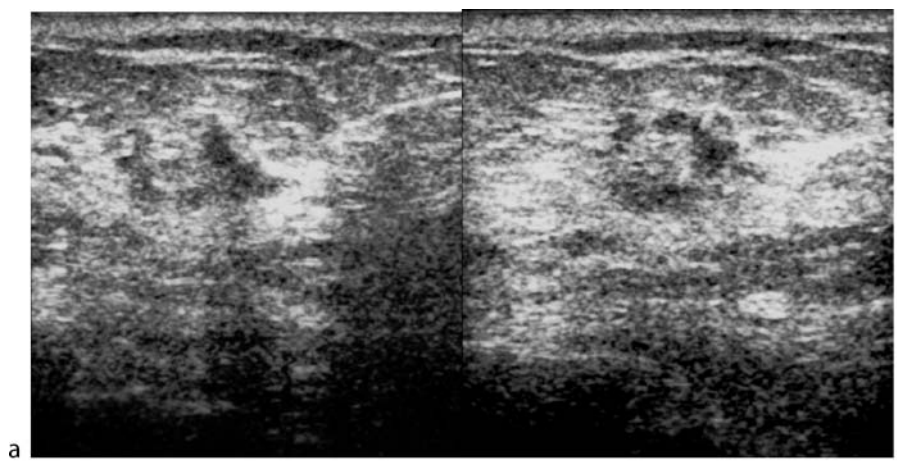

a

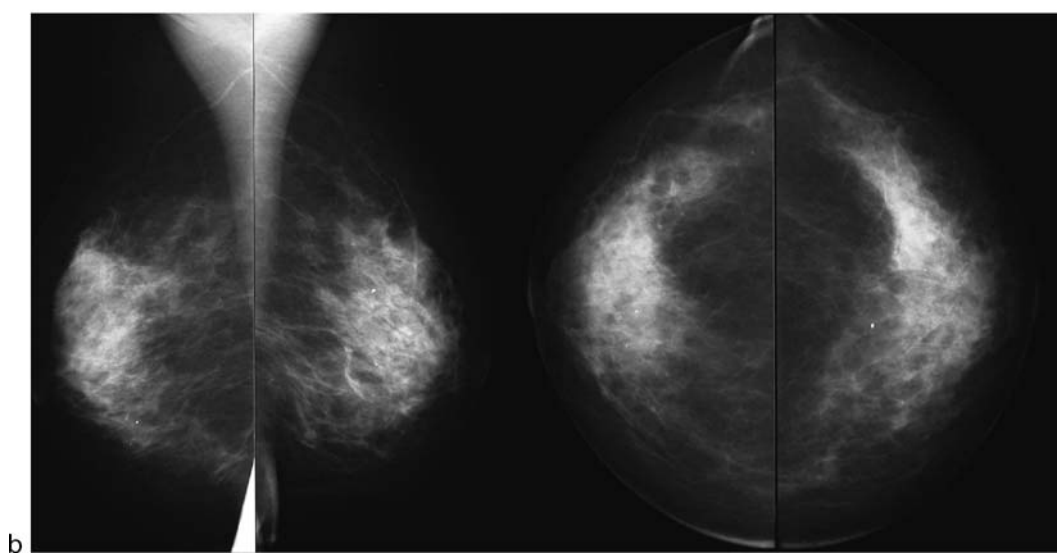

b

Carcinoma, Other, Invasive, Breast. Figure 1 Continued

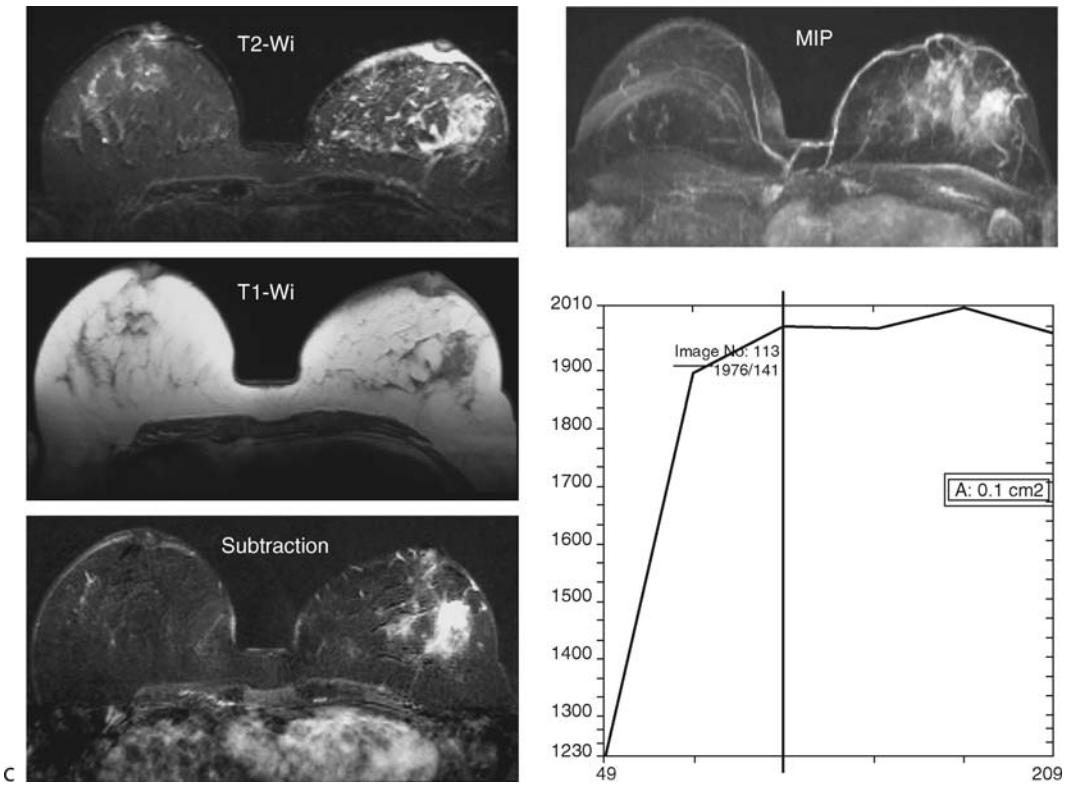

Carcinoma, Other, Invasive, Breast. Figure 1 Mass with irregular border and inhomogeneous echo inside is shown on an ultrasound image (a). Mass on the left side is masqueraded by parenchyma on the mammography. However, higher density on the left outer quadrant is seen (b). MR mammography reveals edema and skin thickening of the left breast on T2-weighted imaging. A mass on the left upper outer quadrant is seen with surrounding edema and contrast media enhancement. On T2-weighted imaging the mass is hyperintense. Signal intensity curves reveal an initial rise of about 100% and a postinitial plateau (c). Histology: papillary carcinoma.

Papillary Carcinoma

Two types are distinguished; the solid form that has a higher tendency to invade and the cystic form that may develop in a dilated lobule or duct. On gross pathology, a well-circumscribed mass is seen, often containing hemorrhage and cystic areas. On microscopy, an absent myoepithelial layer distinguishes the invasive form from a benign papillary lesion. Usually, the lesion is not associated with necrosis or calcifications. Invasive elements are often seen in the periphery of the tumor.

Inflammatory Carcinoma

Breast skin changes such as erythema, thickening, and peau d'orange are common. A diffuse infiltrating tumor without a well-defined tumor mass is found. The tumors are often poorly differentiated, are estrogen-receptor negative, and intralymphatic dermal tumor emboli are seen.

Clinical Presentation

Medullary Carcinoma

Most of these lesions are palpable, soft, and mobile masses usually located in the upper outer quadrant.

Mucinous Carcinoma

The tumors are often soft on palpation and may be perceived as benign.

Tubular Carcinoma

The tumors may be palpable, but most of them are detected on images.

Papillary Carcinoma

A firm, but not hard, mass that may be palpable. Nipple discharge is seen in up to one-third of patients.

Inflammatory Carcinoma

The patient presents with breast erythema, warmth, skin thickening, peau d'orange, pain, and sometimes a palpable mass.

Imaging

Medullary Carcinoma

These tumors are often oval or lobulated circumscribed masses (Figs. 1–3).

Mucinous Carcinoma

This tumor entity often appears as a well-circumscribed and round mass.

Tubular Carcinoma

The tumor is typically a small spiculated mass.

Papillary Carcinoma

The size of the invasive component is often small in relation to the lesion size.

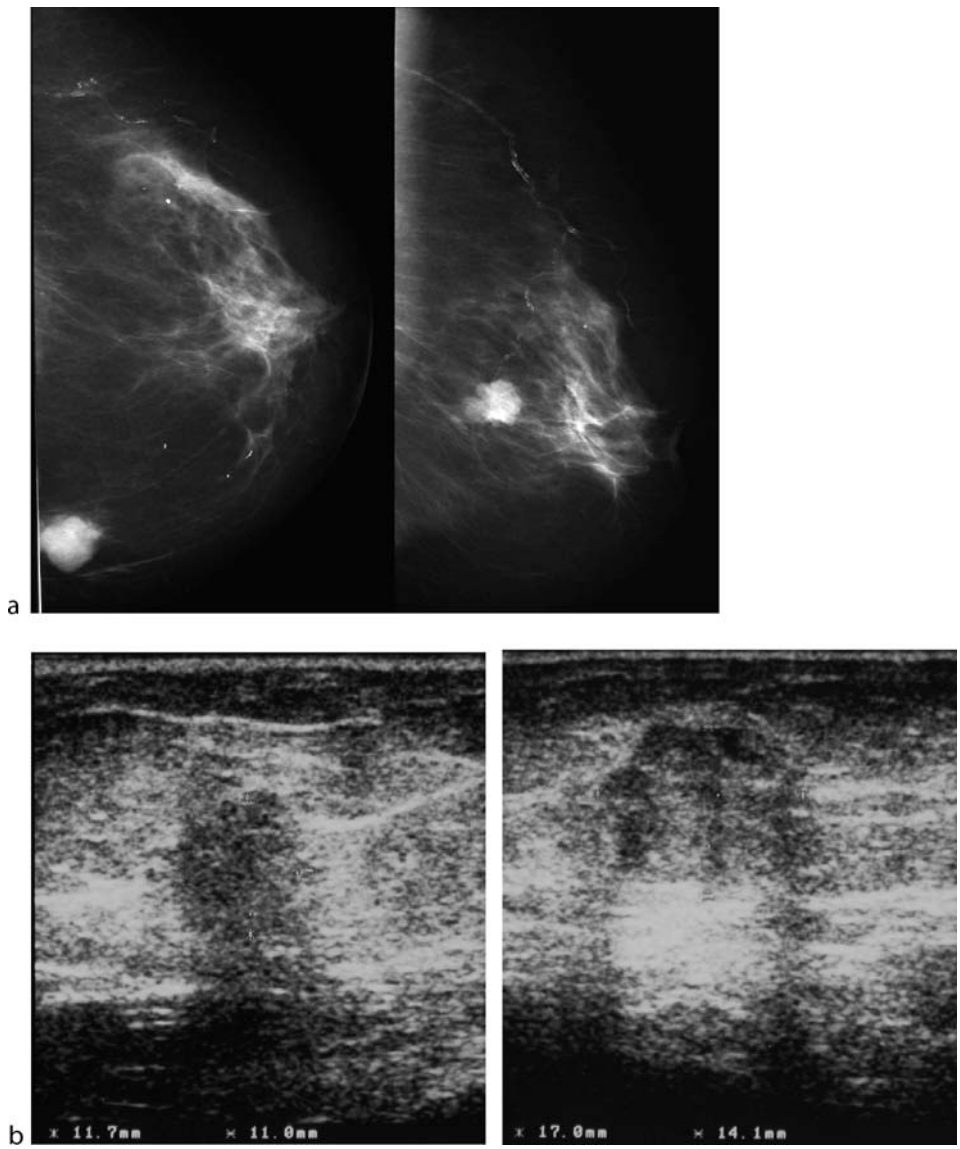

Carcinoma, Other, Invasive, Breast. Figure 2 Continued

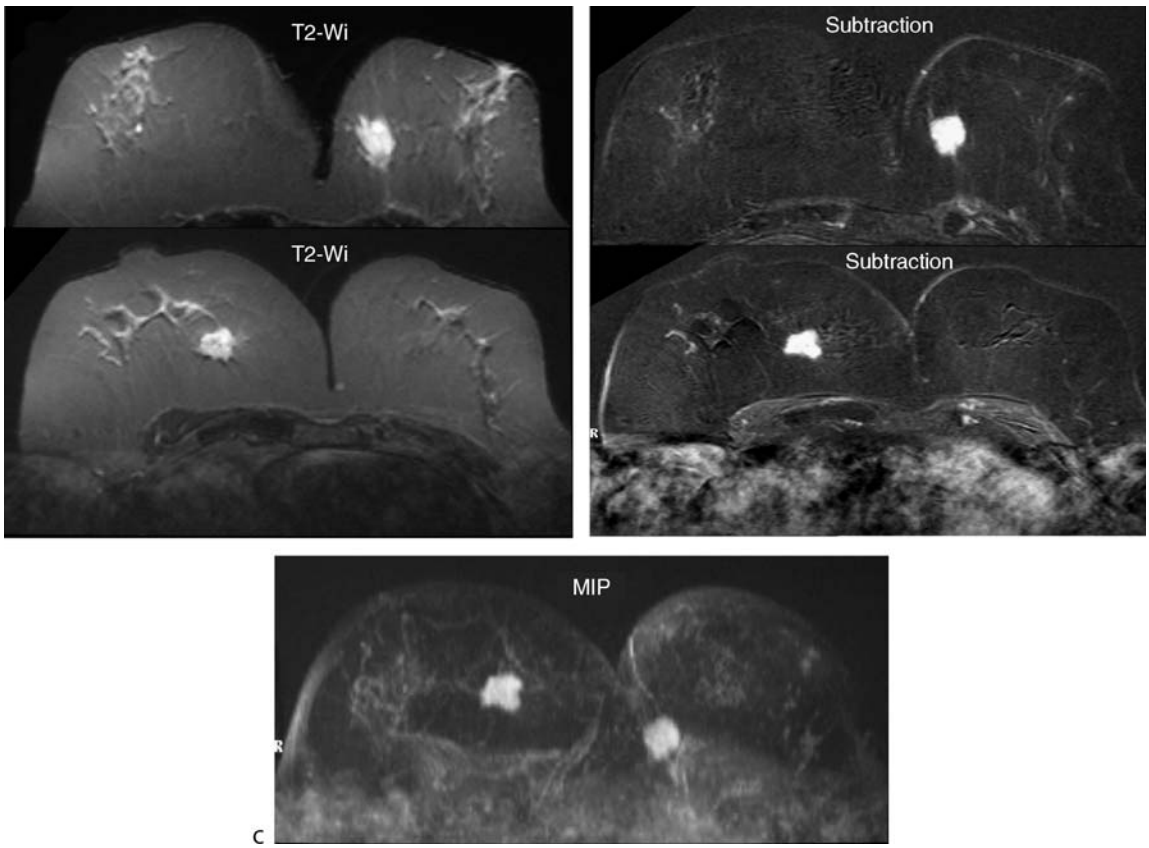

Carcinoma, Other, Invasive, Breast. Figure 2 Mammography of the left side reveals a lobulated mass in the middle inner quadrant without microcalcifications (a). Ultrasound of the lobulated mass with hypoechoic signal and posterior acoustic enhancement (b). MR mammography reveals lobulated masses on both sides of the breasts in the inner quadrant. The masses show hyperintense signal on T2-weighted images and strong contrast media enhancement in the subtraction images (c). Histology shows mucinous carcinomas.

Inflammatory Carcinoma

This tumor entity may be misdiagnosed as benign inflammatory process.

Mammography

Medullary Carcinoma

Typical findings are an oval, lobulated, or round mass with circumscribed margins. Calcifications are very rare.

Mucinous Carcinoma

Typical mammographic findings are a round, well-circumscribed, noncalcified mass. Most commonly the process is solitary at initial presentation and later multiple and bilateral masses are seen as the disease progresses. Spiculations and calcifications are rare.

Tubular Carcinoma

Typical mammographical findings are round or oval masses with spiculations. Sometimes the tumor is seen with architectural distortion, asymmetric density, and microcalcifications.

Papillary Carcinoma

Often a round, oval, or lobulated well-circumscribed mass is seen. Sometimes multiple masses occur. Calcifications and spiculations are rare findings. Pneumocystography may identify an irregular mass. Galactography may be helpful in the evaluation of nipple discharge. Typical findings will be ductal obstruction, wall irregularity, and filling defects.

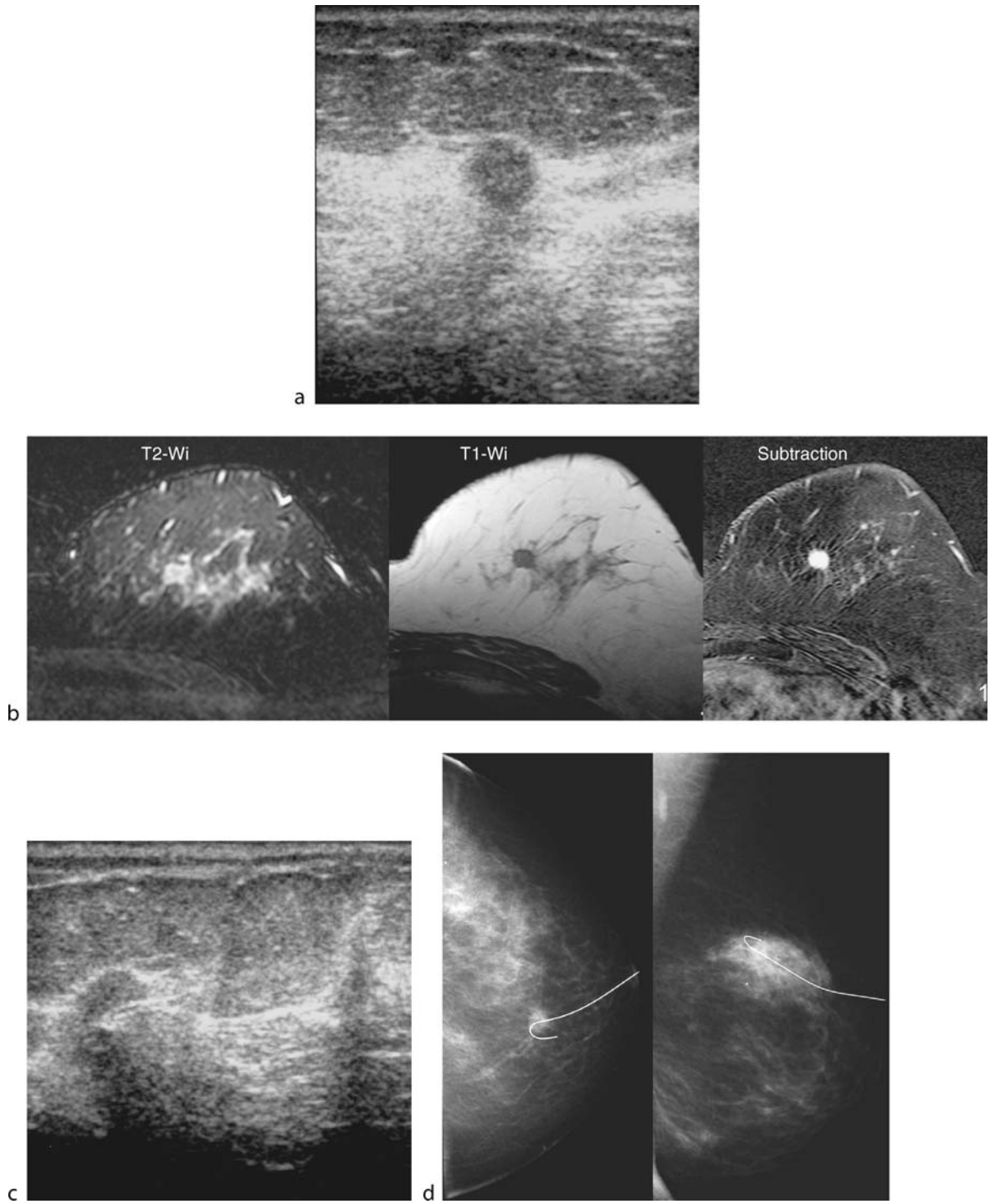

Carcinoma, Other, Invasive, Breast. Figure 3 Ultrasound of a tubular carcinoma revealing a hypoechoic mass, more tall than wide (a). MR mammography shows a round mass on the left side. On T2-weighted images the mass is hyperintense, on T1-weighted images hypointense, and on the subtraction image the mass shows contrast enhancement (b). Preoperative ultrasound-guided localization of the mass was carried out (c). Follow-up mammography after ultrasound-guided wire localization shows a round, partially ill-defined mass in the left upper middle quadrant exactly localized by wire (d). Histology shows tubular carcinoma.

Inflammatory Carcinoma

Common features are skin thickening and diffuse increased breast density. Other findings such as trabecular thickening, axillary lymphadenopathy, architectural distortion, focal asymmetric density, and nipple retraction may be found. Less often, calcifications or masses are found.

Ultrasound

Medullary Carcinoma

Typically, a well-defined, hypoechoic mass is found. Some large lesions may have anechoic areas. A posterior acoustic enhancement is not uncommon.

Mucinous Carcinoma

Typically, a round or oval mass is seen, sometimes with lobulations. The margins are smooth or irregular. There may be internal anechoic echoes. Posterior acoustic enhancement is not common.

Tubular Carcinoma

The tumor shows an ill-defined hypoechoic mass with posterior acoustic shadowing. Sometimes hyperechoic foci represent calcifications.

Papillary Carcinoma

Often a homogeneously solid and cystic mass is seen with posterior acoustic enhancement. Sometimes an intracystic mass or mural nodules can be distinguished. Sequelae of hemorrhage may also be seen.

Inflammatory Carcinoma

On ultrasound, nonspecific findings are seen such as widening of the dermal–subcutaneous fat interface. Edematous changes are, however, indistinguishable from tumor infiltration.

Magnetic Resonance Mammography

Medullary Carcinoma

Often an oval or round, lobulated, heterogeneous, enhancing mass is seen.

Mucinous Carcinoma

Often a round, well-circumscribed, or ill-defined, rim-enhancing mass is seen.

Tubular Carcinoma

The tumor shows the typical enhancement of an invasive ductal carcinoma with an irregular spiculated mass and a strong initial contrast media rim or inhomogeneous enhancement.

Papillary Carcinoma

The solid components show a heterogeneous, well-circumscribed enhancing mass when i.v. contrast media is administered.

In the cystic mass, mural or nodular enhancement with or without hemorrhage is seen.

Inflammatory Carcinoma

Magnetic resonance mammography is not indicated for this tumor entity. Often a diffuse, intense, rapid enhancement is seen, which is indistinguishable from benign inflammatory process.

Bibliography

1. Heywang SH, Wolf A, Pruss E et al (1989) MR imaging of the breast with Gd-DTPA: use and limitations. Radiology 171:95–103
2. Newstead GM, Baute PB, Toth HK (1992) Invasive lobular and ductal carcinoma: mammographic findings and stage at diagnosis. Radiology 184:623–627

Carcinoma, Ovarium

Rosemarie Forstner
Department of Radiology, Paracelsus Private Medical University, Salzburger Landeskliniken, Salzburg, Austria
r.forstner@salk.at

Synonyms

Epithelial ovarian cancer; Epithelial ovarian neoplasm; Malignant ovarian neoplasm; Ovarian cancer; Primary malignant neoplasm of ovary

Definition

Ovarian cancer is the leading cause of death among all gynecologic malignancies. In females, it is the fifth most common cancer. The majority of ovarian carcinomas are epithelial in origin, accounting for approximately 85% of

ovarian malignancies (1). The incidence of ovarian cancer increases with age, with a median age of 61 years at diagnosis (2). Familial evidence of ovarian cancer is the strongest risk factor: ovarian cancer develops in these women when they are one decade younger than the normal population (1). There are significant differences in prognosis between early and advanced ovarian cancer. While early-stage cancer is often curable, advanced-stage ovarian cancer has an overall 5-year survival rate of 38–53% (1). This is attributed to the fact that at the time of diagnosis up to 70–85% of patients present with peritoneal cancer spread outside the pelvis.

Pathology/Histopathology

Macroscopically, ovarian cancer most often presents as uni- or bilateral multilocular cystic tumors with intracystic ►papillary projections or as mixed solid and cystic tumors (3). Rarely, ovarian cancers may be predominantly solid (3). Cystic elements within the tumor may contain serous, hemorrhagic, or turbid fluid. Papillary projections, which are a typical feature of serous ovarian tumors, may fill the cyst cavities. ►Psammoma bodies within the tumor presenting tiny calcifications are detected in 30% of serous adenocarcinomas. Bilateral ovarian involvement is typically found in serous cystadenocarcinoma, which is the most common ovarian cancer; it is rarely encountered in endometrioid cancer (3). Endometriosis is associated with endometrioid cancer and particularly with clear cell cancer (3).

Epithelial ovarian cancers are adenocarcinomas and comprise, depending on their histopathologic features, serous, mucinous, endometrioid, transitional cell, clear cell, undifferentiated, and mixed carcinomas (1). Except for clear cell carcinomas, the histologic type has limited prognostic significance independent of clinical stage (1).

Epithelial carcinomas are characterized by histologic type and the degree of cellular differentiation (grade).

Clinical Presentation

Ovarian cancer usually remains clinically silent in early-stage disease. Rarely, abnormal uterine bleeding may be the first symptom of ovarian cancer. With more advanced stage and tumor masses larger than 10 cm, women often complain of bloating, abdominal discomfort, pelvic pressure, or urinary or rectal discomfort. The disease may also become clinically apparent by ascites-related symptoms including abdominal swelling and pleural effusion with shortness of breath (1).

Imaging

The American College of Radiology (ACR) recommends ►screening for ovarian cancer by ►CA-125 and ultrasound (US) assessment of the ovaries only in high-risk patients (2). These are patients with a positive family history of ovarian cancer or *BRCA1* or *BRCA2* gene mutations.

The role of imaging in suspected ovarian cancer includes characterization of an adnexal mass, ►staging of ovarian cancer, and defining criteria of nonresectability.

Criteria for differentiation between benign and malignant ovarian masses do not differ for the cross-sectional imaging modalities US, computed tomography (CT), and magnetic resonance imaging (MRI). They include tumor size and morphologic criteria of the internal architecture of an adnexal mass including its vascularization (4). Secondary signs supporting the diagnosis of metastatic spread are ascites, peritoneal implants, or lymph node enlargement (4).

Staging of ovarian cancer is based on the extent and location of disease found at explorative laparotomy. The International Federation of Gynecologists and Obstetricians (FIGO) classification system is the most commonly used staging system for ovarian cancer. Although definitive staging of ovarian cancer is based on the findings at surgery, preoperative assessment of the tumor extent by imaging may influence patient management. Accurate preoperative assessment of ovarian cancer may assist in selecting sites for biopsy and may alert to tumor deposits that are difficult to visualize intraoperatively, for example, locations in the upper abdomen and lymph nodes. Furthermore, it may influence surgical strategy, for example, need of subspecialist cooperation or of referral to an oncology center.

Preoperative routine chest radiographs, intravenous urography (IVU), and barium studies have recently been replaced by CT.

In cases of extensive cancer and signs of nonresectability in CT or MRI, candidates who may benefit from neoadjuvant therapy prior to surgery may be selected.

In the assessment of ovarian cancer, *US* is the primary imaging modality for detection and characterization of adnexal masses (2) (Fig. 1).

MRI is currently most commonly used as a problem-solving modality in cases of indeterminate adnexal masses (2). Its advantages over US are superior morphologic assessment of adnexal masses, particularly in hemorrhagic lesions. MRI is superior to US and CT in the evaluation of local pelvic spread of ovarian cancer.

Multidetector contrast-enhanced CT is the modality of choice for preoperative staging and for follow-up of ovarian cancer (2) (Fig. 2). Alternatively, particularly in

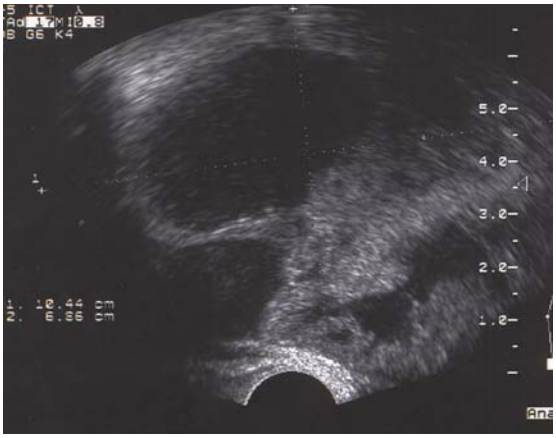

Carcinoma Ovarium. Figure 1 Mucinous adenocarcinoma on US image. A large, complex ovarian lesion consisting of solid and cystic elements is demonstrated in transvaginal sonography. The cyst contains multiple homogeneous echoes presenting hemorrhagic or proteinaceous fluid; the cyst walls are thick and irregular.

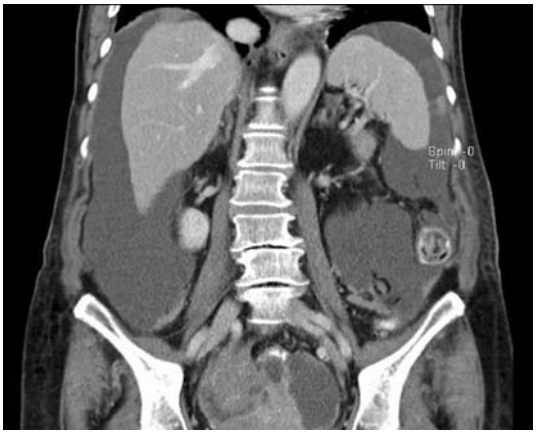

Carcinoma Ovarium. Figure 2 Staging of ovarian cancer by CT. A complex, solid, and cystic ovarian mass is demonstrated on the coronal CT scan. Large amounts of ascites are found throughout the abdomen. Small bilateral diaphragmatic nodules and plaquelike peritoneal thickening in the paracolic gutters show stage IIIb disease.

the case of contraindications for intravenous contrast media, MRI is used for preoperative staging of ovarian cancer. Following the FIGO criteria, CT and MRI perform similarly in staging ovarian cancer, with reported sensitivities of 63–79% and specificity of 100% (5).

Nuclear Medicine

Fluorodeoxyglucose positron emission tomography (FDG PET)-CT is emerging as a new imaging technique for assessing ovarian cancer. Currently it is only recommend complementary to CT for the detection of recurrent ovarian cancer. For preoperative staging of ovarian cancer, recent data suggest that the combination of FDG PET and CT is superior to CT alone.

C

Diagnosis

Ovarian cancers are typically inhomogeneous adnexal masses with a mixed pattern of cystic and solid elements, and are often large at the time of presentation (4). US is the modality of choice for detection and characterization of lesions as yielding a high or low risk for malignancy (2).

MRI is currently used as a problem-solving modality complementary to sonography. Its strength is not to define the exact histology of ovarian cancer, but to predict if a lesion is malignant or not.

The most commonly used imaging criteria suggestive of malignancy in US and MRI are: lesions size larger than 4 cm, thickness of wall or septa exceeding more than 3 mm, papillary projections, necrosis, partially cystic and solid internal architecture, a lobulated solid mass, and presence of tumor vessels (4) (Fig. 3). Doppler assessment in ovarian cancer displays a low resistive index (RI<1) (2).

Contrast-enhanced MRI studies assist in tumor characterization, especially in the depiction of papillary projections and necrosis.

None of these imaging criteria, however, are specific enough as a single factor to diagnose ovarian cancer reliably. The likelihood of malignancy increases with solid nonfibrous elements, thickness of septa, and presence of necrosis. Ancillary findings such as presence of lymphadenopathy, peritoneal lesions, and ascites improve the diagnostic confidence. The combination of tumor size and architecture and ancillary signs improves prediction of malignancy and yields an accuracy of 89–95% in MRI (4).

In a multivariate logistic regression analysis of complex adnexal masses studied by MRI, necrosis within a solid portion of an ovarian mass and vegetations in a cystic lesion were the most predictive signs of malignancy (4). Solid, nonfatty, nonfibrous tissue with or without necrosis has also been reported as a valuable predictor of malignancy. Thick walls and septations are less reliable signs of malignancy, as they may also occur in abscesses, endometriomas, and benign neoplasm such as cystadenofibromas and mucinous cystadenomas.

Large amounts of ascites in a patient with ovarian cancer usually indicate the presence of peritoneal metastases (Fig. 2). Absence of ascites does not exclude ovarian malignancy, as 50% of borderline tumors and 83% of early-stage ovarian cancers are not associated with ascites (2).

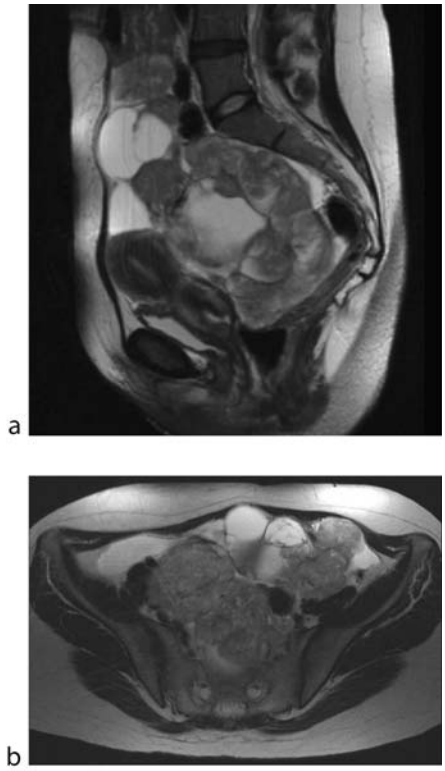

Carcinoma Ovarium. Figure 3 Papillary serous adenocarcinoma in a 46-year-old patient. Sagittal (a) and transaxial (b) T2-weighted MR images demonstrate a complex partly cystic and solid adnexal tumor that is found separate from the uterus and extends to the level of L4. The solid areas are composed of multiple papillary excrescences which also fill the cystic areas. Only small amounts of ascites surround the lesion.

CA-125 is currently the most commonly used tumor marker for ovarian cancer. However, elevation of CA-125 can be observed in other malignant epithelial cancers and in benign conditions, including cirrhosis, pancreatitis, endometriosis, and pelvic inflammatory disease as well as in different stages of the menstrual cycle. More than 80% of women with advanced epithelial ovarian cancer present with CA-125 elevations. However, the sensitivity of CA-125 elevation in early-stage disease is only 25% (2).

Bibliography

1. Hensley ML, Alektiar KM, Chi DS (2001) Ovarian and fallopian-tube cancer. In: Barakat RR, Bevers MW, Gershenson, Hoskins WJ (eds) Handbook of Gynecologic Oncology. Martin Dunitz, London, pp 243–263
2. Togashi K (2003) Ovarian cancer: the role of US, CT and MRI. Euro Radiol 13 (Suppl 4):L87–104
3. Seidman JD, Russell P, Kurman RJ (2002) Surface epithelial tumors of the ovary. In: Kurman RJ (ed) Blaustein's Pathology of the Female Genital Tract. Springer Verlag, New York, pp 791–904
4. Hricak H, Chen M, Coakley FV et al (2000) Complex adnexal masses: detection and characterization with MRI—multivariate analysis. Radiology 214:39–46
5. Tempany CM, Zou KH, Silverman et al (2000) Staging of advanced ovarian cancer: comparison of imaging modalities—report from the Radiology Oncology Group. Radiology 215:761–767

Carcinoma, Pancreatic

Carlo Bartolozzi[1], Laura Crocetti[1], Piero Boraschi[2], Carla Cappelli[1]
[1]Department of Diagnostic and Interventional Radiology, University of Pisa, Italy
[2]2nd Department of Radiology, University Hospital, Pisa, Italy
l.crocetti@med.unipi.it

Synonyms

Adenocarcinoma of the pancreas; exocrine carcinoma of the pancreas; pancreatic ductal adenocarcinoma

Definitions

Pancreatic ductal adenocarcinoma accounts for 90% of all primary malignant tumors arising from the pancreatic gland. It represents the fourth leading cause of cancer death and its incidence tripled over the past 40 years. The peak of incidence occurs in the seventh and eighth decades of life, with an incidence rate slightly higher in men than in women. Despite improvements in diagnostic and surgical techniques and perioperative management, pancreatic carcinoma represents a major health problem and it remains a significant challenge, being the tumor at the time of diagnosis confined to the pancreas in about 10% of patients, locally advanced in 40% of cases, and metastatic in 50% of cases. The poor survival of patients with pancreatic cancer is caused by the late diagnosis and the low resection rate. For all stages combined, the 1-year survival rate is 19% and the 5-year survival rate is 4%. Overall, fewer than 5% of patients undergo resection, but among these, as many as 20% survive 5 years. The median survival is less than 18 months after surgery.

The definitive causative factors that lead to an increased incidence of pancreatic cancer are unknown. Many environmental factors are associated with increased risk of pancreatic cancer, including high-protein and high-fat diets and the exposure to aromatic amines, such as in cigarette smoking or occupations including chemistry or petrochemical work.

The association of pancreatic adenocarcinoma with chronic pancreatitis is still unclear, but individuals with the hereditary type of chronic pancreatitis seem to have a predisposition for pancreatic cancer stronger than that of the general population. Alcohol abuse is seen in 4% of patients and association of alcohol and pancreatic cancer is indirectly related to the development of alcohol-induced pancreatitis. Whether or not diabetes is a risk factor for pancreatic adenocarcinoma remains controversial. Diabetes or impaired glucose tolerance occurs in about 80% of cases at the time of the diagnosis, but recent evidence suggests that diabetes is a consequence of carcinoma rather than a predisposing factor, because of the production of a diabetogenic factor.

There is increasing evidence that some pancreatic cancers are inherited and that genetic predisposition plays a significant role in pancreatic cancer risk. Furthermore some genetic syndromes associated with an increased risk of pancreatic cancer have been identified and these include the familial atypical multiple mole melanoma syndrome (FAMMM), characterized by the germline mutation in the p16 gene; the Peutz-Jeghers syndrome; the hereditary nonpolyposis colorectal cancer (HNPCC) with germline mutations in the DNA mismatch repair genes; the hereditary pancreatitis, caused by mutations in the PRSS1 gene (cationic trypsinogen gene); and the familial breast cancer caused by a mutation of the BRCA2 gene.

Pathology and Histopathology

In the past, numerous classification schemes for pancreatic tumors were proposed. Presently, the most widely adopted is the AFIP classification system, published by the Armed Forces Institute of Pathology in 1995. According to the AFIP system, pancreatic tumors are classified into primary tumors, secondary tumors, and tumor-like lesions. Primary tumors are then classified into exocrine lesions, endocrine lesions, and nonepithelial tumors. All the pancreatic tumors are divided according to their biologic behavior into benign, borderline (with an uncertain malignant potential), and malignant.

The ductal adenocarcinoma and its variants account for the vast majority (about 90%) of malignant pancreatic neoplasms. Microscopically ductal adenocarcinoma is composed of epithelial cells forming glands surrounded by dense fibrous connective tissue. Most adenocarcinomas infiltrate into perineural, lymphatic, and vascular spaces. Some variants of ductal adenocarcinoma include the mucinous noncystic adenocarcinoma or colloid carcinoma, which is characterized by abundant extracellular mucin production; the adenosquamous carcinoma with glandular and squamous components; the signet-ring cell carcinoma composed almost exclusively of cells filled with mucin; and the undifferentiated or anaplastic carcinoma, composed of large cells showing extreme anaplasia.

Between 60% and 70% of ductal adenocarcinomas are located in the head of the pancreas. Carcinomas of the pancreatic head have an intimate relationship with the distal common bile duct and the main pancreatic duct, producing stenosis and eventually obstruction with duct dilatation and fibrous atrophy of the parenchyma (obstructive chronic pancreatitis).

It is now widely accepted that ductal pancreatic adenocarcinomas arise from lesions which represent precursors of the carcinomas, called PanINs (►pancreatic intraductal neoplasms); the development of carcinoma from PanINs lesions involves accumulation of multistep genetic alterations. PanINs lesions are composed of mucin-producing epithelial cells with varying degrees of cytological and architectural atypia that involve the small pancreatic ducts. PanINs can be flat 1A, papillary without atypia 1B, papillary with atypia 2, or may be a carcinoma *in situ* 3. PanINs display some of the genetic changes which are founded in infiltrating carcinomas (mutations in K-ras gene, p16, p53, BRCA2 and DPC4), suggesting that there is a progression from PanIN 1 to PanIN 2 and PanIN 3 to infiltrating adenocarcinoma.

A number of schemes have been proposed in the past for the staging of pancreatic carcinoma. By 1977, they were replaced by the UICC (Union Internationale Contre le Cancer) staging system, which is a TNM staging system. The newest revised version was published in 2002 by the American Joint Committee for Cancer. A more complex stage classification system had been proposed by the Japan Pancreas Society (JPS) in 1987; this classification system primarily relies on the prognostic value of tumor size and local spread, adding other factors to the classification such as serosal invasion, retroperitoneal invasion, and invasion of the portal vein. An important prognostic factor is also the possible presence of residual neoplastic tissue at the level of margins of surgical resection; the extent of resection is graded into R0 (complete resection), R1 (grossly negative but positive microscopic margins of resection), and R2 (grossly and microscopically positive margins of resection).

Clinical Presentation

Clinical symptoms and signs develop late, particularly in tumors of the pancreatic body and tail, thus the vast majority of pancreatic cancers are diagnosed at an advanced, incurable stage. The most common, even nonspecific, symptom associated with carcinoma is abdominal pain, especially in patients with a locally advanced lesion, because it indicates spread of tumor to perineural lymphatics. The typical epigastric pain is frequently accompanied by back pain. Obstructive

jaundice represents the most common finding in patients with a neoplasm arising in the head of the pancreas and obstructing the common bile duct. Dark urine, light stools, pruritis, and palpable gallbladder (Courvoisier's sign) may be present together with jaundice; laboratory tests reveal elevated conjugated bilirubin concentrations and alkaline phosphatase and γ-glutamyl transpeptidase levels. Obstruction of the pancreatic duct or its side branches results in symptoms related to an obstructive pancreatitis. It is important to suspect a pancreatic carcinoma when there are not obvious causes for the acute pancreatitis (such as gallstones, alcohol abuse etc.). Other signs include new onset of diabetes or instability of diabetes that was previously well-controlled and thrombophlebitis (Trousseau syndrome). Weight loss, weakness, and anorexia may be present. Nausea and vomiting can be related to a gastroduodenal obstruction.

The carbohydrate antigen 19.9 (Ca 19.9) blood levels can be increased in patients with pancreatic adenocarcinoma; however 10–15% of individuals do not secrete the Ca19.9. In addition, Ca19.9 levels can be elevated in benign biliary or pancreatic diseases.

Imaging

Ultrasound (US) examination often represents the first level imaging modality performed in patients with pancreatic lesions, the symptoms usually being the symptoms usually nonspecific. Direct visualization of the tumor by US is often difficult and depends on the size and location of the tumor. The lesion may have a variable appearance on US, however the large majority of pancreatic cancers present as hypoechoic, nonhomogeneous lesions with irregular margins. US examination is less sensitive than other modalities in the detection of pancreatic malignancy, particularly when the lesions are smaller than 2 cm. In some cases, the intravenous administration of a contrast medium during the examination can improve the depiction of the pancreatic tumor, showing the lesion a much lower contrast enhancement than the normal pancreatic parenchyma. Indirect signs include dilatation of biliary and pancreatic ducts associated to dilatation of the gallbladder. US can also demonstrate the presence of locoregional lymph nodes enlargement, distant metastases (in particular liver metastases) or peritoneal carcinosis. Despite the advances in US technology, including the employment of US contrast media, the local staging of pancreatic cancer results difficult in the majority of cases. In particular, the relation of the tumor to peripancreatic vessels is demonstrated less reliably with US than with other modalities.

Endoscopic ultrasound (EUS) has been used for early detection of small carcinomas as well as local staging. The close proximity of the transducer to the region of interest permits the use of high ultrasound frequencies, then improving the image resolution. EUS can determine the size and local extent of a pancreatic cancer, also assessing the peripancreatic vascular and lymph node involvement. EUS can also enable the fine needle aspiration.

Intraoperative ultrasound (IOUS) allows to easily identify pancreatic lesions and to precisely define the staging of the tumor, demonstrating the relationships between the tumor itself and adjacent structures (in particular vascular structures) and also highlighting with high sensitivity small hepatic metastases.

Presently, computed tomography (CT) is the most widely used and most sensitive technique for the evaluation of the pancreas. High-resolution spiral CT has represented the preferred noninvasive imaging modality for the diagnosis and staging of pancreatic cancers. However state-of-the-art CT scanning is actually based on multidetector CT, which has allowed a further improvement in resolution and in scan timing, thus obtaining acquisitions in multiple selective phases of contrast distribution. Multidetector CT should be the first-line study for the detection of pancreatic tumor and for evaluating its resectability. Before the CT examination, the distension of stomach and duodenum must be obtained. Water represents the oral contrast agent of choice, associated with the intravenous administration of a hypotonizing drug, just before the scan. Acquisition is performed before and after the intravenous administration of the iodinated contrast medium. After the contrast administration, acquisition with thin slices (1–2 mm) must be performed in the pancreatic phase (delay 35–40 sec) and in the venous phase (delay 70–80 sec). Typically, pancreatic adenocarcinoma is more hypodense than pancreatic parenchyma, especially during the pancreatic phase when the parenchyma shows the highest contrast enhancement. The margins of the lesion usually are poorly defined; central necrosis can be present. Features suggestive of pancreatic cancer include also alterations in morphology of the gland, such as focal enlargement or, more rarely, diffuse enlargement and obliteration of peripancreatic fat (which is suggestive of invasion beyond the margins of the gland). Pancreatic ductal dilatation is often present, associated with a dilatation of the biliary ducts and of the gallbladder when the tumor is localized in the pancreatic head. Chronic obstruction of the pancreatic duct leads to atrophy of the parenchyma distal to the obstruction (Fig. 1) (1–4).

In order to define the staging and resectability of the tumor, the possible infiltration of the adjacent structures (including retroperitoneal fat infiltration), and the presence of lymph node metastases, distant metastases, or peritoneal carcinosis must be identified. Spread to surrounding organs may typically involve the

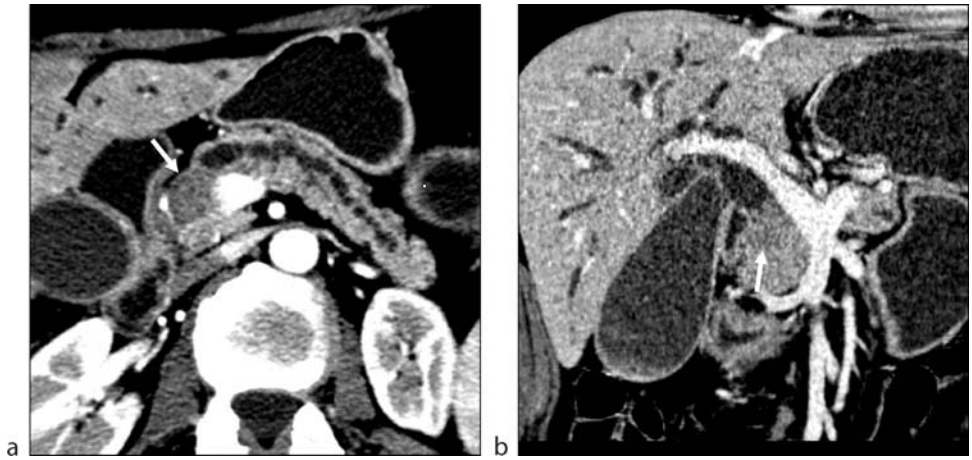

Carcinoma, Pancreatic. Figure 1 Multidetector CT study in a case of ductal adenocarcinoma of the pancreatic head. The lesion causes obstruction of the pancreatic duct which appears dilated; atrophy of the parenchyma distal to the obstruction is associated (a). The multiplanar reconstruction on the coronal plane shows dilatation of the biliary system and the gallbladder in the same case (b).

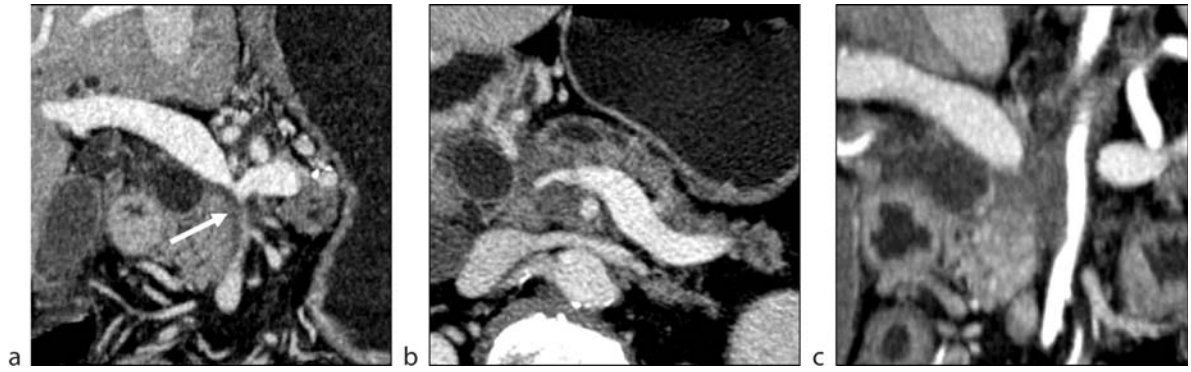

Carcinoma, Pancreatic. Figure 2 Multidetector CT study in a case of ductal adenocarcinoma of the pancreatic head and uncinate process. Stenosis of the portomesenteric junction and the superior mesenteric vein, which suggests infiltration, can be observed (*arrow*, a). The neoplastic tissue obliterates also the retroperitoneal tissue corresponding to the retroportal pancreatic margin reaching the right wall of the superior mesenteric artery (b, c).

duodenum, spleen, stomach, and colon. Pancreatic cancers can involve local vessels, such as the celiac axis, superior mesenteric artery, and venous vessels, including the portal vein, the splenic vein, and the superior mesenteric vein (Fig. 2). When the lesion shows no contact with the vessel, the fatty plane around the vessel result intact, while the presence of neoplastic tissue reaching the vascular wall or variably surrounding the vessel can suggest a vascular involvement. However, the presence of soft tissue surrounding a vessel may also be due to a desmoplastic inflammatory reaction. Vascular encasement is suggested when the vessel occlusion or stenosis is present, sometimes associated to collateral circulation. Initial reports suggested that any degree of tumor to vessel contiguity indicated tumor unresectability. Since the introduction of helical CT, several classifications have been proposed to grade the degree of vascular infiltration, to relate the vascular involvement with the resectability of the tumor, and to establish when the encasement of the vessel represents a certain sign of vascular infiltration. For instance, Lu et al in 1997 proposed a classification including four different grades on the basis of the vascular surrounding, and identified a cut-off of resectability, demonstrating that the mere contiguity between tumor and vascular structure does not automatically mean vascular invasion, while when the tumor surrounds the vessels for more than 50% of its circumference, there is a high likelihood of vascular infiltration. Multidetector CT has further improved the staging of vascular invasion, because of the increased spatial

resolution and the possibility to associate multiplanar and maximum intensity projection reformations and volume rendering images.

Another fundamental aspect in order to stage pancreatic tumors is to value the infiltration of the fat peripancreatic retroperitoneal tissue. In particular, for tumors of the head/uncinate process, it is fundamental to evaluate the fat retroperitoneal tissue infiltration in correspondence of the retroperitoneal resection margin (retroportal margin), which corresponds to the fatty layer localized behind the portal and superior mesenteric vein and comprised between the right margin of the proximal 3–4 cm of the superior mesenteric artery and the left margin of the head/uncinate process of the pancreas, near the origin of the postero-inferior pancreatic arch. Multidetector CT is an accurate technique in order to evaluate retroportal margin involvement, and the suspicion of infiltration arises at CT when the fatty retroperitoneal tissue appears obliterated, irregular, or with abnormal density. Neoplastic infiltration is in fact a critical factor in tumor staging and in surgical planning because it frequently represents a site of persistence and recurrence of disease and it is related to half postsurgical survival (1–4).

Regional lymph node metastases can be suspected at CT only when there is a lymph node enlargement; for this reason nodal staging with CT is reported to be often incorrect. Distant metastases usually involve the liver, while lungs and other organs are less commonly involved. The peritoneal nodules are rarely demonstrated by means of CT, while omental thickening or ascites are often the only finding suggesting the peritoneal carcinosis (1–4).

Recent advances in magnetic resonance (MR) imaging (including high resolution and fast imaging, tissue-specific contrast media, MR colangiopancreatography (MRCP), and functional imaging) improved its ability in diagnosing and staging pancreatic cancer. MR offers the advantage of the simultaneous evaluation of pancreatic parenchyma, vessels, and ductal system during the same examination (5,6).

The normal pancreas shows low signal intensity on T1-weighted images and intermediate signal on T2-weighted images, with a variable amount of fat in the gland parenchyma. Owing to the desmoplastic nature of ductal adenocarcinoma, at MR the tumor is visible as an area of lower signal intensity on T1-weighted images. On T2-weighted images it has variable signal intensity, depending on the degree of desmoplastic reaction, hemorrhage, necrosis, and associated inflammatory changes. Pancreatic cancer can cause pancreatitis distal to the lesion, because of ductal obstruction; this causes a low signal intensity of the pancreatic tissue on T1-weighted images, which results in poor contrast between the tumor and the parenchyma surrounding the lesion (Fig. 3). Following intravenous administration of gadolinium, the tumor may become more conspicuous, since the parenchyma enhances in the early phase but the tumor exhibits poor enhancement. On delayed images pancreatic adenocarcinomas show variable appearance depending on the size of the interstitial space and venous drainage. The administration of the Mn-DPDP can further improve the lesion conspicuity, particularly in case of small tumor, increasing the contrast between the high enhancing pancreatic parenchyma and the lesion; furthermore assessment of the liver is an important factor in the staging of pancreatic cancer patients, since pancreatic tumors tend to metastasize early into the liver. MR examination with Mn-DPDP has been found to be superior to CT in the detection of liver metastases (5,6).

MR colangiopancreatography (MRCP) sequences can be performed, to visualize the pancreatic and biliary ductal systems. When both the common bile duct and the pancreatic duct are involved, two adjacent ring-like ducts (known as the "double duct" sign) are visible within the pancreatic head. Furthermore, dilatation of the

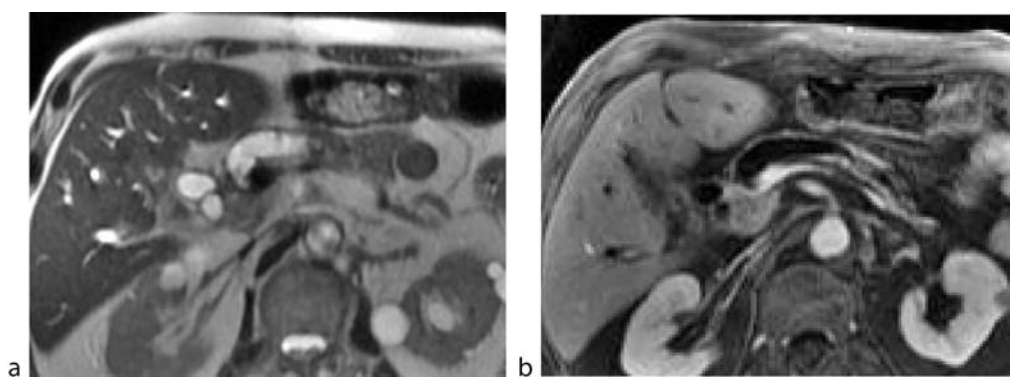

Carcinoma, Pancreatic. Figure 3 MR in a case of ductal adenocarcinoma of the pancreatic head. Axial single-shot fast spin-echo T2w (a) and gadolinium-enhanced fat-suppressed SPGR T1w (b) images demonstrate a hypointense lesion in the pancreatic head causing an abrupt cut-off of the pancreato-biliary system, which is markedly dilated.

intrahepatic bile ducts and of the gallbladder can be seen. The intravenous administration of secretin allows the improvement of the pancreatic ducts delineation; the presence of a ductal obstruction persistent after the secretin administration, sometimes with associated dilatation of the duct proximal to the obstruction, is suggestive for a neoplastic stenosis. MR angiographic sequences can be performed to demonstrate the vascular patency and to assess the vascular involvement (5,6).

Lymph node metastases can be suspected when there is a lymph node enlargement; nodal disease is shown using fat-suppressed T2-weighted images and Gd-enhanced images.

Although the sensitivity of endoscopic retrograde cholangiopancreatography (ERCP) for the diagnosis of pancreatic cancer is quite high, it is now rarely necessary and should not be routinely used. Because of its invasiveness and the high risk of complications, it has been replaced by MRCP, which provide a good alternative. ERCP plays, however, a very important role when used in combination with interventional radiological procedures such as biliary drainage and stent placement. ERCP findings include narrowing of the duct by tumor encasement, duct erosion with contrast extravasation, or complete obstruction associated to dilatation of ducts proximal to the point of obstruction. The pancreatic ducts between the obstruction and the papilla of Vater are usually normal; this finding may help to distinguish pancreatic carcinoma from pancreatitis. Involvement of both the pancreatic and common bile duct, termed double-duct sign, was originally described as being specific for carcinoma, while it also may be seen in pancreatitis.

The use of pancreatic biopsy (percutaneous or endoscopic) in the diagnostic work-up of a patient with a suspected pancreatic cancer is controversial. Complications such as hemorrhage, pancreatitis, fistula, and abscess have been reported and there are reports of tumor seeding along the tract of the needle. Additionally, malignancy cannot be excluded with certainty when malignant cells are not found in the specimen. For these reasons biopsy has no role in patients with a resectable pancreatic mass. Pancreatic biopsy is mandatory in patients excluded for a surgical resection and candidates for palliative treatment. Further biopsy may be performed in the suspicion of more uncommon lesions, such as ▶pancreatic lymphoma, which can be susceptible of chemotherapy treatment.

Nuclear Medicine

Positron emission tomography (PET) with the administration of 18F-FDG has been successfully used in the management of patients with pancreatic cancer for initial diagnosis, pretreatment staging, detection of distant metastases, evaluation of treatment response, and detection of recurrence (1, 7).

Diagnosis

Surgical resection remains the treatment of choice for pancreatic adenocarcinoma. To date, a curative treatment of pancreatic cancer can be achieved only with complete surgical resection. Vascular invasion, infiltration of the adjacent structures, and the presence of lymph node metastases, distant metastases, or peritoneal carcinosis are generally accepted reasons for unresectability. On the other hand, the diagnosis of vascular invasion by pancreatic cancer is one of the most critical issues in imaging; in fact, while in some institutions surgery is precluded in cases of vascular invasion, other surgeons perform aggressive surgery with vascular resection. For these reasons the role of diagnostic imaging is not only to demonstrate the tumor but also to accurately assess the resectability of the lesion, for identifying patients who might benefit from surgery and to avoid unnecessary interventions.

There is much debate concerning the sensitivity and specificity of imaging investigations in the diagnosis and staging of pancreatic carcinoma. Contrast-enhanced multidetector CT is generally accepted to be the first line of investigation in a patient with suspected pancreatic cancer. The reasons for this preference include its wide availability, speed, and the possibility to perform thin sections with high spatial resolution. Several studies have compared CT with MR regarding tumor detection and staging, obtaining similar results with both modalities. The current role of MR is probably more important for the detection and characterization of the lesion, particularly when the lesion is not easily demonstrable with CT. MR is also helpful in evaluating and characterizing liver lesions in patients with pancreatic cancer. In the detection and staging of small tumors, EUS and IOUS can be reliable. In conclusion, multidetector CT or MR should be used first in the detection and staging of pancreatic adenocarcinoma. When CT or MR findings are doubtful, EUS or IOUS should be applied for detection and for the assessment of resectability. PET imaging is usually reserved to confirm the malignancy, to differentiate between a carcinoma and a focal nodular pancreatitis and to recognize distant metastases.

References

1. Saisho H, Yamaguchi T (2004) Diagnostic imaging of pancreatic cancer. Computed tomography, magnetic resonance imaging, and positron emission tomography. Pancreas 28(3):273–278

2. Lepanto L, Arzoumanian Y, Gianfelice D et al (2002) Helical CT with CT angiography in assessing periampullary neoplasms: identification of vascular invasion. Radiology 222:347–352
3. Lu DS, Reber HA, Krasny RM et al (1997) Local staging of pancreatic cancer: criteria for unresectability of major vessels as revealed by pancreatic-phase, thin-section helical CT. AJR Am J Roentgenol 168(6):1439–1443
4. Mc Nulty NJ, Francis IR, Platt JF et al (2001) Multi-detector row helical CT of the pancreas: effect of contrast-enhanced multiphasic imaging on enhancement of the pancreas, peripancreatic vasculature, and pancreatic adenocarcinoma. Radiology 220:97–102
5. Schima W, Fugger R (2002) Evaluation of focal pancreatic masses: comparison of mangafodipir-enhanced MR imaging and contrast-enhanced helical CT. Eur Radiol 12(12):2998–3008
6. Semelka RC, Marcos HB (1998) Nonendocrine Tumors of the pancreas. In: Heuck A, Reiser M (eds) Abdominal and Pelvis MRI. Springer, Berlin-Heidelberg, pp 51–58
7. Diederichs CG, Staib L, Vogel J et al (2000) Values and limitations of 18F-fluorodeoxyglucose-positron-emission tomography with preoperative evaluation of patients with pancreatic masses. Pancreas 20:109–116

Carcinoma, Rectal

S. M. E. Engelen[1,2], G. L. Beets[2]
M. J. Lahaye[1,2], R. G. H. Beets-Tan[1]
[1]Department of Surgery, University Hospital Maastricht, Maastricht, Netherlands
[2]Department of Surgery, University Hospital Maastricht, Maastricht, Netherlands
Rbe@rdia.azm.nl

Definition

In Western countries, colorectal cancer is the second most common malignancy. There are 940,000 new cases yearly worldwide, of which about one-fourth are adenocarcinomas of the rectum (1). The rectum is arbitrarily defined as the distal 12–15 cm of the large bowel. The incidence of rectal carcinoma is increasing.

Pathology/Histopathology

The vast majority of rectal carcinomas are adenocarcinomas originating from adenomatous polyps or glands. The remainder are rare entities i.e. neuroendocrine tumours. Tumours start as intramucosal lesions, gradually growing outward through the rectal wall, invading the muscularis propria, blood and lymphatic vessels, surrounding mesorectal fat, mesorectal lymph nodes and eventually the surrounding structures.

Rectal cancer metastasizes *via* lymphatic and hematogenous routes. Lymphatic spread is mainly to mesorectal nodes, and from there on to the para-aortic nodes in advanced cases. In distal tumours, internal iliac nodes can be involved. Hematogenous spread is through the superior rectal vein, draining into the inferior mesenteric and portal vein. Distant metastases in rectal cancer are therefore most often located in the liver. For distal tumours, venous drainage is *via* the middle and inferior rectal vein into the internal iliac vein into inferior vena cava. Pulmonary metastases are therefore more common in rectal cancer than in colon cancer. Other sites of metastases in rectal cancer are retroperitoneum, ovaria, peritoneal cavity, adrenals, bone and brain.

There are several risk factors for developing rectal carcinoma: age (>50 years), high-fat and low-fibre diet, personal or family history (first degree relative) of colorectal cancer, inflammatory bowel diseases (M. Crohn, Ulcerative Colitis), familial adenomatous polyposis (FAP) and hereditary non-polyposis colorectal cancer (HNPCC). Alcohol consumption, smoking, little physical activity and diabetes mellitus are less well-defined risk factors. Risk factors for rectal carcinoma are mostly associated with Western lifestyle, explaining large variation in incidence of rectal cancer worldwide.

Clinical Presentation

Rectal bleeding and changed bowel habits can be early symptoms of rectal carcinoma. Rectal bleeding of cancer often resembles haemorrhoidal blood loss. Other symptoms include mucus discharge, narrowing calibre of stool, increased frequency of defecation, feeling of rectal fullness and tenesmus. Anal canal involvement of tumour mass may lead to anal pain. Bulky tumours can invade sacrum and sacral plexus, causing pelvic pain and sciatic nerve symptoms.

Signs and symptoms of metastatic disease are weight loss, fatigue, abdominal distention, pain in the right upper quadrant, jaundice and ascites.

Imaging

Imaging in rectal cancer is used for local and distant staging. T stage has long been used as a measure for local extent, and has therefore been subjected to many studies. At present, the importance of prediction of the ►circumferential resection margin (CRM) along the ►mesorectal fascia is accepted as an important feature for the surgeon, as incomplete removal of the lateral spread of the tumour is a main cause of local recurrence (Fig. 1). Another risk factor for local recurrence and therefore of interest in local staging is nodal status. Distant staging concerns liver, lung and further extra hepatic sites.

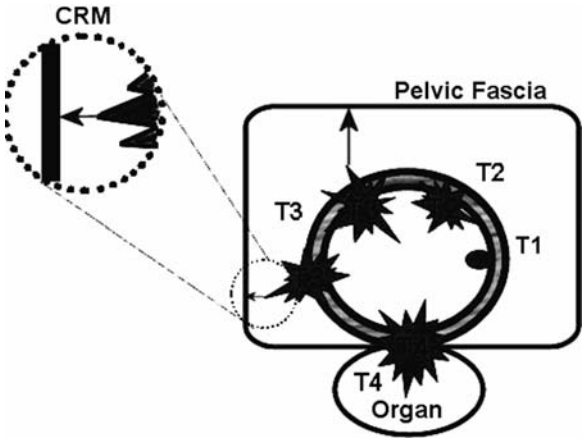

Carcinoma, Rectal. Figure 1 Transverse section through the rectum. Illustration of the circumferential resection margin (CRM) and different T stages. The CRM is defined as the closest distance from tumour to mesorectal fascia (pelvic fascia). This fascia is used as the plane of dissection in rectal cancer surgery. Preoperative identification of a close or involved CRM allows the clinician to use preoperative radiochemotherapy and/or more extensive surgery. The prognostic inhomogeneity of T3 rectal tumours is shown in this figure as well, as T3 tumours can have a wide (upper-left tumour) or close (left-sided tumour) CRM. (Reprint with permission from Lahaye MJ, Engelen SME, Nelemans PJ et al (2005) Imaging for predicting the risk factors—the circumferential resection margin and nodal disease—of local recurrence in rectal cancer: A meta-analysis. Semin Ultrasound CT MRI 26: 259–68.)

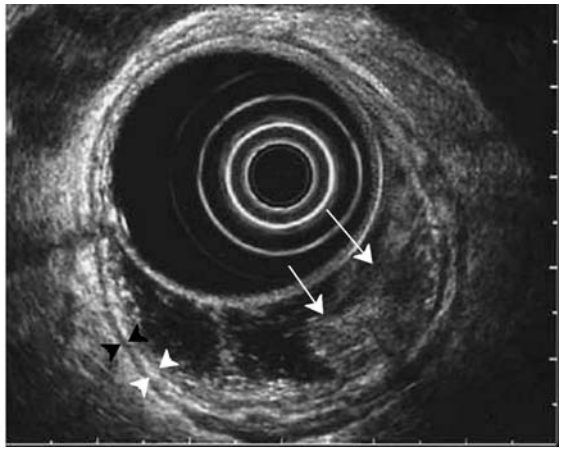

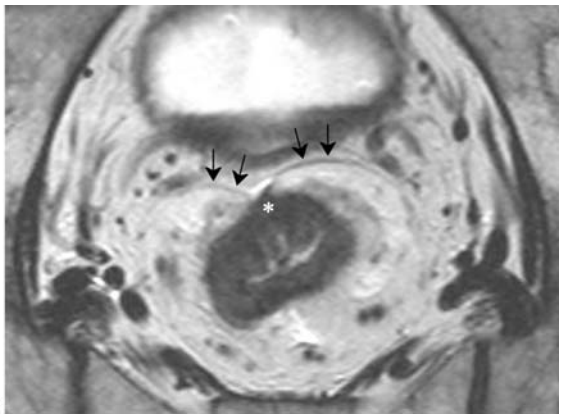

Carcinoma, Rectal. Figure 2 (a) Endorectal sonography of T1 rectal carcinoma confined to mucosa and superficial submucosa. Anteriorly, seminal vesicles are seen (white arrows). (Reprint with permission from Schwartz, DA, Harewood, GC, Wiersema, MJ (2002). EUS for rectal disease. Gastrointest. Endosc. July; 56(1):100–109.) (b) Transverse T2W TSE (TR/TE 3427/150 ms) MR image of a pelvis of a 73-year-old male. T3 rectal carcinoma. Anteriorly, the mesorectal fascia (black arrows), is retracted by the tumour (white asterisk).

Local Extension

Endorectal ultrasound is an accurate modality to depict the bowel wall and therefore to assess superficial tumours, especially T1 and T2 stages (Fig. 2a). Due to its limited field of view, EUS is less useful for non-superficial tumours (T3 and T4) and more proximal or stenosing tumours. Moreover, endorectal ultrasound is an observer-dependent imaging modality with important patient discomfort. This real-time exam is not suitable to be used as road map for the surgeon during operation.

MRI with a dedicated external coil (phased-array coil) has the major advantage of a large field of view, combined with a high spatial and contrast resolution, providing detailed anatomical information on structures in the pelvis. In single-centre studies MRI is a very good tool in preoperative prediction of CRM (2, 3) (Fig. 2b). Multi-centre studies on the routine use of MRI are ongoing. For predicting T-stage, MRI is less accurate in staging superficial tumours, unless an endorectal coil is used, which is however not widely available.

CT can give an impression of the size of the tumour and the proximity of the surrounding structures, and has long been used for staging of fixed tumours. Comparative studies however have shown superiority of MRI in prediction of organ invasion, because of better contrast resolution compared to CT.

Nodal Status

At present, no imaging modality has a sufficient accuracy for reliable prediction of nodal status. This is because current modalities only use morphologic criteria. Furthermore, these morphologic criteria can only be applied in large nodes. It is known however, that small

nodes with metastases are not uncommon in rectal cancer. A recent meta-analysis showed that endorectal ultrasound is slightly but not significantly better than CT and MRI in prediction of nodal status (4).

A new iron specific MR contrast agent (ultra small paramagnetic iron oxide—USPIO) has been developed recently. This contrast agent is taken up by the reticulo-endothelial system of healthy nodal tissue, causing a decrease in signal intensity on T2-weighted MR images. Malignant nodes do not take up the contrast because of lack of normal node anatomy, and therefore appear white (high-intensity) on T2-weighted images. This new contrast agent has been proven to be accurate in prediction of nodal status in prostate, bladder, head and neck malignancies (5). Use of this agent in rectal cancer is under investigation. Results of studies are awaited.

Metastatic Disease

Organs of primary interest in assessing for presence of metastases are liver and lungs. Wide availability as well as low cost make chest X-ray and liver sonography the imaging modalities of first choice. However, CT is more sensitive. Although there are little data on the cost-effectiveness, it is recommended to use CT scanning of liver and lungs at least in high risk patients. The rationale for choosing a more accurate but expensive tool relates to new developments in the treatment of metastatic disease. With combinations of more effective systemic therapy and metastasectomies or local destruction of metastases the prognosis is no longer as grim as it used to be, and some patients even can be cured.

Nuclear Medicine

^{18}FDG PET is a functional imaging method, based on imaging of increased glucose metabolism in neoplastic cells, by detecting fluorine-18 deoxyglucose uptake. So far, there is no consensus about use of ^{18}FDG PET in primary rectal carcinoma.

The main drawback of PET is its low resolution. Therefore, PET can only be used in combination with anatomical imaging such as CT for reliable information on exact tumour localization. A systematic review on hepatic metastases in colorectal cancer has shown that PET is of additional value to CT for the detection of extrahepatic disease which could alter patient management (6). However, randomized controlled clinical trials are lacking on this subject. Drawbacks are inability of PET to localize metastases that are small (<1–2 cm). Also, inflammatory processes have increased glucose metabolism as well, which may cause false-positive findings on PET.

In recurrent rectal cancer, use of ^{18}FDG PET could be valuable to differentiate between recurrent tumour and postoperative fibrosis.

Diagnosis

History taking should include, additional to the specific symptoms mentioned earlier, the family and personal history regarding colorectal polyps and malignancies as well as other malignancies. Only rarely a rectal cancer is diagnosed only by history taking. Digital rectal examination however can be highly specific for mid and distal rectal cancer. Physical examination should also include vaginal examination and palpation of inguinal nodes.

The definitive diagnosis of rectal carcinoma is based on histologic examination of tissue obtained through an endoscopic biopsy. As 3–5% of patients have a synchronous more proximal tumour all patients should have an examination of the complete colon whenever possible.

Treatment Implications

The principal treatment of rectal cancer is surgery. Depending on extension of tumour, surgery consists of local excision (T1 tumours in selected patients), ▶total mesorectal excision (TME) or more extensive surgery (locally advanced tumours). TME is a procedure in which the rectum is removed together with its surrounding mesorectal fat and the enveloping mesorectal fascia. In this way, tumour spread as well as invaded lymph nodes in the mesorectal fat are removed. This surgical technique is at present recognized as standard of care.

Radiotherapy as well as chemotherapy are important as (neo) adjuvant treatment. Preoperative radiotherapy reduces the local recurrence rate significantly. For more extended tumours (Fig. 3), a long course of chemo radiation therapy can provide significant downsizing of the tumour. Adjuvant chemotherapy reduces the likelihood of later metastatic disease, although the evidence is not as strong as in colon cancer. Metastatic disease is treated with chemotherapy with the goal of prolonged palliation. A small number of patients with metastatic disease can be cured with surgical excision of metastases with or without the use of concomitant chemotherapy.

Multi-disciplinary involvement in the decision making is very important for the treatment of rectal cancer. Good quality preoperative imaging plays a key role in this process, leading to an optimal individual treatment.

Bibliography

1. Stewart BW, Kleihues P (eds) (2003) World Cancer Report 2003. Lyon: IARC Press

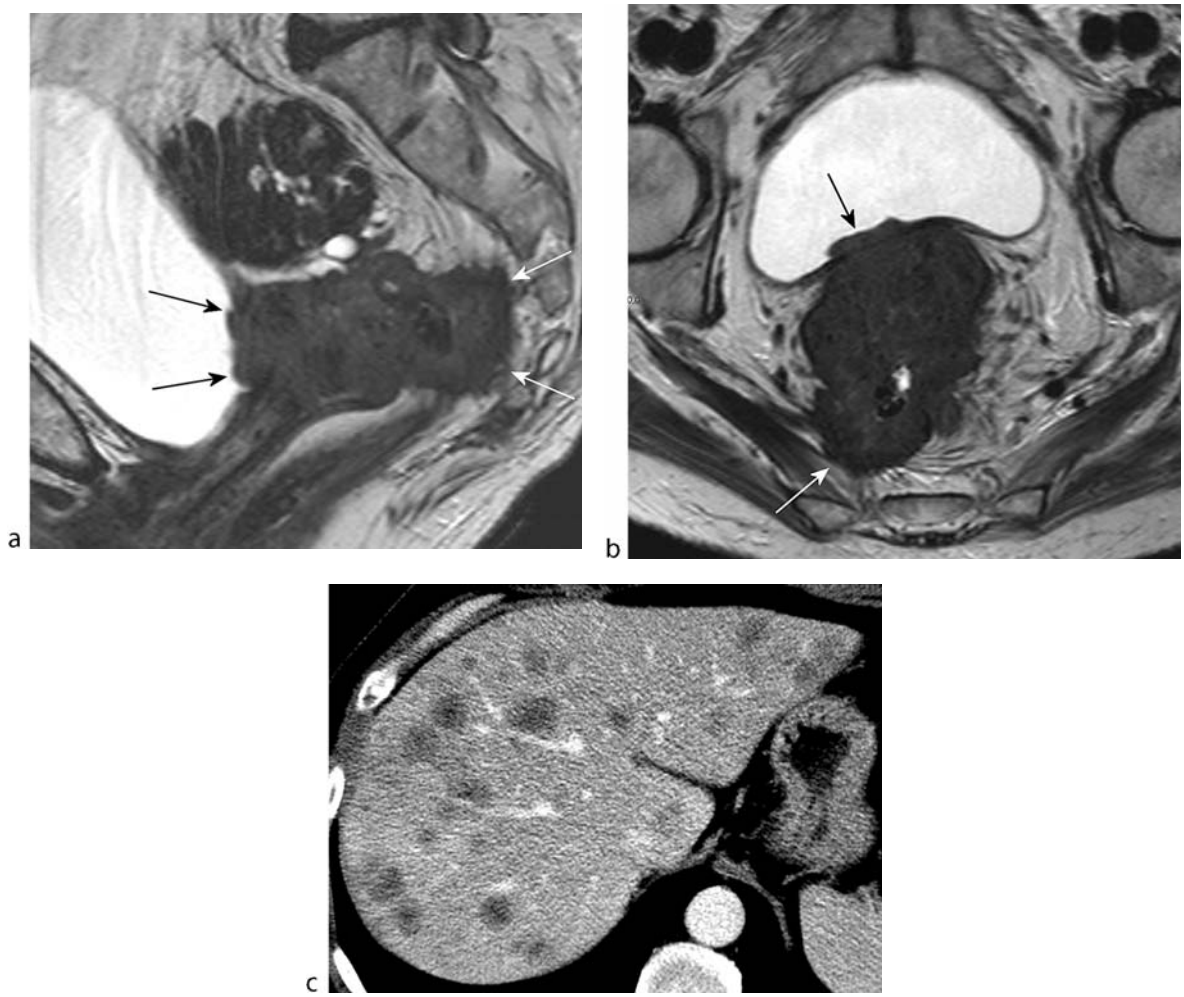

Carcinoma, Rectal. Figure 3 Locally advanced distal rectal cancer. (a) Sagittal T2W TSE (TR/TE 3427/150 ms) MR image of the pelvis of a 77-year-old female. Locally advanced rectal carcinoma, invading the bladder anteriorly (black arrows) and the presacral space posteriorly (white arrows). (b) Transverse T2W TSE (TR/TE 3427/150 ms) MR image of the same patient. Anteriorly, invasion of the bladder is again visible (black arrow). Right posterolateral, invasion of the piriform muscle is indicated by the white arrow. (c) Contrast-enhanced CT scan of a liver (PVP). Multiple liver metastases of a rectal carcinoma in a 59-year-old male.

2. Beets-Tan RG, Beets GL, Vliegen RF et al (2001) Accuracy of magnetic resonance imaging in prediction of tumor-free resection margin in rectal cancer surgery. Lancet 357: 497–504
3. Brown G, Richards CJ, Newcombe RG et al (1999) Rectal carcinoma: thin-section MR imaging for staging in 28 patients. Radiology 211:215–222
4. Lahaye MJ, Engelen SME, Nelemans PJ et al (2005) Imaging for predicting the risk factors—the circumferential resection margin and nodal disease—of local recurrence in rectal cancer: A meta-analysis. Semin Ultrasound CT MRI 26:259–268
5. Harisinghani MG, Barentsz J, Hahn PF et al (2003) Noninvasive detection of clinically occult lymph-node metastases in prostate cancer. N Engl J Med. June 19; 348 (25):2491–2499
6. Wiering B, Krabbe PFM, Jager GJ et al (2005) The impact of fluor-18-deoxyglucose-Positron Emission Tomography in the management of colorectal liver metastases. A systematic review and metaanalysis. Cancer 104:2658–2670

Carcinoma, Renal Cell

Laurence Rocher, Malik Chouli, Yves Menu
Hôpital de Bicêtre, Paris, France
laurence.rocher@bct.ap-hop-paris.fr

Synonyms

Conventional renal carcinoma; Grawitz tumor; Hypernephroma; Kidney cancer

Definitions

Renal cell carcinoma is the most common solid renal neoplasm accounting for 80 to 85% of all malignant renal tumors and for 2% of all cancers. Renal cell cancer (RCC) represents the fifth most common cancer in men (male-to-female ratio is 2:1), with a rising incidence. A solid mass detected in the kidneys can be considered as a renal cell carcinoma until any other possibility is proved. It originates from renal tubular epithelium, usually in the cortex.

Lymphomas, metastases, various sarcomas are other solid rare noncarcinoma malignant tumors of the kidney.

A special group of patients includes those with some hereditary conditions. The most common are Von Hippel–Lindau disease and tuberous sclerosis. Other conditions are the followings: hereditary papillary renal cancer, Birt–Hogg–Dubé syndrome, hereditary leiomyoma renal cell carcinoma, familial renal oncocytoma, hereditary nonpolyposis colon cancer, and medullary carcinoma of the kidney. In these patients, tumor incidence is much higher, multiple synchronous or metachronous tumors are frequent, and age of onset is much lower.

Pathology/Histopathology

Renal cell carcinoma is typically round-shaped, varying from several millimeters to tumors that almost fill the abdomen. A pseudocapsule, related to compressed parenchyma and fibrous tissue is commonly found. Areas of yellowish or brownish components are intermingled with sclerosis, hemorrhage, and necrosis. The tumor can extend into the renal vein and to the inferior vena cava as a tumor cast.

A new histologic classification proposed by the Union Internationale Contre le Cancer (UICC) and the American Joint Committee on Cancer (AJCC) in 1997 is widely accepted. Renal cell carcinoma can be divided into several histologic subtypes like, including clear cell (70–80%), papillary (10–15%), chromophobe cell (5%), collecting duct carcinoma (Bellini duct carcinoma) (1%), medullar carcinoma (1%). Sarcomatoid variant is not considered a type of its own, 4 to 5% are unclassified. Each subtype is associated with a different prognosis indeed: tubulopapillar and chromophobe renal cell carcinomas carry a better prognosis than clear cell renal carcinoma. Since 1998, new entities have surfaced in renal tumor classification included in WHO 2004 classification multilocular renal carcinoma, Xp11 translocation, and low-grade mucinous tubular carcinoma.

Sarcomas included leiomyosarcoma, hemangiopericytoma, liposarcoma, rhabdosarcoma, and malignant fibrous histiocytoma. Sarcomas are usually very large but radiological findings are not specific.

Nuclear grade is the most important microscopic feature that independently correlates with survival for all stages. The most widely used is the Fuhrman classification.

Clinical Presentation

The triad of pain, hematuria, and flank mass is highly indicative for a renal tumor, and generally indicates advanced disease. Other symptoms are related to metastatic disease: pathologic fracture, bone pain, neurologic disorders.

Fever, general status alteration, sudden development of a varicocele, polyglobuly, hypertension, hypercalcemia are other circumstances of diagnosis. Some of them represent paraneoplastic syndromes. Fortuitous detection with US or CT occurs for 40% of renal mass detected. For this reason, the incidence of renal cell carcinoma has apparently increased over the last 20 years, especially concerning small tumors.

Imaging

The aim of any preoperative imaging is to differentiate benign from malignant lesions, to adequately assess tumor size, localization, and organ confinement, to identify visceral metastases and lymph metastatic node, and to reliably predict the presence and extent of any tumor cast into the renal vein and the inferior vena cava.

Imaging Techniques

Intravenous pyelography with nephrotomography is no more the reference standard in case of suspected renal cancer, because of its poor sensibility.

Ultrasonography–Color Doppler

Ultrasound (US) evaluation has a role in the detection of renal masses and has improved recently with technical upgrading of the devices. The sensitivity is 80% for tumors over 3 cm and 60% for tumors less than 2 cm.

The specificity for characterizing solid tumor subtypes is poor but conversely is excellent for distinguishing cystic from solid lesion. When a solid lesion or atypical cystic lesion is detected on US, it must be analysed by CT. Staging with US is nonaccurate as compared with CT, although liver metastases and vein involvement may be confidently detected with US. Contrast-enhanced ultrasonography may facilitate the evaluation of tumor vasculature and venous involvement.

Computed Tomography

CT is the modality of choice for detection, characterization, staging, and follow-up of patients with renal carcinoma.

New technologies, such as multidetector CT (MDCT) with thin collimation and multiplanar reformatting, might result in a diagnostic improvement. Three or four helical phases are required to have the best diagnosis and staging (Fig. 1).

Unenhanced phase provides a baseline from which to measure the enhancement within the lesion after the injection of intra venous contrast material. This enhancement (at least 15 UH) is important in distinguishing hyperdense cysts (no enhancement) from solid tumor. The diagnosis of renal cell carcinoma rests on demonstrating enhancement within a renal mass Renal cell carcinoma usually has an attenuation similar to the surrounding parenchyma but may show higher attenuation in case of hemorrhage. Unenhanced CT scan also demonstrates calcification (30%) in the tumor.

The cortico-medullar phase occurs at about 35–40 sec after the start of injection. This phase is essential for accurate staging of renal cell carcinoma. Maximal opacification of the renal arteries and veins occurs, allowing study of the venous extension of tumoral tissue. This phase allowed vascular reconstruction before partial

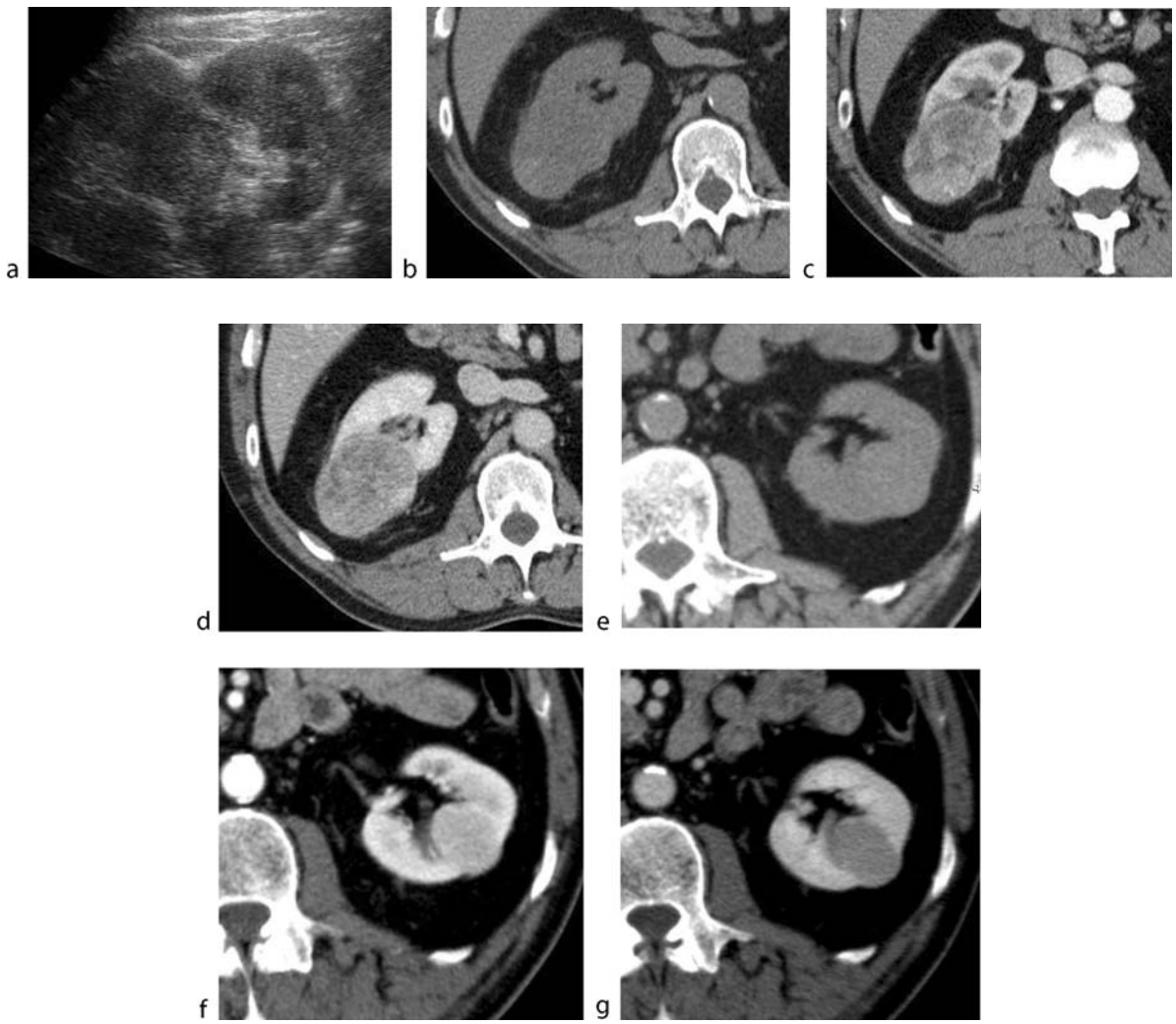

Carcinoma, Renal Cell. Figure 1 US and CT findings in renal clear cell carcinomas. (a) US of the right transverse plane shows a large renal mass. (b, c, d) CT findings. Nonenhanced CT (b) shows slightly high attenuation of the peripheral portion, contrast-enhanced CT in cortical (c) and nephrographic (d) phases show heterogeneous enhancement. (e, f, g): a homogeneous renal tumor in a 71-year-old man. Noncontrast enhanced (e), cortical phase shows an important and early enhancement (f), the tumor is low attenuated on the nephrographic-phase image (g).

surgery. Clear cell carcinoma has a great enhancement at this phase.

Hypervascular metastases of the liver, pancreas, muscles are most visible compared tubular phase. This phase must concern liver and kidney.

The nephrogenic or tubular phase is the more useful phase; it is made up after a scanning delay between 80 and 120 sec after the start of injection. The renal parenchyma enhances homogeneously. That is why the nephrographic phase is the most helpful for detecting renal masses and characterizing indeterminate lesions. The enhancement of papillary tumor is well demonstrated more clearly as at the cortical phase.

The excretory phase is optional. It begins approximately 180 sec after the initiation of injection of iodinated contrast material. This phase is occasionally helpful to better delineate the relationship of a centrally located mass with the collecting system.

Thoracic examination depicts lung or pleural metastasis, mediastinal lymph nodes, and attention is required in axillar regions and thoracic wall.

Pelvic examination may be proposed with the aim to depict peritoneal, pelvic lymph nodes, and pelvic bones metastasis.

Chest and pelvis examination can be carried within a single acquisition, for instance at the cortico-medullar phase, when the examination is performed using MDCT.

Magnetic Resonance Imaging

In the absence of formal contraindications, magnetic resonance imaging (MRI) is helpful in cases of renal failure, because CT with iodine injection cannot be performed. MRI can be a substitute to CT. CT remains mandatory for chest examination that does not require iodine injection. Another advantage of MRI is that it can help in characterizing small and/or cystic lesion.

Abdominal imaging examinations are performed with an abdominal phased array surface coil (which increases signal to noise ratio); breath-hold sequences are helpful to minimize artifacts secondary to respiratory motion and to allow dynamic evaluation after contrast injection.

Precontrast imaging includes axial breath-hold T1-weighted gradient echo sequence performed with in phase and out phase images, to provide anatomical overview, detection of lymphadenopathy, characterization of any associated adrenal mass. Fat-suppressed T1-weighted sequence, which allows differentiation of fat from hemorrhage may also be acquired. A transverse or coronal T2 sequence, usually using a breath-hold technique, is performed to differentiate cystic lesion from hydronephrosis. Fat saturation can be associated as well.

To evaluate the renal vasculature, a high-resolution breath-hold fat-suppressed three-dimensional T1-weighted spoiled GRE sequence is performed in a coronal-oblique or axial plane before and at the arterial phase after dynamic the intravenous administration of gadolinium. Images are displayed either as native two dimensional or reformatted using a maximum-intensity-projection (MIP) algorithm.

Evaluation of the renal parenchyma is subsequently performed with a breath-hold three-dimensional fat-suppressed T1-weighted spoiled GRE sequence in the axial plane at the cortical and tubular phases.

MR urographic images can be provided with a heavily T2-weighted sequence.

Angiography

Today, angiography has a very limited role in renal tumors because CT and/or MRI provide diagnostic images of renal vessels. Angiography is still useful when embolization of the tumor, usually before surgery, is required.

Results

Clear Cell Type

On US, the appearance varies: larger tumors are usually hypoechoic or isoechoic to renal parenchyma, whereas more than half of small renal cell carcinomas are hyperechoic.

On CT, most renal cell carcinomas are solid lesions with attenuation values of 20 HU or greater on plain CT. Small (<3 cm diameter) tumors usually have a homogeneous appearance; whereas larger lesions tend to be more heterogeneous due to hemorrhage or necrosis. Calcifications are detected in up to 30% of cases of renal cell carcinoma. The enhancement is often heterogeneous, important and early, reaching a maximum at the cortico-medullary phase. On nephrographic phase, it appears hypodense compared to the normal renal parenchyma.

On MRI, renal cell carcinomas have variable signal intensity on T1- and T2-weighted sequences, often slightly hypointense on T1-weighted images and isointense to slightly hyperintense on the T2-weighted images, but anyway significantly lower than cystic lesions. Enhancement after gadolinium injection is early and strong.

Renal clear cell carcinoma may have a cystic appearance.

Identification and characterization of complex cystic renal mass relies on Bosniak classification, which is based on CT criteria but is also employed also for MRI. The criteria include the plain attenuation of cyst, the presence of calcifications, number of septae, the thickness (regular

or nodular) of the wall or septae, the presence or absence of enhancing soft tissue components.

The categories I and II are benign lesions, the categories III and IV with thick enhancing walls or septae or thick nodular enhancing soft tissue components, are suspicious of malignant lesions and surgery is therefore indicated (Fig. 2).

Tubulopapillar Carcinoma

It is commonly a small (<3 cm) and sometimes multifocal or bilateral. It can appear hyperechoic at ultrasonography, and mimic an angiomyolipoma: the rule is that any lesion that is not clearly a simple cyst on US must be studied further by CT. Enhancement appears lower and delayed as compared with the clear cell type. It may appear hypointense on T2-weighted sequences, which is an indicator for this diagnosis (Fig. 3).

Chromophobe Renal Cell Carcinoma

It usually appears large, often homogeneous, and lobulated, showing a low enhancement. In some cases, a spoke-wheel-like enhancement with a central scar like an oncocytoma may be seen, but early enhancement is usually lacking.

Bellini Duct Carcinoma, Medullar Carcinoma

They are localized in the renal medulla, show a mass effect on the collecting system but there is no modification of the cortical line. Postcontrast enhancement is weak. It may present as a large infiltrating tumor. Prognosis is poor.

Staging

The prognosis of renal cell carcinoma is related to the tumor stage.

Robson classification has been widely used. The stages are following:

I: tumor within the renal capsule
II: tumor spread to the perirenal fat and/or adrenal gland
IIIA: venous tumor invasion
IIIB: regional lymph node metastasis
IIIC: venous invasion and regional node metastasis
IVA: direct invasion beyond Gerota's fascia
IVB: distant metastasis.

TNMV classification is now more used (from the TNM atlas, 6th edition, 2003):

T0: no evidence of primary tumor
T1a: tumor ≤4 cm in greatest dimension
T1b: tumor >4 cm and ≤7 cm
T2: >7 cm
T3a: tumor invades adrenal gland or perinephritic tissue but not beyond Gerota's fascia
T3b: tumor grossly extends into renal vein or vena cava
T3c: tumor grossly extends into the vena cava above the diaphragm
T4: tumor invades beyond Gerota's fascia

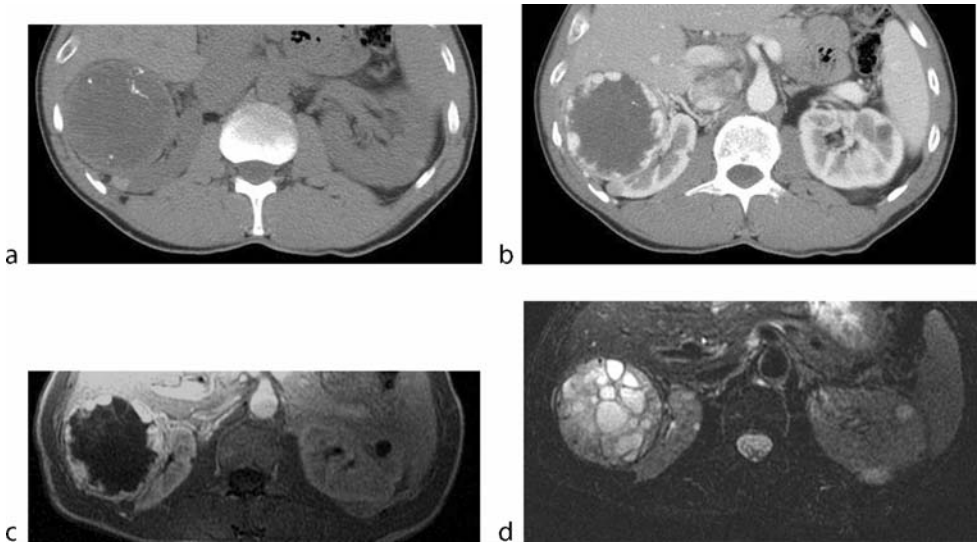

Carcinoma, Renal Cell. Figure 2 Cystic renal cell carcinoma. (a) nonenhanced CT shows small calcifications in the mass. (b, c) contrast-enhanced CT (b) and gadolinium-enhanced T1-weighted MR image (c) show well-enhancing nodules at the peripheral portion, septa are not well seen. (d) T2-weighted MR fat-suppressed image well demonstrate irregular septa.

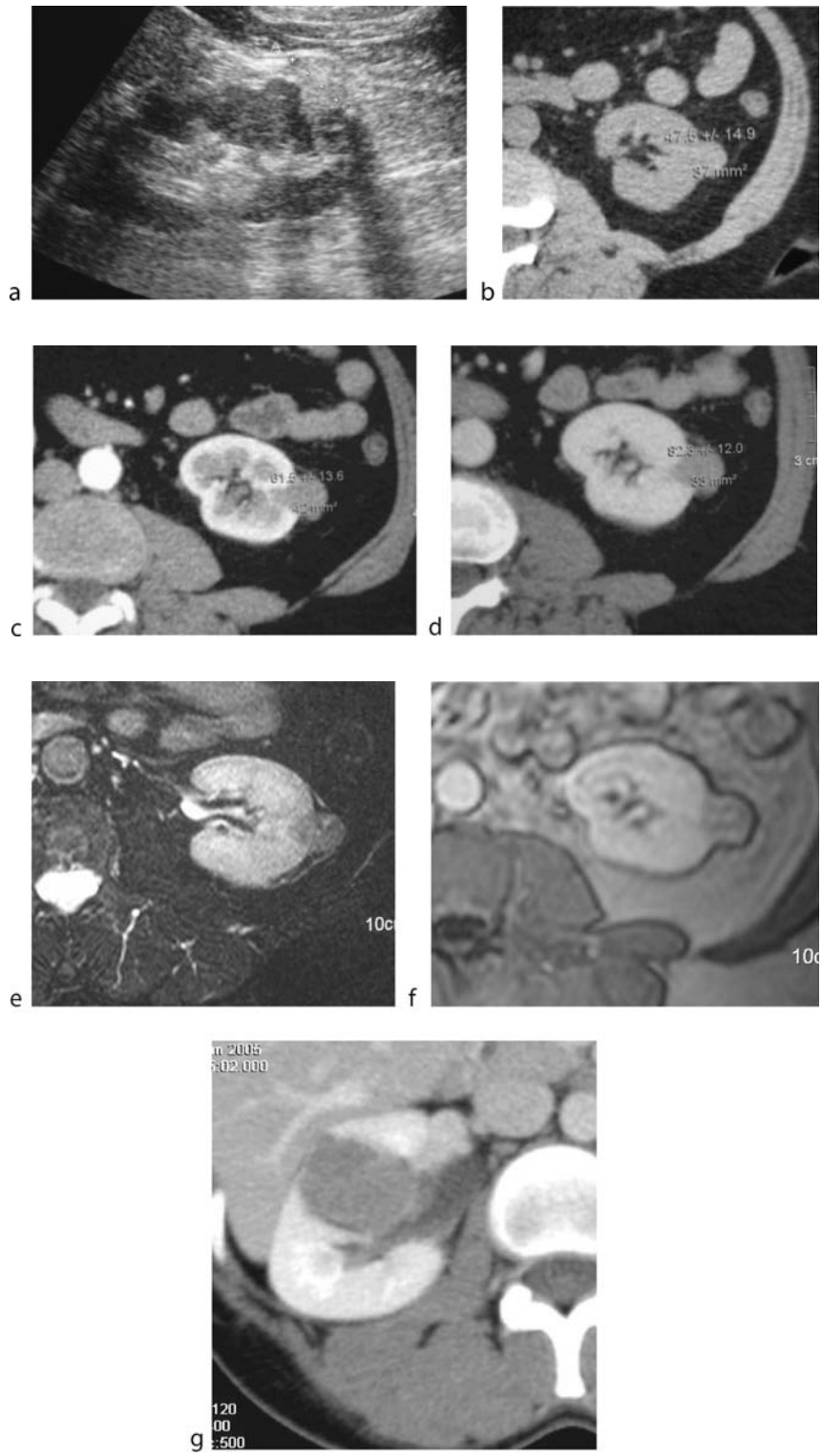

Carcinoma, Renal Cell. Figure 3 US, CT, and MRI in papillary type renal cell carcinomas. (a) US shows a hyperechoic small mass growing exophytically. (b, c, d) CT shows a homogeneous low and delayed enhancement of the tumor. (e) T2-weight MR fat saturation sequence shows the low signal of the mass than that of he renal parenchyma. (f) contrast-enhanced T1-weighted image demonstrates low enhancement of this lesion. (g) Papillary tumor in a 27-year-old woman with hematuria. Contrast-enhanced CT illustrates a low-attenuated lesion growing in the renal sinus.

N0: no regional lymph nodes metastasis
N1: metastasis in a single lymph node
N2: multiple lymph nodes
M0: no distant metastasis
M1: distant metastasis.

Description of the Extension

Local Extension

Perinephric spread of tumor is demonstrated by the presence of an enhancing nodule in the perinephric space. This sign is highly specific but is encountered in only 46% of the cases. Perinephric stranding does not reliably indicate tumor spread; indeed it may be caused by edema, vascular stasis, or previous inflammation.

The involvement of ipsilateral adrenal gland is not frequent, reported at less 5%.

Direct extension of renal cell carcinoma outside the Gerota fascia (stage T4) is difficult to diagnose with certainty unless there is a demonstrable focal change in attenuation within an organ.

The extension into collecting system is evaluated on excretory phase.

Regional Extension

Venous Spread of tumors is very well studied on MDCT and MRI. After detection, precising the exact level of the

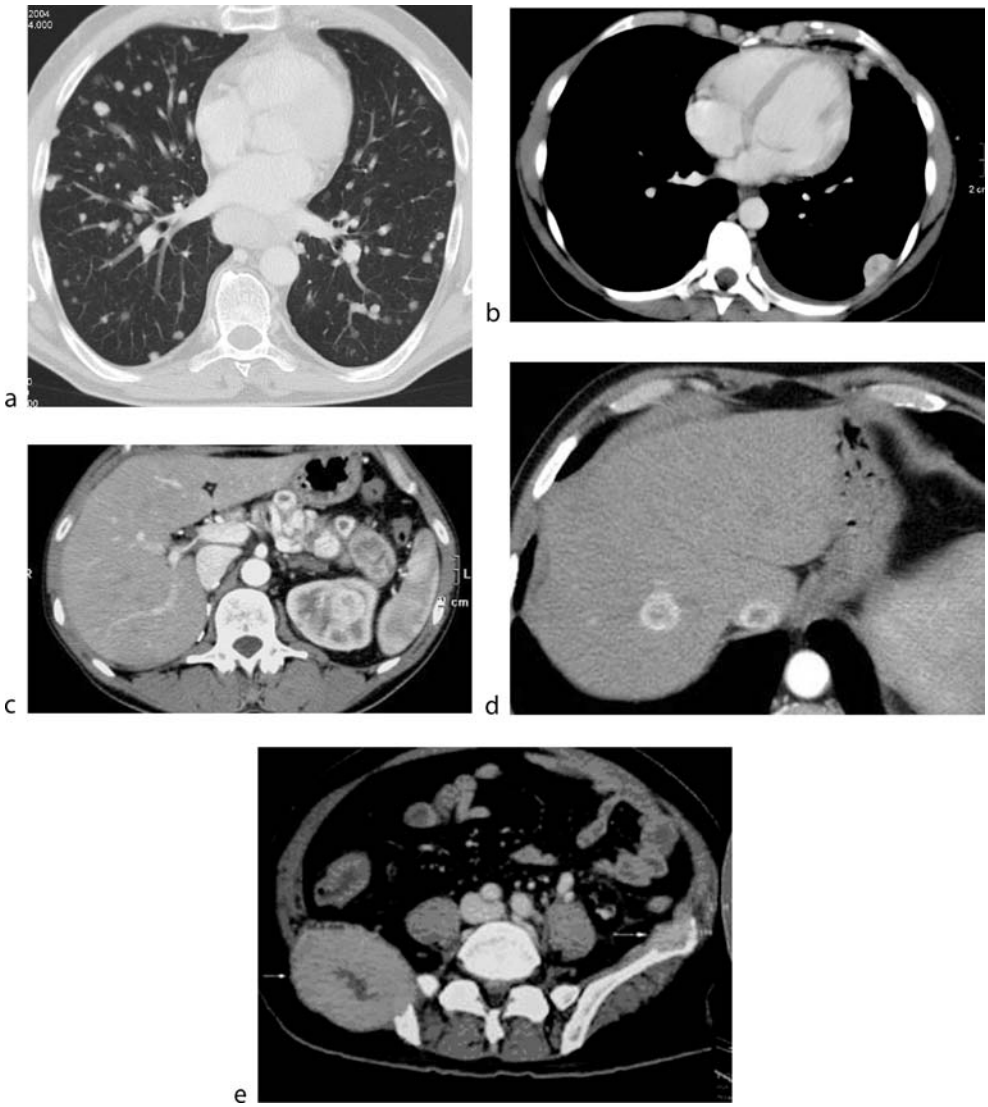

Carcinoma, Renal Cell. Figure 4 Examples of distant and lymph nodes metastasis. Pulmonary (a), pleural (b), pancreatic (c), hepatic (d), and osseous (e) metastasis of renal clear cell type carcinomas.

cast is of dramatic importance. It is mandatory for the surgeon to know if the tumor cast is limited to the renal vein, prolapses in the inferior vena cava, and in this case, how far is the tumor cast from the right atrium. This may have a major impact on surgical technique, some patients requiring extra corporeal circulation and even the combined surgery with a cardiovascular surgeon.

Regional lymphadenopathy should be detected, the number evaluated and the representative size reported.

General Extension

Metastases involve mainly lung parenchyma, pleurae, bone, liver, pancreas, muscle and rarely, thyroid, ovarian, small bowel, colon, peritoneal fat, vagina, bladder. Liver and pancreas metastasis have usually a strong and early enhancement, more clearly visible at an abdominal arterial phase (Figs 3 and 4).

Nuclear Medicine

It does not play a role in the diagnosis of renal tumor. Nevertheless it can predict, before surgery, residual renal function after total or partial nephrectomy.

PET with FDG may be helpful in the evaluation of "equivocal findings" on conventional studies, including bone scan, and also in the differentiation between recurrence and post treatment changes. The value of other PET tracers in renal cell carcinoma is under investigation.

Diagnosis

The final diagnosis requires histopathology and is most often provided by the analysis of material from surgical resection. Percutaneous biopsy is not justified in most cases because surgery will be necessary in most cases, including patients with regional or general extension, who can benefit from the resection of the primary tumor. Percutaneous CT or US guided trucut biopsy may be helpful in selected cases of atypical lesion, multifocality, metastatic patient and/or patient with operative risk.

Renal cell carcinoma can be mimicked by benign tumors like angiomyolipoma (fat component objectived at CT or MRI), oncocytoma (in some cases, cartwheel-like central scar may suggest the diagnosis, but specificity is low).

Chronic infection like xanthogranulomatous pyelonephritis may present as an infiltrative tumor.

Lymphoma or metastasis is usually hypovascular and multiple, but some atypical cases can simulate renal cell carcinoma.

Interventional Radiological Treatment

The number of detected renal cell carcinomas has been increasing, and many are early-stage lesions. Nephron-sparing surgery has been proposed as a more appropriate treatment for small (≤4 cm) renal cell carcinomas. Percutaneous thermal ablation therapies, principally radiofrequency (RF) ablation, have been advocated recently as an alternative to surgery. Preliminary data are promising. Cryotherapy has been performed by using open, laparoscopic, and percutaneous approaches and is likely just as effective in ablating cancerous tissues as is RF ablation. In palliative or not operable cases, embolization arteriography can be used in bleeding lesion. In cases of postoperative complications, embolization and percutaneous drainage can be used.

Bibliography

1. Sheth S, Scatarige JC, Horton KM, et al (2001) Current concepts in the diagnosis and management of renal cell carcinoma: role of multidetector CT and three-dimensional CT (review). Radiographics October 21 Spec No:S237–S254
2. Israel GM, Bosniak MA (2005) How I do it: evaluating renal masses. Radiology August 236(2):441–450
3. Kim JK, Kim TK, Ahn HJ, et al (2002) Differentiation of subtypes of renal cell carcinoma on helical CT scans. Am J Roentgenol June 178(6):1499–1506

Carcinoma, Vulva

Martin Unterweger
Diagnostic Radiology, Cantonal Hospital Baden, Baden, Switzerland
Martin.Unterweger@ksb.ch

Synonyms

Vulvar cancer

Definition

Carcinomas of the vulva are rare tumors, which account only for about 35% of female genitourinary malignancies. They present as polypoid vulvar masses and can be easily

reached for biopsy. The patients are normally post-menopausal.

Pathology/Histopathology

Over 90% of vulvar carcinomas are squamous cell carcinomas. The rest are uncommon tumors, e.g. basal cell carcinoma, vulvar intra-epithelial neoplasia, vestibular papilloma and sarcomas.

Clinical Presentation

Staging of vulvar carcinoma depends on local extension and lymphadenopathy (Table 1). Local extension can involve the urethra, vagina, peritoneum and anus. More distant infiltration of the pelvic floor and bladder is also possible. Initially, lymphatic metastatic spread is into the superficial inguinal nodes, in the deeper inguinal nodes and the iliac nodes. If lymph node spread is found, 5-year survival is only 40%. Therapeutic options in vulvar carcinomas

Carcinoma, Vulva. Table 1 Staging of vulvar carcinoma according to TNM and FIGO

TNM	FIGO	
Tis	0	Carcinoma *in situ*
T1	I	Tumor confined to the vulva with a dimension <2 cm
T2	II	Tumor confined to the vulva with a dimension >2 cm
T3	III	Tumor involves the lower urethra, vagina and anus
	III	FIGO III or if regional lymph nodes are present in T1 or T2
T4	IVA	Tumor invades bladder mucosa, rectal mucosa or tumor fixed to bone
	IVA	only in FIGO staging if N2 (retroperitoneal lymph nodes are present) in T1 or T2
	IVB	Any T with a metastasis (M1)

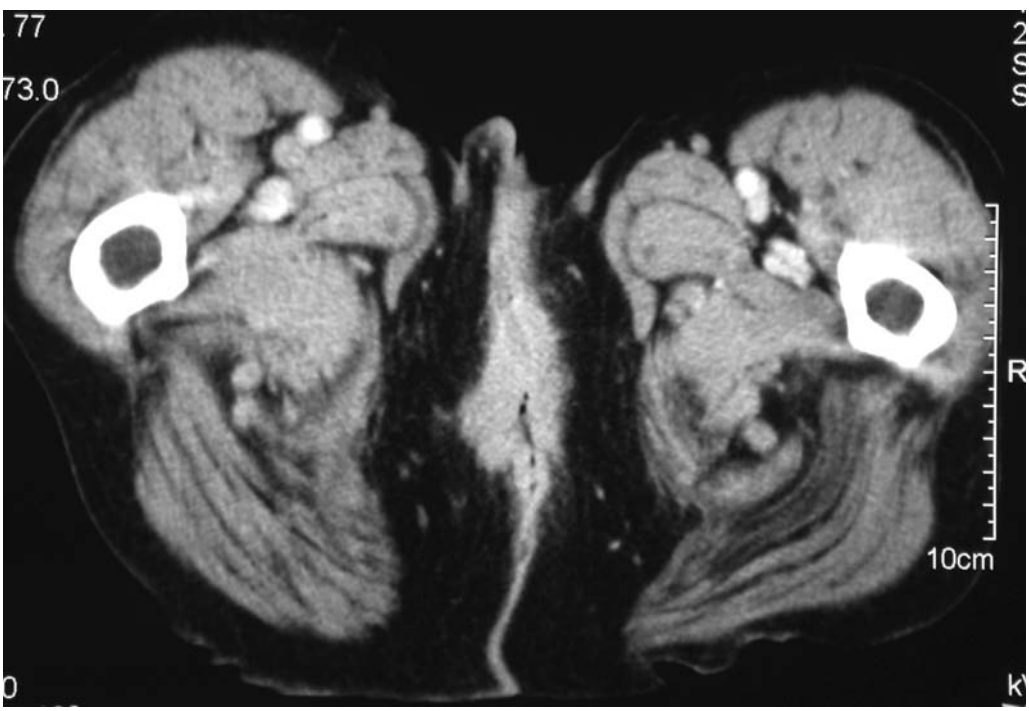

Carcinoma, Vulva. Figure 1 Axial CT demonstrates a contrast-enhanced thickened vulva in an assay of a female patient with histologically confirmed vulvar cancer (*arrow*). No pathological lymph nodes were seen in the abdominal CT.

include a radical vulvectomy or local resection of the tumor in smaller carcinomas. If metastases are present, a combined radio- and chemotherapy could be applied.

Imaging

With CT or MRI the infiltrating of the surrounding soft tissue of the vulva and the lymphatic spread can be demonstrated. However, CT is limited in the evaluation of the primary tumor in the vulva (Fig. 1a). Due to its higher tissue contrast, MRI is more accurate for the assessment of local tumor spread and involvement of surrounding structures. Lymph nodes with a size over 1 cm are defined as pathologic (Fig. 1b).

Diagnosis

The diagnosis is normally clinically suspected and then pathologically confirmed with a biopsy or after the tumor resection.

Bibliography

1. Semelka R (2002) Abdominal Pelvic MRI. Wiley-Liss, New Jersey
2. Sohaib SA, Richards PS, Ind T et al (2002) MR imaging of carcinoma of the vulva. Am J Roentgenol 178(2):373–377
3. Hawnaur JM, Reynolds K, Wilson G et al (2002) Identification of inguinal lymph node metastases from vulva carcinoma by magnetic resonance imaging: an initial report. Clin Radiol 57(11):995–1000
4. Outwater E, Kressel HY (1992) Evaluation of gynaecologic malignancy by magnetic resonance imaging. Radiol Clin North Am 30(4):789–806 (Review)
5. Tavassoli FA, Deville P (2003) Tumor of the Breast and Female Genital Organs. WHO classification of tumors

Carcinomatous Cirrhosis

Desmoplastic reaction induced by a diffusely infiltrative cancer of the liver.

▶Cirrhosis, Hepatic

Carcinosarcoma

The main presentation of this rare malignant tumor is a polypoid lesion in the lower esophagus. Rarely, this tumor has been described in the gallbladder and stomach. Both carcinomatous and sarcomatous tissues are involved in this malignancy.

▶Neoplasms, Gallbladder

Cardiac Enlargement

Increase of size of cardiac Chambers that could produce esophageal compression due to the close relationship between them.

▶Compression, Extrinsic, Esophagus

Cardiac Radiology

Albert de Roos
Department of Radiology, C2-S,
Leiden, The Netherlands
A.de_Roos@lumc.nl

Cardiac radiology encompasses the use of several imaging technologies, including conventional chest radiography, ultrasound, X-ray angiography, nuclear medicine techniques, and more recently computed tomography (CT) and magnetic resonance imaging (MRI). Traditionally, in many countries cardiac ultrasound and coronary X-ray angiography are performed by cardiologists, although exceptions may exist. A discussion of the anatomy and pathology as defined with X-ray angiography constitutes a basis for the interpretation of other technologies that depict the left ventricle and coronary artery tree. Some understanding of functional aspects as assessed by cardiac ultrasound may provide a basis for understanding similar pathophysiological concepts with MRI and CT.

In this review these imaging technologies are discussed with special emphasis on chest radiology, multidetector CT, and MRI.

1. Chest radiology: Chest radiographs are routinely obtained in patients with suspected cardiac disease. A number of useful observations on the presence of heart failure and underlying valvular and other cardiac pathologies can be made from chest radiographs. The size and shape of the heart can provide a clue as to the presence of certain valvular abnormalities. The size and position of the great arteries may also provide diagnostic clues. Abnormal calcifications (coronary, valvular, etc.) can help to identify certain valve

abnormalities. The appearance of the lungs and interstitium is routinely interpreted so as to detect imminent or overt heart failure. The presence of signs of heart failure on chest radiographs has clinical importance for the guidance of treatment as well as prognostic implications.

2. Nuclear medicine imaging: A number of advanced nuclear techniques are available [single photon emission CT (SPECT), positron emission tomography (PET)], which have widespread application and are accepted in routine clinical practice as they have proven their clinical value in terms of patient management and predicting prognosis. Rest-stress perfusion is most commonly applied for the detection of ischemic heart disease. Newer techniques also allow accurate evaluation of regional and global left ventricular function. PET scanning has traditionally been the gold standard for the assessment of myocardial viability, but for detailed viability imaging it is currently challenged by MRI.
3. Cardiac ultrasound allows regional and global function assessment both at rest and under pharmacological stress testing. This application is widely used for the detection of wall motion abnormalities as a sign of underlying ischemic heart disease. The accuracy and success rate of MRI have recently challenged ultrasound for rest–stress function analysis. Ultrasound is still the first-line tool for cardiac function analysis. It also allows comprehensive and sophisticated flow analysis across valves and other hemodynamics. For example, tissue Doppler techniques allow detailed analysis of systolic as well as diastolic heart function. Many functional features of ultrasound are now also becoming possible and applicable with MRI. Some structures are better visualized and quantified with MRI than with ultrasound; therefore, MRI can complement ultrasound in complex pathologies or when patients lack adequate acoustic windows.
4. X-ray coronary angiography is the mainstay of coronary artery imaging. Treatment and stent placement are guided by high-resolution X-ray technology. Understanding the anatomy from traditional angiographic projections can provide a good basis for the interpretation of current multidetector CT and MRI images that attempt to present the coronary artery tree in similar projections.
5. MRI has made much progress over the last few years in terms of technology and clinical applications for cardiac imaging. Recent MRI pulse sequences are optimized for cardiac imaging and today allow routine high-quality imaging. Both anatomy and function can be well evaluated by black-blood and bright-blood techniques, respectively. Coronary artery imaging has also become feasible and some clinical indications have become evident. Further technological advancement is still required for reliable imaging of coronary artery stenosis and atherosclerotic plaque in the small-sized coronary vessels. MRI is currently the new gold standard for functional assessment of ventricular function. Another routine application currently is the assessment of myocardial viability by using delayed enhancement imaging. Many aspects of ischemic heart disease are currently assessable by MRI. Furthermore, MRI has proved to be a valuable tool for the assessment of clinically relevant issues in the follow-up of patients with (repaired) congenital heart disease.
6. Multidetector CT has rapidly developed into a reliable tool for coronary and bypass imaging. In particular, 16-row technology has advanced the clinical utility of CT significantly. High-quality coronary imaging is now possible routinely for diagnostic studies, with a high success rate. Cardiac CT is also developing into a tool for functional analysis as well as perfusion imaging. Ultimately, integration of these techniques may allow comprehensive evaluation of ischemic heart disease. In addition, other cardiac applications have shown clinical relevance (e.g., pulmonary vein imaging preablation). In general, thoracic vascular imaging (e.g., aortic dissection, pulmonary embolism) has greatly benefited from recent multidetector CT applications.

Caries

Gino Ghigi
University of Bologna, Bologna, Italy
gghigi@alma.unibo.it

Synonym

Tooth decay

Definition

Dental caries is one of the most common dental diseases for humans, and it consists in a progressive demineralization of the tooth surface.

Pathology/Histopathology

Pathogenesis is due to a combined effect of different factors, such as dental plaque, carbon hydrates, receptiveness, and time. Within the dental plaque several bacteria grow (streptococci and lactobacilli), which usually induce the production of acids and a pH reduction to a value lesser than 5.5. This is the consequence of a combination between bacteria and the fermentation of carbon hydrates, which can lead to the demineralization of the enamel (1).

Clinical Presentation

Enamel carious lesion is asymptomatic and in its initial stage it looks like a white spot that affects only the enamel. During this period, the carious lesion could change its color and become darker, as a consequence of an attempt to mineralize it. Later on, if not treated, the enamel carious lesion could involve dentin and become symptomatic, suffering from physical, chemical, and thermal stimuli.

Imaging

The radiological image of dental caries is a radio transparency because of the loss of mineral tissue. Bitewing radiographs and intraoral dental films, with the central ray perpendicular to the tooth's vertical axis, are the most common techniques. Recently conventional radiographs have been substituted by phosphor images (2).

Plain X-rays are usually the main imaging tools in investigating caries, but sometimes tomography could be useful to highlight small caries at their initial stage.

Nuclear Medicine

Bone scintigraphy has not any role in the assessment of dental diseases such as dental caries.

Diagnosis

Radiology usually subdivides dental caries into four classes, on a penetration level basis:

- 1st class: carious lesion that involves lesser than a half of the enamel
- 2nd class: carious lesion that involves more than a half of the enamel
- 3rd class: carious lesion that involves dentin only in its external portion
- 4th class: carious lesion that involves more than a half of the dentin and perhaps also dental pulp

Interproximal dental caries develops within the area between two contiguous dental crowns, and so it can be well estimated with bitewing radiograms (Fig. 1).

Occlusal dental caries cannot be easily detected by radiology till the carious lesion starts involving dentin. Vestibular and lingual dental caries can be easily recognized by a clinical approach, and radiology is poorly useful.

Radicular caries involves cementum and perhaps dentin. Radicular caries has a radiological aspect of radio transparencies localized where portions of root are exposed because of gingival recession.

Recurrent dental caries develops in proximity to a carious lesion treatment (Fig. 2). Recurrent caries sometimes cannot be easily recognized because of the overlapping radio opacity or radio transparency of the treatment.

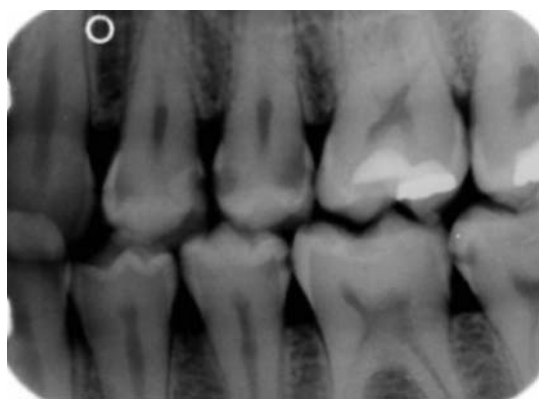

Caries. Figure 1 Digital bitewing radiograph: interproximal caries of different classes.

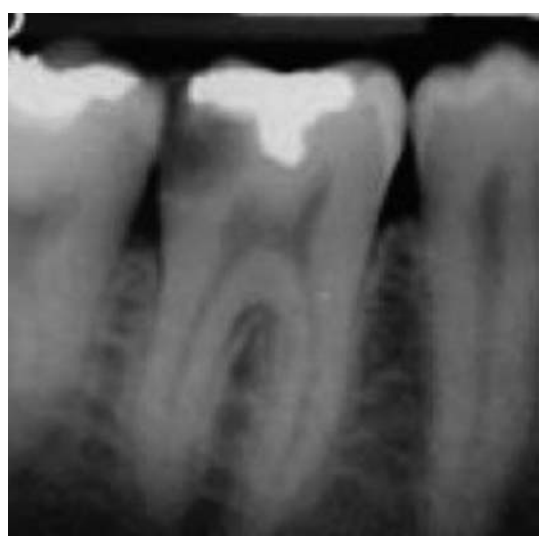

Caries. Figure 2 Recurrent caries.

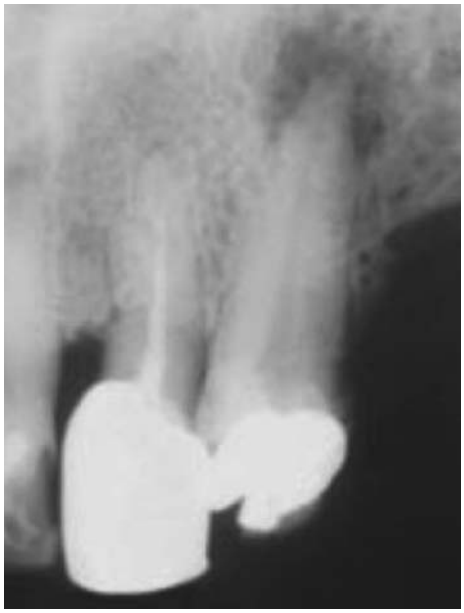

Caries. Figure 3 Periapical granuloma.

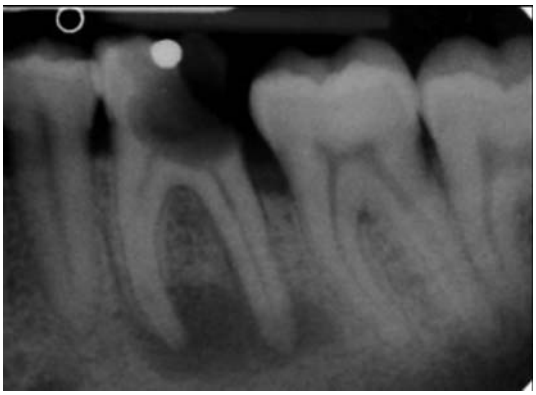

Caries. Figure 4 Periapical roundish granuloma, similar to a cyst.

A pulpal disease, if no treatment is provided, is followed by diffusion of bacteria toward the dental apex, with a phlogosis of the periapical region, the so-called acute periapical diseases. The diffusion could spread also to the structures in proximity.

From a radiological point of view, a homogeneous lacuna with a shaded outline can be observed. If the phlogistic process becomes chronic, in this case an expansion of the apical periodontal region with areas of surrounding osteosclerosis can be observed. Chronic periapical diseases are commonly indicated as apical granuloma.

Granuloma is usually asymptomatic and in radiology it is represented by a periapical transparency (Fig. 3), sometimes roundish and similar to a cyst (Fig. 4). The periapical bone infection can spread to tissues in proximity and can cause odontogenic abscesses, fistulas, and sinusitis.

Bibliography

1. De Florio L, Ghigi G (2005) Compendio di Radiologia Odontostomatologica Napoli, Idelson Gnocchi 2nd ed.
2. Wenzel A (2000) Digital imaging for dental caries. Dent Clin North Am 44:319–338

Carcinoma, Prostate

Jurgen J. Fütterer, Stijn W. T. P. J. Heijmink
Department of Radiology, University Medical Centre Nijmegen, Nijmegen, The Netherlands
j.futterer@rad.umcn.nl

Synonym

Prostatic adenocarcinoma

Definition

Prostate cancer is a malignant tumor of glandular origin in the prostate.

Characteristics

Epidemiology

Prostate cancer is the sixth most common cancer in the world. In 2005, an estimated 232,090 new cases and 30,350 deaths of prostate cancer are expected in the United States (1, 2). The lifetime risk of men developing clinically diagnosed prostate cancer is approximately one in six. With an ever-aging population, these figures are likely to increase in the coming decades. The use of prostate-specific antigen (PSA) testing has facilitated an earlier awareness of abnormalities in prostate health, resulting in a more frequent biopsy diagnosis of this disease (3). There has been an increase in the prevalence of prostate cancer, possibly due to increased importance of etiological factors such as diet and lifestyle.

Prostate Cancer Pathophysiology

Prostate cancer is a multifactorial disease. Age and a positive family history of prostate cancer are the main risk factors. Other factors are the type of diet, lifestyle-related

factors, and certain genetic defects (3). There is also a distinct geographical and racial difference in prostate cancer incidence with higher rates in Western countries and among black men, as compared to Asian countries and white men, respectively.

The main task of the prostate gland is to lubricate the sperm produced in the testes during ejaculation. In healthy prostatic epithelial cells, the enzyme aconitase is inhibited by high levels of zinc present in the cells. This, in turn, blocks the oxidation of citrate in the Krebs cycle, thus accumulating citrate in the prostatic lumina.

The earliest determinable pathological changes in the characteristics of the healthy prostatic cells are atrophic and inflammatory changes. A cascade of these and other factors may lead to the histopathologically defined precursors of prostatic intraepithelial neoplasia.

Normal Prostate Anatomy

On the basis of embryological origins, the prostate is anatomically divided into three zones that are eccentrically located around the urethra: the innermost transition zone, the central zone, and the outermost peripheral zone. Knowledge of the zonal anatomy of the prostate is very useful, considering that many prostatic diseases have a zonal distribution. Up to 70–80% of prostate cancer is located in the peripheral zone, whereas about 20% emerge in the transitional zone, and 10% in the central zone (4). Radiologically, in older patients the transitional zone and central zone cannot be distinguished due to compression of the central zone by benign prostatic hyperplasia and are referred together as the central gland. Most central gland tumors have additional tumor foci in the peripheral zone. Another aspect of the prostate anatomy that is relevant to radiologic imaging relates the prostatic capsule. The prostate is surrounded by a thick layer of fibromuscular tissue corresponding to the capsule. The "true" prostatic capsule, however, is a thin (0.5–2 mm) layer of connective tissue that is located externally to the peripheral zone. Around this layer there is the pelvic fascia, often called the "false" prostatic capsule.

Transrectal Ultrasonography

Nowadays, in regular clinical practice, prostate biopsies are performed under gray-scale transrectal ultrasonography (TRUS) guidance. Although prostate cancer traditionally appears as a hypoechoic lesion in the peripheral zone on TRUS (Fig. 1), nonmalignant conditions such as prostatitis, atrophy, and prostatic intraepithelial neoplasia may also present as hypoechoic lesions (5, 6). Thus, a hypoechoic lesion has a chance of 17–57% of being prostate cancer. More than 40% of prostate cancer lesions are isoechoic whereas only 5% are hyperechoic. Color Doppler imaging detects blood flow by determining its velocity and direction. An increased blood flow related to tumor neovascularity is a characteristic of prostate cancer. Use of Doppler imaging thus increased the accuracy rate of prostate cancer detection to 40–90%, with sensitivity and specificity outcomes being widely spread (52–75% and 40–82%, respectively). Application of gas-filled microbubble contrast agents enhances the visibility of the prostatic vasculature. This may lead to increased prostate cancer detection rate. Reported sensitivities and specificities of prostate cancer detection using contrast agents were 53–87% and 46–79%, respectively (7–9).

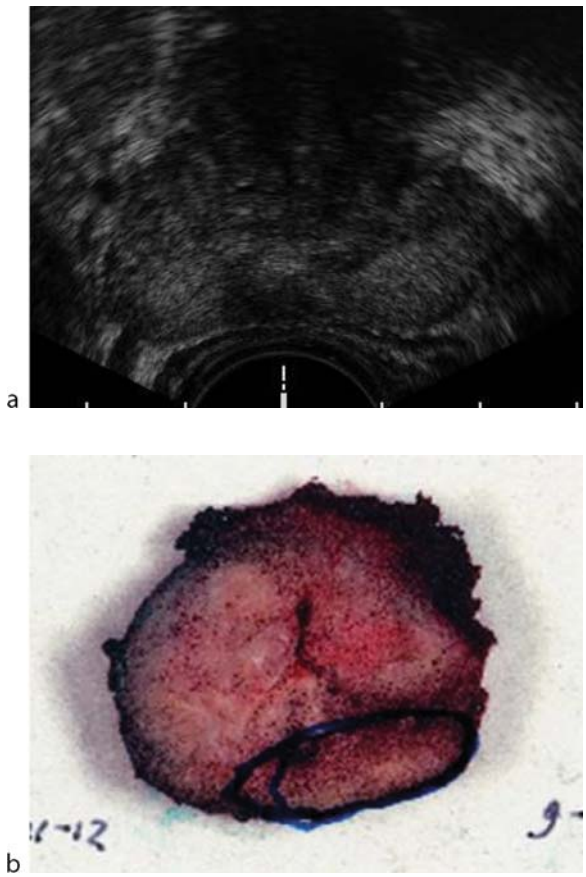

Carcinoma, Prostate. Figure 1 (a) Transrectal ultrasound image through the prostate demonstrating a hypoechoic area in the right peripheral zone indicating prostate carcinoma. This was confirmed with (b) whole mount section histopathology.

Computed Tomography

In general, computed tomography (CT) scanning has too little soft-tissue contrast resolution to differentiate the tissues intraprostatic (Fig. 2a). An additional disadvantage of CT is that the patient is exposed to a significant dose of radiation. Two studies revealed low sensitivity (26–29%) with reasonably high specificity (80–89%) in

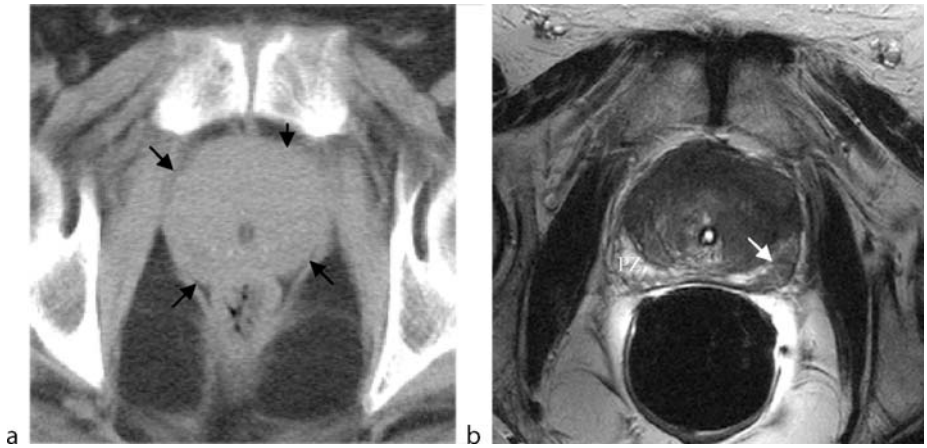

Carcinoma, Prostate. Figure 2 A 56-year-old patient with biopsy-proven prostate cancer. (a) Axial CT slice through the prostate (arrows indicate prostate contour). Prostate tumor is not visible. (b) Axial T2-weighted MR image in the same patient. A low signal intensity (arrows) in the left peripheral zone (PZ) indicating prostate cancer, which was confirmed with whole mount section histopathology.

staging prostate cancer (10, 11). Thus, CT has little value for staging and detection of prostate cancer.

Magnetic Resonance Imaging

Contrary to CT scanning, magnetic resonance (MR) imaging has a high soft-tissue contrast resolution. On T2-weighted MR images, normal prostate tissue displays an intermediate to high signal intensity whereas the central gland has lower signal intensity than the peripheral zone (12, 13). Conversely, the prostate has homogeneous, intermediate signal intensity on T1-weighted images. This means that the differentiation between peripheral and central zone cannot be perceived.

On T2-weighted MR images, prostate carcinoma displays as a low signal intensity area in a bright normal peripheral zone (Fig. 2b). In addition to carcinoma, the differential diagnosis of an area of low signal intensity includes postbiopsy hemorrhage, prostatitis, benign prostatic hyperplasia, effects of hormone or radiation treatment, scars, calcifications, smooth muscle hyperplasia, and fibromuscular hyperplasia (14). Detecting prostate carcinoma in the central gland on T2-weighted images is difficult because this area is often involved with benign prostate hyperplasia, which has signal intensity similar to that of carcinoma and the inner gland structure is more inhomogeneous. Postbiopsy hemorrhage can also appear as a low signal intensity lesion, but can be differentiated from prostate cancer as it is hyperintense using T1-weighted sequences (Fig. 3).

MR imaging obtained high sensitivities (77–81%), whereas specificities were lower (46–61%), in localizing prostate cancer. The addition of 3D proton MR spectroscopic imaging to anatomical MR imaging increased the localization specificity up to 91% (15). Because of typical tumor contrast enhancement characteristics, cancer can be differentiated from normal tissue on fast dynamic contrast enhanced MR imaging (16). Engelbrecht et al. (17) showed that prostate cancer demonstrated different enhancement patterns compared to both onset time, time to peak, peak enhancement, and washout.

The current general opinion is that the localized prostate cancer can be treated successfully by radical prostatectomy in the patient group with a life expectancy of 10 to 15 years or more. Accurate staging is therefore especially important for the proper management of prostate cancer. The most reliable criteria for the detection of extracapsular extension of prostate carcinoma are asymmetry of the neurovascular bundle, obliteration of the rectoprostatic angle, tumor bulge into the periprostatic fat, broad tumor contact with the surface of the capsule, an extracapsular tumor, and the radiologists' overall impression (18, 19). The most common but misleading MR sign of extraprostatic extension, e.g., irregular bulging (especially in nonpalpable tumors), is not often used. Wedge shape, diffuse extension without mass effect, and size are the morphological features of low-intensity lesions in the peripheral zone on prebiopsy T2-weighted MR images that give the best prediction of malignancy. Seminal vesicle invasion can be identified as an asymmetric area of low signal intensity in the seminal vesicles that is visible on T2-weighted MR images (18). Thickening of the tubular walls and asymmetric widening of the seminal vesicles have to be avoided as criteria because these are nonspecific signs. Senile amyloidosis can mimic extraprostatic spread. Prostate MR imaging should be obtained at a minimum of 2 to 4 weeks after prostate biopsy, as hemorrhage decreases staging accuracy. Endorectal MR imaging findings are significant predictors for the detection of extracapsular disease when

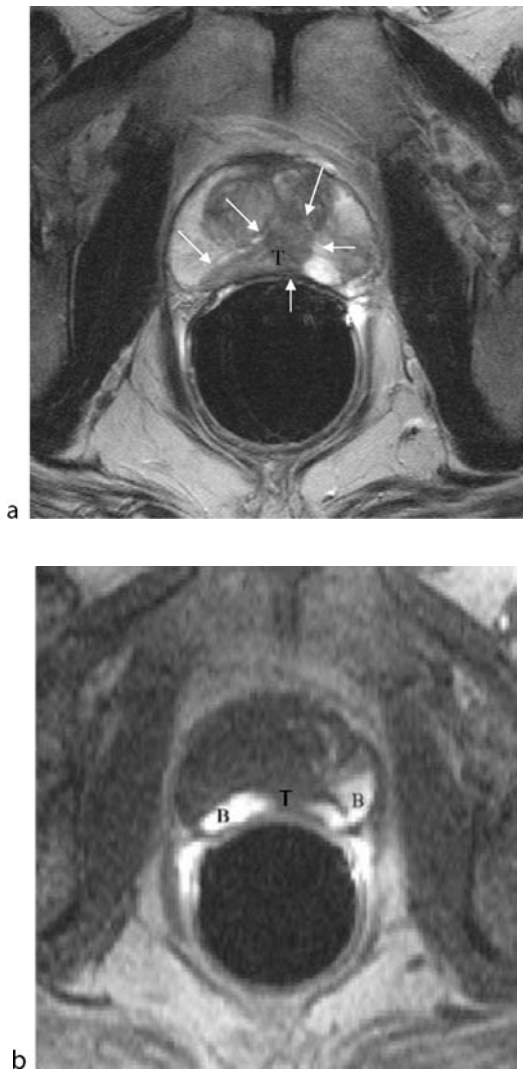

Carcinoma, Prostate. Figure 3 A 64-year-old patient with prostate cancer underwent MR imaging 2 weeks after transrectal ultrasound-guided biopsy. (a) Axial T2-weighted image through the prostate demonstrates a low signal intensity area in almost the whole peripheral zone (arrows). However, the T1-weighted axial image (b) at the same level revealed high signal intensity areas in the peripheral zone which were biopsy artifacts (B). Only in the mid-peripheral zone, tumor (T) was present which was confirmed with whole mount section histopathology.

MR images are interpreted by genitourinary radiologists experienced with MR imaging of the prostate. Engelbrecht et al. (20) suggested in their meta-analysis that the use of turbo spin-echo MR sequences, an endorectal coil, and multiple imaging planes can improve staging performance of MR imaging. Addition of dynamic contrast enhanced MR imaging to the anatomic images revealed a significantly improved staging accuracies for less-experienced readers (21). Addition of 3D proton MR spectroscopic imaging to MR imaging improved staging accuracies, most significantly for less-experienced readers.

Bibliography

1. Jemal A, Murray T, Ward E et al (2005) Cancer statistics 2005. CA Cancer J Clin 55:10–30
2. Parkin DM, Bray FI, Devesa SS (2001) Cancer burden in the year 2000. The global picture. Eur J Cancer 37(Suppl 8):S4–S66
3. Barry MJ (2001) Prostate-specific-antigen testing for early diagnosis of prostate cancer. N Engl J Med 344:1373–1377
4. McNeal JE (1981) Normal and pathologic anatomy of the prostate. Urology 17:11–16
5. Lee F, Gray JM, McLeary RD et al (1986) Prostatic evaluation by transrectal sonography: criteria for diagnosis of early carcinoma. Radiology 158:91–95
6. Meirelles LR, Billis A, Cotta AC et al (2002) Prostatic atrophy: evidence for a possible role of local ischemia in its pathogenesis. Int Urol Nephrol 34:345–350
7. Unal D, Sedelaar JP, Aarnink RG et al (2000) Three-dimensional contrast-enhanced power Doppler ultrasonography and conventional examination methods: the value of diagnostic predictors of prostate cancer. BJU Int 86:58–64
8. Halpern EJ, Rosenberg M, Gomella LG (2001) Prostate cancer: contrast-enhanced US for detection. Radiology 219:219–225
9. Frauscher F, Klauser A, Berger AP et al (2003) [The value of ultrasound (US) in the diagnosis of prostate cancer]. Radiologe 43:455–463
10. Tarcan T, Turkeri L, Biren T et al (1996) The effectiveness of imaging modalities in clinical staging of localized prostatic carcinoma. Int Urol Nephrol 28:773–779
11. Barbieri A, Monica B, Sebastio N et al (1997) [Value and limitations of transrectal ultrasonography and computer tomography in preoperative staging of prostate carcinoma]. Acta Biomed Ateneo Parmense 68:23–26
12. Sommer FG, Nghiem HV, Herfkens R et al (1993) Determining the volume of prostatic carcinoma: value of MR imaging with an external-array coil. AJR Am J Roentgenol 161:81–86
13. Schnall MD, Imai Y, Tomaszewski J et al (1993) Prostate cancer; local staging with endorectal surface coil MR imaging. Radiology 178:797–802
14. Schiebler ML, Schnall MD, Pollack HM et al (1993) Current role of MR imaging in the staging of adenocarcinoma of the prostate. Radiology 189:339–352
15. Scheidler J, Hricak H, Vigneron DB et al (1999) Prostate cancer: localization with three-dimensional proton MR spectroscopic imaging—clinicopathologic study. Radiology 213:473–480
16. Barentsz JO, Jager GJ, van Vierzen PBJ et al (1996) Staging urinary bladder cancer after transurethral biopsy: the value of fast dynamic contrast-enhanced MR imaging. Radiology 201:185–193
17. Engelbrecht MR, Huisman HJ, Laheij RJF et al (2003) Discrimination of prostate cancer from peripheral zone and central gland tissue using dynamic contrast-enhanced MR imaging. Radiology 229:248–254
18. Outwater EK, Petersen, RO, Siegelman ES et al (1994) Prostate carcinoma: assessment of diagnostic criteria for capsular extension on endorectal coil images. Radiology 193:333–339
19. Yu KK, Hricak H, Alagappan R et al (1997) Detection of extracapsular extension of prostate carcinoma with endorectal and phased-array coil MR imaging: multivariate feature analysis. Radiology 202:697–702

20. Engelbrecht MR, Jager GJ, Laheij RJ et al (2002) Local staging of prostate cancer using magnetic resonance imaging: a meta-analysis. Eur Radiol 12:2294–2302
21. Futterer JJ, Engelbrecht MR, Huisman HJ et al (2005) Staging prostate cancer with dynamic contrast-enhanced endorectal MR imaging prior to radical prostatectomy: experienced versus less experienced readers. Radiology 237:541–549

Caroli's Disease

Caroli's disease, first described by Jacques Caroli in 1958, is a rare, autosomal recessive condition characterized by segmental, non-obstructive saccular or fusiform dilatation of the intrahepatic bile ducts. Other typical pathologic features are the presence of intraluminal bulbar protrusions, bridges across the dilated lumina and portal radicles partially or completely surrounded by dilated bile ducts. The abnormality may be segmental or diffuse. The pure form of the disease is quite rare, while a various degree of congenital hepatic fibrosis is usually associated. Caroli's syndrome is the condition in which features of both congenital hepatic fibrosis and Caroli's disease are simultaneously present.

▶Cystic-Like Lesions, Hepatic
▶Congenital Malformations, Bile Ducts

Caroli's Syndrome

Caroli's syndrome is the condition in which features of both congenital hepatic fibrosis and Caroli's disease are simultaneously present.

▶Cystic-Like Lesions, Hepatic

Carotid and Vertebral Artery Pathology

Jonathan Gillard, Daniel Scoffings
Cambridge University Hospitals Foundation Trust, Cambridge, UK
Jhg21@cam.ac.uk

Definitions

Carotid atherosclerosis is characterised by lipid deposition, macrophage infiltration and fibrous cap development in the arterial wall with subsequent luminal narrowing. Stenoses occur most often at the bifurcation of the common carotid artery (CCA). Stenoses are quantified as percentages, which vary according to the method of measurement. The most common methods are those of the North American Symptomatic Carotid Endarterectomy Trial (NASCET) and the European Carotid Surgery Trial (ECST). The NASCET method compares the narrowest luminal diameter of the carotid artery to that of the normal distal internal carotid artery (ICA), beyond any post-stenotic dilatation. The ECST method compares the minimal luminal diameter to the predicted normal luminal diameter at the same level. A 50% NASCET stenosis corresponds to a 70% ECST stenosis. NASCET showed benefit from endarterectomy for symptomatic 70–99% stenoses, with a 17% reduction in ipsilateral stroke at two years. The Asymptomatic Carotid Atherosclerosis Study found some benefit for endarterectomy for asymptomatic stenoses greater than 60%, with a 5.9% reduction in stroke over 5 years.

Dissection indicates intramural haemorrhage in an artery. Typically the blood tracks between the tunica intima and media, less often between media and adventitia.

The term non-atheromatous vasculopathy includes intrinsic arterial diseases such as fibromuscular dysplasia (FMD), systemic diseases that affect the arteries such as neurofibromatosis type 1 and Marfan syndrome, and extrinsic processes such as tumour, infection and radiation injury.

Pathology/Histopathology

Plaques and their precursors can be classified into asymptomatic early lesions and advanced lesions, which may or may not be symptomatic. The earliest lesions, fatty streaks, are composed of layers of lipid-loaded macrophages and intimal smooth muscle cells in a proteoglycan matrix. Advanced lesions are characterised by a thickened, disorganised intima with deformation of the arterial wall. Lesions may have a fibrous cap of connective tissue overlying the lipid core and may be complicated by surface disruption, calcification, hemorrhage or thrombosis.

In a sub-intimal dissection haemorrhage lies between the intima and media and narrows the arterial lumen. In a sub-adventitial dissection the blood may extend beyond the adventitia to form a pseudoaneurysm. The most common site of carotid dissection is the cervical ICA just beyond the bulb. Intracranial carotid dissection is uncommon, but usually involves the supraclinoid ICA. Vertebral artery dissection typically occurs between C2 and the skull base.

Three types of FMD affect medium sized arteries. Medial FMD (90–95%) consists of fibrous proliferation

and smooth muscle hyperplasia in the tunica media. Intimal and adventitial FMD are rare. Marfan syndrome is associated with cystic medial necrosis. Radiation injury causes fibrinoid necrosis, endothelial damage and accelerated atherosclerosis.

Clinical Presentation

Carotid stenoses are often asymptomatic but may be detected by finding a bruit at physical examination. Embolisation of plaque components after ulceration or haemorrhage can result in a transient ischaemic attack or cerebral infarct.

Carotid or vertebral dissection is usually associated with neck pain or headache. Horner's syndrome may occur with ICA dissection. Deficits due to ischaemia in the territory supplied by the dissected artery also occur, dissection underlying 5–20% of strokes in young patients.

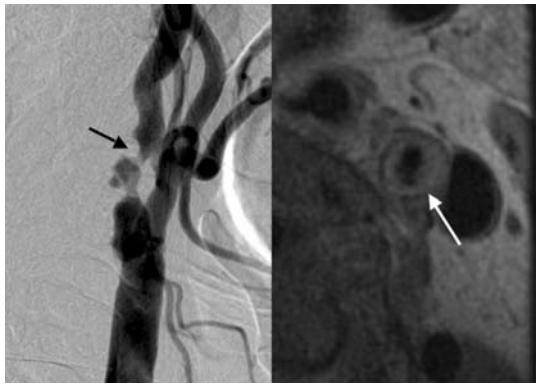

Carotid and Vertebral Artery Pathology. Figure 1 Right carotid stenosis. Catheter angiogram (a) shows an irregular, ulcerated plaque of the proximal internal carotid causing a tight stenosis (*arrow*). High-resolution axial MR (b) shows the extraluminal component of the plaque (*arrow*).

Imaging

Atherosclerosis

Digital Subtraction Angiography (DSA)

This remains the gold standard for measuring carotid stenosis though its use has declined as non-invasive imaging has improved. Studies should include AP, lateral and oblique views of each carotid bifurcation. Views of the distal carotid siphon and the intracranial circulation are necessary to detect tandem lesions, present in 20%, and to evaluate collateral circulation. The lumen at the site of maximum stenosis is often non-circular so that standard angiographic views do not accurately show the true minimum luminal diameter. (Fig. 1) Plaque ulceration is shown as a niche of at least 2 mm, a double density of contrast, or marked luminal irregularity. The detection of plaque ulceration by DSA is sub-optimal.

Ultrasound

A consensus statement has been issued regarding the use of US in the diagnosis of carotid stenosis, requiring the use of gray scale, colour Doppler and analysis of spectral Doppler waveforms (2). The angle of insonation should be 60° or less to the long axis of the artery to reduce measurement errors. The peak systolic velocity (PSV) is the most reproducible measure. Doppler measurements cannot predict the exact percentage stenosis, rather the result is stratified within one of the following groups. Normal: PSV <125 cm/s, no intimal thickening or plaque. Less than 50% stenosis: PSV <125 cm/s with intimal thickening or plaque on gray scale US. 50–69% stenosis: PSV 125–230 cm/s, plaque visible. Greater than 70% stenosis but less than near occlusion: PSV >230 cm/s, plaque and luminal narrowing seen on gray scale and colour Doppler imaging. Total occlusion is diagnosed by absence of flow on colour Doppler. Morphological assessment of plaques with ultrasound has not been conclusively shown to be of clinical value, but fibrous plaques tend to be of homogeneous reflectivity whilst heterogeneous plaques, containing lipid, haemorrhage and calcification, are associated with a greater incidence of neurologic events.

CT

With multislice CT machines, volumetric data acquisition during the injection of iodinated contrast allows fast, minimally invasive angiography of the cervicocephalic arteries. Different post-processing techniques are available: ►*shaded surface display* underestimates stenoses while ►*maximum intensity projections* (MIPs) can be performed quickly but overestimate stenoses. Multiplanar, or curved planar reformats are the preferred post-processing technique, allowing stenosis measurement. An advantage of CT over DSA is its depiction of the plaque and arterial wall beyond the lumen. Plaque calcification can be detected and quantified. Similarly, CT can differentiate between plaques that are lipid-rich or mostly fibrous. Attenuation of 60 HU is the optimal cut off to distinguish lower attenuation lipid-rich plaques from fibrous plaques. With automated methods plaque area and volume can also be measured from CT. Such techniques have yet to reach mainstream clinical practice.

MRI

Carotid magnetic resonance angiography (MRA) allows non-invasive measurement of stenoses without the risks of ionising radiation or iodinated contrast. Two-dimensional ▶time-of-flight (TOF) MRA uses sequential acquisition of thin slices, which are then stacked and MIPs obtained. Flow gaps correlate well with significant stenosis, the method is sensitive to slow flow and background suppression is good. The long TE used results in signal loss in areas of turbulent flow, however. Three-dimensional TOF-MRA excites a slab of tissue and sub-divides it with phase encoding gradients. Advantages over 2D TOF-MRA include better signal to noise ratio due to excitation of a volume of tissue and better through plane resolution because thinner slices can be reconstructed. Progressive saturation of protons as they move into the slab can be avoided by multiple overlapping thin slab acquisition (▶MOTSA). With fast gradient echo sequences images can be acquired during the first pass of a bolus of gadolinium chelate injected at 2–3 mL/sec. A correct timing is vital for contrast-enhanced MRA (CE-MRA).

Dedicated phased array coils enable high-resolution MR of the plaque, using 'black-blood' techniques with T1 and T2 weighting. This allows assessment of the plaque surface and its components.

Dissection

Smooth, or slightly irregular luminal narrowing over a long segment are the typical DSA findings. The degree of narrowing varies from minimal to complete occlusion, which can have a 'rat's tail' appearance. Intimal flaps are specific but seen in only 10%. Similar appearances are shown by CT and MR angiography. Acute intramural haematoma appears as a periarterial cuff of isointense or slightly hyperintense signal on T1 and T2 weighted MR, becoming hyperintense on T1 weighted images after a few days (Fig. 2) (3). Fat-suppressed T1 weighted sequences improve detection of the haematoma. Ultrasound can show a hyperreflective intimal flap, mural haematoma, or absence of colour flow in the false lumen, but dissection is more often inferred from abnormal Doppler indices in the absence of visible plaque.

Non-atheromatous Vasculopathy

Fibromuscular dysplasia results in segments of alternating stenosis and dilatation, the 'string of beads' appearance at angiography. It tends to spare the carotid bifurcation and bulb and is most common at the C2–3 levels. Vasculopathy due to neurofibromatosis type 1 and Marfan's syndrome manifest as areas of fusiform ectasia and tortuosity. Infections, such as retropharyngeal abscess or necrotising otitis externa can also narrow or displace the carotid. Radiation injury produces areas of stenosis or arterial occlusion, with moyamoya vessels intracranially.

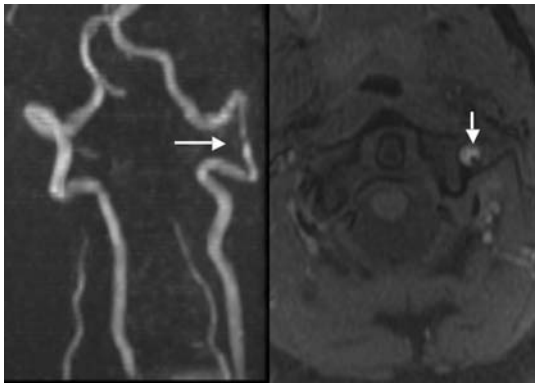

Carotid and Vertebral Artery Pathology. Figure 2 Left vertebral artery dissection. 3D-time-of-flight MR angiogram (a) shows short segment of narrowing of the vertebral artery between C1 and C2 (*arrow*). Fat-suppressed T1-weighted MRI (b) shows intramural haematoma as a crescent of high signal (*arrow*).

Diagnosis

The use of DSA in diagnosing carotid stenosis has declined with improving non-invasive techniques. A cost-benefit analysis using an analytical model recommended use of Doppler US and CE-MRA (4). This has been supported by a recent meta-analysis of the accuracy of non-invasive imaging (5). This showed that for 70–99% NASCET stenosis, sensitivities and specificities were: CE-MRA 94%, 93%; MRA 88%, 84%; Doppler US 89%, 84; CTA 76%, 94%. There was a paucity of reliable data for 50–69% stenosis.

References

1. Gillard J, Graves M, Hatsumaki T et al (eds) (2006) Carotid disease: the role of imaging in diagnosis and management., Cambridge University Press, Cambridge
2. Grant EG, Benson CB, Moneta GL et al (2003) Carotid artery stenosis: gray-scale and Doppler US diagnosis - Society of Radiologists in Ultrasound Consensus Conference. Radiology 229:340–346
3. Provenzale JM (1995) Dissection of the internal carotid and vertebral arteries: imaging features. Am J Roentgenol 165:1099–1104
4. U-King-Im JM, Hollingworth W, Trivedi RA et al (2005) Cost-effectiveness of diagnostic strategies prior to carotid endarterectomy. Ann Neurol 58:506–515
5. Wardlaw JM, Chappell FM, Stevenson M et al (2006) Accurate, practical and cost-effective assessment of carotid stenosis in the UK. Health Technol Assess 10:1–200

Carotid Artery Steal

Reversed flow in the right carotid artery caused by a significant stenosis in the origin of the innominate artery. Similar steal may involve the external carotid artery in the case of ipsilateral common carotid artery occlusion.
▶Steal Syndrome Vertebral

Carotid Endarterectomy

Open Surgery in order to resect atherosclerotic plaques out of the internal carotid artery in order to normalize the arterial diameter and treat a potential source of cerebral emboli.
▶Stroke, Interventional Radiology

Cartilage Destruction

Cartilage destruction in rheumatoid arthritis typically leads to a concentric pattern of joint space diminution, which is, together with bone destruction, one of the three radiologic key symptoms of arthritis (the other two are synovial soft tissue swelling and collateral phenomenon).
▶Rheumatoid Arthritis

Cartilage T2 Relaxation Time

Molecular motion of cartilage water protons and the structure of the extracellular matrix influence spin–spin relaxation. Therefore, quantitative T2 measurements may serve as a non-invasive tool to measure cartilage matrix integrity. In cartilage degeneration an increase in cartilage T2 is observed.
▶Degenerative Joint Disease, Peripheral Joints

Caspases

Proteolytic enzymes belonging to the family of aspartyl-specific cysteine proteases, which are not only essential for the starting event in the DISC but also for the execution of apoptosis.
▶Apoptosis

Cationic Lipophilic Complexes

The cationic lipophilic complexes ^{99m}TC sestamibi and ^{99m}TC tetrofosmin have recently replaced other gamma emitting radiopharmaceuticals with similar biological properties but less favorable physical characteristics. They are used as perfusion and tumor imaging agents.
▶Single Photon Emission Computed Tomography

Cauda Equina Syndrome

Syndrome of muscle paresis, saddle aneasthesia, sphincter disturbance and/or micturition disturbance due to involvement of multiple lumbosacral nerve roots, frequently caused by large median disc herniations.
▶Conservative Therapy for Lumbosacral Radicular Syndrome

Caudal Agenesis—Caudal Regression

▶Congenital Malformations, Spine and Spinal Cord

Caval Vein Occlusion

▶Thrombosis, Caval Vein, Inferior

Cavernous Angioma

Congenital vascular malformation formed by thin-walled, endothelial-lined sinusoidal vascular spaces, filled by slow-flow blood, with no intervening brain tissue. Also known as cavernoma and cavernous hemangioma. The term “occult vascular malformation” is obsolete.
▶Congenital Malformations, Vascular, Brain

Cavitary Necrosis

Multiple fluid- and air-filled cavities without rim-enhancement found in low attenuation lung parenchyma representing necrotizing pneumonia.
▶Pneumonia in Childhood

CCAM

▶Congenital Cystic Adenomatoid Malformation (CCAM)

CDH

▶Congenital Diaphragmatic Hernia (CDH)

Celiac Artery Stenosis

Celiac artery stenosis may be due to atheromatous disease or, in the younger patient, impingement by the diaphragmatic crura or median arcuate ligament. Atherosclerotic lesions tend to occur in the proximal or mid-proximal part of the artery. Clinical features of a severe celiac artery stenosis include postprandial epigastric pain, weight loss, and abdominal bruit. At Doppler US evaluation, the Doppler spectrum shows an elevated peak velocity and spectral broadening, findings consistent with turbulence. The diagnosis is usually confirmed by conventional angiography; however, CT angiography or MR angiography may be also useful.
▶Transplantation, Hepatic

Cell Cycle

The series of stages in which cells proceed from a resting state to cell division. The cell cycle includes interphase (consisting of G1-, S-, and G2-phases) followed by the mitotic phase, in which the replicated DNA is separated into two groups of chromosomes followed by division of the entire cell.
▶Proliferation of Neoplasms

Cell Doubling

▶Proliferation of Neoplasms

Cell Growth

▶Proliferation of Neoplasms

Cell Membrane-based System

Cell membrane-based reporter systems utilize gene products that are associated with the cell membrane.
▶Reporter Systems

Cellulitis

Cellulitis is a diffuse, spreading, acute inflammation within solid tissues, characterized by hyperemia, WBC infiltration, and edema without cellular necrosis or suppuration.
▶Gout
▶Infection, Soft Tissue
▶Oral Cavity, Inflammatory Diseases

Cemento-Ossifying Fibroma

Benign fibro-osseous lesion characterized by fibrous and calcified tissues associated with mature and immature bone/cement. Histologically, this lesion is very similar to fibrous dysplasia and the diagnosis is often difficult. It usually occurs in the jaws; localizations in the paraorbital region are rare.
▶Fibro-Osseous Lesions, Facial Skeleton

Central Facial Nerve Paralysis (CFNP)

Is a clinical condition characterized by paralysis of the muscles of the lower two thirds of the face secondary to supra-nuclear insults. Whereas fibres that project to the part of the motor nucleus that innervate the forehead muscles decussate only partially, those that project to the part of the nucleus that innervate the muscles of the lower two thirds of the face decussate completely. Henceforth, lesions of the upper motor neuron result in contralateral facial palsy sparing the upper face.

▶Facial Nerve Palsy

Central Neurofibromatosis

▶Neurofibromatosis, Musculoskeletal Manifestations

Cephalocele

▶Congenital Malformations, Cerebrum

Cerebellar Dysgenesis

Cerebellar Dysgenesis can involve the vermis and/or the hemispheres. This general term includes entities such as rhombencephalosynapsis, molar tooth malformations, and different abnormalities of foliation and fissuration.

▶Congenital Malformations, Cerebellar

Cerebral Aneurysm

▶Aneurysm, Intracranial

Cerebral Herniation

Secondary traumatic lesion that is the result of increased intracranial pressure. Herniation of the uncus/parahippocampal gyrus and herniation of the tonsils are the two most common types.

▶Trauma, Head, Accidental

Cerebral Infarction

The irreversible damage of the brain caused by inadequate blood supply.

▶Stroke, Children

Cerebral Infections

▶Infection, Opportunistic, Brain

Cerebral Neonatal Disease (Neuro View)

T. A. Huisman
Johns Hopkins University, Baltimore, USA
thierry.huisman@kispi.unizh.ch

Synonyms

Encephalopathy of the newborn; Neonatal diseases of the central nervous system; Perinatal cerebral injury

Definition

Neonatal cerebral disease refers to pathologies of the CNS that are present at birth or become symptomatic within the first weeks of life. These pathologies may have been acquired pre-, peri-, or postnatally.

Pathology and Histopathology

Neonatal cerebral diseases include a wide variety of pathologies like malformation, infection, tumor, hemorrhage, focal or generalized ischemia, and trauma. In addition, the timing of injury may vary, lesion may result

from prenatal (e.g., intrauterine fetal infection), perinatal (e.g., hypoxic-ischemic encephalopathy, HIE), or postnatal (e.g., germinal matrix hemorrhage) events (1, 2).

Hypoxia-ischemia or perinatal asphyxia is one of the leading causes of severe neurological deficit for all gestational ages. The exact etiology and cascade of events in HIE as well as the identification of the principal and supporting/mediating factors that determine severity of brain injury are the focus of ongoing research. Clinical presentation and outcome vary significantly with gestational age. Additional cardio-pulmonary diseases (e.g., congenital heart disease) may aggravate injury. HIE is characterized by the combination of cerebral ischemia (cerebral hypoperfusion) and cerebral injury due to global hypoxia (reduced blood oxygenation). Experimental studies showed however, that ischemia rather than hypoxia is responsible for most of the tissue injury. Neuronal and glial cell death is induced by many factors that are only partially understood. Primary and secondary energy failure with collapse of the normal aerobic pathway of glucose metabolism and shift into an anaerobic glycolysis result in a loss of transmembranous ion exchange, an excessive influx of calcium, failure of the neuronal resting membrane potential, lactic acidosis (anaerobic glycolysis) and cellular damage by release of free radicals and neurotoxic excitatory amino acids (glutamine and glutamate).

In contrast to adult brain, HIE in neonates is characterized by a selective vulnerability of different anatomical areas of the brain. This selective vulnerability is believed multifactorial and is tightly bound with the stage of brain maturation at the time of injury. The rapid biochemical, metabolic, cellular and anatomical changes are factors that determine vulnerability. This explains, at least partially, why the premature brain shows different patterns of injury compared with the term neonate. Generally, in preterm infants the white matter is more vulnerable while in term neonates the central and cortical gray matter is more susceptible. In addition, the maturation of the cerebral vasculature with progressive migration of the watershed zones from the periventricular areas to the subcortical regions explain the periventricular, confluent linear extension of white matter injury in preterm neonates while in term neonates wedge-shaped cortical/subcortical injuries are observed. These wedge shaped lesions match the border zones between the anterior, middle, and posterior cerebral arteries.

Focal infarction in neonates results from acute thrombo-embolic occlusion of major cerebral arteries. Ischemic infarction in neonates is rare. It is most frequently observed in neonates with congenital heart disease, coagulopathies, or hemoglobinopathies. Arterial dissection due to a traumatic birth seldom occurs.

Germinal matrix hemorrhages (GMH) are the most frequent intracranial hemorrhages in the newborn period. Premature born neonates are at increased risk for GMH. Based on their extension, GMH are classified into three different grades. Extension into the ventricular system may result in a hydrocephalus. Compression of the subependymal veins by the hematoma may induce a hemorrhagic venous infarction.

Neonatal infections can be acquired *in utero* due to (a) transplacental maternal–fetal transmission, (b) by ascending vaginal infections, or (c) during the passage through the birth canal during delivery. Neonatal infections may interfere with normal brain development if acquired *in utero*. Timing of infection in relation to the gestational age determines extent and kind of injury. Early in pregnancy, developmental brain anomalies occur with different degrees of migrational disturbances, microcephaly, cerebellar and brainstem hypoplasia as well as injuries/malformations of the eyes, and inner ear. Later in gestation, already developed and differentiated brain structures may become injured resulting into encephaloclastic lesions. Intracerebral calcification frequently develops. Most infections belong to the TORCH acronym. They include Toxoplasmosis, Other (HIV), Rubella, Cytomegalovirus, and Herpes simplex. Neonatal herpes simplex type II infection is typically acquired during birth while passing through an infected birth canal. Pre- and postnatal Herpes simplex-II infections are rare. In the case of a complicating meningoencephalitis, the prognosis is poor. Extensive perivascular infiltrates with ischemic and hemorrhagic infarction are usually fatal.

Metabolic diseases are rare, but initial symptoms may present shortly after birth with poor primary adaptation, seizures, respiratory distress, hypotonia, developmental delay, hypoglycemia, etc.

Clinical Presentation

Neonates with acute perinatal asphyxia present with low Apgar scores, low umbilical cord pH, bradycardia, and respiratory insufficiency. In addition, the amniotic fluid is often meconium stained. Additional signs of neonatal encephalopathy that may develop during the initial days of life include irritability, neonatal seizures, stupor, lethargy, generalized muscular hypotonia (floppy child), and poor reflexes (Moro, Gag, Suck). Clinical symptoms may parallel the cascade of primary and secondary energy failure characterized by an initial period of severe neurological symptoms, followed by a phase of partial recovery which is again followed by a lasting phase of neurological deficits.

Focal infarction in neonates may be clinically silent or present with focal seizures that can become generalized. Focal neurological deficits depend on the anatomical location of infarction respectively on the involved functional center.

Clinical signs in GMHs depend on the location and especially grade of hemorrhage. A grade I GMH is frequently an incidental finding on routine ultrasonography in preterm neonates. Neonates with higher grade GMHs will present with various neurological symptoms that are especially determined by the degree of hydrocephalus.

Clinical findings in neonatal infections are determined by the timing of infection in relation to the gestational age. The earlier the onset of infection, the more extensive the developmental anomalies will be. Clinical symptoms are frequently complex with signs of significant developmental delay as well as deafness, poor vision and seizures. In the case of late infection during gestation, focal neurological deficits and seizures are encountered. Cerebral malformations are discussed in the chapter "Congenital malformations" (cerebral).

Imaging

Patterns of brain injury in acute perinatal hypoxia have been studied extensively and differ between premature and term neonates. In premature neonates, the white matter is predominantly involved while in term neonates the gray matter is involved. These patterns of injury reflect the different vulnerability of different cerebral structures.

Ultrasound

The sonographic imaging of the brain immediately after the ischemic event maybe normal. In the premature infant the periventricular white matter may become echogenic as a result of coagulation necrosis and edema. The distinction between hemorrhagic and nonhemorrhagic periventricular leukomalacia however is difficult. Over the course of the subsequent 1–2 weeks the echogenicity decreases and cysts may develop at 10–14 days and beyond. These cysts usually coalesce and disappear as the ventricles enlarge and the damaged tissue is resorbed. In the term infant the cortex becomes echogenic with moderate to severe edema and this maybe diffuse or focal. Ventricular size is a nonspecific finding as small slit-like ventricles maybe seen as a normal finding in the term infant. Later cystic encephalomalacia, ventricular enlargement, and atrophy may develop in severe cases. Routine sonography through the anterior fontanelle may miss the peripheral areas of the parieto-occipital lobes, the sites of watershed infarction. These areas are now better visualized using the newer high frequency ultrasound probes and all available acoustic windows. In infants with thalamic and basal ganglia infarction there maybe focal or diffuse increased echogenicity in these regions.

Magnetic Resonance Imaging

In hypoxic-ischemic injury, T1-hypointense and T2-hyperintense white matter edema narrows the ventricular system as well as the subarachnoid spaces (Fig. 1a). A T1-hyperintense cortical highlighting following the cortical ribbon is seen due to intracortical petechial hemorrhages. This T1-hyperintensity is matched by a T2-hypointensity. Additional cortical necrosis will result in a diminished cortico-medullary differentiation. Moreover, signal alterations are seen within the basal ganglia/thalamus, hippocampus and posterior limb of the internal capsule (PLIC). In particular, the loss of the normal T1-hyperintense signal of the white matter tracts within the PLIC has been shown to correlate with degree of hypoxic-ischemic injury and outcome. On T2-weighted imaging a corresponding loss of the T2-hypointensity is observed. Finally, in many cases a linear, centripetal T2-hypo- and, T1-hyperintensity is seen within the cerebral white matter due to a stasis/thrombosis within the medullary veins. MR-spectroscopy may identify lactate within the ischemic white or gray matter as well as a reduction of the normal metabolites within the brain (Fig. 1b). Diffusion weighted imaging allows to differentiate between cytotoxic edema and vasogenic edema.

On follow-up after HIE, a multicystic encephalopathy ensues with *ex vacuo* enlargement of the CSF spaces. Depending on the gestational age, a multicystic periventricular leukoencephalopathy (Fig. 2) is seen or a more classical appearance of cortical–subcortical watershed ischemias.

Imaging appearance of GMH is discussed in the chapter titled: hemorrhage, intracranial, neonates. Ultrasonography is the primary imaging modality. In cases where ultrasonography cannot explain neurological symptoms, computer tomography (CT) or even better MRI should be performed.

In neonatal infections MRI is the imaging modality of choice to identify the associated disorders of development (Fig. 3). CT can be helpful to identify parenchymal calcifications, chorioretinitis, and malformations of the inner ear.

In metabolic diseases functional MRI techniques like MR-spectroscopy and diffusion tensor imaging are especially helpful in narrowing differential diagnosis.

Diagnosis

Diagnosis in neonatal disease should always rely on the combined analysis of clinical history, clinical-neurological findings, laboratory tests, and imaging findings. In neonatal encephalopathy without an obvious history or signs of acute perinatal hypoxia/injury other causes of neonatal

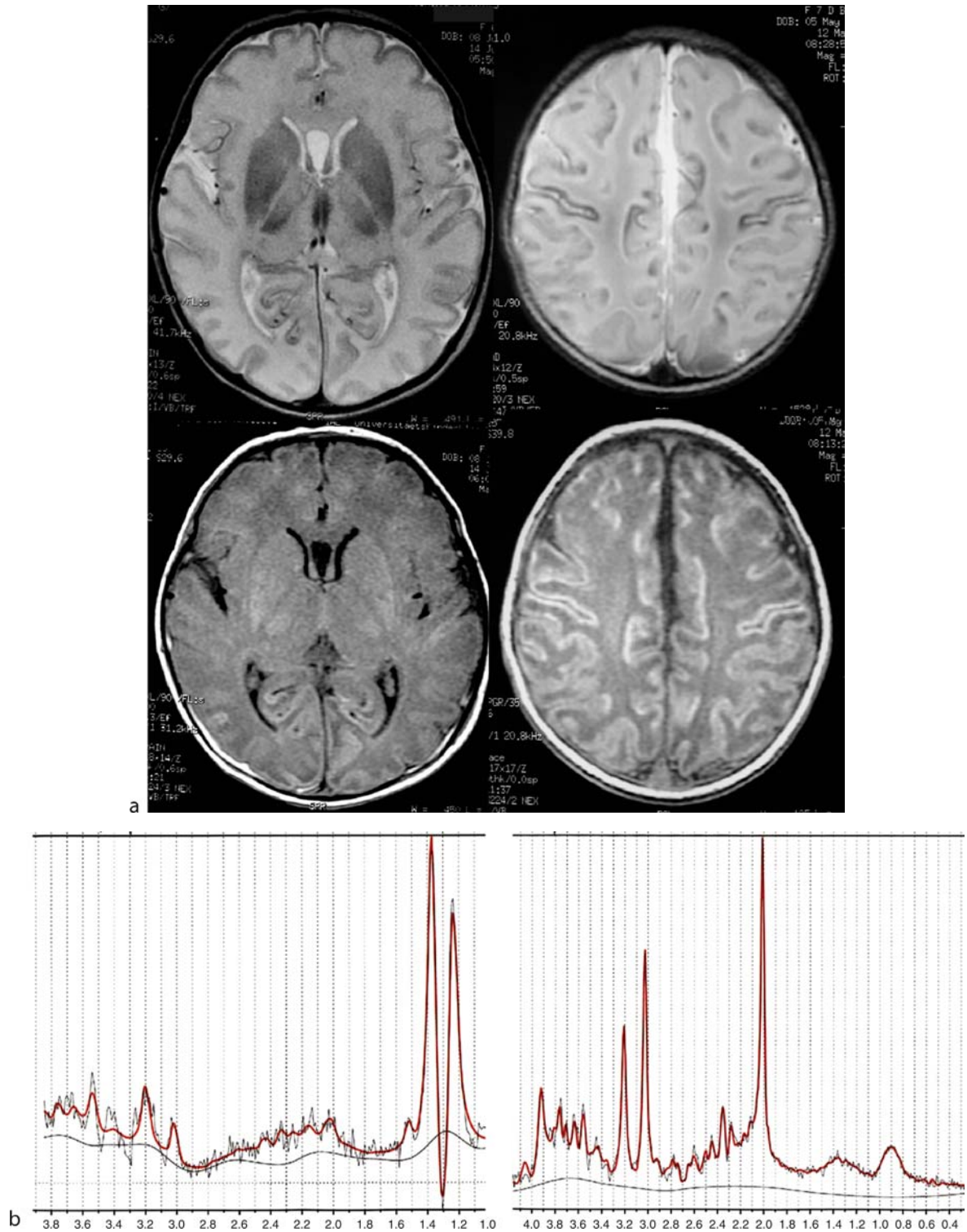

Cerebral Neonatal Disease (Neuro View). Figure 1 (a) Axial T2-FSE (upper row) and T1-SE (lower row) images of a term neonate with HIE. A diffuse white matter edema is seen with narrowing of the adjacent CSF-spaces. In addition, the T1-hyperintense and T2-hypointense signal intensity of the PLIC is missing. Finally, a T1-hyper- and T2-hypointensity is seen within the cortical ribbon of the central region due to intracortical petechial hemorrhages. (b) 1H-MRS of a child with severe HIE (left spectrum) compared with a 1H-MRS of healthy neonate (right spectrum) shows a significant lactate doublet

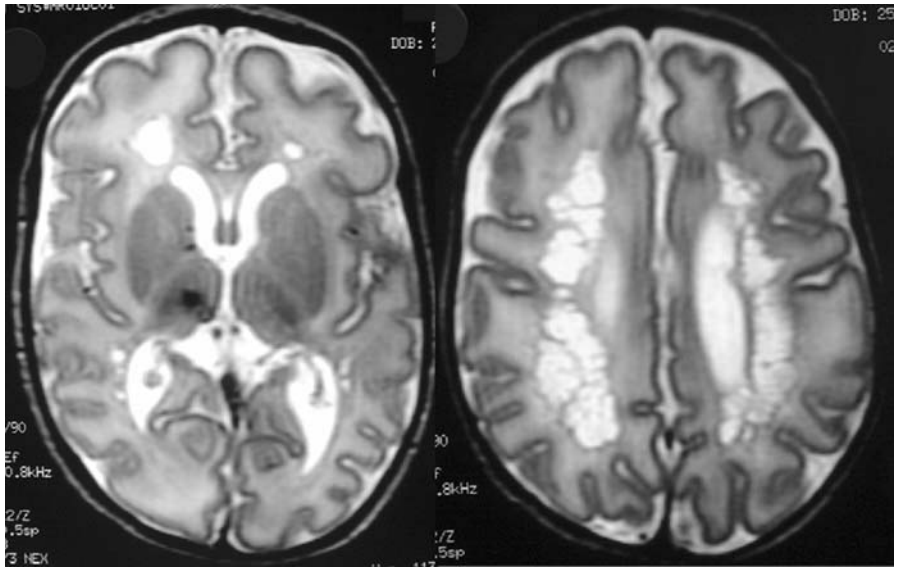

Cerebral Neonatal Disease (Neuro View). Figure 2 Axial T2-FSE in a 4 months old, premature born child with severe HIE. Multicystic leukoencephalopathy within the periventricular white matter is observed with a mild vacuo enlargement of the ventricular system.

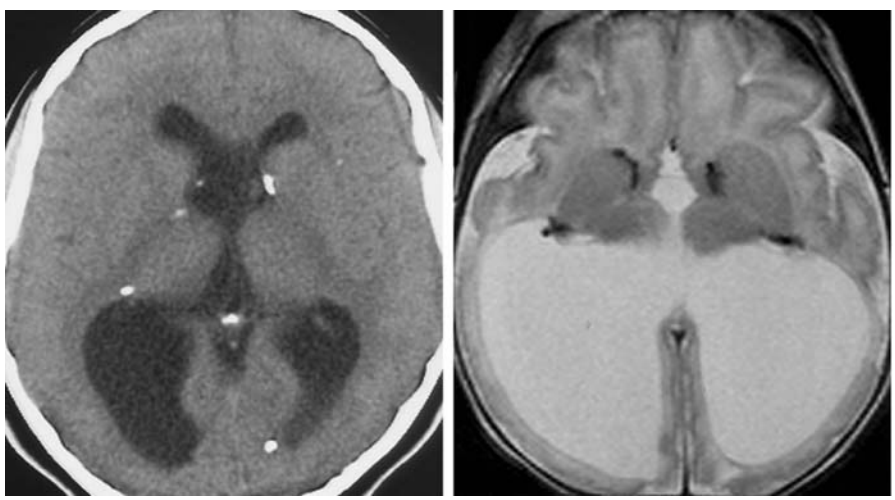

Cerebral Neonatal Disease (Neuro View). Figure 3 Axial CT and T2-FSE in two children with congenital toxoplasmosis infection. CT reveals multiple tiny, subependymal calcifications as well as a ventriculomegaly. MRI shows an identical pattern with T2-hypointense calcifications and a significant ventriculomegaly.

encephalopathy like e.g., neurometabolic diseases, hyperbilirubinemia, congential infections or malformations should be excluded. In addition, dual injury should be considered in complex or unexplained cases of neonatal encephalopathy. Furthermore, additional systemic diseases outside the central nervous system may complicate or aggravate neurological disease (e.g., congenital heart disease). Neuroimaging is increasingly combining anatomical–morphological data with functional results like diffusion tensor imaging, perfusion weighted imaging and qualitative and quantitative proton MR-spectroscopy. The functional data increasingly serves as predictors of outcome.

Bibliography

1. Triulzi F, Baldoli C, Parazzini C (2001) Neonatal MR imaging. Magn Reson Imaging Clin N Am 9(1):57–82
2. Paneth N, Rudelli R, Kazam E et al (1994) Brain Damage in the Preterm Infant (Clinics in Developmental Medicine) pp 22–137

Cerebral Tumors in Childhood

▶Neoplasms, Brain, Supratentorial, Pediatric

Cerebral Vasculature

The blood vessels that supply the brain. The arterial supply comprises the anterior (internal carotid) and posterior (vertebrobasilar) circulations that are linked through the circle of Willis.

▶Stroke, Children

Cerebral Venous Thrombosis

Shelley Renowden
Department of Neuroradiology, University of Bristol, Bristol, UK
shelley.renowden@north-bristol.swest.nhs.uk

Definition

One to two percentage of all adult strokes result from cerebral venous sinus thrombosis (VST). The real incidence of VST is unknown.

The sinuses most commonly affected are the superior sagittal (70–80%), transverse and sigmoid sinuses (70%) and less often, the cavernous and straight sinuses. In one third, more than one sinus is involved and in 30–40%, cerebellar and cortical vein thrombosis is associated. Venous anatomy is illustrated in Fig. 1.

Aetiology

There are many causes of VST but aetiology is unknown in one-third (1). Often multiple factors contribute. The most common are pregnancy and the puerperium, the contraceptive pill, coagulopathies and intracranial infections. Others causes include all causes of deep venous thrombosis, head and neck infections and cranial tumours.

Clinical Features

Presentation varies and may be acute, sub-acute or chronic, dependent upon venous collaterals, thrombus location and rate of progression (1).

Headache is the most common symptom in 74–90% of patients and reflects venous congestion. In 15%, presentation mimics sub-arachnoid haemorrhage (SAH).

Venous occlusion and hypertension may significantly elevate intracranial pressure (ICP) and additionally cause dizziness, nausea, visual disturbance and papilloedema, mimicking idiopathic intracranial hypertension (IIH).

Focal neurological deficits and seizures, which may be focal, occur and may be associated with a Todd's paresis.

Deep venous involvement may result in infarction of the basal ganglia, thalamus, and hypothalamus and these patients may deteriorate rapidly with coma and long tract signs.

Diagnostic Imaging

Cranial CT

Routine cranial CT is normal in 20% but is often the first line of investigation.

Pathognomonic signs of VST are the cord sign (in 25%) and the empty delta sign (in up to 46%) (Fig. 2). Thrombosed cortical veins and sinuses appear dense on plain CT (Fig. 3a). Unfortunately, interpretation is sometimes difficult (2). Flowing venous blood often may mimic dense clot in a sinus. Beam hardening artifact from the skull vault may mimic dense thrombus in the transverse sinuses and partial volume artifact may obscure clot within the horizontal portion of the superior sagittal sinus (SSS) or the transverse sinus (TS).

Other signs include generalised (48%) (Fig. 3) or focal brain swelling (3%), white matter oedema (12%), venous infarction (13%) (Fig. 3), parenchymal haemorrhage (33%), sub-dural haematoma (8%) and tentorial or falcine enhancement indicating venous stasis or dural hyperaemia (19%).

CT Venography

Multichannel helical CT enables 3D vascular imaging. Large volumes of tissue may be scanned during peak venous enhancement with high spatial resolution and triplanar reconstruction clearly demonstrates the veins and sinuses. CTV is unaffected by flow related artifacts

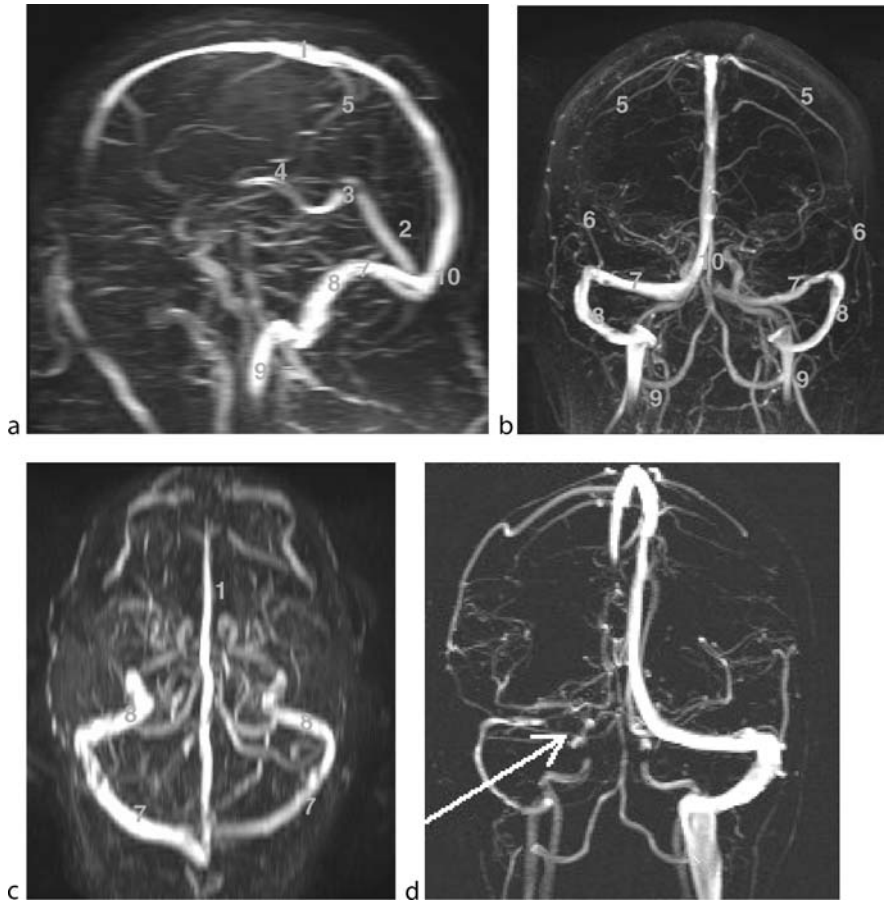

Cerebral Venous Thrombosis. Figure 1 Lateral (a) and frontal (b) 3D phase contrast reformatted MR venograms demonstrate venous sinus anatomy (1 = superior sagittal sinus; 2 = straight sinus; 3 = vein of Galen; 4 = internal cerebral veins; 5 = cortical vein; 6 = vein of Labbe; 7 = transverse sinus; 8 = sigmoid sinus; 9 = jugular vein; 10 = torcula).

(3). It may be used in uncooperative patients as acquisition times are very short and it is clearly useful in those in whom MRI is contraindicated. There may however be problems with background bone suppression and optimal timing of image acquisition is important to minimize arterial and venous superimposition.

Magnetic Resonance Imaging (MRI)

MRI is the preferred method (combined with magnetic resonance volumetry [MRV]) for diagnosis and follow up in our institution. Parenchymal abnormalities are seen more readily on MRI than on CT. It is important, at least for the initial diagnosis, to combine MRI in different planes with MRV. This combination importantly minimises confusion with sinus aplasia/hypoplasia (seen as a flow gap on MRV) and flow related artifacts with thrombus.

On T1W a thrombus appears isointense in the first days, then remains hyperintense during approximately 10 days and becomes isointense again after 2–3 weeks.

On T2W the thrombus appears hypointense during approximately 10 days and then becomes hyperintense (Fig. 4) (4).

MRV

Two dimensional or three dimensional time-of-flight (TOF) or phase contrast (PC) sequences may be used.

The author favours 3D PC sequences. Although TOF sequences have shorter acquisition times, good spatial resolution, and cover a larger volume, optimal signal is only returned when the slices are aligned perpendicular to direction of flow and signal loss arises from the in-plane saturation effect and from slow flow and intravoxel phase

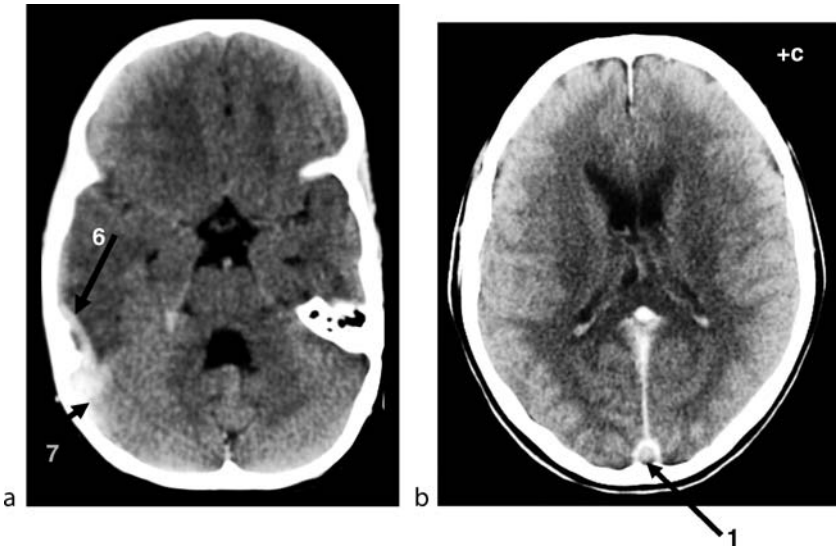

Cerebral Venous Thrombosis. Figure 2 **Axial unenhanced cranial CT scan (a) demonstrates the cord sign as dense thrombus in the right vein of Labbe (6, thin arrow) and right transverse sinus (7, thick arrow). Contrast enhanced axial cranial CT scan (b) demonstrates the "empty data sign" (arrow). Intraluminal thrombus is seen as a filling defect within the enhanced walls of the superior sagittal sinus (I).**

dispersion with turbulent flow. An additional problem associated with TOF MRA is that the hyperintense signal from methaemoglobin within clot may mimic flow.

PC is not associated with maximum intensity projection (MIP) or in plane saturation artifacts but the disadvantages are longer acquisition times, aliasing artifacts and intravoxel phase dispersion.

A hypoplastic/aplastic sinus may mimic sinus occlusion on MRV and must be differentiated by examination of the source images and triplanar MRI. 'Flow gaps' in the transverse sinuses due to hypoplasia may be seen in nearly one third of normals mostly in the non-dominant sinus or co-dominant sinus (5).

Small filling defects may also result from fat, fibrous bands and septae and arachnoid granulations.

Cerebral Angiography

Cerebral angiography is not generally used for diagnosis of VST and is usually only performed as part of local thrombolysis. Partial or complete non-opacification of venous sinuses and veins, dilated cortical collateral veins with a corkscrew appearance, increased cerebral circulation transit time and flow reversal away from the obstructed sinus or vein are signs that may be present.

Treatment

VST is poorly understood, unpredictable, diverse in presentation and causation, with variable sinus/venous involvement, and while potentially life-threatening (see Fig. 3) has a high incidence of spontaneous recovery. Treatment regimens are therefore impossible to compare and should be somewhat individualised.

Although there are few randomised control trials, heparin is considered by most to be the drug of first choice. Complications are rare and haemorrhagic infarction is not a contraindication. Heparin may act by limiting thrombus extension and promote its dissolution and is usually followed by oral anticoagulation for 3–6 months or longer with coagulopathies.

Pharmacological local thrombolysis is performed at our institution if the patient is in coma at the outset or if there is clinical deterioration despite full anticoagulation. It involves the selective delivery of thrombolytic agent directly into the occluded sinus. Local thrombolysis is usually performed *via* the transvenous femoral route. The patient is anticoagulated using heparin. Either urokinase or rt-PA is delivered directly into the clot using either bolus hand injections or an infusion. Recombinant tissue-type plasminogen activator (rt-PA) is often preferred because it has a greater affinity for plasminogen bound to fibrin rather than circulating plasminogen and thus has a reduced systemic effect. Recanalisation is faster with rt-PA than with urokinase. Extensive mechanical disruption of the clot by the micro-guide wire is important and clot maceration may be further enhanced if necessary using a balloon catheter or microsnare device.

The objective in most cases is complete recanalisation but while this is desirable, experience suggests that

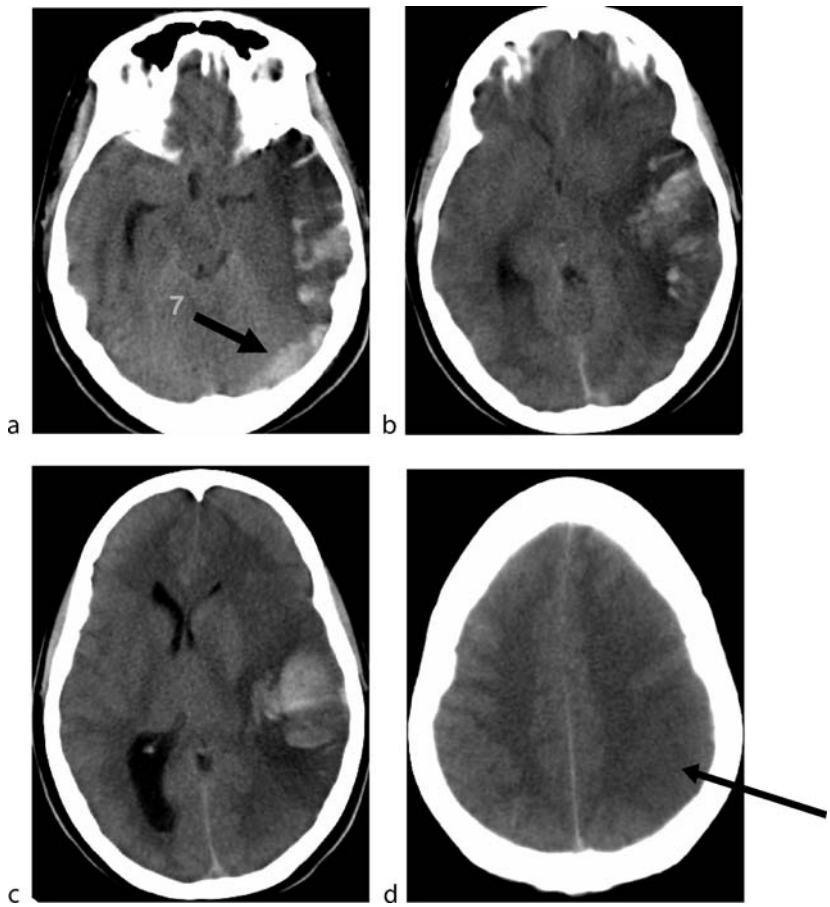

Cerebral Venous Thrombosis. Figure 3 Axial unenhanced cranial CT images (a–d) demonstrate severe consequences of venous sinus thrombosis, rapidly fatal in this 17-year-old girl, despite local thrombolysis. The dominant left TS, sigmoid sinus and jugular vein are occluded. Thrombus extended up to the torcula and then started to propagate in a congested SSS. The right TS is hypoplastic unfortunately. There is generalised cerebral swelling with effacement of the sulci, basal cisterns and third ventricle. There is bilateral uncal herniation with midbrain compression (a, b). Haemorrhagic venous infarction (a–c) involves the left temporal lobe and additional swelling has resulted in compression of the left lateral ventricle, midline shift and contralateral hydrocephalus. Parenchymal oedema reflecting venous hypertension is present in the left parietal and frontal lobes (d, arrow). There is a small amount of blood in the right occipital horn.

complete recanalisation is not always necessary for a good outcome.

Catheter mediated thrombectomy using a saline jet vacuum device has also been described and is used together with local pharmacological thrombolysis. It should probably be reserved for those with extensive thrombosis and malignant intracranial hypertension.

Outcome

Outcome is often favourable. Mortality ranges between 5.5–30% and a further 15–25% will incur permanent neurological deficits. Mortality is high in those presenting with a rapid onset, in coma, in infancy, in the aged and with involvement of the cortical, deep and cerebellar veins. VST recurrence is estimated in about 12% of patients.

Dural and pial arteriovenous fistulae may occasionally occur following VST thrombosis. Venous hypertension may promote growth of microscopic arteriovenous-shunts within the vasa vasorum of the normal pachymeninges and/or may stimulate the release of angiogenic factors.

References

1. Van Gijn J (2000) Cerebral venous thrombosis: pathogenesis, presentation and prognosis. J Royal Society of Medicine 93:230–233
2. Provenzale JM, Joseph GJ, Barboriak DP (1998) Dural sinus thrombosis: findings on CT and MR imaging and diagnostic pitfalls. AJR 170:777–783

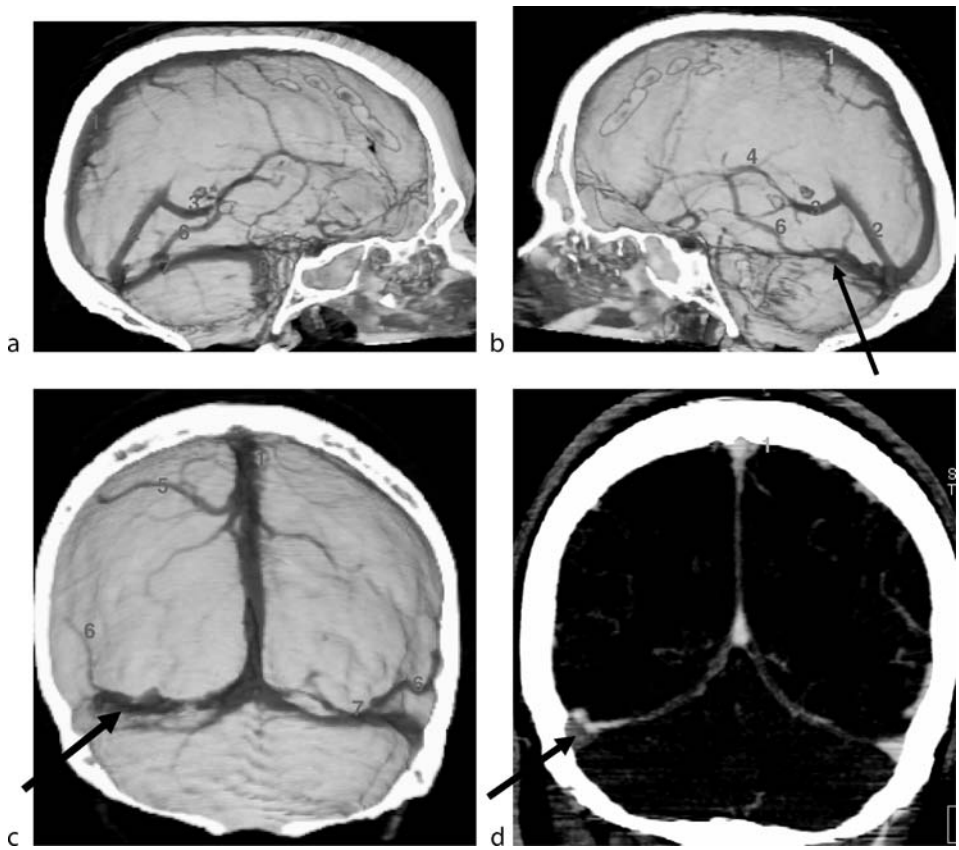

Cerebral Venous Thrombosis. Figure 4 CT venography with sagittal (a, b) and coronal (c) reconstructions and a mipped coronal image (d) demonstrate thrombus in the right transverse sinus. Venous antomy is again well demonstrated and the numbering is as in Figure 1.

3. Ozsvath RR, Casey SO, Lustrin ES et al (1997) Cerebral venography: comparison of CT and MR projection venography. AJR 169: 1699–1707
4. Bianchi D, Maeder Ph, Bogousslavsky J et al (1998) Diagnosis of cerebral venous thrombosis with routine magnetic resonance: an update. European Neurology 40:179–190
5. Ayanzen RH, Bird CR, Keller FJ et al (2000) Cerebral MR venography: normal anatomy and potential diagnostic pitfalls. AJNR 21:74–78

Cervical Carcinoma

▶Carcinoma, Cervix Uteri

Cervicomedullary Angle

Cervicomedullary angle is the angle between two lines on, respectively, the ventral side of the medulla oblongata or brainstem and the cervical cord, in degrees. A decrease <135° is a risk factor for the development of myelopathy in patients with rheumatoid arthritis with cervical spine affection.

▶Rheumatoid Arthritis

Cervix

The cervix is the lower and narrow part of the uterus, which forms a canal that opens into the vagina.

▶Carcinoma, Cervix Uteri

CEUS

Contrast-enhanced ultrasound.

▶Contrast Media, Ultrasound, Safety and Adverse Reactions

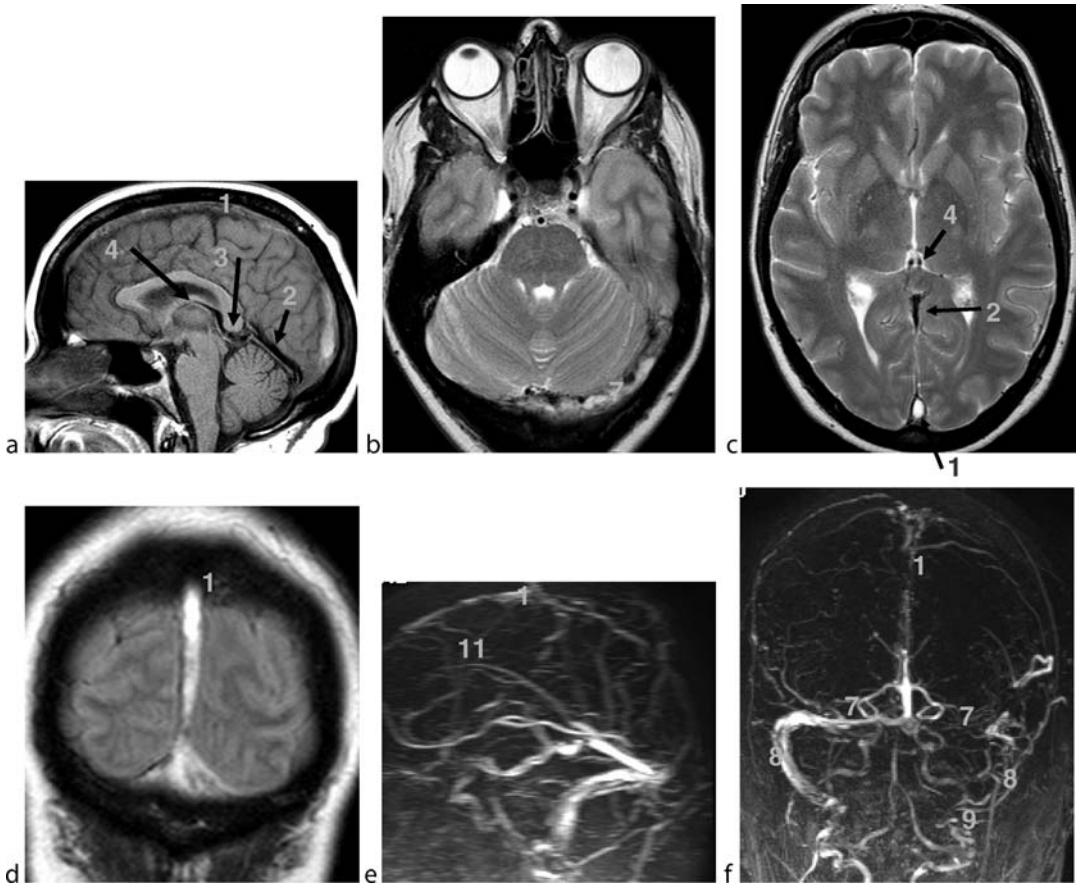

Cerebral Venous Thrombosis. Figure 5 T1W sagittal (a) and T2W (b, c) axial and coronal FLAIR (d) MR images demonstrate signal from sub-acute clot in the SSS and left TS, hyperintense on both T1W and T2W. Note the normal flow voids seen in the SS and deep venous system (a, c). Lateral (e) and frontal (f) projections of a 3D PC MR venogram in the same patient confirm occlusion of these sinuses and the left sigmoid sinus and jugular vein. The patient suffered increasingly severe headaches over 3–4 weeks. The clinical severity here is much less than the patient in Fig. 3 almost certainly reflecting the less rapid onset and superior venous collateralisation.

CEUS – Contrast-Enhanced Ultrasound of the Kidneys

▶Contrast Media, Ultrasound, Applications in Kidney Tumor

CFNP

▶Central Facial Nerve Paralysis (CFNP)

Charcot Neuroarthropathy

▶Neuropathic Joint Disease

CHARGE Association

The acronym refers to a clustering of malformations that occurs more frequently together than expected on the basis of chance. The diagnosis is firmly established when

all major criteria or three major and three minor criteria are present. Major criteria are coloboma (C), choanal atresia (A), typical external ear anomaly and/or hearing defects (E) and brain stem and cranial nerve dysfunction. Minor criteria are heart defects (H), genital hypoplasia (G), orofacial clefting, tracheoesophageal fistula, short stature and developmental delay (R).

▶Congenital Malformations, Nose and Paranasal Sinus

Chelator

Linking molecule between vector and radionuclide. The chelator defines with which radionuclides a vector can be labeled. Stable binding of the radionuclide by the chelator is mandatory for application of a radiopharmaceutical in patients.

▶Receptor Studies, Neoplasms

Chemoembolization

Thomas Rand
Allgeneines Krankenhfus-Universitätzkliniken
Vienna, Austria
thomas.rand@akhwien.at

Synonyms

Liver embolization; TACE

Definition

Transarterial chemoembolization (▶TACE) is based on the injection of a chemotherapeutic agent, mixed with an embolic material, into selected branches of the hepatic arteries feeding a liver tumor. This concept derives from the pathophysiological background of liver perfusion: Hepatocellular carcinoma (HCC) tumors are hypervascular and receive their blood supply from the hepatic artery. Normal liver receives approximately 70% of its blood supply from the portal vein and 30% from branches of the hepatic artery. The rational for TACE is that the infusion of a drug such as Doxorubicin, Mitomycin C, and Cisplatin with a viscous material (e.g. lipiodol) followed by embolization of the blood vessel with Gelfoam, PVA particles or spherical embolic agents will occlude arterial blood supply to the tumor causing an infarct and subsequent necrosis of the tumor. The advantage of TACE is that higher concentrations of the drug can be delivered to the tumor with decreased systemic exposure as compared with systemic chemotherapy.

Other hypervascular malignancies that might be considered derive from gastrointestinal neuroendocrine tumors that have been currently extensively reclassified. Management of these tumors nowadays include a more radical surgical approach of treatable tumor masses and treatment of liver metastases by embolization or thermoablation (1, 2).

Pathology/Histopathology

(HCC is the fifth most common cancer in the world and represents more than 5% of all cancers with an estimated annual incidence of about 1 million cases. Approximately 500,000 cases of HCC are diagnosed each year and it is the third cause of cancer-related deaths (3). There are wide geographical variations in the incidence of the disease with the highest rates in the developing countries of Asia and Africa. However, the incidence of HCC is increasing in North America and Europe (4). HCC tends to develop in cirrhotic livers due to hepatitis B and C virus, iron overload states, or alcohol abuse.

Clinical Presentation

Despite advances in diagnosis and treatment, the overall 5-year survival rate is only 2%. It is generally accepted that surgical resection, liver transplantation, and percutaneous tumor ablation are the only curative treatment options for patients with early stage HCC. Curative surgical resection is not feasible in many patients, therefore palliative approach is frequently considered to limit tumor progression. Today, several treatment modalities are discussed and compared. Multiple specialities are required for optimal treatment. Treatment options and prognosis depend on tumor stage and the cirrhotic background. Untreated HCC carries a poor prognosis and is directly related to the degree of underlying cirrhosis and tumor stage. Early detection offers the only possibility for cure. In patients with large tumor mass and Child C cirrhosis, patient survival is not more than 6 months. Patients with small HCCs (<5 cm diameter) and stable liver function have a better prognosis with 2-year survival rates of up to 56% (5).

Approximately 75% of HCC patients are not candidates for curative treatments either due to poor liver function or the presence of advanced disease. Nonsurgical treatments for unresectable HCC include systemic chemotherapy and radiotherapy, but these treatments have not

been found to prolong survival in randomized clinical studies. Chemotherapeutic agents (e.g. Doxorubicin) can be infused directly into the systemic circulation. However, serious side effects may arise, such as pain, nausea, vomiting, myelosuppression, and alopecia, or even cardiac toxicity.

From therapeutic aspects, arterial embolization achieves partial response in 15–55% of patients and significantly delays tumor progression and vascular invasion (6–9). Two major studies have reported the benefits for chemoembolization in selected patients. Llovet et al reported 1- and 2-year survival probabilities of 82% and 63% with objective response sustained for at least 6 months in 35% of cases (9). Lo et al found significant improvement in survival for Asian HCC patients treated by chemoembolization with a Lipiodol/Cisplatin emulsion and gelatin sponge (8). A systemic review and meta-analysis of randomized clinical trials for unresectable HCC has shown a survival benefit of chemoembolization (10). Innovative studies dealt with potential application of TACE in patients scheduled for liver transplantation: Graziadei and Jaschke et al demonstrated that TACE can be highly effective in preventing tumor progression in patients listed for liver transplantation, but failed to show beneficial effects on patient survival in advanced-stage HCCs (11). Thus, the best candidates for chemoembolization are those with preserved liver function and asymptomatic multinodular tumors without invasion or extrahepatic spread.

New strategies are also in discussion regarding technical aspects and innovations in mixture and application of chemotherapeutic and embolic agents.

Until now, generally superselective application of the chemotherapeutic drug to the tumor was followed by its embolization with microparticles, each procedure done as one step. Recent studies (12) have shown advantages of application of the embolic agents (microspheres) that are already loaded with doxorubicin.

Imaging

The procedure itself is monitored by fluoroscopy and digital subtraction angiography (DSA).

Interventional Radiological Treatment

Before Embolization

Clinical status, residual liver function, and blood parameters must be evaluated before the embolization procedure.

Contraindications for transarterial embolization are advanced tumor stages and/or advanced cirrhotic disease (Child C, Okkuda III) or other stages of uncontrolled liver disease, bacterial infection, presence of complete portal vein thrombosis, and contraindications for arterial access.

Informed consent for the embolization procedure must be obtained and the palliative aspect of chemoembolization should be evident.

Embolization Procedure

Transarterial embolization is performed according to a standardized technique. Hydration, analgesics, and antiemetics are administered before and during treatment. The femoral artery is catheterized under local anesthesia, and diagnostic angiography of the celiac trunk and superior mesenteric artery is usually performed with use of Sidewinder-configurated catheter. After identification of the vascular anatomy, a superselective highly flexible coaxial 3French microcatheter, is advanced into the hepatic arteries.

Arterial embolization is performed, when possible, through catheterization of feeding arteries of the tumor as selectively as possible.

When separately applied, the chemotherapeutic agents are administered prior embolization with microparticles. Embolization particles are then mixed with the contrast media and injected under fluoroscopic control, according to the location of the HCC, using sizes from 100 nm up to 700 nm (Fig. 1). Alternatively, as an innovative technique, microparticles can also be loaded directly with the chemotherapeutic agent and be used as a carrier and embolization agent at the same time. This technique shows very promising results. The procedure ends when complete occlusion of the arteries feeding the tumor is achieved. When injecting contrast agents, stasis is observed. Later embolizations are performed identically when CT follow-up indicates tumor progression or inadequate treatment response.

Dose Selection

The standard doxorubicin dose mixed with Lipiodol is adjusted to the serum bilirubin level as follows: bilirubin value of <1.5 mg/dL-75 mg/m^2 doxorubicin; bilirubin value of 1.5–3 mg/dL-50 mg/m^2. On average, patients receive 50–100 mg of doxorubicin in a single session. Embolization particles are used in sizes from 100 nm up to 700 nm. Treatment is applied periodically after 2–4 months, accounting for 2–4 treatments per year.

Further Medication, Follow-Up

Pain medication and antibiotics are given systematically, further conservative medication might be necessary in

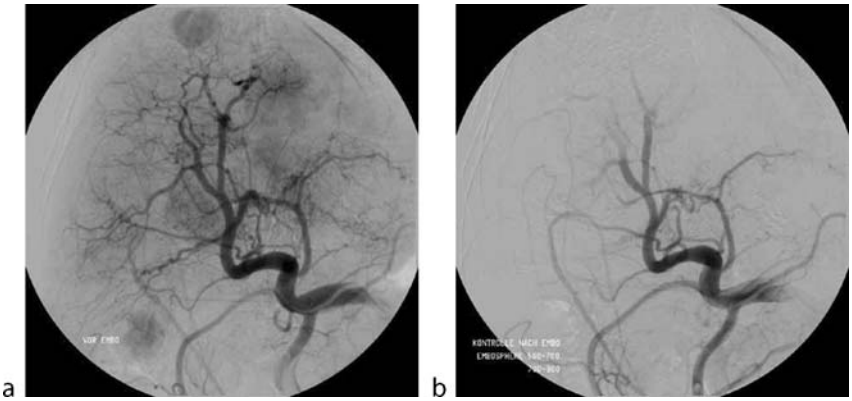

Chemoembolization. Figure 1 Multicentric HCC before (Fig. 1a) and after (Fig. 1b) TACE.

cases of a postembolic syndrome. Follow-up should be performed by CT or MR imaging and is usually applied 5–6 weeks postembolization.

References

1. Marlink RG, Lokich T, Robins SR et al (1990) Hepatic arterial embolization of metastatic hormone secreting tumors. Cancer 65:2227–2232
2. Kloeppel G, Heitz PU, Capella C et al (1996) Pathology and nomenclature of human gastrointestinal neuroendocrine 8carcinoid) tumors and related lesions. World J Surg 20:132–141
3. Parkin DM, Bray F, Ferlay J et al (2001) Estimating the world cancer burden: Globocan 200. Int J Cancer 94(2):153–156
4. El-Serag HB, Mason AC (1999) Rising incidence of hepatocellular carcinoma in the United States. N Engl J Med 340(10):745–750
5. Barbara L, Benzi G, Gaiani S et al (1992) Natural history of small untreated hepatocellular carcinoma in cirrhosis: a multivariate analysis of prognostic factors of tumor growth rate and patients survival. Hepatology 16:132–137
6. Lin DY, Liaw YF, Lee TY (1988) Hepatic arterial embolization in patients with unresectable hepatocellular carcinoma-a randomised controlled trial. Gastroenterology 94(2):453–456
7. Pelletier G, Roche A, Ink O et al (1990) A randomized trial of hepatic arterial chemoembolization in patients with unresectable hepatocellular carcinoma. J Hepatol 11(2):181–184
8. Lo CM, Ngan H, Tso WK et al Randomized controlled trial of transarterial lipiodol chemoembolization for unresectable hepatocellular carcinoma. Hepatology 35(5):1164–1171
9. Llovet JM, Real MI, Montana X et al (2002) Arterial embolization or chemoembolization versus symptomatic treatment in patients with unresectable hepatocellular carcinoma: a randomised controlled trial. Lancet 359(9319):1734–1739
10. Llovet JM, Bruix J (2003) Systemic review of randomised trials for unresectable hepatocellular carcinoma: chemoembolization improves survival. Hepatology 37(2):429–442
11. Graziadei IW, Sandmueller H, Waldenberger P et al (2003) Chemoembolization followed by liver transplantation for hepatocellular carcinoma impedes tumor progression while on the waiting list and leads to excellent outcome. Liver Transpl 9(6):557–563
12. Lammer J (2005) Prospective Study of Doxorubicin in the Treatment of Hepatocellular Carcinoma (HCC) by Drug-Eluting Bead Embolisation (PRECISION V-Study) The Vienna Experience. CIRSE, presentation

Chemonucleolysis

A proteolytic enzyme called chymopapain is injected into the centre of the intervertebral disc in order to induce hydrolysis of the proteoglycan molecules that form the nucleus pulposus. The resulting proteoglycan fragments have limited water-binding abilities, which leave intradiscal water molecules free to diffuse into the surrounding tissues. The resulting loss of water causes a decrease of intradiscal pressure. This causes the herniated portion of the nucleus pulposus to recede towards the centre of the disc, relieving pressure on the nerve root.

▶Percutaneous Interventions for Lumbar Radicular Syndrome

Chemoperfusion

THOMAS RAND
Allgeneines Krankenhfus-Universitätzkliniken
Vienna, Austria
thomas.rand@akhwien.at

Definition

Chemoperfusion is a locoregional treatment used as an adjuvant therapy in locally advanced tumors and as palliation in inoperable tumors. Intra-arterial locoregional chemoperfusion has been performed as a palliative therapy in bleeding bladder cancer, in the therapy of head and neck carcinomas, in inoperable pancreatic

carcinomas and local recurrence, and in hepatic metastases from breast carcinoma (1, 2). However, serious side effects have been observed, and in light of innovative embolic agents with the option of combining chemotherapy and embolic procedures, arterial chemoperfusion is only rarely applied today. As a nonvascular variation, intraperitoneal hyperthermic chemoperfusion is performed in tumors originating from the genital and gastrointestinal systems, in addition to surgical debulking of tumor masses (3, 4).

Characteristics

Locoregional Chemoperfusion

Clinical Background

Locoregional chemoperfusion of inoperable pancreatic carcinoma or of cases of local recurrence has been used to reduce side effects and provide clinical benefits. However, only a small series of patients have been studied (2).

Locoregional therapy of head and neck carcinomas (PEC) has been performed with the superselective application of cisplatin (5). The concept of this therapy is based on the simultaneous transarterial locoregional application of cisplatin and the systemic venous application of sodium thiosulfate. After its arterial passage, cisplatin is bound to the circulating sodium thiosulfate in a complex that makes the cisplatin ineffective and thus prevents systemic side effects of the chemotherapeutic agent. Additional pain medication is mandatory.

Technique

Locoregional application of chemotherapeutic agents is performed *via* superselective arterial catheterization, with the introducer sheet in the femoral artery. Selective angiographies are performed to evaluate the tumor feeding arteries and the arterial vascularization of the neoplasm.

Arterial embolization is performed, when possible, through catheterization of feeding arteries to the tumor as selectively as possible using a highly flexible coaxial 3 French microcatheter, analogous to transarterial chemoembolization (TACE). In contrast to TACE, however, only the chemotherapeutic agent is applied, without further embolization.

Hyperthermic Perfusion Chemotherapy

Clinical Background

Intraperitoneal hyperthermic perfusion chemotherapy (IHCP) is a locoregional treatment modality that is used as adjuvant treatment in locally advanced operable tumors and as palliation in inoperable tumors with the goal of treating peritoneal seedings and peritoneal micrometastases.

The intraperitoneal administration of cytotoxic agents has been used since 1980 (6, 7). The first aim of this method is the eradication of microscopic residual disease. It has the benefit of higher concentrations of drugs being delivered locally to the tumor site, while preventing the systemic toxic effects compared with intravenous administration. The efficacy of a drug is calculated by the ratio of the peritoneal cavity area under the concentration/time curve to the plasma area under the concentration/time curve. This ratio is between 250 and 1400 for 5-fluorouracil, 12 and 20 for cisplatin, and 75 and 80 for mitomycin C. The efficacy is increased with the slow absorption rate of cytotoxic drugs. Hydrophilic drugs like 5-fluorouracil, cisplatin, and mitomycin C are absorbed very slowly from the peritoneal surface, and therefore they are the most useful drugs for IHCP. Beyond this, the direct tumor absorption of drugs occurs up to a level of 5 mm beneath the tumor surface, which means tumor nodules exceeding 5 mm are not suitable for IHCP. In this technique, the cytotoxic effect of hyperthermia also enhances the efficacy by maximizing the diffusion of the drugs to the tumoral nodules.

In gastric cancer, IHCP can also be used as a neoadjuvant (preoperative) substance for down-staging, but the most preferential use is the adjuvant route. Takahashi and Hagiwara used activated carbon particles in the peritoneal cavity, which adsorbed a large amount of mitomycin C, in gastric cancer patients with definite serosal involvement (8, 9). They found a 2- and 3-year survival advantage of 14 and 18%, respectively, compared with control groups. In other studies that used cisplatin or mitomycin C in early postoperative intraperitoneal chemotherapy, statistically significant survival advantages were found against control groups and it was determined that this advantage occurred especially in stage III diseases. Fujimura et al reported 40% complete remission and 1- and 2-year survival rates of 67 and 40%, respectively, after IHCP in gastric cancer patients with peritoneal seeding (10).

Technique

Cytoreductive surgery consists of the removal of all gross tumors and involved organs or peritoneum. At the end of the operation two drains are inserted in the peritoneal cavity and after the closure of the abdomen, an extracorporeal circuit is used to conduct IHCP,

allowing perfusate circulation at 300–500 ml/min and hyperthermia ranging from 40 to 42°C for 60–90 min. The perfusate consists of 3 L of saline solution with cytotoxic drugs, for example, 10 mg/L mitomycin C is recommended because of its high penetration rate to micronodules and low absorption rate across the peritoneal surface. At the end of the perfusion, 1 L of perfusate is emptied and the rest is left in the abdomen for 12 h.

Bibliography

1. Textor HJ, Wilhelm K, Strunk H et al (2000) Locoregional chemoperfusion with mitoxantrone for palliative therapy in bleeding bladder cancer compared with embolization. Rofo 172(5):462–466
2. Vogl TJ, Heller M, Zangos S et al (2003) Transarterial chemoperfusion of inoperable pancreas carcinoma and local recurrence. Rofo 175(5):695–704
3. Reichman TW, Cracchiolo B, Sama J et al (2005) Cytoreductive Surgery and Intraoperative Hyperthermic Chemoperfusion for advanced ovarian carcinoma. J Surg Oncol 90:51–58
4. Erhan E, Haluk A (2004) The effectiveness of adjuvant intraperitoneal hyperthermic chemoperfusion after cytoreductive surgery in locally advanced gastric cancer. Indian J Surg 66:277–280
5. Rohde S, Kovacs AF, Zanella FE et al (2005) [Local chemotherapy for squamous cell cancer of the oral cavity and oropharynx] Radiologe Sep 45(9):843–50
6. Spratt JS, Adcock RA, Muskovin M et al (1980) Clinical delivery system for intraperitoneal hyperthermic therapy. Can Res 40:256–260
7. Howell SB (1980) Pharmacokinetic principles of regional chemotherapy. Contr Oncol 29:1–8
8. Takahashi T, Hagiwara A, Shimotsuma M (1994) Intraperioneal chemotherapy with mitomycin C bound to activated carbon particles for patients with advanced gastric cancer. Eur J Surg Oncol 20:183–184
9. Hagiwara A, Takahashi T, Kojima O et al (1992) Prophylaxis with carbon- absorbed mitomycin against peritoneal recurrence of gastric cancer. Lancet 339:629–631
10. Fujimura T, Yonemura Y, Fushida J et al (1990) Continuous hyperthermic peritoneal perfusion for the treatment of peritoneal dissemniation in gastric cancers and subsequent second-look operation. Cancer 65:65–71

Chemotherapy

This is a treatment with anticancer drugs that may be given intravenously or orally. The drugs travel through the bloodstream to reach cancer cells in most parts of the body. When used as *adjuvant therapy* after breast conservation therapy or mastectomy, chemotherapy reduces the risk of breast cancer recurrence. Chemotherapy given before surgery is called *neoadjuvant therapy.*

▶Breast, Therapy Effects

Chest

Hans-Ulrich Kauczor
Department of Radiology, German Cancer Research Center, Heidelberg, Germany
hu.kauczor@dkfz-heidelberg.de

C

Chest radiology is one of the recognized subspecialty areas of radiology. In the last decade remarkable advances in the ability to vividly image both normal anatomic and pathophysiologic aspects of the lungs and other thoracic structures have been accomplished. All the different imaging modalities, such as projection radiography, computed tomography (CT), magnetic resonance imaging, ultrasonography, angiography, and nuclear medicine examinations are applied to imaging of pulmonary, pleural, and mediastinal diseases. Cardiac and vascular diseases are covered separately. This entry focuses on adult radiology; pediatric radiology is covered separately.

Chest radiology is oriented toward disease entities and not imaging modalities. Thus, readers will become familiar with and understand the utility and limitations of all modalities for each particular disease and clinical situation much easier by retrieving the respective information.

To understand the imaging findings in chest radiology and their interpretation, a profound knowledge base of anatomy, histochemistry, and physiology of the lung as well as pathology and pathophysiology of lung diseases is necessary, because such radiological-pathological as well as structural-functional correlations are important.

The chest consists of three major anatomic compartments: (1) lungs, (2) chest wall, and (3) mediastinum.

1. Lungs. The lungs are divided into lobes by fissures, then further into segments, and continue to divide down to the alveolar space represented by pulmonary lobules and acini. The airspaces are supported by airways that have a continuous dichotomous branching structure starting from the trachea, carina, and main stem bronchi, going down to the small airways and bronchioles. The airways are surrounded by connective tissue, and there are distinct bronchovascular bundles and lymphatic and venous pathways within this lung structure.

2. Chest wall. The chest wall itself consists of the rib cage, respiratory muscles including the diaphragm, and soft tissue. The lung is surrounded by the visceral pleura, which has areas of invagination that give rise to the interlobar fissures. The chest wall is covered by the parietal pleura. Between the pleural surfaces is a small amount of fluid, which allows for smooth sliding of the lung during inspiration and expiration.

3. Mediastinum. Apart from the heart and fat, the mediastinum contains multiple different anatomical structures such as arteries, veins, nerves, and lymphatics as well as the esophagus (which belongs to the gastrointestinal tract), the tracheobronchial tree (which belongs to the respiratory tract) and finally, a primary mediastinal organ, the thymus. All of them can be the origin of disease in the mediastinum and also involve other structures. Additionally, adjacent structures such as lungs, pleura, and pericardium can afflict the mediastinum by means of continuous infiltration. The mediastinum is divided into anterior, middle, posterior, and superior parts.

The regular anatomy of the chest can be visualized by all the different modalities, which have particular advantages and disadvantages related to their respective properties. Abnormalities of the normal anatomy require the depiction of normal variants and the diminishment or enlargement of particular structures or organs. It is important to recognize normal image characteristics, structures, and patterns, which can be solitary, multiple, or disseminated. For radiology of the lungs, specific correlations between normal anatomy and pathological changes as well as image morphology have been established. The observations of individual findings can represent "signs" or they can merge to complex patterns that are based on radiological morphology. Such parameters relate radiological-morphological findings to anatomic-pathological substrates. Additionally, the correlation of abnormalities to particular pathophysiologic phenomena or pathological entities is facilitated by the use of image patterns. To understand image patterns, a profound knowledge base of normal anatomy, pathophysiology, and pathology is mandatory for applying these patterns to detect primary vascular, pulmonary, or pleural disease as well as diseases of the mediastinum or chest wall, and in establishing the differential diagnosis of cardiac diseases.

The lung has only a limited number of possible reactions to the wide array of different noxious substances that are related to different disease entities. The radiological patterns reflect the macroscopic consequences of lung disease, and the number of different patterns is thus also limited. The accurate analysis of imaging findings with regard to size, number, morphology, localization, and distribution is the prerequisite for detecting and using image patterns. Image patterns are first of all divided according to the predominant type of the change of attenuation (increase, decrease), the potential change of structure (destruction of lung architecture) and the morphological appearance, including extensive (alveolar, interstitial) or localized (nodular, reticular, reticulonodular), generalized, or focal. Although the commonly used modalities—radiography, CT, and angiography—mainly focus on visualizing structure, the application of magnetic resonance imaging, ultrasonography, and nuclear medicine is directed at elucidating function. Magnetic resonance imaging and nuclear medicine look for disease activity, vascularization, and blood flow as well as ventilation and perfusion, while ultrasound looks for respiratory motion and blood flow.

Signs and Patterns in Chest Radiology

- Air bronchogram—indicates a parenchymal process, including nonobstructive atelectasis, as distinguished from pleural or mediastinal processes
- Air crescent sign—indicates a lung cavity, often due to fungal infection
- Deep sulcus sign on a supine radiograph—indicates pneumothorax
- Continuous diaphragm sign—indicates pneumomediastinum
- Ring around the artery sign (around the pulmonary artery on lateral chest radiograph)—indicates pneumomediastinum
- Fallen lung sign—indicates a fractured bronchus
- Gloved finger sign—indicates bronchial impaction
- Hampton's hump—indicates a pulmonary infarct
- Silhouette sign—loss of the contour of the heart or diaphragm, used to localize a parenchymal process (for example, a process involving the medial segment of the right middle lobe obscures the right heart border, a lingula process obscures the left heart border, and a basilar segmental lower lobe process obscures the diaphragm)
- Scimitar sign—an abnormal pulmonary vein seen in venolobar syndrome
- CT angiogram sign—enhancing pulmonary vessels against a background of low attenuation material in the lung
- Halo sign—suggests invasive pulmonary aspergillosis in a leukemic patient
- Kerley A and B lines
- Honeycombing
- Cystic pattern
- Nodular pattern
- Reticular pattern
- Septal thickening
- Perilymphatic distribution patterns
- Bronchiolar opacities
- Tree-in-bud
- Air trapping
- Ground-glass opacities
- Egg-shell calcifications of lymph nodes
- Cavitation
- Unilateral hyperlucent lung

Lung Diseases

Lung diseases can be divided into several major groups:

Interstitial Lung Disease

- Scleroderma
- Drug toxicity
- Congestive heart failure—enlarged cardiac silhouette, pleural effusions, vascular redistribution, interstitial and/or alveolar edema, Kerley lines
- Asbestos-related pleural disease and asbestosis
- Pneumoconiosis, silicosis, coal worker's pneumoconiosis
- End-stage lung disease
- Sarcoidosis
- Progressive massive fibrosis
- Langerhans cell histiocytosis
- Lymphangioleiomyomatosis

Alveolar Lung Disease

- Acute alveolar lung disease (ALD)
- Pulmonary-renal syndrome
- Acute respiratory distress syndrome (ARDS)
- Cryptogenic organizing pneumonia (COP; bronchiolitis obliterans organizing pneumonia, or BOOP)
- Fat embolization
- Alveolar proteinosis

Atelectasis and Airway and Obstructive Lung Disease

- Partial or complete atelectasis
- Bronchiectasis, cystic fibrosis
- Asthma
- Chronic obstructive pulmonary disease (COPD)
- Tracheomegaly
- Tracheal and bronchial stenosis
- Emphysema and bulla, alpha-1-antitrypsin deficiency
- Kartagener's syndrome

Solitary and Multiple Pulmonary Nodules

Neoplasms

- Non-small cell lung cancer
- Small cell lung cancer
- Adenoid cystic and carcinoid tumors

Chest Trauma

- Contusion, laceration
- Tracheobronchial tear

Infection

- Bacterial pneumonia, typical, atypical
- Tuberculosis
- Fungal pneumonia, including *Pneumocystis carinii* pneumonia and invasive aspergillosis
- Viral pneumonia, including cytomegalovirus pneumonia
- Acquired immune deficiency syndrome (AIDS)
- Posttransplant lymphoproliferative disorders

Congenital Lung Disease

- Pulmonary venolobar syndrome
- Intralobar and extralobar sequestration
- Bronchial atresia

Pulmonary Vascular

- Acute pulmonary embolism, venous thromboembolic disease
- Pulmonary arterial hypertension

Diseases of the Chest Wall

Chest Wall, Pleura, and Diaphragm

- Pneumothorax, tension pneumothorax
- Pleural effusion
- Pleural calcification, asbestos exposure, tuberculosis
- Subdiaphragmatic abscess
- Diaphragm rupture
- Phrenic nerve paralysis
- Involvement with lung cancer
- Serothorax, fibrothorax
- Malignant mesothelioma
- Pleural metastases
- Fractured ribs, clavicle, spine, scapula

Diseases of the Mediastinum

- Bronchogenic, pericardial, thymic, or esophageal duplication cyst, goiter, lymphoma, germ cell tumors, neurogenic tumors
- Pneumomediastinum

Chest Pain

Chest pain is often a symptom leading to referral of patients for a barium meal study, and for which the diagnostic

concerns include cardiac disease, gastro-oesophageal reflux and musculo-skeletal disorders.

►Gastroesophageal Reflux in Adult Patients: Clinical Presentations, Complications, and Imaging

Chest Trauma

Jürgen Biederer
German Cancer Research Center, Heidelberg, Germany
j.biederer@dkfz.de

Definitions/Pathology/Histopathology

Chest trauma is defined by lesions to the chest that are induced by physical or chemical force. The chest is considered as a functional unit of the lung parenchyma, visceral pleura, airways, vasculature, and the surrounding structures with parietal pleura, mediastinum, chest wall, and diaphragm. The genuine task of this complex system is to guarantee gas exchange by ventilation and perfusion. Any trauma to single or multiple of these structures directly or indirectly involves all parts of the system. The pattern of lesions and the structures involved is directly related to the mechanism, intensity, and duration of the effective forces. The spectrum of mechanisms covers perforating and blunt trauma, barotrauma and aspiration of foreign bodies or (aggressive) gases and fluids, or any combination of these.

Perforating trauma is typically related to stab trauma or gunshot. Trauma mechanisms are directly related to cut and tear along the path of the impacted material. Impact with high kinetic energy (bullets, etc.) can combine this with mechanisms similar to blunt trauma (shockwaves with compression/decompression mechanisms).

The typical scenarios for *blunt trauma* of the chest are motor vehicle accidents or deep falls with deceleration injury. Blunt trauma to the chest wall may result in soft and bony tissue lesions. Rib fractures for themselves are usually of minimal clinical importance, but dislocated fragments can lacerate the pleura, lung, or abdominal organs thus combining blunt trauma with perforating mechanisms. Paradoxical movement of a ►flail chest due to multiple rib fractures can impair respiratory mechanics, promote atelectasis, and impair pulmonary drainage. Fractures of the thoracic spine, sternum, clavicle, or scapula are less relevant for the respiratory function of the chest, but indicative of extreme forces and associated with a high probability of life-threatening injury.

►Traumatic diaphragmatic hernia predominantly occur on the left side (4/5 cases) and may present with acute or delayed herniation of abdominal organs depending on the extent of the initial tear.

The mechanisms of blunt trauma to the lungs are direct or indirect deceleration, compression, or decompression. Deceleration becomes effective at transitions between fixed and elastic structures and results in destructive shear forces, e.g., between bronchovascular structures and blood-filled lung parenchyma. Compression and decompression effects occur along shockwaves with either abruptly elevated or lowered pressure. Both lead to local contusion or even rupture of lung parenchyma (laceration). Injuries may be visible either at the side of trauma or on the opposite side. The leading patterns include contusion (most frequent), laceration, aspiration, and atelectasis. These may even occur with intact chest wall. Conditions affecting primarily extrathoracic sites may have indirect effects on the lungs causing ARDS or fat embolism syndrome. Traumatic pulmonary pseudocysts are relatively rare sequelae of blunt chest trauma with lung contusion. ►Tracheobronchial lesions are rare (incidence ~1%) in blunt chest trauma but potentially life-threatening. Due to the underlying forces, concomitant blunt aortic injuries and myocardial contusion are frequently found. Cardiac contusion is the most common injury of the heart, but other injuries, including coronary injuries, pericardial tears, rupture of the free wall, septum, and heart valves, tamponade, as well as conduction defects, may be found. Cerebral air embolism is a rare, but severe complication of lung contusion.

Clinical Presentation

Seventy percent of the patients with severe thoracic injury are polytraumatized and present with shock symptoms. In perforating trauma, the combination of relatively small externally visible lesions with life-threatening intrathoracic complications is critical. Patients with blunt trauma present with more or less obvious chest wall injury. Pneumothorax and lung contusions lead to dyspnea, tachypnea, and cyanosis. If a tension pneumothorax is present these are combined with tachycardia and arterial hypotension. Contrarily to lung lacerations, lung contusions usually present without hemoptysis. Patients with massive intrathoracic bleeding (►hemothorax due to rupture of intercostal arteries or ►lung laceration) present with signs of respiratory failure, hypovolemia, and finally shock symptoms. The triad of arterial hypotension, elevated central venous pressure and

dampened heart sound can be indicative for cardiac tamponade. Clinical signs of tracheobronchial lesions are hemoptysis, pneumothorax, ►pneumomediastinum, subcutaneous emphysema, or an insufficient expansion of the lungs after drainage of a pneumothorax.

Imaging and Diagnosis

Respiratory failure related to chest trauma is a major cause of mortality during the "golden hour" of polytrauma. Immediate, life-threatening conditions that require prompt diagnosis are airway obstruction, pneumothorax (simple, open or tension pneumothorax), flail chest, cardiac tamponade, and massive hemothorax ("the lethal six"). Very often, initial treatment requires just simple procedures, such as chest tube insertion or pleural drains. Algorithms of polytrauma management therefore include chest X-ray and ultrasound as the primary survey with CT as second line imaging modality for the hemodynamically stable patient (Fig. 1). An alternative concept is based on initial whole body Multislice CT as the primary survey ("emergency room CT"). It is superior for the fast diagnosis of the "lethal six" when the dedicated workflow for transportation, scanning, data management, reading and reporting is fulfilled. Contrast administration is mandatory to exclude blunt vessel injury since CT-Angiography has replaced diagnostic DSA.

Further, potentially life-threatening injuries to be detected by CT ("the hidden six") are pulmonary contusion, tracheobronchial rupture, diaphragmatic tear, thoracic aortic rupture, ►esophageal rupture, and myocardial contusion. Further, impact from CT comes from the detection of pericardial hemorrhage, major thoracic vascular injury, small pneumothorax, and from the definition of the extent of contusion, laceration, and pulmonary pseudocysts, which is considered an important prognostic factor (Figs. 2, 3). Catheter misplacements can also be clearly identified. On chest X-ray and CT, the

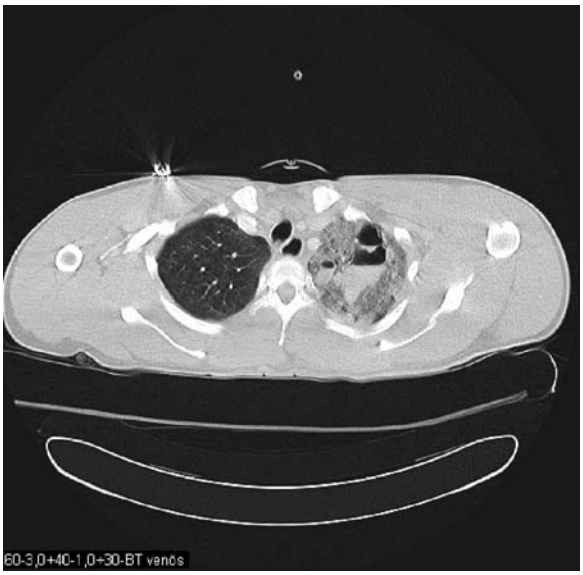

Chest Trauma. Figure 2 Lung laceration and severe lung contusion in the left upper lobe after blunt chest trauma with formation of hematopneumoceles.

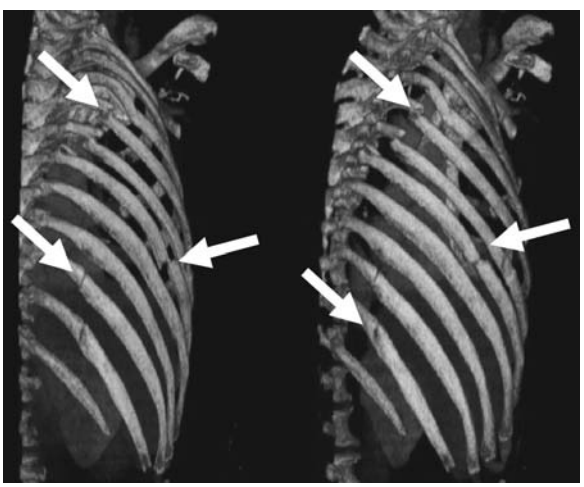

Chest Trauma. Figure 1 Volume renderings in posterior and latero-posterior views of the right chest wall indicating flail chest after blunt chest trauma with serial rib fractures and rib fragmentation (*arrows*).

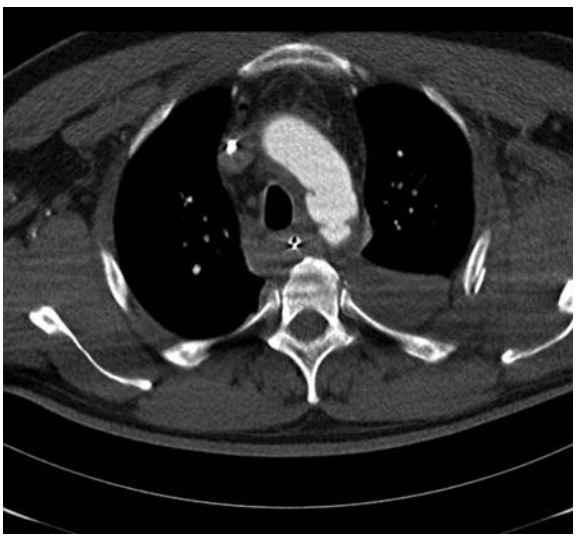

Chest Trauma. Figure 3 Traumatic aortic dissection at the typical location in the upper descending aorta with concomitant left-sided hemothorax and small mediastinal hematoma.

"fallen lung sign" is indicative for main stem bronchial rupture, but incomplete tracheobronchial rupture may be overlooked and definite diagnosis of airway lesions is usually made by endoscopy. A pneumomediastinum is not necessarily related to direct rupture of the tracheobronchial tree (►Macklin effect). The usual procedure for follow-up of chest trauma is chest X-ray with additional CT as far as necessary.

Nuclear Medicine

Nuclear medicine does not contribute to the diagnostic procedures of acute chest trauma.

Interventional Radiological Treatment

Except for endograft implantation for the treatment of thoracic aortic rupture, endovascular procedures do not contribute to the treatment of chest trauma. Endobronchial stenting for tracheobronchial lesions might replace surgical repair in selected patients.

Bibliography

1. Gavant ML (1999) Helical CT grading of traumatic aortic injuries. Impact on clinical guidelines for medical and surgical management. Radiol Clin North Am 37:553–574
2. Gavelli G, Canini R, Bertaccini P, et al (2002) Traumatic injuries: imaging of thoracic injuries. Eur Radiol 12:1273–1294
3. Miller LA (2006) Chest wall, lung, and pleural space trauma. Radiol Clin North Am 44:213–224
4. Reuter M (1996) Trauma of the chest. Eur Radiol 6:707–716
5. Stahel PF, Schneider P, Buhr HJ, et al (2005) Emergency management of thoracic trauma [Article in German]. Orthopäde 34:865–879

Chest, Neonatal

Veronica Donoghue
Radiology Department, Children's University Hospital, Dublin, Ireland
veronica.donoghue@cuh.ie

Synonyms

Congenital Neonatal Pneumonia; Hyaline Membrane Disease; Idiopathic Respiratory Distress Syndrome; Meconium Aspiration Syndrome; Pleural Effusions; Transient Tachypnoea of the Newborn

Definitions

The various medical causes of newborn respiratory distress depend largely on the gestational age of the infant. In the premature infant, the commonest abnormality is ►hyaline membrane disease, sometimes referred to as idiopathic respiratory distress syndrome or surfactant deficiency disease.

In the term infant, the causes include ►transient tachypnoea of the newborn, also referred to as retained foetal lung fluid or wet lung syndrome, amniotic fluid aspiration, ►meconium aspiration syndrome, which is defined as respiratory distress in an infant born through meconium stained amniotic fluid where symptoms cannot be otherwise explained, ►neonatal pneumonia, spontaneous pneumothorax/pneumomediastinum and ►pleural effusions.

Congenital abnormalities of the lung bud and vascular development include pulmonary agenesis and hypoplasia, pulmonary venolobar or Scimitar syndrome, horseshoe lung, congenital lobar emphysema, bronchial atresia, congenital cystic adenomatoid malformation, pulmonary sequestration, bronchopulmonary foregut malformations, oesophageal lung, bronchogenic cysts, neuroenteric cysts, pulmonary vascular malformations, congenital pleural effusions which include chylothorax, and situs abnormalities.

Abnormalities of the diaphragm include congenital diaphragmatic hernia of the Bochdalek and Morgagni types, eventration of the diaphragm and accessory diaphragm. The majority of these congenital and diaphragmatic abnormalities are discussed elsewhere.

Pathology/Histopathology

Hyaline Membrane Disease: In this condition, the abnormality is a deficiency of the lipoprotein surfactant superimposed on structural immaturity of the lungs. The surfactant is produced by the alveolar cells. Without it alveolar surface tension is raised, there is a reduction in alveolar distensibility and as a result collapse of the alveoli. The alveolar ducts and terminal bronchioles are distended and lined by hyaline membranes containing fibrin, cellular debris and fluid. Hyaline membranes are thought to result from a combination of ischaemia, barotrauma and increased oxygen concentrations delivered by assisted ventilation. In the very premature infant in particular there is also associated pulmonary haemorrhage and interstitial and airspace oedema later in the course of the disease. It is suggested that the presence of oedema is due to the fact that immature arterioles in these infants have a highly permeable basement membrane

which is aggravated by anoxia and acidosis. In addition immature vessels in these infants may lack sufficient smooth muscle to compensate for haemodynamic and osmotic changes. As a result there is capillary leaking and water is drawn into the alveoli. At low lung volumes negative interstitial pressure reduces fluid movement into the lymphatics.

Pulmonary Haemorrhage occurs because of an immature sequence of clotting factors, platelet sequestration or vitamin K and enzyme deficiency (1).

Transient Tachypnoea of the Newborn: During foetal life the lungs are expanded with fluid, an ultrafiltrate of foetal serum which contributes to amniotic fluid volume. During and after birth the fluid is removed by the pulmonary lymphatics and capillaries. In transient tachypnoea of the newborn there is slow or incomplete removal of the lung fluid. The incidence is increased in infants delivered by caesarian section. It is postulated that the absence of squeezing of the thorax during passage through the vaginal canal results in retention of lung fluid. The condition is also reported in infants with hypoproteinaemia, hyponatraemia, maternal fluid overload, small hypotonic or sedated infants and infants who have experienced a precipitous delivery (2).

Amniotic Fluid Aspiration: If intra-uterine foetal distress occurs the foetus may gasp and aspiration of amniotic fluid may occur. Debris in the amniotic fluid may contain squames and lanugo hair.

Meconium Aspiration Syndrome: Passage of meconium in utero is associated with ante- or intrapartum foetal acidaemia. It is widely accepted that foetal hypoxia causes an increase in intestinal peristalsis with anal sphincter relaxation and as a result passage of meconium. It is also thought that oligohydramnios may result in compression of the foetal head and umbilical cord, which may precipitate a vagal response and passage of meconium. Meconium aspiration syndrome may be secondary to aspiration of meconium *in utero* or at birth, maybe related to alterations in the pulmonary vascular system, which occurs as a result of asphyxia or indeed the presence of meconium itself. It appears that the degree of symptomatology is directly related to the viscosity of the meconium and large amounts of thick meconium can completely obstruct the airways. It is however more common for the meconium to migrate distally into the peripheral airways causing complete or partial obstruction. Complete obstruction causes atelectasis and ventilation—perfusion mismatch and partial obstruction causes a 'ball-valve' effect, whereby gas flows into the distal airways during inspiration, but becomes trapped distally during expiration due to the smaller diameter. After several hours there is an inflammatory response to the presence of meconium resulting in the presence of polymorphonuclear leucocytes diffusely throughout the lungs. These cells release chemical mediators which adversely affect the tissues. In addition the presence of bile salts in the meconium causes specific toxicity in type (II) pneumocytes. All contribute to the picture of chemical pneumonitis which leads to pulmonary vasoconstriction and in turn persistent pulmonary hypertension of the newborn (3).

Neonatal Pneumonia: Although the foetal environment is considered relatively protected neonatal sepsis can occur even in the presence of intact amniotic membranes. Congenital infections can occur through transplacental spread of organisms most commonly the 'TORCH' group (cytomegalovirus, herpes, rubella, toxoplasmosis) and are rare. Perinatal infections can be acquired *via* ascending infection from the vaginal tract which also causes chorioamnionitis sometimes referred to as amnion infection syndrome, transvaginally during the birth process and nosocomially in the neonatal period. It is postulated that most organisms causing neonatal pneumonia gain entry during the birth process as the foetus takes the first gasping efforts at breathing. This may occur earlier in the asphyxiated infant who may aspirate in response to non-specific stressful events. It is important therefore to treat chorioamnionitis aggressively once diagnosed. Approximately half of all the infections are due either to group B streptococcus or *E. Coli* (3).

Spontaneous Pneumothorax/Pneumomediastinum: This condition maybe the result of the infants own forceful initial respiratory effort or may result from resuscitation.

Pleural Effusions in the neonatal period are most likely due to chylothorax. Less common causes include hydrops foetalis, non-immune hydrops and cardiac disease.

The cause of chylothorax is unknown. Birth trauma to the thoracic duct has been suggested but is unlikely, as the effusion is seen on antenatal ultrasonography. Late maturation of the thoracic duct has also been suggested.

Hydrops Foetalis most commonly results when a Rhesus-negative mother becomes sensitised to Rhesus-positive blood. This results in the development of antibodies which enter the foetal circulation causing haemolysis and anaemia. When severe this may result in soft tissue oedema, pleural effusions, ascites and pericardial effusions.

The commonest causes of non-immune hydrops are twin–twin transfusion, foetomaternal transfusion, cardiac arrhythmias and tumours, cystic adenomatoid malformations, pulmonary arteriovenous malformations, lymphangiectasia and intra-uterine infection.

Clinical Presentation

Hyaline Membrane Disease: Clinically these infants are usually symptomatic within minutes of birth, with grunting, nasal flaring, intercostals retraction, tachypnoea

and cyanosis. The degree of symptomatology varies with the severity of disease. Prenatal steroid administration to mothers during the 2 days prior to delivery is safe and significantly reduces the incidence of the disease in premature infants. It promotes endogenous surfactant production and lung maturation in addition to inducing anti-oxidant enzymes. A similar response can occur when maternal steroid production is increased because of stress caused by prepartum maternal infection, toxaemia or other forms of prepartum stress. These situations however need to exist for 24 h or more prior to delivery. The condition results in poor gas exchange, hypoxia, hypercarbia and acidosis.

Transient Tachypnoea of the Newborn: Mild to moderate respiratory distress without cyanosis is typically present at birth or in the first couple of hours in this condition. Clinically resolution usually occurs within 48 h and often within 24 h.

Amniotic Fluid Aspiration: Tachypnoea is the most common clinical finding and its severity varies with the degree of aspiration.

Meconium Aspiration Syndrome: Clinically these infants demonstrate pallor, cyanosis, apnoea, grunting and intercostal retraction. Respiratory and metabolic acidosis may develop due to hypoxaemia and hypercarbia secondary to ventilation—perfusion mismatch.

Neonatal Pneumonia: The clinical signs and symptoms in neonatal pneumonia are frequently non-specific. The infant maybe listless, have pallor, apnoea, tachypnoea, tachycardia, bradycardia or feeding intolerance. Laboratory tests may also be non-specific. These infants usually present after 48 h of birth and have a less fulminant course. Those infants who present in the first 48 h of life tend to have a more severe clinical picture of hypotension, shock, disseminated intravascular coagulation and multi-organ failure. Mortality rates are high in this form of the disease especially when due to *B. streptococcus*.

Spontaneous Pneumothorax: Pneumothorax causes varying degrees of respiratory distress. They are usually transient and do not need intervention.

Pneumomediastinum is for the most part asyptomatic.

Pleural Effusions: This condition is frequently diagnosed by antenatal ultrasonography and if large may be treated antenatally by thoracocentesis and/or thoracoamniotic shunt.

After birth if the effusion is large the infants present with respiratory distress. The condition maybe bilateral.

Imaging

The chest radiograph is the most useful imaging modality in the investigation of the various medical conditions which cause respiratory distress in the newborn period.

It is also very important in determining the position of various tubes which are introduced during therapy, together with their complications. The most common of these is a misplaced endotracheal tube which ideally should be positioned above the level of the carina and the origin of the right upper lobe bronchus. Failure to do this may result in bronchial occlusion and atelectasis. Endotracheal and nasogastric tubes may perforate the trachea or oesophagus and cause a pneumothorax or pneumomediastinum.

The position of pleural chest tubes to drain pneumothoraces and pleural effusions can also be assessed on the chest radiograph. Misplacement may result in diaphragmatic paralysis as a result of phrenic nerve damage.

Positioning of intravenous and intra-arterial lines in the heart is not ideal as they may predispose the infant to thromboembolism. The venous catheters are best positioned in either the superior or inferior vena cava. Perforation of the superior vena cava resulting in hydrothorax and haemothorax has been reported. Umbilical arterial line tips are best located in the aorta proximal to the origins of the main arterial branches in order to avoid thrombosis and ischaemia to the dependant organs.

Hyaline Membrane Disease: Although the initial radiographic findings maybe noted shortly after birth, occasionally the maximum findings are not present until 6–24 h of life. Prior to commencement of assisted ventilation, typically the radiographic findings are those of underaeration of the lungs with fine granular opacification and air bronchograms which are diffuse and symmetrical. This is due to collapsed alveoli with distended terminal bronchioles and alveolar ducts. When distension is very poor there is more generalised opacification and a frank whiteout of the lungs (3) (Fig. 1a). Very small infants less than 26 weeks gestation may have clear lungs initially or mild perihilar haziness (4). Their lungs are biochemically and structurally immature and require prolonged ventilatory support. Several technologies have significantly altered the radiographic evolution. The clinical use of artificial surfactant is a very important recent therapeutic advance. It is given at birth, frequently prior to performing the first chest radiograph with up to 3–4 additional doses in some patients. It is given through the endotracheal tube and radiographic improvement can occur quickly. It is often not evenly distributed throughout the lungs and it is common to see residual areas of atelectasis alternate with areas of improved aeration. In addition the surfactant may reach the level of the acini causing sudden distension which produces a radiographic picture similar to interstitial pulmonary emphysema (3). It is therefore essential to correlate the image closely with the clinical findings

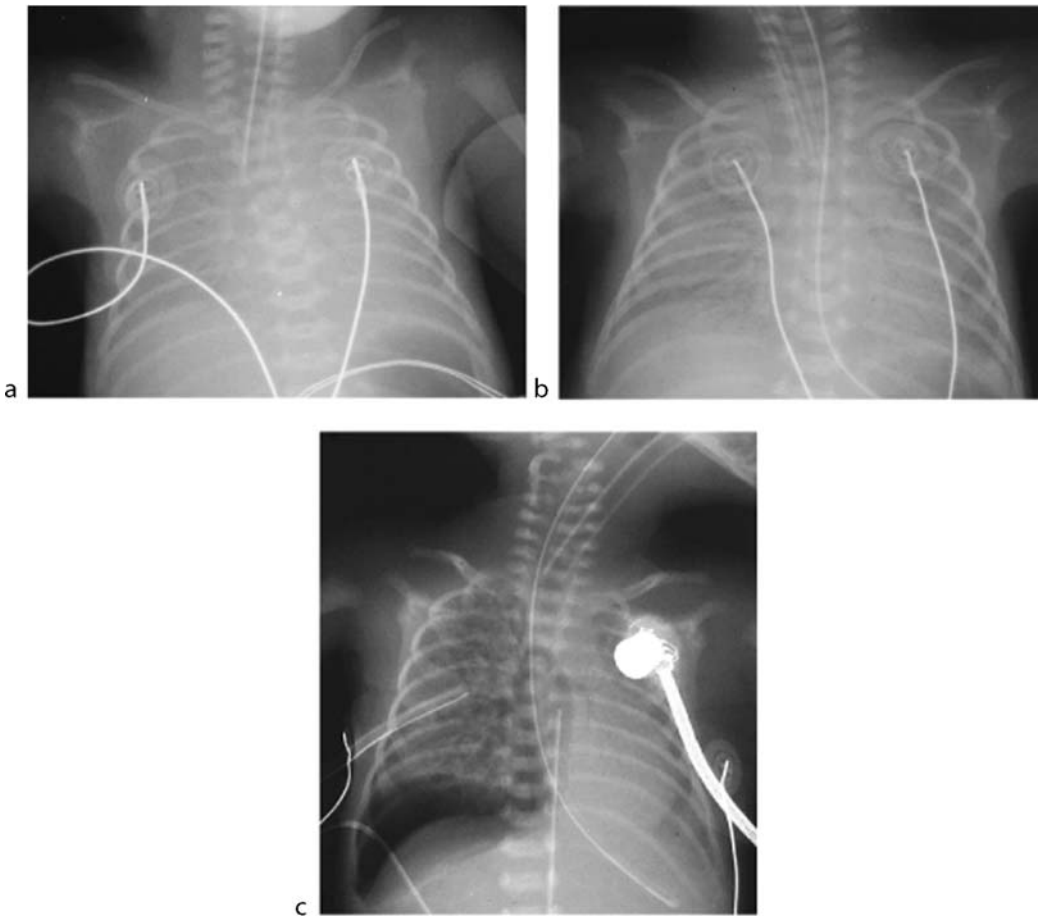

Chest, Neonatal. Figure 1 (a) Severe hyaline membrane disease showing almost complete 'whiteout' of both lungs with some air bronchogram visible bilaterally. (b) Premature infant with patent ductus arteriosus. The heart is bulky. There is distortion of the left main bronchus and marked pulmonary opacification due to pulmonary oedema. (c) Ventilated premature infant. There is right pulmonary interstitial emphysema and a right inferior and medial pneumothorax. A right chest drain is in position.

when interpreting the radiographs. Smaller infants, less than 27 weeks gestation may not respond well to surfactant therapy. Their lungs, although becoming clear with surfactant therapy are very immature with fewer alveoli than normal, leading to inadequate gas exchange and the need for prolonged ventilation which in turn leads to chronic lung problems, most commonly a hazy to opaque appearance on the chest radiograph. This is due to the presence of haemorrhage and pulmonary oedema, the latter is sometimes referred to as the 'leaky-lung' syndrome (2). Less commonly the radiograph demonstrates a much coarser irregular pattern similar to that seen in *bronchopulmonary dysplasia*.

A *patent ductus arteriosus* is common in premature infants and is thought to contribute to the lung disease. In the early stages of hyaline membrane disease the rigid lungs together with hypoxia and hypercarbia result in persistent pulmonary vasoconstriction. This may lead to right-to-left shunting through the ductus. With surfactant therapy and improved oxygenation there is a reduction in pulmonary resistance and left-to-right shunting may occur leading to pulmonary oedema. Radiographically in addition to pulmonary oedema there may be evidence of sudden cardiac enlargement with left atrial enlargement causing elevation or distortion of the left main bronchus (Fig. 1b). Treatment with indomethacin may result in ductal closure but occasionally surgery is necessary.

High frequency ventilation may also be employed to reduce the incidence of barotrauma. This method employs supra-physiological breathing rates and tidal volumes frequently less than dead space. This allows oxygenation and carbon dioxide removal without pressure induced injury. The aim is to achieve maximum alveolar recruitment without overdistending the lungs as

overdistended lungs compromise the systemic circulation. The chest radiograph in infants on high frequency ventilation is the best diagnostic tool for assessing overinflation of the lungs. Ideally the dome of the diaphragm should project over the 8–10th posterior ribs if the main airway pressure is appropriately adjusted. Otherwise the chest radiograph is not different from those infants receiving conventional ventilation.

Positive pressure ventilation in these premature infants is the most common cause of complications such as pneumothorax, pneumomediastinum, pneumopericardium and pulmonary interstitial emphysema. These air leaks are less common since the more routine use of artificial surfactant and high frequency ventilation. When a terminal airway ruptures—most often as a result of air being forced into the collapsed alveoli of hyaline membrane disease—air leaks into the pulmonary interstitial tissues and lymphatics and results in pulmonary interstitial emphysema. This causes stiff lungs which do not empty with expiration. Gas exchange is poor as a result and pulmonary blood flow maybe compromised and there is a need to increase ventilatory requirements. Radiographically, pulmonary interstitial emphysema is seen as bubbles often radiating from the hilum to the lung periphery (Fig. 1c). It maybe unilateral, bilateral or confined to part of a lung and may cause mass effect and mediastinal shift. If interstitial air reaches the pleural surface of the lungs and if a bleb bursts, a pneumothorax develops (Fig. 1c). If air dissects centrally it may leak into the mediastinum, pericardial space or downwards into the peritoneal cavity. Large pneumothoraces are easily identified radiographically but smaller pneumothoraces maybe subtle as sick infants are nursed in the supine position and free air may accumulate over the anterior surface of the lung producing a large hyperlucent lung and increased sharpness of the mediastinal edge. A pneumopericardium is recognised radiographically by the presence of air completely surrounding the heart and the pericardial sac maybe visible as a white line. Skin folds should not be mistaken for pneumothoraces. They can be seen to continue beyond the lung edge.

Focal atelectasis, due to malposition of the endotracheal tube, poor clearance of secretions or mucous plugging is also a common complication of surfactant deficiency.

Radiographically there is pulmonary opacification with volume loss or ipsilateral mediastinal shift proportional to the degree of atelectasis.

Infants with hyaline membrane disease are also at risk of pneumonia. The radiographic picture may be identical to that of the underlying condition. However, the lungs are usually more compliant and the infants require lower levels of ventilation relative to the degree of opacification present. More commonly however, there is evidence of patchy pulmonary opacification (5).

Pulmonary haemorrhage may also develop in infants with hyaline membrane disease secondary to severe hypoxia and capillary damage. Mild cases are difficult to detect on the chest radiograph. In severe cases blood may ooze from the nose, mouth or endotracheal tube. Radiographically the lungs may show homogeneous opacification and appear airless (3).

Bronchopulmonary dysplasia, a long-term consequence of neonatal lung disease is discussed elsewhere.

Though it does not serve as a substitute for the chest radiograph ultrasonography has been shown to be useful for assessing the severity of hyaline membrane disease and documenting the success of artificial surfactant. The persistence of retrodiaphragmatic hyperechogenicity beyond day 9–18 has also been demonstrated as a predictor for the development of bronchopulmonary dysplasia.

Transient Tachypnoea of the Newborn: The most common appearance is mild overaeration of the lungs, perihilar interstitial shadowing, prominent blood vessels and the presence of fluid in the horizontal fissure (Fig. 2). Occasionally there is a small pleural effusion and mild cardiomegaly. The radiographic findings maybe more marked on the right side and to date this finding remains unexplained. When the changes are marked there should be close clinical correlation to help distinguish this condition from meconium aspiration syndrome and neonatal pneumonia. Typically the appearances clear rapidly within 24–48 h.

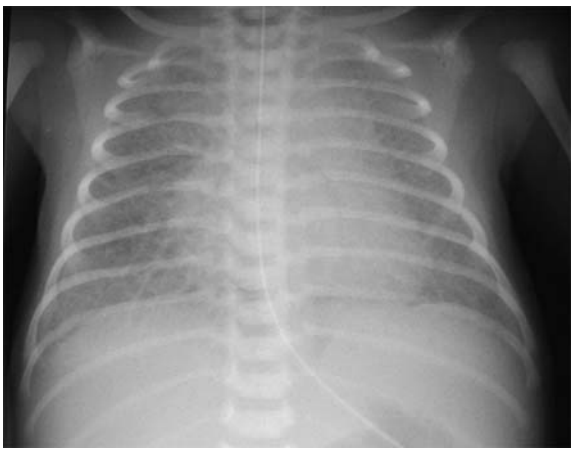

Chest, Neonatal. Figure 2 Transient tachypnoea of the newborn. There is mild cardiomegaly, bilateral perihilar shadowing most marked on the right and a small right basal pleural effusion.

Amniotic Fluid Aspiration: The radiographic findings vary with the volume of fluid aspirated and the amount of debris it contains. If aspiration is severe the chest radiograph may show marked nodular opacification. This however clears rapidly over the next 24 h which helps distinguish the condition from meconium aspiration.

Meconium Aspiration Syndrome: The chest radiographic picture includes any combination of diffuse patchy coarse infiltrates which maybe asymmetric or symmetric and focal or general, overinflation, air leaks, pleural effusions and cardiomegaly (Fig. 3).

Infiltrates are the result of atelectasis due to airway occlusion and alveolar oedema as a consequence of inflammation. The hyperinflation and air leaks result from partial airway occlusion and air trapping. Alveoli may rupture with free air dissecting into the pleural spaces and mediastinum. Pleural effusions are also the result of the inflammatory process.

Cardiomegaly may be the result of direct intra-uterine asphyxia or *persistent pulmonary arterial hypertension* (3). One-third of infants with meconium aspiration syndrome require assisted ventilation. As air leaks are a common complication they are exacerbated by using positive end expiratory pressure or continuous positive airway pressure ventilation. High frequency ventilation is also used and has the benefits of less barotrauma and better attainment of respiratory alkalosis in an attempt to achieve pulmonary vascular vasodilatation in those infants with associated persistent pulmonary arterial hypertension. The latter is also treated with inhaled nitric oxide. Surfactant deficiency is also seen in infants with meconium aspiration syndrome and this may be treated with artificial surfactant. It is probably caused by inhibited surfactant function or alterations in its composition. Infants who are resistant to the above therapies are treated with extra-corporeal membrane oxygenation. The technique is discussed elsewhere in this section.

Neonatal Pneumonia: The radiographic changes in neonatal pneumonia are non-specific to the extent that it is not possible to determine a causative organism from the appearances. In addition many neonates do not suffer from pneumonia in isolation but it may complicate other conditions. The radiographic pattern may mimic hyaline membrane disease or transient tachypnoea of the newborn. The presence of some overinflation associated with airspace disease has been reported as suggestive of pneumonia. Also the presence of pleural effusions with opacification is more suggestive of pneumonia especially group B streptococcus. A diffuse, bilateral alveolar pattern which develops in the first 4–6 h of life is characteristic though not specific (3) (Fig. 4).

Spontaneous Pneumothorax: Large pneumothoraces are easily identified radiographically, but smaller pneumothoraces may be subtle as sick infants are nursed in the supine position and free air may accumulate over the anterior surface of the lung producing a large hyperlucent lung and increased sharpness of the mediastinal edge. The thymus may also be compressed and elevated giving the appearance of a superior mediastinal mass. A medial

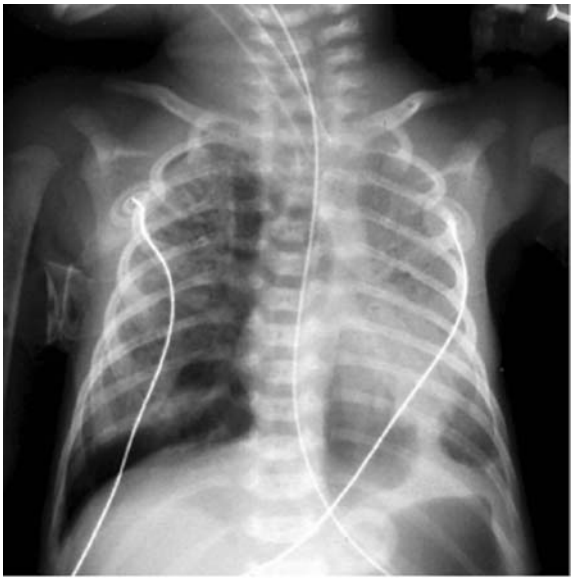

Chest, Neonatal. Figure 3 Meconium aspiration syndrome. There is coarse bilateral pulmonary opacification, hyperinflation and bilateral air leaks with some mediastinal shift to the left side.

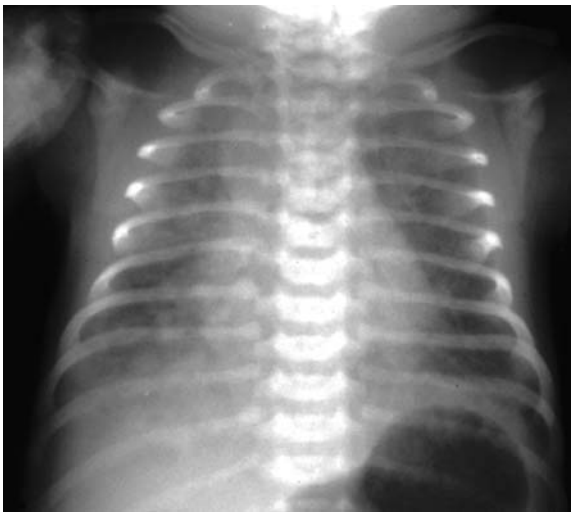

Chest, Neonatal. Figure 4 Group B streptcoccus neonatal pneumonia. There is diffuse bilateral coarse pulmonary opacification.

pneumothorax may be difficult to differentiate from a pneumomediastinum.

Pleural Effusions: The condition maybe diagnosed antenatally using ultrasonography. Antenatal MR imaging may also be helpful to delineate the extent of the effusion and to assess the presence of an underlying abnormality such as *cystic adenomatoid malformation*. After delivery radiography will demonstrate the effusion which maybe bilateral. If large enough it may opacify the entire hemithorax and cause shift of the mediastinum to the contralateral side.

Ultrasonography is the easiest way to confirm the presence of an effusion and is useful to guide thoracocentesis. Underlying causes such as cardiac abnormalities and cystic adenomatoid malformation may also be detected prior to aeration of the cysts. CT scan may be necessary to delineate the extent of conditions such as cystic adenomatoid malformation and rarer anomalies such as pulmonary lymphangiectasia, arteriovenous malformations and arteriovenous malformations. The latter can also be imaged using MR imaging. The treatment of chylothorax is by thoracocentesis and multiple aspirations may be necessary prior to resolution.

Diagnosis

In neonatal chest disease close correlation with the clinical history is very important in arriving at the correct diagnosis. In the premature infant hyaline membrane disease is the most serious pulmonary abnormality. The presence of the classic chest radiographic findings as described above, in these premature infants is diagnostic. In the term infant tachypnoea of the newborn, amniotic fluid aspiration, meconium aspiration syndrome and neonatal pneumonia may be difficult to distinguish radiographically. A finding of meconium below the vocal cords on laryngoscopic examination together with the presence of coarse pulmonary opacification and air leaks on the chest X-ray is highly suggestive of meconium aspiration syndrome. A history of prolonged rupture of the membranes during later pregnancy or the diagnosis chorioamnionitis in the mother together with coarse patchy pulmonary opacification is a strong pointer towards neonatal pneumonia. Transient tachypnoea of the newborn and amniotic fluid aspiration are benign conditions causing mild clinical symptoms that are transient and seldom require ventilatory support despite the fact that the radiographic changes are occasionally quite marked. Resolution is usually complete in 24–48 h.

The definitive cause of a pleural effusion may be made by examining the aspirated fluid. In infants with a chylothorax the fluid will have a high lymphocyte count. After feeding has been established the fluid will have a milky appearance.

Bibliography

1. Wood BP, Davitt MA, Metlay LA (1989) Lung disease in the very immature neonate: radiographic and microscopic correlation. Pediatr Radiol 20:33–40
2. Swischuk LE (2003) Respiratory system. In: Swischuk LE (ed) Imaging of the Newborn, Infant and Young Child. 5th edn. Williams and Wilkins, Baltimore
3. Donoghue V (ed) (2002) Radiological Imaging of the Neonatal Chest. Springer-Verlag, Berlin Heidelberg New York
4. Newman B (1999) Imaging of medical disease in the newborn lung. Radiol Clin North Am 37:1049–1065
5. Cleveland RH (1995) A radiologic update on medical disease of the newborn chest. Pediatr Radiol 25:631–637

Chest, Thromboembolic Diseases

Edwin J. R. van Beek
Department of Radiology
Carver College of Medicine, University of Iowa Hospitals and Clinics,
Iowa City, USA
Edwin-vanbeek@uiowa.edu

Synonyms

Chronic thromboembolic pulmonary hypertension (CTEPH); Fat embolism syndrome; Pulmonary embolism (PE); Venous thromboembolic disease

Definition

Thromboembolic pulmonary arterial diseases are a spectrum involving the embolization of either blood clot or fat/marrow droplets into the pulmonary arterial circulation.

The vast majority of the spectrum relates to *acute pulmonary embolism (PE)*. This is a syndrome caused by the dislodgement of thrombus within the context of deep vein thrombosis (1). The thrombus material will be caught in the pulmonary arteries, and depending on size and extent of the thrombotic material lung perfusion will be impaired.

Chronic Thromboembolic Pulmonary Hypertension (CTEPH) is the condition that results from recurrent PE or incomplete resolution of significant or extensive acute

pulmonary emboli. The pulmonary arterial bed becomes obstructed, and the result is an increase in pulmonary arterial pressure.

The more generic term for acute pulmonary embolism and deep vein thrombosis is *venous thromboembolic disease* (1) in the acute form. Chronic forms include postphlebitic syndrome, varicose veins, and chronic thromboembolic pulmonary hypertension.

Fat embolism syndrome is a specific type of pulmonary embolism, which occurs in the course of large bone fractures and/or orthopedic manipulations and surgery. This syndrome usually occurs subclinical, but in multiple fractures or with extensive bone marrow surgery (such as the introduction of intramedullary nails), the bone marrow fat will enter the venules from where the central venous system will be reached. As a result, fat droplets will obstruct the pulmonary vascular bed and a rise in pulmonary artery pressure will occur. There is also a humoral response, leading to acute respiratory distress syndrome and (often extensive and fatal) pulmonary edema.

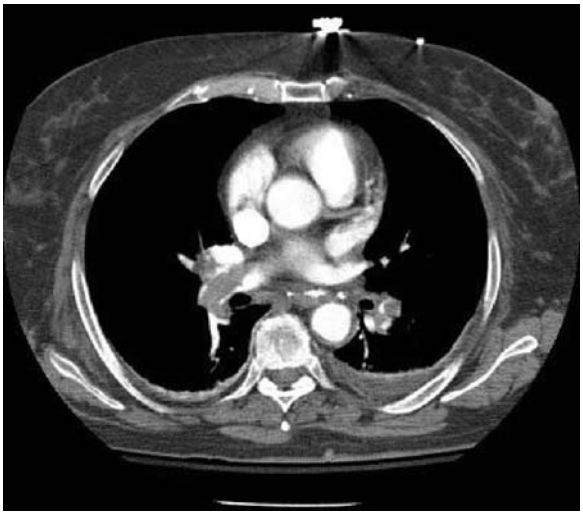

Chest, Thromboembolic Diseases. Figure 1 CT pulmonary angiography demonstrating filling defects in the right main and bilateral lobar pulmonary arteries.

Pathology/Histopathology

The pathology and histopathology depends on the clinical syndrome. The main pathological findings are:

1. Acute pulmonary embolism: this will cause a thrombus mass occluding the lumen of the pulmonary arterial tree. Depending on the extent of the emboli, the heart may also demonstrate acute right over-load, including atrial and ventricular dilatation. A saddle embolus is the term applied to a central large embolus that straddles the main pulmonary artery bifurcation. This type of PE is often (but not always!) immediately fatal. (Fig. 1) demonstrates acute embolism as seen on CT pulmonary angiography.
2. Chronic thromboembolic disease: this will cause mural adherent thrombus mass and intimal hyperplasia due to the incorporation of thrombus material into the vessel wall. This type of disorder will also cause webs (fibrous bands), vessel wall fibrosis, and stenosis as part of the recanalization of thrombus material. (Fig. 2) demonstrates the findings of a mural thrombus in an extremely dilated pulmonary artery as part of the CTEPH spectrum on CT pulmonary angiography (2a) and on MR pulmonary angiography in a different patient (2b). Other examples of findings in CTEPH are included in the Chapter on pulmonary hypertension.CT pulmonary angiogram in a patient with CTEPH demonstrates aneurysmal dilatation of the left upper lobe pulmonary artery with vessel remodeling in the presence of extensive mural thrombus. CTEPH in a different patient demonstrates similar findings as above in a MR angiogram, this time involving the right main pulmonary artery.
3. Fat embolism syndrome is diagnosed by demonstration of fat droplets in the pulmonary capillary bed. In significant fat embolism, there is rapidly increasing obstruction of the peripheral pulmonary arterial bed, resulting in a rapid rise of pulmonary arterial pressure and acute right heart failure and death. To deal with this new pressure gradient, right-to-left shunts may become apparent, such as seen in patients with patent foramen ovale. In these circumstances, paroxysmal embolization and a clinical course similar to that seen in septic endocarditis may develop.

Clinical Presentation

The clinical presentation of thromboembolic pulmonary arterial diseases is highly variable. For PE, it can be divided into acute major events, acute minor events, and chronic insidious development of symptoms. This has led to the introduction of the terminology acute massive PE, acute submassive PE, acute nonmassive PE, and chronic PE (2).

a. Acute massive PE: Patients with large pulmonary embolism or with occlusion of a significant portion of the vascular tree will present with symptoms that are acute in onset and the result of perfusion decrease and strain on the right ventricle. Up to 10% of patients suffer acute coronary arrest or will die within the first

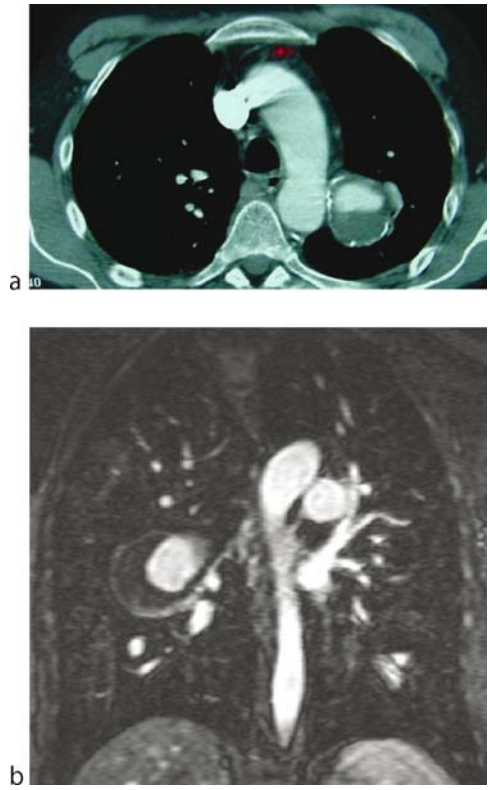

Chest, Thromboembolic Diseases. Figure 2 Chronic thromboembolic pulmonary hypertension. (a) CT pulmonary angiogram in a patient with CTEPH demonstrates aneurysmal dilatation of the left upper lobe pulmonary artery with vessel remodelling in the presence of extensive mural thrombus. (b) CTEPH in a different patient demonstrates similar findings as above in a MR angiogram, this time involving the right main pulmonary artery.

hour of this catastrophic embolism syndrome. Patients will present with circulatory instability (shock), dyspnea and/or chest pain and the "fear of dying."

b. Acute submassive PE: Patients with this level of embolism will present similarly to those with massive PE, with the exception that they are not suffering from hemodynamic instability using routine measures of blood pressure and heart rate. However, right heart strain and right ventricular dysfunction may be diagnosed using echocardiography.

c. Acute nonmassive PE: Many patients with nonmassive PE will present with a plethora of symptoms, ranging from asymptomatic to chest pain, dyspnea, tachycardia, and hemoptysis.

d. Chronic thromboembolic pulmonary hypertension (3): Patients with chronic thromboembolism often present with gradual, progressive shortness of breath, dyspnea on exertion and general lack of energy. They may suffer intermittent episodes of more significant symptoms as discussed above.

e. Deep vein thrombosis and clinically silent PE (1): A significant number of patients will present with leg symptoms, rather than chest symptoms. This is the group of patients who will present with deep vein thrombosis: swelling, calf pain, and red discoloration. Upon further questioning, many will have symptoms of PE, but a significant proportion of PE in this group of patients will be completely asymptomatic.

f. Fat embolism syndrome always presents in the presence of long-bone and/or pelvis fractures. It is often an acute progressive syndrome, leading to right heart failure and in the presence of patent foramen ovale will yield systemic fat embolism (petecchiae, neurological syndromes) similar to left-sided endocarditis.

Imaging

Chest radiography is only helpful in detecting disorders that may mimic PE: pneumothorax, heart failure, pleural effusions, and rib fractures (1, 3). PE can present with pulmonary infarction in 10–15% of patients (usually those with limited cardiorespiratory reserve), which will demonstrate a peripheral area of lung consolidation (►Hampton hump). Other findings include pleural effusions and hyperlucency of lung areas due to vascular obstruction more centrally (►Westermark sign). However, the vast majority of patients with proven PE will have a (nearly) normal chest radiograph.

Pulmonary angiography has long served as the reference method for the diagnosis of PE. However, as it is an invasive technique, this method never gained much popularity. With the increased capabilities of CT, invasive pulmonary angiography has all but vanished from the radiological arsenal (1, 3, 4).

The technique is still important for interventions in extremely sick patients with massive PE (thromboendarterectomy and fragmentation devices have been successfully developed) and as part of the work-up during right heart catheterization in patients with pulmonary hypertension.

CT pulmonary angiography is now the method of choice for the diagnostic management of PE (3, 4). Not only is it capable of detecting PE in central down to subsegmental vessels (Fig. 1), it can also give important alternative diagnoses that help in the management of patients with chest symptoms. It is not surprising, therefore, that there has been a huge demand for this technology in the acute hospital setting. As a result, the prevalence of PE using CT-pulmonary angiography

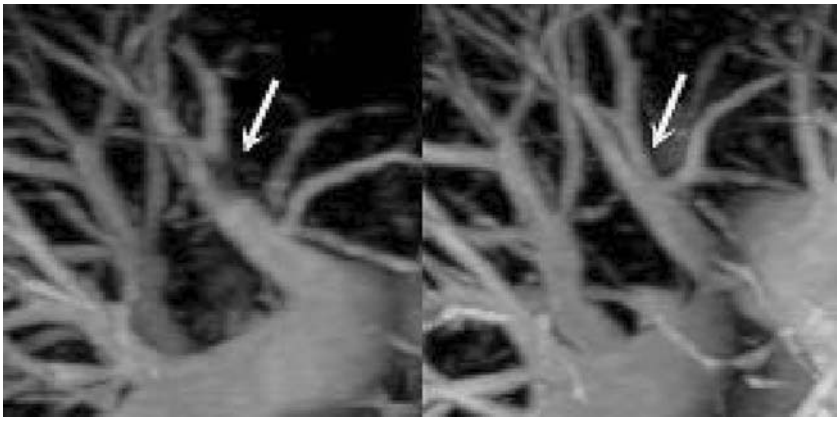

Chest, Thromboembolic Diseases. Figure 3 MR pulmonary angiogram (detail) of patient with pulmonary embolism (left) and following treatment (right).

has decreased from 40–50% in early studies to less than 10–15% in current clinical practice.

Important studies have shown that it is safe to withhold anticoagulant therapy in patients with suspected PE and normal CT pulmonary angiography provided the quality of the study was good. Unfortunately, up to 7% of studies will suffer from technical problems, although this number is decreasing with increasing detector rows in the CT systems.

Echocardiography is the method of choice in patients with massive PE, as it is both bed-side and capable of demonstrating large PE and the sequellae on the heart (1, 2). It has also been applied for assessment of patients with submassive PE and for evaluation of fibrinolytic therapy effectiveness.

Ultrasonography of the leg veins may be applied to detect deep vein thrombosis in the context of venous thromboembolism (1, 2, 4). Both compression and Doppler color ultrasonography have excellent sensitivity and specificity for detection of thrombi in symptomatic patients. However, in asymptomatic patients the diagnostic accuracy of this technique is less favorable, and may not be cost-effective (5).

Magnetic Resonance Imaging has many different techniques, which may be employed for the diagnosis of pulmonary vascular diseases, including MR perfusion, MR angiography, and direct clot imaging (6). Excellent anatomical detail can be obtained (Fig. 3), but presently the technique is usually reserved for difficult cases or where ionizing radiation or iodine contrast agents must be avoided.

Nuclear Medicine

Traditionally, perfusion (-ventilation) lung scintigraphy was the main diagnostic test for pulmonary vascular disease demonstrating the typical mismatch of a perfusion defect and preserved ventilation. With the advent of CT and MRI, this technology has been largely omitted from the diagnostic work-up of acute pulmonary embolism.

Diagnosis

The diagnosis of acute PE is based on demonstration within the pulmonary artery of a filling defect within a pool of contrast. Secondary signs include a cut-off vessel (no contrast at all), (sub) segmental consolidation, or nonenhancement of lung parenchyma.

In CTEPH, both the wall-adherent thrombus material and the secondary signs, including pulmonary artery dilatation, right ventricular and atrial dilatation, right ventricular hypertrophy, and bronchial artery hypertrophy may be demonstrated using CT or MRI.

Fat embolism syndrome is generally diagnosed at autopsy or by broncho-alveolar lavage. Acute right heart failure, ARDS and multiple organ failure are the most common findings, within a setting of long bone and/or pelvis fractures.

Interventional Radiological Treatment

The main interventional treatments for pulmonary vascular diseases are reserved for patients with acute massive PE (thrombo-endarterectomy and fragmentation devices) and for the treatment of right-left shunts in patent foramen ovale with paroxysmal embolization.

Inferior vena cava filters may be employed to support patients with contraindications for anticoagulant therapy, those in whom this therapy fails or in patients who are scheduled to undergo or already underwent pulmonary thrombo-endarterectomy.

Bibliography

1. Oudkerk M, van Beek EJR. Ten Cate JW eds (1999) Pulmonary embolism - epidemiology, diagnosis and treatment. Blackwell Science Publishers, Berlin
2. ESC Task Force on Pulmonary Embolism (2000) Guidelines on management of acute pulmonary embolism. Eur Heart J 21:1301–1336
3. Schoepf UJ, Costello P (2004) CT angiography for diagnosis of pulmonary embolism – state of the art. Radiology 230:329–337
4. Sohne M, ten Wolde M, Buller HR et al (2005) Pulmonary embolism. In: Lipson DA, van Beek EJR. Functional lung imaging. Taylor and Francis, New York, pp 480–498
5. Turkstra F, Kuijer PMM, van Beek EJR et al (1997) Value of compression ultrasonography for the detection of deep venous thrombosis in patients suspected of having pulmonary embolism. Ann Intern Med 126:775–781
6. Van Beek EJR, Wild JM, Fink C et al (2003) MRI for the diagnosis of pulmonary embolism. J Magn Reson Imaging 18:627–640

Chiari Malformation

Chiari Malformation comprises three different cerebellar malformations. The Chiari 1 malformation can occasionally be acquired, but all Chiari malformations are usually congenital. They are due to a lack of expression of the surface molecules, and imaging shows an abnormally small posterior fossa.

►Congenital Malformations, Cerebellar

Child Abuse

►Battered Child Syndrome

Children, Imaging Techniques

Anne Paterson
Royal Belfast Hospital for Sick Children, Belfast, UK
annie.paterson@royalhospitals.n-i.nhs.uk

Definition

The selection of an imaging modality depends largely upon the clinical question that is being asked, but local availability of equipment, the potential risks to the patient from the possible use of sedation or anaesthesia, and the radiation dose involved all need to be considered before the patient is investigated. Communication between radiologists and their clinical colleagues, the use of imaging protocols in common clinical scenarios and the review of request forms by senior radiologists also play an important role in the choice of a particular imaging technique.

Pathology

Imaging

Projection Radiography (Plain Films)

Over a 100 years have passed since the discovery of X-rays by Wilhelm Röntgen and since that time there have been considerable advances in diagnostic imaging techniques, yet plain film radiography remains the most frequently requested radiological investigation.

Basic principles: X-rays are generated, attenuated as they pass through the patient and the resultant X-ray beam emerging from the patient is then made visible by a variety of detectors:

- ►Film-screen (FS): Photographic film is sandwiched between two intensifying screens (made of rare earth materials). The screen fluoresces when it is irradiated and exposes the film. The latent image produced can only be 'read' when the film is (chemically) developed.
- ►Computed radiography (CR) uses a radiographic screen containing a type of phosphor (photostimulable phosphor plate, storage phosphor imaging plate, digital cassette). When the plate is exposed to X-rays, a latent image is formed and stored as electronic charges. A laser beam is used to stimulate the plate and the emitted light is directed to a photomultiplier tube, the electrical output signal of which is digitised. The digitised image can then be read by the radiologist (either on 'hard-copy' laser-printed films or 'soft-copy' workstations). A host of post-processing techniques can be used to improve the quality and appearance of the soft-copy image.
- ►Digital radiography (DR) makes use of caesium iodide (CsI) layered onto an amorphous silicon photodiode panel as a detector. When the CsI crystals absorb X-ray photons, they emit light, which is immediately converted into an electronic charge by the photodiode (no latent image is formed by this technique). Read-out electronics convert this information into an image (which can be printed onto film or viewed on a monitor). As with CR systems, the soft-copy image can be post-processed by the reporting radiologist.

CR and more recently DR are now replacing FS systems. One of the main reasons for this, is the potential

to reduce the rate of repeat films due to poor exposure technique (1), making them a popular choice in paediatric radiology. Both CR and DR systems operate over a wide dynamic range, in contrast to FS systems. An underexposed FS radiograph produces a 'white' film, an overexposed one the familiar 'black' film. The radiologist can read neither and the image must be repeated, increasing the radiation dose to the patient. The separation of image acquisition from display in both CR and DR allows these systems to compensate for inappropriate exposure factors and produce an image of consistent appearance. The phenomenon of 'exposure factor creep' is becoming increasingly recognised in the literature (2); radiographers often choose higher exposure factors, as the images produced are less grainy, and the increased radiation dose can go unnoticed unless regular quality assurance (QA) checks are in place. DR systems perform more efficiently than CR and the potential for dose reduction is greater (3).

Advantages, limitations and uses of projectional radiography: Regardless of the detector system used, projectional radiography is considered a low dose imaging technique. The risk to the patient can be further reduced by the judicious use of lead shields (e.g. for the breast and gonads). Radiographs are rapidly obtained, require no patient preparation, are painless, readily available and relatively cheap.

Projectional radiography is principally used to investigate the skeleton and chest. Only four different anatomical densities can be detected by the radiologist:

- Bone (and other calcifications)
- Soft tissue/fluid
- Fat
- Air

It is also possible to distinguish other densities foreign to the body, such as metal or radiographic contrast media (containing barium or iodine). The radiologist can only appreciate the outline of a structure on a plain radiograph when it is adjacent to a different density: blood vessels (fluid density) are seen coursing through the lungs on a chest radiograph because the surrounding alveoli are filled with air. Many disease processes (particularly those involving the soft tissues) have similar appearances on plain radiographs, and the possible differential diagnoses are vast. Relevant clinical findings and laboratory data help to tailor this list.

Fluoroscopy

Basic principles: Fluoroscopy is an enhanced X-ray technique that utilises an image intensifier tube connected to a closed circuit television system. The function and structure of body systems can be evaluated in real time, for both diagnostic examinations and as a prelude to interventional procedures. In addition, stationary images may be captured and can be viewed immediately on the television monitor. The static images may be radiographic exposures (if high spatial resolution is required), 'fluorograb' images taken during screening or as 'last image hold' from the television monitor. The latter techniques do not involve any further radiation to the patient and are commonly employed in paediatric radiology. Pulsed (as opposed to continuous) fluoroscopy is now considered imperative in paediatric radiology, as radiation dose reductions of over 90% can be achieved, whilst still maintaining imaging quality (4).

Uses: Fluoroscopy is most commonly used to evaluate the gastrointestinal and genitourinary tracts. Contrast media containing either barium sulphate or iodine in solution, can be ingested or introduced per rectum (or via stomas) to give detailed images of bowel anatomy, or instilled via a urinary catheter to outline the bladder. Iodine containing contrast media can also be injected intravenously or intra-arterially to demonstrate vascular anatomy. Angiographic examinations are improved by the use of digital subtraction techniques, whereby the anatomic background detail is removed to leave images showing only the contrast-enhanced vascular tree.

Interventional procedures in paediatric radiology usually require that the patient be sedated or receive an anaesthetic. Fluoroscopic guidance may be employed to place drainage catheters (e.g. into abscess cavities or nephrostomy tubes), for hydrostatic or pneumatic reduction of intussusception, during oesophageal, vascular or tracheal dilatations, and for vascular embolisation procedures.

Computed Tomography

Computed tomography (CT) is now estimated to account for around 15% of a radiology department's workload, but it is a high radiation dose technique and is responsible for 70–75% of the collective population dose from medical radiation (5, 6). Baseline axial 2D image sets are created by this technique, but newer single and multi detector helical scanners allow the radiologist to produce 2D images in any plane, using a workstation. Post-processing techniques can also be used to produce sophisticated 3D reconstructions, which can be of huge benefit to surgical colleagues in operative planning, and have also led to CT being utilised to perform non-invasive peripheral and cardiac angiography, and virtual endoscopy (both bronchoscopy and colonoscopy) examinations.

Basic principles: CT scanners consist of a rotating X-ray tube and a curved bank of detectors both housed within a gantry. The X-ray beam passes through the patient, is recorded by the detectors and an electronic

signal is generated, which is then used to reconstruct the image. In CT, there is a complex relationship between the radiation dose received by the patient and image quality, and the radiologist and radiographer must carefully plan each examination. This is of particular relevance in paediatric CT studies, given the stochastic risks from ionising radiation (7).

The anatomic detail given by CT images is excellent and post-processing techniques can be used to study the different body tissues. Modern CT scanners acquire image data rapidly, lessening the need for sedation and anaesthesia in younger children. Patient preparation is minimal; for some examinations, the child may be required to drink oral contrast medium (a dilute solution of barium or a water-soluble iodinated agent), though this can generally be mixed with juice or flavourings to improve palatability. An indwelling IV cannula is also commonly required and the distress at its insertion can be minimised by the use of topical anaesthetic agents. The cannula allows IV contrast medium to be injected during the examination, for easier inspection of solid organs and for direct visualisation of blood vessels. Contrast agents are valuable in paediatric CT scanning, not least because many children lack body fat, making interpretation of the abdomen and pelvis difficult without the benefits of contrast media.

Uses: Traditionally, CT has been particularly useful in the staging and follow-up of tumours, for evaluating trauma and infections, to study the lung parenchyma and mediastinal structures, and for cranial imaging. More recently, CT use has increased to include the investigation of suspected appendicitis or renal calculi, and to provide detailed anatomy of fracture sites (both acutely and following surgery).

Ultrasound

Basic principles: Piezoelectric crystals, contained within an ultrasound (US) probe (transducer), emit high-frequency sound waves when subjected to an alternating current. These sound waves pass through the patient's body, being reflected back towards the probe when tissues of different acoustic properties interface. The sound 'echoes' generate a signal within the crystal that is used to form the image. This process occurs so rapidly, that the images can be generated in real time. Bone absorbs the sound completely, air reflects it, which is why acoustic 'shadows' are seen behind them. Fluid-filled structures, such as the bladder transmit sound well, which is why a stronger 'echo-signal' is seen behind them. The time taken for the echoes to return to the crystal is used to determine a tissue's location in the body.

Techniques, advantages and uses: In medical US, transducer frequencies of between 1 and 15 MHz are used. Higher frequency probes provide exquisite detail, but have only limited tissue penetration. The converse is true for lower frequency probes, which are needed to image larger patients or deeper structures. The small size and lack of obesity in many children mean US images of excellent quality can be obtained. In addition, the anatomy of the growing skeleton, means that non-ossified bone can be imaged, e.g. to allow visualisation of the spinal cord or the hip joints. The fontanelles in an infant's skull allow imaging of the brain that is not possible in adult patients. US is commonly used to examine the solid intra-abdominal organs, the heart in echocardiography, superficial organs such as the thyroid gland and testes, and soft tissue masses. Bowel US for suspected hypertrophic pyloric stenosis and appendicitis are regularly requested, and the use of US as a guidance imaging modality for interventional procedures, voiding cystourethrograms and reduction of intussusception are common. The choice of US as the imaging modality for some of these clinical problems will be largely dependent upon local expertise.

The major advantage of US in paediatric radiology is that it does not involve ionising radiation, meaning it is safe to use in all patients, and can be performed repeatedly. US is portable and widely available. It is painless, requires little in the way of patient preparation and patient sedation is unnecessary, given that the examinations can generally be performed rapidly. High-quality US images do, however, require a skilled paediatric sonographer to perform the examination.

Newer developments in the field of US include tissue harmonics, which particularly improve the image quality in larger patients and the increased use of 3D imaging. The term '4D' US has been coined; it simply refers to 3D images being obtained in real time, with time representing the fourth dimension.

Colour Doppler and Doppler Interrogation

Basic principles and uses: The information obtained from an US examination can be increased with a technique that utilises the Doppler effect (a perceived change in the frequency of a sound emitted by a moving source). In US exams, the moving sources are erythrocytes, with the echo undergoing a frequency shift depending upon the speed and direction of blood flow within a vessel. This data can be colour-coded (by convention, flow towards the probe is red and away from the probe is blue, but this is arbitrary) or can be presented in graphical form to show the shape of the pulse wave and the velocity of the flowing blood. In paediatric radiology, Doppler is especially useful to look for vessel patency in children with central lines (before and after insertion), to assess vessels in relation to

new and known malignancies, following organ transplantation, for assessment of renal blood flow in children with suspected acute pyelonephritis and also during echocardiography. US contrast media are also available, though their use in paediatric radiology is currently limited. They may be used in echocardiography, particularly in the assessment of suspected arteriovenous malformations, in sonocystography, to aid the detection of vesicoureteric reflux and in the assessment of organ and tumour perfusion. These agents are injected intravenously and contain numerous microbubbles, which act as strong reflectors of the US beam.

Magnetic Resonance Imaging

Basic principles: Magnetic resonance imaging (MRI) is technically the most complex of the currently available imaging modalities, and gives vast anatomic and physiological detail of the body. In their most simplistic terms, the physics of MRI involve the patient being placed in a strong magnetic field. Here, those atoms in the body, which have magnetic moment (more protons than neutrons in the nucleus), align themselves with the magnet. A radiofrequency (RF) pulse is then applied to disturb this formation. When the RF pulse is switched off, the atoms realign with the main magnetic field and give off a signal as they do so. This signal is minute, but multiplied many millions of times, due to the number of (hydrogen) atoms within the human body; it is this signal that is used to create the image. Many RF pulses are required to form the image, and the timing, length and type of the RF pulses, give the different sequences used in modern MRI. An individual MR sequence can take less than 1 to longer than 15 min, and each examination is comprised of several sequences. The total time taken for an MR study is between 30–60 min. Small amounts of patient motion can destroy the images, as they cannot be reconstructed until an entire sequence is complete. Many children cannot hold still for the length of time required and frequently require sedation or general anaesthesia for this type of examination.

Both oral and IV contrast media are utilised in MRI, though not frequently in children. Oral MR contrast agents consist of ferrite compounds that accumulate in the reticuloendothelial system. Gadolinium chelates are the most common IV contrast agents; they work by shortening the T1-relaxation times of protons, increasing the signal from tissues and organs on T1-weighted sequences.

Advantages and uses of MRI: Excellent contrast resolution and multiplanar imaging are the major benefits of MR. The most commonly performed MR examinations are those of the central nervous system; posterior fossa detail and grey/white matter differentiation are well demonstrated. MR is also the imaging modality of choice to evaluate many musculoskeletal problems: trauma, tumours (both benign and malignant, pre- and post-operatively), bone marrow disorders and joint disease. Other indications include tumour staging and follow-up, the mapping of vascular malformations and their blood supply, assessment of the airway, examination of both children and adults with congenital heart disease, the study of genito-urinary tract anatomy and in the case of the kidneys themselves, function.

Newer techniques include diffusion-weighted MR studies (based upon the Brownian motion of the water molecules in a tissue), which are useful in the detection of tissue ischaemia, functional MRI (based upon the increase in blood flow to the local vasculature that accompanies neural function), as an adjunct to neurosurgical planning and contrast-enhanced dynamic MRI. The latter technique is useful in cardiac studies, to calculate for example, the ventricular ejection fraction and blood flow across septal defects, within shunts and in stenotic vessels. Contrast-enhanced dynamic MRI is also useful in MR urography (often in conjunction with a dose of diuretic), where renal function can be mapped to provide information analogous to a radioisotope MAG 3 study.

Nuclear Medicine

Basic principles: A radiopharmaceutical is a minute quantity of a drug to which a radionuclide is tagged. This compound may then be injected, ingested or inhaled and is delivered to a specific organ or body tissue. Once it reaches its target, the radionuclide emits gamma radiation, which is detected by a scintillation (gamma) camera. Computer software aids in image reconstruction, based upon the position in the body from which the radiation was emitted. Using nuclear medicine techniques, it is possible to study the function of different organs, tissues and bones. Most commonly, 2D planar images are produced, but using a technique called SPECT (▶single photon emission computed tomography), the images can be reconstructed in multiple planes. The anatomic detail obtained in nuclear medicine is limited.

Advantages and uses of nuclear medicine: Nuclear medicine studies are divided broadly into two types: dynamic and static. The former may be used to study, for example gastro-oesophageal or vesicoureteric reflux, regional blood perfusion, gastric emptying, biliary or renal excretion. Static studies may be used to study more specific radiotracer absorption, such as by the kidneys to evaluate for acute pyelonephritis or focal renal scars, or by the bone cortex when evaluating for metastatic disease, osteomyelitis or fractures. Other commonly requested paediatric radioisotope studies include the study of

primary tumours, such as neuroblastoma, lung function assessment and to aid in the evaluation of children with epilepsy.

New developments: Probably the fastest developing area in nuclear medicine is the use of PET (►positron emission tomography) and PET-CT. These techniques make use of short-lived, positron-emitting isotopes, to study biochemical and physiological processes within the body. The most commonly used isotope is ^{18}F-fluorodeoxyglucose (FDG), which is a glucose analogue that accumulates in normal cells, inflammatory lesions and malignant tumours. The technique works upon the principle that the abnormal tissues take up and metabolise the isotope at a faster rate than do normal tissues. In common with other nuclear medicine examinations, the anatomical information from a PET scan is limited, but fusing the axial PET images with the corresponding CT study, is a sensitive technique for localising a lesion. PET and PET-CT are not yet widely available. They rely upon on-site or regional isotope production in a cyclotron; with express delivery of the isotope to the nuclear medicine department (the isotopes are very short-lived). The technique is expensive and delivers a higher radiation dose to the patient, than do the more common nuclear medicine examinations. Due to the length of time a study takes, a child is likely to require sedation or anaesthesia. In paediatric radiology, PET has mainly been used in the staging and follow-up of children with lymphomas and in the pre-operative assessment of children with epilepsy.

Diagnosis

There are important anatomic, physiological and psychological differences between children and adults, and whilst the paediatric radiologist has all of the imaging modalities his or her adult colleagues have at their disposal, the choice of which modality to use in a given clinical scenario, will be governed in part by the special needs of an individual child. Communication skills are vital to all radiologists, but a paediatric radiologist must be able to explain procedures and answer questions in a language that is comprehensible to both a patient's (adult) carers, and to the child himself. The cooperation of a child for a particular study is likely to depend upon how successful the radiologist has been in this task, and dictates whether or not the images obtained are of diagnostic quality.

Bibliography

1. Don S, Albertina MJ, Ammann DL et al (1995) Soft-copy computed radiography in neonatal and pediatric intensive care units: cost savings analysis. Radiology 197:501–505
2. Willis CE, Slovis TL (2004) The ALARA concept in pediatric CR and DR: dose reduction in pediatric radiographic exams—a white paper conference executive summary. Pediatr Radiol 34 (Suppl 3): S162–S164
3. Samei E, Hill JG, Frey GD et al (2003) Evaluation of a flat panel digital radiographic system for low-dose portable imaging of neonates. Med Phys 30:601–607
4. Brown PH, Thomas RD, Silberberg PJ et al (2000) Optimization of a fluoroscope to reduce radiation exposure in pediatric imaging. Pediatr Radiol 30:229–235
5. Linton OW, Mettler FA (2003) National conference on dose reduction in CT, with an emphasis on pediatric patients. Am J Roentgenol 181:321–329
6. Wiest PW, Locken JA, Heintz PH et al (2002) CT scanning: a major source of radiation exposure. Semin Ultrasound CT MR 23:402–410
7. Brenner DJ, Elliston CD, Hall EJ et al (2001) Estimated risks of radiation-induced fatal cancer from pediatric CT. Am J Roentgenol 176:289–296

Chloroma

►Hepatic Sarcoma

Cholangiocarcinoma, CC

►Neoplasms, Bile Ducts

Cholangiocellular Carcinoma, CCC

►Neoplasms, Bile Ducts

Cholangiography

Introduced in 1954 as intravenous cholangiography for the visualization of the common bile duct, it consists in intravenous injection of an iodinated contrast medium that is excreted by hepatocytes allowing the opacification of the biliary ducts. Gallbladder visualization was not included in cholangiography. Intravenous cholangiography has been replaced by direct cholangiography, which includes percutaneous transhepatic cholangiography

(PTC), endoscopic retrograde choledochopancreatography (ERCP), perioperative cholangiography, and trans-Kehr cholangiography.
►Biliary Anatomy

Cholangitis

Thomas Helmberger[1], Carlo Bartolozzi[2], Paola Vagli[2]
[1]Clinic of Radiology and Nuclear Medicine, University Hospitals Schleswig-Holstein Campus, Luebeck
[2]Department of Diagnostic and Interventional Radiology, University of Pisa, Italy
thomas.helmberger@uni-luebeck.de
bartolozzi@do.med.unipi.it

Synonyms

Acute cholangitis; AIDS cholangiopathy; Ascending cholangitis; Bacterial cholangitis; Bile duct inflammation; Chemotheraphy-induced cholangitis; Cholangitis due to scolicidal agents; Clonorchiasis; Eosinophilic cholangitis; fascioliasis; Fungal cholangitis; Ischemic cholangitis; Primary sclerosing cholangitis; Recurrent pyogenic cholangitis

Definition

Cholangitis means inflammation of the bile ducts. The term applies to inflammation of any portion of the biliary ducts, from the liver to the gallbladder and intestine. The inflammation is produced by infection or some other cause (toxic agents or ischemic or autoimmune disorders). Bile duct inflammation, in either the acute or chronic form, may result in a fibrosing process in some instances (primary or secondary sclerosing cholangitis).

Pathology/Histopathology

Cholangitis, Bacterial

►Cholangitis, bacterial also called ►cholangitis, ascending or ►cholangitis, acute is an acute infection of the biliary tree with the potential to cause significant morbidity and mortality. The pathogenesis of cholangitis requires stasis or obstruction of bile flow, which predispose to subsequent infection. Choledocholithiasis is the most common cause of obstruction. Strictures, stenosis, tumors, choledochal/biliary cysts, and ►sump syndrome have also been described as causes of bile stasis and cholangitis. Recently, endoscopic manipulation and stents placement have increasingly been reported as causes of benign strictures and subsequently of cholangitis. Hepatobiliary or pancreatic head malignancies are less common causes of biliary obstruction and subsequent bile contamination.

Bacteria are not normally present in bile or are present only in very small amounts; however, the incidence of bactibilia increases in cases of gallbladder and common bile duct stones. The most common organisms found are *Escherichia coli*, *Klebsiella*, *Enterobacter* species, enterococci, and group D streptococci. Bacteria most frequently infect the bile directly from the gut or through the lymphatics or vascular supply; infection thereby ascends into the hepatic ducts. The development of increased biliary pressure pushes the infection into the biliary canaliculi, hepatic veins, and perihepatic lymphatics, leading to bacteremia. The infection can present suppurative features.

Cholangitis is reported in all races but is relatively uncommon in Western countries, where it occurs in association with other diseases that cause biliary obstruction and bactibilia. The condition is reported in both females and males and has no clear predominance. Otherwise, gallstones are more common in women, and cholangitis due to gallstones shows a higher prevalence in females. The condition mostly occurs in adults, with a reported median age at onset of 50–60 years (1, 2).

Cholangitis, Sclerosing Primary

►Primary sclerosing cholangitis (chol, PS) (PSC) is a chronic, idiopathic, fibrosing inflammatory disorder affecting the bile ducts (both intrahepatic and extrahepatic) leading to bile duct obliteration, cholestasis, and biliary cirrhosis. The term "primary" is used to differentiate this condition from biliary strictures due to bile duct injury, cholelithiasis, ischemia, and chemical injury (secondary sclerosing cholangitis). Peak incidence occurs in the third and fourth decades of life, and a male predominance appears to exist. The etiology remains unknown, although most authors believe it to be an autoimmune process because it may be associated with other autoimmune diseases such as retroperitoneal fibrosis, mediastinal fibrosis, and Sjögren syndrome. A strong association with inflammatory bowel disease, especially ulcerative colitis, has also been noted.

Pathophysiologically, the biliary injury may be initiated by an immune-mediated destruction of the hepatobiliary tract that is perhaps caused by transient infection or the absorption of bacterial products in genetically predisposed individuals with colonic disease.

Bacteria, toxins, viral infections (reovirus and cytomegalovirus), and genetic factors (increased frequency of HLA-B8 and HLA-DR3) have also been proposed as predisposing agents. These lend support to the theory that immunologic and genetic mechanisms may both be involved in the pathogenesis. Histological findings include nonspecific features such as periductal concentration of mononuclear cells, ductular proliferation, aspects resembling chronic active hepatitis, and specific findings including concentric obliterative fibrosis of interlobular bile ducts with the presence of intrahepatic cholangiectasis and ductal obliteration. Bile ducts grossly display multiple short strictures, pseudodiverticula, and wall thickening. Saccular dilatations like those seen in Caroli's disease are uncommon.

The diagnosis is based on a combination of clinical features and a cholestatic biochemical profile, along with typical cholangiographic abnormalities confirmed by liver histology and the exclusion of secondary causes of sclerosing cholangitis. PSC is usually progressive, leading to cirrhosis, portal hypertension, and liver failure. An increased incidence of cholangiocarcinoma and gallbladder carcinoma is reported in these patients. In adult patients, the median period of survival from the time of diagnosis is 9–11 years but is shorter for patients who are symptomatic at the time of diagnosis. Treatment is usually palliative and includes medical therapy with choleretic or immunosuppressive therapy or endoscopic or percutaneous mechanical dilation of dominant strictures. Liver transplantation remains the only effective therapeutic option for patients with end-stage liver disease from PSC (3).

Cholangitis, Recurrent Pyogenic

Recurrent pyogenic cholangitis, also called oriental cholangiohepatitis, intrahepatic pigmented calculus disease, or hepatolithiasis, is a complex hepatobiliary disease characterized by chronic inflammation of the bile ducts attributed to parasite influx. In endemic areas (Southeast Asia), parasites such as *Clonorchis sinensis* and *Ascaris lumbricoides* can inhabit the bile ducts, causing ductal damage and strictures. Other parasites such as *Opistorchis viverrini*, *Fasciola hepatica*, and *Entamoeba* have also been implicated. Recurrent pyogenic cholangitis is rarely observed in Western countries but may be diagnosed in native Asian people, in whom it tends to be less severe. The infection is typically chronic and recurrent, leading to progressive destruction of the bile ducts and secondary biliary cirrhosis. The primary histopathologic changes of recurrent pyogenic cholangitis are proliferative fibrosis of bile ductal walls, with inflammatory infiltration of the portal tracts and periductal abscesses. Grossly multiple strictures associated with marked dilatation upstream from the stenotic tracts can be observed both in the intrahepatic and extrahepatic bile ducts. Marked enlargement of intrahepatic and extrahepatic ducts may be present. The nidus for stone formation is provided by the presence of secondary bacterial infection, whereas brown-pigmented bile stones can be frequently observed inside bile ducts. Intraductal stones can lead to progressive biliary obstruction and recurrent infection, resulting in the formation of multiple cholangitic hepatic abscesses, biliary strictures, and, eventually, severe hepatic destruction, cirrhosis, and portal hypertension. An increased incidence of cholangiocarcinoma is also reported (4).

Clinical Presentation

Cholangitis, Bacterial

Cholangitis ranges from light forms to fulminant destructive sepsis associated with multiple organ failure. In 1877, Charcot described a triad of findings related to cholangitis: right upper quadrant pain, fever, and jaundice. In 1959, Reynolds and Dargon described a more severe form, adding two other signs: septic shock and mental confusion (Reynolds pentad). A history of past symptoms of gallbladder colic or recent biliary tract manipulation associated with fever, right upper quadrant pain, and jaundice is highly suggestive of cholangitis. Other signs and symptoms include chills, rigor, itching, acholic or hypocholic stools, and mild hepatomegaly. Laboratory findings include leukocytosis, hyperbilirubinemia (patients with malignant obstruction generally have significantly higher bilirubin levels than those with benign obstruction), and elevated alkaline phosphatase levels. Elevation of transaminases and serum amylase levels is possible in cases of concurrent pancreatitis due to stone impaction at the ampulla of Vater and secondary obstruction of the pancreatic duct. Blood culture findings are positive in nearly half of the patients. Bile culture findings are positive in nearly all patients. With increasing degrees of sickness, there is an increased likelihood of complications such as liver failure, hepatic abscesses, bacteremia, gram-negative sepsis, and acute renal failure. The prognosis is usually severe, although it improves with early antibiotic treatment and appropriate drainage and decompression of the biliary tract as needed. Factors associated with poor prognosis include advanced age, female gender, acute renal failure, preexisting cirrhosis, and malignant biliary obstruction (1, 2).

Cholangitis, Sclerosing Primary

The onset and progression of PSC tend to be insidious, and some patients may be affected without having

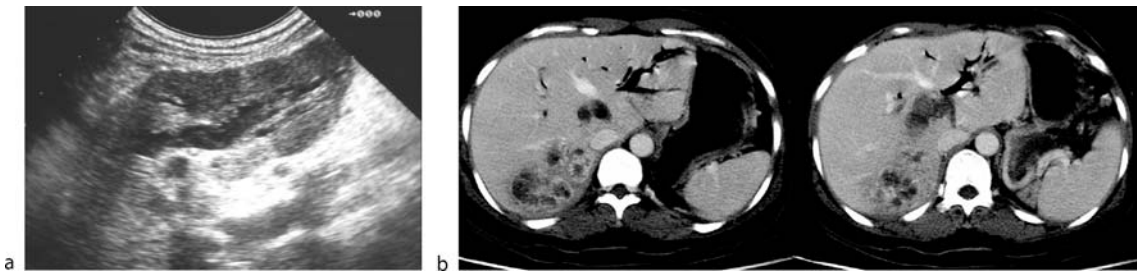

Cholangitis. Figure 1 (a) Bacterial cholangitis. Ultrasound examination shows echogenic material within a dilated bile duct in the left lobe. (b) Bacterial cholangitis. Computed tomographic image displays aerobilia in the left lobe and inflammed, dilated bile ducts in the right lobe. Inflammed biliary walls are concentrically thickened, enhancing after contrast medium administration and surrounded by parenchymal hypodensity due to edema.

symptoms. Patients may present with nonspecific signs, including progressive fatigue, abdominal pain, fever, and intermittent jaundice, or with cholestasis and complications of cholestasis such as pruritus, cholangitis, and fat malabsorption. Additionally, some patients may show the stigmata of chronic liver disease and cirrhosis at the time of presentation.

Biochemical analysis reveals increased levels of serum bilirubin and alkaline phosphatase in most patients, with a mean increase in the alkaline phosphatase level to three times the upper limit of normal. Serum transaminase levels may be normal or elevated. Perinuclear antineutrophil cytoplasmic antibodies (pANCAs) have been found in most patients with PSC. The presence of pANCAs is associated with a more severe course of autoimmune liver disease (3).

Cholangitis, Recurrent Pyogenic

Clinical presentation is characterized by recurrent attacks of abdominal pain, fever, and jaundice caused by intrahepatic ductal strictures and calculi. The therapeutic approach is ruled by the complete clearance of calculi and debris from the biliary tract and the elimination of bile stasis to prevent recurrent attacks of the disease. Therefore, hepatolithiasis is difficult to eradicate, and for effective treatment, accurate topographic cholangiographic evaluation of disease distribution is required before surgical intervention (surgical resection of the affected portion of the liver and the creation of biliary–enteric anastomosis to allow adequate biliary drainage) (4).

Imaging

Cholangitis, Bacterial

Computed tomography (CT) and ultrasound (US) are commonly employed to diagnose biliary dilation. Endoscopic retrograde cholangiopancreatography (ERCP) or percutaneous transhepatic cholangiography (PTC) may directly visualize the biliary ducts and treat the obstruction in a unique session. A paramount view of the biliary tree may also be achieved by means of magnetic resonance cholangiopancreatography (MRCP). Conventional radiography plays an inferior role in the diagnosis of acute cholangitis, showing only indirect signs such as adynamic ileus, radiopaque gallstones, and aerobilia after endoscopic manipulation or in cases of bilioenteric fistula.

US is the modality of choice for gallstones and cholecystitis but is not completely reliable for choledocholithiasis in all patients. US is also sensitive for diagnosing and differentiating intrahepatic from extrahepatic dilatation, including common bile duct dilatation, but it may fail in establishing the cause of stenosis (stone vs. stricture). Purulent bile can be identified as intraluminal echogenic material within dilated bile ducts (Fig. 1a). Furthermore, US can display other abdominal organs (gallbladder, aorta, pancreas, liver), thereby excluding other potential causes of acute abdominal pain. Complications such as liver abscess can also be detected.

CT depicts biliary dilatation and adds further information to provide the precise site of obstruction and also displays inflammation of the biliary tree walls or eventual aerobilia. Thickening of the bile duct walls, either concentric or diffuse, may be underlined after contrast enhancement; increased attenuation of bile or aeroblia may also be displayed (Fig. 1b). Cholangitis may also be present with no visible sign on CT. Potential causes and complications of cholangitis (ampullary tumors, liver abscesses) or pathologies that clinically mimic cholangitis and must be distinguished from cholecystitis, biliary colic, mesenteric ischemia, or ruptured appendix may be displayed by CT.

Magnetic resonance (MR) imaging resembles CT findings without further specific contribution to the diagnosis. Cholangiographic acquisitions depict irregularities of the walls of the bile ducts associated with filling

defects that may be due to stones or sludge, and can accurately determine the site of blockage.

ERCP and PTC may be used for diagnostic and therapeutic purposes, allowing stones to be removed and strictures resolved. Endoscopic biliary drainage and decompression have mostly replaced surgery as the initial treatment of severe cholangitis. In unstable patients, a reasonable option for decompressing the biliary tract is percutaneous biliary drainage (2).

Cholangitis, Sclerosing Primary

US findings may be normal in about half of the patients. In some patients, US may show only unspecific features, including intrahepatic and extrahepatic ductal dilatation, or signs of cirrhosis such as increased echogenicity and heterogeneity of liver parenchyma. Splenomegaly and ascites are observed in cases of portal hypertension. US cannot display bile duct abnormalities unless there is dilatation. Sludge or stones may be present in long-standing cases, presenting as echogenic intraductal structures. Wall thickening and intraductal protrusions may be depicted in the common bile duct. CT signs of primary sclerosing cholangitis are quite specific, including randomly dilated small peripheral ducts without apparent connection to the central duct, which are referred to as skip dilatation or knoblike appearance. After contrast medium administration, regular or nodular wall thickening may be appreciated.

Peripheral wedge-shaped areas of high T2 signal intensity and dilatation of bile ducts are characteristic MR findings in PSC.

Cholangiographic techniques (both invasive PTC/ERCP and noninvasive MRCP) may depict typical changes in intrahepatic and extrahepatic bile duct morphology.

The cholangiographic findings depend on the stage of the disease and include multifocal, intrahepatic bile duct strictures alternating with normal-caliber ducts, which sometimes produce a beaded appearance. Early phases present with short annular intrahepatic strictures, randomly distributed, alternating with normal or slightly dilated segments, with a distinctive acute-angle branching pattern. Strictures usually occur at the bifurcation of ducts and are out of proportion with respect to proximal ductal dilatation. Progressive fibrosis and periductal inflammation cause an increase in strictures and duct obliteration, avoiding opacification of peripheral ducts on ERCP, and producing a "pruned tree" appearance. Irregular narrowing with small diverticular marginal protrusions or shaggy contours is typically found in extrahepatic ducts. Nonspecific cholangiographic findings include webs, diverticula, and stones.

ERCP shows a higher success rate in the absence of dilated intrahepatic ducts with respect to PTC and represents the standard of reference for diagnosing PSC because the clinical, biochemical, and hepatic histological findings are usually nonspecific. ERCP provides a high sensitivity regarding peripheral intrahepatic duct abnormalities and allows interventional procedures such as mechanical dilation of obstructing strictures, stent placement, and biopsy.

MRCP is a suitable noninvasive alternative method for detecting and localizing bile duct obstruction and choledocholithiasis. By using heavily T2-weighted sequences, the signal of static or slow-moving fluid-filled structures such as biliary and pancreatic ducts is greatly increased, resulting in increased duct-to-background contrast. Advantages of MRCP include better demonstration of ducts proximal to an obstruction or tight stenosis, and when combined with conventional T1- and T2-weighted sequences, the ability to generate an anatomical imaging of extraductal disease. However, MRCP provides less spatial resolution than ERCP, thereby decreasing the sensitivity to peripheral ductal abnormalities. On MRCP, the presence of stenoses is usually deduced when there is prestenotic dilatation (Fig. 2); however, in the initial stages of stenosis, there is only temporary dilatation. As a result, these early stenoses may remain undetected at MRCP. In addition, the extent of a focal short stricture, especially of the common hepatic duct, may be overestimated at MRCP for the ducts collapsed downstream of the stenosis. The visualization of mildly dilated peripheral ducts that do not connect to the central ducts is a characteristic sign on MRCP (3).

Cholangitis, Recurrent Pyogenic

Pigmented intrabiliary calculi are hardly visualized by conventional radiography due to their low opacity. US

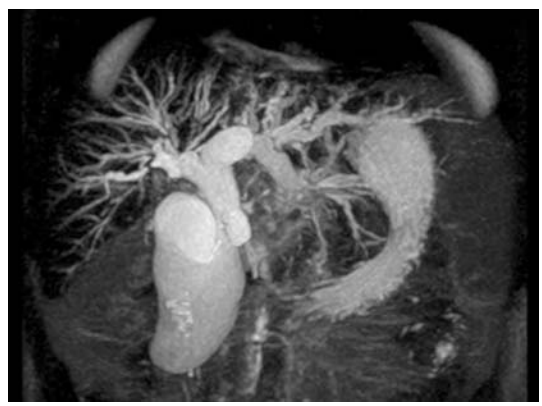

Cholangitis. Figure 2 Magnetic resonance cholangiography. This three-dimensional MIP reconstruction shows the typical aspect of sclerosing cholangitis. (Courtesy of Dr. Piero Boraschi)

can visualize intrahepatic and extrahepatic bile duct dilatation, biliary stones, and coexisting parenchymal abnormalities, such as hepatic atrophy, abscess, and biloma. Other suggestive US features are localized dilatation of the lobar or segmental bile ducts, increased periportal echogenicity, and fibrous thickening of the duct walls with increased wall echogenicity. Pigmented stones usually show a medium echogenity with a variable degree of acoustic shadowing, and the association in some instances of aerobilia determines a low capacity of US for detecting ductal stones. Also, US poorly visualizes dilated ducts completely filled by sludge or calculi.

CT may depict pigment stones as hyperdense to isodense structures relative to their degree of calcification. CT can also better appreciate on precontrast scans the presence of calculi inside significantly dilated ducts and provides assessment of the spatial extent of ductal involvement. A significant enhancement of the involved ductal walls as well as of periductal tissues, suggesting inflammation, can be observed after contrast medium administration. CT even allows accurate depiction of coexisting hepatic parenchymal complications such as intrahepatic abscesses, biloma, and segmental or lobar atrophy.

Cholangiographic findings include multifocal strictures and dilatation of the intrahepatic bile ducts, disproportionate dilatation of the extrahepatic bile ducts unrelated to strictures or stones, straightening and rigidity of the ducts, a right-angle branching pattern, and decreased arborization. In rare instances, cholangiectasis or "bile lakes" can occur from progressive obstruction and inflammation. Stones determine filling defects in the opacified bile ducts. When the calculi completely obstruct the orifice of the segmental or subsegmental bile ducts, they cannot be detected (missing duct sign). Direct cholangiography, such as ERCP and PTC, has been the most accurate way to obtain an accurate topographic description of the biliary tree by depicting the full spectrum of ductal changes and calculi. However, these techniques have limitations, especially in cases of high-grade stenosis, impacted calculi, and complete ductal obstruction, and are invasive with an increased risk of septic complications. Conversely MRCP rendering of the stationary fluids allows noninvasive depiction of the entire biliary tree despite obstruction or stenosis. Parenchymal atrophy is seen as slightly hyperintense areas with reduced volume, while bile duct dilatation and biloma may be depicted regardless of their communication with the bile duct (4).

Nuclear Medicine

Cholangitis, Bacterial

Biliary scintigraphy with ^{99m}Tc-radiolabeled molecules such as iminodiacetic acid derivatives is a functional study showing high sensitivity. It is associated with positive results before the ducts result in enlargement on US, but high bilirubin levels may decrease the study's sensitivity. Obstruction of the common bile duct causes a lack of visualization of anatomic details and of activity within the small intestine.

Diagnosis

Cholangitis, Bacterial

The diagnosis is obtained in most cases on the basis of clinical and laboratory findings and should be suspected in patients with a history of past symptoms of gallbladder colic or recent biliary tract manipulation. A diagnostic imaging work-up must be done to confirm the diagnosis and to depict potential causes and the site of biliary obstruction.

Cholangitis, Sclerosing Primary

Diagnosis is usually achieved by means of the typical cholangiographic pattern. Histological analysis is used only for confirmation because it shows only nonspecific inflammatory fibrosis of the portal triads and a paucity of bile ducts. Differential diagnosis must encompass other causes of secondary sclerosing cholangitis or nonsclerosing processes that mimic primary sclerosing cholangitis at cholangiography. These include strictures or stones complicating chronic bacterial cholangitis, parasitic or ►fungal infection of the bile, cholangitis related to acquired immunodeficiency syndrome (AIDS), ischemia due to treatment with chemotherapeutic agents or to hepatic arterial thrombosis complicating liver transplantation, previous bile duct surgery, congenital biliary anomalies, and rare entities such as ►eosinophilic cholangitis.

In definitely dilated ducts that simulate primary sclerosing cholangitis, one should consider other sclerosing ductal processes, such as ascending cholangitis or primary sclerosing cholangitis complicated by cholangiocarcinoma (3).

Cholangitis, Recurrent Pyogenic

In patients from endemic areas, the presence of a characteristic clinical history associated with imaging features including predominantly left-sided findings should prompt consideration of this diagnosis. Diffuse, uniform dilatation of the intrahepatic bile ducts, particularly in the periphery of the liver, with thick enhancing walls and the absence of extrahepatic biliary dilatation, should also raise suspicion for ►clonorchiasis. Other causes of sclerosing and chronic cholangitis must be excluded (4).

Bibiliography

1. Lipsett PA, Pitt HA (1990) Acute cholangitis. Surg Clin North Am 70(6):1297–1312
2. Balthazar EJ, Birnbaum BA, Naidich M (1993) Acute cholangitis: CT evaluation. J Comput Assist Tomogr 17(2):283–289
3. Vitellas KM, Keogan MT, Freed KS et al (2000) Radiologic manifestation of sclerosing cholangitis with emphasis on MR cholangiopancreatography. Radiographics 20(4):959–975
4. Park MS, Yu JS, Kim KW et al (2001) Recurrent pyogenic cholangitis: comparison between MR cholangiography and direct cholangiography. Radiology 220(3):677–682

Cholangitis due to Scolicidal Agents

Form of secondary sclerosing cholangitis due to injection of scolicidal agents into hydatid liver cysts directly communicating with the bile duct system.
▶Cholangitis

Cholangitis, Acute

Acute bacterial infection of the bile ducts
▶Cholangitis

Cholangitis, Ascending

Also called bacterial cholangitis, ascending cholangitis is usually determined by bacterial (gram-negative) contamination of an obstructed biliary system. The role of MRCP or ERCP is to enable diagnosis of the underlying cause of the obstruction, while the diagnosis of ascending cholangitis is clinical. Clinical presentation usually occurs with the classic Charcot triad of abdominal pain, fever, and jaundice. Complications such as liver abscess and sepsis can occur when increased ductal pressure causes necrosis of the duct wall with reflux of infected bile into the portal triads.
▶Cholangitis

Cholangitis, Bacterial

Also called ascending cholangitis or acute cholangitis, this is a bacterial infection of the biliary tree. Development of cholangitis requires stasis or obstruction of bile flow, which subsequently becomes infected. Diagnostic imaging may confirm diagnosis and reveal the causes or the site of obstruction.
▶Cholangitis

Cholangitis, Chemotherapy-induced

Secondary sclerosing cholangitis characterized by the presence of strictures in the common hepatic duct occurring in patients with metastatic liver disease, treated by means of hepatic arterial infusion of chemotherapeutic agents such as floxuridine. Hepatic toxic effects can develop because of a high rate of extraction on the first pass through the liver. Characteristic features include an inflammatory, fibrosing process in the portal triads, causing narrowing or occlusion of the bile ducts that simulates primary sclerosing cholangitis at conventional cholangiography. The mechanism of injury is either a direct effect of treatment or ischemia secondary to thrombosis of the intrahepatic arterial branches. According to the specific arterial supply of the biliary ducts, intrahepatic bile ducts and the lower portion of the common bile duct are unimpaired in most cases. Bile duct strictures occur as early as 2 months after therapy and may decrease if the intraarterial infusion is interrupted. The most common cholangiographic findings are narrowing of the bifurcation of the common hepatic duct with sparing of the distal common bile duct. Cross-sectional imaging is usually required to exclude worsened metastatic disease in these patients.
▶Cholangitis

Cholangitis, Eosinophilic

Presence of multiple strictures of the bile ducts due to eosinophilic infiltration of the hepatobiliary system usually associated with eosinophilic gastroenteritis. This rare condition is reversible, responds rapidly to corticosteroid therapy, and may result in radiographic and histological features in accordance with cholangitis, cholecystitis, or chronic hepatitis.
▶Cholangitis

Cholangitis, Fungal Infection

Form of secondary sclerosing cholangitis characterized by diffuse inflammation and strictures determined by various fungal infections of the liver and the biliary tree. Imaging features resemble those of primary sclerosing cholangitis.
▶Cholangitis

Cholangitis, Ischemic after Liver Transplantation

Biliary strictures occurring in liver recipients can be classified into anastomotic and nonanastomotic types and can be caused by iatrogenic injury, hepatic arterial thrombosis or stenosis, prolonged preservation time, recurrence of primary liver disease, chronic rejection, or cholangitis. Anastomotic strictures are mostly extrahepatic ductal, due to iatrogenic trauma with consequent ischemia and scar formation. In these cases, ascending cholangitis may result in formation of intrahepatic bile duct strictures that simulate primary sclerosing cholangitis. Nonanastomotic strictures are mostly due to arterial ischemia and are unrelated to iatrogenic bile duct injury. The hepatic artery represents the unique arterial supply to the transplanted liver, since the peribiliary collaterals from the hepatic, gastroduodenal, celiac, and superior mesenteric arteries are absent in the transplanted liver. Therefore, the presence of hepatic artery obstruction, mostly determined by arterial thrombosis, may result in severe ischemia and bile duct or hepatocyte necrosis. Other causes of nonanastomotic strictures are prolonged preservation time, bacterial or viral cholangitis, and rejection.
▶Cholangitis

Cholangitis, Recurrent Pyogenic

Also called oriental cholangiohepatitis, intrahepatic pigmented calculus disease, or hepatolithiasis, this is a complex hepatobiliary disease characterized by chronic inflammation of the bile ducts and is attributed to parasite invasion. In endemic areas (Southeast Asia), parasites such as Clonorchis sinensis and Ascaris lumbricoides can inhabit the bile ducts, causing ductal damage and strictures. Other parasites such as Opistorchis viverrini, Fasciola hepatica, and Entamoeba have also been found.
▶Cholangitis

Cholangitis, Sclerosing Primary

Chronic, idiopathic, fibrosing inflammatory disorder affecting the bile ducts that eventually leads to bile duct obliteration, cholestasis, and biliary cirrhosis. The term "primary" is used to differentiate this condition from bile duct strictures due to bile duct injury, cholelithiasis, ischemia, or chemical injury (secondary sclerosing cholangitis). The peak incidence occurs in the 3rd and 4th decades of life, and a male predominance appears to exist. It is believed to be an autoimmune process because it is frequently associated with other autoimmune diseases such as ulcerative colitis.
▶Cholangitis

Cholecystitis

Thomas Helmberger[1], Carlo Bartolozzi[2], Paola Vagli[2], Giuliano Mariani[2]
[1]Clinic of Radiology and Nuclear Medicine, University Hospitals Schleswig-Holstein, Campus Luebeck, Germany
[2]Department of Diagnostic and Interventional Radiology and of Nuclear Medicine, University of Pisa, Italy
thomas.helmberger@uni-luebeck.de
bartolozzi@do.med.unipi.it

Synonyms

Cholecystitis acute; Cholecystitis acute acalculous; Cholecystitis chronic; Cholecystitis emphysematous; Cholecystitis gangrenous; Cholecystitis necrotizing; Cholecystitis xanthogranulomatous; Inflammation of the gallbladder

Definition

Cholecystitis is the inflammation of the gallbladder occurring most commonly in cases of obstruction of the cystic duct caused by gallstones. In a very small percentage

(about 10%) of cases, cholecystitis occurs without gallstones (►acalculous cholecystitis). The inflammation often initiates without contamination, and infection may develop later; therefore, bacterial proliferation may be a result of cholecystitis and not the precipitating factor. Severe disease, alcohol abuse, and rarely, tumors of the gallbladder can also be the cause of cholecystitis. Cholecystitis may develop either as an acute or a chronic process. ►Acute cholecystitis is the abrupt onset of inflammation of the gallbladder, resulting in severe upper abdominal pain (biliary colic), which may occur repeatedly. ►Chronic cholecystitis is a long-standing inflammation of the gallbladder characterized by repeated episodes of pain (gallbladder attacks) over a prolonged period.

Pathology and Histopathology

Cholecystitis, Acute

Acute calculous cholecystitis is the acute inflammation of the gallbladder, caused in most instances by obstruction of the cystic duct (usually by gallstones or sludge), leading to distension of the gallbladder and resulting in acute inflammation of the gallbladder wall. As the gallbladder becomes distended, blood flow and lymphatic drainage are compromised, leading to mucosal ischemia and necrosis. Cholelithiasis is the major risk factor for cholecystitis; therefore, risk factors for cholecystitis reflect those for cholelithiasis and include age, female gender, certain ethnic groups (native Americans), obesity or rapid weight loss, and some drugs. Acute cholecystitis complicates the course of symptomatic gallstones in 10–20% of patients. Early acute histological findings include edema and venous congestion. Signs of acuteness are usually overlapped by histological features suggestive of ►chronic cholecystitis. Specific findings include fibrosis, flattening of the mucosa, and chronic inflammatory cells. Mucosal herniations known as Rokitansky–Aschoff sinuses are related to increased hydrostatic pressure and are present in half of the cases. Focal necrosis and infiltration of neutrophils may also be present. In advanced cases, gangrene or perforation may develop (1–4).

Cholecystitis, Acute, Acalculous

Acalculous cholecystitis is defined as an acute inflammation of the gallbladder in the absence of visible stones. It occurs most likely in elderly men secondary to major injuries such as major surgery, trauma, sepsis, burns, cardiac events, and a widespread severe disease particularly in people receiving prolonged intravenous feeding. The most common predisposing factors are biliary stasis associated to prolonged fasting, immobility, and hemodynamic instability. About half of the cases of acute cholecystitis in pediatric patients are acalculous disease, perhaps originating as an infection (viral or other). The exact pathogenesis of acalculous cholecystitis is unclear, although current theory is related to the histotoxicity of concentrated, stagnant, retained bile developing in cases of prolonged fasting where the gallbladder never receives a stimulus to empty. Ischemia is considered another potential cause of direct injury. In some patients, infection may be the primary event, as has been described in cases of typhoid fever or AIDS cholangiopathy. Complications such as gallbladder wall necrosis, gangrene (diffuse or focal), and perforation are common. The mortality is very high because of the fulminant course and coexistent disease (1,4).

Cholecystitis, Emphysematous

►Emphysematous cholecystitis is a severe condition associated with a high mortality and characterized by the presence of gas within the wall and the lumen of the gallbladder.

It can be considered either as a complication of acute cholecystitis (occurring in about 1% of cases), in particular acalculous, or as a separate entity. It occurs most commonly in elderly males and diabetics and is less frequently associated with cholecystolithiasis than other forms of acute cholecystitis. Pathogenesis of this type of disease is related to ischemia (obstruction of the cystic artery) and bacterial overgrowth with gas-forming agents such as *Escherichia coli*, *Clostridium perfringens* or *Clostridium welchii*, anaerobic streptococci, and *Klebsiella* species. Whether these bacteria represent the primary cause of the disorder or are secondary invaders remains unclear. Histologically the layers of the gallbladder wall become separated, leading to the characteristic tissue crepitus, while colonies of bacteria can be observed forming intramural abscesses and the gallbladder content is often purulent. The frequent occurrence of gangrenous evolution and perforation, associated to the septic course and comorbidities, explains the high morbidity and mortality rate (1).

Cholecystitis, Chronic

►Chronic cholecystitis represents the chronic inflammation of the gallbladder wall associated to recurrent mild attacks of acute cholecystitis. This condition occurs predominantly in patients with long-standing cholecystolithiasis and shows a female predominance with an increased incidence in elderly patients. Although rare, cases of chronic acalculous cholecystitis have been reported. Repeated attacks of acute inflammation, usually caused by stones, lead to a progressive damage of the

gallbladder that becomes deformed (scarred, and shrink) with wall thickening due to the fibrosing inflammatory reaction. Additionally, the gallbladder may lose its function of concentrating and storing bile. The gallbladder usually contains sludge or gallstones that often cause obstruction of the gallbladder neck or the cystic duct. Long-standing gallstones may determine erosion of the gallbladder walls causing complications such as bilioenteric fistulas and ►gallstone ileus, and they are also considered the most important risk factor for gallbladder carcinoma.

Cholecystitis, Xanthogranulomatous

►Xanthogranulomatous cholecystitis (XGC) is an uncommon form of chronic cholecystitis, formally characterized by Christensen and Ishak, and previously called by many pseudonyms such as "ceroid granulomas," "ceroid-like histiocytosis," and "fibroxanthogranulomatous inflammation". XGC was initially reputed as a malignant disease for its pseudotumoral appearance. Currently, it is considered benign, showing similar behavior and histological pattern to other xanthogranulomatous lesions occurring in other organs such as the kidney (xanthogranulomatous pyelonephritis), female genital tract, lymph nodes, and urinary bladder. It occurs predominantly in middle-aged females, and frequently the patients are misdiagnosed as having cholelithiasis or a primary cancer. Early phases are histologically characterized by the collection of lipid-loaded macrophages with acute and chronic inflammatory cells in areas of destructive phlogosis, replaced by increasing fibrosis in the late stages. The gross appearance is that of yellowish tumor-like masses in the gallbladder wall typically extending into the adjacent structures (liver bed and surrounding viscera) and leading to perforation, fistula formation, abscess, biliary ductal stricture or obstruction, and ascending cholangitis. An increased association of underlying carcinoma in patients with XGC than in those with ordinary cholecystitis has been reported. Associated cholesterol gallstones are a common finding. The pathogenesis is not clear but it is assumed that a chronic inflammation determined by stones or obstruction of gall flow determines the formation of lysolecithin in bile, resulting in further damage to the gallbladder mucosa. The upgrading from cholecystitis to XGC is related to the occlusion by means of inspissated bile and mucin of the Rokitansky–Aschoff sinuses. These develop into rupture when the wall tension of the distended gallbladder exceeds its natural compliance, leading to the spreading of inflammation into the adjacent tissues. Histiocytes add to the catabolism of bile phagocyting insoluble cholesterol and bile salts, generating the characteristic XGC appearance of loaded macrophage and foamy histiocytes, and resulting in the formation of xanthoma cells (5).

Clinical Presentation

Cholecystitis, Acute

Upper abdominal pain, often radiating to the right scapula in patients with a history of biliary pain or documented gallstones, is the most common presenting sign. Signs of peritoneal irritation consisting of tenderness in the right upper quadrant or in the epigastric region may be present, often with guarding or rebound and positivity of the Murphy sign.

Characteristically, the pain begins in the epigastric region and then localizes to the right upper quadrant. Initially it is described as intermittent, becoming persistent in nearly all cases. Other common signs include nausea, vomiting, and fever that can be less evident in elderly or diabetic patients. Jaundice indicates common bile duct obstruction and is not commonly reported. The persistence of constant severe pain for more than 6 h helps to differentiate cholecystitis from biliary colic. A complete remission is achieved in most cases, although some patients require surgery or develop important complications such as pericholecystic abscess, empyema of the organ, bilioenteric fistulas and gallstones ileus, ►emphysematous cholecystitis, sepsis, perforation, and gangrene. These complications are often suggested by the persistence of the abdominal pain for more than 2–3 days and the appearance of high fever, chills, ileus, and a marked increase in the white blood cell count. If the diagnosis is certain and the risk of surgery is low, the gallbladder is usually laparoscopically removed during the first 2 days from the onset. If a complication is suspected, immediate surgery is required. After gallbladder removal for cholecystitis with gallstones, a small percentage of people develop new or recurring episodes of pain, like gallbladder attacks, probably resulting from an abnormal function of the sphincter of Oddi or from residual stones in the biliary tree.

Cholecystitis, Acute, Acalculous

Individuals presenting with acalculous cholecystitis are typically older hospitalized patients with microvascular disease or other severe comorbidities without prior history of gallbladder disease. Usually the onset is characterized by abrupt excruciating pain in the upper abdomen, although often patients may present with fever and sepsis alone, without signs of acute cholecystitis. The most frequent physical and laboratory findings are nonspecific including fever, right upper quadrant pain, nausea, leukocytosis, and elevation of liver-associated enzymes and bilirubin. Abdominal pain is present in nearly all patients; however, the pain is often not localized to the right upper quadrant. Surgical removal of the diseased gallbladder is required in almost all cases and is considered the reference treatment (2).

C

Cholecystitis, Emphysematous

The clinical scenario is not significantly different from that of acute cholecystitis, consisting of right upper quadrant pain radiating to the back, unrelated to the patient's position. Other unspecific signs include leukocytosis, fever, tachycardia, tenderness in the right upper quadrant, diminished bowel sounds, or a palpable mass. However, in elderly and diabetic patients this condition may present with few or no localizing symptoms or signs. The transient decrease of abdominal pain associated to peritoneal signs suggests perforation.

Cholecystitis, Chronic

Chronic cholecystitis is usually asymptomatic if there are no associated complications. A clinical history or recurrent attacks of acute cholecystitis or biliary colic may be reported. A palpable mass in the right upper quadrant due to fibrous involvement of the gallbladder is uncommon. The reduced ability of the gallbladder in concentrating bile may hinder the ingestion of a fatty meal. Recommended therapy includes surgical removal of the gallbladder, usually in a laparoscopic fashion, once the acute episode subsides.

Cholecystitis, Xanthogranulomatous

Clinical features resemble those observed in acute or chronic inflammation of the gallbladder, such as acute or chronic pain in the right upper quadrant, fever, and anorexia.

Imaging

Cholecystitis, Acute

Conventional radiography does not play a primary role in the diagnosis of cholecystitis, allowing only detection of indirect signs, such as calcified gallstones that suggest cholelithiasis with or without cholecystitis. The presence of gas limited to the gallbladder wall or lumen indicates gangrenous or ▶emphysematous cholecystitis. Ultrasound (US) suggests the diagnosis of cholecystitis in most instances showing a very high sensitivity and specificity for detecting gallstones and gallbladder sludge that is usually visualized as nonshadowing and inhomogeneous echogenic material, which tends to form a fluid–fluid level. The main US features suggestive of acute cholecystitis include pericholecystic fluid from perforation or exudation, gallbladder distension (diameter >4 cm, length >10 cm), gallbladder wall thickening greater than 3–4 mm, and sonographic Murphy's sign. The thickened wall usually shows a multilayered aspect due to the visualization of a hypoechoic middle layer between two outer hyperechoic layers, which is related to the edema and cellular infiltration of subserosa and submucosa (Fig. 1). A sonographic Murphy's sign is the presence of pain (not related to breathing), evoked by direct pressure of the probe over a sonographically localized gallbladder. The presence of gallstones also aids to confirm the diagnosis, and a dilated common bile duct or dilated intrahepatic ducts indicate common bile duct stones. US also identifies complications (perforation, empyema, abscess). Color Doppler US of the cystic artery at the level of the anterior wall of the gallbladder may demonstrate increased flow. However, this finding may also be observed in other conditions associated with gallbladder wall thickening. Computed tomography (CT) may be adequate for detecting complications such as empyema or suppurative cholecystitis, and it also provides more accurate information of the surrounding structures than US. In particular, the extent and the exact anatomical localization of the pericholecystic abscesses are well visualized on CT. CT is also superior to US in correctly identifying small pericholecystic gas collections

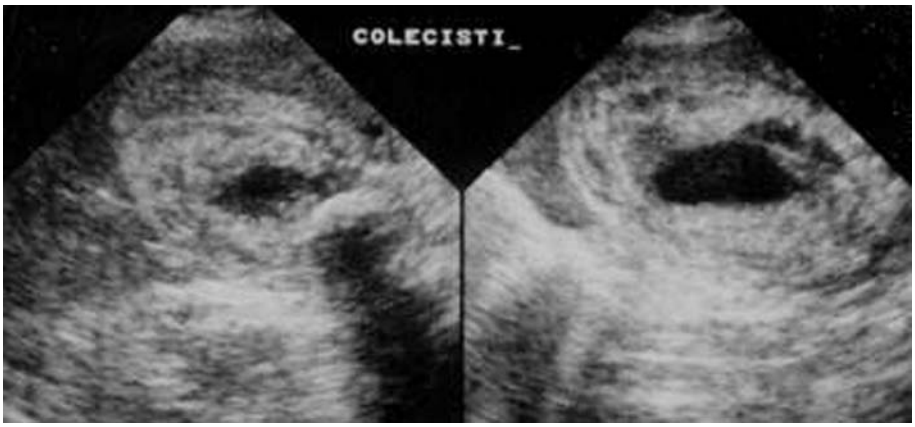

Cholecystitis. Figure 1 Acute cholecystitis. US shows a thickened wall with a multilayered aspect due to the visualization of a hypoechoic middle layer between two outer hyperechoic layers.

and distinguishing them from bowel gas as well as in detecting a gallstone lying outside the lumen of the gallbladder. CT may also depict calcified stones in the gallbladder or in the cystic duct, biliary tree dilatation, focal or diffuse thickening of the gallbladder wall (more than 3–4 mm in cases of noncontracted gallbladder), fluid in the gallbladder fossa, enlargement of the gallbladder, and infiltration of the surrounding fat. The presence of a hypodense concentric band surrounding the gallbladder may indicate fluid collection in the gallbladder bed (in the absence of ascites) or edema in the outer layers of the gallbladder wall. The gallbladder content may show an abnormally elevated density indicating hemobilia. After contrast medium administration, a significant increase in attenuation values of the gallbladder wall as well as increased contrast accumulation in the inflamed hyperemic area surrounding the liver parenchyma can be observed (Fig. 2). The presence of an inflammatory reaction in the pericholecystic fatty tissue is a specific CT sign and appears as a band-like structure with soft tissue density around the gallbladder. Nevertheless, CT misses 20% of gallstones because the stones may be of the same radiographic density as bile. Morphological features of acute cholecystitis in magnetic resonance imaging (MRI) resemble those of CT. On T2-weighted images, inflammatory pericholecystic changes are displayed as high-signal linear structures around the gallbladder. Gadolinium-enhanced T1-weighted images show the same inflammatory changes of the gallbladder wall, pericholecystic fat, and intrahepatic periportal tissues as those displayed on enhanced CT.

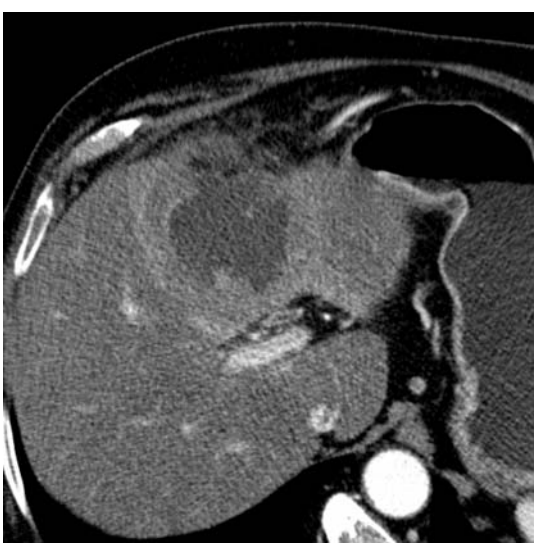

Cholecystitis. Figure 2 Acute cholecystitis. CT shows a diffuse thickening of the gallbladder wall and infiltration of the surrounding fat. A significant enhancement of the gallbladder wall as well as increased contrast accumulation in the inflamed hyperemic surrounding liver parenchyma can be observed.

Endoscopic retrograde cholangiopancreatography (ERCP) provides both endoscopic and radiographic visualization of the biliary tract. ERCP can be diagnostic and therapeutic by direct removal of common bile duct stones and may be particularly useful in patients at high risk for common duct stones if signs of common bile duct obstruction are not present (1–4).

Cholecystitis, Acute, Acalculous

Conventional radiography is of limited use (as stated for acute calculous cholecystitis), allowing detection of indirect signs such as the presence of air in emphysematous complications. The presence of gas has a high association with gangrene and perforation. US is the first approach and may depict nonspecific signs of distension of the gallbladder and sludge (echogenic bile), while more specific signs include gallbladder wall thickening with hypoechoic regions within the wall (striated gallbladder, i.e., gallbladder wall edema) and the presence of pericholecystic fluid or intraluminal membranes. Gangrenous and emphysematous complication is characterized by the presence of gas. Major criteria for US diagnosis are gallbladder wall thickening greater than 3–4 mm (measured in the transverse plane in a noncollapsed gallbladder), the presence of pericholecystic fluid (that suggests advanced disease or perforation), and mucosal sloughing, whereas gallbladder distension (more than 4 cm transverse), and echogenic bile (sludge) are considered minor criteria.

CT is the imaging technique of choice in patients with abdominal pain with fever or leukocytosis of undefined etiology, offering the advantage of evaluating the entire abdomen. The normal gallbladder wall is barely perceptible as a thin enhancing rim on contrast-enhanced CT and the following CT signs in the appropriate clinical setting are suggestive of the diagnosis: gallbladder wall thickening, subserosal halo (i.e., gallbladder wall edema), mucosal irregularity and sloughing, intraluminal hemorrhage, localized pericholecystic fluid collections, perforation of the gallbladder wall or inflammation of pericholecystic fat, and indistinctness of the liver–gallbladder interface. Mucosal sloughing and intramural gas are infrequent specific findings. Isolated local pericholecystic fluid collections and pericholecystic inflammatory changes are relatively specific and suggest advanced disease, but they lose specificity in the setting of concurrent ascites or recent abdominal surgery (1, 4).

Cholecystitis, Emphysematous

Conventional radiography contributes to the diagnosis by showing the presence of an air–fluid level in the right

upper quadrant representing gas in the gallbladder lumen, a curvilinear gas collection conforming to the gallbladder wall in the case of intramural gas, or multiple small air bubbles in the Rokitansky–Aschoff sinuses. The classic picture observed on abdominal radiographs is believed to represent a late phase in the evolution of ▶emphysematous cholecystitis and may predict a poor outcome. If perforation occurs, mottled pericholecystic air accumulation is visible. Aerobilia can be associated in rare instances. US shows the gallbladder lumen as containing hyperechoic structures with blunt acoustic shadowing that cause obscuration and render differentiation from intestinal gas difficult. Gas within the gallbladder wall is usually depicted as a ring due to hyperechoic tiny structures located around the fluid-filled gallbladder. Curvilinear gaseous artifacts in the gallbladder, the "ring down effect" or "comet tail" signs, are diagnostic but not frequent signs of emphysematous cholecystitis. An original feature called "effervescent bile" may be observed if the gas leaks from the wall of the gallbladder into the bile. CT should be performed if US and conventional radiography are not diagnostic. CT can better depict the presence of extra- and intraluminal gas and may also demonstrate possible extension into the pericholecystic tissue and the hepatic ducts (1, 4).

Cholecystitis, Chronic

Imaging features (both US and CT) of ▶chronic cholecystitis are not specific, including a contracted gallbladder associated with gallbladder wall thickening and cholelithiasis. US can show a diffuse gallbladder wall thickening with shadowing or nonshadowing particles within the gallbladder lumen.

Cholecystitis, Xanthogranulomatous

US and CT features are nonspecific and frequently suggestive of malignancy. Suspect findings include irregular or nodular marked thickening of the gallbladder wall with an indistinct separation from the liver parenchyma especially when the inflammatory process extends to involve the adjacent liver. US shows hypoechoic bands or nodules within the thickened gallbladder wall. These hypoechoic nodules represent abscesses or foci of xanthogranulomatous inflammation. Other findings include disruption of the mucosal line, pericholecystic fluid, stones, and intrahepatic biliary dilatation. CT shows low attenuation foci in the gallbladder wall corresponding to the hypoechoic nodules seen at US. CT can also depict the presence of a mass in the gallbladder wall with inhomogeneous density and moderate to marked enhancement after contrast medium administration, which may extend to the liver or to other adjacent organs. Associated infiltration of the surrounding fatty tissue that presents a striate appearance is commonly reported (2, 5).

Nuclear Medicine

Cholecystitis, Acute

Hepatobiliary scintigraphy with ^{99m}Tc-labeled iminodiacetic acid (IDA) derivates has been found to be very accurate in diagnosing ▶acute cholecystitis. These tracers are intravenously administered and secreted by hepatocytes into the bile, enabling a morphofunctional study and the visualization of the gallbladder, biliary tree, and small bowel filling in about 30 min. Since acute cholecystitis is initiated and characterized by cystic duct obstruction, cholescintigraphy that detects cystic duct obstruction should correlate better with acute cholecystitis with respect to the presence of cholelithiasis. In the case of cystic duct obstruction, on radionuclide scans there is no visualization of the gallbladder at 60 min as the bile is excreted directly into the duodenum. If the gallbladder is not visualized, morphine may be administered intravenously causing increased resistance to flow through the sphincter of Oddi, resulting in a filling of the gallbladder if the cystic duct is patent, thus reducing the number of false positives in patients who are critically ill and immobilized with viscous bile. The persistent nonvisualization of the gallbladder within 60 min after tracer administration, despite morphine injection or delayed images, is the characteristic pattern of acute cholecystitis. The reported negative predictive value of a normal cholescintigraph in excluding acute cholecystitis is greater than 98%. In patients with persistent gallbladder nonvisualization, it is important to detect the rim sign on the 45–60-min post-morphine images, because this connotes a complicated cholecystitis (gangrenous forms with or without perforation) indicating inflammatory spread into adjacent liver parenchyma with impairment of local hepatic tracer excretion. Radionuclide studies also have the advantage of revealing an obstructed cystic duct in the case of a normal gallbladder appearance on US imaging.

Cholecystitis, Acute, Acalculous

Cholescintigraphy is considered very sensitive but not specific. The absence of the gallbladder filling can be a manifestation of both mechanical and functional obstruction. The gallbladder filling can also be observed, although an early filling excludes acalculous cholecystitis. Additional findings include the presence of an area of increased pericholecystic radiotracer accumulation in the gallbladder fossa (rim sign) that is associated with complications such

as gangrene. Radiotracer extravasation can rarely be visualized in the setting of perforated ►gangrenous cholecystitis if the cystic duct remains patent.

Cholecystitis, Chronic

In patients with signs and symptoms suggestive of biliary induced pain, but normal US examination for the presence of biliary stones, cholescintigraphy can document gallbladder dysfunction even before stone formation. Signs suggestive of gallbladder dysfunction include delayed gallbladder visualization, persistent gallbladder nonvisualization, or abnormal responses to cholecystokinetic agents. The visualization of the gallbladder within 30-min after morphine injection or in delayed images is a sign of chronic cholecystitis. Hepatobiliary scintigraphy has been used to assess whether chronic ►acalculous cholecystitis is present and to predict the symptomatic response to cholecystectomy. The determination of maximum gallbladder ejection fraction (GBEF) response to a 3-min infusion of sincalide (0.02 μg/Kg) is useful in detecting symptomatic acalculous biliary disease (GBEF > 35% suggests that the patient's symptoms are not related to chronic acalculous biliary disease, 91% NPV), thus confirming the current role of cholescintigraphy in the assessment of patients with chronic biliary pain and normal US.

Diagnosis

Cholecystitis, Acute

The patient's symptoms, associated to the laboratory tests that suggest gallbladder inflammation, together with US features of gallstones or gallbladder wall thickening may lead to the diagnosis. However, many conditions unrelated to gallbladder disease may cause thickening of the gallbladder wall. The most frequent are hepatitis, hypoalbuminemia, ascites, congestive heart failure, and carcinoma. Diagnostic imaging has to contribute substantially to the differential diagnosis and to the detection of complications. Particular attention should be paid to complicated cases in which imaging features such as diffuse or focal wall thickening, as well as infiltrative changes in the pericholecystic lipomatous tissue, can be similar to the findings present in gallbladder carcinoma (1–4).

Cholecystitis, Acute, Acalculous

Often, the diagnosis is difficult and delayed because of the presence of comorbidities that decrease the diagnostic accuracy of both clinical and imaging evaluation. Early imaging evaluation is required, although no single imaging study is sufficient. The different imaging techniques are usually complementary and better suited to excluding, rather than confirming, the disease. It is unusual for ►acalculous cholecystitis to develop in the presence of a normal gallbladder, although this finding can occur early in the course of the disease (4). The differential diagnosis is broad for the presence of nonspecific signs in patients with many co-morbidities. Almost any infectious or inflammatory process can result in such nonspecific findings. In patients with more localized symptoms, the primary differential diagnoses include calculous cholecystitis, ascending cholangitis, acute hepatitis, and pancreatitis.

Cholecystitis, Emphysematous

Clinically, the differential diagnosis must include acute cholecystitis (nonemphysematous), both calculous and acalculous. The radiologic differential diagnosis includes all causes of gas in the biliary tree such as bilioenteric fistula, after ERCP or in cases of cholangitis caused by gas-producing agents.

Cholecystitis, Chronic

US and CT findings may resemble those seen in gallbladder carcinoma. Although the presence of a diffuse mural thickening instead of a focal involvement associated to specific clinical features may help to differentiate benign from malignant affections, pronounced or focal wall thickening when associated to irregularity and lymphadenopathy should suggest malignancy.

Cholecystitis, Xanthogranulomatous

Imaging techniques are well suited for diagnosing complications, while only a histological examination of a surgical specimen will accurately give the final diagnosis of XGC excluding malignancy or a ►gallbladder abscess. It should also be considered that XGC can coexist with malignancy (2, 5).

References

1. Bennett GL, Balthazar EJ (2003) Ultrasound and CT evaluation of emergent gallbladder pathology. Radiol Clin North Am 41 (6):1203–1216
2. Zissin R, Osadchy A, Shapiro-Feinberg M et al (2003) CT of a thickened-wall gallbladder. Br J Radiol 76(902):137–143
3. Adusumilli S, Siegelman ES (2002) MR imaging of the gallbladder. Magn Reson Imaging Clin N Am 10(1):165–184
4. Hanbidge AE, Buckler PM, O'Malley ME et al (2004) From the RSNA refresher courses: imaging evaluation for acute pain in the right upper quadrant. Radiographics 24(4):1117–1135
5. Chun KA, Ha HK, Yu ES et al (1997) Xanthogranulomatous cholecystitis: CT features with emphasis on differentiation from gallbladder carcinoma. Radiology 203:93–97

Cholecystitis, Acute

Acute inflammation of the gallbladder due to obstruction of the cystic duct, usually caused by gallstone or sludge, and leading to distension of the gallbladder. Advanced cases may develop gangrene or perforation.
▶Cholecystitis

Cholecystitis, Acute, Acalculous

Acute inflammation of the gallbladder in the absence of demonstrated stones occurring most likely in elderly adults affected by severe comorbidities. Complications such as gallbladder wall necrosis, gangrene (diffuse or focal), and perforation are common and mortality is very high.
▶Cholecystitis

Cholecystitis, Chronic

Chronic inflammation of the gallbladder caused by repeated attacks of ▶acute cholecystitis in patients with long-standing gallstones. Chronic ▶acalculous cholecystitis has rarely been reported. The gallbladder presents a deformed and thickened wall due to fibrous involvement. Complications include bilioenteric fistulas and ▶gallstone ileus.
▶Cholecystitis

Cholecystitis, Emphysematous

Severe condition associated with a high mortality, characterized by the presence of gas within the wall and the lumen of the gallbladder. It can be considered either as a complication of ▶acute cholecystitis, in particular acalculous, or as a separate entity. It occurs most commonly in elderly males and diabetics. Pathogenesis is related to ischemia and bacterial overgrowth with gas-forming agents. The development of gangrene and perforation are frequently reported.
▶Cholecystitis

Cholecystitis, Gangrenous

Gangrenous or necrotizing cholecystitis is a severe advanced form of ▶acute cholecystitis with a higher morbidity and mortality rate than uncomplicated acute cholecystitis. It results from marked distension of the gallbladder with increased tension of the wall. Associated inflammation leads to ischemic necrosis, with or without associated cystic artery thrombosis. Clinical and laboratory findings are often nonspecific and indistinguishable from those of patients with acute cholecystitis without gangrene. A typical US sign of gangrenous cholecystitis is the presence of heterogeneous or striated thickening of the gallbladder wall, which is often irregular with projections into the lumen and the pericholecystic fluid collections. The presence of intraluminal membranes representing desquamative gallbladder mucosa is a specific finding but is less common. US findings, typically for uncomplicated acute cholecystitis, may be absent in this subset of patients. CT findings in gangrenous cholecystitis are better appreciated after contrast medium administration, and include intraluminal membranes, intraluminal hemorrhage, and an irregular or absent wall.
▶Cholecystitis

Cholecystitis, Necrotizing

Complicated form of acute cholecystitis (both calculous and acalculous) synonymous to gangrenous cholecystitis.
▶Cholecystitis

Cholecystitis, Xanthogranulomatous

Uncommon form of chronic cholecystitis occurring predominantly in middle-aged females characterized by the collection of lipid-loaded macrophages and a gross appearance of yellowish tumor-like masses in the gallbladder wall, typically extending into the adjacent structures (liver bed and surrounding viscera) and leading to perforation.
▶Cholecystitis

Cholecystography

This radiological technique, now considered obsolete, allowed the opacification and visualization of the gallbladder with an orally administered agent owing to the ability of the gallbladder to concentrate the oral medium.

▶Biliary Anatomy

Cholecystoses

Thomas Helmberger[1], Carlo Bartolozzi[2], Paola Vagli[2]
[1]Clinic of Radiology and Nuclear Medicine, University Hospitals Schleswig-Holstein, Campus Luebeck, Luebeck, Germany
[2]Department of Diagnostic and Interventional Radiology, University of Pisa, Italy
thomas.helmberger@uni-luebeck.de
bartolozzi@do.med.unipi.it

Synonyms

Adenomyomatosis gallbladder; Cholesterolosis; Hyperplastic cholecystosis; Porcelain gallbladder; Strawberry gallbladder

Definition

Cholecystosis is a generic term introduced by Colesson and Jutras used to describe a group of noninflammatory, nonlithiasic benign diseases of the gallbladder wall. However, a chronic aspecific inflammatory process seems to be much more frequent than is believed and often this condition is associated with lithiasis. Cholecystoses have been classified into hyperplastic or accumulating forms. The hyperplastic forms are characterized by normal growth with hyperplasia of the cellular wall components, while in the accumulating forms there is an overload of the wall with organic substances or minerals such as lipids or calcium salts (thesaurismosic forms). The hyperplastic forms include both the presence of limited thickening of the wall (focal and segmental cholecystosis) and more extensive thickening. The most common forms of cholecystoses are adenomyomatosis and cholesterolosis (hyperplastic forms) and calcified or ▶porcelain gallbladder (thesaurismosic forms). The clinical picture resembles that of inflammation of the gallbladder caused by stones.

Pathology and Histopathology

Adenomyomatosis, Gallbladder

Adenomyomatosis of the gallbladder is a common, benign condition, with tumor-like features, of unknown cause, characterized by hyperplastic changes of the wall and therefore named hyperplastic cholecystosis. This condition is characterized by overgrowth of the surface epithelium with associated glandular formation and out-pouching into or through the thickened muscular wall, causing formation of intramural diverticula or sinus tracts termed Rokitansky–Aschoff sinuses. Adenomyomatosis of the gallbladder and the associated Rokitansky–Aschoff sinuses may involve the gallbladder in a focal, segmental, or diffuse form. A septum or an annular thickening causing circumferential narrowing of the lumen is frequently associated with adenomyomatosis and must be differentiated from a congenital fold of the gallbladder wall (▶Phrygian cap), which is usually thinner and smoother and localized to the fundus, whereas adenomyomatosis may involve any portion of the gallbladder. Adenomyomatosis occurs most frequently in middle-aged females and its etiology remains unclear (1, 2).

Cholesterolosis, Gallbladder

Cholesterolosis is a benign condition and represents a type of hyperplastic cholecystosis, resulting from the macrophage accumulation of triglycerides and cholesterol esters mainly in the submucosal layer or lamina propria of the gallbladder wall. The true incidence and etiology of cholesterolosis remain unclear, and a causal association with cholesterol gallstones, super saturation of bile with cholesterol, hyperlipidemia, obesity, or atherosclerosis remains unconfirmed. Nevertheless, this condition is often seen in gallbladders containing stones. Two types have been described: a diffuse form, also called "strawberry" gallbladder, and a polypoid form.

The gross appearance of ▶strawberry gallbladder includes a diffuse thickening and the presence of yellowish, diffuse, granular, lipid deposits, varying in distribution and size, in the gallbladder mucosa that resemble a strawberry. The polypoid form is characterized by single or multiple, small (up to 1 cm in some cases), discrete polypoid excrescences composed of cholesterol-filled macrophages. Malignant degeneration has not been described (2).

Porcelain Gallbladder

This condition also called calcified gallbladder, calcifying cholecystitis, and cholecystopathia chronica calcarea refers to the presence of extensive dystrophic calcifications within the chronically inflamed gallbladder wall with associated fibrosis in the muscular layer. The term porcelain gallbladder emphasizes the brittle consistency and blue discoloration of these calcifications that may appear as a broad continuous band in the muscularis conferring a sac-like appearance or multiple punctate calcifications in the mucosal glandular spaces. The most accredited origin of the calcification is secondary to the chronic inflammation of the gallbladder wall due to cholecystitis, but intramural hemorrhage and an imbalance in calcium metabolism also seem to be implicated.

Gallstones are documented in 90% of cases. Porcelain gallbladder has a low prevalence but its clinical importance lies in a significant association with gallbladder carcinoma especially in cases of diffusely calcified gallbladder. A significant female prevalence has been reported with a male-to-female ratio of 1:5.

Clinical Presentation

Adenomyomatosis, Gallbladder, Cholesterolosis, Gallbladder

Usually these conditions remain asymptomatic or are characterized by aspecific features such as vague abdominal pain. Cholecystectomy is rarely required to treat these affections, and may be considered for patients with convincing symptoms or coexisting cholelithiasis.

Porcelain Gallbladder

This condition is usually asymptomatic and incidentally diagnosed. Although asymptomatic, surgical removal of the gallbladder is recommended because the occurrence of carcinoma in porcelain gallbladder is remarkably high.

Imaging

Adenomyomatosis, Gallbladder

Conventional radiography by means of cholecystography is considered obsolete and has been replaced by other imaging modalities. On cholecystograms, the patent Rokitansky–Aschoff sinuses appear as single or multiple oval or rounded extraluminal pouches filled with contrast medium, ranging in size (between 1 and 10 mm), and separated from the lumen by at the most 2-cm-thick band representing both the mucosa and the muscular wall ("pearl necklace" sign).

Ultrasound (US) is the examination of choice showing the mural thickening, especially if the cystic spaces are visible as small anechoic extraluminal structures. These cystic spaces appear as anechoic diverticula and may show echoic foci and/or reverberation artifacts together. Association of cystic spaces with full or partial thickening of the gallbladder wall is considered to be the key diagnostic findings (Fig. 1). Intradiverticular echoic foci are caused by the presence of sludge or stones, and reverberation artifacts due to cholesterol crystals are "V" shaped and shorter in length than artifacts from air. If intramural diverticula are not identified, differentiating adenomyomatosis from other causes of gallbladder wall thickening especially if segmental or focal, such as cholecystitis or carcinoma, is difficult. Exceptionally bright echogenic dots due to debris-filled Rokitansky–Aschoff sinuses may be detected. Gallstones are often associated with adenomyomatosis (1).

Computed tomography (CT) and magnetic resonance imaging (MR) can be used as problem-solving modalities, especially to differentiate hyperplastic cholecystosis from gallbladder carcinoma.

CT shows a thickened gallbladder wall with the "string of beads" sign when the multiple intramural cystic spaces are visualized crossways. This sign is caused by the enhanced proliferative mucosal epithelium of the intramural diverticula surrounded by the unenhanced hypertrophied muscular layer of the gallbladder.

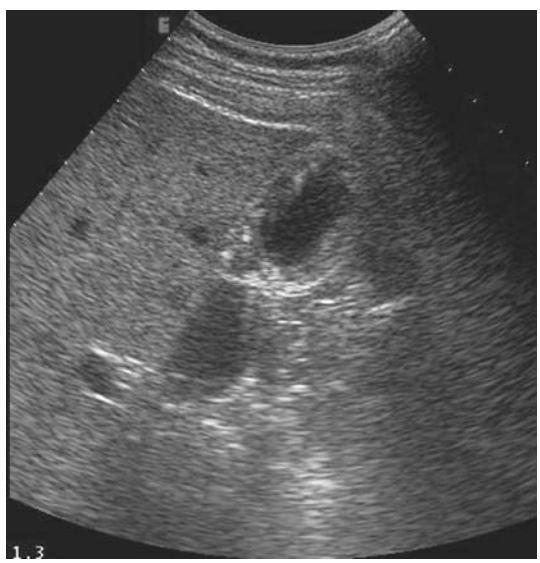

Cholecystoses. Figure 1 ►*Adenomyomatosis gallbladder*. **US shows a segmental mural thickening involving the fundus and partially the body. Rokitansky–Aschoff sinuses appear as anechoic diverticula associated with echoic foci and short reverberation artifacts.**

MR helps to differentiate adenomyomatosis from cholesterolosis and benign from malignant thickening of the gallbladder wall. MR signs suggestive of adenomyomatosis are gallbladder wall thickening with multiple intramural cystic components from Rokitansky–Aschoff sinuses, readily visualized as markedly hyperintense spots on the images, especially using heavily T2-weighted MR breath-hold sequences. Early mucosal enhancement, followed by a serosal enhancement, is a typical feature of the diffuse type of adenomyomatosis. Localized adenomyomatosis displays homogeneous enhancement, showing smooth continuity with the surrounding gallbladder epithelium (3).

Cholesterolosis, Gallbladder

Today, oral cholecystography has been largely replaced by US and to a lesser degree by MR cholangiopancreatography for the evaluation of cholesterolosis. This technique usually shows a functioning gallbladder with single or multiple, fixed, filling defects with a slightly irregular surface caused by the larger, polypoid cholesterol deposits. These filling defects may occur anywhere in the gallbladder and project into the lumen rendering the edges of the gallbladder unsharp. These excrescences appear as fixed lucencies in the opacified gallbladder lumen and are distinguished from calculi thanks to their fixity with compression and positional change.

US shows the lesions as nonshadowing, immobile, intraluminal echoic structures. In fact, cholesterol polyps rarely produce a degree of shadowing. However, in some cases acoustic shadowing may occur, mimicking adherent stones. A comet tail pattern due to parietal deposits of cholesterol may also be detected. US features of the diffuse form of cholesterolosis are not specific and more difficult to recognize (2).

Porcelain Gallbladder

Conventional radiography and CT exhaustively depict calcifications shaped by the gallbladder globular contour in the right upper quadrant, with superior characterization by CT. On conventional radiograms these calcifications appear rather pathognomonic enabling the differentiation from other causes of calcifications in the right upper quadrant. US features are unspecific, referring to extensive gallbladder calcifications and the presence of a nonfunctioning gallbladder. Gallbladder calcifications may show different sonographic patterns including hyperechoic linear or semilunar structures with posterior acoustic shadowing that simulates a stone-filled gallbladder, biconvex curvilinear echoic structures with variable acoustic shadowing, irregular conglomeration of echoes with posterior acoustic shadowing, and an echogenic gallbladder wall without acoustic shadowing. Usually a well-demarcated shadow is associated to this condition, although in the case of heavy calcifications or emphysematous cholecystitis a fuzzy shadowing with reverberation may be observed (4–5).

Nuclear Medicine

Cholesterolosis, Gallbladder

Fluorodeoxyglucose positron emission tomography (FDG-PET) can easily differentiate small polypoid lesions of diffuse cholesterolosis from gallbladder carcinoma, showing a focal tracer uptake at the site of gallbladder carcinoma, whereas there is no marker uptake in cholesterol polyps.

Porcelain Gallbladder

Radionuclide scans, with hepatobiliary tracers (^{99m}Tc imminodiacetic acid analog), provide unspecific features depicting a nonfunctioning gallbladder.

Diagnosis

Adenomyomatosis, Gallbladder

The differential diagnosis includes all conditions causing intraluminal polypoid masses such as adenomatous, hyperplastic, and cholesterol polyps, intramural hematoma, and malignancies (gallbladder carcinoma, carcinoid tumor, metastases). The differential diagnosis is mandatory especially in the case of lesions larger than 10 mm and/or associated to focal gallbladder thickening. A typical enhancement pattern on MR images may lead to the diagnosis (3). The clinical setting may aid in excluding other causes in cases of diffuse thickening such as cholecystitis (acute or chronic), nonfasting state, chronic hypoalbuminemia, hepatitis, and congestive heart failure.

Cholesterolosis, Gallbladder

Differentiating between adenomyomatosis and cholesterolosis can be difficult. Solitary polyps located in the fundus of the gallbladder usually cannot be differentiated from adenomyoma. Also, in cases of diffuse forms the preservation of the multilayered pattern of the gallbladder wall may help to differentiate from carcinoma.

Porcelain Gallbladder

Porcelain gallbladder must be differentiated from large, solitary, calcified gallstones, and milky bile syndrome, where the radiopaque content produces features comparable to

porcelain gallbladder both on conventional radiography and US. Calcified hydatid cysts can mimic porcelain gallbladder on plain abdominal radiograms; however, US or CT images promptly lead to the diagnosis. Regarding the differential diagnosis, other causes of calcifications in the right upper quadrant including schistosomiasis, other granulomatous disease, old healed liver infarcts, calcified renal cysts, calcified nonparasitic liver cysts, calcific primary, and metastatic liver tumors must be excluded.

The US appearance alone may lead to the erroneous diagnosis of emphysematous cholecystitis or a stone-filled gallbladder. However, emphysematous cholecystitis usually causes "dirty" shadowing that can be separated by ring down shadows caused by gas within the gallbladder wall or lumen, while a stone-filled gallbladder produces the wall echo shadow sign that is characterized by two parallel echoic bands separated by a hypoechoic space with distal shadowing. The echoic bands correspond to the interface of the gallbladder wall and the liver and the anterior surface of the gallstone, while the hypoechoic one corresponds to the gallbladder wall itself.

Bibliography

1. Hwang JI, Chou YH, Tsay SH et al (1998) Radiologic and pathologic correlation of adenomyomatosis of the gallbladder. Abdom Imaging 23(1):73–77
2. Berk RN, van der Vegt JH, Lichtenstein JE (1983) The hyperplastic cholecystoses: cholesterolosis and adenomyomatosis. Radiology 146 (3):593–601
3. Yoshimitsu K, Honda H, Jimi M et al (1999) MR diagnosis of adenomyomatosis of the gallbladder and differentiation from gallbladder carcinoma: importance of showing Rokitansky-Aschoff sinuses. Am J Roentgenol 172(6):1535–1540
4. Kane RA, Jacobs R, Katz J et al (1984) Porcelain gallbladder: ultrasound and CT appearance. Radiology 152(1):137–141
5. Versaci A, Terranova M, Rossitto M et al (1999) Authors' experience with the role of preoperative ultrasonography in the study of benign lesions of the gallbladder. G Chir Aug-Sep 20(8–9):354–358

Cholecystosis, Hyperplastic

This term is used to describe both cholesterolosis and adenomyomatosis of the gallbladder.

▶Cholecystoses

Choledochal Cyst Type V

▶Congenital Malformations, Bile Ducts

Choledochal Cysts

Congenital anomalies of the bile ducts consisting of cystic dilatations (saccular or fusiform) of the extrahepatic biliary tree, intrahepatic biliary radicles, or both.

▶Congenital Malformations, Liver and Biliary Tract
▶Congenital Malformations, Bile Ducts

Choledochocele

Type III choledochal cysts arising from the intraduodenal portion of the common bile duct.

▶Congenital Malformations, Liver and Biliary Tract
▶Congenital Malformations, Bile Ducts

Cholestasis

▶Occlusion, Bile Ducts

Cholesterolosis, Gallbladder

A type of hyperplastic cholecystosis resulting from the accumulation of triglycerides within macrophages and cholesterol esters mainly in the submucosal layer or lamina propria of the gallbladder wall. A causal association with cholesterol gallstones, super saturation of bile with cholesterol, and hyperlipidemia remains unconfirmed. Two types have been described: a diffuse form, also named "strawberry" gallbladder, and a polypoid form. The gross appearance of strawberry gallbladder includes a diffuse thickening and the presence of yellowish, diffuse, granular, lipid deposits, varying in distribution and size, in the gallbladder mucosa that resemble a strawberry. The polypoid form is characterized by single or multiple, small, discrete polypoid excrescences composed of cholesterol-filled macrophages.

▶Cholecystoses

Chondroblastoma

Chondroblastoma (Codman tumor) is a benign chondroid tumor with a chondroblast-like cellular component and limited matrix production.

▶Neoplasms, Bone, Benign

Chondrocalcinosis

A condition characterized by deposits of calcium pyrophosphate dihydrate (CPPD) crystals in one or more joints that eventually results in damage to the affected joints. It most often affects the knee, wrist, and pubic symphysis.
▶CPPD

Chondrolysis (of Cartilage)

▶Osteonecrosis, Childhood

Chondrosarcoma

Chondrosarcoma is the second most frequent malignant bone tumour and produces cartilage matrix. Frequently arises from benign cartilage lesions such as osteochondroma or enchondroma (secondary chondrosarcoma). It is usually found in middle aged and older adults. Matrix calcifications may be found and cortical bone destruction is a typical finding.
▶Neoplasms, Bone, Malignant

Chronic Bronchitis

▶Airway Disease

Chronic Cystic Mastitis

▶Fibrocystic Disease, Breast

Chronic Intestinal Pseudo Obstruction

▶Hirschsprung Disease and Related Disorders

Chronic Liver Disease

▶Cirrhosis, Hepatic

Chronic Lung Disease of Prematurity

▶Dysplasia, Bronchopulmonary

Chronic Lymphatic Thyroiditis

▶Thyroid Autoimmune Diseases

Chronic Obstructive Pulmonary Disease (COPD)

▶Airway Disease

Chronic Polyarthritis

▶Rheumatoid Arthritis

Chronic Thromboembolic Pulmonary Hypertension (CTEPH)

▶Chest Thromboembolic Diseases

CIN

▶Contrast Induced Nephrotoxicity

Circumferential Resection Margin

The circumferential resection margin is the distance from rectal tumour to the resection plane (mesorectal fascia) when viewed in a transverse section through the rectum. A complete resection of rectal cancer is defined as a CRM of >2 mm. The CRM can be predicted preoperatively on MRI. In this way, radiologist can predict a narrow margin and indicate at which location a wider excision is needed for radical resection.

▶Rectal Carcinoma

Circumscribed Carcinoma

▶Carcinoma, Other, Invasive, Breast

Cirrhosis, Hepatic

Massimo Bazzocchi, Bartolozzi Carlo, Giuseppe Como, Chiara Franchini
Università degli Studi di Udine, Udine, Italy
massimo.bazzocchi@med.uniud.it

Synonyms

Chronic liver disease; Liver cirrhosis

Definition

Chronic liver disease characterized by diffuse widespread disruption of normal liver architecture with necrosis, fibrosis and formation of ▶regenerative nodules that is caused by various aetiology.

Pathology and Histopathology

Cirrhosis is the final result of chronic liver injury characterized by extensive fibrosis and regenerative nodules replacing the normal liver parenchyma. The process is initiated by necrosis, followed by connective tissue formation and nodular regeneration, leading to distortion of the lobar and vascular liver architecture (1). Regenerating nodules may vary from micronodules (lesser than 3 mm in diameter) to macronodules (3 mm to several centimeters in diameter). The causes of liver cirrhosis could be divided into toxic, inflammation, biliary obstruction, vascular, nutritional, hereditary and idiopathic. The most common causes of liver cirrhosis are chronic viral hepatitis C (HCV) and B (HBV) and alcoholic liver disease. Less frequent are biliary diseases, haemochromatosis, Wilson's disease, galactosemia, tyrosinosis and drug-induced cirrhosis. Cirrhosis is the most important cause of portal hypertension. The obstacle to the portal flow is intrahepatic, being related to compression of hepatic sinusoids caused by regenerative nodules and fibrosis.

Cirrhosis is a premalignant condition: the development of hepatocellular carcinoma (HCC) represents a common long-term complication. Different types of hepatocellular nodules can be found in the cirrhotic liver: regenerative nodule, low-grade and high-grade ▶dysplastic nodule hepatic, HCC. A stepwise carcinogenesis for HCC has been proposed. Ordinary cirrhotic nodules are termed regenerative nodules. The term dysplastic nodule replaces older terms like adenomatous hyperplasia and refers to a nodular region of hepatocytes with dysplasia but without definite malignancy. They are considered premalignant nodules. In the de novo pathway, a single cell may give rise to a focus of small HCC that will develop into a large HCC (2). In the progression from regenerative nodule to overt HCC, there is a reduction in portal blood supply and development of new arterial anomalous vessels, called non-triadal arteries.

Clinical Presentation

Cirrhosis may be clinically silent. It gives non-specific symptoms such as anorexia, weight loss and weakness. Clinical manifestations may be related to portal hypertension: ascites, oesophageal varices, splenomegaly, hepatic encephalopathy. Death usually occurs for progressive liver failure, complications related to portal hypertension, development of HCC.

Imaging

The role of imaging is assessing intrahepatic and extrahepatic signs of cirrhosis and, above all, revealing the presence of HCC.

Ultrasound

Intrahepatic signs of cirrhosis are related to changes in size, morphology, margins and echostructure of the liver. In the early-stage of the disease, the liver may show normal or slightly increased dimensions. In more advanced

stages, hypertrophy of the caudate lobe and the lateral sector of the left lobe associated to atrophy of the right lobe can be observed. This leads to an increased ratio of the size of the caudate lobe to the right lobe that is widely accepted as a sign of cirrhosis (caudate lobe to right lobe size ratio >0.65) (3). The atrophy of the right lobe may result in a widening of the great interlobar fissure and prehepatic colonic interposition. The medial segment of the left hepatic lobe may also be atrophic; this results in enlargement of periportal and pericholecystic spaces (gallbladder fossa), filled by adipose tissue (4). Peculiar sign of cirrhosis is superficial nodularity, best demonstrated using high-frequency probes (Fig. 1). Nodular regeneration may also determine alteration of the profile of hepatic vessels, particularly hepatic veins (5). Cirrhotic liver may show a normal homogeneous parenchymal echostructure, or have an aspecific 'bright liver pattern', with fine, tightly packed echoes distributed throughout the liver parenchyma, as observed also in hepatic steatosis and hepatic fibrosis. The so-called 'coarse pattern' is considered a specific sign of cirrhosis: it consists in inhomogeneous, coarse, thick, echoes, with or without multiple small hypoechoic nodules in the liver tissue (5). A common finding is enlarged lymph nodes at the porta hepatis.

Extra-hepatic signs are related to the portal hypertension: they include ascites, splenomegaly, dilatation and reversal of flow in portal, splenic and superior mesenteric veins, portal vein thrombosis and demonstration of portosystemic collaterals. The diameter of the main portal vein should not exceed 13 mm. In portal hypertension, the normal calibre variation during respiration is not present. Doppler US gives information about flow direction and velocity in the portal vein. A mean velocity <16 cm/sec in the portal trunk suggests portal hypertension. The presence of hepatofugal flow within the main portal vein or reversal of flow in the splenic vein is the indicative for portal hypertension. Patients with cirrhosis are at high risk of developing portal thrombosis. At conventional US chronic portal thrombosis is depicted as hyperechoic material within the portal veins. Recent thrombosis is anechoic and could be not appreciated on conventional US, while can be detected with colour-Doppler US. US is able to demonstrate portosystemic collaterals, such as paraumbilical vein, gastro-oesophageal veins and spleno-renal shunt. The spleen may be enlarged, usually with a homogeneous parenchymal echostructure. Ascites is a common and serious complication of advanced cirrhosis. Gallbladder and stomach wall oedema resulting from portal hypertension may also been observed.

US is the imaging modality of choice in the screening for HCC in cirrhotic patients. The detection of a nodule at US in a cirrhotic liver should raise the suspicion of HCC and require further imaging investigations. The imaging criterion which allows the diagnosis of HCC is the

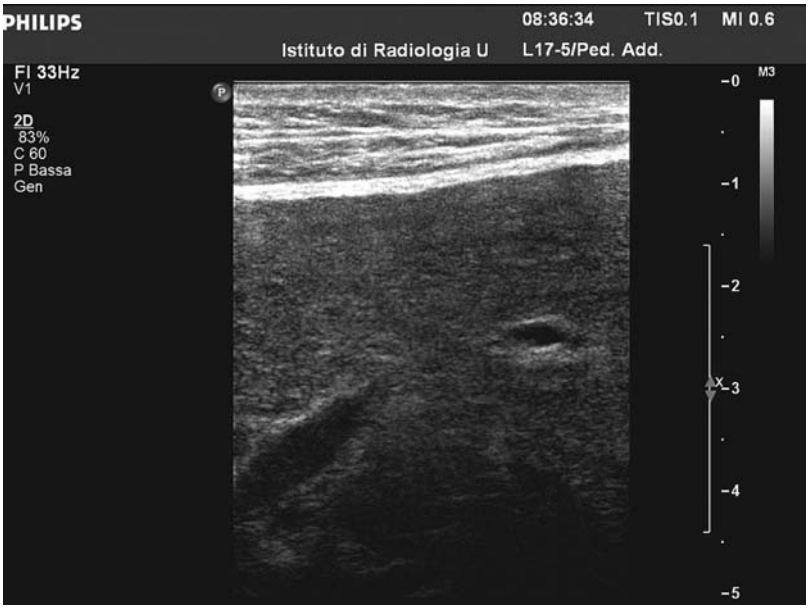

Cirrhosis, Hepatic. Figure 1 US scan with high frequency linear probe. Peculiar sign of cirrhosis is superficial nodularity, best demonstrated using high-frequency probes. We can see so called 'coarse pattern' that is considered a specific sign of cirrhosis: it consists in inhomogeneous, coarse, thick, echoes, with multiple small hypoechoic nodules in the liver tissue.

demonstration of arterial hypervascularization. The use of US contrast media can reliably demonstrate the hypervascularity of HCC.

Computed Tomography

At CT, the cirrhotic liver may appear normally sized or slightly enlarged in the early-stage disease; in advanced stage the global size tends to decrease and the typical is atrophy of the right lobe and hypertrophy of the caudate lobe and of the lateral sector of the left lobe. Atrophy of the medial sector of the left lobe (IV segment) may occur, with consequent enlargement of the gallbladder fossa and the periportal space, filled by adipose tissue. The margins may be irregular, with a nodular appearance. The parenchymal structure may be normal or inhomogeneous. The density of the regenerative nodules rarely differs from that of the cirrhotic liver tissue. Sometimes they show a slight hyperdensity on unenhanced scans, due to their iron content, or a slight hypodensity, due to fatty changes. Regenerative nodules may also become evident for causing mass effect on intrahepatic vessels, which appear compressed or displaced. Contrast-enhanced CT study in cirrhotic liver always includes the arterial phase and the portal–venous phase. The arterial phase is crucial in detecting HCC nodules which typically have a hypervascular pattern. Regenerative nodules do not have a prevalent arterial blood supply. In the arterial phase they usually appear hypodense, sometimes isodense, in the portal–venous phase they are hypo-isodense. A frequent finding is the presence of areas of anomalous perfusion during the arterial phase. These anomalies are called 'transient hepatic attenuation differences' (THAD), because the hyperdensity observed in the arterial phase disappears in the portal–venous scans. THAD are due to small arterial–portal fistulas and have a triangular shape, a peripheral location and do not show mass effect. The portal–venous phase is important in assessing the patency of portal system's veins and the presence of porto-systemic collaterals. Portal thrombosis appears as a defect of contrast enhancement within portal vessels. Large oesophageal varices are often recognizable. Splenomegaly and ascites are accurately demonstrated at CT (Fig. 2).

Magnetic Resonance

Cirrhosis alone does not markedly alter the T1 and T2 relaxation times because fibrous bands and scars constitute a small fraction of liver volume. Cirrhosis is diagnosed by MR using morphologic features analogous to those at US and CT: hypertrophy of the left hepatic and caudate lobes (caudate lobe to right lobe size ratio >0.65), a nodular appearance of the liver surface, and distortion or compression of intrahepatic vessels. In the micronodular form of cirrhosis, the liver surface shows a subtle irregular appearance. MR is much more sensitive than CT in demonstrating regenerative nodules. Regenerative nodules appear as small (<2 cm) nodular lesions, with low signal intensity on T2-weighted images and variable signal intensity on T1-weighted images (Fig. 3). When they contain iron (siderotic nodules) they appear hypointense both on T1-weighted and in T2-weighted

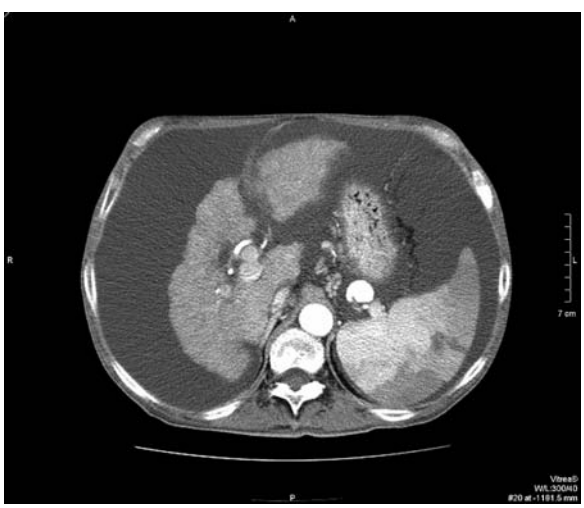

Cirrhosis, Hepatic. Figure 2 CT axial scan of cirrhotic liver in advanced stage: the global size decrease. The margins are irregular, with a nodular appearance. The parenchymal structure is inhomogeneous. There are signs of portal hypertension with the spleen that is enlarged and with inhomogeneous density.

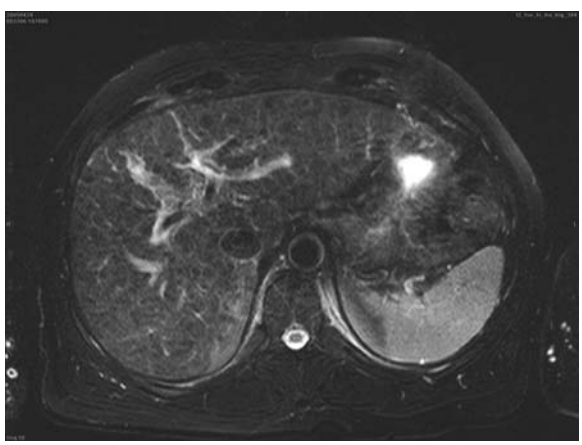

Cirrhosis, Hepatic. Figure 3 MR TSE T2 axial scan: We can see a nodular appearance of the liver surface with distortion of intrahepatic vessels. MR is much more sensitive than CT in demonstrating regenerative nodules. Regenerative nodules appear as small nodular lesions, with low signal intensity on T2-weighted images.

scans. Regenerative nodules may present increased signal intensity on T1-weighted images due to high triglyceride content in zones of fatty degeneration. They are never hyperintense on T2-weighted images. Regenerative nodules show no enhancement on arterial phase gadolinium-enhanced images (2). They appear hypointense with a better demarcation in contrast to the surrounding liver parenchyma using delayed images. Dysplastic nodules and early HCCs show similar features regarding signal intensity, although the latter may be hyperintense on T2-weighted images. Like regenerative nodules, dysplastic nodules can be siderotic. HCC may arise within a high-grade dysplastic nodule. These lesions have a nodule-within-a-nodule appearance on MR images, consisting of one or more hyperintense internal foci within a low signal intensity nodule on T2-weighted images. The central nodule usually also shows enhancement during the arterial phase at gadolinium-enhanced dynamic study (1, 2). HCC shows high signal intensity on T2-weighted images and variable signal intensity on T1-weighted images. However, the differentiation of HCC from regenerative nodules and dysplastic nodules relies on the arterial blood supply of HCC responsible of the typical intense enhancement during the arterial phase of dynamic gadolinium-enhanced imaging of HCC (2). Findings in portal hypertension include enlargement of the extrahepatic portal–venous system (portal vein diameter >13 mm), presence of portosystemic collaterals and splenomegaly. Siderotic nodules in the spleen, called Gandy-Gamna nodules, appear as tiny hypointense foci on T2-weighted images. They are pathognomonic of portal hypertension. Ascites, gallbladder and small bowel wall oedema are manifestations of associated hepatic failure (1).

Interventional Radiology

In cirrhotic patients, hepatic resection for HCC may worsen the hepatic function so interventional procedures can be performed for the treatment of HCC. The rationale is destroying the tumoural tissue, sparing the non-tumoural tissue. Percutaneous ethanol injection (PEI), thermal ablation and transcatheter chemioembolization (TACE) are the main non-surgical therapeutic tools for the treatment of HCC.

Transjugular intrahepatic porto-systemic shunt (TIPSS) is used for the treatment and the prevention of oesophageal variceal bleeding in portal hypertension.

Diagnosis

Cirrhosis may be suspected on the basis of symptoms and laboratory. The diagnosis can be suggested at imaging. Imaging techniques (US, CT, MR) are able to identify hepatic and extrahepatic manifestations of liver disease. The definite diagnosis of cirrhosis is traditionally established with biopsy.

Bibliography

1. Lencioni R, Bartolozzi C (2003) Diffuse liver disease. In: Magnetic Resonance Imaging in Liver Disease, pp 163–197. Thieme: Stuttgart-New York
2. Hussain SM, Zondervan PE, IJzermans JNM et al (2002) Benign versus malignant hepatic nodules: MR imaging findings with pathologic correlation. Radiographics 22:1023–1036
3. Awaya H, Mitchell DG, Kamishima T et al (2002) Cirrhosis: modified caudate-right lobe ratio. Radiology 224(3):769–774
4. Ito K, Mitchell DG, Gabata T et al (1999) Expanded gallbladder fossa: simple MR imaging sign of cirrhosis. Radiology 211(3):723–726
5. Caturelli E, Castellano L, Fusilli S et al (2003) Coarse nodular US pattern in hepatic cirrhosis: risk for hepatocellular carcinoma. Radiology 226(3):691–697

Classification of the American College of Radiology (ACR)

▶BI-RADS, Lexicon

Claudication Brachial

Elias N Brountzos
2nd Department of Radiology, Athens University, Medical School, Greece
ebrountz@cc.noa.gr

Synonyms

Upper extremity claudication; Arm claudication

Definition

Arm, hand, or brachial claudication is described as forearm or hand pain or disabling discomfort arising during exercise.

Pathology

This symptom is characteristic of chronic ischemia of the upper extremity.

Clinical Presentation

Depending on the degree of the reduction of arterial perfusion, the claudication appears with minimal activity such as hair combing, or requires prolonged activity. Brachial claudication represents the most common indication for upper extremity arterial revascularization (1).

See ►Brachial Ischemia

Bibliography

1. Whitehouse Jr (2000) Upper extremity revascularization. In: Rutherford RB (ed) Vascular Surgery, WB Saunders, Denver, Colorado, pp 1162–1170

CLD

►Dysplasia, Bronchopulmonary

Clear Cell Renal Carcinoma

The most common type of RCC, accounting 70% to 80% of the cases in surgical series. This type is diagnosed by histologic and cytogenetic criteria.

►Nodules, Pulmonary, Solitary

Cleft Lip, Palate, and Alveolus Defects

Cleft abnormalities of the lip, palate, and alveolus are the most common congenital disorder of the oral cavity and result from developmental defects with incomplete fusion of the lips, palate, and/or alveolus.

►Congenital Malformations, Oral Cavity

Cloaca

A cloaca is defined as an opening in an involucrum. Pus or sequestra can be discharged through a cloaca in chronic Osteomyelitis.

►Osteonecrosis, Adults

Clonorchiasis

Parasitic infestation by a metacercaria (Clonorchis sinensis) endemic in Southeast Asia and China that most frequently causes a fibrosing cholangitis. The ingestion of contaminated uncooked fresh fish can cause infection in humans.

►Cholangitis

Closed Loop Obstruction

Closed loop obstruction occurs when a segment of bowel is obstructed at both ends, such as in a hernia or by a dense adhesion and becomes distended with a potential to twist on its mesentery.

►Occlusion and Subocclusion, Small Bowel in Adults
►Small Bowel, Postoperative

Clubbed Digits

Digital clubbing is a bulbous digital deformity with a watch-crystal deformity of the fingernail, associated with intrathoracic malformations, neoplastic or inflammatory conditions, as well as with hypertrophic osteoarthropathy.

►Hypertrophic osteoarthropathy

CM

►Spinal Cord Cavernous Malformation

CNS

Central nervous system.

►Tumors, Spine, Intradural, Extramedullary

CNS Toxicity

►Toxic Disorders, Brain

Coarse Liver

Ultrasonographic finding consisting with hepatic cirrhosis. It is characterized by the presence of inhomogeneous, coarse, thick, echoes, with or without evidence of multiple small hypoechoic nodules diffusely distributed throughout the liver tissue.

▶Cirrhosis, Hepatic

Coating of Ultrasound Contrast Media

▶Contrast Media, Ultrasound, Influence of Shell on Pharmacology and Acoustic Properties

Cobb Angle

Standard technique to measure the angle of scoliosis. Lines are drawn in extension of the uppermost and lowermost endplates of the neutral vertebrae. Neutral vertebrae have parallel endplates with—in contrast to the other vertebrae—minimal or no change in shape and are maximally tilted to the horizontal line.

▶Scoliosis

Codman's Angle

Usually suggests an aggressive lesion, found in rapidly growing lesions that penetrate through the cortex causing separation of the periosteum and formation of lamellated new bone, once the periosteum elevates to a significant degree, it can break forming an acute angle. However, findings similar to Codman's angle may also be shown in benign pathologies such as osteomyelitis and subperiosteal hematoma.

▶Neoplasms, Bone, Malignant

Coiling

Application of wire-coils with special configurations and sizes into vascular malformations, mainly into saccular aneurysms, in order to decrease the risk of rupture and hemorrhage.

▶Stroke, Interventional Radiology

Colic

According to Dorland's Medical Dictionary, colic is an acute abdominal pain; characteristic intermittent visceral pain with fluctuations corresponds to smooth muscle peristalsis. Renal colic is pain produced by thrombosis or dissection of the renal artery, renal infarction, intrarenal mass lesions, the passage of a stone within the collecting system, or thrombosis of the renal vein; called also nephric colic.

▶Colic, Acute, Renal

Colic, Acute, Renal

Darja Babnik Peskar, Eveline Smrtnik
University Medical Center Ljubljana,
Ljubljana, Slovenia
darja.babnik@kclj.si

Synonyms

Kidney stones; Renal colic; Ureteral colic; Urinary stones

Definition

Renal colic is a symptom complex characteristic for the presence of obstructing urinary tract calculi. It is defined as pain caused by stone passage within the collecting system (1). According to Dorland's Medical Dictionary, it may also be caused by thrombosis or dissection of the renal artery, renal infarction, intrarenal mass lesions, or thrombosis of the renal vein.

Acute renal colic is more correctly termed ureteral colic, as it is predominantly the result of a ureteral calculus. It is characterized by an abrupt onset of severe pain in the flank or kidney area, radiating anteriorly and caudally to the groin and anterior thigh. During passage, stones cause partial or complete obstruction,

local spasm, proximal dilatation, and stretching of the collecting system, which are responsible for the pain characteristics.

Pathology/Histopathology

►Urinary stones affect 2–3% of the population, usually the middle age group, with a 2:1 male predominance (1, 2). Up to 75% of stones are composed of calcium oxalate, the rest of struvite (magnesium ammonium phosphate), uric acid, hydroxyapatite, or cystine. Stone formation can be associated with primary metabolic abnormalities, primary hyperparathyroidism, prolonged immobilization, recurrent urinary tract infection, malignancy, sarcoidosis, Crohn's disease, laxative abuse, jejuno-ileal bypass, renal tubular acidosis, and gout.

The typical pain of renal colic is caused by distension of the renal pelvis and calices and stretching of the renal capsule in the acutely enlarged kidney. Nausea and vomiting occur due to the common innervations of the renal pelvis, stomach, and intestines through the celiac axis and vagal nerve afferents. In the midureter and lower ureter, pain is predominantly generated by increased peristalsis, muscle spasm, local irritation, and edema.

In ►Urinary Obstruction, Acute, autoregulatory changes of renal blood flow, glomerular filtration rate, and tubular function affect intrarenal hydrostatic pressure (1, 2). The initially increased renal blood flow preserves the glomerular filtration rate in the first hour. Together with an increase of hypotonic urine production and hyperperistalsis, they make an attempt to overcome obstruction. If passage is not attained after 3–5 h, preglomerular arteriolar vasoconstriction causes blood flow to decrease, while hydrostatic pressure continues to rise. After 5 h, both renal blood flow and pressure start to decrease, gradually leading to reduction of pain. Other changes that reduce renal pelvic hydrostatic pressure in the early phase are pyelolymphatic or pyelovenous backflow, and urine leakage into the renal parenchyma and perinephric soft tissues from forniceal rupture in 20% of cases (1, 2). In complete ureteral obstruction, irreversible loss of renal function will already be present after 48 h. Interstitial nephritis and fibrosis may cause atrophy of renal tissue.

Obstructive uropathy from ureteral calculus refers to acute, partial and one-sided obstruction, where renal function is preserved but lowered. A complete recovery of function is expected if blockade is eliminated in time. If obstruction is eliminated after 24 h renal function may recover in 7 to 10 days. Obstruction that lasts 2 to 3 weeks causes renal tubular function to be permanently damaged, thus leading to obstructive nephropathy. Four to eight weeks from onset of obstruction, renal function ceases and we speak of the afunctional kidney.

Clinical Presentation

The classic presentation of renal colic (1) is the acute onset of severe flank or kidney pain radiating to the groin or testicle in the male, and in the labia majora in the female, or in the anterior thigh, with either gross or microscopic hematuria (85%), nausea and vomiting (50%), tachycardia, hypertension, and costovertebral angle tenderness. When ureteral stones are near the bladder urinary frequency and urgency develop. Fever and the presence of leukocytosis, pyuria, or bacteriuria suggest the possibility of infected urinary lithiasis or pyonephrosis. Urinanalysis may reveal original urine crystals. Patients should be encouraged to retrieve stones for analysis.

Pain in renal colic is constant, and lasts for minutes to hours; however, exacerbation of pain with intervals of no pain may occur due to stone passage. Patients tend to move constantly to relieve pain, while patients with an acute abdomen try to be motionless.

Most symptomatic upper urinary tract stones are less than 5 mm in diameter, and the majority of them pass spontaneously in 24–48 h (1). Spontaneous stone passage depends on stone diameter, shape, location, and anatomy of the urotract. In absence of ureteropelvic junction (UPJ) obstruction or ureteral stricture, 4 mm or smaller stones may pass spontaneously in 90%, calculi between 5 and 10 mm in 50% of cases, while larger stones usually require intervention.

Imaging

►Plain film of the kidney, ureter, and bladder (KUB) can be diagnostic of urinary stones, since 90% are radiopaque (1). KUB is necessary for the follow-up of stones that do not pass spontaneously, and for lithotripsy planning and survey. KUB can miss small stones, radiolucent stones (uric acid, xanthine, dihydroxyadenine, indinavir, triamterene stones), or stones overlying bone. Phleboliths, vascular calcifications, calcified lymph nodes, appendicoliths, granulomas, various calcified masses, and even bowel contents can sometimes be confused with urinary tract stones.

When clinical presentation and KUB are not diagnostic, other imaging methods help in the early diagnosis of renal colic. ►Intravenous urography (IVU) is still the gold standard (1), and is preferred by urologists. The main advantages of IVU are the demonstration of renal

function, the precise outlining of the urinary collecting system, the detection of mild or local dilatation, and the differentiation of the obstructing stone from calcium deposits in medullary sponge kidneys (MSK), from abdominal calcifications, and from other intra- or extraluminal pathology. Indirect signs, such as delayed excretion and persisting nephrogram, pyelosinus backflow and extravasation of contrast around the collecting system, are highly suggestive or positive for acute stone obstruction (Fig. 1). After obtaining a KUB and 5 min postcontrast film, either a 10–15 min supine, full abdomen film is obtained to visualize the normally functioning urotract, or a prone film is obtained to spill contrast in the collecting system from the opacified calices on the affected side. A standing oblique film should be obtained under fluoroscopic control, to opacify the ureter to the level of obstruction and to differentiate ureteral stones from other calcifications. If the collecting system is not ready opacified, 1–2 delayed films are required up to a few hours later, and rarely after 24 h. A conducted IVU consists of 4–6 films, depending on the delay. IVU remains price and radiation risk competitive with unenhanced CT (UHTC).

►Ultrasound (US) is a noninvasive, radiation-free method, and may be the initial method in the evaluation of renal colic. It is accepted as a follow-up investigation for monitoring spontaneous stone passage after extracorporeal shock wave lithotripsy (ESWL) or surgical treatment. US can demonstrate obstruction and the obstructing stone based on its echogenicity and dorsal acoustic shadowing. It has certain limitations in evaluating obstruction and depicting small midureteral stones. Its effectiveness is also operator-dependent. In acute colic, with or without a dilated collecting system, duplex ►Doppler US suggests stone obstruction by the assessment of an elevated intrarenal resistive index (RI > 0.7; 92% sensitivity, 88% specificity) or a difference of RI between both kidneys larger than 0.04 (1, 3). False-negative RI results in the first hours after onset may be explained by initial vasoregulation and spontaneous pelvocaliceal rupture (4) (Fig. 3). A characteristic slow or absent ureteral jet in the bladder, and the twinkling artifact behind stones help in the diagnosis of stone obstruction.

►Retrograde pyelography refers to direct ureteral contrast injection through a catheter inserted at cystoscopy. It is the most precise imaging method for diagnosing any type of ureteral pathology, but is rarely performed; mostly when obtaining material for cytology, and prior to ureterorenoscopy (URS) or the placement of double-J stents. When the insertion of double-J stents fails, therapeutically inserted percutaneous nephrostomes (PNS) can also be used for *anterograde pyelography* (1, 2) (Fig. 2).

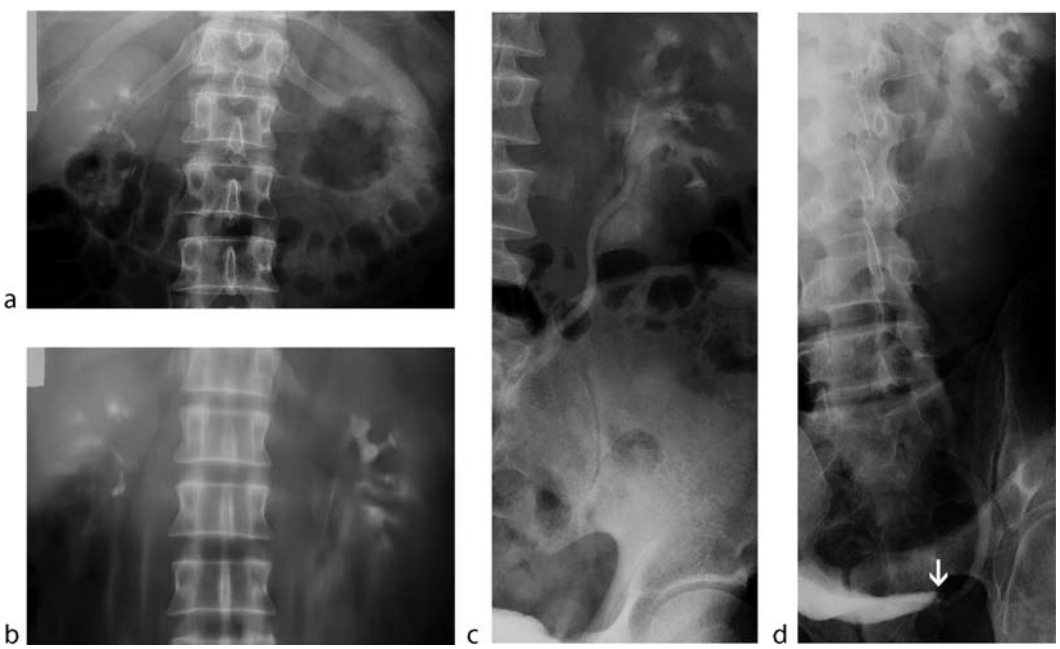

Colic, Acute, Renal. Figure 1 IVU examination in a 55-year-old man with acute renal colic demonstrates (a) slightly delayed excretion on the left 5 min after 30 mL nonionic contrast injection, (b) extravasation around the nonopacified pyelon and proximal ureter after spontaneous caliceal rupture on tomography, (c) in prone position pyelon and ureter opacify 10 min postcontrast, (d) visible level of obstruction at the UVJ due to a small left ureteral calculus *(arrow)*.

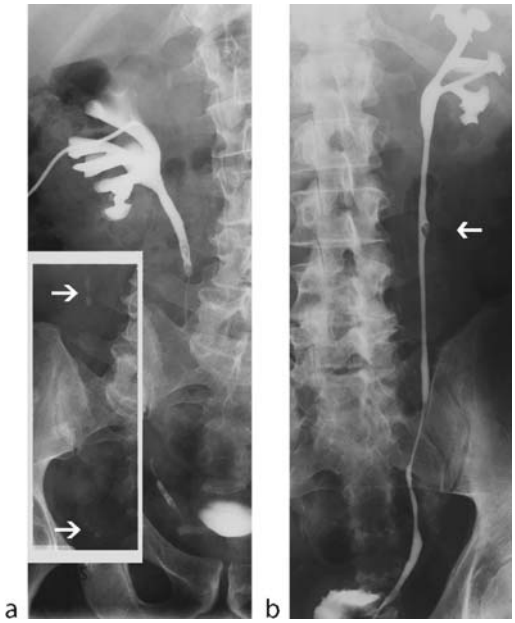

Colic, Acute, Renal. Figure 2 (a) Small radio-opaque right-sided urinary stones detected at KUB *(arrows)* in a female with acute renal colic after ESWL. Percutaneous nephrostoma was inserted after unsuccessful double-J insertion. On anterograde urography these radiopaque and severely obstructing stones were demonstrated as less radiopaque than contrast. (b) Retrograde urography in 64-year old man with acute renal colic and suspected radiolucent left ureteral calculi. An atypical eccentric filling defect is delineated *(arrow)*. IVU was inconclusive, but US confirmed a ureteral stone.

UHCT has proved to be more accurate than IVU for the diagnosis of urinary calculi and equal in demonstrating dilatation (5). It is indicated in patients with a high risk for use of contrast media, in nonfunctioning kidneys, or when urography is inconclusive. Other advantages of CT over IVU are the demonstration of other abdominal pathology. Thin section (3.5 or 5 mm) UHCT has a sensitivity of 97%, and specificity of 96% for the investigation of renal colic (1). Secondary signs typical for the acute phase are periureteral or perirenal tissue stranding and the tissue rim sign due to edema in the ureter wall around small calculi. A split bolus technique of contrast administration and scanning during the nephrographic and excretory phase provides evaluation of renal function and parenchymal alterations, and delineates the collecting system. The advent of multislice-computed tomography (MSCT) provides the ability to perform CT urography with a spatial resolution closer to that obtained at IVU. High-resolution multiplanar (MPR), maximum-intensity (MIP), and average-intensity (AIP) images of the collecting system are generated from unenhanced and enhanced CT data (Fig. 4a).

MR urography is regarded as a diagnostic test of secondary reference following IVU, US, and CT (6). Two different techniques of MRI, depending on the clinical situation, are available. Static-fluid MR urograms are obtained with heavily T2-weighted turbo spin-echo sequences. Dynamic or excretory MR urograms are obtained with gadolinium contrast agent administration and T1-weighted gradient-echo sequences (Fig. 4b, c).

Diagnosis

The diagnosis of an obstructive urinary stone is essential for the exclusion of acute surgical abdominal pathology (appendicitis or abdominal aortic aneurysm). Urinary tract infection, cardiac ischaemia, bowel ischaemia or obstruction, hepatic capsulitis, musculo-skeletal pain, and biliary colic, are also considered in the differential diagnosis.

In patients with acute flank pain, the diagnosis of ureteral calculi can be apparent according to positive history, physical examination, and laboratory studies. In presence of hematuria, calculi are confirmed with 96% accuracy by a positive KUB. Radiological imaging is required to evaluate the location of the stone, the exact size, shape, orientation, radiolucency, all necessary for treatment planning. Kidney function and the presence of infection are assessed. Until recently, IVU was performed to evaluate stone obstruction in inconclusive cases, with a sensitivity of 95%. Recently, abdominal US supersedes IVU in patients with positive KUB. It is the test of choice if KUB is negative, since it can effectively demonstrate radiolucent stones, or exclude other causes of abdominal pain. The reported sensitivity of US for stone detection varies, the highest is 98%. US easily demonstrates larger stones within the renal pelvis and stones in the dilated ureter near the UPJ and ureterovesical junction (UVJ). In the absence of dilatation (35%), duplex Doppler US can assess an elevated RI in the affected kidney, and asymmetry of ureteral jets, thus helping to exclude false-negative cases. It reduces the number of false-positive results by assessing nonobstructive dilatation in cases of extrarenal pelvis, UPJ obstruction, prominent vasculature, residual dilatation, vesicoureteral reflux, megacalices, papillary necrosis, pyelonephritis, full bladder, and diabetes insipidus (2).

UHCT of the abdomen may be helpful as an alternative or in the clarification of equivocal US findings. UHCT of the abdomen is more sensitive and more likely to yield a diagnosis than plain radiographs and US.

Management of urinary stones (1) comprises the insertion of a double-J stent in cases of uncontrollable

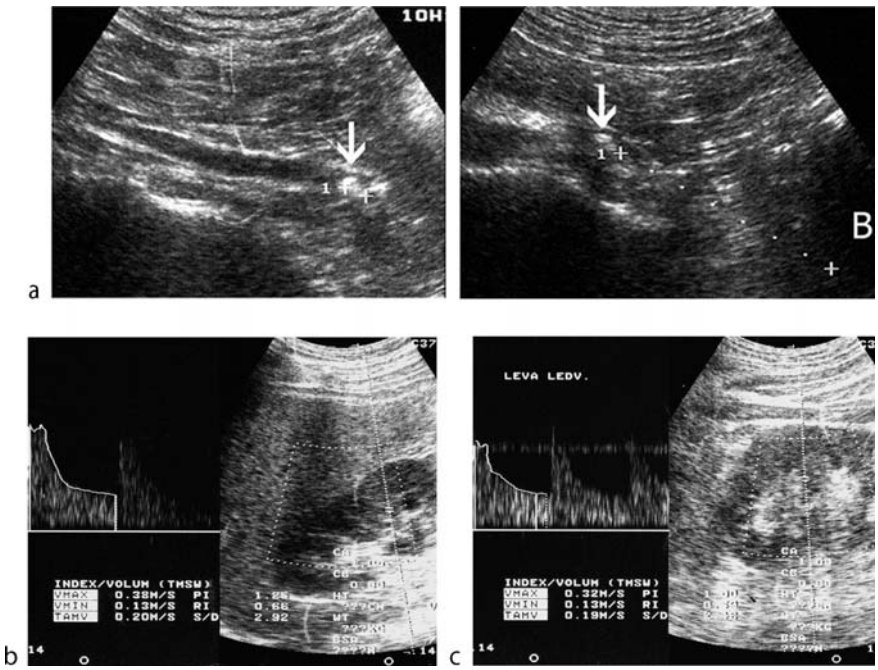

Colic, Acute, Renal. Figure 3 US examination in acute renal obstruction showing (a) ureteral dilatation due to calculus *(arrow)* 6.8 cm from the bladder *(B)*, and (b, c) increased RI in the affected kidney with a significant RI difference of 0.07 between both kidneys. (Contributed by A. Visnar-Perovic)

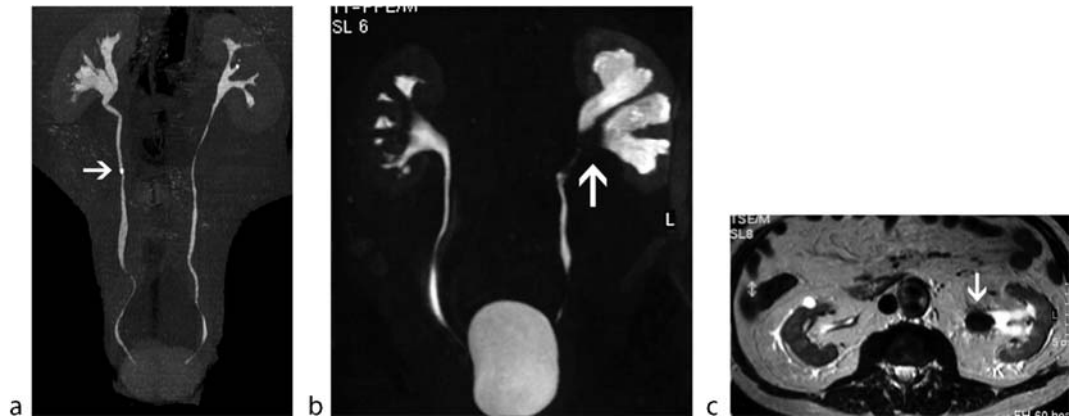

Colic, Acute, Renal. Figure 4 (a) CT urography in 40-year old patient presenting with right-sided flank pain and gross hematuria was performed in a pain-free interval. The MIP image shows a calculus (*arrow*) within the right ureter with sufficient contrast material passage and only slight dilatation of the pelvicaliceal system. In addition, a small infundibular concrement can be appreciated on the left side. (Contributed by J. Kemper) (b, c) MRU case showing a calculus inside the left renal pelvis obstructing the UPJ in a 64-year old man with recurrent left-sided flank pain. (b) MIP from a gadolinium-enhanced T1-weighted breath-hold 3D-gradient-echo-sequence displaying the urographic overview and (c) axial standard T2-weighted TSE-image showing the signal void of the calculus (*arrows*). (Contributed by C. Nolte-Ernsting)

pain, complete obstruction with severe urinary infection or urosepsis, in solitary obstructed kidneys, in large stones that are considered unlikely to pass spontaneously, or in suspected ureteral strictures. Percutaneous nephrostomes are inserted when the insertion of double-J fails. Ten to twenty percent of all urinary stones require surgical removal. Percutaneous nephrostolithotomy (PNL), URS, and ESWL successfully compete to open surgery. Most

urinary stones pass spontaneously in 24–48 h and do not require special treatment other than pain relief, hydration and antiemetics.

Bibliography

1. Menon M and Resnic MI (2002) Urinary lithiasis: etiology, diagnosis, and medical management. In: Campbell MF, Walsh PC, and Retik AB (eds) Campbell's Urology. Urinary Lithiasis and Endourology. WB Saunders Company, Philadelphia, pp 3229–3305
2. Platt JF (1996) Urinary obstruction. Radiol Clin North Am 34 (6):1113–1129
3. Platt JF, Rubin JM, Ellis JH, et al (1989) Duplex Doppler US of the kidney: differentiation of obstructive from nonobstructive dilatation. Radiology 171:515–517
4. Roy C, Tuchmann C, Pfleger D, et al (1998) Potential role of duplex Doppler sonography in acute renal colic. J Clin Ultrasound 26:427–432
5. Smith RC, Verga M, McCarthy S, et al (1996) Diagnosis of acute flank pain: value of unenhanced helical CT. Am J Roentgenol 166:97–101
6. Nolte-Ernsting CC, Staatz G, Tacke J, et al (2003) MR urography today. Abdom Imaging 28:191–209

Colitis, Ulcerative

Francesca Maccioni[1], Sara Parlanti[1], Francesca Siliquini[1], Viola Garbarino[1], Valeria D'Ovidio[2]
[1]Department of Radiological Sciences, Policlinico Umberto I, University of Rome "La Sapienza", Italy
[2]Department of Clinical Sciences, Gastroenteroly Unit, Policlinico Umberto I, University of Rome "La Sapienza", Italy
francesca.maccioni@uniroma1.it

Synonyms

Ulcerative colitis; Ulcerative proctitis; Ulcerative sigmoiditis; Ulcerative pancolitis

Definitions

Ulcerative colitis (UC) was described in 1859 by Sir Samuel Wilks (1824–1911), a British physician who firstly differentiated it from bacterial dysentery.

The greatest incidence of chronic UC is in the second, third and fourth decades of life. The condition is more common in white women. The disease may vary greatly in its severity, course, and prognosis. It has an unknown etiology and a chronic relapsing–remitting course. To date, the pathogenesis of UC still remains unknown, although recent studies showed an important role of environmental enteric, immune, and genetic factors. These studies suggest that UC may result from the loss of tolerance of the immunocompetent intestinal system versus the normal intestinal flora, in genetically susceptible individuals.

UC is characterized by a predictable course and localization, extending continuously from the rectum to the colon, involving first the left colon, then the transverse and right colon, and very rarely the distal ileum. The different patterns of ulcerative colitis are commonly called as "ulcerative proctitis," "ulcerative sigmoiditis," "left-sided colitis," or "pancolitis." A recto-sigmoid localization is present in up to 95% of the patients. The mucosal inflammation of the terminal ileum, is rarely observed in UC, developing only in presence of a pancolitis (the so-called "►backwash ileitis"); in those cases, UC can be hardly differentiated from Crohn's disease (CD).

Pathology/Histopathology

Cryptitis or abscesses of the crypts of Lieberkühn are hallmarks of ulcerative colitis. They form ulcerations that reach the lamina propria, or may produce excrescences also called as "pseudopolyps." With the lateral extension of the ulcers, large areas of bowel wall muscle may be almost completely denuded. Microscopically, UC is characterized by moderate wall thickness, leukocyte infiltrates in the mucosal and submucosal layer, disruption of mucosal elements and aphthoid ulcers, mucosal edema, inflammatory pseudopolyps, without extra-wall lesions neither significant signs of perivisceral inflammations in the majority of cases. Fatty deposition in the submucosal layer is a common finding in long-standing disease. Macroscopically, the chronic inflammatory bowel process of UC determines loss of haustration, moderate strictures, mild diffuse colonic wall thickening, widening of the presacral space, and occasionally severe complications such as massive bleeding, toxic megacolon, tight bowel strictures, or perforation.

The disease is intermittently acute and in the quiescent phase the mucosa may completely heal, but more frequently it appears atrophic with rare crypts, with distorted mucosal architecture and thickening of the lamina propria.

Clinical Presentation

Three degrees of severity are distinguished as mild (about 60–80% of cases), moderate (25%), and severe or fulminant.

Eighty percent of patients have only proctitis or proctosigmoiditis in the early phases of the disease, although in 50% of them a proximal extension later occurs. Only 20% have extensive colitis at the onset of symptoms, the course of the disease can vary widely. Spontaneous remission from a flare-up occurs in 20% to 50% of the patients, although 50% to 70% have a relapse during the first year after diagnosis. The relapse rate is higher in younger patients.

In acute phases, bleeding results from friable and hypervascular granulation tissue; diarrhea with urge incontinence results from damage that impairs the ability of the mucosa in reabsorbing water and sodium. If the disease is more severe, it may extend beyond the mucosa and submucosa into the muscularis mucosa (rarely to serosa) and this explains the dilation of the colon, by loss of motor tone, in cases of toxic megacolon.

Severe disease is indicated by large volumes of diarrhea, weight loss, large amount of blood in the stool, high fever, elevated C-reactive protein, elevated erythrocyte sedimentation rate, low hematocrit value, and hypoalbuminemia. Approximately 65% of patients with UC have positive perinuclear antineutrophil cytoplasm antibodies (pANCA), also present in patients with primary sclerosing cholangitis.

The prevalence of the extraintestinal manifestations such as arthritis, uveitis, pyoderma gangrenous, sacroiliitis, spondylitis, or erythema nodosum, may vary depending on the geographic area, population, location and duration of the disease, medication, and diagnostic accuracy. Patients with ulcerative colitis have an increased risk of developing colorectal cancer. The current procedure to diminish this risk is colonoscopy surveillance and histopathological evaluation of biopsy specimens. This method is not unquestioned and is undergoing continuous evaluation.

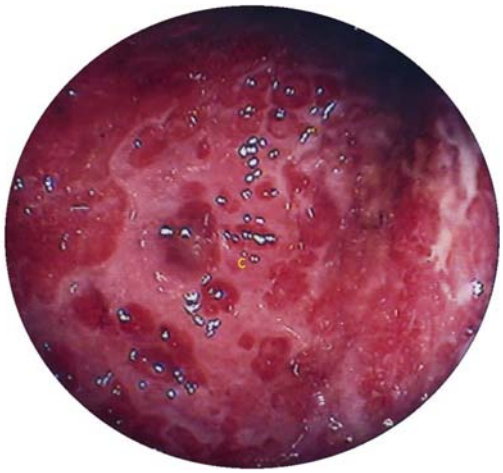

Colitis, Ulcerative. Figure 1 Endoscopic view of the colonic mucosa, as appears in severe ulcerative, very friable, with spontaneous bleeding. Furthermore, loss of vascularity, hemorrhage, and ulcers with fibrin and mucous are well appreciable.

Imaging

Endoscopy

Endoscopy (ES) is definitely a primary examination in the evaluation of UC. The disease is, in fact, usually confined to the colonic mucosa, which is completely accessible to endoscopy. Moreover, endoscopic biopsies, although confined to the mucosa and submucosa layer, may adequately evaluate the severity of colonic wall inflammation, which usually spares the outer muscular and serosa layers.

Typical endoscopic findings include reddening of the mucosa, increased vulnerability, mucosal bleeding, irregular ulcers, pseudopolyps, granularity, loss of vascular architecture, loss of haustration, and occasionally strictures. These changes are continuous in the colon, and the rectum is always involved (Fig. 1).

However, although ES is widely considered the first examination for the diagnosis UC, it can be contraindicated, refused or incomplete in up to 30% of patients with UC. It is an invasive examination causing patient discomfort and associated with possible complications, above all colonic perforation, whose incidence may vary according to the operator's experience, ranging between 0.1% and 3%. Moreover, ES is absolutely contraindicated in the acute phases of severe colitis, due to the higher risk of perforation; in these phases, however, a diagnostic support is crucial to plane an effective treatment. Finally, late complications of UC, particularly tight strictures, can partially or completely prevent the passage of an endoscope. In all these cases other imaging modalities, including barium studies and ►cross-sectional imaging, may add important information on the disease (Fig. 2).

Conventional Radiographs

Barium studies may be an alternative modality to endoscopy to assess luminal changes, particularly when performed with a double-contrast technique. Single- or double-contrast barium enema (BE) may easily visualized the typical mucosal changes of the disease.

In the first phase, BE may show superficial changes related to edema and granulation tissue; occasionally the only sign of inflammation in the early phases is the blunting of the normally acute angles of the rectal valves.

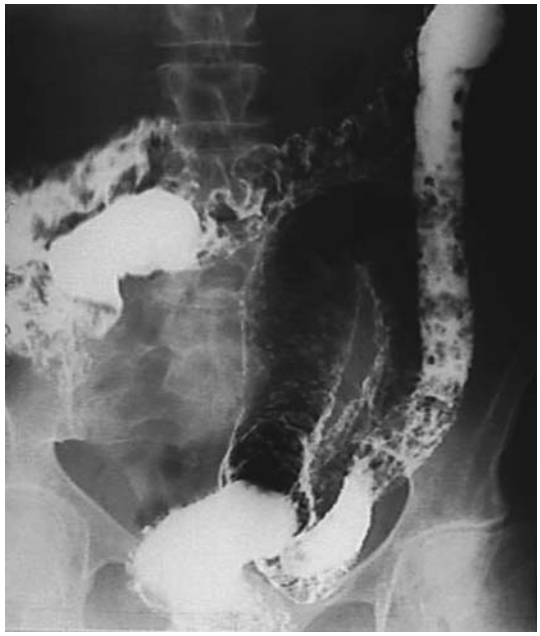

Colitis, Ulcerative. Figure 2 Barium studies, performed with a double contrast technique, shows lack of haustrations and tubular narrowing of the left-side colon, characterized by multiple pseudopolyps and ulcers showing a "collar-button" appearance. (Courtesy of Panzironi G, Department of Radiology, Policlinico Umberto I. Rome, Italy.)

When the disease progresses, using a double-contrast BE, ulcers seen in profile have a "collar-button" appearance. The demonstration of ulcerations by radiographic means is important because these changes indicate clinically and pathologically severe diseases. Between denudated and ulcerated areas, a large number of pseudopolyps may be observed, representing elevation of inflamed mucosa. Secondary changes can be easily seen on both single- and double-contrast BE examinations. Main signs of chronic disease are foreshortening of the colon, lack of haustrations, and tubular narrowing of the colon that gives the large bowel the appearance of a garden hose or stovepipe. Barium studies, although not useful in assessing the clinical activity of UC, can be indispensable in distinguishing between the two diseases (Goldberg et al. 1979; Gore et al. 1997).

In very severe hyper acute phases, a BE may be contraindicated. In such phases a plain film of the abdomen is the best option, being crucial in the identification of the toxic megacolon. This complication is usually well identified at plain films as a severe colonic distention exceeding the 8 cm in diameter in the left colon and the 10 cm in diameter in the right colon. Colonic perforation and free peritoneal air can be easily identified at plain films in upright position as well.

Cross-Sectional Imaging: Ultrasonography, Computed tomography, and Magnetic Resonance Imaging

Cross-sectional studies may play a complementary role in the assessment of UC.

Transabdominal ultrasonography (TUS) is a non-invasive cross-sectional imaging modality that can be helpful in the diagnosis of ▶inflammatory bowel disease (IBD). The main purpose of US is to exclude the involvement of the distal ileum, in order to distinguish UC from CD. High-resolution US, performed with a 7.5 MHz probe, is a well accepted modality to evaluate the wall thickening of the distal ileum in Crohn's disease, therefore it may be extremely useful to differentiate the two diseases, whenever ES or histology are doubtful. Moreover, in more severe colitis, the mild wall thickening, particularly the left and sigmoid colon, if equal or superior to 4 mm, can be well-depicted at high-resolution US. Finally US can be useful in the investigation of biliary complications of the disease, including biliary stones, cholangitis, and cholangiocarcinoma.

Usually cross-sectional modalities cannot assess the typical mucosal changes of UC, but they (CT and MRI above all) can evaluate the mild wall thickening, the increased wall vascularity associated with an active disease, as well the changes in the morphology of the colon. In some cases, cross-sectional imaging may substitute ES and BS, particularly when they are contraindicated in very severe phases.

Thanks to their panoramic and multiplanar capability, both CT and MRI are usually able to distinguish between a proctitis, a left-sided colitis or a pancolitis, according to the findings observed either on axial and coronal planes. MRI Coronal or CT multiplanar reconstructions are very useful to exclude involvement of the terminal ileum, thus helping in differentiating UC from CD, similarly to US. In the evaluation of rectal disease, the mid-sagittal imaging plane offered by MRI better displays the typical widening of the recto-sacral space.

Recently, MRI has been proposed to evaluate the degree of wall inflammation (disease activity) especially in the follow up of patients (thanks to lack of radiations) (Fig. 3). At MR, wall gadolinium enhancement is frequently observed in severe active UC associated marked wall thickening; on the other hand, in moderate disease a moderate wall enhancement can still be present, but

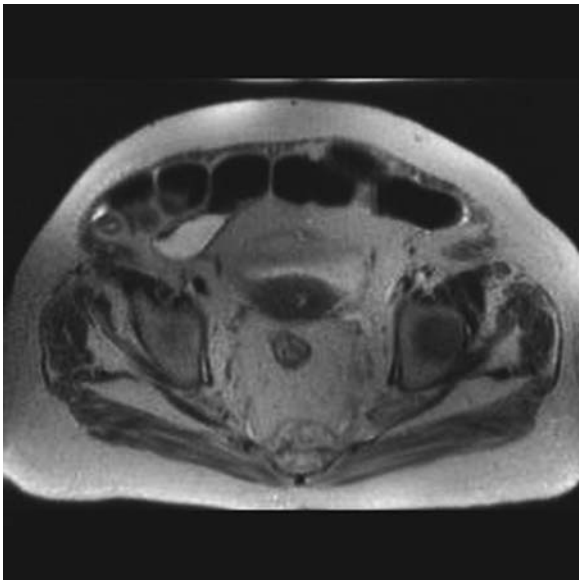

Colitis, Ulcerative. Figure 3 Colitis, Ulcerative. The T2-weighted MR image, acquired on the axial plane, shows a mild case of ulcerative colitis, localized on rectum, demonstrating diffuse thickening and high wall T2 signal of the rectal wall, which is surrounded by abundant fat tissue proliferation, both signs of chronic inflammatory disease.

associated with lower thickening; finally, inquiescent disease, wall enhancement can be very low or absent.

CT and MRI can detect complications of UC requiring surgery, such as diffuse dilatation of the colonic lumen (toxic megacolon), tight strictures, and rectal cancer.

The toxic megacolon can be diagnosed with the same criteria of conventional abdominal plain films: a marked and diffuse colonic dilation (upper normal limit 5.5–6.5 cm in the transverse and left colon) with severe mucosal disease is the typical appearance.

Nuclear Medicine

Radionuclide studies have a useful role in acute fulminant colitis when colonoscopy or BE study is contraindicated, similarly to CT or MRI. Radionuclide studies are also useful in depicting disease activity and the extent of disease and in monitoring the response to therapy. Promising results have been published about the clinical use of technetium 99m white blood cells (WBC) in the assessment of IBD in adults and in a small series of children. In patients with active UC, inflammation is visualized with 99mTc-exametazime-labeled leucocytes or 99mTc-labeled antigranulocyte antibodies. The antibody technique offers the advantage of *in vivo* labeling, but is less reliable than the exametazime method for imaging of colonic inflammation.

Treatment

The treatment of patients with IBD depends on knowledge of the location, extent, and activity of the inflammation. Clinical evaluation (Truelove and Witts classification or the more recent Powell–Tuck index) and ES are usually sufficient to assess the extent and severity of UC, since the inflammatory process involves the colon only, sparing the small bowel. Moreover, biopsy specimens obtained during ES, necessarily limited to the mucosa and submucosa layer, can usually detect most of the pathologic features of UC, since the inflammatory process does not extend beyond the submucosa layer. Clinical data (acute phase reactants, etc.) together with endoscopic evaluation are usually adequate to estimate the disease extent in most of patients with mild to moderate disease. In case of complicated or very severe disease, if endoscopy is limited or contraindicated, or in case doubtful cases, the diagnostic modalities above mentioned may complete the diagnostic procedure, helping to reach a final correct diagnosis.

Generally, most patients with mild to moderate disease are effectively treated with drugs. Occasionally, however, the disease may be extremely severe, thus requiring urgent colectomy if it does not respond to pharmacological therapy promptly.

The drugs of first choice for the treatment of an acute flare-up of UC are 5-ASA-releasing preparations and glucocorticoids.

The efficacy of glucocorticoids and the beneficial effects of sulfasalazine have been known for half a century. The 5-ASA influences a wide variety of immunologic and inflammatory reactions, such as a chemotaxis of white blood cells, cytokine release, and release of reactive oxygen species.

The extent of the disease influences the strategy of treatment.

Left-sided colitis is better treated with rectal administration of drugs, whereas more extensive colitis requires oral or intravenous treatment, depending on the disease severity.

Active distal UC should initially be treated with 5-ASA. If treatment is otherwise

ineffective, steroid enemas and preferably steroid foams, can be used.

If the colitis involves the left colic flexure, rectal treatment is not sufficient. In patient with mild or moderate disease oral administration of 5-ASA preparation is effective.

In more severe cases, or if 5-ASA fails, glucocorticoids should be used orally or intravenously and 60–100 mg of prednisolone equivalent is useful in the majority of patients.

Among those with very severe colitis, however, only half of the patients respond.

When adequate doses of glucocorticoids fail to improve severe UC, a colectomy should be performed, particularly in patients with fulminant colitis and toxic megacolon.

Azathioprine or 6-mercaptopurine is effective in chronic active colitis. However, considering the possible side effects and the need for long term therapy this option should be weighted against colectomy and ileoanal pouch surgery.

Maintenance of remission with sulfasalazine should be used and decreases the relapse rate by about 50%. Azathioprine should be used only in patients who cannot be kept in remission with 5-ASA and who are not willing or able to undergo colectomy.

The most frequent indication for surgical resection in UC is severe inflammation of the large intestine and rectum that is refractory to conservative therapy, also in patients who suffer from the side effects of the medication.

Toxic colitis with or without megacolon can be complicated by perforation. Operation within 3.5 days is prognostically associated with a better outcome than operation after a long, futile treatment attempt with considerable worsening of the patient's general conditions.

Three classic surgical interventions are performed in UC: conventional proctocolectomy with terminal ileostomy (without preservation of the anal sphincter), ileorectal anastomosis (only if the rectum is not extensively involved), or restorative proctocolectomy with ileo-anal pouch, which is nowadays considered the first choice procedure. In the last procedure (total colectomy with ileo-anal pouch), the rectum is completely resected whereas the anal sphincter muscles apparatus is spared; therefore there is no risk of recurrence, and at the same time the ileo-anal pouch ensures a reservoir function. Sometimes the ileal pouch may undergo to chronic wall inflammation, and the so-called "pouchitis" endoscopy is the modality of choice to evaluate the degree of wall inflammation in a pouch. Cross-sectional imaging, particularly MRI or CT, may be useful in evaluating the morphology of the pouch and possible complications.

Bibliography

1. Goldberg HI, Caruthers SB Jr, Nelson JA et al (1979) Radiographic findings of the National Cooperative Crohn's Disease Study. Vol 77: 925–933, Gastroenterology
2. Gore RM (1995) Characteristic morphologic changes in chronic ulcerative colitis: Abdom Imaging. Vol 20:275–278
3. Gore RM, Ghaharemani GG, Miller FH et al (1997) Inflammatory Bowel Disease: Radiologic Diagnosis. In Syllabus of the radiological Society of North America, Categorical Course in Gastrointestinal radiology: 95–109, RSNA Publications
4. Miner PB (2000) Clinical Features, course, laboratory findings, and complications in ulcerative colitis. In: Kirsner JB (ed) Inflammatory Bowel Disease. 5th edn. WB Saunders, Philadelphia, pp 299–304
5. Maccioni F (2004) In: Chapmann AH (ed) MRI of Colitis in Radiology and Imaging of the Colon. Springer-Verlag, Heidelberg, pp 201–214
6. Maccioni F, Colaiacomo MC, Parlanti S (2005) Ulcerative colitis: value of MR imaging. Abdom Imaging 30:online (May)
7. Scholmerich J, Herfarth C In: Cremer M et al (eds) (1999) Ulcerative colitis in Gastroenterology and Hepatology. McGraw-Hill, New York, pp 382–392

Collateral Phenomenon

Collateral phenomenon is an nonspecific finding of periarticular demineralization, which occurs, for example, due to disuse or neighborhood inflammation. Today the terms "regional osteoporosis" and "periarticular demineralization" are more common.

▶Rheumatoid Arthritis

Collimator

In a radionuclide imaging device, a collimator is a block of radiation-attenuating material with one or more apertures defining the field of view and limiting the angular spread of the radiation that can reach the radiation detector assembly.

▶Scintigraphy

Colloid Carcinoma

▶Carcinoma, Other, Invasive, Breast

Coloboma

▶Congenital Malformations, Orbit

Colon, Postoperative

Ashley S. Shaw[1], Alan H. Freeman[2]
[1]Consultant Radiologist
Cambridge University Hospitals NHS Trust
Cambridge, UK
[2]Consultant Radiologist
Cambridge University Hospitals NHS Trust
Cambridge, UK

Synonyms

Abdominal Surgery; Complications; Abdomen; Post-operative

Colonic resection may be performed for a number of conditions, most commonly malignancy, diverticular disease, inflammatory bowel disease (ulcerative colitis, Crohn's disease) or ischaemic bowel. Equally, a wide variety of procedures may be performed, from short segmental resection to complete pan-proctocolectomy. When imaging patients who have undergone colonic surgery, it is important for the radiologist to establish what the underlying condition is, when and what procedures have been performed, and whether there has been any adjuvant chemo- and/or radiotherapy (1). It is only with this information to hand that one is able to identify the most likely pathology, perform the most appropriate study and interpret the images.

Paralytic Ileus

Often referred to simply as 'ileus' (alternatively adynamic or non-obstructive ileus), paralytic ileus is atony of the intestine resulting in failure to propel the bowel contents distally. Ileus is common after any operation where the stomach, small or large bowel have been handled, although the aetiology is complex. It may be exacerbated by biochemical abnormalities (e.g. renal failure, diabetes mellitus, hypokalaemia), anti-cholinergic drugs, reflex sympathetic inhibition (e.g. retroperitoneal haematoma), sepsis or other systemic illness.

Clinical Presentation

Ileus is considered normal for the first few days following colonic surgery. The patient will have little appetite, absent bowel sounds on auscultation and will not pass any flatus or faeces. If this persists for greater than 4–5 days, particularly in the absence of any of the correctable causes detailed above, it may herald the presence of intra-abdominal sepsis or haemorrhage and require investigation.

Imaging

The key differential diagnosis is large bowel obstruction. The supine abdominal radiograph typically demonstrates distension of both small and large bowel (±gastric distension). Ileus, unlike obstruction, often demonstrates multiple loops of dilated bowel with normal calibre bowel in between. In addition, the presence of a gas filled dilated rectum is strongly suggestive of ileus. Serial films often show the degree of bowel dilatation to reduce over time. Oral contrast medium will pass slowly through the dilated bowel, being increasingly diluted by small bowel fluid and is usually unhelpful. Rectal contrast medium may be used to confirm the absence of a colonic stricture (free passage of contrast into the most distal dilated bowel loop confirms ileus). Where ileus persists, cross-sectional imaging with computed tomography (CT) may be helpful to determine whether there is a surgically remediable cause (e.g. abscess or haematoma).

Anastomotic Leak

Following the resection of a segment of colon, the two free ends are usually joined together using sutures or staples. The exceptions to this are Hartmann's procedure, complete pan-proctocolectomy and abdomino-perineal resection, where an ileostomy or colostomy is fashioned. Failure of the anastamosis occurs in a small proportion of patients, but is significantly more common when there is active inflammation or infection at the time of surgery. Segmental ischaemia or radiotherapy also contribute to friable tissue. For this reason, many surgeons may either electively perform a loop ileostomy to temporarily rest or 'defunction', the colon or perform the operation in two stages.

Clinical Presentation

Breakdown of the surgical anastomosis usually occurs towards the end of the first post-operative week. The patient commonly presents with a fever and/or pelvic pain, indicating the presence of an underlying abscess. Preliminary investigations may demonstrate an elevation of the white blood cell count and inflammatory markers.

The presence of a pelvic abscess may lead to an ileus, development of a fistula, peritonitis or mechanical obstruction.

Imaging

A supine abdominal radiograph is often the first investigation but is non-specific. It may show dilated loops of bowel from either ileus or obstruction. A *gastrografin* enema will delineate any ongoing leaks at the anastomosis (Fig. 1) and perhaps identify a fistula. It should be borne in mind that a proportion of leaks will seal spontaneously, but may leave the patient with a pelvic abscess. To assess the pelvis for a collection, cross-sectional imaging with CT is indicated (Fig. 2). CT may be performed following administration of rectal contrast in order to help define the often complex post-operative anatomy. Whilst CT will demonstrate the anatomy, it may be difficult to differentiate haematoma from abscess, particularly when there is often a combination of the two. Where there is clinical concern, percutaneous drainage of any fluid collections is often required, both to confirm the diagnosis and treat the abscess. Failure of radiological management or the development of peritonitis will usually necessitate a repeat laparotomy.

Nuclear Medicine

Occasionally, it may not be possible to clearly demonstrate ongoing infection within the pelvis on cross-sectional imaging, particularly where there is no discrete abscess. In these cases, particularly where there is delayed presentation, a radiolabelled white cell scan may be of use in proving the diagnosis before committing the patient to a prolonged course of antibiotics or further surgery.

Tumour Recurrence

Following diagnosis of colorectal carcinoma, approximately 70% of patients will undergo 'curative' surgery. The reported rates of tumour recurrence vary considerably, with the liver the most common site of metastatic disease (2). Local recurrence, at or near the surgical anastomosis or within the surgical bed, is seen in approximately 10–15% of cases and is more common in rectal than colonic tumours.

Clinical Presentation

The majority of recurrences occur within the first 2 years following surgery. Tumour recurrence at the surgical anastomosis may lead to rectal bleeding or even mechanical obstruction. However, more often there are no local symptoms and it is identified on routine post-operative surveillance, either at CT or endoscopy.

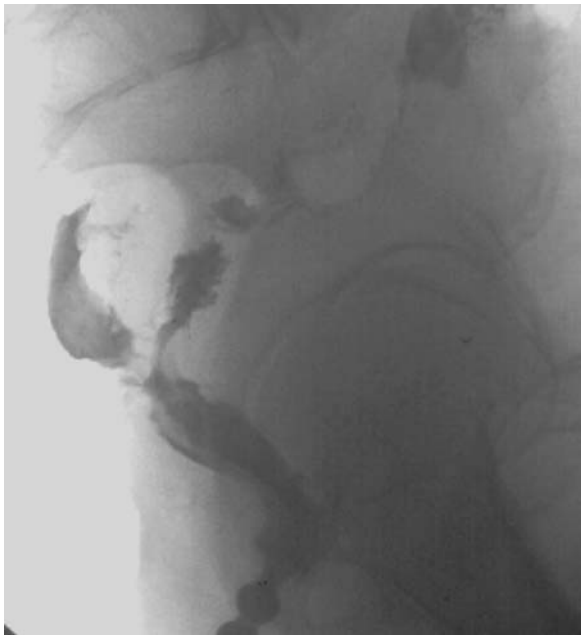

Colon, Postoperative. Figure 1 Contrast enema demonstrating an anastomotic leak in a patient shortly after undergoing an anterior resection.

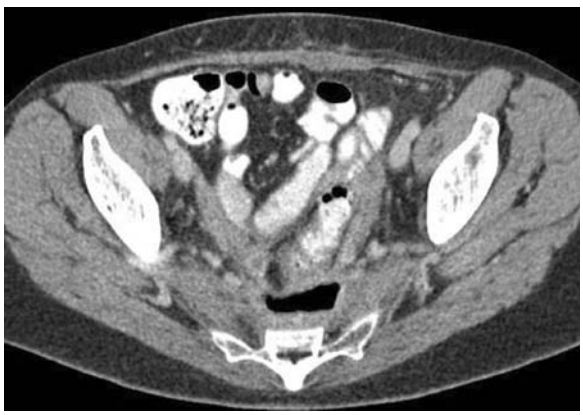

Colon, Postoperative. Figure 2 CT demonstrates a cavity in the pre-sacral space containing air and fluid, indicating the presence of an abscess. The patient had recently undergone an anterior resection.

Imaging

CT is the mainstay of post-operative surveillance following resection of colorectal cancer, usually performed at

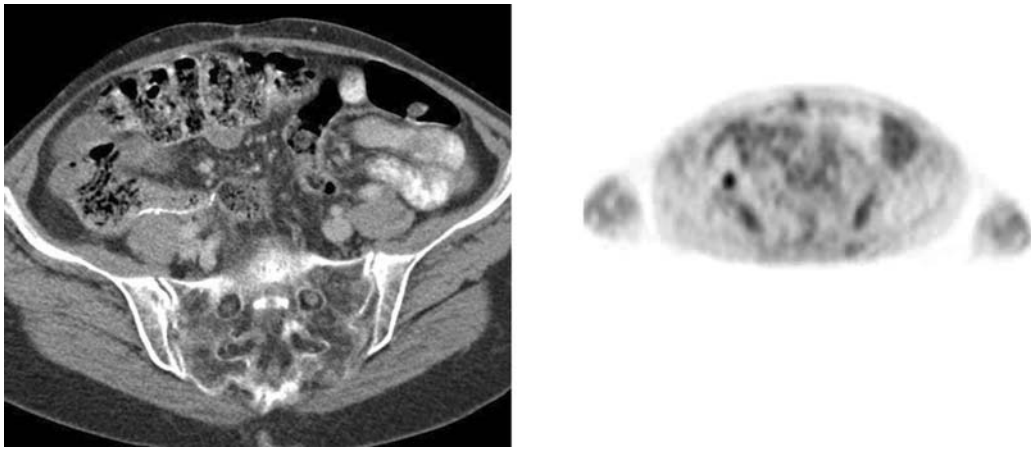

Colon, Postoperative. Figure 3 Patient with previous right hemicolectomy for Dukes B adenocarcinoma. CT does not show any abnormality, but the PET study demonstrates a focal area of recurrence at the anastomosis, confirmed at surgery.

6–12 monthly intervals for 2–3 years after surgery. This will reliably detect liver, peritoneal and nodal metastases. Recurrence at the anastomotic site will be seen as a nodule or plaque of abnormal soft tissue. The difficulty lies in differentiating such areas from post-operative fibrosis or haematoma. Previously, one could either choose to 'watch and wait' or attempt a biopsy of such lesions. This has been superseded in many centres by the use of functional imaging (Fig. 3).

Nuclear Medicine

Positron emission tomography (PET) uses radiolabelled isotopes (principally ^{18}fluoro deoxyglucose-FDG) to identify areas of abnormally increased metabolism within the body. This complements the anatomical imaging offered by CT, enabling differentiation of abnormal soft tissue, and often identifies hitherto unsuspected disease. Sites of recurrent colorectal cancer are detected with a sensitivity of 97% and specificity of 76%, resulting management changes in between one quarter and one third of patients (3). False positive results may occur at sites where there is active inflammation or infection, thus PET may be more difficult to interpret in the early post-operative period.

Bowel Obstruction

Obstruction following colonic surgery has a number of possible causes: recurrence of disease (tumour, Crohn's disease); adhesions; and fibrous strictures at the surgical anastomosis.

Clinical Presentation

Increasing abdominal distension, abdominal pain and the absence of flatus or bowel motions are the typical presenting symptoms of bowel obstruction, with 'tinkling' bowel sounds on auscultation. Bowel obstruction following resection is typically a late complication and occurs at the anastamosis site with an incidence of 2–8% (1). The use of staples, rather than hand sewing the anastamosis, appears to increase the frequency of stricturing.

Imaging

Anastomotic strictures may be evaluated by a number of methods, including double-contrast barium enema (DCBE), colonoscopy and CT. DCBE will allow evaluation of the mucosal surface and identify any fistulae, whereas CT permits evaluation of the extracolonic structures. Recent advances in CT colonography increasingly allow evaluation of the mucosal surface, but in cases where there is suspicion of tumour recurrence, evaluation with FDG-PET or direct visualisation with endoscopy will be required.

Crohn's Disease

Crohn's disease may affect any part of the gastrointestinal tract, most commonly the terminal ileum and not infrequently the colon. A significant proportion of patients with Crohn's disease will require abdominal surgery at some point during the course of their disease, either to resect a fistula or a symptomatic intestinal stricture.

Clinical Presentation

Following surgery for colonic Crohn's disease, approximately one-third will relapse within the next 10 years. Most typically, this involves the neo-terminal ileum leading up to the anastomosis following an ileo-colic resection. However, recurrence may occur elsewhere. The patient will often present with abdominal pain or bleeding per rectum and has often lost weight. Fistulae may extend to the skin surface and result in severe perianal pain.

Imaging

The plain abdominal film may demonstrate mechanical obstruction, but a barium enema is the investigation of choice to evaluate the colonic mucosa. Cross-sectional imaging with CT or MRI will enable imaging of any associated abscesses and fistulae. Imaging perianal and rectal fistulae are now performed using MRI. Suppression of the signal from the pelvic fat allows the demonstration of any abnormal fluid tracks and collections, together with their relationship to the sphincters.

Bibliography

1. Scardapane A, Brindicci D, Fracella MR et al (2005) Post colon surgery complications: imaging findings. Eur J Radiol 53:397–409
2. Faria SC, Tamm EP, Varavithya V et al (2005) Systematic approach to the analysis of cross-sectional imaging for surveillance of recurrent colorectal cancer. Eur J Radiol 53:387–396
3. Huebner RH, Park KC, Shepherd JE et al (2000) A meta-analysis of the literature for whole body FDG PET detection of recurrent colorectal cancer. J Nucl Med 41:1177–1189

Colonic Atresia

A congenital abnormality, usually due to an ischaemic insult in embryological development resulting in complete occlusion of the lumen of the colon.

▶GI Tract, Paediatric, Congenital Malformations

Colonoscopy

Colonoscopy is the "gold standard" for the detection of colonic neoplasms and the preferred colorectal cancer screening strategy.

▶Neoplasms, Benign, Large Bowel
▶Neoplasms, Large Bowel, Malignant

Color Doppler Ultrasound

This uses standard ultrasound methods to produce a picture of a blood vessel. In addition, a computer converts the Doppler sounds into colors that are overlaid on the image of the blood vessel and that represent the speed and direction of blood flow through the vessel.

▶Breast, Therapy Effects
▶Lymphadenopathy

Colorectal Adenomas

Colorectal adenomas are benign polypoid neoplasms, pedunculated or sessile arising from the epithelial cells of the colorectum, with varying degrees of cellular atypia. Although benign, they are the direct precursors of adenocarcinomas and follow a predictable cancerous temporal course unless interrupted by treatment.

▶Neoplasms, Benign, Large Bowel

Colorectal Cancer

Colorectal cancer is the most common cancer of gastrointestinal tract with approximately 150,000 new cases every year. Despite these statistics, mortality from colon cancer has decreased over the past 30 years, possibly because of earlier diagnosis through screening and better treatment modalities.

▶Neoplasm, Large Bowel, Malignant

Colovescical Fistula

Complication of sigmoid diverticulitis presenting with frequency, UTI and pneumoturia. CT confirms diagnosis with findings of thickened bladder mucosa, fistulous track and gas in the bladder.

▶Diverticulitis

Colpocystogram

Invasive radiological technique to assess pelvic floor descent. Progressively replace by MRI.

▶Incontinence, Urinary

Column of Bertin

Normal variant of the renal cortex, which may simulate tumors (pseudotumor).
▶Contrast Media, Ultrasound, Applications in Kidney Tumor

Columnar Lined Oesophagus

▶Reflux, Gastroesophageal in Adults

Comedomastitis

▶Duct Disease, Breast

Communicating Dissection

Dissection with dual lumen and visible tears in the intimal flap.
▶Dissection, Aortic, Thoracic

Compartment Anatomy

Is the concept of tumor anatomical site and definition of borders. The intracompartmental remaining tumor, which respects anatomical borders such as adjacent fascia, has a better prognosis over the tumor, which is already extracompartmental at presentation. The extracompartmental tumor is one that has already spread beyond the anatomical site of origin and requires more extensive surgery. Involvement of an adjacent joint or space such as the popliteal fossa, is extracompartmental, and may necessitate amputation, if limb salvage procedures are not possible.
▶Neoplasms, Soft Tissues, Malignant

Complex Cyst

Cyst with internal masses, thick septations, or thick or irregular wall.
▶Cyst, Breast

Complex Partial Epilepsy (CPE), Focal Epilepsy: Temporal lobe epilepsy (TLE): TLE accounts for approximately 70% of all chronic CPE

▶Seizures, Complex, Partial

Complex Regional Pain Syndrome

Characteristic disabling joint and soft tissue abnormalities of poorly understood etiology. Also known as reflex sympathetic dystrophy, the most common theory of its pathogenesis is an injury to nerves resulting in painful afferent stimuli. These afferent stimuli are thought to activate increased sympathetic tone and other efferent discharge. Symptoms include pain, dysesthesia, swelling, and vasomotor instability. Early changes on scintigraphy are characteristic and demonstrate bilateral asymmetric increased activity in the affected juxta-articular region on all three phases of bone scanning. Decreased unilateral activity occurs in chronic disease. Radiographs may demonstrate periarticular swelling, osteopenia, and subchondral resorption. Preservation of joint space is an important feature in differentiation from an inflammatory arthritis.
▶Fractures, Peripheral Skeleton

Complex Sclerosing Lesion

▶Radial Scar, Breast

Complicated Cyst

Cyst with diffuse internal echoes.
▶Cyst, Breast

Complication of Kidney Graft

▶Transplant Kidney, Complications

Compression, Extrinsic, Esophagus

Luis H. Ros Mendoza,
M[a] Eugenia Guillén Subirán,
Cristina Gutiérrez Alonso
University Hospital Miguel Servet, Department of Radiology, Zaragoza, Spain
lhros@wanadoo.es

Synonyms

Contour wall alteration; Notches; Wall displacement

Definition

Morphologic alteration of the esophagus related to a neighboring mass or space-occupying lesion.

Pathology/Histopathology

Pathology depends on the cause of the extrinsic compression, with the main causes classified as congenital, inflammatory, or tumoral.

In congenital cases, the pathologic findings are related only to the compressive phenomena without the presence of inflammatory signs or tumoral infiltration, which might be present in the two other groups.

Non-neoplastic mediastinal cysts form a group of uncommon benign lesions of congenital origin (1). Neuroenteric and duplication esophageal cysts are localized in the posterior mediastinum, and they might cause this kind of alteration (Fig. 1).

Other cases present an inflammatory origin, such as retropharyngeal abscesses or mediastinal pancreatic pseudocysts. Mediastinal masses associated with chronic pancreatitis should raise suspicion for the extension of the inflammatory process to the mediastinum (Fig. 2).

Tumoral masses located between the esophagus and the tracheobronchial tree, mainly related to bronchogenic carcinoma, can lead to esophageal infiltration and compression (2). Neurogenic tumors (neurilemmoma, paraganglioma, neuroepithelioma, and neurogenic sarcoma) might also compress the esophagus because of their frequent posterior mediastinal location. Leiomyoma, the most frequent benign tumor of the esophagus, can sometimes grow in an eccentric way, making it difficult to differentiate from an extramural mass (Fig. 3).

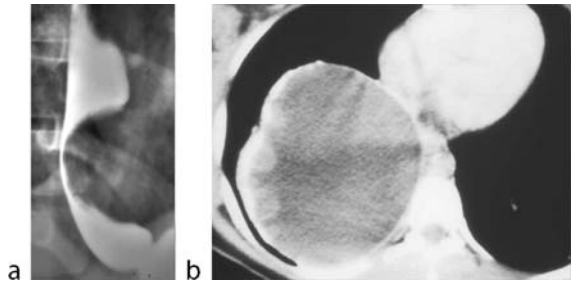

Compression, Extrinsic, Esophagus. Figure 1 Extrinsic esophageal compression related to a noncommunicating esophageal duplication cyst. The barium study (a) shows a significant compression over the esophagus with smooth contours and obtuse angles. Computed tomography (b) identifies a cystic mass, with thick walls and well-defined contours, located in close relationship to the anatomic area of the esophagus.

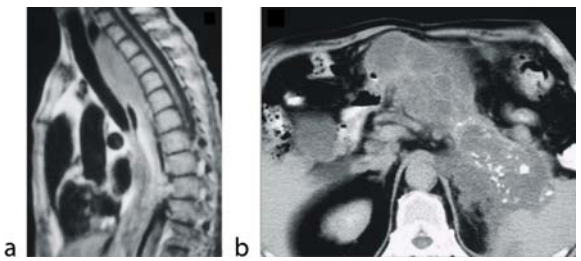

Compression, Extrinsic, Esophagus. Figure 2 Extrinsic compression of the esophagus related to a mediastinal pancreatic pseudocyst. The sagittal plane of the magnetic resonance study (a) shows a mass in the posterior mediastinum that is compressing the thoracic esophagus. The mass corresponds to a pancreatic pseudocyst. Abdominal computed tomography (b) demonstrates the inflammatory pancreatic involvement. Magnetic resonance imaging by means of the sagittal and coronal planes is a very useful tool for studying the esophagus, as it shows this structure in its major longitudinal plane.

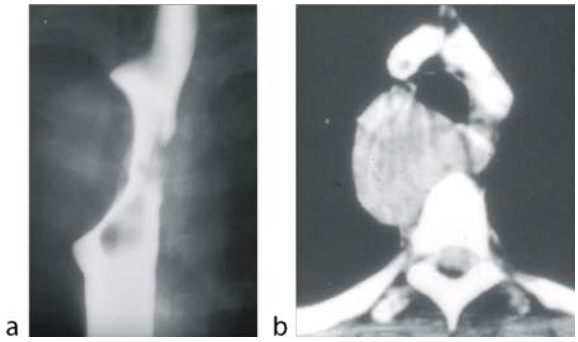

Compression, Extrinsic, Esophagus. Figure 3 Esophageal compression due to an intramural leiomyoma. The barium study (a) shows an esophageal compression that is difficult to classify as intrinsic or extrinsic by only the classic semiological criteria. The compression presents smooth contours and the marginal angles are wide open, almost obtuse. Computed tomography (b) defines a tumoral mass, located in the anatomic area of the esophagus, which is also compressing the trachea, with attenuation values very similar to those of the muscular structures.

Apart from the three groups mentioned earlier, there are other causes for esophageal extrinsic compression:

1. *Vascular compression*: Aberrant right subclavian artery (ARSA) is an anomaly with a reported incidence of 0.5–2%. The aberrant artery usually follows a retroesophageal course; it rarely takes an anterior course to the esophagus or trachea. Anomalies associated with ARSA are nonrecurring inferior laryngeal nerve paralysis, aortic coarctation, right-sided aortic arch, and a common origin of the carotid arteries.
   Other vascular causes of compression include anomalies of the aortic arch, an enlarged ascending aorta, a malpositioned descending aorta, and enlarged pulmonary arteries.
   Enlargement of the left atrium causes compression of the superior part of the distal esophagus, whereas global cardiomegaly can produce compression of the inferior part.
2. *Lymphadenopathies*: Mediastinal lymphadenopathies (from a tuberculous, metastatic, or lymphomatous origin) can also compress the esophagus and cause dysphagia (3).
3. *Thyroid and parathyroid gland enlargement*: Enlargement of the thyroid gland, with either a benign or malignant origin, might produce lateral displacement of the esophagus, which is well seen on the anteroposterior view of a barium swallow study. In secondary hyperparathyroidism, there is a generalized hyperplasia of parathyroid glands that, in some cases, can produce esophageal compression (4).
4. *Cervical osteophytes*: These are found in approximately 20–30% of the aged population. In most of these patients bony spurs are asymptomatic, although they may be associated with neck stiffness and localized or radiating pain. However, large osteophytes that protrude from the anterior edge of the cervical vertebrae can impinge on the upper esophagus, causing dysphagia and odynophagia.
5. *Zenker's diverticulum*: This is a protrusion of the mucosal wall of the hypopharynx through the weakened muscular layer between the oblique fibers of the inferior constrictor of the pharynx and the transverse fibers of the cricopharyngeal muscle. When large, it might compress the cervical esophagus.
6. *Retropharyngeal hematoma*: If this occurs, it is located just in front of the cervical spine. Trauma or anticoagulant therapy can lead to its development.
7. *Esophageal pseudomass*: A narrowed sagittal diameter of the thoracic inlet is recognized as an anatomic variant that causes dysphagia because of extrinsic compression of the esophagus between the trachea and vertebral bodies, resulting in a pseudomass appearance.
8. *Pleural, lung or mediastinal scars*: These can retract the esophagus to the involved side.

Clinical Presentation

The most frequent symptom related to extrinsic esophageal compression is mechanical dysphagia, first for solids and in cases of advanced obstruction, for both solids and liquids. The point at which the patient experiences this symptom is useful for localizing the level and cause of the compression.

Some of the illnesses responsible for the esophageal compression can present specific manifestations:

- Coughing is frequent in patients with ARSA, and stridor is frequent in those with right-sided or double aortic arch.
- Hiccups suggest involvement of the distal esophagus.
- Zenker's diverticulum is characterized by regurgitation, gurgling sounds, and aspiration.
- Large osteophytes (greater than 10 mm) can produce aspiration.
- Mediastinal masses, when large, might produce unilateral sibilants and dysphagia because they compromise both the esophagus and the tracheobronchial tree.
- Thyroid and parathyroid gland alterations can present endocrine symptoms associated with esophageal manifestations (4).

- Fever, night sweats, odynophagia, and weight loss are common manifestations of lymphoma.
- Chronic pancreatitis produces chronic abdominal pain.

Imaging

In some cases, conventional chest radiology might show findings that are suggestive of this condition, including intrathoracic goiter; posterior mediastinal masses; pleural, lung or mediastinal retractions; left atrium enlargement; cardiomegaly; aortic arch anomalies or other vascular alterations.

Lateral neck radiographs can also be useful for showing the presence of osteophytes, localized retropharyngeal masses, or posttraumatic vertebral fractures.

But the most specific semiological criteria are obtained by means of a barium swallow study (5). An intraluminal or intramural mass usually presents its center within or along the contour of the esophageal lumen; as a result, the angles produced by the esophageal wall and the lesions are acute. An extramural mass presents its center out of the contour of the lumen, with these angles being obtuse (Fig. 1a). This is called the spheroid sign.

In some cases, the barium swallow shows fixation and traction of the mucosal folds with a teething appearance suggestive of parietal infiltration.

By means of a barium swallow, it is also possible to differentiate between the esophageal displacement due to a mediastinal mass, which usually causes a narrowing of the lumen, and the retraction due to a neighboring scar, which produces a widening of the esophageal lumen.

In general, the filling defects with smooth or slightly lobulated edges correspond to extramural masses.

On some occasions, ultrasound (US) can be useful for characterizing a posterior mediastinal mass as solid or cystic or an enlargement of the thyroid gland. US-guided fine needle aspiration can be performed in selected cases.

Endoscopic ultrasound (EUS) is being increasingly used as a less invasive alternative to mediastinoscopy to obtain a diagnosis of mediastinal involvement; EUS-guided fine needle aspiration can provide material to establish the histologic diagnosis.

Cross-sectional imaging modalities, computed tomography (CT) and magnetic resonance imaging (MRI), are also very useful tools for evaluating this situation. They confirm the presence of the extrinsic compression and allow a precise evaluation of its cause in the different spatial planes (Figs 1 and 2). MRI angiography demonstrates with great accuracy the different vascular causes of dysphagia and allows a definite evaluation of the cardiac chambers.

Nuclear Medicine

Nuclear medicine techniques might be useful in studying some entities that can produce an extrinsic esophageal compression. Thyroid pathology is well defined by means of nuclear scintigraphy, and mediastinal lymphomatous masses or adenopathies might be identified by means of gallium citrate scintigraphy. The radionuclide study of choice for parathyroid location is single photon emission CT using technetium-99m sestamibi (2-methoxyisobutylisonitrile).

Diagnosis

The initial diagnosis of extrinsic esophageal compression, which can be suspected when the clinical symptoms suggest it, is commonly made during a barium contrast study or during an upper digestive endoscopy that shows a mass or impression covered by normal-appearing epithelium.

The first problem to solve is to differentiate between an extrinsic compression versus a lesion arising from the wall itself. The semiological criteria previously defined—spheroid sign, characteristics of the edges of the compression, teething appearance—can be the key findings to establish the differential diagnosis, although this is not always easy (Fig. 3). Some entities can present specific manifestations on the barium swallow that help determine the specific diagnosis:

- ARSA appears as a characteristic posterior compression, an oblique notch "in bayonet."
- Intrathoracic goiter presents the cervicothoracic sign, compressing and displacing both trachea and esophagus.

The second problem is to determine the origin (cause) of the extrinsic compression. CT and MRI are very useful tools for this because they allow not only identification of the esophageal compression but also identification of its etiology, with the possibility of a detailed evaluation in the different spatial planes. Some entities show specific findings:

- Tuberculous mediastinal adenopathies show a hypodense, necrotic center.
- Narrowing of the thoracic inlet diameter (normal: 6.2 cm in the sagittal plane, range 5–8.7 cm) occurs in cases of esophageal pseudomass (apparent external compression on the upper esophagus from the right side with displacement to the left and narrowing of the esophageal lumen, which is suggestive of a mass that should be excluded with CT).

In some cases, the diagnostic algorithm might be completed by means of a percutaneous puncture under US or CT guidance to obtain sample material for pathologic study.

Interventional Radiological Treatment

Nonresectable malignant esophageal stenosis, in some cases related to parietal infiltration from a neighboring tumor, might be treated using self-expanding stents. The self-expanding plastic stent is removable, induces less hyperplasia than metal stents, and can be used to treat benign esophageal conditions.

Bibliography

1. Trojan J, Mousset S, Caspary WF et al (2005) An infected esophageal duplication cyst in a patient with non-Hodgkin's lymphoma mimicking persistent disease. Dis Esophagus 18(4):287–289
2. Simchuk EJ, Low DE (2001) Direct esophageal metastasis from a distant primary tumor is a submucosal process: a review of six cases. Dis Esophagus 14(3–4):247–250
3. Nagi B, Lal A, Kochhar R et al (2003) Imaging of esophageal tuberculosis. Acta Radiol 44(3)329
4. Weber AL, Randolph G, Aksoy FG (2000) The thyroid and parathyroid glands. CT and MR imaging and correlation with pathology and clinical findings. Radiol Clin North Am 38(5):1105–1129
5. Levine MS, Rubesin SE (2005) Diseases of the esophagus: diagnosis with esophagography. Radiology 237(2):414–427

Compression, Extrinsic, Stomach and Duodenum

Luis H. Ros Mendoza,
Cristina Gutiérrez Alonso,
M[a] Eugenia Guillén Subirán
University Hospital Miguel Servet, Department of Radiology, Zaragoza, Spain
lhros@wanadoo.es

Synonyms

Contour wall alteration; Notches; Wall displacement

Definition

Extrinsic compression of the stomach and duodenum is a morphologic alteration of the gastric and duodenal contour related to a neighboring space-occupying lesion.

Pathology/Histopathology

Pathology depends on the cause of the compression. The most frequent etiologic factors in gastric compression are liver and spleen enlargement, pancreatic pathology (tumors, cysts, and pancreatitis), gallbladder alterations, retroperitoneal lymphadenopathies, renal masses, and collections in the lesser sac.

In duodenal compression, the main causes include hepatomegaly, gallbladder enlargement, coledocal compressions, right renal and adrenal masses, periportal adenopathies, and hepatic angle and transverse colon alterations (1).

According to the histological characteristics, compressions can be classified as congenital (duplication cysts of the stomach or duodenum), inflammatory (acute and chronic pancreatitis, Morrison pouch abscesses), or tumoral (pancreatic adenocarcinoma, hepatic carcinoma, renal cell tumor).

In the first case, the pathologic findings will be related only to the compressive phenomena without the presence of inflammatory signs or tumoral infiltration, which might be present in the two other groups.

Special attention should be given to *gastric duplication* with its special pathologic characteristics: it can be cystic (the most frequent type), tubular, or tubulocystic. The duplication wall is close to the gastric wall, and its muscular layer fuses with the gastric one, although it rarely communicates with the gastric lumen. The duplication contains gastric epithelium (which can become ulcerated) or ectopic pancreatic epithelium (which can develop into pancreatitis).

Clinical Presentation

The patient can have no symptoms, with the extrinsic compression being a casual finding.

If symptoms are present, obstruction is the most frequent one, causing epigastric pain, abdominal distension, early satiety, and nausea and vomiting during or immediately after food intake. Vomiting usually alleviates the symptoms. Significant weight loss may occur (2). In low gastric and duodenal obstructions, "gastric splashing" can be found during clinical examination.

Some illnesses causing extrinsic compression have special clinical manifestations:

- Acute pancreatitis: Nonstop superior abdominal pain that radiates to the back.
- Chronic pancreatitis: Severe abdominal pain that is relieved at the genupectoral decubitus and when the patient sits leaning to the front, together with appetite loss, steatorrhea, and diabetes. Duodenal obstruction is more frequent in cases of alcohol-related pancreatitis.

- Annular pancreas: Bilious vomiting, growth failure, abdominal pain, duodenal obstruction, pancreatitis, and obstructive jaundice.
- Duodenal and gastric duplications: In neonates and infants, they produce vomiting, abdominal distention, volvulus, intussusception, and an abdominal mass. In adults, peptic ulcer or pancreatitis of the ectopic pancreatic tissue may occur. A duplication might get infected, and if it ruptures in the peritoneal cavity, peritonitis occurs.
- Duodenal diverticula: About half of the diverticula are found incidentally. When they are symptomatic, the most common clinical presentation is abdominal pain, gastrointestinal bleeding, and perforation.
- Internal hernias: Might cause small bowel obstruction (closed-loop or strangulating obstruction). They can also produce chronic intermittent intestinal obstruction.
- Superior mesenteric artery syndrome: Appears in cases of significant weight loss, sometimes postsurgical, and in cases of severe burns. The symptoms are a sensation of gastric fullness and abdominal distention after food intake, bilious vomiting, and colicky pain in the middle part of the abdomen, which eases in the prone decubitus and in genupectoral positions.

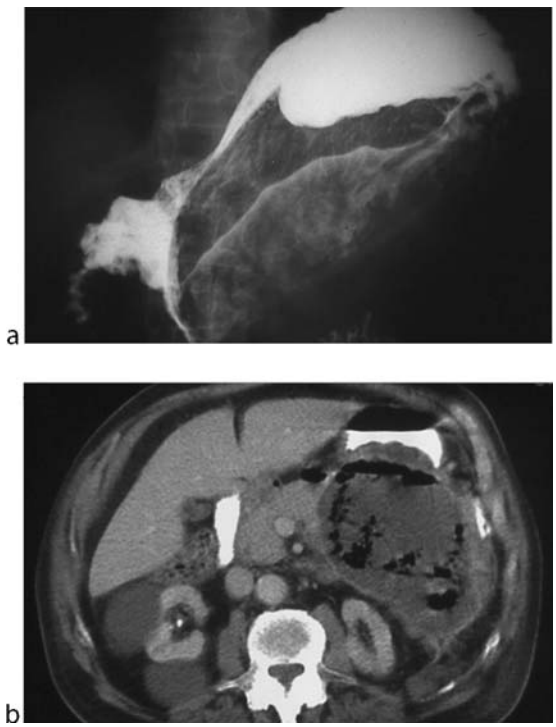

Compression, Extrinsic, Stomach and Duodenum.
Figure 1 Extrinsic compression of the stomach related to a pancreatic abscess. The upper gastrointestinal tract barium study (a) shows a significant extrinsic compression of the posterior gastric wall, with smooth contours and obtuse angles. Computed tomography (b) demonstrates the presence of a large pancreatic abscess as the cause of the extrinsic gastric compression. The stomach is identified by the presence of positive oral contrast within its lumen; the abscess, identified by the presence of gas bubbles, is located in close relationship to the posterior gastric wall.

Imaging

In an *abdominal plain film*, displacement of the gastric luminogram can be identified in some cases.

In *barium contrast examination*, the most common findings are a wide base compression or notch in the luminal contour of the stomach or duodenum, usually accompanied by displacement of the organ, along with a poorly defined area of low density (Fig. 1a). The location of the barium column alteration depends on the cause of the compression (Tables 1 and 2).

By means of *computed tomography* (CT) and *magnetic resonance imaging* (MRI) in the different spatial planes (axial, coronal, sagittal), these same vectors of displacement can be identified, enabling evaluation not only of the extrinsic compression but also of its cause (Figs 1b and 2).

Nuclear Medicine

Gastrointestinal duplications that contain gastric mucosa can be identified with technetium-99m-pertechnetate or

Compression, Extrinsic, Stomach and Duodenum. Table 1 Causes of gastric extrinsic compression

Body: right anterior wall	Hepatomegaly, gastric varicose veins
Body: left posterior wall	Splenomegaly
Body: posterior wall	Paraduodenal and lesser sac hernias
Antrum: anterolateral face	Enlargement of the gallbladder
Antrum: posterolateral face	Internal hernias through Winslow's hiatus
Antrum: posterior face ("antral pad")	Pancreatic masses (tumors, cysts, pancreatitis), retroperitoneal adenopathies, left renal masses, lesser sac collections
Great curvature	Gastric duplication

Compression, Extrinsic, Stomach and Duodenum. Table 2 Causes of duodenal extrinsic compression

First and second portions: medial displacement	Common bile duct (lineal notch), distended gallbladder (carcinoma), hepatomegaly (caudate lobe), focal hepatic lesions, periportal adenopathies, Morrison pouch collections, colonic hepatic angle distension or neoplasms, internal hernias through Winslow's hiatus
Second portion: posterolateral compression	Right renal and adrenal tumors, right renal ptosis
Second portion: annular compression	Annular pancreas
Second portion: medial wall compression (widening of the duodenal arch)	Pancreatic masses (tumors, cysts, pancreatitis), peripancreatic adenopathies (metastatic, lymphomatous), retroperitoneal masses
Second and third portions	Duodenal duplication cysts
Third portion: anterior compression	Pancreatitis (mesenterium involvement), mesenteric masses, superior mesenteric artery syndrome
Third portion: posterior compression	Retroperitoneal hematoma, aortic aneurysms
Fourth portion: medial displacement	Abdominal aortic aneurysms
Fourth portion: anterior compression	Transverse colon distension or neoplasms

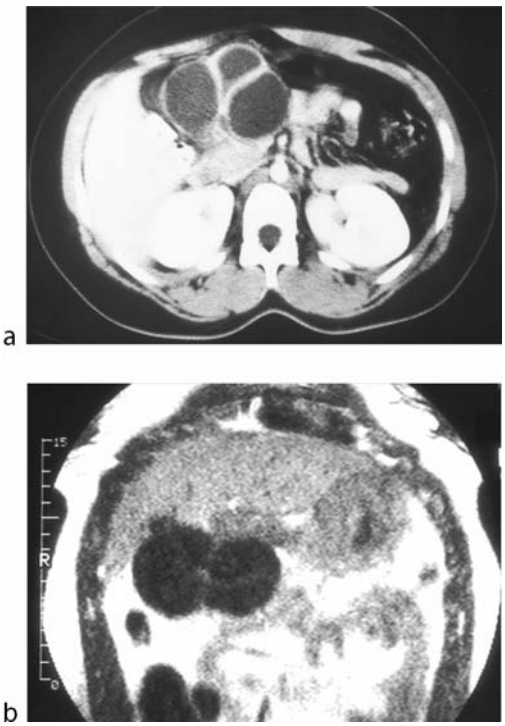

Compression, Extrinsic, Stomach and Duodenum. Figure 2 Extrinsic compression of the duodenum due to a cystic duodenal duplication. Computed tomography (a) shows the presence of a cystic mass with thick walls in the anatomic area of the pancreatic head. The patient had no antecedents of pancreatitis. The coronal plane of the abdominal magnetic resonance study (b) shows that the cystic mass is closely related to the duodenal walls. This and the thick walls (because congenital duplications "duplicate" all the layers of the wall of the digestive tube) are the key findings for suspected duodenal duplication cyst.

technetium-99m diethyltriamine pentaacetic acid scintigraphic evaluation, visualizing the functioning ectopic gastric mucosa simultaneously with the stomach in gastric duplications and even earlier in the case of duodenal duplications (3).

Diagnosis

The initial diagnosis of extrinsic compression of the stomach or duodenum is commonly suspected during an upper digestive endoscopy, with the visualization of a mass or impression covered by normal-appearing epithelium, or during a barium contrast study that presents the findings previously described.

The *first problem* to be solved is the differential diagnosis between extrinsic compression—caused by a normal or abnormal structure adjacent to the involved organ—versus a lesion arising from the wall itself.

In the upper gastrointestinal tract barium study, if the largest part of the lesion projects out of the gastric or duodenal lumen, and if the angle produced by the gastric or intestinal wall and the mass is obtuse, then the cause is more likely extrinsic (Fig. 3). In addition, the notches related to an extrinsic compression are not constant, changing under the actions of gravity and breathing.

Although during the upper endoscopy the finding can be evaluated by means of endosonography and, in some cases, an endosonographically guided fine needle aspiration can be performed (4), transabdominal ultrasound, CT, and MRI are more useful for defining the origin and extent of the extramural masses.

The *second problem* is to determine the origin of the extrinsic compression. In the barium study, the location and characteristics of the extrinsic compression (tubular,

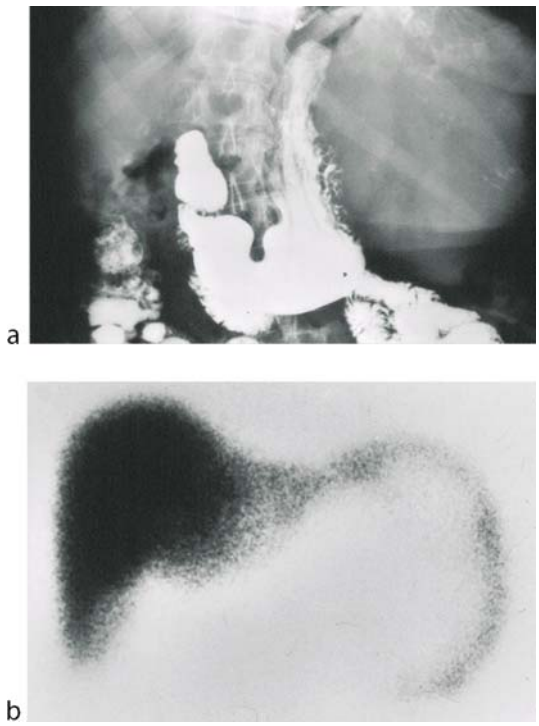

Compression, Extrinsic, Stomach and Duodenum.
Figure 3 Extrinsic compression of the stomach related to a massive splenomegaly. The upper gastrointestinal tract barium study (a) shows the deformity of the great curvature of the stomach, which suggests an extrinsic compression depending on the spleen. A mass effect, with high radiologic density, could be identified in the splenic area. The isotopic study (b) shows the absence of the radioisotope uptake by the spleen due to a massive acute splenic infarct. Edema at this acute stage of the splenic infarct results in the splenomegaly.

serpiginous notches in the case of gastric varicose vein) can be indicative of the cause (Tables 1 and 2), but in general, the cross-sectional imaging modalities, CT and MRI, are more useful in this respect, confirming the findings of the barium study, differentiating intrinsic from extrinsic compression in doubtful cases, and showing the cause of the compression.

Some entities, which are detailed later, present more diagnostic difficulties:

- *Gastric duplications* are more frequently found in the great curvature and duodenal duplications in the anteromedial contour of the first and second portions, and they are usually noncommunicating duplications. They appear on CT as rounded lesions that present a water density and are closely related to the gastrointestinal lumen (Fig. 2). On ultrasonography they appear as cystic structures, with the internal mucosal wall presenting a bright appearance, being the external muscular layer hypoechoic. In doubtful cases, a fine-needle aspiration biopsy under endoscopic ultrasound guidance or nuclear medicine techniques that allow the identification of gastric mucosa can be performed.
- The preoperative diagnosis of *internal hernia* can be made with barium studies, but in the presence of small bowel obstruction, CT plays an important role, allowing the identification of a sac-like mass or cluster of small bowel loops at an abnormal anatomic location, with a stretched and displaced mesenteric vascular pedicle and converging vessels at the hernial orifice.
- *Superior mesenteric artery syndrome* appears on CT as a sharpening in the middle of the third duodenal portion, with retrograde distension. On barium study there is an abrupt lineal compression with dilatation of the first and second duodenal portions and a fluctuant appearance of the barium column, as well as delayed gastric emptying.
- *Gastric varicose* veins are easy to identify on CT. They appear as serpiginous lesions that present intense enhancement after the intravenous contrast administration.
- *Annular pancreas* causes, in the barium study, a filling defect with annular morphology in the descendent portion of the duodenum at the level of the Vater ampulla, with a homogeneous dilatation of the proximal duodenum and inverted peristalsis of this area. To establish the diagnosis of this entity, endoscopic retrograde cholangiopancreatography, pancreatic CT, and MRI are very useful tools.
- *Pancreatic neoplasms* produce characteristic signs in the barium study when they have a long evolution. Enlargement of the duodenal arch and the Frostberg inverted-three sign (compression of the duodenal loop with fixation of the middle portion at the level of Vater papilla) are very well known. In cases with muscular infiltration or mucosal edema, contour spiculation and blurring of mucosal folds are produced; however, these signs are not specific to tumoral lesions, also appearing in acute and chronic pancreatitis.

Interventional Radiological Treatment

In patients with advanced neoplasms that compress the stomach or duodenum, an alternative to traditional surgical palliative treatment (gastrojejunostomy and duodenojejunostomy) is gastroduodenal stent placement, which can be done under fluoroscopic guidance or with a combination of fluoroscopic and endoscopic techniques. Stent placement reduces postsurgical complications, provides better gastric emptying, and is more cost-effective than surgical palliation (5).

Bibliography

1. Martín ES, Pedrosa CS (2000) El tubo digestivo: semiología radiológica. In: Pedrosa CS, Casanova R (eds) Diagnóstico Por Imagen. Tratado de Radiología Clínica. McGraw-Hill-Interamericana de España, Madrid, pp 335–378
2. Feldman M, Friedman LS, Sleisenger MH (2004) Enfermedades Gastrointestinales Y Hepáticas: fisiopatología, Diagnóstico Y Tratamiento. Editorial Médica Panamericana, Buenos Aires
3. Kumar R, Tripathi M, Chandrashekar N et al (2005) Diagnosis of ectopic gastric mucosa using 99Tcm-pertechnetate: spectrum of scintigraphic findings. Br J Radiol 78(932):714–720
4. Hwang JH, Kimmey MB (2004) The incidental upper gastrointestinal subepithelial mass. Gastroenterology 126:301–307
5. Lopera JE, Brazzini A, Gonzales A et al (2004) Gastroduodenal stent placement: current status. Radiographics 24:1561–1573

Computed Radiography (CR)

After passing through the patient, the emergent X-ray beam is detected by a photostimulable phosphor plate, forming a stable latent image. A laser then stimulates the plate, light is emitted and a digital signal produced (via a photomultiplier tube) than is converted into the image. The resultant image can be read either on laser-printed film or as soft copy on a workstation.

▶Children, Imaging Techniques

Computed Tomographic Colonography

CTC is a novel imaging modality for the evaluation of the colonic mucosa in which thin-section spiral CT provides high resolution two-dimensional (2D) axial images; CT data sets are edited off-line in order to produce multiplanar reconstructions (coronal and sagittal images) as well as three-dimensional (3D) modeling, including endoscopic-like views.

▶Neoplasms, Benign, Large Bowel

Computed Tomography

Diagnostic modolity based on X-rays able to obtain cross-sectional images of the human body is a non invassive manner.

▶Ischemic Heart Disease, CT

Congenital (or Dysgenetic) Pancreatic Cyst

Congenital pancreatic cyst is an intrapancreatic cystic lesion non-communicating with the duct system and lined by a single layer of flat epithelium. The cysts are usually enclosed in a thin fibrous capsule and they are filled with a mucoid or serous fluid. They may range from microscopic lesions up to 3–5 cm in diameter. They are believed to result from anomalous development of the pancreatic ducts. Unlike cysts in the liver and kidneys, asymptomatic simple pancreatic cysts are uncommon. Most of these cysts are multiple and associated with von Hippel–Lindau disease or, rarely, with inherited polycystic kidney disease. Macroscopic pancreatic cysts are occasionally seen in patients with cystic fibrosis. At imaging, congenital cysts appear as well-defined cystic lesions with smooth walls and without intramural excrescences or septations. Associated renal and hepatic cysts may be seen.

▶Cystic Neoplasms, Pancreatic

Congenital Abnormalities, Pancreatic

Huisman TA[1], Carla Cappelli[2]
[1]Johns Hopkins University, Baltimore, USA
[2]Department of Diagnostic and Interventional Radiology, University of Pisa, Italy
thierry.huisman@kispi.unizh.ch
bartolozzi@do.med.unipi.it

Synonyms

Pancreatic congenital anomalies; Pancreatic congenital variants; Pancreatic developmental anomalies

Definitions

The pancreas arises from dorsal and ventral anlages that fuse at 6 weeks of gestation. The ventral anlage develops into a part of the pancreatic head and the uncinate process while the dorsal part gives rise to the pancreatic body and tail as well as a second part of the pancreatic head. Congenital variants of the pancreas are seen in

approximately 10% of children and include pancreatic agenesis, hypoplasia, ectopia, ►pancreas divisum, and ►annular pancreas.

Complete pancreatic agenesis is extremely rare and is usually associated with other major malformations. In agenesis of the dorsal anlage only the pancreatic head develops, e.g., in combination with polysplenia syndrome.

In pancreatic hypoplasia, the exocrine elements or more rarely also the endocrine elements are underdeveloped.

Pancreatic ectopia is defined as pancreatic tissue in ectopic locations (e.g., stomach, duodenum, jejunum, appendix, Meckel's diverticulum). These lesions have no contact with the normal pancreas and possess its own ductal system and blood supply. It is usually found at autopsy or as an incidental finding at laparotomy. The incidence varies between 1% and 15%.

In pancreas divisum, the dorsal and ventral anlages did not fuse resulting in two separate pancreatic portions which drain separately into the duodenum: the major drainage (body and tail) is performed by the duct of Santorini through the minor papilla, while the main duct of Wirsung drains only the posterior part of the pancreatic head through the major papilla. The accessory duct of Santorini becomes the main excretory pathway of the gland. This anomaly is the most common pancreatic anomaly (4–14% of all children).

The annular pancreas results from a premature fusion of the dorsal and ventral anlages. This anomaly is characterized by a ring of pancreatic tissue that encircles the second portion of the duodenum. A second embryological theory is that an annular pancreas may also result from an anomaly of the ventral bud rotation. Duodenal obstruction may occur. Incidence is increased in children with Down syndrome and other congenital anomalies.

Pathology and Histopathology

While in complete pancreatic agenesis no pancreatic tissue is found at all, in partial agenesis parts of the pancreas can be identified in the pancreatic region. The histology of the pancreatic tissue is normal.

In pancreatic hypoplasia, lipomatous hypertrophy of the pancreas with extensive atrophy of the exocrine acinar tissue is seen while the endocrine system is preserved; in cases of an associated endocrine hypoplasia the Langerhans cells are also atrophic.

Ectopic pancreatic tissue includes all histological elements of the exocrine and the endocrine pancreas, although the ducts of the exocrine pancreatic tissue are not arranged in the normal anatomical pattern. In gastrointestinal ►ectopic pancreas, the pancreatic tissue is usually found in the submucosa. The ectopic pancreatic tissue may be functionally active and secreting, causing local ulceration of the mucosa. Inflammation of the ectopic pancreas with pseudocyst formation or the development of benign or malignant pancreatic tumor has also been described.

Pancreas divisum occurs when the ductal systems of the ventral and dorsal pancreatic ducts fail to fuse. Grossly pancreas divisum is characterized by a completely separated pancreatic ductal system in an undivided gland. In pancreas divisum the predominant drainage is performed by the dorsal duct of Santorini through the minor papilla. In patients with pancreas divisum, signs of acute or chronic pancreatitis can be found in the dorsal duct distribution while normal pancreatic tissue is seen in the ventral duct distribution. It is suggested that the duct of Santorini and the minor papilla are too small to adequately drain the large amount of secretions which may lead to a relative outflow obstruction with resulting pancreatitis.

Annular pancreas is believed to result from an early fusion of the ventral and dorsal anlages or from a failure of normal pancreatic tissue to rotate around the duodenum. The annulus represents the ventral part of the pancreas that remains fixed to the duodenum. In the extramural type, the pancreatic tissue is drained by a duct originating at the anterior surface of the duodenum, passing posteriorly around the duodenum and opening into the main pancreatic or common bile duct near the ampulla. In the intramural type, pancreatic tissue is found within the duodenal wall and small ducts drain directly into the duodenum.

Clinical Presentation

Pancreatic agenesis is usually associated with severe forms of intractable neonatal diabetes mellitus. Complete pancreatic agenesis is usually characterized by severe morbidity and mortality.

In pancreatic acinar hypoplasia the endocrine pancreatic function is usually intact while the exocrine cells are atrophic. The exocrine pancreatic insufficiency results in malabsorption with weight loss and chronic diarrhea. Congenital pancreatic hypoplasia should always be kept in mind when a child manifests with gross steatorrhea and responds well to pancreatic enzyme replacement therapy. ►Shwachman–Diamond syndrome (SDS) is a rare autosomal recessive disorder characterized by exocrine pancreatic insufficiency associated with bone marrow dysfunction and skeletal anomalies (metaphyseal chondrodysplasia). In affected children the pancreatic acinar cells do not develop in utero and are replaced by fatty tissue.

Ectopic pancreas is a relatively rare entity, usually of no clinical importance and found incidentally during laparotomy or in autopsy. If present, symptoms are nonspecific, including abdominal pain, nausea, vomiting, and gastrointestinal bleeding. Specific symptoms can develop in case of complication. Pancreatitis can occur in ectopic pancreas, leading to typical symptoms and laboratory findings; the ectopic insulin secretion may cause hypoglycemia. Exocrine or endocrine tumors may develop in the ectopic pancreatic tissue. Obstructive symptoms are mainly related to the localization of the ectopic pancreas (gastrointestinal obstruction, obstructive jaundice); intestinal mechanical obstruction can be related to intussusception.

Most patients having pancreas divisum are asymptomatic, although some reports have suggested a high incidence of abdominal pain and acute and chronic pancreatitis with typical clinical and laboratory findings. It has been suggested that the relative stenosis of the accessory papillary orifice, the major outflow tract for pancreatic secretions, is the cause of problems.

In many instances annular pancreas is discovered incidentally during radiological imaging studies performed for other reasons. Symptoms develop when complications occur, including pancreatitis, biliary obstruction, and peptic ulcer. If the annular pancreas forms a complete ring, there may be total obstruction of the duodenum and diagnosis is rapidly evident in the neonate; if the ring is incomplete, obstruction may occur later in life or may never produce symptoms. A history of polyhydraminos and other anomalies such as intestinal malrotation, duodenal atresias, and cardiac anomalies are often associated.

Imaging

Ultrasound (US) is a highly sensitive, nonionizing bedside primary imaging modality that can locate, identify, and characterize pancreatic tissue. Computed tomography (CT) and magnetic resonance imaging (MRI) are second line imaging modalities; dynamic contrast-enhancement pattern may increase sensitivity and specificity. Magnetic resonance cholangiopancreatography (MRCP) can be a noninvasive alternative for endoscopic retrograde cholangiopancretography (ERCP).

In complete pancreatic agenesis, no pancreatic parenchyma can be found in the expected locations. In partial agenesis the pancreatic tissue has a normal aspect on US, CT, and MRI.

Pancreatic hypoplasia can be demonstrated by imaging because of the presence of pancreatic lipomatosis with the replacement of the normal pancreatic parenchyma by fat.

Ectopic pancreatic tissue is unlikely to be identified by US, CT, or MRI. Ectopic pancreas in the stomach and duodenum can occasionally be identified on barium studies as submucosal masses. Their appearance is however nonspecific mimicking any kind of submucosal mass in the gastrointestinal tract. Ectopic pancreatic islands in the stomach and duodenum can display a central depression, which corresponds to the opening of a duct. Gastric locations are typically located along the greater curvature in the proximity of the pylorus, whereas in the duodenum, they are mostly found proximally between the bulb and the ampulla of Vater. Ectopic pancreas located in the gallbladder can be visualized by US, which will display hyperechoic nodular mural thickening without acoustic shadowing; however this appearance is not specific.

In pancreas divisum CT and MRI can occasionally demonstrate a separate dorsal and ventral pancreatic portion divided by a thin fat plane. Definite diagnosis of pancreas divisum is obtained by MRCP or ERCP. MRCP may demonstrate a short (1–6 cm) and thin main duct of Wirsung and a larger accessory duct of Santorini which drains almost the entire pancreas from the tail to the anterior part of the head. The identification of the separated ducts can be enhanced by secretin stimulation. In rare cases, pancreas divisum is associated with a focal dilatation of the duct near the papilla, called santorinicele.

Annular pancreas is usually demonstrated by barium enema studies. Asymmetric extrinsic narrowing of the lateral and medial borders of the second portion of the duodenum with normal mucosal pattern is a typical finding. On US, CT, or MRI the annular pancreas may appear as duodenal wall thickening, as an apparent enlargement of the pancreatic head or as a well-defined ring of pancreatic tissue encircling the duodenum. The presence of calcification can suggest an associated chronic pancreatitis. MRCP demonstrates the presence of the annular duct which drains into the main pancreatic duct.

Nuclear Medicine Diagnosis

In patients with unexplained and persisting signs of cholangitis, pancreatitis, jaundice, recurrent abdominal pain, nausea, and vomiting, a congenital anomaly of the pancreatic or bile duct must be considered. Because clinical findings are usually nonspecific, US, CT, and MR are essential for diagnosis. In case of ectopic pancreatic tissue, diagnostic imaging can fail in detection because of the presence of obscuring complications such as pancreatitis and duodenal perforation. In such cases only the histopathological findings can demonstrate the presence of pancreatic tissue. There is however limited value for nuclear medicine imaging in congenital anomalies of the pancreas.

Interventional Radiological Treatment

ERCP is used for therapeutic intervention in patients with pancreas divisum. Several endoscopic and/or surgical procedures have been proposed in an attempt to improve the pancreatic outflow through the minor papilla in patients with acute recurrent pancreatitis. These include endoscopic sphincterotomy, ductal balloon dilatation, and pancreatic duct stent placement.

Bibliography

1. Leyendecker JR, Elsayes KM, BI Gratz et al (2002) MR cholangiopancreatography: spectrum of pancreatic duct abnormalities. Am J Roentgenol 179:1465–1471
2. Fulcher AS, Turner MA (1999) MR pancreatography: a useful tool for evaluating pancreatic disorders. Radiographics 19:5–24
3. Roberts- Thomson IC (2004) Images of interest. Hepatobiliary and pancreatic: annular pancreas. J Gastroenterol Hepatol 19:464
4. Nijs E, Callahan MJ, Taylor GA (2005) Disorders of the pediatric pancreas: imaging features. Pediatr Radiol 35:358–373
5. Nagi B, Kochhar R, D Bhasin et al (2003) Endoscopic retrograde cholangiopancreatography in the evaluation of anomalous junction of the pancreaticobiliary duct and related disorders. Abdom Imaging 28:847–852

Congenital Adrenal Hyperplasia

A group of inborn errors of metabolism arising from enzyme defects in the biosynthesis pathways of adrenal corticosteroids, resulting in inadequate production of glucocorticoids and mineralocorticoids and excess production of adrenal androgens.

►Adrenogenital Syndrome
►Ambiguous Genitalia

Congenital Anomalies of the Pancreas

F.E. Avni[1], C. Matos[1], J.-F. Chateil[2]
[1]Department of Medical Imaging, University Clinics of Brussels—Erasme, Brussels, Belgium
[2]Department of Pediatric Imaging, Hospital Pellegrin, Bordeaux, France
favni@ulb.ac.be

Synonyms

Agenesis of dorsal pancreas; Annular pancreas; Congenitally short pancreas; Ectopic pancreas; Pancreatic cyst(s); Pancreas divisum; Pancreatic lipomatosis

Definitions

Anatomical Anomalies (1–4)

- Pancreas divisum is the most common anatomic variant of the pancreas. Its incidence varies from 4–14% of autopsies. It is characterized by an incomplete fusion between the dorsal and ventral ducts. Only the duct of Wirsung drains into the ampulla of Vater. The duct of Santorini drains into the minor papilla. Stenosis and pancreatitis may ensue.
- Annular pancreas possibly results from abnormal adherence of the ventral duct to the duodenum that results in a complete ring of pancreatic tissue around the duodenum. About 50% of the patients are present in the neonatal period with an associated duodenal obstruction. Other associated anomalies are Trisomy 21, congenital heart disease, and tracheo-esophageal fistula.
- Congenitally short pancreas corresponds to an absence of the pancreatic neck, body, and tail. There is an increased risk of diabetes and associated malformations.
- Ectopic Pancreas: ectopic pancreatic tissue is an aberrant rest of "normal" pancreatic tissue that can be seen in various locations (stomach, jejunum, liver, spleen, umbilicus, Meckel's diverticulum, and so on). It may ulcerate or remain asymptomatic.
- True single congenital cyst of the pancreas may be isolated or associated to ano-rectal, kidney or limbs anomalies. Intestinal duplication cysts may be sequestrated within the pancreas.

Congenital anomalies resulting from systemic diseases that affect the pancreas (1–4)

- Pancreatic lipomatosis is characterized by fatty infiltration of the pancreas associated with deficient secretion of pancreatic enzymes. It is a common finding in the ►Shwachman–Diamond and ►Johanson–Blizzard syndromes already in infants. The lipomatosis develops progressively in cystic fibrosis (CF). In CF, multiple cysts may develop in late childhood (cystosis).

These congenital causes must be differentiated from acquired causes such as lipomatosis following steroid therapy.

- Multiple cysts in the pancreas are seen in Von Hippel Lindau disease and in Dominant Polycystic kidney disease, but usually in adult patients.
- Pancreatomegaly is observed in ►Beckwith–Wiedemann syndrome.
- Congenital tumors: congenital tumors are very rare but perinatal diagnosis of pancreatoblastoma (exocrine tumor) and insulinoma (endocrine tumor) has

been reported. Among endocrine tumors, nesidioblastosis corresponds to ill defined tumors leading to intractable neonatal hypoglycemia.

Pancreatic cysts may be acquired and appear in the course of cystic fibrosis (cystosis).

Pathology/Histopathology

The histopathological anomalies observed on the pancreas will depend upon the type of the primary lesion and complications that have occurred. For instance, inflammatory lesions or fibrosis will be observed in case of pancreatitis associated to pancreas divisum. Fatty infiltration of the gland will be observed in case of Shwachman disease. Islet cells hypertrophy or a circumscribed tumor can be identified in case of nesidioblastosis.

Clinical Presentation

Congenital anomalies of the gland will be clinically evident either because of an antenatal diagnosis of pancreatic tumor (cyst) or because of an abdominal mass palpated at clinical examination. Other symptoms that orient toward a pancreatic anomaly are evidence of pancreatic insufficiency (fatty diarrhea, failure to grow, diabetes) or abdominal pain related to complications of the malformation.

A pancreatic endocrine tumor should be suspected in case of seizures associated with neonatal hypoglycemia (1–4).

Imaging

Ultrasound is the primary screening tool to evaluate the pediatric pancreas. Its size varies with age. The head and the tail increase ±1.0 cm at birth and 2 cm at 10–15 years. The body varies from 0.5 to 1 cm. The gland's echogenicity is slightly hyperechoic to liver at birth, relatively hypoechoic in children.

The width of the pancreatic duct should not measure above 1.5 mm at 1 year and 2.2 mm at 15 years.

The pediatric pancreas is well seen on contrast-enhanced CT. The technique is well suited to visualize pancreatic calcifications, tumors, or complication of traumatism.

MRI can be used for similar indications than CT. Furthermore, the technique using special ▶MRCP sequences provides important supplementary information about the pancreatic duct and biliary tract. A normal MRCP may obviate the need for ▶ERCP.

ERCP is useful whenever MRCP does not provide sufficient information or when a therapeutic maneuver is planned.

In selected cases, peripancreatic venous sampling can be performed in order to localize nesidioblastosis or other ill defined pancreatic endocrine tumors (1–5).

Nuclear Medicine

Not applicable

Diagnosis

The first imaging tool for evaluating the pancreas is ultrasound. The technique will allow evaluation of its size, form, and echogenicity. Its relation with the portal system will be evaluated. Whenever a mass is observed, CT or MRI should be performed.

Whenever a dilatation of the pancreatic duct is observed and whenever an anomaly of the gland morphology is observed, MRCP should be performed (Figs 1 and 2).

Abnormal hyperechogenicity should suggest lipomatosis (Fig. 3) and other symptoms of an associated syndrome should be looked for (1–5).

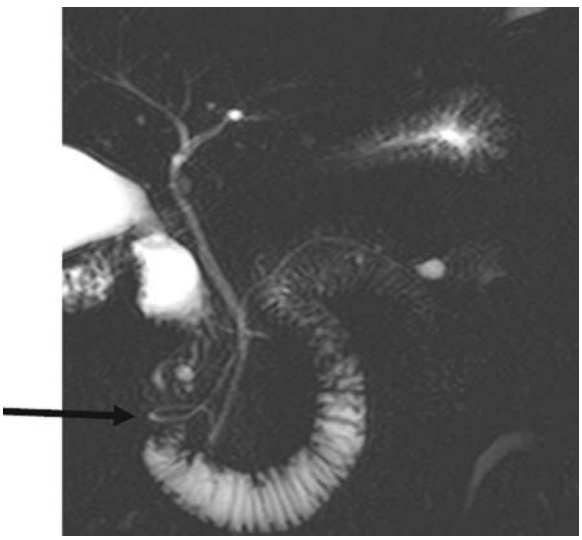

Congenital Anomalies of the Pancreas. Figure 1 Annular pancreas: MRCP demonstrating the pancreatic ducts and the typical annular appearance of the pancreatic duct (arrow).

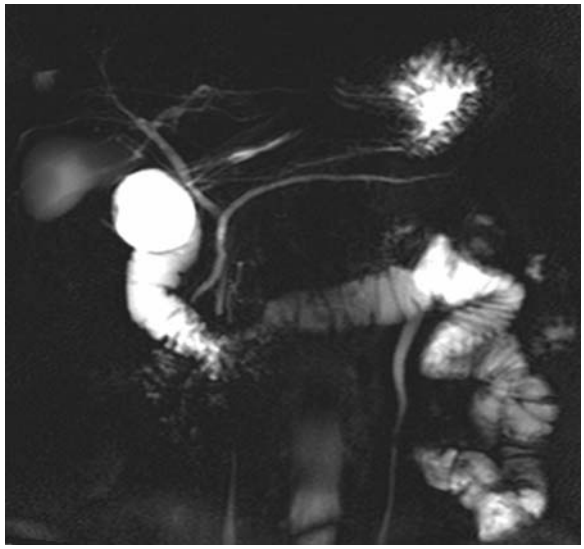

Congenital Anomalies of the Pancreas. Figure 2 Pancreas divisum: MRCP demonstrating separately the main pancreatic and Sontorini ducts.

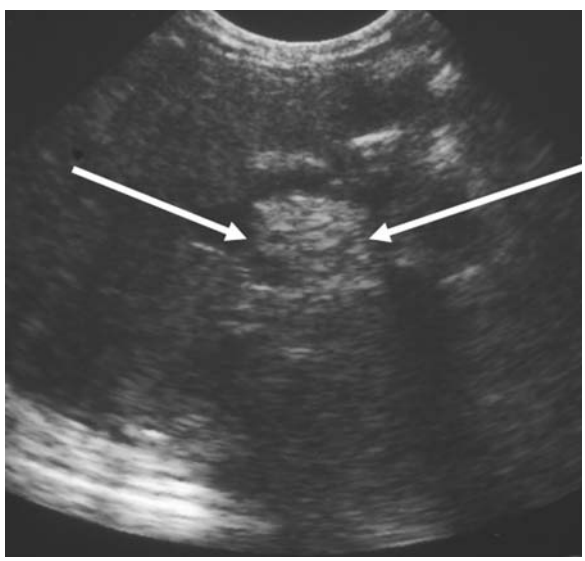

Congenital Anomalies of the Pancreas. Figure 3 Pancreatic lipomatosis in a case of Shwachman syndrome. Ultrasound of the pancreas; the hyperechogenicity of the pancreatic head is striking (between arrows).

Bibliography

1. Enriquez GE, Vasquez E, Aso C (1998) Pediatric Pancreas: an overview. Eur Radiol 8:1236–1244
2. Nijs E, Callahan MJ, Taylor GA (2005) Disorders of the pediatric pancreas: imaging features. Pediatr Radiol 35:358–373
3. Synn AY, Mulvihill SJ, Fonkalsrud EW (1988) Surgical disorders of the pancreas in infancy and childhood. Am J Surg 156:201–205
4. Lerner A, Branski D, Lebenthal E (1996) Pancreatic disease in children. Pediatr Clin North Am 43:125–156
5. Arcement CM, Meza MP, Arumanla S et al (2001) MRCP in the evaluation of pancreatico-biliary disease in children. Pediatr Radiol 31:92–97

Congenital Anomalies of the Uterus

▶Congential Malformations, Mullerian Duct

Congenital Anomalies or Malformations of the Urinary Tract

▶Congential Malformations, Genitourinary Tract; Including Ureter and Urethra

Congenital Abnormalities, Splenic

Huisman TA, Chiara Franchini
Johns Hopkins University, Baltimore, USA
thierry.huisman@kispi.unizh.ch

Synonyms

Inborn Splenic Abnormalities; Splenic Congenital Abnormalities; Splenic Malformations

Definition

Congenital splenic anomalies include inborn anomalies of shape, location, number, and size of the spleen due to aberrant embryologic development.

Pathology and Histopathology

Accessory Spleen

The spleen is a mesodermal derivative, which first appears as a mesenchymal cell condensation inside the dorsal mesogastrium. Sometimes, additional smaller splenic condensations appear and give origin to ▶accessory spleens, representing by far the most common congenital

abnormality of the spleen. Accessory spleens resemble the splenic structure. They may be located anywhere in the abdomen; the most common sites are near the splenic hilum and the tail of the pancreas. Other possible locations are along the splenic vessels, in the gastrosplenic and splenorenal ligaments, in the mesentery, and in the omentum. When splenectomy is performed for hypersplenism, hypertrophy of an accessory spleen may cause recurrent disease (1, 2) (Fig. 1).

Shape Abnormalities

Splenic clefts, notches, and lobules may persist in adult life as variations of the normal shape and are common (1) (Fig. 2).

Abnormal Location

The spleen may be seen in a variety of locations. In congenital diaphragmatic hernia, in Bochdalek diaphragmatic hernia and in eventration of the diaphragm, the spleen may be intrathoracic. If the lateral peritoneal recess is particularly deep the spleen is found posteriorly to the left kidney. The spleen may also be located in the right hypochondrium (1).

Spleno-Gonadal Fusion and Spleno-Renal Fusion

►Spleno-gonadal fusion is a rare anomaly. Due to the close relationship between the developing spleen and

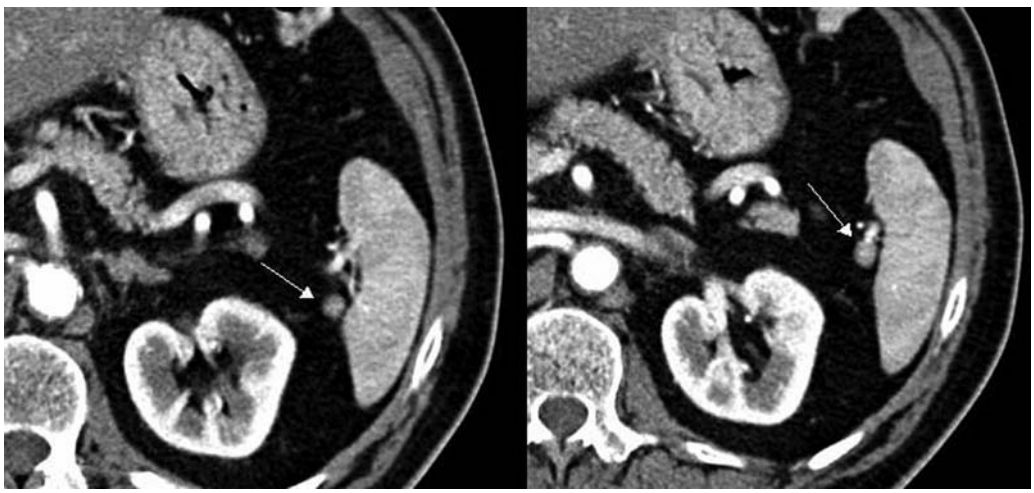

Congenital Abnormalities, Splenic. Figure 1 Accessory spleen CT study shows two small round masses near the splenic hilum (arrows). In the contrast-enhanced arterial phase, they have a strong inhomogeneous enhancement, analogous to that of the normal spleen.

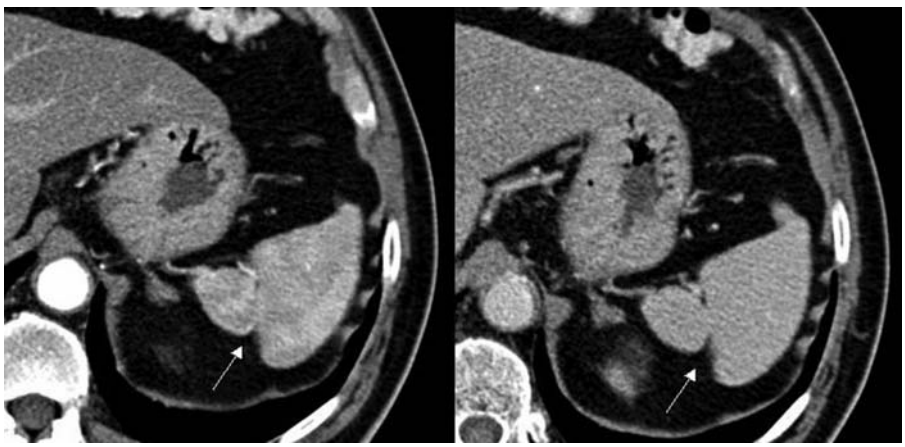

Congenital Abnormalities, Splenic. Figure 2 Splenic cleft CT contrast-enhanced arterial phase. A fissure is appreciable along the posterior margin of the spleen. The smooth edges and the absence of contrast extravasation suggest a congenital splenic cleft.

left gonadal-mesonephric structures, an accessory spleen may be found attached to the left ovary or kidney or may be located within the scrotum. Spleno-gonadal fusion can be classified into two types: continuous (direct connection between the spleen and gonad) and discontinuous (no anatomic connection between ectopic splenic tissue and the principal spleen). This anomaly predominates in males. It can occur as an isolated condition or can be associated with other abnormalities, such as cryptorchismus and orofacial or limb abnormalities (1, 3).

Wandering Spleen

Absence, laxity, or excessive length of ligaments of the spleen leads to an abnormal mobility of the organ. Torsion of the long vascular pedicle may occur, followed by vascular occlusion and splenic infarction (1, 4).

Asplenia and Polysplenia

The absence of the spleen (►asplenia) or the presence of multiple small spleens (►polysplenia) is a rare condition usually associated with other congenital malformations, especially cardiovascular anomalies. Polysplenia or asplenia may associate with abdominal situs ambiguous and are known as asplenia and polysplenia syndrome. Asplenia syndrome is most frequently encountered in males and may be associated with severe cyanotic congenital heart diseases. The typical anatomic features of asplenia syndrome are trilobed lungs with bilateral minor fissures and epiarterial bronchi, bilateral systemic atria, midline liver, and a variable location of the stomach. Polysplenia syndrome is more common in females. The typical anatomic features of classic polysplenia syndrome are bilobed lungs with bilateral hypoarterial bronchi, bilateral pulmonary atria, midline liver, and multiple spleens of variable size and number that may be located in either the left or right abdomen. In rare cases these patients have a single, lobulated spleen or even a normal spleen. Malrotation of the bowel is a frequent finding in heterotaxy syndrome (1, 5).

Splenic Atrophy

Congenital ►splenic atrophy is quite uncommon and is associated with recurrent bacterial infections (1).

Clinical Presentation

Accessory spleens and splenic shape abnormalities are typically an incidental finding at imaging.

Spleno-gonadal fusion may manifest as a mobile and painless left scrotal mass. Other presentations include cryptorchismus, testicular torsion, and inguinal hernia. Spleno-gonadal fusion is often asymptomatic in females.

In case of an intrathoracic location of the spleen, patients usually have respiratory symptoms.

The ►wandering spleen usually is symptomatic in the childhood and may present with an abdominal mass and acute, chronic, or intermittent symptoms due to torsion of the vascular pedicle.

In children with asplenia and polysplenia syndromes, the clinical manifestations may be related to congenital heart disease, immune deficiency (splenic absence), or volvulus due to intestinal malrotation (1).

Imaging

Accessory Spleen

Accessory spleens may vary in number and size, usually ranging from a few millimeters to several centimeters in size. Typically, they appear as round or oval masses near the splenic hilum, but they may be found anywhere in the abdomen. Intrapancreatic accessory spleen, typically in the tail, can mimic a neoplastic mass. Imaging features are identical to those of normal splenic tissue. At computed tomography (CT), the attenuation values before and after contrast administration are identical to those of the spleen. The characteristic inhomogeneous enhancement during the arterial phase is crucial to demonstrate the nature of the mass. On magnetic resonance images (MRI), the spleen is hypointense on T1-weighted scans and hyperintense on T2-weighted scans with respect to the liver and the pancreas. The use of reticuloendothelial-targeted contrast media can confirm the splenic nature of the mass (1, 2).

Shape Abnormalities

Splenic clefts, notches, and lobules are quite common findings and must be distinguished from traumatic lesions. The demonstration at US and CT of characteristic smooth edges and the absence of contrast extravasation suggests a congenital splenic cleft (1).

Spleno-Gonadal Fusion and Spleno-Renal Fusion

In case of left scrotal mass, US is usually the first examination; the splenic tissue appears as a homogeneous, well-encapsulated mass with the same echotexture as the normal spleen. At Doppler US, a vascular architecture analogous to that of the spleen is seen. If spleno-gonadal

fusion is suspected, a cord-like structure connecting the spleen to the mass should be searched for. CT may be helpful to demonstrate associated splenic-renal fusion or cryptorchismus. The typical enhancement pattern confirms diagnosis. In women, spleno-gonadal fusion is usually an incidental finding at US or CT (1, 3).

Wandering Spleen

On plain abdominal X-ray, the absence of the normal splenic outline in the left upper quadrant in association with a soft-tissue mass in the abdomen or pelvis may be noted. US and CT confirm the absence of the spleen in its expected location and the presence of an ectopic splenic location. Torsion of the vascular pedicle may lead to infarction. The congested or infarcted spleen may have a normal echotexture or may be hyperechogenic due to secondary hemorrhage. The spleen's comma-shaped configuration is usually preserved. Splenomegaly with rounded edges of the organ is suggestive for torsion and is attributed to venous congestion. The lack of a flow signal on Doppler US will confirm hypoperfusion. US contrast media can increase sensitivity. Doppler spectral analysis may show a low diastolic velocity with an elevated resistive index in the splenic artery. Unenhanced CT usually shows a decreased density of the spleen; after contrast medium injection a partial or total lack of enhancement may be seen. A whirlpool appearance of the splenic vessels within the splenic hilum indicates torsion (1). Dense splenic vessels (dense artery sign), corresponding to acute thrombosis, are occasionally observed. MR can provide useful information about the precise location of the wandering spleen, the viability of the splenic parenchyma and the splenic vessel anatomy (MR angiography) (4).

Polysplenia and Asplenia

In polysplenia, numerous small splenic masses can be seen predominantly in the right upper quadrant at US, CT, MR, or scintigraphy.

Identification of a missing spleen is more difficult than confirmation of its presence. Scintigraphy remains the gold standard (1, 5).

Nuclear Medicine

99m-Technetium sulfur colloid scintigraphy and 99m-technetium-labeled heat-damaged red blood cells offer functional images and are highly specific for differentiating splenic tissue from other masses. Although nuclear medicine offers the most specific imaging techniques for identifying ectopic splenic tissue, CT and MR offer superior anatomic resolution (2). Scintigraphy is used to confirm the presence of normally functioning splenic tissue in cases of accessory spleens, ectopic spleen, spleno-gonadal and ▶spleno-renal fusion or polysplenia. Scintigraphy is also the examination of choice in documentating the absence of the spleen. However, the absence of a detectable radiotracer uptake can also occur in so-called "functional asplenia," in which the splenic phagocytic function is markedly reduced, despite the presence of

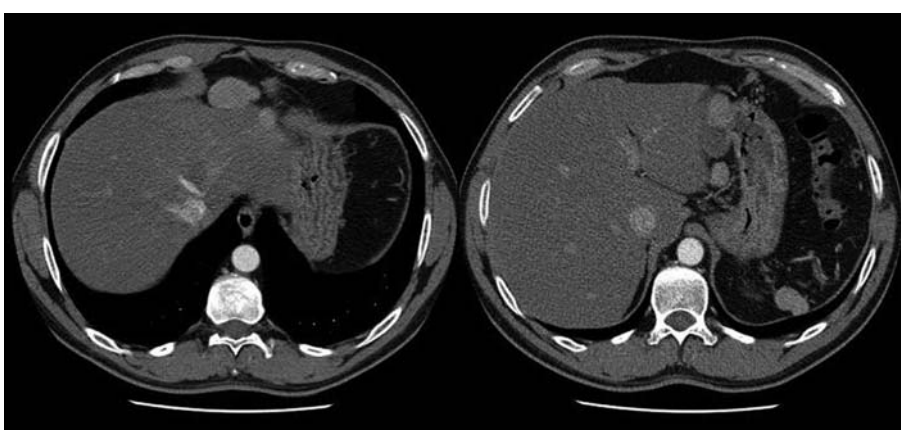

Congenital Abnormalities, Splenic. Figure 3 Splenosis CT study demonstrates multiple masses scattered throughout the abdomen (liver surface, liver hilum, and left hypochondrium) in a patient who had a posttraumatic splenectomy several years before. The masses have regular margins. In the contrast-enhanced arterial phase, the masses typically have a strong inhomogeneous enhancement, analogous to that of the normal spleen.

splenic tissue. Functional asplenia may occur in sickle cell disease, secondary to radiation therapy and chemotherapy, secondary to tumor invasion of the spleen, in splenic anoxia or after bone marrow transplantation (1).

Diagnosis

Ectopic splenic tissue may mimic neoplasms and lymphadenopathies. Imaging can make a definite diagnosis avoiding biopsy. Ectopic splenic tissue shows imaging features identical to those of the spleen in all imaging modalities. The enhancement pattern, especially the inhomogeneity in the arterial phase, is very specific. The combination of different MR sequences increases the confidence in diagnosis. MR reticuloendothelial-targeted contrast media can confirm the splenic nature of the mass. 99m-Technetium sulfur colloid scintigraphy and 99m-technetium-labeled heat-damaged red blood cells represent the most specific imaging techniques to confirm the presence of functioning splenic tissue.

In spleno-gonadal fusion presenting with scrotal mass, US is the first examination to be performed. The homogeneity of the echotexture, the regularity of the vascular architecture and the presence of well-defined margins suggest a nonneoplastic nature of the mass. When spleno-gonadal fusion is suspected, a comparison with the US appearance of the spleen and a study directed to the visualization of a cord-like structure connecting the mass with the normal spleen should be performed. A definitive diagnosis cannot be made solely on the basis of US findings. Nuclear medicine imaging can confirm the presence of splenic areas of activity. However, surgical exploration is generally required to rule out malignancy. Nevertheless, orchiectomy can be avoided because splenic tissue can be dissected away from the tunica albuginea (3).

Accurate preoperative diagnosis of wandering spleen with or without torsion represents an imaging challenge and can be made with US, CT, and MR. Perfusion and viability of the splenic parenchyma can be assessed by contrast-enhanced CT and MR, Doppler ultrasonography, and scintigraphy. Information concerning splenic perfusion and viability is important for the surgeon, especially in younger children where splenopexy instead of splenectomy is the treatment of choice in uncomplicated wandering spleen.

Multiple splenic masses, usually in the abdomen, may be seen in case of multiple accessory spleens, polysplenia, and ►splenosis (autotransplantation of splenic tissue occurring after splenic trauma or after splenectomy) (Fig. 3). History of previous splenectomy suggest the diagnosis of splenosis; in case of polysplenia, other congenital abnormalities are associated.

Bibliography

1. Paterson A, Frush DP, Donnelly LF et al (1999) A pattern-oriented approach to splenic imaging in infants and children. Radiographics 19(6):1465–1485
2. Miyayama S, Matsui O, Yamamoto T et al (2003) Intrapancreatic accessory spleen: evaluation by CT arteriography. Abdom Imaging 28(6):862–865
3. Pomara G (2004) Splenogonadal fusion: a rare extratesticular scrotal mass. Radiographics 24(2):417
4. Deux JF, Salomon L, Barrier A et al (2004) Acute torsion of wandering spleen: MRI findings. Am J Roentgenol 182 (6):1607–1608
5. Applegate KE, Goske MJ, Pierce G et al (1999) Situs revisited: imaging of the heterotaxy syndrome. Radiographics 19(4):837–852; discussion 853–854

Congenital Cystic Adenomatoid Malformation

Intrapulmonary multicystic mass of pulmonary tissue with an abnormal proliferation of bronchial structures.

►Congenital Malformations, Tracheobronchial Tree

Congenital Diaphragmatic Hernia (CDH)

A congenital defect in the diaphragm that allows abdominal contents including bowel and solid abdominal organs to herniate into the chest, most commonly occurring in utero, and resulting in lung hypoplasia on the affected side (left sided in 90%).

►Hernia, Diaphragm, Congenital

►Contrast Media, Ultrasound, Influence of shell on Pharmacology and Acoustic Properties

Congenital Duplication Cyst

Space-occupying lesion of a congenital origin that "duplicates" the different layers of the wall of the digestive tube. It can be communicating or noncommunicating. It is more frequent in the gastric great curvature and in the anteromedical contour of the first and second portions of the duodenum. It presents a water density on CT and a hypoechoic appearance on ultrasonography.

Congenital Heart Disease and Great Vessel Disease, MRI

A. van Straten, G. L. Guit, A. de Roos
Radiology Department, Kennemer Gasthuis, Haarlem, Noord-Holland, The Netherlands
straten@knmg.nl

Definition

Congenital heart diseases (CHD) form a wide range of cardiac malformations. The most common cyanotic congenital heart disease is Tetralogy of Fallot (TOF). Other relatively common CHD are: transposition of the great arteries, atrioventricular septal defects and various kinds of valvular diseases. The most widely used classification is based on the sequential segmental analysis in which the heart is divided into three segments: the atrial chambers, the ventricular mass and the great arteries. In this model, the first step is identification of the arrangement of the atrial chambers (situs). Then ventricular morphology and topology are determined, for example type of atrioventricular connection and morphology of atrioventricular valves. Thirdly, the morphology of the great arteries is assessed (type of ventriculoarterial connection, morphology of arterial valves and infundibulum). Associated cardiac malformations are also noted as well as the cardiac position (position of the heart within the chest and the orientation of the cardiac apex).

Pathology

Most cases of CHD occur spontaneously and aetiology is multifactorial. However, a recent prospective study has shown that patients with CHD have an increased risk of having offspring with a similar CHD (1). The recurrence risk varies between 3 and 8% and is dependent on the cardiac defect and the gender of the involved parent. In general, the risk of recurrence is highest for atrioventricular defects and lowest for TOF. Further evidence of a genetic aetiology is provided by numerous reports of families comprising multiple members with CHD that follow a mendelian pattern of inheritance. This suggests a single gene defect as the specific cause of the CHD. An example of a specific disorder in which the gene defect has been elucidated is the Holt–Oram syndrome. This is an autosomal dominant disorder characterized by atrial and ventricular septal defects as wells as upper limb abnormalities. The affected gene (TBX5) is a member of the T-box family of transcription factors.

Clinical Presentation

Patients with CHD usually present shortly after birth (e.g. transposition of the great arteries), or in (early) childhood. The clinical symptoms are usually failure to thrive and cyanosis. In some cases, patients present at a much later stage or even in adulthood, for example 'pink Fallots', when right ventricular outflow tract obstruction is only mild. When a patients presents with symptoms that would suggest a CHD, history is very important. In the workup of these patients, the electrocardiogram and chest film may provide further insight into the type of cardiac malformation, however, for a definite diagnosis, echocardiography or cardiac magnetic resonance (CMR) imaging is often needed.

With an incidence of 0.3–0.5 per 1,000 live births, TOF is the most common cause of cyanotic CHD (Fig. 1) (2). Traditionally, corrective surgery was preceded by a palliative shunt connecting the systemic arterial circulation to the pulmonary arterial system. It was thought that these shunts would promote growth of the pulmonary arteries and total correction could be delayed until the patient was larger. Nowadays, patients undergo total repair in infancy, which may decrease the risk of late sudden death, but may increase the severity of residual pulmonary regurgitation (PR) in some patients, due to the higher number of trans-annular patch procedures needed in young infants.

Imaging

The clinical role of MR imaging in diseases of the heart and great vessels is rapidly evolving. CMR has become an established non-invasive imaging modality for the assessment of various cardiac disorders, such as cardiac masses, cardiomyopathies, aortic and pericardial diseases and congenital heart diseases. Moreover, due to its accuracy

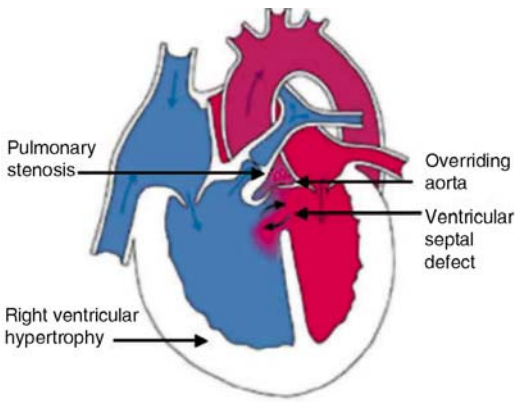

Congenital Heart Disease and Great Vessel Disease, MRI. Figure 1 Schematic view of the Fallot heart.

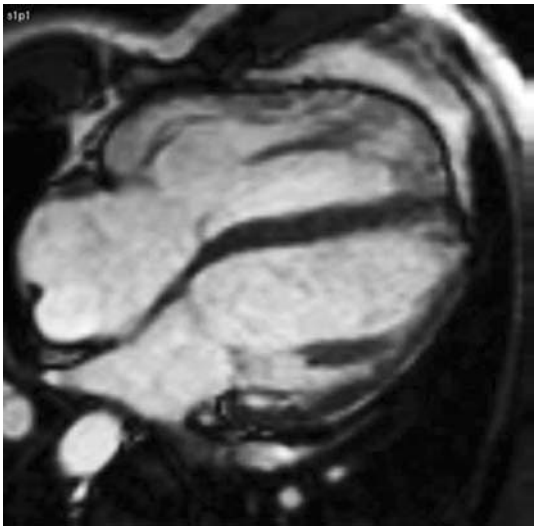

Congenital Heart Disease and Great Vessel Disease, MRI. Figure 2 MR four-chamber view of an adult with TOF and RV hypertrophy due to residual pulmonary stenosis.

and reproducibility, CMR is currently considered the gold standard for quantification of ventricular volumes, function and mass (Fig. 2) (3). Comprehensive functional assessment is possible by CMR due to its capability to measure flow velocity and flow volume, which is a basic requirement to quantify lesion severity in valvular heart disease. Over the past few years, major technical advances have considerably improved acquisition speed and image quality making CMR a useful tool for the evaluation of patients with ischemic heart disease as well. Although the clinical robustness of coronary magnetic resonance angiography still needs improvement, CMR currently provides valuable information to detect reversible ischemia, myocardial infarction and residual viability.

Transthoracic echocardiography is still the most commonly used technique in the non-invasive assessment of CHD, especially in young children whose small thoracic diameter provides an optimal acoustic window. After surgical intervention, however, the use of ultrasound is often restricted because of scar tissue and thoracic deformations. Unlike echocardiography, CMR provides unlimited access to the thoracic cavity and different techniques are available for detailed visualization and accurate measurement of the complex post-surgical morphology and functional status. Biventricular volumes and blood flow can be accurately measured during a single examination, allowing complete evaluation of both right and left ventricular systolic and diastolic function as well as intracardiac and vascular flow.

In the seriously ill or uncooperative patient CMR imaging is often limited, and it is contraindicated in patients with pacemakers. CMR studies are also time-consuming and may require patient sedation. Ultrasound has been the imaging modality of choice for many years, however, recently the role of electron beam CT and multidetector CT (MDCT) has been established in the evaluation of congenital heart disease.

The advantages of MDCT compared to MR imaging should be considered in selecting the optimal imaging modality for a child with CHD. Because MDCT takes less time and has fewer requirements for sedation than does MR imaging, it can be more easily performed in an unstable patient who needs intensive monitoring and care. Failure to wean the patient off the ventilator post-operatively may result from the airway compression caused by the vascular structure. The relationship between the airway and vessel can be accurately evaluated at MDCT. This information is useful for surgical management and cannot be provided by any other imaging modality. On the other hand, MDCT has several disadvantages, such as the need for iodinated contrast agents and radiation exposure, although the latter can be minimized by using a low-dose MDCT protocol.

Nuclear Medicine

The role of radionuclide angiography is limited nowadays since non-invasive imaging modalities such as cardiac CMR and MDCT offer detailed information on cardiac morphology as well as biventricular function.

Diagnosis

Presently, the vast majority of CHD can be surgically repaired. However, even after corrective surgery, the right ventricle (RV) may remain subject to an abnormal pressure and/or volume overload, due to longstanding residual pulmonary stenosis and/or PR. Hence, RV function has shown to be a major determinant of clinical outcome in CHD patients. With the growing number of long-term survivors amongst CHD patients, the need for accurate follow-up becomes increasingly important in clinical management. Careful monitoring of functional parameters such as cardiac function and vascular flow will help to allow early detection of the most important post-operative complications and aid in the timing of re-interventions (4). Timely detection of late complications requires adequate assessment of right ventricular size and function as well as quantification of intracardiac blood flow in these patient groups. Widely used techniques, such as echocardiography and radionuclide studies, have limitations when applied for this purpose, especially in patients with abnormal RV morphology.

Interventional Radiological Management

The recent implementation of fast CMR sequences along with the ability of MR imaging to acquire images in any given orientation and with high soft-tissue contrast makes this technique attractive for guiding interventional procedure. Razavi et al showed that cardiac catheterization guided by MR imaging is safe and practical in a clinical setting, allows better soft-tissue visualization, provides more pertinent physiological information, and results in lower radiation exposure than do fluoroscopically guided procedures (5). MR guidance could become the method of choice for diagnostic cardiac catheterization in patients with CHD, and an important tool in interventional cardiac catheterization and radiofrequency ablation. MR guided cardiopulmonary interventions, however, are challenging due to motion artefacts caused by the beating heart and respiration. Moreover, the tortuous anatomy of the right cardiac chambers and pulmonary arteries makes monitoring of the passage of guide wires and endovascular catheters and the deployment of stents with MR imaging more difficult. Kuehne et al showed that interactive real-time MR imaging has the potential to guide stent placement in the pulmonary valve or main pulmonary artery and measure blood flow volume in the stent lumen immediately after the intervention (6). Several other authors have reported the use of MR imaging—compatible catheters and guide wires. However, none of the investigated instruments contained properties required for complex cardiovascular interventions, such as (a) fast and reliable detection of the tip; (b) curvature of the shaft and (c) material properties such as tip flexibility, torque and tracking ability, shaft strength and flexibility. More work is needed to develop new MR imaging—compatible catheters and guide wires that are appropriate for use in cardiovascular interventions. In the future, research methods such as use of resonance circuits as fiducial markers should be investigated to provide tip and shaft detection without incorporating the risk of heating effects inherent with active catheter tracking methods.

Bibliography

1. Burn J, Brennan P, Little J et al (1998) Recurrence risks in offspring of adults with major heart defects: results from first cohort of British collaborative study. Lancet 351:311–316
2. Ferencz C, Rubin JD, McCarter RJ et al (1985) Congenital heart disease: prevalence at livebirth. The Baltimore-Washington Infant Study. Am J Epidemiol 121:31–36
3. de Roos A, Doornbos J, van der Wall EE et al (1995) Magnetic resonance of the heart and great vessels. Nat Med 1:711–713
4. Vliegen HW, Van Straten A, de Roos A et al (2002) Magnetic resonance imaging to assess the hemodynamic effects of pulmonary valve replacement in adults late after repair of tetralogy of Fallot. Circulation 106:1703–1707
5. Razavi R, Hill DL, Keevil SF et al (2003) Cardiac catheterisation guided by MRI in children and adults with congenital heart disease. Lancet 362:1877–1882
6. Kuehne T, Saeed M, Higgins CB et al (2003) Endovascular stents in pulmonary valve and artery in swine: feasibility study of MR imaging-guided deployment and postinterventional assessment. Radiology 226:475–481

C

Congenital Hepato-Biliary Anomalies

▶Congenital Malformations, Liver and Biliary Tract

Congenital Lesions of the Adrenal Gland

▶Congenital Malformations, Adrenals

Congenital Lobar Emphysema

Congenital progressive overdistension of a lung lobe.
▶Congenital Malformations, Tracheobronchial Tree

Congenital Lymphatic Malformation

▶Lymphangioma

Congenital Malformations, Adrenals

ROSEMARY ARTHUR
Department of Pediatric Radiology, Leeds General Infirmary, Clarendon Wing,
Leeds, UK
r.arthur@ukonline.co.uk

Synonyms

Congenital lesions of the adrenal gland

Definition

Congenital lesions of the adrenal gland arise from disordered embryogenesis, ►inborn errors of metabolism, or the occurrence of disease processes identified in the fetus or early neonatal period.

Histology/Pathology

The fetal adrenal cortex develops around 6 intrauterine weeks from coelomic mesodermal tissue and between 8 and 12 weeks it is invaded by ectodermal sympathetic cells of the neural crest to form the adrenal medulla producing catecholamines. The fetal adrenal cortex differentiates into an outer definitive zone and a larger inner fetal zone producing androgenic precursors for the placental synthesis of estriol. The fetal adrenal gland is proportionately very large, but soon after birth the fetal zone involutes disappearing by 1 year. At the same time the definitive zone of the cortex differentiates to form the glomerulosa (15%), lying peripherally and producing aldosterone, and the fasciculata (75%) and the reticularis (10%), lying next to the medulla both producing glucocorticoids and androgens. The glomerulosa becomes fully differentiated around 3 years of age, whereas the reticularis is not fully differentiated until approximately 15 years. In the adult a normal adrenal gland weighs approximately 4–5 g (1, 2).

Abnormalities in Embryogenesis

A number of developmental abnormalities of the adrenal gland result from disordered embryogenesis. Most are asymptomatic and discovered incidentally, although some are associated with other developmental anomalies (2–5).

Adrenal agenesis is rare and usually occurs in conjunction with ipsilateral renal agenesis. Ten percent of infants with renal agenesis will have adrenal agenesis. In these cases, the renal/adrenal agenesis is thought to be due to the failure of the mesonephric ridge to develop, whereas the majority of cases of renal agenesis (i.e., those not associated with adrenal agenesis) develop as a result of the failure of the ureteric bud to develop normally.

Adrenal hypoplasia of the adrenal glands in anencephalic infants is associated with triploidy and prenatally acquired pituitary and CNS degenerative disorders due to ACTH deficiency. Hypoplasia is also seen in neonatal adrenoleukodystrophy and Zellweger's syndrome.

Accessory adrenal glands are found in up to 50% of autopsies in children, and contain both adrenal cortical and medullary tissue. They may be hormonally active becoming overproductive following adrenalectomy. They are found around the celiac axis, along the line of the gonadal vessels and around the ovaries in girls and around the testes, epididymis, and hernial sacs in boys.

Straight adrenal refers to a discoid-shaped adrenal gland that appears elongated and straight on both longitudinal and transverse imaging rather than having the normal Y, Z, or V shape. This anomaly is seen in association with renal agenesis, hypoplasia, or ectopia and is thought to result from the failure of the renal tissue to indent into the adrenal gland during early development.

Horseshoe adrenal is a single mass of adrenal tissue that lies across the midline, generally posteriorly to the aorta and anteriorly to the inferior vena cava (IVC), but when associated with asplenia is always seen anteriorly to the aorta. Coexisting anomalies occur frequently including 52% asplenia, 37% neural tube defects, 29% renal anomalies, and in 3% Cornelia de Lange syndrome. Horseshoe adrenal does not occur in association with polysplenia, a differentiating feature from asplenia.

Circumrenal adrenal gland is a further anatomical variant describing the finding where there is fusion of two limbs of one gland extending down and around the kidney.

Adrenohepatic fusion and adrenorenal fusion are uncommon anomalies. These occur when the adrenal gland becomes incorporated within the capsule of the liver or kidney and is thought to be due to the disruption of intervening coelomic epithelium allowing these adjacent organs to fuse.

Clinical Presentation

With the exception of adrenal agenesis and severe hypoplasia, these anatomical variants of fusion are associated with normal adrenal function and histologically normal tissue. Adrenal tissue in ectopias, straight adrenal, and fusion anomalies usually show the characteristic pattern of normal adrenal glands on ultrasound (Figs 1 and 2).

Congenital adrenal hyperplasia is a group of inborn errors of metabolism arising from enzyme defects in the biosynthetic pathways of adrenal corticosteroids resulting in inadequate production of glucocorticoids and mineralocorticoids and the excess production of adrenal androgens. (*Give link to CAH/Ambiguous genitalia essays*)

►*Wolman's disease* is an inborn error of metabolism due to a deficiency of the enzyme acid esterase leading to an accumulation of triglycerides, cholesterol, and its esters within many organs particularly the inner layers of the adrenal cortex. The infants develop massive enlargement of the adrenal glands, hepatosplenomegaly, jaundice, vomiting, steatorrhea, abdominal distension, and failure to thrive.

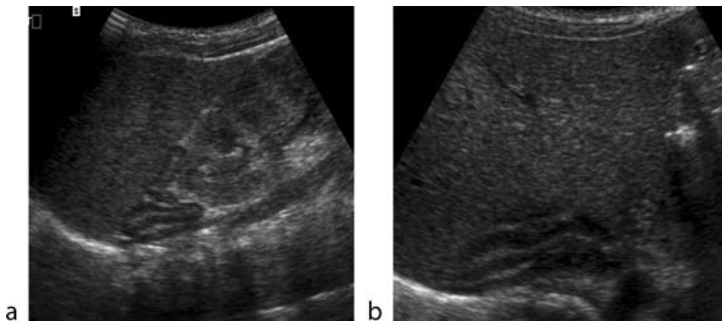

Congenital Malformations, Adrenals. Figure 1 (a) US (longitudinal US) and (b) (transverse US), of a normal, right neonatal adrenal gland.

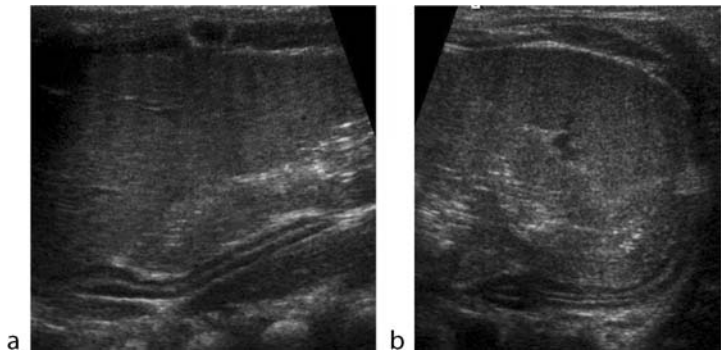

Congenital Malformations, Adrenals. Figure 2 (a) US (longitudinal US) and (b) (transverse US; both same patient as Figure 1), the straight or discoid left adrenal gland associated with left renal agenesis.

The condition generally presents early in infancy and is rapidly progressive resulting in death during the first year.

A number of pathological processes result in *cystic adrenal lesions* that need to be differentiated from simple adrenal cysts and include cystic ▶neuroblastoma, adrenal hemorrhage, adrenal abscess, epidermoid cysts, and intraabdominal extralobar pulmonary sequestration (ELPS) that may be sited within or adjacent to the adrenal glands. Careful imaging should help to differentiate these lesions from the cystic or dysplastic upper moiety of a duplex kidney.

Adrenal congestion and hemorrhage occur in the perinatal period in response to perinatal asphyxia and stress. Hypoxic damage to the endothelial cells results in adrenal congestion which may be followed by hemorrhage and hemorrhagic infarction. Prolonged abdominal compression in labor, particularly in infants born to diabetic mothers, and underlying bleeding diatheses and are also considered etiological factors. Adrenal hemorrhage may be bilateral but is more commonly unilateral affecting the right gland in 70% of cases on account of direct drainage of the right adrenal vein into the IVC. The condition is often asymptomatic, recognized as a result of a palpable kidney displaced by an enlarged adrenal gland, or may present clinically with jaundice, anemia, and rarely hypovolemic shock. If hypertension and/or impaired renal function is present, the possibility of a coexistent ipsilateral renal vein thrombosis should be considered. This occurs more commonly on the left where the adrenal vein drains into the left renal vein. Hemorrhage may track down the retroperitoneal tissues and into the scrotum causing scrotal swelling. Long-term adrenal insufficiency is unusual but may develop when more than 90% of both glands are affected.

Neuroblastoma is the commonest extracranial solid pediatric neoplasm and may present prenatally or be diagnosed at birth, although more commonly it presents in the preschool years. The tumor is variable in size at presentation, and is more commonly cystic than tumors presenting later in childhood. The tumor may be

asymptomatic and discovered incidentally, but when large or associated with hepatomegaly it may result in early neonatal respiratory distress. Neonatal metastatic spread to the liver, skin, and bone marrow sometimes occurs, and when found in association with a localized adrenal primary is staged 4S. These 4S tumors have a favorable prognosis, in contrast to prenatal presentation with hydrops and intraspinal extension, which is associated with a poor prognosis. (*Link to tumors/neuroblastoma essay*)

Adrenal endothelial cysts are seen infrequently in the adrenal glands and are often found incidentally during an ultrasound examination for an unrelated problem. Cysts can be huge and multiloculated, and they are generally filled with blood. They are usually unilateral but may be bilateral and generally decrease in size over time.

Adrenal abscess is unusual in the neonate and is most commonly seen in association with a resolving adrenal hemorrhage following *Neisseria meningitidis*, *Escherichia coli*, β-hemolytic streptococcal, or *Staphylococcus aureus* septicemia.

Imaging

The normal adrenal gland is Y, Z, or V shaped, closely related to the upper pole of the kidneys, and is easily seen in the neonate on *ultrasound imaging* using a high-frequency transducer (Fig. 1). The adrenal gland is a difficult organ to measure on account of its shape, but the thickness of the adrenal limbs should be approximately equal and less than 4 mm in width. Ultrasonically, the neonatal gland has a thin central hyperechoic stripe representing the medulla, central veins, and connective tissue with a surrounding hypoechoic cortex. With increasing age, the differentiation between the cortex and medulla disappears. The contour should be smooth or gently undulating but should not show any marked nodularity (4, 5).

Imaging findings in *Wolman's disease* are fairly characteristic, demonstrating a massive increase in the size of both glands that tend to retain their overall shape in conjunction with areas of calcification. Lymph node enlargement and bowel wall thickening may also be noted (Fig. 3).

A number of *cystic abnormalities* develop in the adrenal glands as discussed earlier and these may be difficult to differentiate on the basis of imaging characteristics alone. Simple adrenal cysts usually appear as simple, thin-walled cysts, whereas resolving hemorrhage and abscess will usually have a thicker wall, and the fluid may contain echoes or even a fluid–fluid level. *Adrenal hemorrhage* presents as an echopoor mass within a mildly enlarged adrenal and tends to become smaller and resolve over 2–4 weeks, often leaving a densely calcified involuted adrenal gland (Fig. 4). Neuroblastoma may also present as a cystic mass, and should be suspected if the wall shows some nodularity. However, the mass may be homogeneous and indistinguishable from other benign or malignant tumors. The differential diagnosis of a complex cystic/solid adrenal lesion should also include an ELPS. These are commonly left-sided and are often first seen in the second trimester on ultrasound, whereas a congenital neuroblastoma is generally first seen in the third trimester

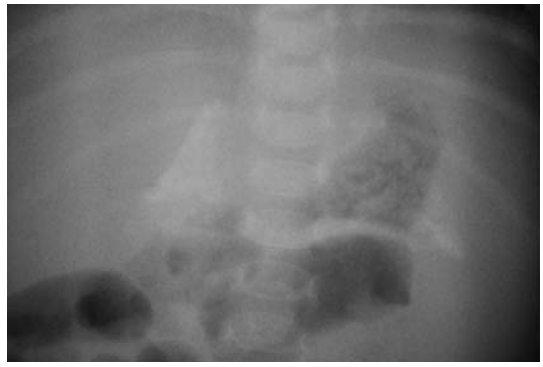

Congenital Malformations, Adrenals. Figure 3 Abdominal X-ray demonstrating calcification in enlarged adrenal glands. Normal overall shape is maintained. (From Paterson A (2002) Adrenal pathology in childhood: a spectrum of disease 12:2491–2508).

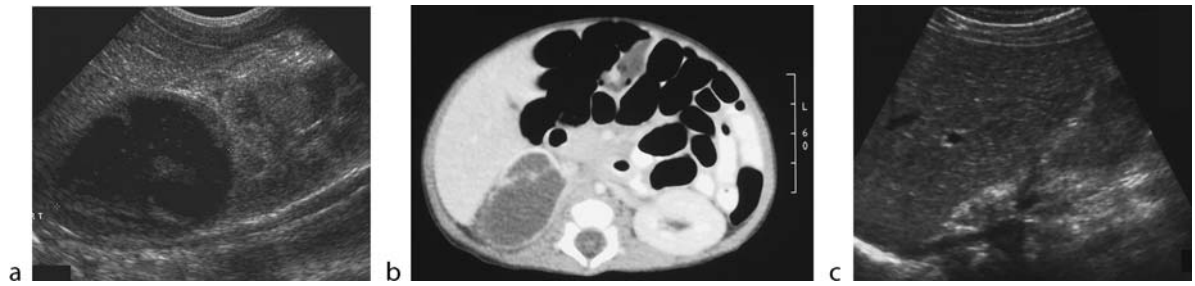

Congenital Malformations, Adrenals. Figure 4 (a) Early US (b) CT, and (c) later ultrasound images of large adrenal hemorrhage, which involutes and become calcified.

following a normal second trimester scan and is more commonly right-sided. EPLS may show increased vascularity, and the identification of a systemic arterial supply helps to clinch the diagnosis.

Abdominal radiography is useful in the assessment of abdominal distension, and in Wolman's disease it will show enlarged and densely calcified adrenal glands, whereas in neuroblastoma the calcification is more focal. In the older child a triangular, dense, calcified adrenal gland may be noted following perinatal adrenal hemorrhage.

CT and MRI scanning of the neonate are rarely helpful in clearly differentiating hemorrhage from a cystic neuroblastoma or adrenal abscess, although helical CT and MRI may be useful to further delineate a mass lesion, particularly when solid and large, and to identify any metastases associated with neuroblastoma. Helical CT and MRI are also useful for the detection of aberrant vessels suggesting the presence of an ELPS. Metaiodobenzylguanidine scintigraphy is only indicated in cases of neuroblastoma.

Diagnosis

The main difficulty in diagnosis is differentiating between the various cystic, complex, or homogeneous masses. A clinical history of perinatal hypoxia should point to the possibility of adrenal congestion and/or hemorrhage, and these lesions should gradually become smaller over the first few weeks of life. Failure to involute is suggestive of more significant pathology, for example, neuroblastoma. Although the potential diagnosis of neuroblastoma is of concern in the case of both cystic and solid congenital adrenal lesions, the outlook for 4S lesions is very good and it is generally considered safe to wait several weeks, particularly in cystic lesions, to see if they involute. Percutaneous/open biopsy will be required for a definitive diagnosis in solid lesions or cystic lesions that fail to involute. Unfortunately, vanillylmandelic acid estimations, a noradrenalin metabolite, are generally unhelpful in the neonatal period.

Bibliography

1. Miller WL (1997) The adrenal cortex and its disorders. In: Brook C, Clayton P, Brown R (eds) Brook's Clinical Pediatric Endocrinology. Blackwell Publishing, pp 293
2. Paterson A (2002) Adrenal pathology in childhood: a spectrum of disease. Eur Radiol 12:2491–2508
3. Strouse PJ, Haller JO, Berdon WE et al (2002) Horseshoe adrenal gland in association with asplenia: presentation of six new cases and review of the literature. Pediatr Radiol 32:778–782
4. Daneman A (2004) The adrenal gland. In: Kuhn JP, Slovis TL, Haller JO (eds) In Caffey's Paediatric Diagnostic Imaging. Mosby, pp 239–251
5. Siegel MJ (2002) Adrenal glands, pancreas and other retroperitoneal structures. In: Siegel MJ (ed) Pediatric Sonography, Raven Press, pp 475–527

Congenital Malformations, Bile Ducts

F.E. Avni, C. Matos, M. Cassart
Department of Medical Imaging, University Clinics of Brussels, Erasme Hospital, Brussels, Belgium
favni@ulb.ac.be

C

Synonyms

Alagille syndrome: Ductular paucity of intrahepatic bile ducts; Bile duct cyst; Biliary atresia; Caroli's disease; Choledochal cyst; Choledochocele; Choledochal cyst type V; Communicating cavernous ectasia of the intrahepatic bile ducts; Extrahepatic atresia; Progressive familial cholestasis; Syndromic hepatic ductular hypoplasia; Watson-Alagille syndrome

Definition

In the infant/neonatal age group, biliary atresia (BA) is the predominant surgical malformation followed by choledochal cyst (CC) and spontaneous perforation of the common bile duct (CBD) (1, 2).

BA consists of a severely complete or partial interruption of the extrahepatic biliary tree (EHBT). It occurs in 1:10,000 to 1:25,000 births. It is thought to result from a progressive *in utero*, inflammatory disease of the entire biliary tract.

There are multiple different anatomic types depending on the extent of the inflammatory and fibrotic process. This leads to numerous variants including (partial) patency of the CBD or gallbladder but also some cystic dilatation of bile ducts (3, 4).

CC consists of a spectrum of malformations of the extrahepatic and intrahepatic bile ducts. The primary anomaly is apparently related to an abnormal pancreaticobiliary junction. There is a common segment that is too long, with reflux of pancreatic juice into the CBD. It occurs in 1:100,000 births.

An early classification indicated three groups of CC. Type I, fusiform or cystic dilatation of the CBD, represents 90% of the patients. Type II corresponds to a diverticulum of the CBD. Type III represents a choledochocele that protrudes into the duodenal lumen.

More recently, two types have been added: type IV corresponds to the presence of multiple extrahepatic bile duct cysts, either as an isolated anomaly (IVa) or in association with intrahepatic biliary cysts (IVb; Caroli's-like disease). Type V is a cystic dilatation of the

intrahepatic bile ducts equivalent to Caroli's disease. Caroli's disease itself is a congenital cystic dilatation of the intrahepatic bile ducts that communicate with the biliary system. The disease can be associated with autosomal recessive polycystic kidney disease, hepatic fibrosis, or both; the condition is then referred as Caroli's syndrome (1–3).

Spontaneous perforation of the CBD is a very rare condition of unknown origin (ischemic lesion is a possible explanation). The perforation is always located at the junction of the cystic duct and the CBD. It may or not be associated with the very rare neonatal biliary lithiasis or biliary plug syndrome.

Intrahepatic bile duct tree congenital anomalies include Byler's disease (progressive familial cholestasis) and ►Alagille syndrome (intrahepatic ductular paucity).

The spectrum of congenital anomalies of the biliary tree also includes rare cases of agenesis, duplication, and septation of the gallbladder (anomalies that are usually without clinical consequences) (1, 2).

Pathology/Histopathology

In BA, the entire EHBT is involved. The biliary ducts are atretic and hypoplastic. Early in the course of the disease, there are tiny but patent biliary structures in the perihilar tissue at the porta hepatis that disappear progressively after 4 months. Some infants may have sparing of the distal BD (patent gallbladder, cystic duct, and CBD). Some others present segmental patency with a pseudocyst-like structure at the level of the CBD or liver hilum. Microscopic evaluation of the liver reveals cholestasis, distorted bile ducts, and a distorted portal vascular system. Extensive fibrosis is also visible (1, 2).

In CC, a long common biliopancreatic channel is observed with partial obstruction of the CBD. The CBD is thickened and fibrotic without a muscular layer. The mucosa is ulcerated. In the case of Caroli's disease, pathology demonstrates saccular or fusiform ductal dilatation of the intrahepatic biliary tree (IHBT). Depending on the age of the patient, evidence of cholangitis, periductal fibrosis, and cirrhosis may be demonstrated as well.

Clinical Presentation

In the neonatal period, most congenital malformations of the BT will be suspected in cases of persistent jaundice, hepatomegaly, and acholic stools. This is the case for up to 80% of patients with BA.

CC is classically suspected with the association of abdominal pain, a right upper quadrant mass, and fluctuant jaundice. Antenatal diagnoses have been reported.

Other clinical symptoms are related to the (later) complications of the congenital malformations (cirrhosis, biliary stones, or rupture of varices).

Imaging

Various imaging techniques provide information about the biliary tract.

1. Conventional X-ray of the spine can be done to demonstrate butterfly vertebrae (Alagille syndrome).
2. Ultrasound (US) is the primary technique used to image the biliary tract, especially in neonates.

The first structure to be identified is the CBD. Yet a normal CBD is difficult to visualize; it has to be differentiated from the hepatic artery. Dilatation should be considered when the diameter is >2 mm, and CC when >7 mm.

The intrahepatic bile ducts are dilated when their diameter exceeds the diameter of the parallel portal branch.

Evaluation of the gallbladder (GB) is more controversial because, even in cases of BA, it may be present and normal in size (2.5–3.5 cm in length). An empty GB after a meal does not exclude the diagnosis; on the contrary, an enlarging GB after 4 h of fasting excludes BA. Ultrasound is helpful in detecting intrahepatic or extrahepatic biliary cysts. It is also important when the triangular cord sign is demonstrated; this consists of a triangular echogenic irregular structure (the fetal biliary duct) at the level of the porta hepatis. Color Doppler analysis is important to detect frequently associated vascular anomalies (preduodenal portal vein, interrupted inferior vena cava).

Periportal fibrosis, portal hypertension, and polysplenia are other possible anomalies demonstrable by US (4).

Magnetic resonance imaging (MRI) can be used in infants and even neonates to demonstrate a normal or abnormal biliary tract. Using T2-weighted MR cholangiography (MRCP), images of the normal or dilated biliary tract can be easily obtained as in adults, and the technique helps to exclude BA.

In cases of BA, the MR equivalent of the US triangular cord sign has been described: a triangular area of high intensity at the level of the porta hepatis can be observed. The status of the liver (periportal fibrosis) and/or vascular anomalies can be analyzed using T1 (without and with gadolinium) and echogradient sequences (5).

Endoscopic retrograde cholangiopancreatography (ERCP) can be performed at any age to assess the patency of the EHBT or IHBT. Its yield is greater in cases of dilated biliary ducts where it has replaced transhepatic opacification of the biliary tract. Its advantage lies in a possible therapeutic maneuver and an easier interpretation than with the imaging.

A perioperative cholangiogram is mandatory to confirm the diagnosis of BA, to determine its type and to differentiate BA with biliary cysts from CC.

Nuclear Medicine

Nuclear medicine scans are of utmost importance for the differential diagnosis of ►neonatal cholestasis and a presumptive diagnosis of BA.

^{99m}Tc-disofenin (DISIDA) has the highest hepatic extraction and the highest diagnostic yield. After proper preparation with phenobarbital (for 5 days), the examination can be performed in neonates. Lack of hepatic captation of the tracer favors hepatic insufficiency (i.e., neonatal hepatitis), and lack of excretion into the intestine on a 24-h delayed scan is highly suggestive of BA. Excretion into the intestine excludes the diagnosis (1, 2).

Diagnosis

Once neonatal cholestasis or obstructive jaundice is suspected, US should be performed to evaluate the liver and biliary tract.

Absence of a visible GB despite 4 h of fasting, a nondilated CBD, the presence of triangular cord sign (Fig. 1), a periportal biliary cyst, echogenic kidneys, and polysplenia are signs suggestive of BA. In equivocal cases, MRCP may provide additional information and eventually exclude the diagnosis.

Nuclear medicine scanning should rapidly be performed (Fig. 2), and during surgery a cholangiogram is mandatory.

If the EHBT or IHBT is dilated on US, MR imaging may be performed to better understand the biliary tract and liver anatomy. Whenever an obstructive jaundice is confirmed, ERCP can be proposed as an alternative to surgery to precisely assess the diagnosis and eliminate any obstructive sludge or lithiasis.

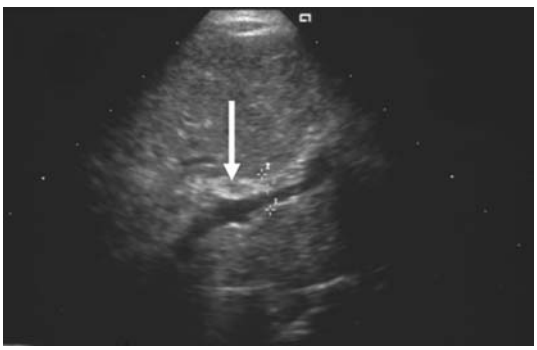

Congenital Malformations, Bile Ducts. Figure 1 Biliary atresia in a neonate. Ultrasound demonstrating the triangular cord sign (*arrow*). Oblique view through the porta hepatic.

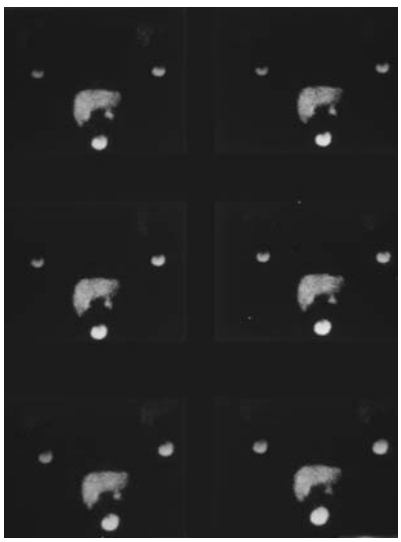

Congenital Malformations, Bile Ducts. Figure 2 Biliary atresia. DISIDA hepatic scan in a neonate. The tracer has been correctly metabolized by the liver but not excreted because no bowel has opacified, despite delayed views.

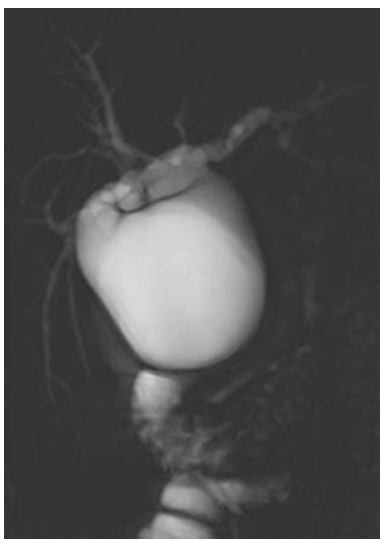

Congenital Malformations, Bile Ducts. Figure 3 Choledochal cyst type 1. Magnetic resonance cholangiopancreatographic demonstration (heavily T2-weighted sequence) of the typical cystic dilatation of the common bile duct.

Both MRCP and ERCP are useful for assessing communication between intrahepatic or extrahepatic cysts and the biliary tract as observed in CC (Fig. 3) or Caroli's disease.

Again, when surgery is elected, a preoperative cholangiogram will be necessary.

Whenever Caroli's disease or syndrome is suspected, the kidneys should be assessed to confirm associated kidney disease.

Bibliography

1. Karrer FM, Hall RJ, Stewart BA et al (1990) Congenital biliary tract disease. Surg Clin North Am 70:1403–1418
2. Benya EC (2002) Pancreas and biliary system: imaging of developmental anomalies and diseases unique to children. Radiol Clin North Am 40:1355–1362
3. Levy AD, Rohrmann CA Jr, Murakata LA et al (2002) Caroli's disease: radiologic spectrum with pathologic correlation. Am J Roentgenol 179:1053–1057
4. Lee HC, Yeung CY, Chang PY et al (2000) Dilatation of the biliary tree in children: sonographic diagnosis and its clinical significance. J Ultrasound Med 19:177–182
5. Norton KI, Glass RB, Kogan D et al (2002) MR cholangiography in the evaluation of neonatal cholestasis: initial results. Radiology 222:687–691

Congenital Malformations, Bone

Alan E. Oestreich
Cincinnati Children's Hospital Medical Center, Cincinnati, Ohio, USA
Alan.Oestreich@cchmc.org

Synonym

Deformity or other structural abnormality of skeletal elements present at (or before) birth

Definitions

Abnormality such as deformity of skeletal elements that is present at or before birth. It may be due to a genetic cause, intrauterine position, or effects of adverse intrauterine conditions, including amniocentesis physical injury, other trauma, prenatal surgery, irradiation, infection substances including medicines ingested by the pregnant mother, or maternal metabolic disease or malnutrition. The abnormalities may affect bone, cartilage, joints, and muscles and tendons, as well as vessels, nerves, and surrounding soft tissues. Those conditions that manifest later in childhood, but are due to causes already present at birth, may be considered as related to congenital malformations.

Pathology/Histopathology

Malformations of bone do not have a specific histopathologic abnormality in general. What one sees on imaging is what the malformation would be on gross pathological examination. Associated vascular and neuromuscular changes are also generally matters of gross pathology, such as the small anterior tibial artery associated with clubfoot. One exception is congenital bony malformation in neurofibromatosis-1, in which mesodermal tissue abnormality is found.

Clinical Presentation

The clinical presentations of congenital malformations are as varied as the malformations. Limp and leg length discrepancy are common to many. Some, including Down syndrome and Williams syndrome, have characteristic associated facies. Skin lesion (such as café-au-lait spots), small rib cage, and fingernail abnormalities are present in some conditions.

Imaging

Although malformations are initially evaluated on plain radiographs, additional modalities are appropriate for specific situations. For example, not yet ossified growth center bones of the foot may be revealed by ultrasound, computed tomography (CT), or magnetic resonance imaging (MRI). For positional relationships of the lower extremity, weight-bearing or simulated weight-bearing images are necessary. For vertical talus diagnosis and evaluation, a maximum plantar flexion lateral view is necessary. The anterior nose or anterior protrusion of the calcaneus on lateral images (1) predicts presence of calcaneonavicular coalition, which is then demonstrated nicely with the everted oblique view (of Slomann) of the foot; CT is not required. The inverted oblique view of the foot, incidentally, nicely shows accessory navicular centers of the foot, although the weight-bearing anteroposterior (AP) view that shows alignment abnormalities should also be obtained.

Scoliosis evaluation requires upright images whenever possible. The flexibility of curves may be checked with supine maximal passive bending of the patient as additional views. Cervical spine evaluation for C1 or C2 malformation or for transverse ligament weakness uses flexion and extension lateral images. To evaluate for

lateral clavicle hook (a sign of upper extremity reduction deformity or weakness); the arms should be at the side of the chest (2). To evaluate an area of upper or lower extremity for unilateral growth disturbance, comparison with the contralateral side is appropriate.

In proximal focal femoral dysplasia, MRI is advisable early in life to determine the presence of cartilaginous centers and to reveal if seemingly nonconnected bony parts of the femur might be connected by cartilaginous (or fibrous) tissue. Ultrasound can yield similar information, but in less exquisite detail.

For pectus excavatum, CT images allow documentation of the severity of the deformity as well as its effects on the heart and other thoracic structures.

In utero imaging for malformation begins with high-detail ultrasound, including 3D imaging. Questions that arise may then be further investigated with fetal MRI. If the answer is still not given, but is important, selected radiographs of the mother's abdomen may be considered, under close supervision by a specialized pediatric radiologist. If possible, radiographs of one twin should be avoided if the other is considered unaffected, for radiation protection considerations.

Nuclear Medicine

If, in malformation, the question arises of whether a bone has capability of growth at a site, bone scanning can indicate the presence of a functioning growth plate. Furthermore, it may be of use in determining if two adjacent carpal or tarsal centers are fused to each other, and if less than normal, or no, growth plate activity occurs between them.

Diagnosis

Several congenital malformations arise related to intrauterine position, including clubfoot, kyphoscoliosis of the tibia, manifestations of amniotic bands, and perhaps developmental dysplasia of the hip and ▶Poland syndrome. Clubfoot is a combination of varus of hindfoot and forefoot, equinus position of the ankle, retarded maturation/small size of tarsal bones, and hypoplasia (or absence) of the anterior tibial artery. The angulation relationship of the talus and calcaneus is observed especially on maximal dorsiflexion lateral images and simulated weight-bearing frontal images. Kyphoscoliosis of the tibia is a posteriorly and medially convex deformation, seen also in the fibula, which improves as a child gets older. Amniotic bands, from damage to a fetal part that was trapped through a gap in the amniotic cavity, cause constriction of bony and soft-tissue elements

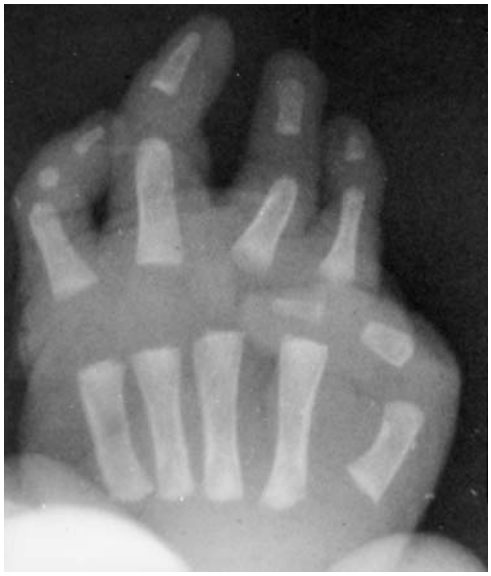

Congenital Malformations, Bone. Figure 1 Poland syndrome. This infant had ipsilateral pectoral muscle hypoplasia. Note the absent middle phalanges 2–4 and hypoplastic middle phalanx 5, with some soft-tissue syndactyly between the middle three fingers. (From Oestreich AE, Crawford AH (1985) Atlas of Pediatric Orthopedic Radiology. Thieme Verlag, Stuttgart p 167)

and perhaps hypoplasia or aplasia distal to the (Streeter) band site. In Poland syndactyly (Fig. 1), middle phalanges of one hand are absent or hypoplastic, soft-tissue syndactyly occurs between involved fingers, ipsilateral ribs are small, the pectoral muscle is small on that side, sometimes with nipple hypoplasia, and a dextroposition of the heart sometimes accompanies left-sided disease. Dr. Josef Warkany suggested that the clenched fist repeatedly beating on the chest in utero may be the causative factor for the unusual combination of findings.

Some congenital malformations may be acquired from intrauterine intervention or the intrauterine environment. For damage from amniocentesis, history of the event is important, as is the case for other trauma or surgery. Heavy metal burden from the mother, lead or bismuth, can yield dense metaphyseal and metaphyseal-equivalent bands in the fetal bones. Magnesium citrate therapy of the mother late in pregnancy yields instead similar lucent bands. Malformations in fetal alcohol syndrome include narrow distal phalanges.

Variation in bone number or connectiveness results from homeobox (hox) gene variations. More complex genetic conditions have recognizable patterns: in cerebrocostomandibular syndrome, gaps appear within ribs and the mandible is small. The mandible is also small in Seckel's syndrome and camptomelic dysplasia, as well as

in ►Pierre-Robin sequence. In cleidocranial dysplasia, a portion or all of the clavicles are missing, wormian bones are present, the pubic symphysis is wide, pseudoepiphyses of the metacarpals and metatarsals are prominent, and vertebral bodies are biconvex. In Down syndrome, trisomy 21, the middle phalanx of the little finger is small, acetabular and iliac angles are low, the sternal manubrium has two centers in series, and the spinal canal behind the dens may be small. About 15–20% of normal children also have two manubrial centers in series. Dislocation of the proximal radius is seen in several genetic syndromes, including Williams syndrome and 4p- (Wolf-Hirschhorn) syndrome. Many upper cervical column abnormalities are seen in ►22q11.2 deletion, including fusions of C2 and C3, platybasia, unfused posterior arch of C1, and upswept posterior lamina and other posterior elements (the C2 swoosh) (3). Wide distal phalanges of the great toes and thumbs, wide tufts of distal phalanges, high incidence of azygos fissure, and low acetabular and iliac angles are findings in Rubinstein-Taybi syndrome. The ►domed talus association (4) includes the ball-in-socket ankle, tarsal bone coalitions (seen on plain images in the second decade of life; on MRI detectable earlier), less than five rays of the feet, short fibula (and often tibia with absent superior tibial spines), and proximal focal femoral dysplasia, in various combinations.

In this article, we were only able to cite a few of hundreds of malformations, which are increasingly being associated with specific genetic findings.

In the equinus tibiocalcaneal relationship, often due to a tight heel cord, the front of the calcaneus is lower than normal in its relationship to the tibia, resembling the "q" in the front of the lower case word equinus that extends below the row of the other letters; in the calcaneus tibiocalcaneal relationship, the front of the calcaneus is higher than normal, like the "l" of the lower case word calcaneus (Fig. 2). In a *valgus* relationship, the distal part heads further from the midline than normal compared to the proximal part, judged with the proximal part in anatomic position; in *varus*, the distal part heads closer to the midline than normal. Mnemonic: the va**r**us proximal right femur looks like a lower case "r" and the valgus right femur looks like a lower case "l."

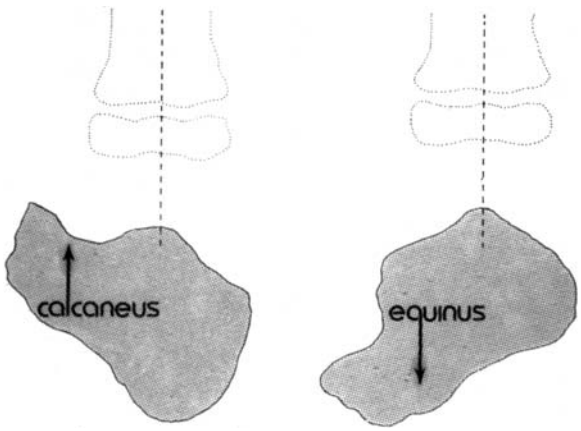

Congenital Malformations, Bone. Figure 2 Calcaneus and equinus mnemonic diagram, by Tamar Kahane Oestreich, see text. (From Oestreich AE, Crawford AH (1985) Atlas of Pediatric Orthopedic Radiology. Thieme Verlag, Stuttgart p 115)

Bibliography

1. Oestreich AE, Mize WA, Crawford AH et al (1987) The "anteater nose"; a direct sign of calcaneonavicular coalition on the lateral radiograph. J Pediatr Orthop 7:709–711
2. Oestreich AE (1981) The lateral clavicle hook-an acquired as well as a congenital anomaly. Pediatr Radiol 11:147–150
3. Ricchetti ET, States L et al (2004) Radiographic study of the upper cervical spine in the 22q11.2 deletion syndrome. J Bone Joint Surg Am 86-A:1751–1760
4. Pistola F, Ozonoff MB, Wintz P (1987) Ball-and-socket ankle joint. Skeletal Radiol 16:447–451

Congenital Malformations, Cerebellar

Philippe Demaerel
Department of Radiology, University Hospitals, Leuven, Belgium
philippe.demaerel@uz.kuleuven.ac.be

Synonyms

Congenital malformations; Hindbrain; Posterior fossa

Definition

Congenital cerebellar malformations involve all malformations of the vermis and cerebellar hemispheres. They are classified on the basis of anatomical and embryological knowledge. Several genes, proteins, and molecules are involved in the various stages of cerebellar development, and it is expected that this knowledge will influence the classification of congenital cerebellar malformations in the future.

Pathology/Histopathology

Although the anatomy of the cerebellum is straightforward, the understanding of embryology is still limited.

Approximately during the fourth week of gestation, the rhombencephalon divides into the metencephalon (pons and cerebellum) and the myelencephalon (medulla oblongata). The metencephalon will give rise to the vermis and the hemispheres, while the cavity in the rhombencephalon will expand to become the fourth ventricle. The roof of the fourth ventricle is divided into an anterior and a posterior membranous area; the posterior membranous area will ultimately communicate with the subarachnoid space at the foramen of Magendie. The posterior membranous area plays a role in several forms of cerebellar hypoplasia related to the ▶Dandy–Walker malformation.

In the formation of the cerebellar cortex, there is first an outward migration of the Purkinje cells and granular cells. Later an inward migration takes place, forming the internal granular cell layer.

The vermis has formed by the 16th week of gestation and the hemispheres 4–8 weeks later. The formation of the vermis is closely related to formation of the hemispheres. The foliation and fissuration occur at least partly simultaneously and are triggered by the migration of Purkinje and granular cells. These processes explain at least to some extent the malformations of fissuration and foliation.

Clinical Presentation

The role of the cerebellum as a center for coordination, motor learning, and higher cognitive functions is well known. Cerebellar abnormalities will usually cause cerebellar signs and symptoms, such as ataxia, cranial nerve palsies, delayed language and speech development, eye movement disorders (nystagmus, oculomotor dyspraxia, and so on), and head/body turning attacks. Epilepsy and mild cognitive deterioration can also be part of the clinical spectrum.

The Chiari I malformation appears to be asymptomatic in up to 14% of the patients in a large series. Magnetic resonance (MR) imaging is not useful in differentiating these patients from symptomatic patients. The typical symptom is occipital headache when coughing or otoneurological disturbances, but the presentation is often more ambiguous.

Joubert syndrome is a separate entity within the molar tooth malformations and is characterized by episodic hyperpnea, abnormal eye movements, ataxia, and mental retardation.

Imaging

MR imaging is the modality of choice in the diagnostic work-up of cerebellar malformations. Computed tomography is not suited to assess intrinsic cerebellar abnormalities. Imaging in different planes is required, and if available, three-dimensional T2-weighted images can be helpful.

A classification is not yet available today, but using knowledge of anatomy, embryology, and histopathology, a provisional classification can be presented.

The two groups of cerebellar malformations are cerebellar hypoplasia and ▶cerebellar dysgenesis. Cerebellar hypoplasia includes the Dandy–Walker malformation. Cerebellar dysgenesis can further be divided into vermian and/or hemispheric dysgenesis. It seems inevitable that there will be some overlap between the two groups of malformations.

The ▶Chiari malformations are not included in the classification and are discussed separately.

Diagnosis

The imaging aspects of the common cerebellar malformations will be briefly reviewed.

The *Chiari I malformation* is defined as a caudal herniation of the cerebellar tonsils over a distance of at least 5 mm through the foramen magnum (below a line from the basion to the opisthion on a sagittal image; Fig. 1a). When the herniation is less than 5 mm, the term "tonsillar ectopia" can be used. This malformation is likely to be the result of an abnormally small posterior fossa and/or the occurrence of craniovertebral anomalies.

The *Chiari II malformation* is a complex entity thought to be due to a lack of expression of surface molecules that cause a persistent aperture of the posterior neuropore. The posterior fossa remains too small, and the cerebellum extends downward, upward, and around the brainstem. Not only the tonsils but parts of the vermis and even the fourth ventricle can herniate through the foramen magnum (Fig. 1b). A lumbar myelomeningocele is associated in more than 85% of cases.

The *Chiari III malformation* consists of a Chiari II malformation with an associated cephalocele (Fig. 1c).

The *Dandy–Walker malformation* is a typical example of vermian and/or hemispheric hypoplasia. It consists of (i) a variable degree of vermian agenesis, (ii) a dilatation of the fourth ventricle with cyst formation, and (iii) an enlarged posterior fossa (Fig. 2a, b). It is thought that a genetic mutation causes an abnormal development of the roof of the fourth ventricle. The posterior membranous area of the roof normally forms the foramen of Magendie. This does not happen in the Dandy–Walker malformation. The Dandy–Walker malformation can be associated with other congenital malformations and has been reported in several syndromes. In the differential diagnosis, one should consider the *persisting Blake's pouch*, the result of a nonperforation of the foramen of

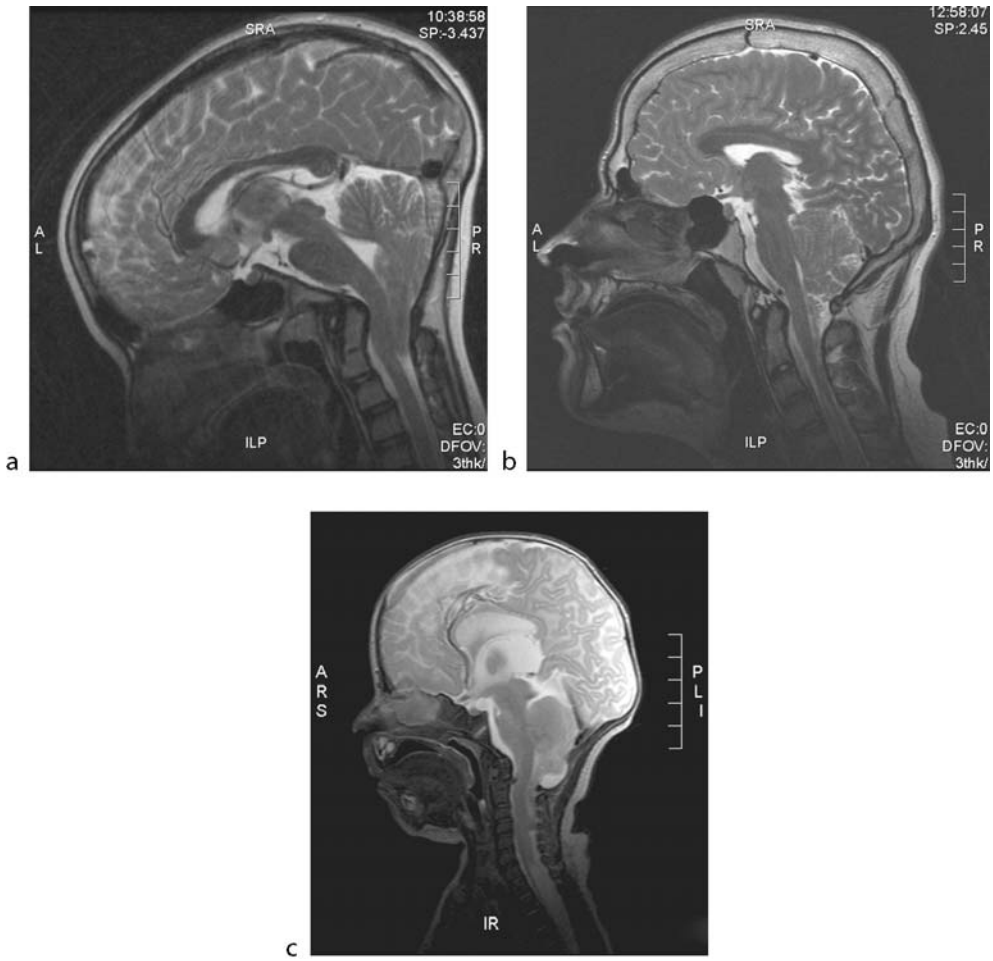

Congenital Malformations, Cerebellar. Figure 1 (a) Sagittal T2-weighted image, Chiari I malformation. Note the herniation of the cerebellar tonsils through the foramen magnum reaching the level of the endplate of C2. (b) Sagittal T2-weighted image, Chiari II malformation. Note the displacement of the fourth ventricle and the herniation of cerebellar tissue to the level of C3. There is tectal beaking and a concave lining of the clivus. The posterior fossa is small. (c) Sagittal T2-weighted image, Chiari III malformation. In addition to the typical finding of a Chiari II malformation, there is a craniocervical cephalocele.

Magendie (Fig. 2c). This malformation resembles *megacisterna magna*, but hydrocephalus is not seen in the latter. Megacisterna magna is asymptomatic but is sometimes considered a mild form of Dandy–Walker malformation. A late opening of the foramen of Magendie has been suggested as an underlying cause. *Arachnoid cysts* in the posterior fossa can resemble a megacisterna magna, but they usually cause symptoms and are often located laterally in the posterior fossa.

Cerebellar dysgenesis can involve the vermis only, the hemispheres only, or both.

The *molar tooth malformations* include several syndromes with *vermian dysgenesis*. Joubert syndrome is the best-known entity. A midline cleft is seen together with a peculiar shape of the fourth ventricle. These malformations are named after the molar tooth appearance of the midbrain on axial images (Fig. 3a, b). This is due to the horizontal course of the superior cerebellar peduncles (due to a lack of decussation of the superior cerebellar peduncles) and a narrow pontomesencephalic junction.

Rhombencephalosynapsis consists of vermian agenesis or severe hypogenesis, fusion of the hypoplastic cerebellar hemispheres, and fusion of the dentate nuclei. Dilated lateral ventricles, fusion of the thalami, and absence of the septum pellucidum can be associated. The disorder is possibly induced by a genetic mutation of the Lmx 1a gene, which regulates events at the pontomesencephalic junction between the fourth and the sixth weeks of gestation. Because of this early timing, metencephalosynapsis might be a more appropriate term. The vermis fails to differentiate, while the hemispheres remain undivided.

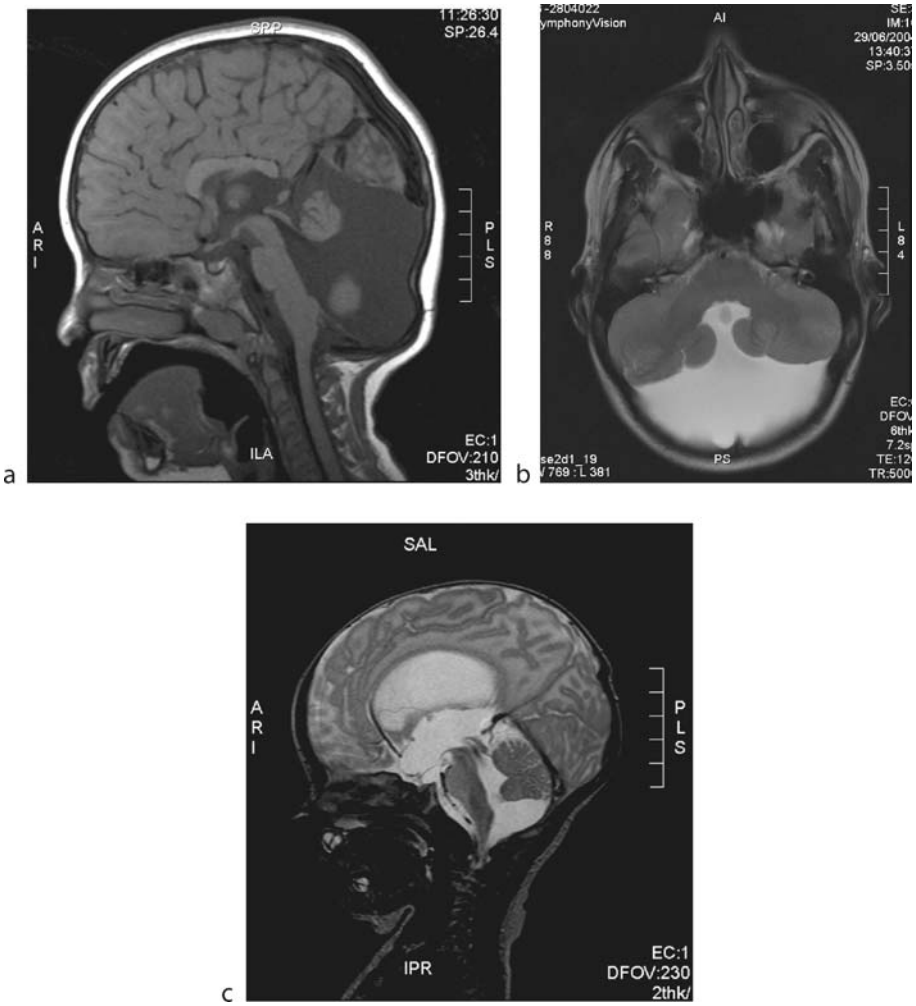

Congenital Malformations, Cerebellar. Figure 2 (a) Sagittal T2-weighted image, Dandy–Walker malformation. The posterior fossa is enlarged. There is an upward rotation of the remaining part of the superior vermis, and there is a large posterior fossa cyst. Note the displacement of the sinus rectus and the hypogenesis of the corpus callosum. (b) Axial T2-weighted image, Dandy–Walker malformation. There is a large communication between the fourth ventricle and the posterior fossa cyst. The hypoplastic cerebellar hemispheres appear "winged outward." (c) Sagittal T2-weighted image, persisting Blake's pouch. There is a large communication between the fourth ventricle and the subarachnoid space, and there is supratentorial hydrocephalus. The vermis is reasonably developed.

Recently, a series of abnormalities have been reported consisting of *vermian and/or hemispheric dysgenesis*.

When only the vermian fissures are involved, this is almost always an asymptomatic incidental finding (*type 1a*; Fig. 3c). Some patients also have an abnormal foliation of the anterior lobe and part of the posterior lobe of the vermis (*type 1b*). Hemispheric extension can occasionally be encountered. Cerebellar signs are frequently seen in this subgroup.

In abnormalities of foliation and fissuration *type 2*, three different hemispheric malformations can be recognized: (i) cortical dysgenesis, (ii) cortical hypertrophy, and (iii) aberrant orientation of the folia. These abnormalities can be seen together or separately. Cortical dysgenesis can be associated with small cyst-like inclusions (Fig. 3d, e). Similar abnormalities have been described in rare syndromes, including Fukuyama muscular dystrophy and Walker–Warburg syndrome, but they can also be observed in the absence of these syndromes. In 60% of the children with type 2 abnormalities, type 1b abnormalities are present, and more than 50% of these children have congenital cerebral anomalies.

The pathogenesis of Lhermitte–Duclos–Cowden remains incompletely elucidated. Although the lesion is classified as a dysplastic gangliocytoma according to

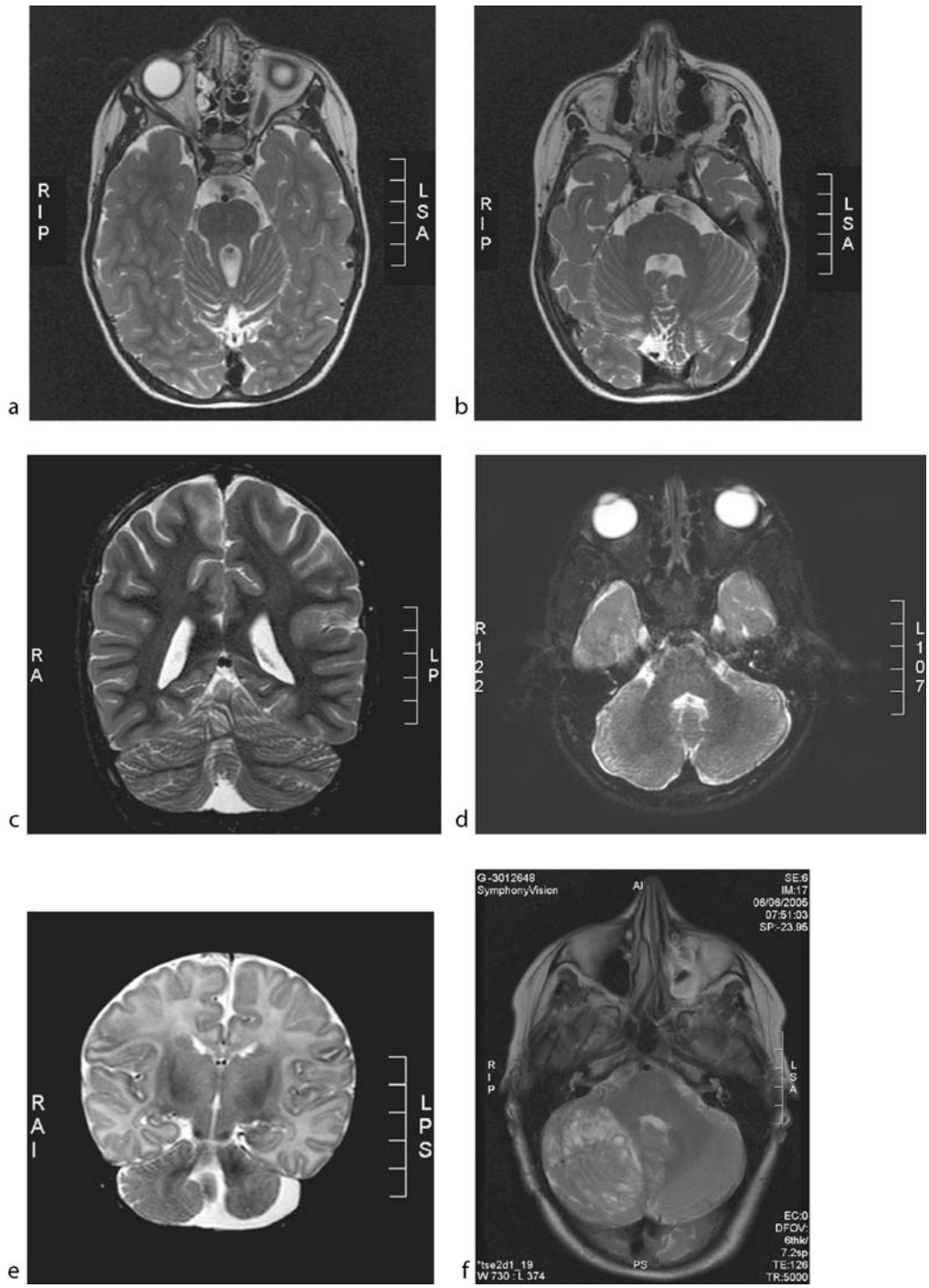

Congenital Malformations, Cerebellar. Figure 3 (a) Axial T2-weighted image, molar tooth malformation. Note the molar tooth appearance due to the horizontal course of the hypoplastic superior cerebellar peduncles. (b) Axial T2-weighted image, molar tooth malformation. The vermian cleft is seen with the "bat wing" appearance of the fourth ventricle. (c) Coronal T2-weighted image, type 1 abnormality of fissuration. The abnormal orientation of the fissures is noted. (d) Axial T2-weighted image, type 2 abnormality of foliation and fissuration. An abnormal foliation is seen, with multiple cyst-like inclusions in the cortex. (e) Coronal T2-weighted image, type 2 abnormality of foliation and fissuration. The cortical dysgenesis is clearly visible in the left hypoplastic cerebellar hemisphere compared with the normal right hemisphere. (f) Axial T2-weighted image, Lhermitte–Duclos–Cowden disorder. A masslike lesion is observed in the right cerebellar hemisphere with a striated folial pattern.

the World Health Organization, there are indications that it might represent a congenital malformation. The imaging appearance is that of a masslike abnormality with, to some extent, a striated pattern of the enlarged folia (Fig. 3f).

Bibliography

1. Barkovich AJ (2005) Pediatric Neuroimaging. 4th edn. Lippincott Williams & Wilkins Philadelphia, Baltimore, New York, London, Buenos Aires, Hong Kong, Sydney, Tokyo
2. Tortori-Donati P, Rossi A (2005) Pediatric Neuroradiology. Springer, Berlin, Heidelberg, New York
3. Demaerel P (2002) Abnormalities of cerebellar foliation and fissuration: classification, neurogenetics and clinicoradiological correlations. Neuroradiology 44:639–646

Congenital Malformations, Cerebral (Neuro View)

Thierry T. A.[1], Veronica Donoghue[2]
[1]Johns Hopkins University, Baltimore, USA
[2]Children's University Hospital, Dublin, Ireland
thierry.huisman@kispi.unizh.ch
veronica.donoghue@cuh.ie

Synonyms

Developmental cerebral anomalies; Disorders of neurulation

Definition

Congenital cerebral malformations result from an erroneous organogenesis, histiogenesis or cytogenesis of the central nervous system (CNS). The aetiology is multifactorial and includes genetic defects, intrauterine destructive events, ischaemia, infections and environmental agents (1–3).

Pathology and Histopathology

Malformations of the CNS are frequent (1:100 births) and may have a significant impact on the quality of life. Cerebral malformations encompass a wide variety of lesions ranging from tiny cortical dysplasias to extensive, highly complex pathologies.

The development of the brain is a highly complex, programmed sequence of interacting processes in which up to 100 billion neurons connect and communicate with each other using countless synapses. While the embryogenesis is most active during the first trimesters of gestation, maturational processes may extend into the second decade of life. The exact anatomical, maturational and functional development of the brain remains the focus of countless research projects.

Classical cerebral malformations should be distinguished from acquired cerebral malformations. Classical malformations result from an erroneous development of the brain which may be genetically encoded while acquired malformations relate to secondary malformations due to a destruction of initially correctly developed brain structures.

A significant overlap between these categories is present. Identical malformations may have different etiologies (e.g. infection, focal hypoperfusion or haemorrhage). In addition, identical 'destructive events' (e.g. focal hypoperfusion due to an arterial embolus) can result in a spectrum of pathologies. The timing of the 'event' in relation to the gestational age is a key feature. Moreover, an increasing number of gene defects are identified in congenital and so-called acquired cerebral malformations. Variable expressions of genetically mediated malformations may result in a spectrum of malformations. Finally, it is increasingly recognized that a predisposition for the development of malformations may be encoded in the chromosomes, a trigger is however necessary to induce the cascade of events.

Cerebral malformations are typically classified into disorders of (a) organogenesis, (b) histiogenesis and (c) cytogenesis. In disorders of organogenesis an altered brain development is combined with a normal histiogenesis while in disorders of histiogenesis, the overall brain structure is normal however anomalous cells persist and continue to differentiate. Inborn errors of metabolism or leukodystrophies represent disorders of cytogenesis.

Clinical Presentation

The spectrum of neurological symptoms varies widely and is often unpredictable. The extent of malformation correlates inconsistently with the severity of neurological symptoms or deficits. Large lesions may be discovered as incidental findings on neuroimaging. Neuronal and functional plasticity of the developing brain with relocation of functional centre may prevent overt neurological deficits. On the other hand, small lesions may present with significant neurological symptoms, e.g. a discrete cortical dysplasia may be causative for intractable seizures preventing normal development. Next to focal neurological deficits, many malformations result in cognitive deficits with different degrees of mental retardation.

Posterior fossa malformations may be present with ataxia. In combined brainstem and cerebellar malformations (e.g. Joubert syndrome) brainstem symptoms may accompany cerebellar symptoms. In callosal malformations and disorders of diverticulation hypothalamic–pituitary malfunction and facial malformations — '*the face predicts the brain*' — occur.

Imaging

Frequent disorders of organogenesis include posterior fossa malformations, callosal or commissural malformations. Disorders of diverticulation or cleavage disorders are less frequently encountered. Malformations of cortical development are described in the chapter on gyration disorders. Ultrasound (US) may serve as a first line imaging tool in neonates. Magnetic resonance imaging is applied when US or CT suspected complex malformations.

Posterior Fossa Malformations

Chiari I Malformation. The cerebellar tonsils herniate into the upper cervical spinal canal (>5 mm below the level of the foramen magnum). The tonsils may be compressed/deformed. Associated syringohydromyelia is seen in 20–25% of cases. There is no increased risk for additional cerebral malformations.

Chiari II Malformation. Complex malformation most probably resulting from too small a posterior fossa in patients with open neural tube defects. The spectrum of findings include varying degrees of downward displacement of the cerebellum with herniation of cerebellar structures into the upper cervical spinal canal, kinking of the upper cervical spinal cord, embracement of the brainstem by the cerebellar hemispheres, tectal plate deformation, supratentorial hydrocephalus, prominent interthalamic adhesion and fenestrations of the falx cerebri with interdigitation of the cerebral hemispheres. Frequently an associated callosal dysgenesis is observed (Fig. 1).

Chiari III Malformation. Very rare malformation of the posterior fossa represented by the spectrum of findings encountered in Chiari II malformation in combination with a low occipital or high cervical meningo-encephalocele.

Rhomboencephalosynapsis. Single lobed cerebellum with vermian agenesis, fusion of both cerebellar hemispheres, dentate nuclei and superior cerebellar peduncles. The cerebellar fissures typically course over the entire cerebellar surface without interruption. Additional malformations are frequent.

Joubert syndrome. Congenital vermian hypoplasia or aplasia. The IV ventricle is deformed and resembles a bat-wing or umbrella while the brainstem resembles a molar tooth on axial imaging. Associated ocular and renal lesions are known.

Cystic Posterior Fossa Malformations

Dandy Walker Malformation. Cystic dilatation of the IV ventricle in combination with varying degrees of vermian hypoplasia. The posterior fossa may be normal in size or enlarged, the torcula is frequently elevated and the vermian remnant rotated upward. The brainstem may be compressed against the clivus. The choroid plexus within the IV ventricle is usually absent, the tentorium cerebelli hypoplastic. Associated malformations are seen in up to 60% of patients, most frequently including callosal dysgenesis, polymicrogyria, cephaloceles and ventricular dilatation. The wide open IV ventricle often resembles a keyhole (Fig. 2). Dandy Walker malformations are believed to result from a combined defective development of the velum medullare anterior and posterior.

Blake's Pouch Cyst. Outpouching of the velum medullare posterior most probably resulting from an incomplete or absent rupture of the velum medullare posterior during development. The posterior fossa may be enlarged, the torcula elevated. The vermis and falx cerebelli is normally developed, the IV ventricle choroid plexus may be displaced dorsally. Associated cerebral malformations are rare.

Retrocerebellar Arachnoid Cyst and Mega Cisterna Magna. The differentiation between an arachnoid cyst and a mega cisterna magna can be difficult. The posterior fossa may be enlarged the cerebellar hemispheres and vermis can be displaced. The IV ventricle choroid plexus is in its normal location. Associated cerebral malformations are rare.

Callosal or Commissural Malformations

In the evaluation of callosal malformations it should be noted that the normal corpus callosum (CC) has a wide variability in size and shape. In addition, it is essential to determine if the encountered callosal anomaly is a primary malformation or a secondary anomaly in shape due to e.g. an adjacent white matter ischemia with focal callosal atrophy or a callosal thinning in chronic severe hydrocephalus.

The CC develops in a programmed sequence (genu, truncus, splenium, rostrum). Callosal agenesis may be partial or complete. Associated cerebral malformations are seen in 50% of cases.

On sagittal images the defective CC is easily identified. In addition, the medial surface of the cerebral hemisphere reveals a radiating pattern of sulci due to the missing cingulate sulcus (no inversion of the cingulate gyrus). On coronal images, the III ventricle may extend superiorly between the hemispheres. The lateral ventricles are displaced laterally and show a trident shape due to the impression by the Probst bundles. The hippocampi may be malrotated. On axial images, the lateral ventricles show

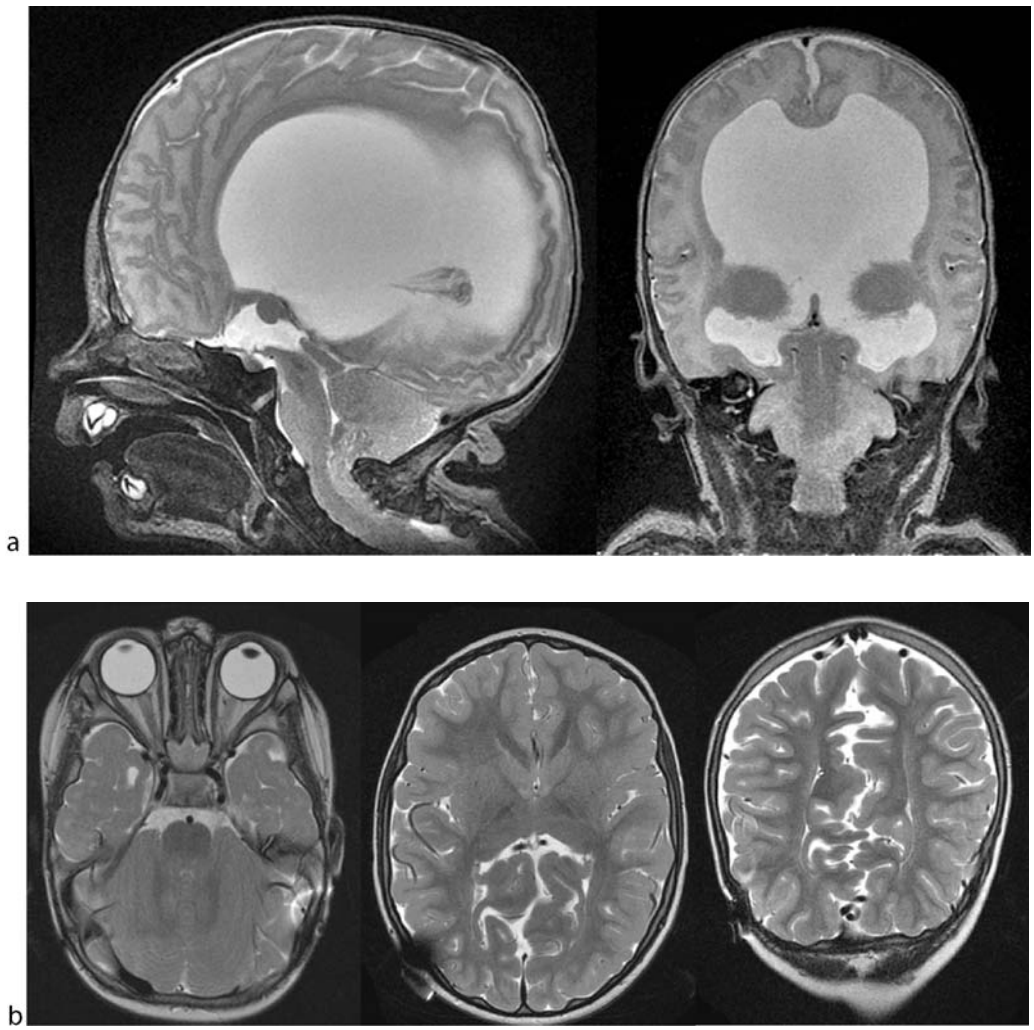

Congenital Malformations, Cerebral (Neuro View). Figure 1 (a) Chiari II malformation: Sagittal, and coronal T2-FSE MRI reveals a small posterior fossa with herniation of the cerebellar tonsils into the upper cervical spinal canal, displacement and compression of the brainstem against the clivus and supratentorial hydrocephalus. (b) Chiari II malformation: Axial and coronal T2-FSE MRI shows a characteristic embracement of the brainstem by the cerebellar hemispheres, a prominent adhesion interthalamica and a fenestration of the falx cerebri with interdigitations of both cerebral hemispheres.

a parallel course, the occipital horns may be enlarged (Fig. 3). Occasionally, an associated interhemispheric lipoma is encountered.

Callosal agenesis is frequently only one component of a more extensive commissural malformation. Consequently, in callosal anomalies, the anterior and posterior commissure as well as the fornix and hippocampi should be studied.

Disorders of Diverticulation or Cleavage Disorders

These anomalies are also known as disorders of ventral induction. They include the holoprosencephaly spectrum. An increasing number of gene defects are identified in holoprosencephaly. Basically, holoprosencephaly results from an incomplete or absent cleavage of the prosencephalon. The spectrum of malformation depends on the degree of cleavage.

Alobar Holoprosencephaly. Most severe form characterized by a small holosphere, monoventricle, fused thalami, missing III ventricle, no falx or CC and no interhemispheric fissure. Frequently, associated malformations of the circle of Willis are encountered.

Semilobar Holoprosencephaly. Partial cleavage of the prosencephalon. The anterior parts of the brain are fused while the posterior brain is split. The thalami are partially separated, a small III ventricle is present, rudimentary temporal horns are seen. The falx cerebri

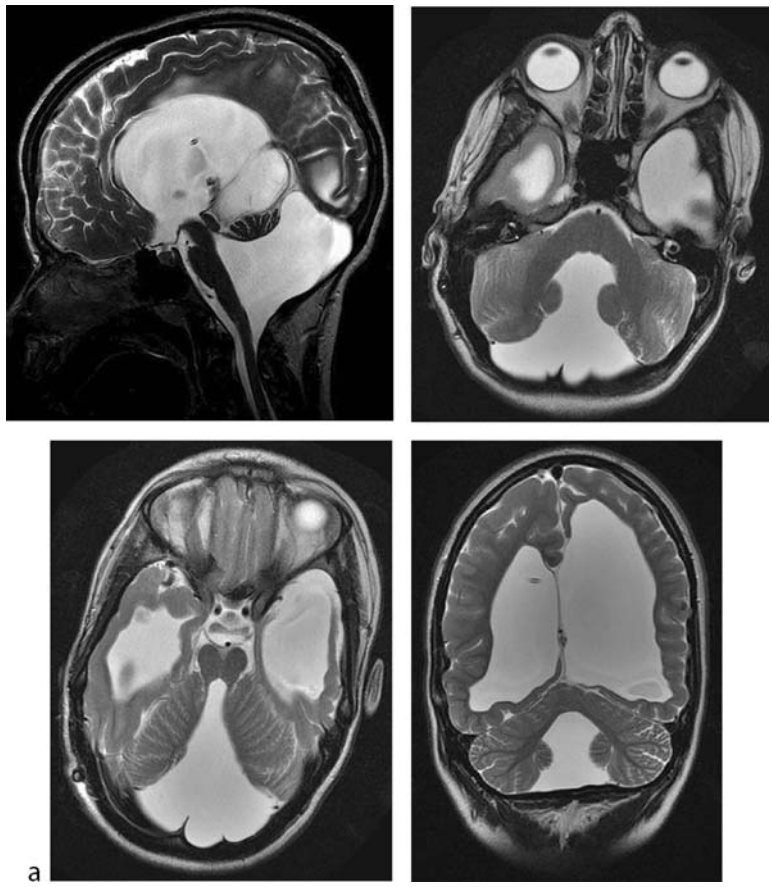

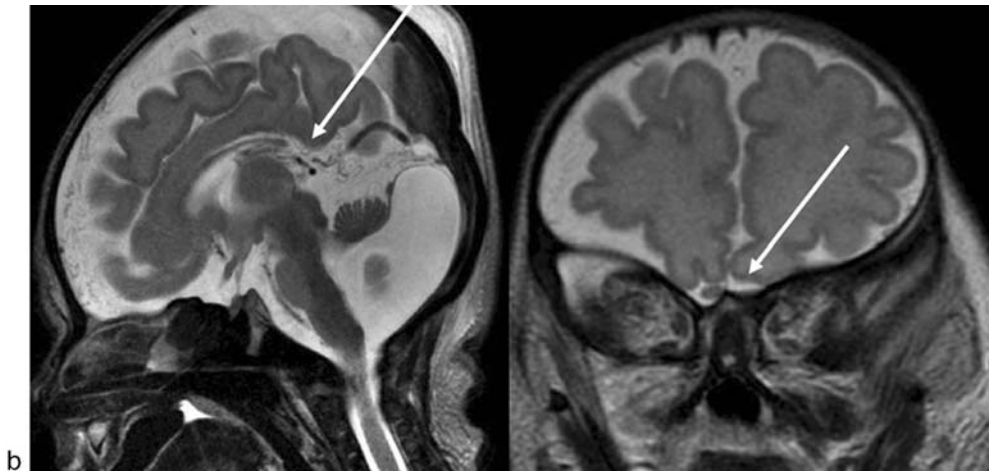

Congenital Malformations, Cerebral (Neuro View). Figure 2 (a) Dandy Walker malformation: Sagittal, axial and coronal T2-FSE MRI reveal a classical Dandy Walker malformations with a cystic dilatation of the IV ventricle, in combination with a hypoplastic, upward rotated superior vermis. No IV ventricle choroid plexu is seen. The brainstem is hypoplastic. On axial images the IV ventricle mimics a key hole. In addition, a supratentorial hydrocephalus is seen. (b) Dandy Walker malformation: Sagittal and coronal T2-FSE MRI may identify a variety of coexisting malformations like e.g. a hypoplastic corpus callosum or a hypoplastic olfactory bulb.

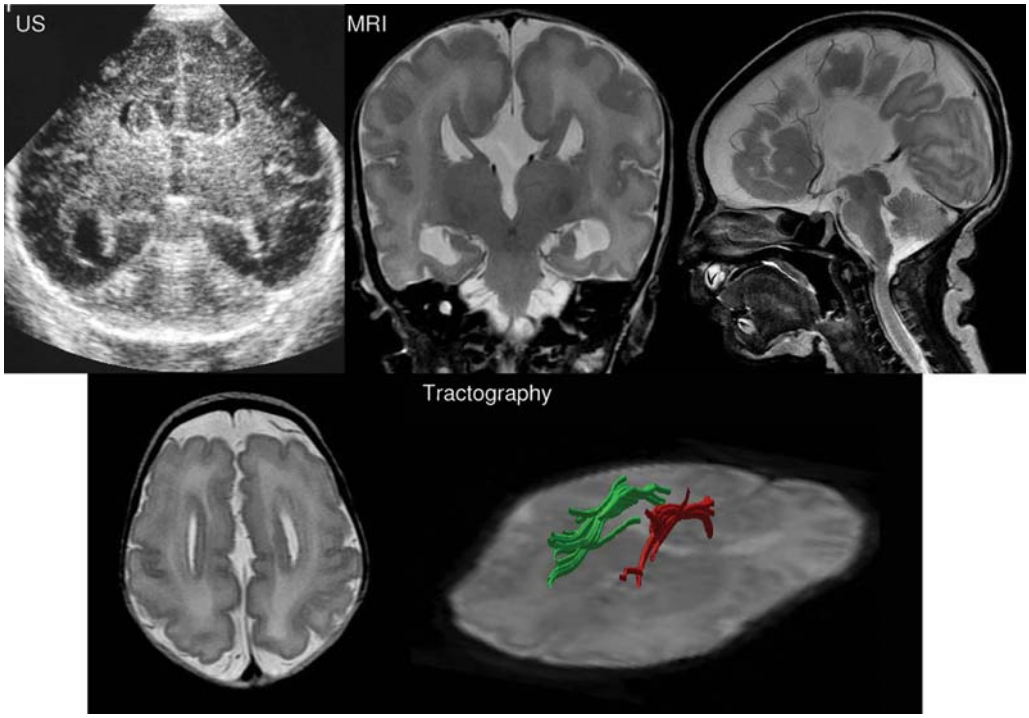

Congenital Malformations, Cerebral (Neuro View). Figure 3 Callosal dysgenesis: Coronal US identifies the characteristic trident shape of the lateral ventricles due to callosal dysgenesis. Coronal, sagittal, and axial T2-FSE reveal the characteristic findings of a callosal dysgenesis including an enlarged, interhemispheric extending III ventricle, a radial gyral pattern of the medial brain surface, a trident shape of the lateral ventricles on coronal images, a parallel course of the lateral ventricles on axial images and T2-hypointense Probst bundles along the medial surface of the lateral ventricles. Tractograhy reconstructions based on diffusion tensor imaging confirms the anterior–posterior course of the Probst bundles.

and interhemispheric fissure is present in the dorsal parts of the brain. This is the only callosal malformation where the dorsal parts of the CC may be present without the anterior part. The optic nerves and olfactory bulbs are frequently hypoplastic.

Lobar Holoprosencephaly. Near complete cleavage of the prosencephalon results in a lobar brain with hypoplastic frontal lobes and rudimentary frontal horns. The falx cerebri extends frontally, the temporal horns are formed.

Septo-Optic Dysplasia. Septo-optic dysplasia is considered to be the mildest variant of lobar holoprosencephaly characterized by an absent septum pellucidum, hypoplastic optic nerves and chiasm. The olfactory bulbs are frequently hypoplastic. Associated cerebral malformations are seen in up to 60% of cases.

Diagnosis

Ultrasound may serve as a first line imaging tool in neonates. Especially when a hydrocephalus is suspected, ultrasound is highly sensitive and may show additional gross parenchymal abnormalities next to the ventricular enlargement. A complete identification of the exact extent and degree of cerebral malformation is essential to guide treatment, may give information concerning prognosis and outcome and should be used for counselling of future pregnancies. Definite diagnosis consequently relies on high resolution triplanar neuroimaging. MRI has proven to be most reliable. With the advance of functional MRI techniques, such as diffusion tensor imaging and tractography (Fig. 3) detailed structural-functional informations can be collected. In the evaluation of malformations of the central nervous system, each radiologist should be aware that if they find one malformation they should look for additional malformations. Frequently, the most obvious lesion is just the tip of the iceberg. A proper knowledge of the complex embryology and maturation of the brain is mandatory.

Bibliography

1. Barkovich AJ (2000) Pediatric neuroimaging, 3rd edn. Lippincott Williams & Wilkens, Philadelphia, pp 251–381
2. Osborn AG (2004) Diagnostic imaging: brain. Amirsys, Salt Lake City, pp I-1–4–78
3. Tortori-Donati P (2005) Pediatric Neuroradiology: Brain. Springer Verlag, Berlin, Heidelberg, pp 41–198

Congenital Malformations, Cerebrum

Pieter Waer, Philippe Demaerel
Dept of Radiology, University Hospitals K.U. Leuven, Leuven, Belgium
philippe.demaerel@uz.kuleuven.ac.be

Synonyms

Anomalies of the cerebral commissures; Cephalocele; Dorsal induction anomalies; Neuronal migration disorders; Ventral induction anomalies

Definition

Depending on the time of insult, different malformations may occur during cerebral development. Often, this will be multifocal involving several brain structures.

It is important to realize that most malformations can display mild, moderate, or extensive changes and that different malformations often occur simultaneously.

Cortical developmental malformations are by far the most common cerebral malformations. Terminology has not always been straightforward, but nowadays a good and flexible classification for the cortical developmental malformations is available which allows the inclusion of new observations (1).

Pathology/Histopathology

A brief review of the embryology of the brain is necessary in the understanding of the pathology of cerebral malformations (2, 3).

Although the cause of cephaloceles remains not fully elucidated, it is believed they may result from a failure of neural tube closure. Other authors have suggested that they might be due to an event occurring after the closure of the neural tube.

The anterior part will form the prosencephalon, mesencephalon, and rhombencephalon at around 30 days of gestation. At this time, the corpus callosum will develop from the commissural plate at the rostral end of the neural tube. The genu of the corpus callosum is formed before the truncus and the splenium. At the end, a more anterior part of the genu and the rostrum become visible. This sequence of formation will be important in analyzing partial agenesis of the corpus callosum. Remnants of the meninx primitiva give rise to the interhemispheric lipomas.

In holoprosencephaly there is a failure of cleavage into hemispheres and sometimes even a failure of separation of the telencephalon from the diencephalon.

The most commonly encountered cerebral malformation is the cortical developmental malformation. The formation of the cerebral cortex begins during the seventh week of gestation with the period of neuronal and glial proliferation in the germinal matrix. The second period consists of a migration of the neurons from the germinal zone along the so-called guiding radial glial fibers. This process takes place between the eighth and twenty-fourth week of gestation. The six-layered cortex can be recognized in the sixteenth fetal week. The thickness does not exceed 4.5 mm. The period of migration is followed by cortical organization, leading to the complex three-dimensional structure of the mature cortex.

Up to the eighteenth week, the hemispheric surface is smooth. At this time, the callosal and parieto-occipital sulci and the calcarine fissure are visible. From 20 weeks onwards, a progressive sulcation can be observed until the thirty-second to thirty-fourth week of gestation.

Clinical Presentation

Minor congenital cerebral malformations can remain asymptomatic. However, often developmental delay, mental retardation, spasticity, hypotonia, epilepsy, hemiplegia, or diplegia are seen in children with a cerebral malformation.

Macro- or microcephaly can also be a sign of an abnormal development.

When the cerebral malformations are part of a syndrome, extracranial anomalies can be encountered.

Imaging

In imaging cerebral malformations, one should always obtain T1- and T2-weighted images, because the ongoing myelination may mask possible malformations during the first 2 years of life on one of these sequences. Additional three-dimensional imaging, using either a T1-weighted gradient-echo sequence or a T2-weighted sequence, will be extremely helpful in displaying the abnormalities.

Diagnosis

The list of cerebral malformations is very extensive and detailed. Here, only the most common malformations are discussed.

Skull and skull base defects are often referred to as "*cephaloceles*." The defect can contain meninges, brain tissue, and/or cerebrospinal fluid.

The terms hypogenesis or complete agenesis are preferably used for partial or complete absence of the corpus callosum. In hypogenesis, the anterior part of the corpus callosum is usually present. The imaging findings of agenesis are quite specific. A radial pattern can be seen on sagittal images (Fig. 1). This is due to the eversion of the cingulate gyri and radial orientation of the medial hemispheric sulci from the region of the roof of the third ventricle. Colpocephaly, corresponding to the dilatation of the trigones and posterior horns of the lateral ventricles, is typically seen on axial images. The third ventricle is widened and extends superiorly. Interhemispheric cysts can be found, and different subtypes have been recognized. Interhemispheric lipomas have frequently been described in association with partial or complete absence of the corpus callosum (4). A curvilinear type of lipoma often appears to be an incidental finding, while the tubulonodular lipoma is usually associated with a more severe abnormality of the corpus callosum and tends to be symptomatic.

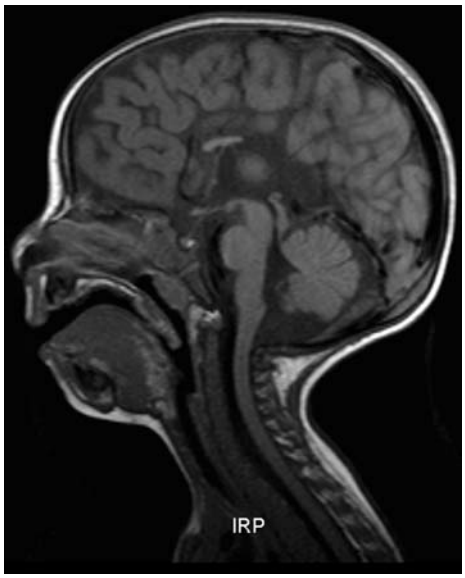

Congenital Malformations, Cerebrum. Figure 1 Agenesis of the corpus callosum. Sagittal T1-weighted image. The typical radial pattern on a mid-sagittal image is due to the radial orientation of the medial hemispheric sulci. The structure visualized is an enlarged hippocampal commissure and does not correspond to the genes of the corpus callosum.

Alobar, semilobar, and lobar *holoprosencephaly* have been distinguished, but significant overlap exists between the different types. The septum pellucidum and the olfactory bulb are always absent in the three subtypes. The lobar form is the least severe from the clinical point of view and the abnormalities can sometimes be very subtle. This latter form is also closely related to septo-optic dysplasia. *Septo-optic dysplasia* or de Morsier's syndrome consists of hypoplasia of the optic nerves and chiasm with absence of the septum pellucidum (Fig. 2). Magnetic resonance (MR) imaging has been used to further classify patients with optic nerve hypoplasia. In 25% of the patients, no associated abnormalities could be demonstrated. The septum pellucidum was absent in 20% of the children. An ectopic neurohypophysis was observed in 15% of the patients. An associated cortical developmental anomaly was found in 15% of the patients with optic nerve hypoplasia. There was evidence of antenatal or prenatal brain injury in the remaining 25% of the children.

Three groups of *cortical developmental malformations* are distinguished: (i) abnormalities of neuronal and glial proliferation, (ii) abnormalities of neuronal migration,

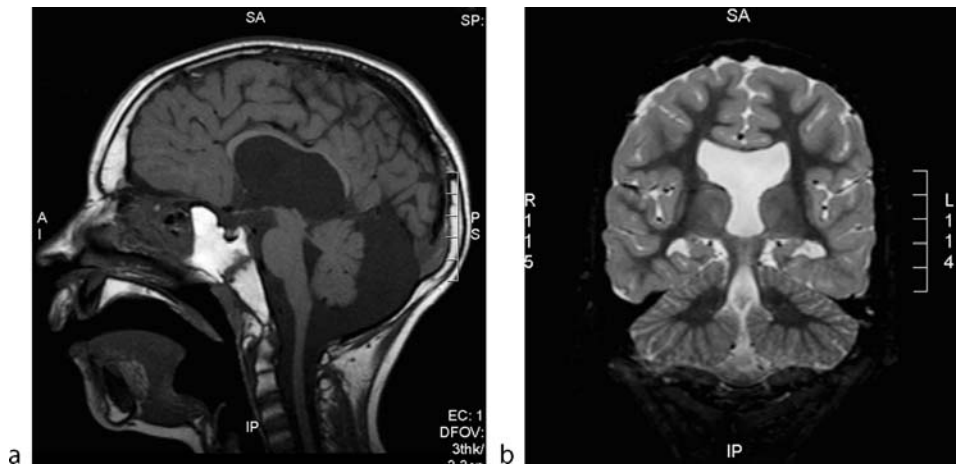

Congenital Malformations, Cerebrum. Figure 2 Septo-optic dysplasia. Sagittal T1-weighted (a) and coronal T2-weighted (b) images. The optic chiasm is hypoplastic (a). The septum pellucidum is absent (b).

and (iii) abnormalities of cortical organization. These malformations can result from several environmental factors including maternal exposure to ethanol and radiation, ischemia, or *in utero* infection, but an increasing number of genetic causes are being identified (5, 6).

The *abnormalities of neuronal proliferation* occur in the early days of cortical development and they often show a high signal on T2-weighted images. Focal cortical dysplasia, first described by Taylor, consists of a focal disorganized cortex with abnormally large neurons, called balloon cells because of their histopathological appearance. On imaging the cortex may appear normal or thinner, usually with blurring of the gray–white matter interface, a useful sign for differentiating focal cortical dysplasia from polymicrogyria (Fig. 3). The high signal on T2-weighted images may be due to gliosis and/or the presence of balloon cells.

Hemimegalencephaly may involve part of one hemisphere or the whole hemisphere and hemicranium. The affected area appears strongly enlarged and has heterogeneous signals reflecting dysmyelination and abnormalities of proliferation, migration, and cortical organization. The abnormalities may undergo changes over time.

The *abnormalities of neuronal migration* occur during the migration of the neurons from the germinal matrix to their final destination, the cortex. They typically have a signal similar to that of gray matter. Lissencephaly is also referred to as agyria-pachygyria complex. Some patients have been shown to have chromosomal mutations, the best known clinical entity being the autosomal dominant form of the Miller–Dieker syndrome. A variable involvement of the cortex can be observed, usually correlating with the severity of the symptoms. In pachygyria the cortex is thickened and the sulci are incompletely formed (Fig. 4). The junction between gray and white matter is regular as opposed to the junction in polymicrogyria.

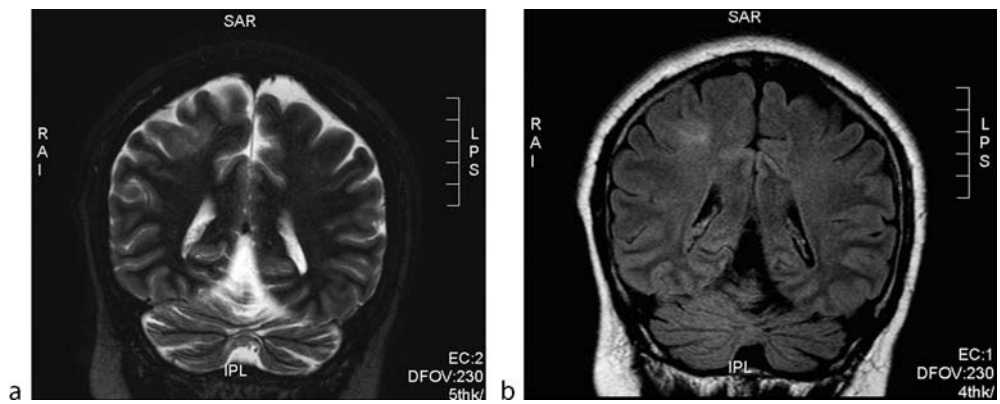

Congenital Malformations, Cerebrum. Figure 3 Focal cortical dysplasia of Taylor. Coronal T2-weighted (a) and fluid-attenuated inversion recovery (b) images. The abnormalities in the cortex and in the subcortical white matter of the right parietal lobe are better seen on the second image (b).

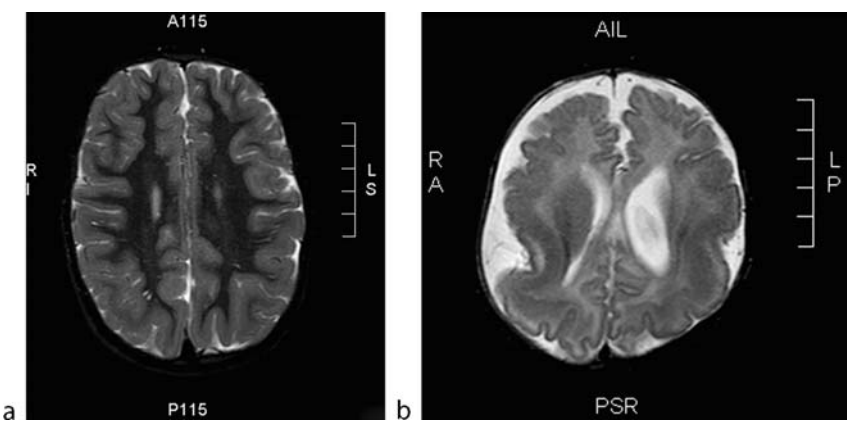

Congenital Malformations, Cerebrum. Figure 4 Pachygyria. Axial T2-weighted (a, b) images. Bilateral focal pachygyria in the parietal lobe (a) and more extensive pachygyria in a 3-month-old infant (b).

Heterotopic gray matter can be located in the subependymal region, in the subcortical region, or in between at any point along the route of migration from the subependymal region to the subcortex (Fig. 5). Heterotopia refers to normal structures in an abnormal site.

Later during gestation, *malformations of cortical organization* can be observed. Polymicrogyria refers to an abnormal gyration consisting of an increased number of gyri. Cortical maldevelopment is due to a process affecting mainly the deep cortical layers, reducing vascularization and arresting growth. Excessive proliferation of the outer layers results in the increased number of gyri. Whereas in the past it was debatable whether polymicrogyria could be diagnosed on MR imaging or only histopathologically, it is now accepted that the diagnosis can be given on imaging (Fig. 6). The inner border is sharp but irregular, which allows the differential diagnosis with pachygyria to be made, where the inner border is sharp but smooth. Bilateral perisylvian polymicrogyria is a well-recognized entity. Usually the opercular and perisylvian cortex are involved.

The term schizencephaly merely refers to an abnormal cleft. The cleft is lined by a polymicrogyric cortex and extends from the subependymal region to the pia. Bilateral and unilateral schizencephaly can be observed, most often in the perisylvian area. The terms open and closed lip schizencephaly refer to the separated and adjacent walls of the cleft.

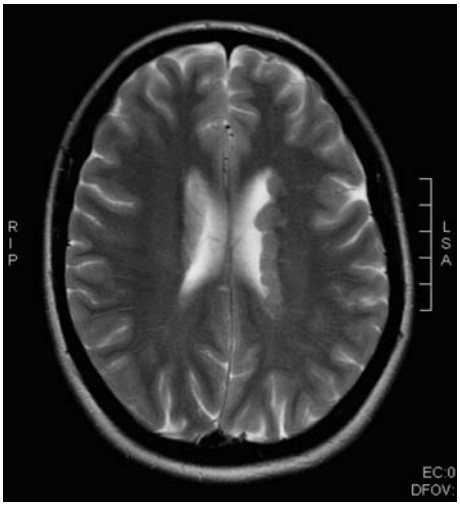

Congenital Malformations, Cerebrum. Figure 5
Subependymal heterotopia. Axial T2-weighted image. Heterotopic gray matter nodules are seen in the subependymal region on the left side.

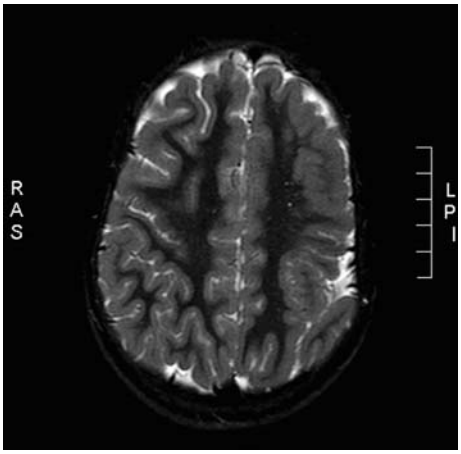

Congenital Malformations, Cerebrum. Figure 6
Polymicrogyria. Axial T2-weighted image. Numerous small abnormal gyri are seen in the left parietal lobe. Note the difference with pachygyria.

Bibliography

1. Barkovich AJ, Kuzniecky RI, Dobyns WB et al (1996) Classification scheme for malformations of cortical development. Neuropediatrics 27:59–63
2. Barkovich AJ (1996) Congenital malformations of the brain and skull. In: Barkovich AJ (ed) Pediatric Neuroimaging. 2nd edn. Lippincott-Raven Publishers, Philadelphia, pp 177–276
3. Sidman RL, Rakic P (1982) Development of the human central nervous system. In: Haymaker W, Adams RD (eds) Histology and Histopathology of the Central Nervous System. Thomas, Springfield, pp 3–145
4. Vandegaer Ph, Demaerel Ph, Wilms G et al (1996) Interhemispheric lipoma with variable callosal dysgenesis: relationship between embryology, morphology, and symptomatology. Eur radiol 6:904–909
5. Barkovich AJ (2002) Magnetic resonance imaging: role in the understanding of cerebral malformations. Brain Dev 24:2–12
6. Blaser SI, Jay V (2002) Disorders of cortical formation: radiologic-pathologic correlation. Neurosurg Clin N Am 13:41–62

Congenital Malformations, Liver and Biliary Tract

Huisman TA[1], Paola Vagli[2]
[1]Johns Hopkins University, Baltimore, USA
[2]Department of Diagnostic and Interventional Radiology, University of Pisa, Italy
thierry.huisman@kispi.unizh.ch
bartolozzi@do.med.unipi.it

Synonyms

Congenital hepato-biliary anomalies; Hepato-biliary malformations

Definition

Congenital anomalies of the liver and biliary system present early in life and may result from hereditary or developmental errors.

Introduction

Congenital hepato-biliary anomalies include a wide spectrum of malformations involving the liver, the biliary tree, and the gallbladder. Children may be asymptomatic or suffer from significant disease, e.g., neonatal jaundice. The most frequent congenital anomalies include ►biliary atresia, ►Alagille syndrome, ►choledochal cysts, ►Caroli's disease, congenital hepatic fibrosis, ►polycystic liver disease, and ►gallbladder anomalies. In neonates with unexplained persisting jaundice hepato-biliary anomalies should be excluded.

Pathology and Histopathology

Biliary Atresia

Persisting neonatal jaundice results in one-third of cases from biliary atresia. Biliary atresia is characterized by a (sub-) total obliteration of the extrahepatic biliary system. Fetal cholangitis due to a malformed biliary tree is believed to be the causative. To prevent permanent hepatic damage, early surgical correction is mandatory. Biliary atresia is associated with situs inversus, congenital heart disease, vascular anomaly, trisomy 17, 18, 21, and polysplenia syndrome.

Alagille Syndrome

Autosomal dominant disorder with chronic cholestasis is due to a hypoplasia of interlobular bile ducts. Associated congenital abnormalities include an abnormal facies, ocular anomalies, butterfly vertebrae, and complex cardiac malformations. Second most common cause of cholestasis in neonates. The incidence is 1 per 100,000 live births. Liver biopsy confirms diagnosis.

Choledochal Cysts

Choledochal cysts encompass a spectrum of common bile duct dilatations that may present with cholestatic jaundice or recurrent cholangitis. The different forms have been classified by Todani. Choledochal cyst type I is the most frequent form (80–90% of cases) characterized by a focal dilatation of the common bile duct. Type I choledochal cysts most probably results from an anomalous proximal insertion of the pancreatic duct into the common bile duct. Reflux of pancreatic enzymes will induce a localized cholangitis with resulting obstruction of the distal common bile duct and proximal dilatation.

Type II choledochal cysts are characterized by focal diverticula of the common bile duct. Type III choledochal cysts are basically ►choledochoceles that protrude into the duodenal lumen. Todani's type IVA shows multiple intra- and extrahepatic cysts while type IVB shows multiple extrahepatic cystic dilatations of the common bile duct. Todani's type V, also known as Caroli's disease, is characterized by segmental nonobstructive dilatations of the intrahepatic bile ducts. This form is associated with stone formation, recurrent cholangitis, and hepatic abscesses. Hepatic fibrosis may develop. Caroli's disease is frequently associated with medullary sponge kidneys, polycystic kidney disease, and nephrothisis. Portal hypertension may develop in disease progress.

Congenital Hepatic Fibrosis

Autosomal recessive disorder occurs with or without associated biliary duct ectasia and infantile or adult polycystic kidney disease. Periportal fibrosis and the presence of irregularly shaped, partially cystic, dilated small bile ducts are the primary pathologic findings. During the course of the disease, hepatomegaly with signs of portal hypertension develops (1).

Polycystic Liver Disease

Two forms are described: the infantile type and the adult type. The infantile type is less common and has an autosomal recessive inheritance while the adult type is autosomal dominant. Children usually present with renal disease are due to the associated polycystic kidney disease. Hepato-biliary cysts may be intrahepatic and/or peribiliary near portal triads or the hepatic hilum.

Gallbladder Anomalies

The gallbladder may be congenitally absent, ectopically located, duplicated, or septated. An absent gallbladder may be an associated finding in polysplenia syndrome. Ectopically located gallbladders are seen within the left hemiabdomen (e.g., situs inversus), in the midline (e.g., asplenia syndrome), intrahepatic, within the abdominal wall, in the falciform ligament ,and in the retroperitoneal area.

Clinical Presentation

Biliary Atresia

Clinical symptoms are related to the neonatal cholestasis. Key findings include jaundice, dark urine, and pale stools. Hepatomegaly may present early, splenomegaly is common

on follow-up due to liver cirrhosis and portal hypertension. Conjugated hyperbilirubinemia and increased levels of alkaline phosphatase, gamma glutamyl transpeptidase and serum aminotransferases may be present.

Alagille Syndrome

The combination of a chronic cholestasis, abnormal facies, ocular abnormalities, butterfly vertebrae, and complex cardiac anomalies are highly suggestive for Alagille syndrome. Most patients if not treated by means of orthotopic liver transplantation will die before the third decade.

Choledochal Cysts

In young children, the lead feature is chronic cholestatic jaundice while clinical presentation in older children may include abdominal pain, obstructive jaundice, and fever. In addition, acholic stools, hepatomegaly, and intermittent episodes of cholangitis and pancreatitis are seen. In untreated cases, recurrent ductal inflammation and biliary stasis may be complicated by hepatic abscesses, cirrhosis, portal hypertension, and cholelithiasis. Laboratory findings are nonspecific. Surgical treatment with complete excision of the cyst and creation of a biliodigestive anastomosis is recommended.

Congenital Hepatic Fibrosis

Principal clinical symptoms are related to the associated renal abnormalities. Initially, liver function may remain preserved, on follow-up hepatomegaly and portal hypertension may develop. Complicating cholangitis occurs.

Polycystic Liver Disease

Most children initially present because of the associated renal disease. Clinical symptoms that are related to the liver include hepatic enlargement by the multiple cysts with compression of adjacent organs as well as the intrinsic bile ducts. In addition, cysts may rupture or hemorrhage. In late stages, hepatic fibrosis may result in portal hypertension.

Gallbladder Anomalies

Gallbladder anomalies are usually asymptomatic and incidentally discovered. Clinical symptoms are related to gallstone formation (2–3).

Imaging

Biliary Atresia

In the majority of children, ultrasound (US) will fail to identify the gallbladder and extrahepatic bile ducts. The intrahepatic bile ducts are usually unremarkable. Because in a minority of affected children, US will show a gallbladder, hepato-biliary scintigraphy is recommended as second imaging modality to rule out biliary atresia. Endoscopic retrograde cholangiopancreatography (ERCP) can be used to confirm diagnosis.

Alagille Syndrome

Imaging features in the newborn period are similar to those in biliary atresia but the identification of the additional components of this syndrome (hypertelorism, butterfly vertebrae, complex cardiac malformations) lead to the correct diagnosis. US of the liver can show hepatomegaly, periportal fibrosis/cirrhosis, and splenomegaly. In less severe forms, US will show a normal liver. Magnetic resonance cholangiopancreatography (MRCP) and ERCP or intraoperative cholangiography may show the patency of the extrahepatic biliary tract.

Choledochal Cysts

Most choledochal cysts are easily identified by US. In addition, sludge and gallstones within the cysts can be seen. US is also helpful in diagnosing complications such as intrahepatic biliary dilatation, portal vein thrombosis, gallbladder or biliary neoplasms, pancreatitis, and hepatic abscesses. On computed tomography (CT), choledochal cysts appear as well-circumscribed hypodense cystic lesions which are separated from the gallbladder. The cyst wall can be thickened due to recurrent cholangitis. On magnetic resonance imaging (MR), choledochal cysts are T2-hyperintense (Fig 1–3). MRCP or ERCP are helpful in classifying the cysts.

Congenital Hepatic Fibrosis

US shows an enlarged hyperechoic liver. Intrahepatic bile duct ectasia and gallbladder enlargement may be seen in case of an associated Caroli's disease. Splenomegaly may result from portal hypertension. Color Doppler sonography should be performed to rule out cavernous transformation. CT and MR show an inhomogeneous pattern with areas of heterogeneously increased or decreased attenuation values or signal intensities.

Polycystic Liver Disease

US reveals multiple, variably sized hypoechoic hepatic cysts. Cysts may show an internal echo due to hemorrhage. The cysts are hypodense on CT, well circumscribed and nonenhancing. On MR, the cysts are T1-hypo and T2-hyperintense without enhancement.

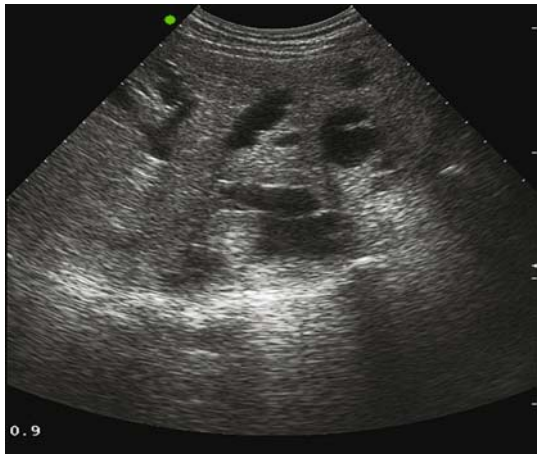

Congenital Malformations, Liver and Biliary Tract. Figure 1 US scan displays the presence of anechoic saccular dilatations of the bile ducts involving both lobes containing intraluminal bulbar protrusions and cross-bridges. The surrounding liver parenchyma shows a normal echostructure.

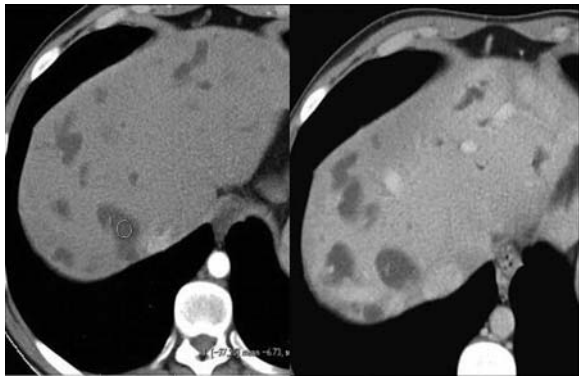

Congenital Malformations, Liver and Biliary Tract. Figure 2 Unenhanced CT scan shows marked intrahepatic ductal dilatation with cystic appearance (*left*). Enhancing central fibrovascular bundles (central dot sign) are identified in many of dilated ducts. These intraluminal dots correspond to intraluminal portal veins, indicating portal radicles surrounded by dilated intrahepatic bile ducts (*right*).

Gallbladder Anomalies

MRCP and US may identify and depict the whole spectrum of these anomalies. In case of an absent gallbladder an ectopic location or an atrophic gallbladder should be excluded.

The spectrum of anomalies can ideally be depicted by MRCP (1–5).

Nuclear Medicine

Biliary Atresia

^{99m}Tc labeled iminodiacetic acid derivates are very sensitive in diagnosing biliary atresia. In case of biliary atresia the liver will show a tracer uptake without excretion into the extrahepatic bile ducts or bowel. Conversely, evidence of intestinal excretion of the radiotracer confirms the patency of the extrahepatic biliary system. The absence of bowel activity after 24 h is an indication for liver biopsy.

Alagille Syndrome

Typically, biliary imaging performed with ^{99m}Tc labeled iminodiacetic acid derivates, fails to show normal excretion of radioisotope into the bowel resembling biliary atresia.

Choledochal Cysts

^{99m}Tc labeled iminodiacetic acid derivates scintigraphy may show the absence of drainage into the intestine in case of complete obstruction of the distal bile duct or the presence of a dilated duct acting as a collecting reservoir (2–4).

Diagnosis

Biliary Atresia

Diagnosis of biliary atresia emerges from recognizing clinical features and imaging findings. US represents the first choice but a normal examination does not exclude diagnosis. Neonatal hepatitis is the number one differential diagnosis. Typically in neonatal hepatitis, US will show a normal gallbladder. Scintigraphy may show a poor tracer uptake in combination with a delayed excretion into the bowel.

Alagille Syndrome

Definitive diagnosis is usually achieved by liver biopsy. The differentiation from biliary atresia can be made by demonstration of an intact extrahepatic biliary tree.

Choledochal Cysts

US findings are diagnostic in many patients, however, in the preoperative setting, complementary studies, such as ERCP, CT, or MR/MRCP may be helpful. Choledochal cyst may resemble hepatic cyst, hepatic abscess, pancreatic pseudocyst, or gallbladder duplications.

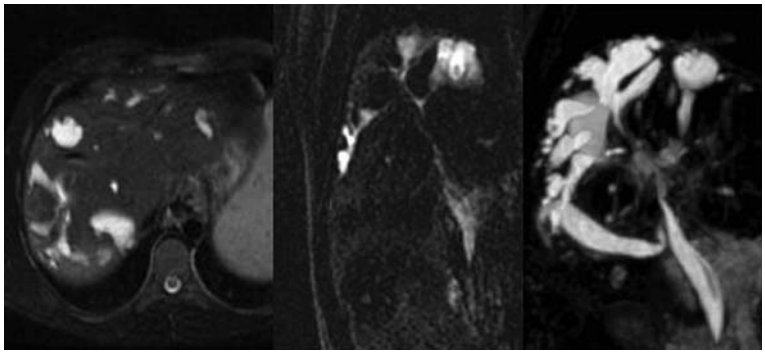

Congenital Malformations, Liver and Biliary Tract. Figure 3 Axial T2-weighted MR image shows multiple hyperintense cystic ectasias involving the entire liver (*left*). MR cholangiogram shows a connection between the saccular dilated segmental bile ducts and the central biliary tree (*middle*). The cystic dilatations communicate with the major biliary tree, and focal narrowing of the major intrahepatic and common bile ducts are depicted by reformatted images (*right*).

Congenital Hepatic Fibrosis

This affection should be suspected in young patients with portal hypertension of unknown origin. Evidence of nephromegaly and renal increased echogenity with polycystic changes support diagnosis. The final diagnosis is dependent on histological findings (biopsy).

Polycystic Liver Disease

The presence of multiple congenital liver cysts in patients with renal disorders suggests diagnosis.

Gallbladder Anomalies

These anomalies are usually an incidental finding on cross-sectional imaging. Most cases are asymptomatic. US may depict the hepato-biliary system anomaly and associated complications. MRCP provides a precise evaluation of the anatomy of the lesions (1–5).

Bibliography

1. Zeitoun D, Brancatelli G, Colombat M et al (2004) Congenital hepatic fibrosis: CT findings in 18 adults. Radiology 231(1):109–116
2. Silverman FN, Kuhn JP (1993) Congenital abnormalities. In: Silverman FN (ed) Caffey's Pediatric X-ray Diagnosis: An Integrated Imaging Approach. Mosby, St. Louis, pp 919–930
3. Taybi H (1979) The biliary tract in children. In: Margulis AR, Burhenne HJ (eds) Alimentary Tract Radiology. Mosby, St. Louis, pp 1504–1516
4. Rizzo RJ, Szucs RA, Turner MA (1995) Congenital abnormalities of the pancreas and biliary tree in adults. Radiographics 15(1):49–68
5. Mortele KJ, Ros PR (2001) Anatomic variants of the biliary tree: MR cholangiographic findings and clinical applications. AJR Am J Roentgenol 177(2):389–394

Congenital Malformations, Musculoskeletal System

Heike E. Daldrup-Link
Department of Radiology, Pediatric Radiology section and Director, Contrast agent Research Group
University of California in San Francisco
USA
daldrup@radiology.ucsf.edu

Congenital malformations are the leading cause of infant mortality in the United States and a major cause of morbidity and mortality throughout childhood. The children with major congenital malformations represent approximately 4% of live births with a higher rate in males than females (4.6% vs. 3.1%), and a higher rate in black children than white children (4.4% vs. 3.8%) (1). Twenty percent of infant deaths are attributed to congenital malformations, a percentage that has increased over time.

Little is known about the causes of congenital malformations. Twenty percent may be due to a combination of heredity and other factors; 7.5% may be due to single-gene mutations; 6% to chromosome abnormalities; and 5% to maternal illnesses, such as diabetes, infections, or anticonvulsant drugs. Fourty to sixty percent of congenital malformations are of unknown origin.

Associations between congenital malformations and environmental agents have been described for radiation

exposure, intrauterine infections (e.g., particular rubella), medications (e.g., thalidomide and anticonvulsants), and toxic waste dumps (e.g., Love Canal and accidents such as Three Mile Island and Seveso). In response, many states began to develop birth defects registries in order to track trends in malformation rates (1).

The musculoskeletal system represents the third most common organ system involved in major congenital malformations (16%). Other potentially involved organ systems are cardiovascular (26%), genitourinary (21%), digestive and clefts (9%), CNS (5%), respiratory (3%), and others (20%). The most common congenital musculoskeletal malformations are dislocation of the hip (22%), varus deformities of the feet (20%), other limb anomalies (10%), anomalies of the skull and face (10%), reduction deformities (6%), valgus deformities of the feet (6%), other feet deformities (3%), and others (23%). A more specific overview over relatively frequent congenital malformations that involve the musculoskeletal system is given in Table 1. The following article provides a brief overview over frequent congential musculoskeletal malformations. Due to its limited length, it cannot be comprehensive. For more detailed information, the reader should consult specific literature for the individual pathologies, mentioned later.

Congenital Malformations of the Hip

►*Hip dysplasia* is the most common congenital malformation and represents an abnormal growth or development of the acetabulum, femoral head, and associated ligaments and soft tissues. It can be associated with instability and/or dislocation of the femoral head. Ultrasonography is the method of choice for the diagnosis and treatment of hip dysplasia and instability in newborns and young infants. The evaluation is typically performed by assessing the alpha angle (which outlines the superior bony acetabulum) and the beta angle (which represents the cartilaginous part of the acetabulum). A normal alpha angle should be greater than 60° and a normal beta angle should be less than 55°. In older children with ossified

Congenital Malformations, Musculoskeletal System. Table 1 Relatively frequent major congenital malformations, that involve the musculoskeletal system

ICD-9	Malformation	Prevalence	Ratio: M/F
090	Congenital syphilis	22.8	1.0
243	Congenital hypothyroidism	3.0	1.1
658.8	Amniotic bands	0.3	0.3
741.0	Spina bifida with hydrocephalus	1.9	0.9
741.9	Spina bifida without hydrocephalus	1.8	0.9
742.1	Microcephalus	5.8	0.8
749.0	Cleft palate	5.8	0.7
749.2	Cleft palate & lip	4.6	1.4
754.3	Congenital dislocation of hip	14.6	0.3
754.51	Talipes equinovarus	11.6	1.7
755.2	Reduction deformities of upper limb	3.0	0.9
755.3	Reduction deformities of lower limb	1.9	1.3
755.8	Arthrogryposis multiplex congentia	1.5	0.9
756.0	Craniosynostosis	4.0	2.1
756.4	Chondrodystrophy	1.1	1.0
756.51	Osteogenesis imperfecta	0.3	0.4
758.0	Down syndrome	10.1	1.0
758.1	Patau syndrome	0.8	1.3
758.2	Edwards syndrome	1.2	0.5
758.7	Klinefelter syndrome	0.6	-
760.71	Fetal alcohol syndrome	2.1	1.4
771.0	Congenital rubella	0.1	1.0
771.1	Congenital cytomegalovirus infection	1.4	1.1
771.2	Other congenital infections	2.3	0.8

Source: From The New York State Department of Health Congenital Malformations Registry: //www.health.state.ny.us.

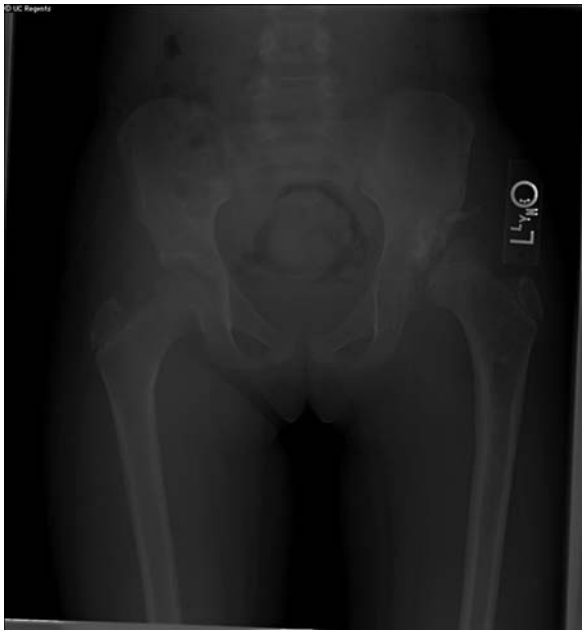

Congenital Malformations, Musculoskeletal System. Figure 1 Hip dysplasia: The left acetabulum is markedly shallow. There is extensive subchondral lucency and sclerosis. There is marked malformation of the left femoral epiphysis. These changes are consistent with congenital hip dysplasia and are unchanged compared to prior study. Ossific fragment is again seen superior to the left femoral head, likely avulsion injury versus heterotopic bone. Several calcific densities are present in the proximal left femoral shaft, which may represent exaggerated trabeculae versus enchondromas.

femoral heads, radiographs are obtained to profile the anterior aspect of the acetabulum (Fig. 1). If any evidence of hip subluxation is present, an additional abducted internal rotation view is added to determine the true neck-shaft angle of the proximal femur. Typical measures for hip joint assessment are the Hilgenreiner line, Perkin line, Shenton Menard line, and acetabular angle (<30° in newborns, decreases with increasing age).

►*Coxa valga* represents an increased angle between the femoral neck and shaft (normal 150° at birth, then gradually decreasing up to 120–130° in adults). The coxa valga usually results from weakness of the abductor muscles and lack of normal weight-bearing forces; it is most commonly associated with neuromuscular disorders such as cerebral palsy, spinal dysraphism, and poliomyelitis, less commonly with some skeletal dysplasias.

►*Coxa vara* represents a decreased angle between the femoral neck and shaft (<120°) and is often associated with shortening of the affected leg, vertical orientation of the capital femoral physis, and femoral anteversion. The congenital coxa vara shows a characteristic radiographic finding of a fragment of bone inferolateral to the proximal femoral physis, which represents a contained area of abnormal calcification.

Congenital Malformations of the Limbs

Congenital malformations of the feet include pes valgus (flat foot) and pes varus (abnormally increased angle between the axis of the calcaneus and second metatarsal), pes planus and pes cavus (decreased or increased longitudinal arch), talipes varus and valgus (abnormally decreased or increased angle between the axes of the ankle and foot), metatarsus varus and adductus (outward or inward bending of the forefoot), and tarsal coalition (abnormal union of two or more tarsal bones).

►Talipes equinovarus (clubfoot) (Fig. 2) involves the talus (ankle) and pes (foot), the heel is elevated (equino—like a horse's) and turned inward (varus). Talipes equinovarus can be idiopathic (most frequent), due to exogenous causes (oligohydramnion, teratogenic agents, e.g., sodium aminopterin, congenital constriction rings) or inherited (autosomal recessive and associated with various syndromes, e.g., diastrophic dwarfism). Radiographic features include parallelism of talus and calcaneus with an AP talocalcaneal angle <20° (normal 25–40°) and lateral talocalcaneal angle of 10–35° (normal 35–50°).

A Rocker bottom foot may occur after inadequate treatment of talipes equinovarus or, more rarely, due to cerebral palsy and other neuromuscular disorders, or due to genetic syndromes, such as trisomy 13, 15, or 18 syndromes. The Rocker bottom foot is diagnosed based on a lateral radiograph, which shows a dorsiflexed forefoot, a plantar flexed calcaneus, a reversed angle between calcaneus and 5th metatarsal, and a reversed angle between a relatively vertical talus and 1st metatarsal.

Reduction defects represent congenital limb malformations (dysmelia), complete absence of a whole limb (amelia) or parts of a limb with only a proximal rudimentary part present (Peromelia), congenital absence of upper and lower arm (leg) with hand (foot) present (phokomelia) or absence of specific bones, e.g., absence of radius/ulna or tibia/fibula (hemimelia). The cause is, in most instances, an exogenous interference with the limb-bud formation in the 3rd–6th week of pregnancy. For example, an increased incidence of dysmelias was noted during the 1950s due to Thalidomide and due to uran intoxication after the wars in Bosnia, Kosovo, and Iraq. Imaging studies of at least the whole affected limb are necessary to fully evaluate dysmelias, since malformations of one bone (e.g., the partial or complete absence of the fibula) are often associated with other malformations of

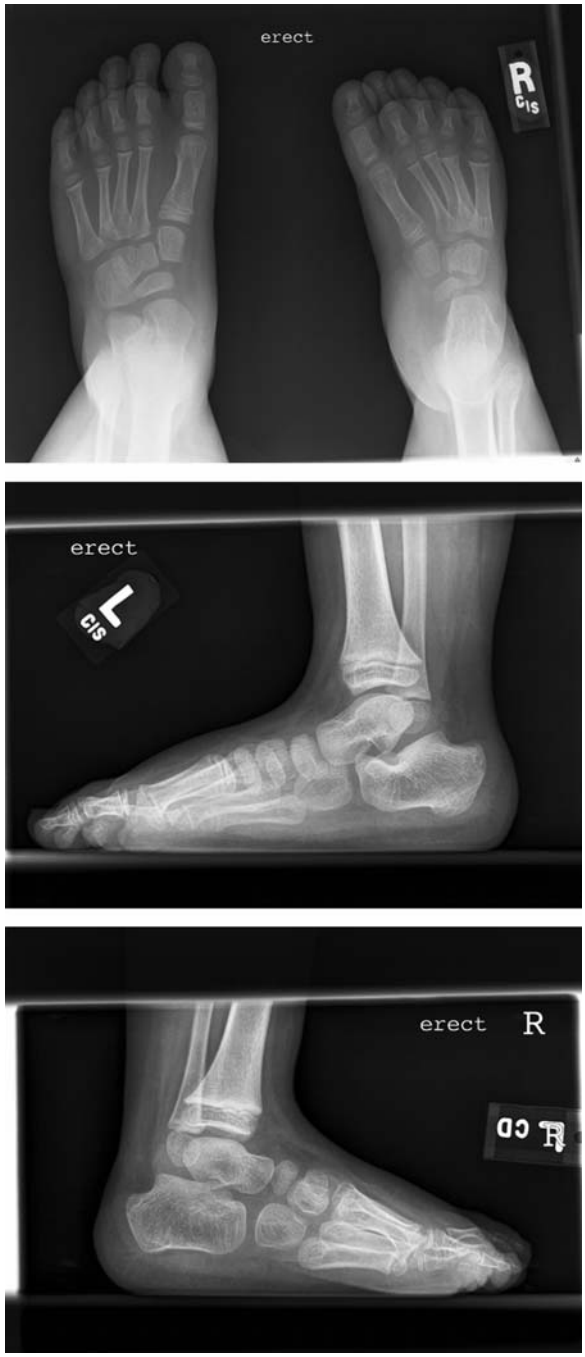

Congenital Malformations, Musculoskeletal System. Figure 2 **Talipes equinovarus.**

Congenital Malformations, Musculoskeletal System. Figure 3 **►Polydactyly: Frontal projection of the left hand demonstrates a well-formed bilateral sixth digit, compatible with polydactyly. This finding can be associated with Ellis-Van Creveld, Meckel-Gruber syndrome, or trisomy syndromes.**

other bones of the same limb (e.g., associated malformations of the femur).

The "lobster claw hand," congenital cleft hand, or split hand (synonyms) may occur isolated or, more frequently, as part of a syndrome with autosomal dominant inheritance and variable penetrance. The split hand is characterized by an absence of the third digital ray, with a deep cleft extending to the carpal bones, dividing the hand into two parts. The syndrome is associated with malformations of the lower legs, especially tibial aplasia.

Other, relatively frequent congenital malformations of the limbs include polydactylies (accessory or supernumerary fingers or toes) (Fig. 3), syndactylies (fused fingers or toes with or without synostosis, webbed fingers or toes) or a combination of both (►polysyndactyly) (3). These may also occur solitary or associated with other abnormalities, e.g., such as in Acrocephalosyndactyly (Apert's syndrome, ►syndactyly and premature closure of sutures of the skull). In addition, fingers or toes may present abnormally short (brachydactyly), abnormally curved (clinodactyly: curving of the fifth finger toward the fourth finger or camptodactyly: fixed in a flexed position), or bifid (bifid digits).

Madelung deformity is characterized by dorsal and lateral bowing of the distal radius, and lateral bowing of the distal radius, shortening of the radius and subluxation of the inferior radio ulnar joint. If congenital, causes are most frequently genetic or dysplastic, less frequently posttraumatic or idiopathic. The most frequently associated genetic syndrome is Turner's syndrome. Associated bone dysplasias are hereditary osteochondromatosis,

achondroplasia, multiple epiphysial dysplasias, and the mucopolysaccharidoses (Hurler and Morquio). The most important associated dysplasia is dyschondrosteosis, a form of mesomelic dwarfism.

Other relatively frequent congenital malformations of the lower limbs include accessory bones, absence of the patella, congenital dislocation of the knee and genu valgum, varum, and recurvatum.

Arthrogryposis multiplex congenita is a rare disease, characterized by multiple limb deformities at birth with gross stiffening of joints and hypotonia or wasting of muscle. The hips are usually dislocated, knees flexed, clubfeet may be present as well as upper extremity deformities similar to Erb's palsy deformity.

Larsen Syndrome represents multiple joint dislocations, mainly hips, and hyperextended or dislocated knee joints. It is associated with cervical kyphosis, which may be life-threatening because of the impingement on the spinal cord at the apex of the kyphosis.

Congential Malformations of the Head and Neck

Deformities of the skull in young babies and infants are most often exogenous, such as forceps delivery or due to positioning (e.g., constant sleeping position on the back causes a flat occiput). Much more rarely, deformities of the skull are due to congenital syndromes with congenital craniosynostosis, such as Apert's syndrome, Crouzon syndrome, Pfeiffer syndrome, or Carpenter syndrome (3). Congenital nose deformities include squashed or bent nose in babies of mothers with oligohydramnion (considered to be due to intrauterine malposition and pressure) and saddle nose in patients with congenital syphilis. A hemicraniofacial microsomia has been associated to exogenous drugs or toxins, such as Thalidomide. Goldenhar syndrome (oculo-auriculo-vertebral syndrome) represents hemifacial microsomia, microtia, abnormal or missing eye, and hemivertebrae (3). ►Hypertelorism, a lateral shift of the orbits, may be due to excessive ethmoid sinus or a midline cleft. In patients with ►hypotelorism, the intercanthal area is narrowed and may be associated with varying degrees of frontonasal hypoplasia. Hypotelorism may be associated with a premature closure of the metopic suture. In the extreme form, the infant looks like a cyclops, this condition is not compatible with life.

Congenital sternocleidomastoid torticollis is the most frequent congenital malformation of the neck, characterized by tilting of the head to one side, rotation of the occiput to that side and the chin to the opposite side due to a unilateral contracture of the sternomastoid muscle. There may be also a facial asymmetry. X-rays may show congenital hemivertebrae or partial fusion of cervical vertebrae, especially in cases where the sternocleidomastoid is normal.

Congenital Malformations of the Spine

►*Congenital scoliosis* is characterized by a lateral curvature of the spine due to congenital vertebral anomalies, such as vertebral absence, partial formation, or lack of separation. Patients with congenital scoliosis require a renal ultrasound to rule out renal anomalies such as a single kidney which is the most common associated finding. MR imaging may be necessary to rule out suspected associated abnormalities of the spinal cord or spinal nerves if clinical neurologic examination findings are present. Early surgical intervention may be required to prevent deformity progression. Other, less frequent patterns of congenital spinal deformity are hyperlordosis and kyphosis.

►*Spina bifida* is a developmental defect of the neuroectodermal tube at the fetal stage, resulting in various degrees of defective closure of the neural arch of the spinal canal. The condition is more common in the western countries. Two main forms should be distinguished: the closed spina bifida (spina bifida occulta), which is usually asymptomatic, and the open spina bifida with meningomyelocele, which is usually associated with neurological deficiencies and sometimes a hydrocephalus.

Congenital spondylolisthesis or dysplastic spondylolisthesis is characterized by presence of dysplastic sacral facet joints, which cause a forward translation of one vertebra relative to another. There is usually no defect in the pars interarticularis. Congenital spondylolisthesis comprise about 14–21% of all cases of spondylolisthesis, occur with a 2:1 female-to-male ratio and typically present around the adolescent growth spurt.

Congenital Platyspondyly is defined as two or more flattened vertebral bodies (single involved vertebra known as vertebra plana) with reduced distance between the endplates and occurs in thanatophoric dysplasia, metatropic dwarfism and osteogenesis imperfecta type IIA. Platyspondyly developing in later childhood occurs in Morquio's disease, spondyloepiphyseal dysplasia tarda, and Kniests dysplasia.

Sacral agenesis or *caudal regression syndrome* refers to a wide range of absent lower portions of the spinal column and pelvis. The incidence is increased in children of diabetic mothers. Sacral agenesis is associated with bowel, bladder or lower extremity motor dysfunction, anorectal malformations, and presacral teratomas or myelomeningoceles.

Klippel Feil syndrome describes a continuity of cervical and upper thoracic vertebrae. It maybe associated with renal

anomalies (38%), sensineural or conductive hearing loss (36%), cardiovascular anomalies (18%) or, less common, limb deficiencies, craniosynostosis, and craniofacial abnormalities.

Malformations of the Chest Wall

Cleidocranial Dysostosis is a developmental and familial disorder of membranous ossification with involvement of the clavicle and the cranial bones. In the typical case, the clavicle may be totally or partially absent and this may be bilateral so that the patient's two shoulders could be brought forward toward the midline to touch each other. The skull is abnormally large with bossing of the parietal and frontal bones. The closure of fontanelles is delayed. The face is small with a relatively large and prognathous mandible and a poorly developed maxilla. The pelvic bones also show poor development with nonfusion of the symphysis pubis and poor development of the sacrum.

►*Sprengel's Shoulder* is characterized by a congenital elevation of the scapula. Developmentally, the scapula has failed to descend from its embryological position in the neck. Radiographs show the elevated position and diminished size of the scapula. It may also show a bony bar connecting the low cervical vertebra with the supero medial angle of the scapula and it is called as the *omovertebral bone.*

Other common congenital malformations of the chest wall are pectus excavatum, funnel chest, and sternum bifidum. Supernumerary ossification centers of the sternum are most commonly seen in association with Down's syndrome.

Osteochondrodysplasias

Relatively common congenital osteochondrodysplasias are osteogenesis imperfecta, McCune Albright Syndrome (polyostotic fibrous dysplasia), osteopetrosis, progressive diaphyseal dysplasia (Camurati Engelmann), enchondromatosis, exostoses, achondrogenesis, thanatophoric dwarfism, chondrodysplasia punctata, achondroplasia, chondroectodermal dysplasia, and spondyloepiphyseal dysplasia. The reader may be referred to the literature for detailed descriptions of these diseases (4).

Bibliography

1. The New York State Department of Health Congenital Malformations Registry: ►//www.health.state.ny.us
2. Graf R (1980) The diagnosis of congenital hip-joint dislocation by the ultrasonic Compound treatment. Arch Orthop Trauma Surg; 97(2):117–133
3. Jones KL, Smith DW (1997) Smiths Recognizable Patterns of Human Malformation. WB Saunders, Philadelphia
4. Spranger JW, Brill PW, Poznanski AK (2003) Bone Dysplasias: An Atlas of Genetic Disorders of Skeletal Development. Oxford University Press, Oxford, England

Congenital Malformations, Neck

Carlos H. Buitrago-Tellez
University of Basel, Head Radiological Institute, Zofingen Hospital, Switzerland
carlos.buitrago@spitalzofingen.ch

Definitions

Malformations of the neck region may initially not be clinically significant but according to their natural history they may change their manifestation and become symptomatic. Generally, congenital malformations can be divided into branchial arch anomalies, ►thyroid malformations, congenital vascular lesions, laryngeal malformations, and congenital dysontogenetic tumors or tumor-like conditions such as the sternocleidomastoid tumor of infancy. The most common anomalies are those associated with abnormal development of the branchial apparatus (1).

Pathology/Histopathology

Branchial Arch Anomalies

First branchial arch anomalies include either cleft cysts or syndrome-associated external auditory canal anomalies. First branchial cleft cysts (BCCs) can be classified according to Arnot (2). In Arnot type I the cleft cyst is located in the parotid gland without communication to the external auditory canal. In type II the cyst is usually located inferiorly to the parotid gland and the cyst tract communicates with the external auditory canal.

First branchial arch anomalies with associated abnormal external ear, external auditory canal stenosis, atresia, or further mandibular malformations include syndromes such as Goldenhar syndrome (Fig. 1), Franceschetti–Treacher-Collins syndrome, Pierre Robin syndrome, or even thalidomide toxicity.

Second branchial arch anomalies include either a persistent stapedial artery or the most common remnants of the second branchial arch. Second BCCs are the most

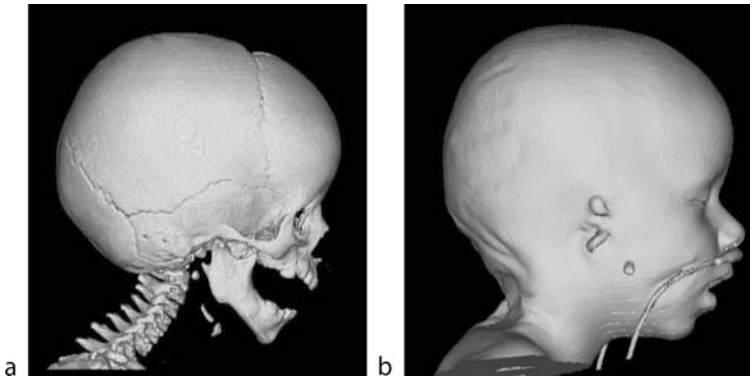

Congenital Malformations, Neck. Figure 1 First branchial arch congenital anomaly: atresia of external auditory canal and abnormal external ear in a 10-month year old baby with Goldenhar syndrome. Note also an accessory apophysis at the ascending ramus of the mandible. (a) Three-dimensional CT reconstruction (Volumen Rendering technique) with osseous display, (b) Three-dimensional CT reconstruction using surface rendering technique with a threshold of −100 HU.

common remnants of the branchial arches, making up around 90% of detected cleft cysts. The Bailey classification system (3) distinguishes four types of second BCC: type I when the cyst lies superficial to the anterior border of the sternocleidoid muscle beneath the cervical fascia and without contact to the internal jugular vein or the carotid arteries.

Type II shows a varying degree of adherence to the internal jugular vein, but no contact with the carotid sheath. In type III the cyst passes between the external and internal carotid arteries and extends further along the lateral pharyngeal wall. Type IV second BCC consist of those cysts located medially to the carotid vessels along the pharyngeal wall.

Third branchial arch anomalies include either the rare DiGeorge's syndrome (absent thymus and third parathyroid gland) or the third BCC. This cyst is located posterior to the sternocleidomastoid muscle and has a sinus tract ascending along the internal carotid artery, passing over the hypoglossal nerve and inferiorly to the glossopharyngeal nerve and then draining into the pyriform sinus.

Fourth branchial arch anomalies may include ►vascular anomalies such as aberrant subclavian artery or the fourth BCCs. These cysts are located around the aortic arch, usually anteriorly on the left, and around the subclavian artery on the right, and their sinus tract may ascend up to the level of the carotid bifurcation draining into the pyriform apex.

►Branchial cleft anomalies may present pathologically as a *fistula*, *sinus*, or *cyst*, based on the degree of completion of development of the anomalous structure. *Fistulae* appear in the case of persistence of both the cleft and the corresponding pouch, thereby forming a communication (i.e., fistula) that is epithelial lined. The fistula lies caudal to the structures derived from that particular arch and has a communication to the skin externally and to the pharynx internally. *Sinuses* may be considered partial fistulae, usually opening externally, with no internal opening.

Congenital Malformations, Neck. Table 1 Vascular congenital lesions of the neck according to the classification of Mulliken and Glowacki (1982)

Hemangiomas
• Capillary hemangioma (superficial)
• Cavernous hemangioma (deep)
• Combined hemangioma
Vascular malformations
• "Low-flow" lesions
Venous malformations
Capillary malformations
Lymphatic malformations (Lymphangioma)
• "High-flow" lesions
Arterial malformations
Arteriovenous malformations
AV Fistulas

Vascular Anomalies

Mulliken and Glowacki (4) proposed a biological classification of vascular birthmarks considering histologic features and clinical behavior. According to their classification system (Table 1), two major categories are distinguished in this setting: vascular tumors and vascular malformations. Vascular tumors include hemangiomas, Kaposiform hemangioendothelioma, and tufted angioma. Vascular malformations comprise high-flow malformations and slow-flow malformations.

High-flow malformations may be arterial or arteriovenous. Slow-flow malformations include venous malformations and capillary and lymphatic malformations. Lymphatic malformations are also known in the literature as lymphangiomas.

The most common vascular tumor is the hemangioma, which in around 30% of cases is visible at birth, the remaining appearing at age 2–4 years. Hemangiomas are most commonly located on the head and neck region. Postnatal growth is rapid and involution is slow.

In contrast, vascular malformations are present at birth in approximately 90% of cases, and depending on their type may manifest clinically at a later age in response to trauma, following incomplete surgical resection, or in altered hormonal states. They also do not involute as hemangiomas and tend to grow with the child.

Hemangiomas can be classified into capillary, cavernous, and capillary cavernous types.

Capillary malformations are groups of tortuous blood vessels in the upper layers of the dermis.

Lymphangiomas or lymphatic malformations are collections of lymph vessels filled with serous fluid. The histology ranges from capillary-sized vessels to macroscopic fluid-filled vessels. They can be divided into four classes clinically and histologically: capillary, cavernous, cystic (hygroma), and lymphangiohemangioma.

Venous malformations grow commensurately with the child. They may expand in response to trauma or hormonal factors. The following histologic characteristics are present: flat endothelium, slow turnover, dysplastic walls in ectatic venous vessels, and thin basement membranes.

Vascular malformations enlarge by hypertrophy. Flat, normal-appearing endothelial cells and ectatic vessels are characteristic findings in vascular malformations.

Hemangiomas rarely affect bone, whereas malformations affect bone in approximately 35% of cases.

Thyroid Malformations

The most common congenital thyroid anomaly is the persistent thyroglossal duct cyst. It occurs along the tract of the thyroglossal duct and is usually in an infrahyoidal location and in the midline. The thyroid gland is usually present and functions normally.

Ectopic thyroid tissue may be located at the base of the tongue in the midline dorsum, but it may also be located along the migration pathway of the thyroid. It is important to consider that in the presence of a lingual ectopic thyroid, the gland is often up to 70% not present at its usual position, so that a preoperative diagnosis is essential to avoid thyroid hormone insufficiency.

Thyroglossal duct cysts may be diagnosed by cytopathological analysis. The cytomorphologic features include colloids, macrophages, lymphocytes, or predominantly neutrophils. The epithelium may be ciliated columnar, metaplastic squamous, or of mature squamous type.

Laryngeal Malformations

The most common congenital anomalies of the larynx are laryngomalacia, bilateral vocal cord paralysis, and congenital subglottic stenosis. Less frequent anomalies comprise laryngeal atresia, laryngeal congenital webs, or vascular anomalies such as subglottic hemangioma or vascular malformations, especially of lymphatic origin (lymphangioma). Congenital laryngeal cysts are very uncommon.

Laryngomalacia is defined as a congenital disorder of the larynx characterized by inspiratory stridor and airway obstruction. It is due to a congenital weakness of the aryepiglottic folds and epiglottis, which are sucked into the airway during inspiration.

Congenital vocal cord paralysis is considered idiopathic. In certain cases, paralysis may occur secondary to central neuromuscular immaturity.

Congenital subglottic stenosis results from incomplete recanalization of the laryngotracheal tube during the third month of gestation. The extreme form of this anomaly is laryngeal atresia. Congenital subglottic stenosis can be classified into two types, membranous or cartilaginous.

Dysontogenetic Tumors or Tumor-Like Conditions

Dysontogenetic cervical tumors include those tumor conditions present at birth and include cervical teratomas, dermoid tumors, and tumor-like conditions as the sternocleidomastoid tumor of infancy or the midline cleft.

The sternocleidomastoid tumor of infancy represents a congenital fibrosis within the muscle and may manifest clinically as a tumor-like mass in the perinatal period.

The midline cervical cleft is a rare congenital anomaly presenting as a midline mass in the form of a pseudonipple located infrahyoidal caudally.

Dermoid cysts are considered the most common form of teratoma and are characterized by a predominance of ectodermal content. Congenital midline cleft histologically consists of a stratified keratinized squamous epithelium with hyperkeratosis, dermal fibrosis, and little or no skin appendages.

Clinical Presentation

Branchial Arch Anomalies

First branchial anomalies associated with external auditory canal atresia or stenosis may present clinically with marked difficulty in hearing, especially if the malformation is bilateral.

First branchial cysts manifest clinically as masses in the parotid gland region, in some cases even up to the submandibular region.

Second to fourth branchial cysts present in a similar way, although the location may be important for diagnosis. Second BCC are typically manifested in the neighborhood of the sternocleidomastoid muscle in the second decade of life. Inflammatory changes may be associated with fistulae formation. Third BCC may also cause an irritation of the hypoglossal or glossopharyngeal nerve in the presence of the typical draining tract.

Vascular Anomalies

Clinically, hemangiomas manifest typically superficially and can exhibit a varied appearance, from a hypopigmented macule to a bruise-like macule. The course of these lesions includes a proliferative postnatal growth phase that lasts for 3–9 months with a gradual involution occurring over 2–6 years. Involution is usually complete by age 7–10 years.

Vascular malformations are by definition present at birth, although in clinical practice 10% may manifest later in the postnatal period. Capillary vascular malformations (i.e., port-wine stains) are the most common type of vascular malformations. The lesions are presents in neonates but darken during adolescence and middle age.

Lymphangiomas present clinically as soft doughy masses that are located in the head and neck region. They may manifest as lymphedema and larger lesions may compromise the airway or the skeletal development of involved structures, such as the mandible. Venous malformations present in a variety of ways, from a slight blue patch to a recurrent growing compressible, soft, blue mass. Episodic painful thrombosis may also occur. Arterial malformations may present with bleeding.

Thyroid Malformations

Thyroglossal duct cysts present as asymptomatic midline masses, although they may occur off the midline in up to 25% of cases. A carcinoma developing in a thyroglossal duct cyst is very rare, but can be responsible for atypical presentation infiltrating surrounding tissues.

A lingual ectopic thyroid gland may manifest with dysphagia, hemorrhage, or airway obstruction.

Laryngeal Malformations

Laryngomalacia may present with noisy respiration and inspiratory stridor that is accentuated by being in the supine position, feeding, and agitation. Vocal cord paralysis also causes an inspiratory stridor and increasing respiratory distress if it is bilateral. Unilateral vocal cord paralysis may cause a hoarse cry.

Congenital subglottic stenosis presents with biphasic stridor with respiratory distress symptoms that may worsen in the case of an upper way infection.

Dysontogenetic Tumors or Tumor-Like Conditions

Cervical teratomas or dermoid tumors as a special form of teratoma present as large masses that may compromise the airway. The sternocleidomastoid tumor of infancy presents as a firm, painless mass in the inferior to the middle third of the muscle in neonates. Congenital midline cleft presents as a midline mass that may be associated with thyroglossal duct cysts, cleft lip/mandible/sternum, cervical contractures, mandibular spurs, microgenia, or bronchogenic cysts.

Imaging

Branchial Arch Anomalies

Branchial cleft anomalies are usually studied by imaging methods, including ultrasound (US) as a basic approach followed by computed tomography (CT) and magnetic resonance imaging (MRI) in more complex anatomic situations.

On US, BCCs present characteristically with a pattern of homogeneous, anechoic, smooth reflections within a well-demarcated, thin and elastic, deformable wall when using a high-resolution transducer. However, some BCCs may present with an inhomogeneous texture and/or irregular walls and hypoechoic characteristics, so that a distinction from inflammatory or neoplastic processes with central necrosis may not be possible. In these cases, CT or MRI may be more useful to rule out associated pathology.

A definitive CT diagnosis of second BCC may be possible in 80–90% of cases. BCCs present a CT appearance of a mass with an enhancing capsule and a lucent center measuring between 20 and 35 HU. To detect sinus or cyst tracts, CT using intravenously administered contrast material, and air as a contrast agent with Valsalva test, may show air along the draining tract proving communication between the internal drainage and the branchial remnant. Three-dimensional CT may be useful in the preoperative planning of craniofacial malformations, including first branchial anomalies, such as the Goldenhar syndrome (Fig. 1).

MRI allows a more detailed analysis of lesion size, morphology, location, relation to the expected course of neurovascular structures, enhancement pattern, attenuation compared to the cerebrospinal fluid (CSF), and T1- and T2-weighted signal intensity (5). This may allow identification of tiny fistulous tracts, especially when using three-dimensional sequences.

Vascular Anomalies

The predominant sonographic features of cavernous *hemangiomas* are well-defined hypoechoic mass lesions with heterogeneous echotexture and the presence of cystic and sinusoidal spaces within, as well as the occasional presence of phleboliths. Color Doppler imaging demonstrates flow inside the mass. MRI is very accurate in detecting hemangiomas, although capillary and cavernous hemangiomas cannot always be differentiated. They show bright signal on T2-weighted, low signal on T1-weighted, and enhancing diffusely without distorted dilated venous vessels.

US with high-resolution transducers can confidently suggest the diagnosis of neck *venous malformations* in up to 90% of cases. The lesions may show well-defined margins, heterogeneous and hypoechoic echo pattern, with sinusoidal spaces and phleboliths on gray-scale imaging, and flow signal on Doppler. In contrast to hemangiomas, large slow-flow venous vessels are present. MRI is superior in the overall characterization of the extent of the venous malformation, showing slow-flow vascular channels, dark on T1-weighted images, bright on T2-weighted images, and enhancing after contrast medium administration. A three-dimensional contrast-enhanced MR angiograph with time resolution or late imaging demonstrates the dilated venous vessels of the malformation.

High-flow vascular malformations contain an arterial component that may be detected by color Doppler US. This may be documented by time-resolved MR angiography, but conventional angiography with selective injection of contrast medium in the involved branch of the external carotid artery or vessels involved is mandatory before therapeutic decisions.

Three-dimensional CT angiography allows detailed description of vascular lesions of the head and neck and offers another effective means of imaging these complex lesions.

Lymphangiomas may be documented by US, CT, or MRI. US may show superficial hypoechogenic multilocular cystic masses with septa of variable thickness, but may fail to demonstrate retropharyngeal, axillary, or mediastinal extensions in all patients. MRI allows a better tissue characterization and lesion extent (Fig. 2).

Lymphangiomas may present as microcystic or macrocystic forms and may be differentiated by MRI. The cysts may usually have variable signal on T1-weighted sequences, from hypointense to brighter signal as CSF, and high signal on T2-weighted sequences. Fluid–fluid levels may be present, especially on the T1-weighted images (see Figs 2a and b).

Thyroid Malformations

The imaging work-up of ectopic thyroid gland requires a thyroid scintigraphy. For further diagnosis of thyroglossal duct cysts, US represents the basic imaging method, followed by CT and MRI. US findings may show anechoic, homogeneous hypoechoic, solid appearing or even heterogeneous midline cervical mass. On MRI the mass may reveal high signal intensity on T2-weighted images and sometimes also on T1-weighted sequences.

Laryngeal Malformations

Plain film radiographs of the cervicothoracic region in the neonate may suggest a diagnosis of laryngomalacia and can exclude anomalies with similar presentation. Inspiratory plain films of the neck may show inferior and medial displacement of the epiglottis and arytenoids. Fluoroscopy may reveal supraglottic collapse and hypopharyngeal dilatation. CT of the larynx region may be necessary if a partial subglottic stenosis or laryngeal atresia is suspected.

Dysontogenetic Tumors or Tumor-Like Conditions

The demonstration of a fat–fluid level on MRI or CT is diagnostic of a cervical dermoid cyst. Other teratomas or tumor-like conditions are also best delineated by CT.

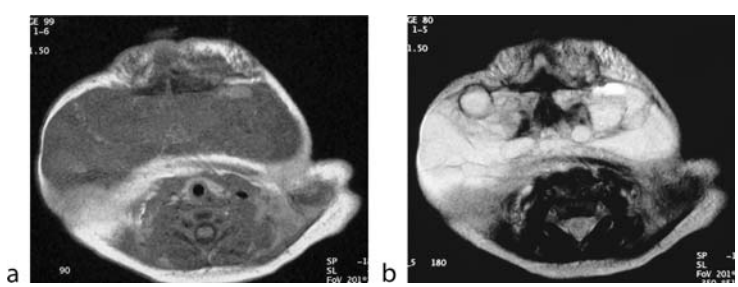

Congenital Malformations, Neck. Figure 2 Lymphangioma of the neck in a 3-day old newborn. (a) T1-weighted axial image at the level of the mandibular symphysis showing a hypointense inhomogeneous mass from the lateral neck crossing the midline. Note hyperintense cysts on the left adjacent to the mandibular body. (b) T2-weigthed image demonstrating high signal intensity together with multiseptate cystic configuration.

Nuclear Medicine

The indications for thyroid scintigraphy pertechnetate using Tc-99m in the setting of congenital thyroid anomalies include investigation of hyperthyroidism, nodularity of the gland, cause of thyroid stimulating hormone elevation, and localization of an ectopic thyroid gland and in the evaluation of a thyroglossal duct cyst.

Diagnosis

Branchial Cleft Anomalies

While the history, physical examination, and imaging findings are the most important parts of the evaluation of neck masses in children, biopsy may be necessary to establish the diagnosis. Image-guided fine-needle aspiration (FNA) is a useful tool in the management of neck masses in children.

Vascular Anomalies

By history and physical examination, 96% of vascular lesions can be classified as hemangiomas or malformations. Knowledge of their natural history as well as their clinical and imaging presentation is essential for making the diagnosis. A biopsy may be accompanied by bleeding.

Thyroid Malformations

As a number of other nonneoplastic and neoplastic lesions can cause cystic midline masses in the neck, FNA may be useful in making a preoperative diagnosis of thyroglossal duct cyst for a more accurate and timely clinical intervention. Histological confirmation is necessary for diagnosis, including the very rare association with carcinoma.

Laryngeal Malformations

A classic history and endoscopic examination usually suffice to establish a diagnosis of laryngomalacia or congenital vocal cord paralysis or congenital subglottic stenosis.

Dysontogenetic Tumors or Tumor-Like Conditions

Surgery with histological evaluation is necessary to establish a diagnosis of dysontogenetic tumors or tumor-like conditions, such as the congenital intramuscular fibrosis present in the sternocleidomastoid tumor of infancy.

Interventional Radiologic Treatment

Patients with hemangiomas are treated surgically by cryosurgery or laser surgery or conservatively according to lesion size and behavior. In patients with venous malformations, percutaneous sclerotherapy is combined with surgical reduction; patients with arteriovenous malformations undergo transarterial embolization before surgical excision of the nidus.

Percutaneous transcatheter arterial embolization plays an increasingly important role in the management of vascular lesions in the neck. Embolization can promote thrombosis within the malformations, reduce bleeding, and decrease the need for transfusion intraoperatively. Moreover, it can facilitate surgical approaches to otherwise unresectable lesions.

Bibliography

1. Mukherji SK, Fatterpekar G, Castillo M et al (2000) Imaging of congenital anomalies of the branchial apparatus. Neuroimaging Clin N Am 10:75–93
2. Arnot RS (1971) Defects of the first branchial cleft. S Afr J Surg 9:93–98
3. Ford GR, Balakrishnan A, Evans JN et al (1992) Branchial cleft and pouch anomalies. J Laryngol Otol 106:137–143
4. Mulliken JB, Glowaki J (1982) Hemangiomas and vascular malformations in infants and children: a classification based on endothelial characteristics. Plast Reconstr Surg 69:412–422
5. Mukherji SK, Tart RP, Slattery WH et al (1993) Evaluation of first branchial anomalies by CT and MR. J Comput Assist Tomogr 17:576–581

Congenital Malformations, Nose and Paranasal Sinus

Fabio Minutoli
Department of Radiological Sciences, University of Messina, Italy
fminutoli@unime.it

Definition

Congenital malformations of the nose and paranasal sinuses are due to discrete faults in the embryological development of the face (1). On the basis of embryogenesis and anatomic location, they can be grouped into four categories: anomalies related to the nasal cavity, nasolacrimal apparatus, nasofrontal region and craniofacial malformations (2).

Pathology/Histopathology

Anomalies Related to the Nasal Cavity

Choanal atresia, the most common congenital abnormality of the nasal cavity, is a developmental defect characterised by lack of communication between the nasal cavity and nasopharynx. Nowadays, it is known that most if not all patients with choanal atresia have bony abnormalities: a combined bony and membranous malformation occurs in about 70% of cases and purely bony atresia is found in about 30% of cases. Choanal atresia seems to be due to persistence of the mesodermal plate, which separates the stomodeum (primitive mouth) from the ectoderm which forms the cranium and brain or of the buccopharyngeal membrane (which separates the stomodeum from the end of the pharyngeal gut). Choanal atresia may be uni- or bilateral. Approximately 75% of children with bilateral choanal atresia have other congenital abnormalities, as exemplificated by the ►*CHARGE association* (1, 3).

Nasal pyriform aperture stenosis is a rare anomaly characterised by narrowing of the anterior bony nasal apertures. It may occur as an isolated anomaly or in association with alobar or semilobar forms of ►*holoprosencephaly*, facial hemangiomas, clinodactyly, hypotelorism, cleft palate, pituitary dysfunction and central megaincisor. Patients with a central megaincisor have an increased incidence of intracranial defects (3).

Congenital absence of the nose (arhinia) with failure of formation of the nose, nares and nasal cavities is rare. It can be associated with various anomalies including maxillary hypoplasia, high arched or cleft palate and ocular and intracranial anomalies.

Nasopharyngeal atresia is an extremely rare malformation that results in complete isolation of the nasal cavity from the oropharynx (3).

Anomalies Related to the Nasolacrimal Apparatus

Congenital nasolacrimal mucocele, a lacrimal sac mucocele with intranasal extension, is an uncommon mass arising in the medial canthal region of the orbit. In such cases, impatency of the distal portion of the nasolacrimal duct results in ballooning of the distal membrane into the nasal cavity, forming a dumbbell-shaped nasolacrimal mucocele. It can become infected determining a dacryocystitis (2).

Anomalies Related to the Nasofrontal Region

In early life, the frontal bone is separated from the nasal bones by the fonticulus frontalis (nasofrontal fontanelle). The nasal bones are separated from the underlying cartilaginous nasal capsule by the prenasal space, which contains a dural diverticulum. This diverticulum regresses, leaving behind the foramen cecum (located anterior to the crista galli).

Congenital herniation of intracranial contents through a defect in the skull with a persistent connection to the subarachnoid space is consistent with cephalocele. Only meninges (meningocele) or both meninges and brain (meningoencephalocele or simply encephalocele) can herniate. According to location, encephaloceles are classified as either occipital (75%), sincipital (15%) or basal (10%). Sincipital encephaloceles occur about the dorsum of the nose, the orbits and the forehead; they are typically either frontonasal (40–60%), nasoethmoidal (30%) or a combination of the two. If brain protrudes through the fonticulus frontalis, a frontonasal encephalocele is formed, whereas brain extending in the prenasal space gives origin to nasoethmoidal encephalocele (the nomenclature is based on the origin of their roof and floor). They have a high prevalence of associated intracranial anomalies.

Midclosure of the dural diverticulum sequestering brain in its distal aspect gives rise to a nasal glioma (nasal cerebral heterotopia). It is composed of dysplastic neurogenic tissue that has become isolated from the subarachnoid space: by definition, it does not contain any CSF-filled space that is connected with either the ventricles or the subarachnoid space of the head. It has no neoplastic features. Nasal gliomas may be intranasal (30%), extranasal (60%) or a combination of the two (10%). Up to 15% of patients with nasal gliomas show multiple cerebral heterotopias.

If the dural diverticulum touches the skin of the nose, it will drag ectoderm with it as it regresses. In 50% of these cases, a dermal sinus will form; in the remaining 50% of cases, an epidermoid or dermoid will be found. Nasal dermal sinuses are thin, epithelium-lined tubes that arise at external ostia situated along the nose and extend deeply for a variable distance, sometimes reaching the intradural intracranial space. Dermoid cysts contain ectoderm with skin appendage and are usually midline with tendency to occur at the glabella. Epidermoid cysts contain ectodermal elements without skin appendages, are usually paramidline and tend to occur near the columella. They may occur in isolation or associated with concurrent malformations (1, 2, 4).

Craniofacial Malformations

Midfacial clefts, the most common craniofacial anomalies, result from deranged development of the frontonasal process and/or failure of adjacent processes to merge successfully. They include the typical unilateral or bilateral common cleft lip and/or cleft palate (98.8% of all facial clefts), the midline craniofacial dysraphisms, an

oblique facial cleft, a transverse facial cleft ('wolf mouth' or macrostomia) and the facial anomalies (including hypoplasia or absence of the nose and intermaxillary segment, and pseudomedian cleft lip) associated with *holoprosencephaly* (4). Midline craniofacial dysraphisms can be divided into two groups: the low group (midline cleft lip), in which the cleft involves the upper lip, hard palate and occasionally the nose; and the high group (median cleft face syndrome or frontonasal dysplasia) in which the cleft involves primarily nose and forehead and, less commonly, upper lip and hard palate (1). Both groups are associated with intracranial anomalies and different kinds of cephalocele.

Many other different syndromic associations involving the midface exist: the syndromes of the first and second branchial arches (including ►*hemifacial microsomia* and ►*mandibulofacial dysostosis*) manifest as deficiencies of tissue and as hypoplasias of the maxillary and mandibular arches; the syndromic craniosynostoses (craniofacial dysostoses) are a group of syndromes (►*Crouzon syndrome* and ►*Apert syndrome* being the most frequent two) that exhibit premature synostoses of cranial sutures as one prominent feature and are frequently associated with maxillary hypoplasia and central nervous system malformations (2, 4).

Clinical Presentation

Congenital arhinia, nasopharyngeal atresia and, when bilateral, choanal atresia, pyriform aperture stenosis and nasolacrimal mucocele determine respiratory obstruction with respiratory distress and cyclical cyanosis. Characteristically, respiratory distress is aggravated by feeding and relieved by crying, since neonates are obligate nose breathers for the first 2–6 months of life. Grunting, snorting, low-pitched stridor and rhinorrhea are other common presenting signs of nasal airway obstruction in neonate or infant. In patients with nasolacrimal mucocele, a tense blue-gray medial canthal mass (due to dilatation of the lacrimal sac) associated with epiphora is appreciable (2, 3).

Anomalies related to the nasofrontal region are usually not associated with airways obstruction. Midface disfigurement, nasal destruction, meningitis and anterior cranial fossa abscesses may occur. Depending on the size of the intracranial connection, cephaloceles may be pulsatile or change in size during crying, the Valsalva maneuver or jugular compression, whereas nasal gliomas, dermoid and epidermoid cysts do not. Dermal sinuses may be associated with intermittent discharge of sebaceous material and/or pus (4).

Clinical presentation of craniofacial malformations is dominated by facial deformities, variously associated with auricular, ocular, musculoskeletal and skin deformities. Moreover, the presence of central nervous system anomalies may be responsible for IQ affection. Midline craniofacial dysraphisms and many syndromic malformations are characterised by hypertelorism, whereas hypotelorism is typically associated with *holoprosencephaly* (1). The nasal and pharyngeal airways may be compromised, increasing the risk of respiratory distress.

Imaging

Computed tomography (CT) is the imaging modality of choice in children with possible malformations related to the nasal cavity or to the nasolacrimal duct. *Magnetic resonance (MR) imaging* is the modality of choice for evaluation of lesions with potential intracranial extension or associated intracranial anomalies, such as congenital midface masses (e.g. dermoid and epidermoid cysts, nasal gliomas, cephaloceles) and craniofacial malformations. However, in many cases, both CT and MR imaging are required to obtain an adequate evaluation of bone, brain and soft-tissue components of midface anomalies (2).

Key imaging features in choanal atresia include narrowing of the posterior choanae to a width of less than 0.34 cm in children under 2 years old, inward bowing of the posterior maxilla, fusion or thickening of the vomer (in children less than 8 years of age the width of the inferoposterior vomer should not exceed 0.34 cm) and the presence of a bone or soft-tissue septum extending across the posterior choanae. Choanal stenosis may appear similar to choanal atresia depending on the degree of narrowing (2).

Imaging features of pyriform aperture stenosis include a shelf of tissue extending across the nostril, just inside the nares, overgrowth and medial displacement of the nasal processes of the maxilla and narrowing of the pyriform aperture (2). A pyriform aperture width less than 11 mm in a term infant has been suggested to be diagnostic of pyriform aperture stenosis (5).

In patients with nasopharyngeal atresia, the posterior choanal passages end blindly, the posterior vomer is wide and both the vomer and the hard palate are fused to the central skull base (3).

The triad of cystic dilatation of the lacrimal sac, dilatation of the nasolacrimal duct and an intranasal cystic mass (homogeneous, well defined, thin-walled) with fluid attenuation is diagnostic of nasolacrimal mucocele. Often, thinning and superior displacement of the inferior turbinate bone occur. Intravenous administration of contrast material may demonstrate slight enhancement of the cyst wall that is more pronounced in dacryocystitis (2).

Imaging features of nasal encephaloceles include a soft-tissue mass that is connected to the subarachnoid

space *via* an enlarged foramen cecum and extends to the glabella or into the nasal cavity. Encephaloceles are isointense relative to gray matter with most MR imaging sequences, but may be hyperintense with T2-weighted sequences because of gliosis. CT may be useful in evaluating bone changes. MR cisternography (hydrographic imaging) may be useful in demonstrating a subarachnoid connection (2).

Nasal gliomas appear as non-enhancing soft-tissue masses; they are isointense to hypointense to gray matter with T1-weighted sequences and hyperintense with proton-density and T2-weighted sequences (2). Extranasal gliomas most commonly lie external to the nasal bones and nasal cavities, typically at the bridge of the nose, to the left or the right of the midline; moreover, they can extend into the maxillary antrum. Intranasal gliomas lie within the nasal or nasopharyngeal cavities, usually between the middle turbinate and the nasal septum. Mixed nasal gliomas consist of extranasal and intranasal components that communicate *via* a defect in the nasal bones or around their lateral edges or, rarely, through defects in the orbital plate of the frontal bone or the frontal sinus (4).

Imaging studies successfully display the course of dermal sinus tracts. They usually appear as isodense fibrous channels or as lucent dermoid channels that extend inward for a variable distance (4).

The imaging of dermoid and epidermoid cysts may overlap, although dermoid cysts are more likely to be midline and fatty, whereas epidermoid cysts usually have fluid attenuation at CT and are isointense relative to fluid at T1- and T2-weighted MR imaging (Fig.1).Diffusion-weighted and magnetization transfer sequences can aid in differentiating solid epidermoid cysts from fluid-containing lesions. In this field, it is very important to recognise normal findings, like septal tubercle (a focal bulge of the anterior nasal septum at the level of the middle turbinate bone) or fatty change within crista galli that may simulate disease (2). Demonstration of an enlarged foramen cecum (normal width: up to 10 mm; avg: 4mm) and distorted crista galli suggests intracranial extension, however it does not prove it (4).

Craniofacial malformations include developmental anomalies of the face and skull that are associated with central nervous system malformations (2). Median cleft face syndrome is characterised by hypertelorism and bony clefting of the nose (with or without cleft upper lip, premaxilla and palate). Associated anomalies may be frontoethmoidal and intraorbital cephalocele, cranium bifidum occultum frontalis, microphthalmos, anophthalmos, intracranial lipomas and callosal agenesis (1, 4).

Midface anomalies in patients with syndromes of the first and second branchial arches or syndromic craniosynostoses are mainly represented by maxillary hypoplasia. It may result in stenosis within the nasal

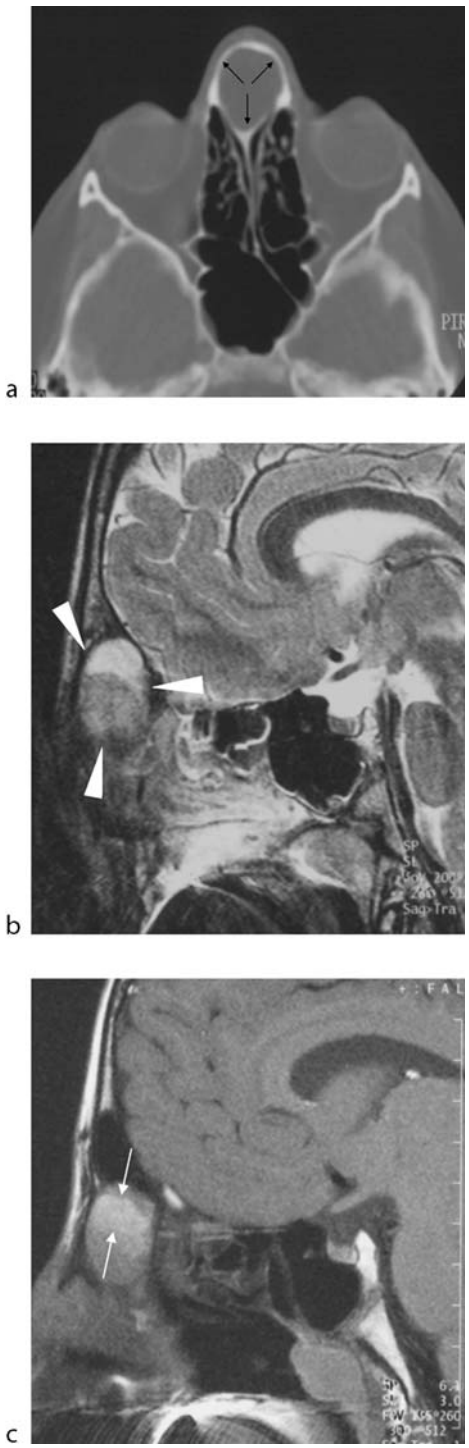

Congenital Malformations, Nose and Paranasal Sinus. Figure 1 Nasal dermoid cyst. Axial CT scan (a) reveals nasal swelling due to a sharply marginated midline lesion with soft-tissue attenuation, which determines broadening of the neighbouring bony structures (*arrows*). Sagittal T2-weighted (b) and sagittal T1-weighted (c) MR images show a inhomogeneous iso- to hyperintense lesion (*arrowheads)* containing areas of fatty-like signal (*arrows*).

cavity; in children with syndromic craniosynostosis, midfacial retrusion is generally associated with narrowing of the entire nasal and nasopharyngeal passages as well as some reduction in choanal dimensions (3).

Nuclear Medicine

Nuclear medicine is of no help in the assessment of congenital malformations of nose and paranasal sinuses.

Diagnosis

Diagnosis of congenital malformations of nose and paranasal sinuses is mainly based on physical examination and imaging. Most patients with craniofacial syndromes can be diagnosed on the basis of the type of anomalies involving the central nervous system and extremities and the presence of similar malformations in relatives (2).

When a congenital midface mass is found, biopsy should not be performed before an intracranial connection is ruled out because of the risk of causing meningitis or cerebrospinal fluid leak.

Only in few cases, the final diagnosis is reached after surgical treatment.

Bibliography

1. Castillo M (1994) Congenital abnormalities of the nose: CT and MR findings. Am J Roentgenol 162:1211–1217
2. Lowe LH, Booth TN, Foglar FM et al (2000) Midface anomalies in children. Radiographics 20:907–922
3. Robson CD, Hudgins PA (2003) Pediatric airway disease. In: Som PM and Curtin HD (eds) Head and Neck Imaging. Mosby Inc., St. Louis, pp 1521–1593
4. Naidich TP, Blaser SI, Bauer BS et al (2003) Embryology and congenital lesions of the midface. In: Som PM and Curtin HD (eds) Head and Neck Imaging. Mosby Inc., St. Louis, pp 3–86
5. Belden CJ, Mancuso AA, Schmalfuss IM (1999) CT features of congenital nasal piriform aperture stenosis: initial experience. Radiology 213:495–501

Congenital Malformations, Oral Cavity

Carlos H. Buitrago-tellez
University of Basel, Head Radiological Institute, Zofingen Hospital, Switzerland
carlos.buitrago@spitalzofingen.ch

Definition

Malformations of the oral cavity may manifest at birth or later, after development of the involved disturbed structures. The oral cavity comprises the anterior two-thirds of the tongue, the buccal mucosa, the gingiva, the soft and hard palate, the retromolar trigone, and the floor of the mouth and is bordered by the maxilla and mandible. Congenital malformations of the oral cavity include ▶cleft lip, palate, and alveolus defects, developmental anomalies of the tongue, vascular anomalies, developmental disturbances of the teeth and/or tooth structure, and congenital dysontogenetic tumors or tumor-like conditions. Most common anomalies of the oral cavity are cleft lip and/or palate and alveolus defects (1).

Pathology/Histopathology

Cleft Lip, Palate, and Alveolus Defects

Cleft abnormalities of the lip, palate, and alveolus are the most common congenital disorder of the oral cavity and result from developmental defects with incomplete fusion of the lips, palate, and/or alveolus. Depending on the association with further malformations, they may be divided into syndromic and nonsyndromic conditions. Among more than 300 syndromes associated with clefts the Pierre-Robin sequence (cleft palate, micrognathia, glossoptosis) and Treacher-Collins malformations (bilateral symmetric anomalies of the structures within the first and second branchial arches) may be mentioned. Nonsyndromic cleft anomalies are considered to be of multifactorial inheritance. Failure of merging of the medial nasal and maxillary processes at the 5th week of embryonic development on one or both sides results in cleft lip. Cleft palate is a partial or total lack of fusion of the palatal shelves.

Complete clefts of the lips and alveolus involve extension into the nose. Incomplete lip clefts do not extend to the nose. Complete clefts of the secondary palate involve both the hard and soft palate. Cleft lips may also be unilateral or bilateral. Unilateral cleft lips result from a failure of mesodermal proliferation, leading to complete or incomplete defects. A complete unilateral cleft lip includes the orbicularis oris muscle where the medial portion of the muscle attaches to the columella and the lateral portion to the nasal ala cartilage. In the bilateral type of cleft, the central part of the muscle is missing.

Clefts of the palate may be of the primary palate (anterior to the incisive foramen through the alveolus) or of the secondary palate, which may have many variants, from bifid uvula to a complete cleft of the hard and soft palate.

Developmental Anomalies of the Tongue

Congenital abnormalities of the tongue include processes that diffusely enlarge the tongue (macroglossia) and processes that cause focal masses.

There are multiple causes of diffuse macroglossia in children, including Down syndrome, hypothyroidism,

mucopolysaccharidosis, Beckwith-Wiedemann syndrome, and congenital duplication. The tongue may be relatively large in patients who have a small mandible (micrognathia), which is seen in children with Pierre-Robin sequence.

Focal masses of the tongue can be caused by vascular malformations or by congenital abnormalities such as thyroglossal duct cyst, lingual thyroid, duplication cyst, or even dysontogenetic congenital tumorous processes such as teratomas (Fig. 1). The most common congenital thyroid anomaly involving the tongue is the persistent thyroglossal duct cyst (see *Congenital Malformations, Neck*).

Ectopic thyroid tissue may also be located at the base of the tongue in the midline dorsum.

Although an intraoral location for duplication cysts is uncommon, when the cysts appear in the oral cavity they usually occur in the tongue. These lesions are usually large and present at birth or on prenatal imaging.

Other congenital malformations of the tongue include aglossia, bifid tongue, adhesions or fissures, hypoglossia or microglossia, which may be associated with skeletal anomalies in the setting of malformation syndromes of the oromandibular region and limbs. Ankyloglossia represents a developmental anomaly defined by the abnormal attachment of the frenum to the floor of the mouth.

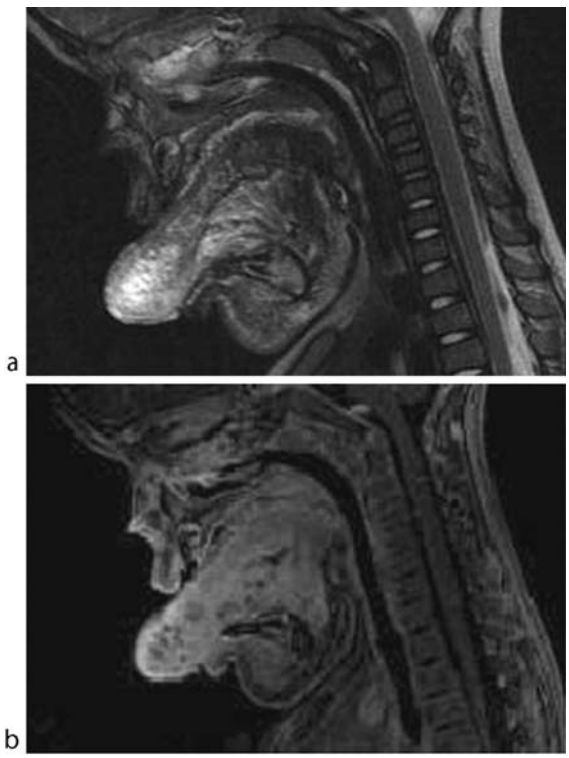

Congenital Malformations, Oral Cavity. Figure 1 Vascular malformation of the tongue with combined lymphangiomatous and venous components: (a) T2-weighted sagittal image showing macroglossia with high signal intensity at the tip of the tongue corresponding to microcystic component, (b) T1- weighted gradient echo sequence image revealing diffuse enhancement with hypointense spaces at the level of the microcystic component and flow voids at the base of the tongue. Patient underwent surgery to relieve macroglossia without complications.

Vascular Anomalies of the Oral Cavity

Mulliken and Glowacki (3) proposed a classification of vascular birthmarks considering histologic features and clinical behavior. Two major categories are distinguished in this setting: vascular tumors and vascular malformations. Vascular tumors include hemangiomas. Vascular malformations comprise high-flow malformations and slow-flow malformations.

High-flow malformations may be arterial or arteriovenous; slow-flow malformations include venous, capillary, and lymphatic malformations. Lymphatic malformations are also known in the literature as lymphangiomas.

The most common vascular malformation in the oral cavity is ▶lymphangioma. Lymphangiomas are collections of lymph vessels filled with serous fluid. The histology ranges from capillary-sized vessels to macroscopic fluid-filled vessels. They can be divided into four classes clinically and histologically: capillary, cavernous, cystic (hygroma), and lymphangiohemangioma.

Cystic lymphangiomas are generally characterized by large sinusoidal spaces, which may have high protein content or hemorrhage within them. Vascular malformations with combined lymphangiomatous and venous components may occur, especially in the tongue, resulting in macroglossia (Fig. 1). Venous malformations grow commensurately with the child. They may expand in response to trauma or hormonal factors.

Developmental Disturbances of the Teeth

Anodontia is a complete lack of tooth development, and hypodontia is a lack of some tooth development. Anodontia is rare, most often occurring in a condition called hypohidrotic ectodermal dysplasia. This is an inherited disease that affects deciduous or permanent teeth. Hypodontia is one of the most common developmental abnormalities. It is often associated with the absence of a dental lamina, which is also associated with many syndromes including Down syndrome and Crouzon syndrome. Hyperdontia is the development of

extraneous teeth. It is believed to be associated with an excess of dental lamina.

Regional odontodysplasia is rare but is most likely to occur in the maxilla and anterior teeth. The cause is unknown. Teeth affected by regional odontodysplasia never erupt into the mouth, have small crowns, are yellow-brown, and have irregular shapes. Supernumerary teeth represent extra teeth found in the dental arches, which result either from formation of extra tooth buds in the dental lamina or from the cleavage of already existing tooth buds. Mesiodens (midline of the maxilla) are the most common supernumerary teeth, and the second most common are the distomolars (distal to the third molar). Abnormalities in the size of teeth include microdontia, in which one or more teeth are smaller than normal, usually the incisors and three molars. In true generalized microdontia, teeth are extremely small, as in midgets. In generalized relative microdontia, teeth are not really small, but they are small compared to the jaw. Macrodontia is uncommon and may appear in the setting of puberty gigantism.

Abnormalities in the shape of teeth include gemination, fusion, concrescence, dilaceration, taurodontism, dens invaginatus, dens evaginatus, and teeth with supernumerary roots. Gemination represents an incomplete twin process with two crowns and one root. Fusion represents union of two normally separated adjacent tooth germs, resulting in one tooth less in dentition. Concrescence means that two adjacent teeth are united by cementum only, and it takes place after tooth formation is complete. In dilaceration, an angle in the root is present. Taurodontism describes elongated, enlarged pulp cavities with short roots. Dens in dente or dens invaginatus represents a tooth in a tooth, meaning an invagination of the enamel organ into the crown before crown formation. In dens evaginatus, an accessory cusp on the occlusal surface is present. Supernumerary roots may result secondary to metabolic dysfunction during root development after birth.

Developmental Tooth Structure Disturbances

Amelogenesis imperfecta is a genetic disorder that results in defective formation of enamel, the hard surface covering the crowns of teeth. Amelogenesis imperfecta either causes problems in the hardening of normal amounts of enamel or causes a smaller amount of normal enamel to be produced. Enamel hypoplasia is associated with a developmental disorder of ameloblasts and may be related not only to amelogenesis imperfecta but also to other factors such as vitamin A, C, or D deficiency or even congenital syphilis. Characteristic teeth changes in the setting of congenital syphilis also include mulberry molars or Hutchinson (screwdriver-like) incisors.

Dentinogenesis imperfecta is a genetic disorder that results in defective formation of dentin, a mineralized material forming the bulk of each tooth. Defective dentin causes the normal enamel layer that covers the tooth to flake off.

Amelogenesis imperfecta and dentinogenesis imperfecta are linked to defects in structural genes that code for proteins necessary for the development of enamel and dentin. Osteogenesis imperfecta is a hereditary disease caused by mutations of genes that produce collagen. A complication of osteogenesis imperfecta that involves the oral cavity in addition to the more generalized effect of fragile bones is a painful dentinogenesis imperfecta-like change in the teeth.

Dysontogenetic Tumors or Tumorlike Conditions

Congenital tumorous lesions of the oral cavity are mainly due to dermoid, epidermoid, or teratoid cysts.

Dermoid cysts are considered the most common form of teratoma and are characterized by a predominance of ectodermal content. The dermoids contain fat or fluid and are usually in the floor of the mouth. Epidermoid cysts usually occur in the sublingual space.

Teratomas involving the tongue are rare. Most cases present at birth with an extremely large mass extruding from the mouth.

Choristomas and mixed hamartomas of the oral cavity are further uncommon lesions that show a variety of clinical presentations, histological appearances, and growth patterns.

Clinical Presentation

Cleft Lip, Palate, and Alveolus Defects

The clinical diagnosis of an orofacial cleft is evident at birth. Clinical problems and manifestations include the risk of aspiration because of communication between the oral and nasal cavities, possible airway obstruction, and potential difficulties in feeding a baby with a cleft and nasal regurgitation.

Developmental Anomalies of the Tongue

When either a diffuse process or a focal mass enlarges the tongue, the tongue may become dysfunctional or obstruct the airway. Thus, airway obstruction may be the basic clinical manifestation of tongue abnormalities. Troubles with eating may also be present.

Thyroglossal duct cysts involving the tongue present as asymptomatic midline lingual masses, although they

may occur off the midline in up to 25% of cases. A carcinoma developing in a thyroglossal duct cyst is very rare, but it may be responsible for an atypical presentation infiltrating surrounding tissues.

A lingual ectopic thyroid gland may manifest with dysphagia, hemorrhage, or airway obstruction. Individuals with ankyloglossia may have speech problems.

Vascular Anomalies

Hemangiomas involving the oral cavity may be asymptomatic but may also manifest clinically with recurrent bleeding, especially if the gingiva or oral mucosa of the soft palate are involved (Fig. 2). The course of these lesions includes a proliferative postnatal growth phase that lasts for 3–9 months, with a gradual involution occurring over 2–6 years. Involution is usually complete by age 7–10 years.

Vascular malformations are by definition present at birth, although in clinical practice 10% may manifest later in the postnatal period.

Lymphangiomas present clinically as soft doughy masses located in the orofacial region. They may manifest intraorally as macroglossia or larger lesions in the mouth floor and can compromise the airway or the skeletal development of involved structures, such as the mandible or maxilla. Venous malformations present in a variety of ways, from a slight blue patch to a recurrent, growing, compressible soft blue mass. Episodic painful thrombosis may also occur. Arterial malformations may present with bleeding.

Developmental Disturbances of the Teeth

There are a number of tooth abnormalities that are not initially clinically evident at birth but are related to development disorders that manifest later on. They may represent not only esthetic problems but also functional disturbances.

Developmental Tooth Structure Disturbances

Dentinogenesis imperfecta causes the teeth to be opalescent and affects both the primary and permanent dentition.

Amelogenesis imperfecta manifests with teeth varying in colors from white opaque to yellow to brown. All teeth are affected, small, and pitted. Teeth have normal pulps and dentin but affected enamel with uneven surfaces. Individuals with amelogenesis imperfecta may be prone to early tooth loss and/or disease of the structures that surround and support the teeth (periodontal disease).

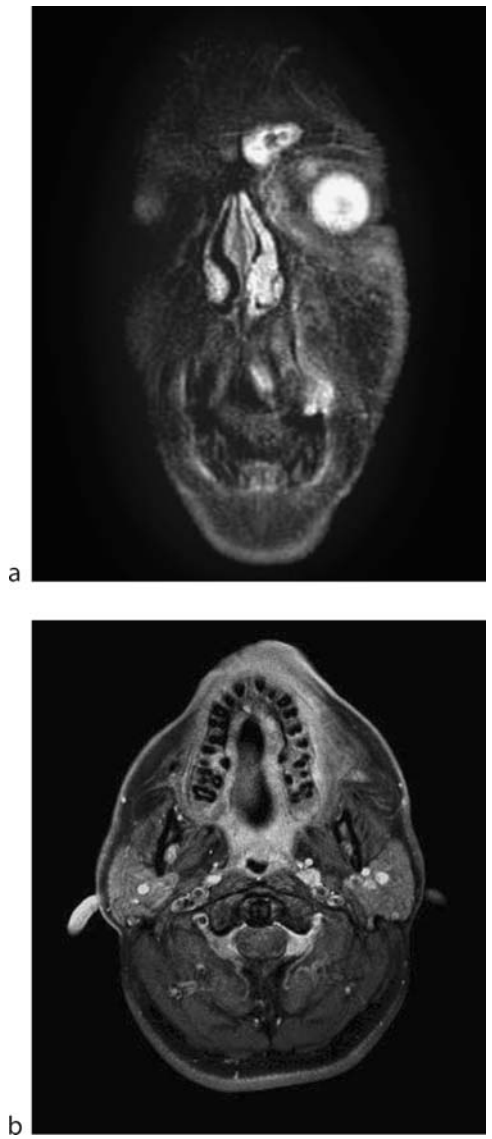

Congenital Malformations, Oral Cavity. Figure 2 Left-sided orofacial hemangioma involving the soft and hard palate on the left. (a) TIRM coronal image at the level of anterior alveolar ridge showing increased signal at the soft palate and gingiva on the left with bone infiltration of the alveolar process marked by high signal intensity. (b) T1-weigthed image after GdDTPA demonstrating diffuse enhancement at the level of the soft-tissue component on the left and the involved alveolar process on the maxilla. Note also the involvement of the upper lip, which was also clinically evident.

Dysontogenetic Tumors or Tumorlike Conditions

Dermoid tumors as a special form of teratoma present as large masses in the floor of the mouth that may compromise the airway.

Imaging

Cleft Lip, Palate, and Alveolus Defects

Cleft lip imaging approaches include ultrasound beyond the second trimester of pregnancy, when the position of the fetal face is located correctly (Fig. 3). Ultrasound diagnosis of cleft palate needs more experience by the examiner to detect atypical movement of the fetal tongue into an open space (cleft) in a lateral view.

Real-time four-dimensional ultrasound has been introduced to prenatal diagnostics of cleft anomalies and may be a useful diagnostic technique in this setting (Fig. 3). Three-dimensional computed tomography (CT) may be useful in preoperative planning in secondary corrections of osseous defects of the hard palate in children.

Developmental Anomalies of the Tongue

Because the tongue is superficially located and presents the initial manifestation of most diseases occurring in the mucosal or lingual surface, these lesions can be easily accessed and diagnosed without imaging analysis. Most congenital lesions of the tongue, however, can manifest as a submucosal bulge and be located in a deep portion of that organ, such as its base. The initial imaging approach is ultrasound. However, the lesions' true characteristics and extent may be recognized only on cross-sectional images such as those obtained by CT or magnetic resonance imaging (MRI).

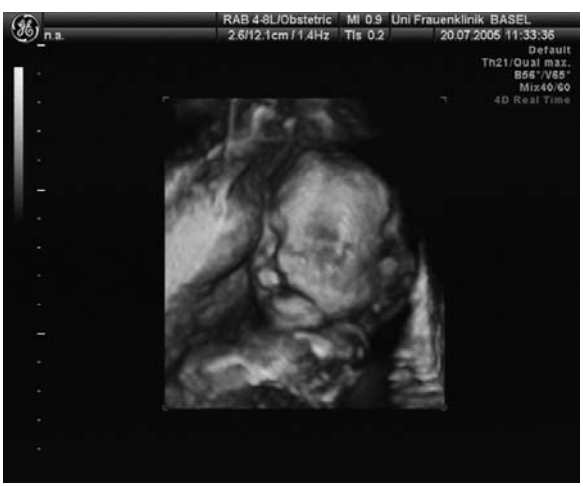

Congenital Malformations, Oral Cavity. Figure 3 Cleft lip palate. Prenatal four-dimensional real-time ultrasound examination showing the right-sided unilateral cleft lip defect clearly. (Image courtesy of PD Dr. S. Tercanli, Department Of Ultrasound, Women's University Clinic, University Hospital Basel)

MRI is superior to CT for evaluating soft tissue lingual lesions. In addition, because it is usually difficult to differentiate congenital lesions from other submucosal neoplasms on the basis of imaging findings alone, clinical history and local examination should be considered when interpreting CT and MR images of the tongue. The imaging work-up of ectopic thyroid gland requires thyroid scintigraphy. For further diagnosis of thyroglossal duct cysts, ultrasound represents the basic imaging method, followed by CT and MRI. Ultrasound findings may show an echoic, homogeneous hypoechoic, solid-appearing, or even heterogeneous midline cervical mass. On MRI the mass may reveal high signal intensity on T2-weighted images and sometimes also on T1-weighted sequences.

Prenatal sonography may be helpful in diagnosing intraoral cystic lesions such as duplication cyst of the tongue. Furthermore, T2-weighted MRI can reveal homogeneous masses that have high signal intensity and variable rings of signal intensity corresponding with mucosa and submucosa in the case of a duplication cyst.

Vascular Anomalies

The predominant sonographic features of cavernous hemangiomas are well-defined hypoechoic mass lesions with heterogeneous echotexture and the presence of cystic and sinusoidal spaces within them, as well as the occasional presence of phleboliths. Color Doppler imaging demonstrates flow inside the mass. MRI is very accurate for detecting hemangiomas, although capillary and cavernous hemangiomas and combined lymphangiohemangioma or lymphatic and venous malformation cannot always be differentiated. They show bright signal on T2-weighted or TIRM sequences (Fig. 2a), low signal on T1-weighted images, and enhance diffusely without distorted dilated venous vessels (Fig. 2b). CT may confirm the infiltration of adjacent bone of the alveolar process of the maxilla.

Lingual venous malformations present on MRI as lobulated masses highly hyperintense on T2-weighted images with respect to normal tongue and slightly hyperintense or isointense on T1-weighted images and/or surrounding muscles. They show a slow and homogeneous filling following intravenous injection of contrast medium. Millimeter-sized hypointense foci and linear hypointense strands are present and may be caused by phleboliths, flow void, or septation.

Lymphangiomas may be documented by ultrasound, CT, or MRI. Ultrasound may show superficial hypoechogenic multioccular cystic masses with septa of variable thickness, but it can fail to demonstrate retropharyngeal, axillary, or mediastinal extensions in all patients. MRI allows better tissue characterization and lesion extent.

Developmental Disturbances of the Teeth

For documentation of developmental disturbances of the teeth, single-tooth radiographs of the suspected anomaly are often adequate. For overall analysis of multiple supernumerary teeth, an orthopantomogram or even CT with three-dimensional reconstructions and dental CT parasagittal reconstructions may be more accurate for therapy planning.

Developmental Tooth Structure Disturbances

Imaging of amelogenesis imperfecta is based on radiographs, including orthopantomogram, palatinal view, and single-tooth images. Radiographically, enamel appears reduced in bulk.

Dysontogenetic Tumors or Tumorlike Conditions

The demonstration of a fat–fluid level on MRI or CT is diagnostic for a dermoid cyst at the mouth floor. Other teratomas or tumorlike conditions are also well delineated by MRI regarding extension and infiltration. CT is superior for detecting calcifications and osseous changes.

Nuclear Medicine

The indications for thyroid scintigraphy pertechnetate using Tc-99m in the setting of congenital disease of the oral cavity include localization of an ectopic thyroid gland and evaluation of a thyroglossal duct cyst to rule out functioning thyroid tissue in other locations.

Diagnosis

Cleft Lip, Palate, and Alveolus Defects

The diagnosis of an orofacial cleft is made based on clinical evidence of the cleft anomaly at birth. Imaging diagnosis using ultrasound allows early detection during pregnancy, especially beyond the second trimester (Fig. 3).

Developmental Anomalies of the Tongue

Because the tongue is superficially located, and the initial manifestation of most diseases occurring there is mucosal change, these lesions can be easily accessed and diagnosed without imaging analysis. However, as previously stated, imaging is necessary to confirm the clinical impression and to delineate lesion extension and characteristics before a surgical or bioptic diagnosis is performed. Because a number of other nonneoplastic and neoplastic lesions can cause cystic midline masses in the neck, fine-needle aspiration may be useful in making a preoperative diagnosis of thyroglossal duct cyst for a more accurate and timely clinical intervention.

Vascular Anomalies

By history and physical examination, 96% of vascular lesions can be classified as hemangiomas or vascular malformations. Knowledge of their natural history and the clinical and imaging presentation is essential for making the diagnosis. Lymphangiomas are the most common soft compressible mass in the orofacial region of children. However, for definite diagnosis a biopsy may be necessary and should be planned based on imaging methods to reduce bleeding risks, especially with associated venous or arterial components.

Dysontogenetic Tumors or Tumorlike Conditions

Surgery with histological evaluation is necessary to establish a diagnosis of dysontogenetic tumors or tumorlike conditions, such as congenital dermoid cyst.

Interventional Radiologic Treatment

Patients with hemangiomas are treated surgically by cryosurgery or laser surgery or conservatively according to lesion size and behavior. In patients with venous malformations, percutaneous sclerotherapy is combined with surgical reduction; patients with arteriovenous malformations undergo transarterial embolization before surgical excision of the nidus.

Lymphangiomas are usually surgically removed. Unfortunately, due to lack of encapsulation, the recurrence rate is high. Alternative treatments include aspiration, percutaneous sclerotherapy, diathermy, and radiation.

Bibliography

1. Eppley BL, van Aalst JA, Robey A et al (2005) The spectrum of orofacial clefting. Plast Reconstr Surg 115:101e–114e
2. Donnelly LF, Jones BV, Strife JL (2000) Imaging of pediatric tongue abnormalities. Am J Roentgenol 175:489–493
3. Mulliken JB, Glowaki J (1982) Hemangiomas and vascular malformations in infants and children: a classification based on endothelial characteristics. Plast Reconstr Surg 69:412–422
4. Lo Casto A, Salerno S, Cannizzaro F et al (2003) MRI findings in lingual venous malformations. Dentomaxillofac Radiol 32:333–336

Congenital Malformations, Orbit

Emanuele Neri, Francesca Cerri, Francesca Turini
Diagnostic and Interventional Radiology, University of Pisa, Pisa, Italy
neri@med.unipi.it

Synonyms

Anophthalmia; coloboma; Cyclopia and synophthalmia; microphthalmos; Septo-optic dysplasia

Definition, Pathology/Histopathology

Anophthalmia, or congenital absence of the eye(s), is a rare, sporadically occurring abnormality usually associated with trisomy syndromes 13–15, Klinefelter's syndrome, and complex craniofacial malformations.

Primary anophthalmia occurs when the optic vesicle does not form. Secondary anophthalmia and congenital cystic eyeball are caused by the same congenital defect: the partial or complete failure of involution of the primary optic vesicle early in the formation of the eye. A small or nonexistent cyst yields the classic appearance of anophthalmia, whereas a large cyst will lead to a congenital cystic eyeball.

Anophthalmia may be difficult to differentiate from severe microphthalmos or orbital hypoplasia. Unlike a child with anophthalmia, a child with microphthalmos, however, has a formed eyeball with lens.

Congenital microphthalmos is a common malformation encountered clinically. Microphthalmos in adults is here defined as eyes of which the axial length is less than 20.4 mm in males and 20.1 mm in females; in children younger than 14 years, it refers to eyes at least three square roots of two-thirds below the mean for age-similar controls.

Although microphthalmos may occur as an isolated event, it is frequently associated with other ocular–orbital abnormalities such as coloboma, glaucoma, cataracts, septo-optic dysplasia, and maternal infections.

Cyclopia and synophthalmia result from total and partial fusion of the optic vesicles, respectively, preventing normal orbital separation.

Cyclopia is the most grotesque developmental abnormality in ophthalmology. The term is commonly used to describe either the abnormality of true cyclopia, in which a single median eye is the only ocular structure present, or synophthalmia, in which two globes are partially fused in a median position. The cause of this malformation is obscure.

Familial occurrence and occurrence in twins and in consanguineous marriages have been documented and would be consistent with a single gene abnormality. However, cyclopia has been produced experimentally in numerous species following exposure to various teratogenic agents, and this has been interpreted as evidence for an environmental cause of cyclopia. In recent years, several isolated case reports of cyclopia in humans have been associated with abnormal chromosomes.

The incidence of the cyclopia/synophthalmia deformity in humans is unknown. By 1963, more than 250 published case reports had been collected. In one hospital, an incidence of approximately 1/40,000 births was reported.

Septo-optic dysplasia is a rare anomaly associated with decreased vision and hypoplasia of the optic nerves. A prominent anterior recess of the third ventricle and a small optic canal are typical. Pituitary insufficiency and absence of or defects in the septum pellucidum are also present. A number of patients with septo-optic dysplasia have schizencephaly and seizures.

Coloboma is a rare congenital abnormality resulting from failure of the embryonic choroid fissure to close properly. It may affect any part of the eye. Morning glory syndrome is a coloboma that affects the optic nerve at the optic disk.

The incidence in the general population, therefore, is probably less than 1/1,000. Typical colobomas are inherited as an autosomal dominant trait, with both variable penetrance (30%) and expression, and they are bilateral in more than 60% of cases. Males and females are affected equally.

A wide variety of environmental agents has been shown to induce the development of coloboma in laboratory animals, but no such association has been proved in humans, although coloboma has been described in a baby whose mother was given thalidomide during pregnancy.

Coloboma at the optic nerve entrance is not uncommon but usually extends to involve a portion of the adjacent retina and choroid. In a relatively small subset of patients, only the proximal part of the fetal cleft fails to close, which results in an isolated defect in the immediate region of the optic disk. Most such colobomas are unilateral, unlike the more extensive defects, although there may be minor cupping of the contralateral optic disk.

Clinical Presentation

The cyclopian deformity is characteristically accompanied by numerous systemic malformations. The infant is small

for estimated age. A microcephalic head has a proboscis over a midline diamond-shaped opening for the single or fused eyes. The ears and mouth are usually of abnormal shape and position. Postaxial hexadactyly may be observed.

At postmortem examination, the forebrain is fused with a single ventricle and a single or absent optic nerve. The olfactory bulbs and tracts are absent, and other cranial nerves may be absent. A significant cardiac abnormality is almost always present (patent foramen ovale, interventricular septal defect, patent ductus arteriosus, dilated atrium or ventricle, or abnormal cardiac valves). The lungs may be atelectatic, edematous, or small. Intestinal lesions range from a small, low-positioned mouth to a high-arched palate; malrotation or Meckel's diverticulum; or a posteriorly located anus. The kidneys may be duplicated, small, polycystic, or hydronephrotic. The data available with these case reports does not permit statistical evaluation of the incidence of specific tissue disorders or of any possible significant differences between the abnormalities present in trisomy D and other different chromosome aberrations, or between trisomy D and the cases with "normal" chromosomes.

A wide variety of clinical findings may be noted at fundoscopic examination of isolated optic nerve head colobomas; they range from slightly increased physiologic cupping to large excavations. The term "morning glory syndrome," first used by Kindler in 1970, refers to the fundoscopic appearance, similar to that of the morning glory flower of the optic nerve head coloboma that involves part of the surrounding retina. There is enlargement and excavation of the optic disk, which has pale glial tissue in its floor and is surrounded by variably pigmented choroid. The remainder of the eye may be normal, but most eyes have associated abnormalities, the most common being microphthalmia and atypical coloboma (i.e., coloboma not originating in the fetal cleft). Other associated abnormalities include optic nerve atrophy, basal (particularly sphenoid) encephalocele, midline craniocerebrofacial clefting, agenesis of the corpus callosum, and many abnormalities not affecting the central nervous system. Vision may be unimpaired or affected by scotomas (blind spots) of varying degree, but blindness is more usual. This leads to strabismus, noted in few patients. Leukokoria may be noted and is important because the differential diagnosis will include retinoblastoma and congenital cataract.

Diagnosis

In most of these syndromes, diagnosis can be made with fetal ultrasound (US). Although the vast majority of these syndromes are exceptionally rare, diagnosis using US cannot be expected without reference values. Eye measurements are easy to obtain and are highly reproducible. Intraocular details such as the lens can also be seen starting from the 22nd week of gestation. In late pregnancy, fetal ocular movements and palpebral movements can be observed. Their significance is not yet established; if there is a relationship between fetal ocular movements and brain maturation, more investigations are clearly needed before fetal ocular movements could be used to assess fetal maturity and development.

Imaging of children with congenital microphthalmos reveals both a small globe and a small, poorly formed orbit. Microphthalmos can be associated with a retrobulbar duplication cyst resulting from a defective closure of the embryonic fissure.

Imaging of children with anophthalmia reveals a poorly formed, shallow orbit with only rudimentary orbital tissue.

The diagnosis of septo-optic dysplasia cannot be made with magnetic resonance (MR) imaging alone. Dysgenesis of the septum is more easily recognized than optic nerve hypoplasia because the chemical shift artifact generated by the interface of orbital fat and the optic nerve obscures the nerve, making accurate assessment of nerve size impossible unless special techniques are used to correct for chemical shift.

In addition, the optic chiasm is difficult to evaluate because its apparent size on MR images is dependent on section thickness, gap, and angle of the chiasm with respect to the plane of the section. Moreover, the intracranial optic nerves, optic chiasm, and optic tracts can be subjectively normal in size on MR images, despite the fact that clinically apparent optic nerve hypoplasia is present.

It appears, therefore, that MR imaging is not sensitive to the small degrees of optic nerve hypoplasia that can be detected clinically. In conclusion, septo-optic dysplasia is a difficult diagnosis to make with MR imaging alone; it requires correlation of the results of ophthalmologic examination with endocrinologic and neuroradiologic studies.

Diagnosis of colobomas is made at fundoscopic examination and is confirmed by imaging, which is indicated to demonstrate the extent of the defect and to exclude associated abnormalities such as those described above. US examination and MR imaging have been suggested as possible modalities. Both techniques, however, require that the patient remain still for relatively long periods with the eyes in a fixed position, as any eye movement will degrade the images obtained and hamper confident interpretation of small scleral defects. For this reason, it is difficult to perform these techniques in children. Also, results of US may be less than satisfactory

due to a variety of technical problems that may make it difficult to image the entire length of the optic nerve. No information is obtained about the brain and the skull base.

MR imaging provides no information that is not readily available with computed tomography (CT), although its lack of ionizing radiation to the eyes is an obvious advantage. The spatial resolution of CT is superior to that of MR imaging, and the inherent contrast between ocular structures and orbital fat permits acquisition of images of excellent quality. Use of the newer fast spin–echo MR imaging sequences, when available, may reduce the overall time required to image the eyes, but the need for multiple sequences, including T1-weighted images, still makes this technique time-consuming. The loud noises produced by the imager during image acquisition cause further difficulties in the sleeping child. CT, with its potential for fast scanning and high resolution is, therefore, presently the technique of choice in children.

Descriptions of the use of CT in diagnosing coloboma are few. These reports describe the findings in several patients with ocular coloboma, but only a small minority confirms the presence of morning glory syndrome at fundoscopic examination. CT findings relate to the extent of the defect. The globe is misshapen, and there is widening of the optic nerve head, which is of water density and is continuous with the vitreous humor. Thinning and eversion of the sclera at the margin of the defect may also be identified. Heterotopic adipose tissue and smooth muscle within the disk have been reported, and these should not be mistaken for tumor. Associated anomalies, including microphthalmos, may be present. CT scans of the brain may demonstrate further associations, including encephalocele and agenesis of the corpus callosum.

Two conditions that may be confused with coloboma at CT are staphyloma at the posterior pole of the globe and microphthalmos with cyst. Staphyloma is an inflammatory condition in which there is localized ectasia of the globe. This is not limited to the inferonasal aspect of the globe, nor does it lead to the classic fundoscopic appearance. Microphthalmos with cyst is a severe malformation of the globe with gross ectasia of the sclera, which results in a cystic structure beside the globe that may be much larger than the globe itself. The important differentiating feature is that the neck of the cyst where it connects with the globe is much smaller than the actual cyst. With thin CT sections confined to the optic nerves, a minimal number of scans will demonstrate the features of optic nerve coloboma. The choroidoscleral defects with cystic expansion of the optic nerve, together with the typical fundoscopic findings, confirm the diagnosis.

References

1. Hopper KD, Sherman JL, Boal DK et al (1992) CT and MR imaging of the pediatric orbit. Radiographics 12:485–503
2. Barkovich AJ, Fram EK, Norman D (1989)Septo-optic dysplasia: MR imaging. Radiology 171(1):189–192
3. Murphy BL, Griffin JF (1994) Optic nerve coloboma (morning glory syndrome): CT finding. Radiology 191:59–61
4. Nippon Ganka Gakkai Zasshi (1994) Microphthalmos and its pathogenic classification. 98(12):1180–2000
5. Benacerraf BR, Frigoletto Jr, Bieber FR (1984)The fetal face: ultrasound examination. Radiology 153:495

Congenital Malformations, Spine and Spinal Cord

Andrea Rossi, Paolo Tortori-Donati
Department of Pediatric Neuroradiology, G. Gaslini Children's Research Hospital, Genoa, Italy
andrearossi@ospedale-gaslini.ge.it

Synonyms

Caudal agenesis—caudal regression; Diastematomyelia—split cord malformation; Lipomyelocele—lipomyeloschisis; Myelocele—myeloschisis; Spinal dysraphism—spina bifida

Definition

Spinal dysraphism is the term used to describe congenital malformations of the spine and spinal cord. Classification of spinal dysraphisms requires a rational correlation of clinical, neuroradiological, and embryological information. Spinal dysraphisms are categorized into open or closed depending on whether the abnormal nervous tissue is exposed to the environment or is covered by the integuments (Table 1).

Spinal dysraphisms are caused by derangements that occur during the three consecutive stages of *gastrulation* (weeks 2–3), *primary neurulation* (weeks 3–4), and *secondary neurulation* (weeks 5–6) (1–5). During gastrulation, the bilaminar embryonic disk, formed by epiblast (future ectoderm) and primitive endoderm, is converted into a trilaminar disk because of formation of an intervening third layer, the mesoderm. Epiblastic cells start migrating toward the primitive streak, a stripe of thickened epiblast composed by totipotential cells, pass inward at the Hensen's node (the cranial termination of the primitive streak), to ingress the interface between the epiblast and the primitive endoderm. Subsequent waves

Congenital Malformations, Spine and Spinal Cord. Table 1 Classification of spinal dysraphisms

Open	Closed				
	With subcutaneous mass		Without subcutaneous mass		
	Lumbosacral	Cervico-thoracic	Simple dysraphic states	Complex dysraphic states	
1. Myelomeningocele	1. Lipomas with dural defect	1. Nonterminal Myelocystocele	1. Intradural lipoma	Disorders of midline notochordal integration	Disorders of segmental notochordal formation
2. Myelocele	1a. Lipomyelomeningocele	2. Meningocele	2. Filar lipoma	1. Diastematomyelia	1. Caudal agenesis
3. Hemimyelomeningocele	1b. Lipomyelocele		3. Tight filum terminale	2. Neurenteric cysts	2. Segmental spinal dysgenesis
4. Hemimyelocele	2. Terminal myelocystocele		4. Persistent terminal ventricle	Dorsal enteric fistula	
	3. Meningocele		5. Dermal sinus		

of epiblastic cells migrating laterally along the interface form the interposed mesoderm, whereas cells migrating along the midline form the notochord, the foundation of the axial skeleton. Establishment of the neural plate under the induction of the notochord marks the onset of primary neurulation on about day 18. Subsequently, the neural plate starts bending, forming paired neural folds that increase in size and approach each other to eventually fuse in the midline to form the neural tube. This process occurs bidirectionally toward the two extremities of the embryo. The cranial extremity of the neural tube (anterior neuropore) closes at day 25, whereas the caudal extremity (posterior neuropore) closes at day 27 or 28. The posterior neuropore corresponds to the 32nd somite, i.e., the future third sacral metamere. The segment of the spine and spinal cord caudad to somite 32 is formed by secondary neurulation. The tail bud, a mass of cells deriving from the caudal portion of the primitive streak, lays down an additional part of the neural tube caudad to the posterior neuropore that undergoes a process of regression, degeneration, and further differentiation, which results in the formation of the tip of the conus medullaris and the filum terminale. The conus medullaris contains a focal expansion of the ependymal canal called terminal ventricle.

Pathology

Myelomeningocele

Myelomeningocele is the principal form of open spinal dysraphism (OSD). In myelomeningocele, the ▶placode herniates, together with the meninges, through a more or less large defect in the midline of the back, typically at a lumbosacral level, and is therefore exposed to the environment. Expansion of the underlying subarachnoid space causes elevation of the surface of the placode above the surface of the skin.

Myelocele

The uncommon myelocele is differentiated from myelomeningoceles by the absence of expansion of the subarachnoid spaces ventrale to the placode. Thus, the placode is flush with the cutaneous surface.

Hemimyelocele and Hemimyelomeningocele

In the setting of a longitudinal cord splitting or diastematomyelia (see later), failure of neurulation of one hemicord produces two additional, very rare forms of OSD, called hemimyelocele and hemimyelomeningocele depending on whether the placode is flush with the skin surface or is elevated.

Lipomyelocele and Lipomyelomeningocele

These are the most common forms of CSD with subcutaneous mass. In both instances, the mass is represented by a lipoma, and the spinal cord is connected to the lipoma at the level of a placode. Differentiation

between the two entities is based on the position of this attachment, the so-called placode–lipoma interface. In lipomyeloceles, the lipomatous tissue creeps into the spinal canal through a posterior bony ▶spina bifida and attaches to the neural placode, i.e., the placode–lipoma interface lies within the spinal canal, whereas in lipomyelomeningoceles, expansion of the subarachnoid spaces pushes the neural placode out of the spinal canal, i.e., the placode–lipoma interface lies outside the spinal canal.

Meningocele

Meningoceles are herniations of a CSF-filled meningeal outpouching through a posterior bony spina bifida. By definition, they do not contain neural elements with the possible exception of redundant nerve roots or the filum terminale.

Myelocystocele

Myelocystoceles are categorized into terminal and nonterminal based on their location along the neuraxis. Terminal myelocystoceles are characterized by herniation of a hydromyelic cavity that involves the terminal portion of the cord into a meningocele. Nonterminal myelocystoceles, either full blown (i.e., containing a hydromyelic cavity) or abortive (i.e., composed of a fibroneural stalk that fans out from the posterior aspect of the spinal cord and crosses a skin-covered meningocele), are located at cervical, thoracic, or high lumbar level.

Intradural and Intramedullary Lipoma

Intradural and intramedullary lipomas are contained within an intact dural sac but are otherwise similar. Large lipomas may displace the cord laterally, resulting in an off midline, flattened, or bumped placode–lipoma interface. In rare instances, lipomas are completely intramedullary.

Filar Lipoma

Filar lipoma is an elementary anomaly of secondary neurulation characterized by a fibrolipomatous thickening of the filum terminale. The incidental finding of fat within the filum terminale in the normal adult population is estimated to be 1.5–5% in unselected MRI studies. In the absence of a ▶tethered cord syndrome (TCS), a fatty filum is therefore considered an anatomic variant.

Tight Filum Terminale

A tight filum terminale is a short, hypertrophic filum that produces tethering and impaired ascent of the conus medullaris. Isolated cases are extremely uncommon, while the abnormality is more frequent in patients with diastematomyelia or dermal sinuses. A low-lying conus medullaris is frequently, albeit not necessarily, associated.

Dermal Sinus

It is an epithelium-lined fistula that extends from the skin surface inward to a variable depth, and sometimes pierces the dura to reach the intradural compartment. The lumbosacral region is the most common location, although cervical, thoracic, and occipital locations are also found. Embryologically, dermal sinus tracts are traditionally believed to result from focal incomplete disjunction of the neuroectoderm from the cutaneous ectoderm.

Persistent Terminal Ventricle

Persistence of the terminal ventricle is embryologically related to preservation of the continuity of the terminal ventricle of secondary neurulation with the central canal of the spinal cord. Differentiation of a persistent terminal ventricle from hydromyelia is based on the location within the conus medullaris immediately above the filum terminale. The size of the cavity usually does not change on follow-up exams.

Diastematomyelia

Diastematomyelia (literally, split cord) refers to a variably elongated separation of the spinal cord in two, usually symmetric halves. There is in fact a continuous spectrum of abnormality ranging all the way between a partially cleft cord contained in a single dural tube at one end, and completely duplicated spinal cord contained within dual dural tubes with an intervening bony spur at the other end. Embryologically, abnormal midline notochordal integration results into a variably elongated segment in which the midline notochord is replaced by two paired notochordal processes separated by intervening primitive streak cells. Each "heminotochord" induces a separate "hemi"-neural plate, which will then neurulate independently to form a "hemi"-neural tube. The resulting malformation essentially depends on the developmental fate of the intervening primitive streak tissue, which is a totipotential tissue capable of differentiating into ecto-, meso-, and endodermal lineages. If this intervening tissue differentiates into cartilage and bone, the two hemicords eventually will be contained into two individual dural sacs separated by an osteocartilaginous spur (type I diastematomyelia). Conversely, if the primitive streak tissue is reabsorbed or only results into a thin fibrous septum, the two hemicords eventually will lie within a single dural tube (type II diastematomyelia).

Caudal Agenesis Syndrome

Caudal agenesis syndrome, also called caudal regression, is a heterogeneous constellation of anomalies that comprise total or partial agenesis of the caudal portion of the spinal column, anal imperforation, genital anomalies, bilateral renal dysplasia or aplasia, pulmonary hypoplasia, and lower limb abnormalities. There is a known association with maternal diabetes mellitus (1% of offspring of diabetic mothers). The degree of vertebral abnormality in CA may range extensively, from isolated agenesis of the coccyx to absence of the sacral, lumbar, and lower thoracic vertebrae. However, the vast majority of these anomalies involve absence of the coccyx and part of, or the whole, sacrum. Caudal agenesis is categorized into two variants depending on the location and shape of the conus medullaris: either high and abrupt (type I) or low and tethered (type II) (23). Embryologically, CA is consistent with abnormal formation of a caudal segment of the notochord and corresponding paraxial mesoderm, resulting in a correspondingly segmental abnormality of neural induction.

Segmental Spinal Dysgenesis

Segmental spinal dysgenesis is defined as the association of (i) segmental agenesis or dysgenesis of the lumbar or thoracolumbar spine; (ii) segmental abnormality of the underlying spinal cord and nerve roots; (iii) congenital paraplegia or paraparesis; and (iv) congenital lower limb deformities. Embryologically, it is related to failure of development of an intermediate segment of the notochord. The spinal cord at level of the abnormality is thoroughly absent, and the bony spine is focally aplastic. As a result, the spine and spinal cord are "cut in two," with resulting acute angle kyphosis.

Clinical Presentation

Because placode ulceration and infection are leading causes of mortality in the untreated newborn, patients with OSDs, including myelomeningoceles, are operated on soon after birth. Unfortunately, surgery cannot restore complete functional recovery, and operated patients usually exhibit a variable association of sensorimotor deficits of the lower extremities, bowel and bladder incontinence, hindbrain dysfunction, hydrocephalus, as well as intellectual and psychological disturbances. Intrauterine myelomeningocele repair has been shown to reduce the incidence of shunt-dependent hydrocephalus and the severity of the Chiari II malformation that is typically associated with OSDs. It is also estimated that 20–40% of individuals with OSDs are allergic to latex. Allergic responses can vary from mild to anaphylaxis, and occur when latex products touch the skin or mucous membranes. Latex-free devices must therefore be used in the MR environment when these patients are studied.

Closed spinal dysraphisms (CSD) are much more heterogeneous than OSDs, and some are not clinically evident at birth. Clinical examination is significantly helpful to restrict the differential diagnosis. A critical factor in this evaluation is the presence of a subcutaneous mass on the patient's back. This will categorize CSDs into those with, and those without, a subcutaneous mass. Affected children usually present with a TCS. TCS includes sensorimotor dysfunction, muscle atrophy, decreased or hyperactive reflexes, urinary incontinence, spastic gait, and orthopedic deformities such as scoliosis or foot and hip deformity. TCS is the main clinical complaint in patients with lipomyeloceles/lipomyelomeningoceles, intradural or filar lipomas, tight filum terminale, diastematomyelia, and caudal agenesis. Several birthmarks are associated with underlying dysraphisms. Among these, focal hirsutism is significantly associated with diastematomyelia. Capillary hemangioma is the least sensitive in predicting underlying malformation, although capillary hemangiomas of the lumbar region are associated with spinal dysraphisms in greater than 10% of cases. Dorsal dimples or ostia can indicate either a dermal sinus or a sacrococcygeal fistula. All fistulas opening above the gluteal crease should be presumed to violate the subarachnoid space until proven otherwise. Conversely, skin pits located within the intergluteal cleft need no further investigation as they are related to simple sacrococcygeal cysts or fistulas. Patients with caudal agenesis may have a rudimentary tail, lower limb abnormalities, or anorectal malformations. Imperforate anus is associated with surgically correctable intradural pathology in at least 10% of patients. Therefore, all patients with imperforate anus should undergo MR imaging studies. Clinically, children with the type I caudal agenesis typically have a stable neurological defect that is due to their "fixed" spinal cord dysplasia, whereas those with the type II will present with a TCS. Patients with segmental spinal dysgenesis typically have a protuberance of bony consistence along their back, corresponding to the apex of a kyphotic gibbus at level of the focal bony aplasia, and are congenitally paraplegic or paraparetic.

Spinal dysraphisms may be part of complex syndromic associations. The OEIS constellation (omphalocele, exstrophy of the cloaca, imperforate anus, and spinal anomalies) can be found in patients with terminal myelocystoceles and caudal agenesis. The latter can also be a part of VACTERL (vertebral abnormality, anal imperforation, cardiac anomalies, tracheoesophageal fistula, renal abnormalities, and limb deformities) and the Currarino triad (partial sacral agenesis, anorectal malformation, and presacral mass: teratoma and/or meningocele).

Imaging

Magnetic resonance imaging (MRI) has greatly ameliorated the diagnosis of these disorders and has enhanced the possibility of earlier and case-tailored treatment, mainly thanks to its multiplanar imaging and tissue characterization capabilities.

Because patients with OSDs (among which myelomeningoceles) are usually operated on soon after birth, only rarely are MRI studies performed prior to surgery. However, preoperative MRI investigation should be performed whenever possible, so as to obtain: (i) anatomic characterization of the various components of the malformation, especially regarding the relationships between the placode and nerve roots; (ii) presurgical evaluation of the entity and morphology of the malformation sequence (hydromyelia, Chiari II malformation, and associated hydrocephalus); and (iii) identification of rare cases with associated cord splitting (hemimyelomeningoceles and hemimyeloceles). MRI of untreated myelomeningoceles shows dehiscence of the subcutaneous fat, fascia, bone, and muscle at level of the spina bifida, and a low position of the spinal cord that forms the dorsal wall of the defect.

On MRI, lipomas are detected as masses that are isointense with subcutaneous fat in all sequences, including those acquired with fat suppression. The appearance of spinal lipomas is variable depending on the presence of dural defects (i.e., lipomyeloceles lipomyelomeningoceles) or absence of them (i.e., intradural and filar lipomas). Lipomyeloceles are characterized by a placode–lipoma interface located within the spinal canal. MRI is the imaging modality of choice to demonstrate both the bony defect and the subcutaneous fat extending into the spinal canal and attaching to the spinal cord. The latter is typically low lying, and the placode–lipoma interface may extend over several vertebral levels. It may be smooth and regular or large and irregular, with stripes of adipose tissue that permeate the spinal cord and penetrate into the ependymal canal. Hydromyelia is usually present in these cases. The size of the spinal canal may be increased in relation to the size of the lipoma, but the size of the subarachnoid space ventral to the cord is consistently normal. Lipomyelomeningoceles may produce a constellation of MRI features and individual cases typically differ from one another because of the variable size of the meningocele and lipoma, as well as the variable orientation of the placode. An archetypal condition in which the placode–lipoma interface lies exactly along the midline is not the rule but, rather, an exception. In most cases, the placode is stretched and rotated eccentrically toward the lipoma on one side, whereas the meningocele develops on the other side. In such an instance, the spinal roots that emerge from the side facing the meningocele have a redundant course and may be at greater risk for damage during surgery, whereas those lying on the side of the lipoma are shorter and cause cord tethering. Unlike with lipomyeloceles, the spinal canal is dilated because of expansion of the ventral subarachnoid spaces. Filar lipomas are detected as hyperintense stripes of adipose tissue with resultant thickening of the filum terminale. Intradural lipomas are larger lipomatous masses that typically connect with an unneurulated spinal cord segment.

In terminal myelocystoceles, MRI shows the terminal portion of the spinal cord that is distended by focal hydromyelia that herniates posteriorly through a wide spina bifida into a meningocele. A subcutaneous lipoma is often associated. Nonterminal myelocystoceles are located along the cervical or thoracolumbar spine; only a thin fibroneurovascular stripe emanating from a limited dorsal myeloschisis and possibly distended by focal hydromyelia enters the meningocele, while the spinal cord remains within the spinal canal. A simple meningocele is detected on MRI as a CSF filled cavity that does not contain the spinal cord. Dehiscence of the subcutaneous fat over the dome of the protruding sac is a common finding to both myelocystoceles and meningoceles.

Diastematomyelia is categorized into two types (see earlier), and a combination of CT and MRI is best suited to evaluate this complex abnormality. In the type I, the radiological hallmark is the osseous or osteocartilaginous septum (the "spur"), which dissects the spinal canal into two separate halves, each containing an independent dural tube, in turn containing a hemicord. Although in the archetypal case the spur connects the vertebral body to the neural arch along a midsagittal plane, "atypical" spurs are common. The spur may course obliquely and may be incomplete, in which case it may originate either from the vertebral body or from the neural arch. In some cases, the spinal canal is divided unequally, resulting in two asymmetric hemicords. There is an indication to CT in order to obtain a three-plane evaluation of the spur for surgical purposes. However, especially in young children, the spur may be mostly cartilaginous, therefore being inadequately visualized on CT; it progressively ossifies as the child grows. MRI is the imaging modality of choice for a thorough investigation of this abnormality. In most cases, the spur is located at the thoracic or lumbar level and lies at the caudal end of the cord splitting. As a consequence, the two hemicords usually surround the spur tightly before fusing with each other to form a normal spinal cord below, whereas rostrally the splitting is much more elongated. Therefore, there is a craniocaudal sequence of partial clefting, complete diastematomyelia within a single dural tube, diastematomyelia with dual dural tubes with intervening spur, and reunion of the two hemicords, an appearance that may recall railway points.

In the type II, there is not an osteocartilaginous spur to divide the spinal canal. As a consequence, there is a single dural tube housing both hemicord. Three variants of diastematomyelia type II exist, i.e., absence of a septum, presence of an intervening fibrous septum, and partial cord splitting. Of these, absence of whatever septum is, by far, the most common. In such case, the diagnosis is relatively straightforward both on correctly placed axial and coronal MRI sequences; on sagittal MR images, the only indicative sign is an apparent thinning of the spinal cord resulting from partial averaging with the intervening subarachnoid space between the two hemicords. A midline, nonrigid, fibrous septum sometimes is detected at surgery; these septa may be identified on axial and coronal T2-weighted images as thin hypointense stripes interposed between the two hemicords. Rare cases of partial cord splitting are characterized by an incomplete separation of the two hemicords, which remain joined by a midline bridge. The conus medullaris is typically low, and there is a strong association with tight filum terminale.

The caudal agenesis syndrome is characterized by a degree of vertebral abnormality that may range extensively, from isolated agenesis of the coccyx to absence of the sacral, lumbar, and lower thoracic vertebrae. However, the vast majority of these anomalies involve absence of the coccyx and part of, or the whole, sacrum. The degree of sacral agenesis may vary, with S1 through S4 present in individual cases. Sacral aplasia may also be asymmetric, with resulting total or subtotal hemisacrum that may, in turn, be unilateral or bilateral. Full appreciation of the heterogeneous spectrum of vertebral malformation requires anteroposterior and lateral X-ray films, which constitute an essential part of the neuroradiological workup. CT may be necessary for clarification of particularly complex conditions. Caudal agenesis is categorized into two variants depending on the location and shape of the conus medullaris: either high and abrupt (type I) or low and tethered (type II).

Bibliography

1. Tortori-Donati P, Rossi A et al (2000) Spinal dysraphism: a review of neuroradiological features with embryological correlations and proposal for a new classification. Neuroradiology 42:471–491
2. Rossi A, Biancheri R, Cama A et al (2004) Imaging in spine and spinal cord malformations. Eur J Radiol 50:177–200
3. Tortori-Donati P, Rossi A, Biancheri A et al (2005) Congenital malformations of the spine and spinal cord. In: Tortori-Donati P (ed) Pediatric Neuroradiology. Heidelberg: Springer Verlag, pp 1539–1596
4. Tortori-Donati P, Cama A, Rosa ML et al (1990) Occult spinal dysraphism: neuroradiological study. Neuroradiology 31:512–522
5. Dias MS, Walker ML (1992) The embryogenesis of complex dysraphic malformations: a disorder of gastrulation? Pediatr Neurosurg 18:229–253

Congenital Malformations, Splenic

F. E. Avni[1], J.-F. Chateil[2]
[1]Department of Medical Imaging, University Clinics of Brussels—Erasme, Brussels, Belgium
[2]Department of Pediatric Imaging, Hospital Pellegrin, Bordeaux, France
favni@ulb.ac.be

Synonyms

Asplenia, polysplenia syndromes; Heterotaxia syndromes, ambiguous situs abdomen; Splenogonadal fusion, wandering spleen

Definitions

A variety of developmental malformations of the spleen may be detected during infancy and childhood (1–3).

- Asplenia: Asplenia is the congenital absence of a spleen. The condition can be isolated or associated with abdominal situs inversus or ▶situs ambiguous and accompanied by congenital heart disease. It is more common in male. In asplenia syndrome, the inferior vena cava (IVC) and the aorta are on the same side. Midgut malrotation, microgastria, and gallbladder duplication may be present.
- Polysplenia: Polysplenia can be isolated or associated with abdominal situs inversus or situs ambiguous and

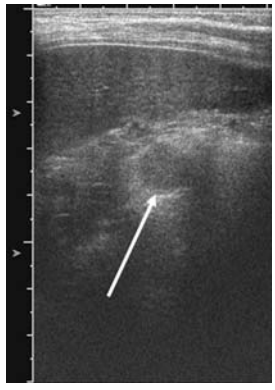

Congenital Malformations, Splenic. Figure 1 Accessory spleen. Incidental finding on ultrasound. Transverse scan of the spleen; the accessory spleen appears as a round well-delineated mass (*arrow*).

accompanied by congenital heart disease. It is more common in females. Polysplenia syndrome includes interruption of the infrahepatic portion of the IVC with azygos continuation, malrotation of the bowel, and absence of gallbladder.

- Splenogonadal fusion: The spleen and/or ectopic splenic tissue may be located anywhere in the abdomen, including attached to the left ovary or within the scrotum, leading to a splenogonadal fusion.
- ►Accessory spleen, cleft notches, and lobules should be considered normal variants.
- In wandering spleen, the ligamentous attachment of the spleen may be lax or absent, leading to an abnormal mobility of the spleen that may undergo torsion.
- True cysts of the spleen may be present in utero and disappear in utero or after birth.
- Lymphangioma and hemangiomas may develop into the spleen. The lesions may be isolated, part of diffuse abdominal disease, or part of syndromes (Klippel Trenaunay Weber, Kasabach–Merritt, Beckwith–Wiedemann, or Turner Syndrome).
- Storage diseases may involve the spleen (►Gaucher disease).

Clinical Presentation

Splenic anomalies by themselves do not produce clinical symptoms unless a mass is present and palpated or unless complications (such as torsion) occur.

Imaging

- *Ultrasound* (*US*): The spleen has a homogeneous pattern, usually hyperechoic compared to the adjacent renal cortex. Its contour is smooth. The technique determines the exact location of the spleen and the presence of accessory glands. Color Doppler evaluation is helpful for evaluation of the vascular anatomy (1, 2). The splenic length measures about 6 cm at 3 months, 7 cm at 12 months, 9 cm at 3 years, and 11 cm at 10 years.
- *Computed tomography* (*CT*): On CT without contrast injection, the spleen appears homogeneous, and its density is around 40 HU. After contrast injection, the helical CT appearance of the spleen depends on the timing of intravenous bolus administration. On early images, the spleen may demonstrate heterogeneous aciform enhancement or a more diffuse pattern that should not be interpreted as disease. This heterogeneity resolves within 70 sec (4).
- *Magnetic resonance* (*MR*) *imaging*: Splenic intensity varies with age in relation with the ratio of white to red blood. In the neonate, before maturation of the lymphoid system and proliferation of white pulp, the spleen is isointense relative to the liver on T1-weighted sequences and isointense to hypointense relative to the liver on T2-weighted sequences. In children older than 8 months, the spleen appears hypointense to the liver on T1-weighted sequences but hyperintense on T2-weighted sequences (5).

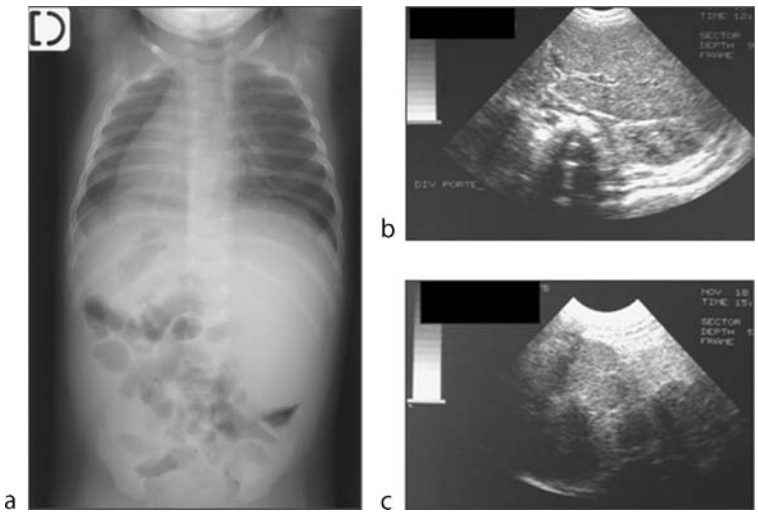

Congenital Malformations, Splenic. Figure 2 Situs inversus and polysplenia. (a) Chest X-ray demonstrating the situs inversus. (b) Ultrasound of the upper left quadrant demonstrating the liver. (c) Ultrasound of the right upper quadrant demonstrating the polysplenia.

Nuclear Medicine

The spleen in normal or abnormal location can be easily identified using Tc99m sulfur-colloid scintigraphy. An accessory or ectopic spleen has imaging characteristics similar to splenic tissue in normal location.

Diagnosis

The diagnosis of splenic anomalies will usually be incidental (Fig. 1), possibly noted on prenatal US examination. Splenic anomalies will be detected on US of the upper abdomen performed as complementary examination in cases of situs inversus or situs ambiguous (Fig. 2).

The spleen is present or absent, unique, or multiple. If absent, nuclear scanning can be done to diagnose ectopic spleen. Isotopic studies can be performed as well in case of splenogonadal fusion.

The diagnosis of a wandering spleen can be suspected on US (Fig. 3). When torsion of a wandering spleen is suspected, CT can be performed to determine the absence of the spleen in its normal location and lack of enhancement of the torsed spleen after contrast injection.

Whenever cystic lesions are demonstrated by US, the differential diagnosis includes benign congenital isolated cyst, ►epidermoid cyst, hydatic cyst, and vascular tumors (lymphangioma, hemangioma).

CT and MR imaging are useful to differentiate between these various diagnoses by showing calcifications, daughter cysts, septa, or abnormal enhancement. In doubtful cases, surgery and histology will be necessary to obtain a definitive diagnosis (3–5).

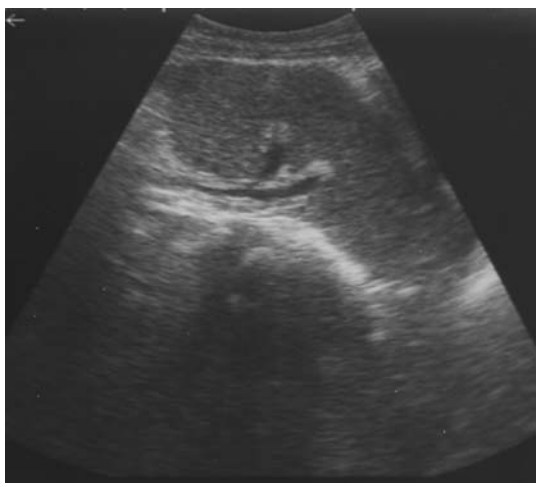

Congenital Malformations, Splenic. Figure 3 Noncomplicated wandering spleen. Ultrasound of the hypogastric area demonstrating a solid mass corresponding to the unattached spleen.

Bibliography

1. Patterson A, Frush DP, Donnelly LF et al (1999) Pattern-oriented approach to splenic imaging in infants and children. Radiographics 19:1465–1485
2. Benya EC (2000) Splenic imaging in infancy and childhood. JBR-BTR 83:217–219
3. Applegate KE, Goska MJ, Pierce G et al (1999) Situs revisited: imaging of heterotaxy syndrome. Radiographics 19:837–852
4. Freeman JL, Kafri ZH, Roberts JL et al (1993) CT of congenital and acquired abnormalities of the spleen. Radiographics 13:597–610
5. Donnelly LF, Emery KH, Bove KE et al (1996) Normal changes in the MR appearances of the spleen during early childhood. Am J Roentgenol 166:635–639

Congenital Malformations, Temporal Bone

Gabriele A. Krombach
Department of Radiology, University Hospital, Aachen, Germany
krombach@rad.rwth-aachen.de

Definitions

Congenital malformations are defined as deviations from the normal anatomical development that lead to functional disorders. They must be differentiated from anatomical variations, which do not cause functional deficiencies and occur more frequently. Congenital malformations can be nongenetic (transplacental) or genetic. In the latter case they may be isolated or syndromal.

Malformations can be classified according to the anatomical structures involved.

Pathology/Histopathology

With respect to the observation that there is a striking resemblance between the various morphological patterns and the stages of inner ear embryogenesis, it has been suggested that malformations result from an arrest of development at a particular stage. Combined malformations of the inner ear and the middle ear with the external ear are rare, since both evolve from mutually independent embryonic origins, namely, from the ectodermal neural crest and the first pharyngeal pouch, respectively.

The bony labyrinth develops between the 4th and 8th week of gestation, grows from the 8th to the 16th week, and ossifies from the 16th to 24th week. The development of the sensory epithelium proceeds until the 25th week. Malformations of the inner ear structures are due to insults between the 4th and 8th week, whereas later injuries affect the sensory epithelium. Owing to these time windows, the majority of patients with sensorineural hearing loss (SNHL) have defects limited to the membranous labyrinth beyond the resolution of the current imaging techniques. Only 20% of patients with congenital hearing loss have anomalies visible on cross sectional imaging.

Microtia, Stenosis, or Atresia of the External Auditory Canal

Microtia indicates a small, abnormally shaped or absent external ear. In approximately 90% of patients it is unilateral. Stenosis (diameter of the external auditory canal 4 mm or less) or atresia of the external auditory canal can be associated with deformities of the middle ear. Microtia is usually divided into four grades: Grade I is a small ear with identifiable structures and a present external auditory canal. Grade II is a partial or hemiear with a stenotic external auditory canal. Grade III is a rudimentary soft tissue structure and atresia of the external ear canal. Grade IV represents absence of the ear, atresia of the external auditory canal, and underdevelopment of the middle ear and deformity of the malleolus and incus.

An *in utero* insult is presumed to cause this malformation. The epithelial cells of the first branchial groove fail to split and canalize, which results in atresia of the external auditory canal.

Ossicular Abnormalities

Congenital abnormalities of the ossicular chain are classified as follows: Class I is the isolated stapedial ankylosis; Class II is the stapedial ankylosis with other ossicular anomalies; Class III is the ossicular anomalies with a mobile stapes; Class IV is the dysplasia of the oval and/or round window.

Nonunion of the incus and stapes is the most common isolated ossicular abnormality and is a result of defects of the long process of the incus.

Oval Window Atresia

The absent cleavage plane between the lateral semicircular canal and the cochlear promontory is associated with a deformed stapes.

Oval window atresia is due to failure of fusion of the primitive stapes with the footplate. If the annular ligament only does not develop, congenital stapes fixation results.

Congenital Cholesteatoma

A cholesteatoma located behind the intact tympanic membrane in a patient with no history of otitis media is presumed to be congenital. Within the temporal bone, it can occur at the petrous apex, mastoid, or middle ear.

Embryonic debris, that is, aberrant epithelial rests of exfoliated keratin within the stratified squamous epithelium, left at the time of closure of the neural tube, can give rise to congenital cholesteatoma.

Michel Aplasia

Michel aplasia is the complete absence of the entire inner ear.

Malformations of the cochlea best demonstrate the "arrest theory," since the distinct anatomical patterns show a remarkable similarity to the appearance of the inner ear at the consecutive stages of embryogenesis. Michel aplasia is the consequence of an arrest of otic placode development in the third gestational week. This extreme form of malformation is very rare and represents less than 1% of inner ear malformations.

Common Cavity Deformity

The common cavity deformity is a single cavity, created from the cochlea and vestibule without the presence of internal architecture.

Arrest of inner ear development between the 4th and 5th week of gestation causes common cavity deformity. At this time, the otic placode has differentiated into the otocyst, but the primordia of the cochlea, vestibule, and semicircular canals have not yet been formed.

Cochlear Aplasia and Cochlear Hypoplasia

In cochlear aplasia the cochlea is absent, whereas in cochlear hypoplasia the cochlea consists of a single turn or less. In both conditions, the vestibule and semicircular canals are present.

An arrest in the development of the cochlear bud during the 5th week of gestation causes cochlear aplasia. Cochlear hypoplasia is due to an arrest during the 6th week.

Mondini Deformity

The cochlea has only 1.5 turns, due to fusion of the middle and apical turns of the cochlea. The osseous spiral lamina and the interscalar septum are missing.

The arrest of inner ear development during the 7th week of gestation causes Mondini deformity. In 20% of patients, it is associated with malformations of the vestibule, semicircular canals, or endolymphatic duct and sac.

Semicircular Canal Aplasia and Dysplasia

This entity refers to partial or complete lack of the development of one or all semicircular canals.

The lateral semicircular canal forms after the superior and posterior semicircular canals have already been formed, between the 6th and 8th week of gestation. The mildest and most common malformation of the inner ear is caused by a late interruption of development and presents as an enlargement of the lateral semicircular canal and the vestibule (Fig. 2a). If development is interrupted at an earlier stage, all three semicircular canals are affected.

Large Vestibular Aqueduct Syndrome

Large vestibular aqueduct syndrome (LVAS) is present if the diameter of the vestibular aqueduct is smaller than 1.5 mm, measured in the middle of the aqueduct (between the common crus and the external aperture). Associated inner ear abnormalities are identified in 60% of the patients, and usually all patients have deficiencies in the modiolus.

LVAS is the most common abnormality in children with SNHL. It results from an arrest of inner ear development in the 7th week of fetal development and follows an autosomal recessive inheritance. There is a female to male predominance of 3:2.

Several mechanisms have been proposed to explain the slow increase of SHNL. Direct transmission of intracranial pressure *via* the vestibular aqueduct to the cochlea can explain deterioration after minor head trauma or barometric pressure changes. Second, accumulation of toxic metabolites in the endolymph might result from dysfunction of the endolymphatic sac and cause cell damage. Third, reflux of hyperosmolar fluid from the endolymphatic sac into the inner ear may cause injury of the cochlear cells. Accordingly, patients with LVAS must be advised to avoid contact sports and scuba diving. They may also benefit from a low-salt diet. In end-stage disease, cochlear implantation is necessary.

Aplasia and Hypoplasia of the Vestibulocochlear Nerve

The normal four nerve branches in the internal auditory canal are lacking.

The internal auditory canal is created by inhibition of cartilage formation at the medial aspect of the otic vesicle in the 9th week of gestation and requires the presence of a vestibulocochlear nerve. The size of the cochlear nerve directly depends on the number of spiral ganglion cells. If the eighth cranial nerve is aplastic, the internal auditory canal will obtain a caliber that depends on the size of the seventh cranial nerve.

Vascular Variants

An aberrant internal carotid artery enters the posterior middle ear cavity and runs along the promontory.

Partial persistence of the stapedial artery represents the intratympanic origin of the middle meningeal artery. It originates from the internal carotid artery between the vertical and horizontal part of the carotid canal, enters the middle ear anteroinferiorly, runs along the promontory, passes between the crura of the stapes, and enters the facial canal. At the level of the first genu, it leaves the facial canal and enters the middle cranial fossa.

Aberrant internal carotid artery: Because of absence of the cervical part of the internal carotid artery and subsequent absence of the vertical part of the bony carotid canal, the tympanic branch of the ascending pharyngeal artery serves as collateral to the horizontal part of the internal carotid artery. Apparently, the vertical segment of the carotid artery enters the temporal bone through the enlarged inferior tympanic canaliculus.

Partial persistence of the stapedial artery: The stapedial artery fails to involute during the third fetal month, so that the developing vessels have to change their course.

Clinical Presentation

Microtia, Stenosis or Atresia of the External Auditory Canal

Conductive hearing loss is the leading symptom in patients with grade II–IV microtia. Up to 90% of patients with stenosis of the external auditory canal develop cholesteatoma as young adults.

Ossicular Abnormalities and Oval Window Atresia

Patients present with congenital conductive hearing loss.

Congenital Cholesteatoma

The most striking finding is a white mass behind an intact tympanic membrane in a young patient with conductive hearing loss. Symptoms depend on the location of the mass if it is not located in the middle ear.

Michel Aplasia, Common Cavity Deformity, and Cochlear Aplasia

Patients present with sensorineural deafness from birth.

Cochlear Hypoplasia

Patients present with a hearing deficit. The severity depends on the degree of membranous labyrinthine development.

Semicircular Canal Aplasia and Dysplasia

If isolated, malformation of the semicircular canals might be asymptomatic.

Mondini Deformity

Mondini deformity is characterized by a low-frequency hearing deficit, due to fusion of the middle and apical turns of the cochlea. High-frequency hearing usually persists to a variable degree.

Large Vestibular Aqueduct Syndrome

The leading symptom is SNHL, which is moderate in early childhood, but gradually deteriorates over a period of years. Usually SNHL deteriorates to profound sensorineural deafness after apparently minor head trauma or sudden changes in barometric pressure.

Aplasia and Hypoplasia of the Vestibulocochlear Nerve

The leading symptom is deafness from birth without change.

Vascular Variants

Aberrant internal carotid artery: Objective or subjective pulsatile tinnitus and conductive hearing loss are common symptoms of an aberrant internal carotid artery. On otoscopy there is a retrotympanic mass that mimics paraganglioma. Biopsy or operation must at all costs be avoided, since it may end disastrously.

Partial persistence of the stapedial artery: Most patients are asymptomatic. In rare cases, pulsatile tinnitus may be present.

Imaging

In general, the history (young age at initial presentation, congenital symptoms) will raise the suspicion of a congenital malformation. High-resolution (HR) thin-slice (1 mm) CT is the imaging technique of choice for patients with suspected congenital malformations of the temporal bone, since it delineates the middle ear and the inner ear. However, neural structures and the fluid-filled labyrinth are only accessible with T2-weighted HR MRI.

Microtia, Stenosis, or Atresia of the External Auditory Canal

CT shows the extent of the malformation with respect to the middle ear (Fig. 1) and provides a roadmap for surgical reconstruction.

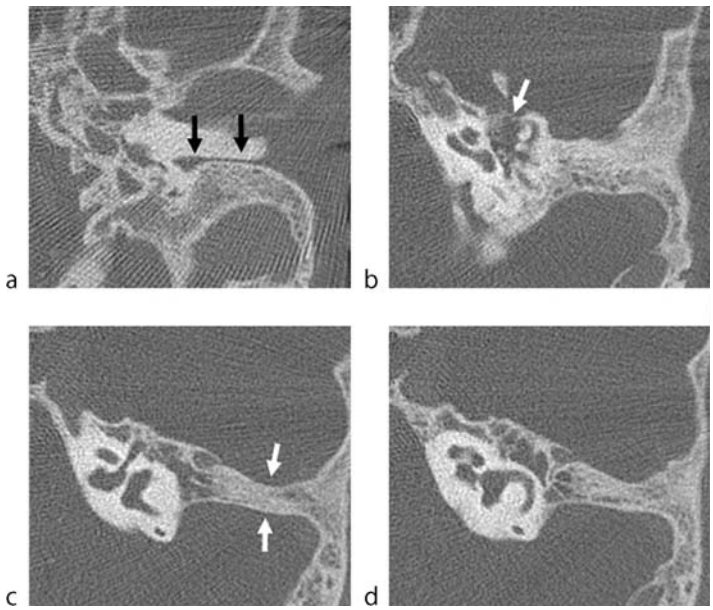

Congenital Malformations, Temporal Bone. Figure 1 Axial HRCT images from a patient with Crouzon syndrome. Stenosis of the external auditory canal is demonstrated (a, *black arrows*). Middle ear opacification is present, due to cholesteatoma (b, *arrow*). The temporal bone itself is small (c, *arrows*), and the inner ear is located near the apex of the temporal bone (d).

Ossicular Abnormalities

HRCT in the axial and coronal plane is required for assessment of the extent of deformities of the ossicular chain.

Oval Window Atresia

HRCT shows the obliteration of the oval window, which is best appreciated in the coronal plane. However, in congenital stapes fixation, which is characterized by absent annular ligament, imaging findings are normal.

Congenital Cholesteatoma

Congenital cholesteatomas of the middle ear present as well-circumscribed masses. The tympanic membrane is intact and the mastoid is well pneumatized. CT without administration of contrast medium is the imaging modality of choice. If glomus tympanicum tumor or facial nerve schwannoma are within the differential diagnosis, contrast enhanced T1-weighted MR images, where congenital cholesteatoma shows a rim enhancement, may be considered.

Michel Aplasia

HRCT demonstrates absence of the cochlea, vestibule, and semicircular canals. The lateral wall of the otic capsule is flat. T2-weighted MR images also do not show inner ear structures; however, complete fibrous or osseous obliteration of the labyrinth is a differential diagnosis in MRI. CT clearly reveals the diagnosis, since in osseous obliteration of the labyrinth, the labyrinthine structures are usually seen with a faded appearance and the lateral wall of the otic capsule is convex, while in Michel aplasia the lateral wall of the inner ear remnant is flat.

Common Cavity Deformity

CT and T2-weighted MRI show a cystic cavity that represents the cochlea and vestibule (Fig. 2a, b). The semicircular canals are absent.

Cochlear Aplasia and Cochlear Hypoplasia

The cochlea is missing (aplasia) or it consists of a single turn or less (hypoplasia). The vestibule and the semicircular canals can be delineated but might be hypoplastic.

Mondini Deformity

The basal turn of the cochlea is normal, whereas the middle and apical turns are fused (Fig. 2c).

Semicircular Canal Aplasia and Dysplasia

Most commonly, the semicircular canals are short and wide (Fig. 2d). They may also be absent or appear as small protrusions in more severe cases.

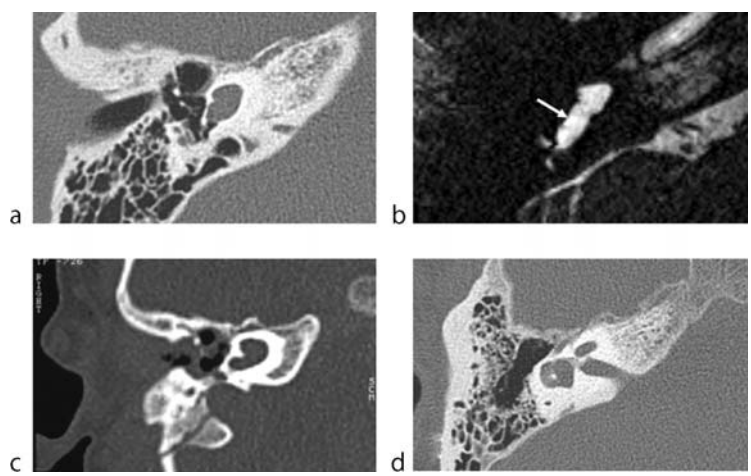

Congenital Malformations, Temporal Bone. Figure 2 Malformations of the inner ear: common cavity deformity (a and b): The axial HRCT image (a) and axial T2-weighted MR image (b) show a cystic cavity (*arrow*, b); Mondini malformation (c). The CT image shows the basal turn, whereas the middle and apical turn are fused. Dysplasia of the lateral semicircular canal. The axial CT image demonstrates the dilated lateral semicircular canal (d).

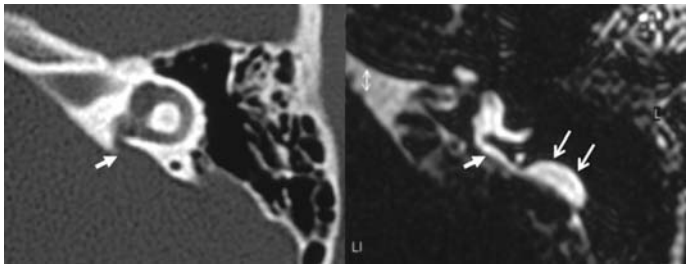

Congenital Malformations, Temporal Bone. Figure 3 Large vestibular aqueduct. The enlarged vestibular aqueduct is visible on the axial CT image (left image, *arrow*) and the axial T2-weighted MR image (right image, *closed arrow*). Only the MR image demonstrates the enlarged endolymphatic sac (*open arrows*).

Large Vestibular Aqueduct Syndrome

Axial HRCT slices show the enlargement of the vestibular aqueduct. Axial T2-weighted MR images demonstrate the enlarged endolymphatic duct within the bony canal and the endolymphatic sac (Fig. 3).

Aplasia and Hypoplasia of the Vestibulocochlear Nerve

HR T2-weighted MRI demonstrates hypoplastic nerves and the narrow internal auditory canal. CT can only show the narrow canal.

Vascular Variants

Aberrant internal carotid artery: CT or MR angiography shows the course of the carotid artery. The vertical part of the carotid canal is missing.

Partial persistence of the stapedial artery: Absent foramen spinosum and enlargement of anterior tympanic facial nerve canal on CT.

Nuclear Medicine

Nuclear medicine is not applied in congenital malformations of the temporal bone.

Diagnosis

Diagnosis of congenital malformations is based on the clinical findings. Congenital conductive hearing loss should raise the suspicion of ossicular abnormalities or oval window atresia. In patients with congenital cholesteatoma, otoscopy shows a white mass behind the intact tympanic membrane. CT shows the extent of the cholesteatoma and possible involvement of the ossicular chain. In patients with SNHL, CT demonstrates the degree of cochlear development. In patients with hypoplasia or aplasia of the vestibulocochlear nerve, sensorineural deafness may raise the suspicion, whereas T2-weighted MRT demonstrates hypoplasia of the nerve. If a very small nerve is present, transtympanic stimulation of the promontory or intracochlear stimulation may be helpful for differentiation between aplasia and hypoplasia.

Bibliography

1. Jackler RK, Luxford WM, House WF (1987) Congenital malformations of the inner ear: a classification based on embryogenesis. Laryngoscope 97(3 Pt 2 Suppl 40):2–14
2. Bamiou DE, Phelps P, Sirimanna T (2000) Temporal bone computed tomography findings in bilateral sensorineural hearing loss. Arch Dis Child 82(3):257–260
3. Casselman JW, Kuhweide R, Ampe W, et al (1996) Inner ear malformations in patients with sensorineural hearing loss: detection with gradient-echo (3DFT-CISS) MRI. Neuroradiology 38(3):278–286
4. Koesling S, Kunkel P, Schul T (2005) Vascular anomalies, sutures and small canals of the temporal bone on axial CT. Eur J Radiol 54(3):335–343

Congenital Malformations, Thymus

Gundula Staatz
Department of Radiology, Division of Radiology
University of Erlangen–Nürnberg, Loschgestr. 15
91054 Erlangen
gu.stz.uni-erlangen@t-online.de

Synonyms

DiGeorge syndrome; Thymus aplasia

Definitions

Congenital malformations of the thymus are rare and include thymus aplasia or hypoplasia, ►ectopic thymus and thymic cysts. *Thymic aplasia or hypoplasia* is defined as an absent or very small thymus, due to an abnormal development of the third and fourth branchial arches encountered in certain immunologic disorders. An absent thymus is most commonly associated with ►*DiGeorge Syndrome*, which is defined as an immunologic disorder characterized by dysmorphic facies, hypoparathyroidism, congenital heart defects and a deficiency in cell-mediated immunity. *Ectopic thymus* is characterized by an aberrant migration of thymic tissue in the superior and posterior mediastinum, bases of the skull, tracheal bifurcation or the cervical region. Ectopic thymus is most frequently located in the cervical region, where it may present as a solid or cystic (*thymus cyst*) mass.

Pathology/Histopathology

Biopsy of the thymus in DiGeorge syndrome reveals no specific histopathologic findings with exception of evidence for thymic hypoplasia. Aberrant cervical thymic tissue histologically contains thymic lobules, lymphoid follicles, Hassell corpuscles, and cysts (1). The cysts can be small or quite large and are lined by a variety of cell types, including non-keratinising squamous, cuboidal, or columnar cells. Cyst contents range from straw-coloured proteinaceous fluid to necrotic debris or old haemorrhage. Cholesterol crystals may be found in the luminal fluid or embedded in the cyst wall. Occasionally parathyroid tissue (also derived from the third pharyngeal pouch) is found in the lesions (1).

Clinical Presentation

The clinical presentation of children with DiGeorge syndrome is primarily characterized by cardiac anomalies, such as tetralogy of Fallot, ventricular septal defect, interrupted aortic arch, pulmonary atresia or truncus arteriosus (2). Arhinencephaly, cleft lip, palate, or uvula, diaphragmatic abnormalities, hydronephrosis, malrotation of the gut and imperforate anus are other anomalies found in DiGeorge syndrome. Hypocalcaemia due to hypoparathyroidism usually begins in the neonatal period and may present with tetany or tonic convulsions. Due to T-cell dysfunction recurrent viral and fungal infections as well as mycobacterial and *Pneumocystis carinii* infections are observed. Ectopic thymus may present as a cervical palpable mass, because it is often located along the anterior border of the sternocleidomastoid muscle lateral to the thyroid gland and near the carotid sheath.

Imaging

The thymus gland can be visualised with use of ultrasound, radiography, CT, MRI and nuclear medicine.

Ultrasound is the modality of first choice for the evaluation of thymic malformations. In fetuses with congenital heart defects, particularly conotruncal anomalies, fetal echocardiography is reliable in diagnosing thymic hypoplasia or aplasia (3). In children below the age of 1 year the incomplete ossification of the sternum and its manubrium provides a comfortable access to the anterior mediastinum, in older children ultrasound of the thymus is performed *via* the jugulum or with use of a parasternal access. Ultrasound is also a reliable tool for the diagnosis of ectopic thymus, especially when the aberrant thymic tissue is located in the neck.

On radiographs the appearance of the thymus is evaluated by the size, configuration and density of the anterior mediastinum.

Computed tomography is a most valuable method for the cross-sectional evaluation of the mediastinum in children, however, because of ionizing radiation, MR imaging is the method of choice for further assessment of thymic malformations beyond ultrasound.

Nuclear Medicine

Fluorine-18 fluorodeoxyglucose (FDG) positron emission tomography (PET) is established as an important diagnostic tool for the diagnosis, staging, and restaging of neoplasms in the mediastinum (4). It plays no role for the assessment of congenital thymic malformations.

Diagnosis

The size and shape of the normal thymus varies considerably with age. In children under 5 years of age, the thymus has a quadrilateral shape with convex lateral contours and gentle undulating borders. In older children and adolescents the thymus shows a triangular configuration with straight lateral margins (5). On chest X-rays the normal thymus presents as a bilateral smoothly outlined mediastinal mass, and particularly on the right side, a characteristic sail-like shadow with a well-defined lateral and inferior margin is often visible (Fig. 1). An absent thymic shadow on the chest X-rays of newborns is

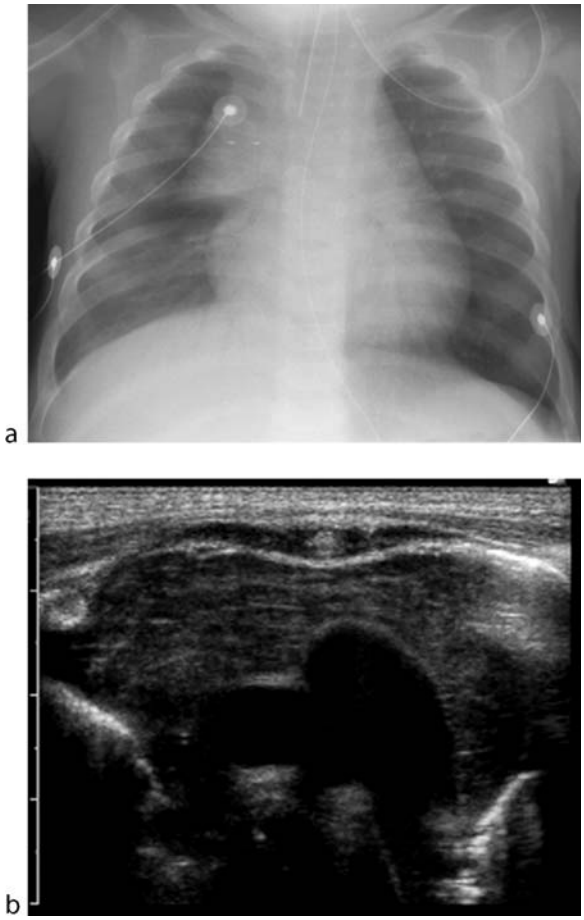

Congenital Malformations, Thymus. Figure 1 (a) Chest radiograph of an intubated neonate from the ICU. Typical sail-like appearance of the right lateral shadow of the thymus with smooth and well-defined margins. (b) US of a normal structured, slightly large thymus in a neonate

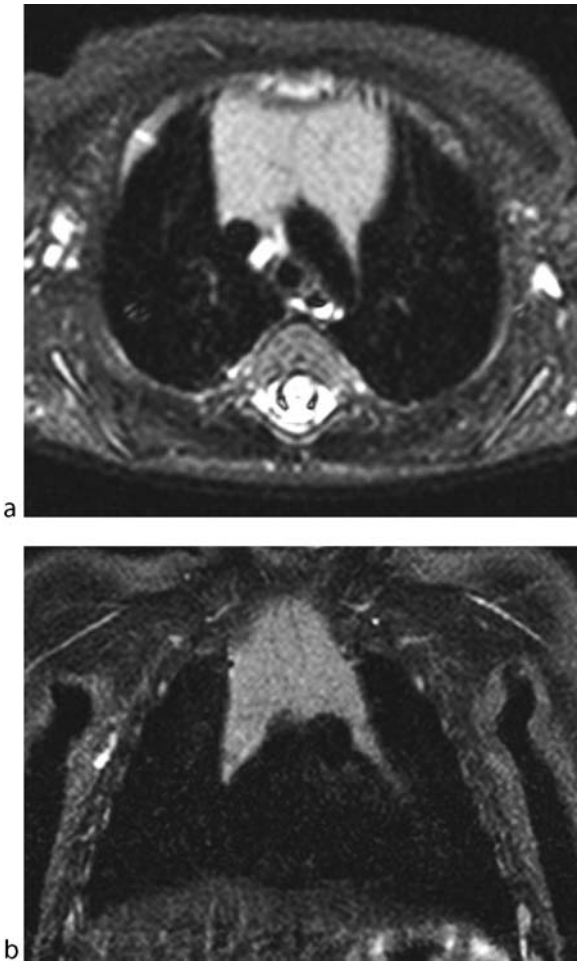

Congenital Malformations, Thymus. Figure 2 Axial (a) and coronal (b) T2-weighted fat-suppressed MR-images of the chest in a 3-month-old girl. The quadrilateral shape of the thymus and the hyperintense signal intensity on T2 weighted images, characteristic for this age group, is demonstrated.

suspicious of thymus hypoplasia or aplasia but the diagnosis has to be confirmed by ultrasound or with MR imaging. On CT images, the normal thymus shows homogenous soft tissue attenuation, with the highest density during infancy, and a homogenous contrast enhancement after intravenous contrast material administration. On MRI, the thymus appears with a signal intensity slightly greater than that of muscle on T1-weighted images, and with a high signal on T2-weighted images (Fig. 2). DiGeorge syndrome is diagnosed by the assessment of the immune system (T-cell function), parathyroid function (parathyroid hormone, PTH) levels, chromosome analysis (microdeletion of 22q11.2), and imaging studies (thymus hypoplasia/aplasia). The diagnosis of aberrant thymus is based on the similar imaging appearance compared to normal thymus. Aberrant thymic tissue may be solid, cystic, or mixed. Cystic lesions are most common and third branchial cleft cysts, lymphangiomas, venous malformations, necrotic or suppurative lymphadenopathy, thyroglossal duct cysts, and epidermoid and dermoid cysts have to be considered as differential diagnosis (1).

Bibliography

1. Cure JK, Tagge EP, Richardson MS et al (1995) MR of cystic aberrant cervical thymus. AJNR Am J Neuroradiol 16:1124–1127
2. Conley ME, Beckwith JB, Mancer JF et al (1979) The spectrum of the DiGeorge syndrome. J Pediatr 94:883–890
3. Chaoui R, Kalache KD, Heling KS et al (2002) Absent or hypoplastic thymus on ultrasound: a marker for deletion 22q11.2 in fetal cardiac defects. Ultrasound Obstet Gynecol 20:546–552
4. Ferdinand B, Gupta P, Kramer EL (2004) Spectrum of thymic uptake at 18F-FDG PET. Radiographics 24:1611–1616
5. Siegel MJ, Glazer HS, Wiener JI et al (1989) Normal and abnormal thymus in childhood: MR imaging. Radiology 172:367–371

Congenital Malformations, Thyroid, and Functional Disorders

Arthur Rosemary
Department of Pediatric Radiology Leeds General Infirmary, Clarendon Wing, Leeds, UK
r.arthur@ukonline.co.uk

Synonyms

Cretinism; Goitre; Grave's disease; Myxoedema

Definition

Congenital disorders of the thyroid gland are developmental disorders, which may present at birth or later in life as a result of abnormal development of the thyroid gland or to inborn errors of metabolism resulting in abnormal hormone production.

Functional disorders of the thyroid gland refer to conditions associated with abnormal production (increased or decreased) or an abnormal somatic response to thyroid hormone or thyrotropin (TSH) and may be the result of a congenital abnormality or be acquired later in childhood.

Pathology and Histology

Development and Hormonogenesis

The thyroid gland develops during the third week of foetal life as a midline outpouching from the floor of the pharynx. During descent into the neck the thyroid gland maintains a connection, the thyroglossal duct, with the base of the tongue until it is obliterated at approximately the seventh intra-uterine week.

During hormonogenesis under the influence of pituitary TSH, thyroid hormone is synthesised by a complex process, where iodine is concentrated from the blood into the follicular cells, oxidised and bound in an organic form to thyroglobulin to produce T3 and T4, the main thyroid hormones. The foetus depends upon low levels of a transplacental maternal thyroid hormone until significant thyroid hormone production begins at about 20 weeks of gestation. Following birth there is a sudden rise in TSH, T4 and T3, followed by a slow progressive fall in childhood to adult levels.

Although thyroid hormone has a number of actions, e.g. thermogenesis, ion transport, and metabolism of amino acids throughout life, it has several unique properties in childhood, being essential for the normal development and maturation of the brain and skeleton. Table 1 indicates the range of thyroid disorders occurring in childhood and the most important congenital and functional disorders will be discussed later.

Congenital Abnormalities

Failure of normal development of the thyroid gland results in *partial or complete agenesis* of one or both lobes, whereas interruption to the normal descent of the thyroid gland will result in the development of *ectopic thyroid tissue* and *thyroglossal duct cysts* (TDC).

Ectopic thyroid tissue maybe found anywhere along the normal descent pathway and maybe found as low as the anterior mediastinum, although a sublingual position is the most common site. Ectopic thyroid tissue is usually associated with a significant degree of hypothyroidism often having poor function, but may enlarge due to compensatory TSH stimulation.

TDC arise from failure of obliteration of the thyroglossal duct in the foetus. They are usually solitary and occur anywhere from the foramen caecum at the base of the tongue to the thyroid gland. Approximately 20% occur above the hyoid bone. In most cases a TDC is

Congenital Malformations, Thyroid, and Functional Disorders. Table 1 Thyroid disorders in children

Congenital
▶Thyroglossal duct cyst
Thyroid dysgenesis
Functional
Hypothyroidism
Congenital hypothyroidism (CH)
Chronic lymphocytic thyroiditis (CLT)
Iodine deficiency
Secondary hypothyroidism (e.g. pituitary disorders)
Hyperthyroidism
Neonatal
Diffuse toxic goitre—Grave's disease
TSH-induced hyperthyroidism
Thyrotoxicosis without hyperthyroidism
Euthyroid
Goitre
Neoplasia
Benign nodules
Adenomas
Cysts
Malignant nodules
Carcinoma—papillary 70%
Lymphoma
Infection
Thyroiditis—pyriform sinus abnormality

present in conjunction with a normally sited and functioning thyroid gland, although in fewer than 5% of TDC, the cyst may contain the only functioning thyroid tissue in the individual.

Clinical Presentation

The clinical presentation dsepends on the underlying condition and usually reflects either a hormonal disorder or consequences of mass effect. Beside the clinical examination, laboratory investigations are essential. Biochemical tests are fundamental in the evaluation of all babies and children with a suspected thyroid abnormality (1). Serum TSH, T3, T4, free T3 and free T4 levels being most important to diagnosis and the results must be related to normal values for age. More complex investigations may be necessary including the identification of TSH receptor antibodies, cytogenetic testing and biochemical investigations to determine the nature of any inborn error of metabolism, thyroid antibody, other autoimmune antibody tests and pituitary function and TRH testing. Screening programmes for congenital hypothyroidism are based on the detection of low levels of thyroxine, and or high levels of TSH in cord blood or a dried blood spot from a heel prick. Programmes based on thyroxine estimation detect both primary and secondary congenital hypothyroidism (CH) but have a low specificity with a high recall rate, whereas those measuring TSH alone will only detect primary CH but are more specific. In those infants with a low TSH, serum TSH and T4 levels are estimated and if confirmed to be abnormal are referred for clinical evaluation (2).

TDC and ►goitre usually present by their mass effect, potentially causing respiratory problems; TDC may also become secondarily infected and present acutely with a painful midline neck mass. The main concern usually affects functional disorders of the thyroid gland.

Functional Disorders

Congenital Hypothyroidism (CH) is the commonest treatable cause of mental retardation world wide, with iodine deficiency as the most important cause. Thyroid dysgenesis is the most frequent cause in Europe where iodine deficiency is rare, occurring in approximately one in 4,000 live births. Table 2 outlines the most common causes of congenital hypothyroidism. In approximately 10% of cases of CH detected by neonatal screening, the condition is transient and resolves within a few weeks of birth. Thyroid dysgenesis accounts for 85–90% of cases of CH with females more commonly affected than males. Most cases are sporadic although the condition is more frequent in children with Down's syndrome. Dysgenesis ranges from agenesis, to hypoplasia of one or both lobes. Unilateral dysgenesis is not usually associated with CH as sufficient thyroid hormone is still being produced. Inborn errors of metabolism resulting in dyshormonogenesis account for a further 10–15% of cases of CH. In contrast to thyroid dysgenesis most cases have an autosomal recessive pattern of inheritance.

Screen detected babies with CH often have no overt clinical manifestations, although severe cases may show clinical signs at birth, including, large tongue, hoarse cry, umbilical hernia, hypotonia, cold extremities, prolonged jaundice, constipation and large fontanelles. Untreated CH will result in severe irreversible developmental and

Congenital Malformations, Thyroid, and Functional Disorders. Table 2 Congenital hypothyroidism

'Transient'
Thyroid dysgenesis (85–90%)
Inborn errors of metabolism (10–15%)
Secondary/tertiary hypothyroidism
Hypothalamic
TRH deficiency
Midline facial brain dysmorphism
Pituitary
TSH deficiency
Multiple hormone deficiencies
TSH resistance
Thyroid hormone resistance

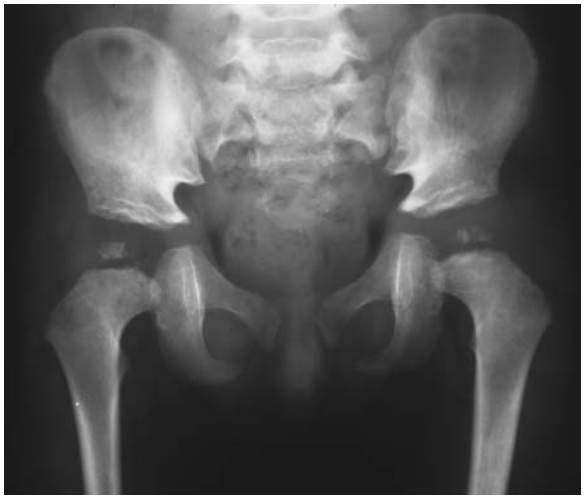

Congenital Malformations, Thyroid, and Functional Disorders. Figure 1 Pelvic X-ray of a young boy presenting with overt signs of ►hypothyroidism, showing delayed and fragmented ossification of the femoral capital epiphyses.

intellectual delay. CH secondary to pituitary or hypothalamic dysfunction may have signs suggestive of hypopituitarism, and can be seen in association with midline facial defects or cerebral malformation; boys may have a micropenis. The presence of a palpable goitre excludes the diagnosis of thyroid dysgenesis, and indicates that the CH is likely to be transient or due to abnormal hormone synthesis resulting in excessive stimulation of the thyroid gland by raised levels of TSH.

The onset of *hypothyroidism in older children* is often insidious, with the development of a *goitre* or identification during child health surveillance due to poor linear growth.

Chronic lymphocytic thyroiditis (CLT) is the most common cause of hypothyroidism presenting beyond infancy although many affected individuals with CLT may initially be euthyroid and present with an asymptomatic goitre. CLT is an autoimmune disorder often affecting adolescent girls with 30–40% having an inherited predisposition to autoimmune disease. The disease is characterised by a destructive process with lymphocytic infiltration and atrophy and fibrosis of the follicles. Goitre occurs in approximately 5% of all children and it is important to distinguish children with goitre due to CLT from those with a simple colloid goitre, by the demonstration of thyroid antibodies in CLT, as the former are at risk of developing hypothyroidism later in life unlike those with a colloid goitre who will remain euthyroid. Children and adolescents with hypothyroidism have an increased incidence of slipped upper femoral epiphyses and puberty may be delayed. In contrast to untreated neonatal hypothyroidism affecting brain development hypothyroidism developing after 3 years of age mainly affects growth and causes delayed skeletal maturation, with no permanent effect on cognitive or neurological development.

Neonatal hyperthyroidism is rare occurring in 2–3% of babies born to mothers with Grave's disease due to the transplacental passage of maternal TSH receptor stimulating antibodies. The condition usually presents towards the end of the first week of life as maternal antithyroid drugs are cleared and is generally transient lasting up to 3 months. The salient features include tachycardia >160, congestive cardiac failure and cardiac arrhythmia. The infant may be irritable, fail to thrive, develop prominent eyes and a goitre may cause airway obstruction. Untreated neonatal ▶hyperthyroidism has a high mortality of approximately 20%. Permanent neonatal hyperthyroidism also occurs as a result of an inherited autosomal dominant genetic mutation in the TSH receptor.

In *older children and adolescents* with hyperthyroidism a large fleshy goitre is common.

Grave's disease, diffuse toxic goitre accounts for 95% of hyperthyroidism in older children generally presenting in adolescent girls with a genetic predisposition to autoimmune disease. Other causes of hyperthyroidism are rare, and include a functioning *thyroid adenoma*, thyrotoxicosis factitia, i.e. ingestion of thyroxine in adolescent girls attempting to lose weight or high levels of TSH secretion, e.g. due to a pituitary adenoma. The absence of a goitre in a thyrotoxic adolescent girl should raise the possibility of thyrotoxicosis factitia. A solitary palpable nodule indicates that an adenoma is the most likely cause. Classical symptoms and signs of thyrotoxicosis develop although ophthalmological signs are less common in children than in adults. Secondary amenorrhoea may occur in association with accelerated bone maturation and linear growth. Cafe au lait spots seen in conjunction with thyrotoxicosis should raise the possibility of McCune Albright Syndrome.

Imaging

X-ray

A number of radiological abnormalities have been described in association with thyroid disease that may serve to point to an underlying thyroid disorder. These include delayed skeletal maturation i.e. bone age, flattened and fragmented femoral epiphyses in hypothyroidism and periostitis and accelerated bone age in hyperthyroidism (Fig. 1). A lateral soft tissue neck may

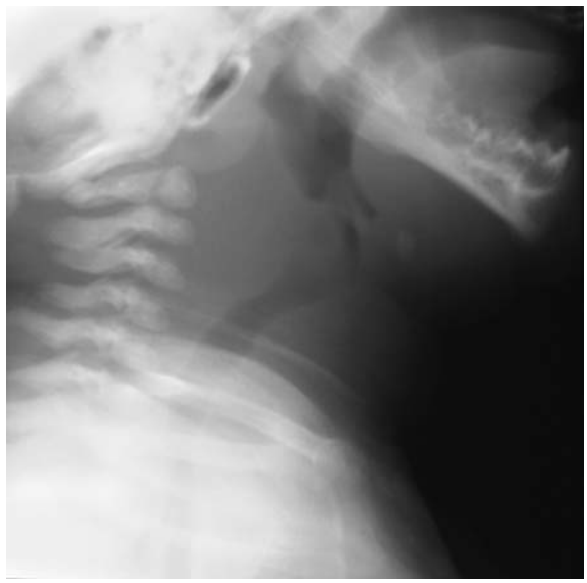

Congenital Malformations, Thyroid, and Functional Disorders. Figure 2 Posterior displacement of the trachea causing mild respiratory distress in a neonate with an enlarged thyroid gland (goitre) due to neonatal hyperthyroidism.

help to demonstrate airway compression in rare cases of airway obstruction, due to an enlarged ectopic thyroid or goitre (Fig. 2).

Thyroid Ultrasound

Ultrasound imaging forms the mainstay of thyroid imaging, to identify the presence or absence of a normal thyroid gland in hypothyroidism, to evaluate any midline swelling thought to be a TDC, and to evaluate a palpable thyroid nodule (Fig. 3). A high frequency transducer is essential (12–15 MHz) and Doppler sonography is useful to assess vascularity of a palpable nodule or ectopic thyroid tissue which is often of increased vascularity (3). A normal thyroid gland in a young child has a lateral lobe measuring approximately 1–1.5 cm in width, 2–3 cm in length and a depth of 0.2–1.2 cm. In CH the finding of a normal thyroid gland indicates that dyshormonogenesis is the most likely cause. In older hypothyroid children where thyroid antibodies are negative and there is no palpable goitre, ultrasound can be helpful to distinguish primary myxoedema i.e. non-goitrous CLT from late presenting thyroid dysgenesis.

There is rarely an indication for ultrasound in a goitre, unless possible mediastinal extension needs to be clarified. The investigation and treatment of solid nodules follows the pathways well established for adult patients, although in children a solitary nodule is more likely to be carcinomatous, particularly papillary carcinoma; functioning adenomas and colloid cysts also occur.

A thyroglossal duct cyst is usually midline but may be found embedded in the strap muscles just to the left of the midline. The wall may be thin and the fluid anechoic, but if there has been previous infection or haemorrhage, the wall may be thickened and the cyst contents may contain echoes. A thyroglossal duct tract may be identified extending deeply to the hyoid bone (Fig. 4).

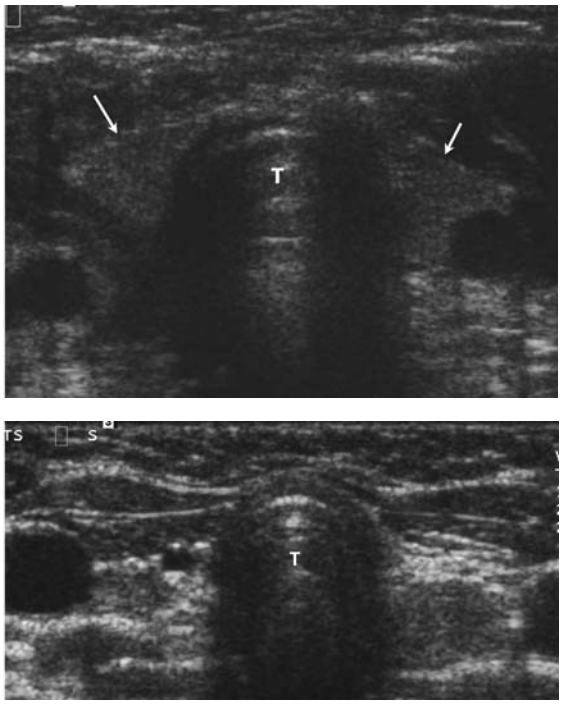

Congenital Malformations, Thyroid, and Functional Disorders. Figure 3 Transverse ultrasound images through the neck. (a) Transverse ultrasound image demonstrating a normal thyroid gland (arrows) in an infant with screen detected congenital hypothyroidism due to an inborn error of metabolism. (b) No thyroid gland could be demonstrated in this infant with thyroid agenesis

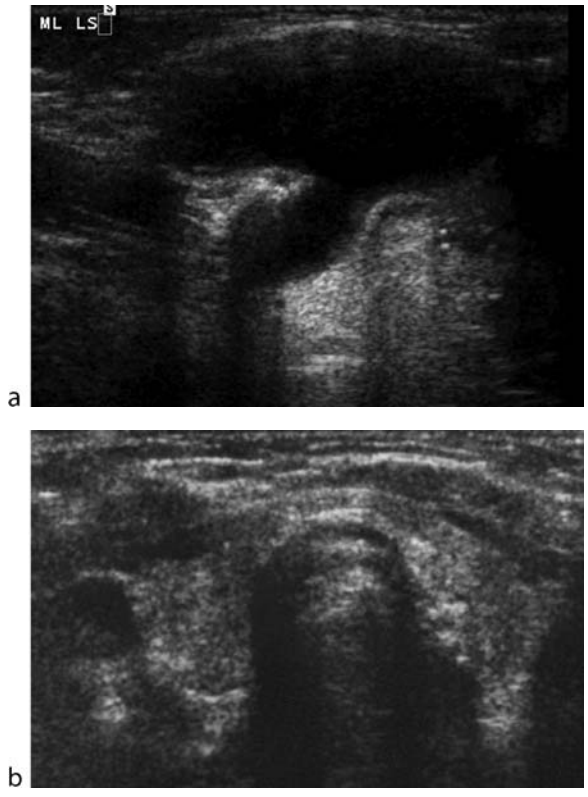

Congenital Malformations, Thyroid, and Functional Disorders. Figure 4 Four year old girl presenting with a high midline neck swelling: (a) Sagittal ultrasound image demonstrating an elliptical cystic structure with posterior and cranial extension towards the hyoid bone typical of a thyroglossal duct cyst (TDC). (b) Demonstrates a normally sited thyroid gland indicating that the TDC can be safely excised.

Thyroid Scintigraphy

Thyroid scintigraphy using technetium-99m pertechnetate and iodine-123 is useful to evaluate both anatomical and functional aspects of a thyroid disease (5). Scintigraphy is essential for the further evaluation of a possible TDC or ectopic thyroid tissue when a normal thyroid gland cannot be identified on ultrasound, as removal of the cyst/ectopic tissue may result in rendering the patient athyroid and dependent on life long thyroid hormone replacement (Fig. 5). Although iodine-123 is more specific and better to quantify dysfunction and inborn errors of metabolism, pertechnetate is cheaper and more readily available, and is the tracer of choice for the initial scan with iodine-123 reserved for further evaluation where the technetium scan is abnormal. In most inborn errors of metabolism the gland is usually enlarged, normally sited and shows increased tracer uptake. Scintigraphy is also used in the evaluation of the solitary thyroid nodule. Identification of a 'hot' nodule suggests the presence of a functioning adenoma and ultrasound

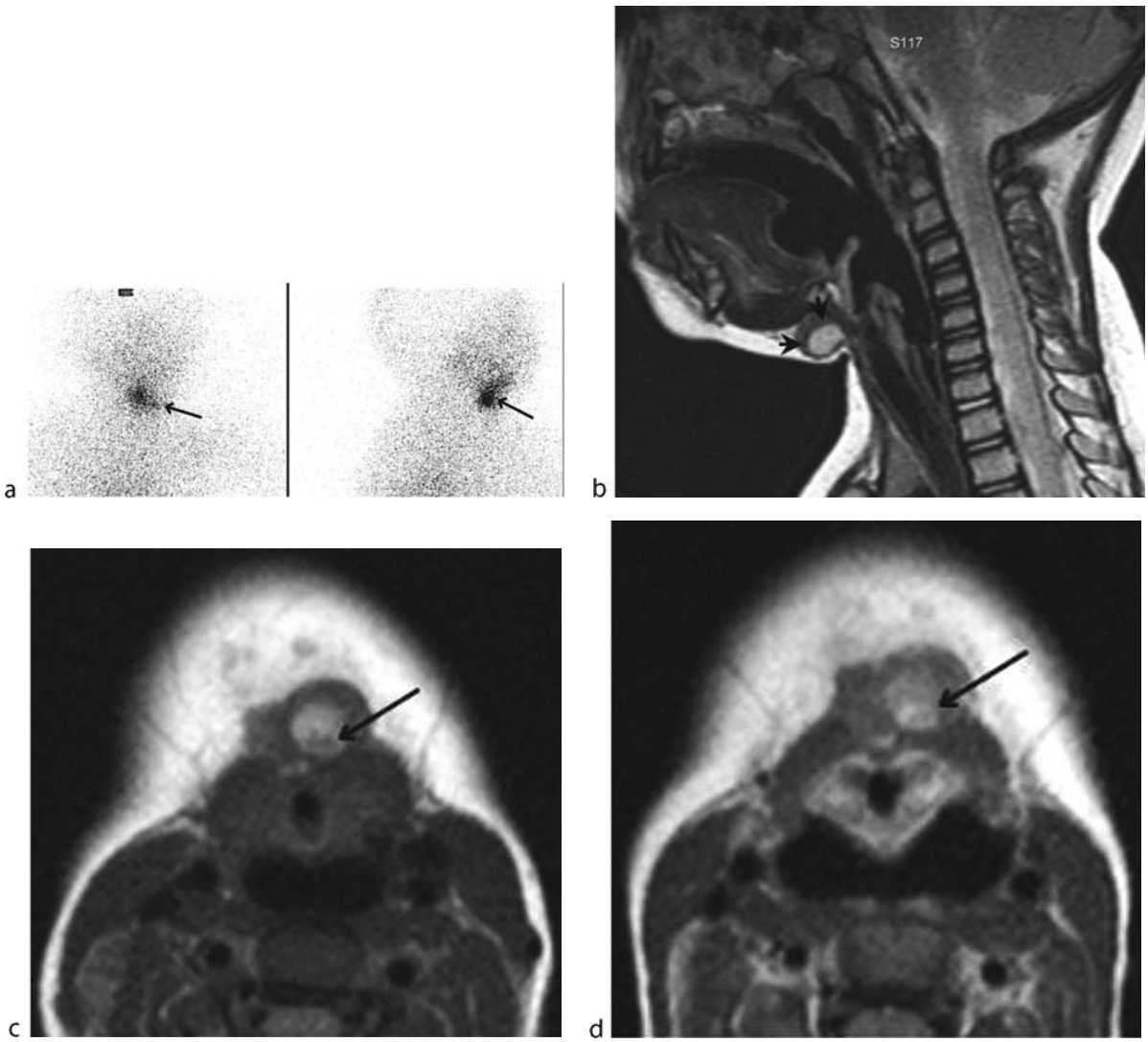

Congenital Malformations, Thyroid, and Functional Disorders. Figure 5 Thyroglossal duct cyst with ectopic thyroid tissue. (a) Thyroid scintigraphy using technetium-99m pertechnetate showing relatively low level uptake of isotope, in frontal and lateral projections, corresponding to the position of the TDC (arrows). No other functioning thyroid tissue was identified, indicating that excision of the TDC would render her athyroid. b-d MRI scans. (b) T2 sagittal, (c) T1 transverse, (d) Contrast enhanced T1 transverse demonstrating a thick walled cystic structure containing proteinaceous fluid in a midline submental region (arrows). No thyroid gland demonstrated elsewhere. There is enhancement of the posterior wall of the TDC following contrast injection (arrows).

Congenital Malformations, Thyroid, and Functional Disorders. Table 3 Important diagnostic features in functional and congenital thyroid disorders

	Disorder	TSH levels	T4 levels	Thyroid gland
Hypothyroidism				
	Dysgenesis	High	Low	Absent/ectopic
	Inborn error of metabolism	High	Low	Normal or enlarged
	TSH resistance	High	Low	Normal/small or not visible
NB (may also be euthyroid or hyperthyroid)	Chronic lymphocytic thyroiditis	High	Normal or low	Enlarged/normal
	Secondary—pituitary or hypothalamic disease	Low	Low	Normal or small
	Thyroid hormone resistance	Normal or low	High	Normal or enlarged
Hyperthyroidism	Neonatal/Graves	Low	High	Normal or enlarged +/– bruit
	Adenoma	Low	High	+/– palpable nodule
	TSH-induced	Normal/ high	High	

fine needle aspiration can then be reserved for evaluation of 'cold' nodules. Open biopsy may be necessary in the younger child.

Cross Sectional Imaging

Cross sectional imaging, i.e. CT or preferably MRI scanning is reserved for the evaluation of more difficult cases, particularly the ectopic sublingual thyroid gland and TDC particularly when recurrent. TDC may be noted to contain contents of intermediate signal intensity on T1 and high signal on T2 if the contents are proteinaceous. Wall enhancement is likely to occur if ectopic thyroid tissue is present (Fig. 5). Nodularity within the mass and the presence of calcification may be an indicator of the development of papillary carcinoma, a complication occurring in approximately 1% of TDC generally during adulthood.

Diagnosis

The diagnoses of the various thyroid disorders depend upon correlation between clinical signs, mode of presentation and the functional status of the thyroid gland, and have been discussed in relation to specific entities earlier. Table 3 summarises the most important findings. The precise pathway for investigation and imaging will depend on the suspected diagnosis. Although initial investigations can be undertaken in a general hospital setting, more complex cases particularly when presenting in the neonate should be referred for specialist investigation and management.

Bibliography

1. Brown RS, Huang S (2005) The thyroid and its disorders. In: Brook C, Clayton P, Brown R (eds) Brook's Clinical Pediatric Endocrinology. Blackwell Publishing, pp 218–253
2. Pollitt RJ, Green A, CJ McCabe et al (1997) Neonatal screening for inborn errors of metabolism: cost, yield and outcome. Health Technol Assess 1:31–35
3. Siegel MJ (1991) Neck. In: Siegel MJ (ed) Pediatric Sonography. Raven Press, pp 63–89
4. Effmann EL (2004) Neck and upper airway. In: Kuhn JP, Slovis TL, Haller JO (eds) Caffey's Paediatric Diagnostic Imaging. Mosby, pp 777–809
5. Schoen EJ, Clapp W, Trinh T (2004) The key role of newborn thyroid scintigraphy with isotropic iodide (123 I) in defining and managing congenital hypothyroidism. Pediatrics 114:683–687

Congenital Malformations, Tracheobronchial Tree

Gundula Staatz
Department of Radiology, Division of Pediatric Radiology, University of Erlangen-Nürnberg Erlangen
gu.stz.uni-erlangen@t-online.de

Synonyms

Bronchial atresia; Bronchogenic cyst; Bronchopulmonary sequestration; Congenital cystic adenomatoid malformation (CCAM); Congenital lobar emphysema; Foregut

malformations, pulmonary and tracheobronchial anomalies such as: bronchial atresia; hypogenetic lung syndrome; Pulmonary arteriovenous malformation; Pulmonary varix; Tracheal bronchus; Tracheal stenosis

Definitions

Congenital malformations of the tracheobronchial tree consist of a heterogeneous group of anomalies, which may be divided into two groups, one with a normal vascular supply, the second group with anomalous vasculature. The most frequent malformations will be addressed in the following chapter.

A *tracheal bronchus* is defined as a right upper bronchus originating in the trachea.

Congenital lobar emphysema is characterised by a progressive overdistension of lung tissue (lobe) without destruction of alveolar septa.

Bronchogenic cysts are foregut duplication cysts developing from an abnormal budding of the ventral foregut and may be located mediastinal, intrapulmonary, or less frequently in the lower neck (1).

Congenital cystic adenomatoid malformation (CCAM) is characterised by an intrapulmonary multicystic mass of pulmonary tissue with an abnormal proliferation of bronchial structures (1). The cysts communicate with the bronchial tree and the vascular supply as well as venous drainage is normal.

Bronchopulmonary sequestration is an embryonic mass of lung tissue disconnected from the tracheobronchial tree with a blood supply from the systemic circulation. Sequestration is divided into an *intralobar* and *extralobar* type. Intralobar sequestration is incorporated within the normal visceral pleura of the lung, has arterial blood supply from the aorta or major aortic branches and drains usually into pulmonary veins. Extralobar sequestration has a separate pleural investment, an arterial blood supply from the aorta or aortic branches and a systemic venous drainage (2).

Pathology/Histopathology

A tracheal bronchus is usually arising from the right lateral wall of the trachea, less than 2 cm above the carina, and is defined as a displaced bronchus, if a single branch of the upper lobe bronchus is missing, and as a supranumary bronchus, if the trifurcation of the right upper lobe is normal (1).

Congenital lobar emphysema is due to a bronchial narrowing, usually caused by an absence or hypoplasia of bronchial cartilage, which leads to an air trapping in the affected lobe. In case of extrinsic compression of a bronchus (e.g. aberrant pulmonary artery), the cartilage rings are malformed, soft and collapsible. The left upper lobe is most often affected, followed by the right middle lobe and the right upper lobe.

The histopathology of a bronchogenic cyst demonstrates a cystic lesion with fibrous walls, which occasionally contain cartilage, lined by ciliated columnar epithelium.

CCAM has been subdivided into three major histological types:

Type 1 (50%)	One or more cysts measuring 2–10 cm in diameter
Type 2 (40%)	Multiple small relatively uniform cysts resembling bronchioles, measuring 0.5–2 cm in diameter
Type 3 (<10%)	Microscopic, adenomatoid cysts, grossly a solid mass without obvious cyst formation

Type 2 and type 3 CCAM may be associated with extralobar sequestration, and receive blood supply from the systemic circulation. The larger cysts of type I lesions are frequently lined by pseudo-stratified columnar epithelial cells, which produce mucine. The cysts of type II lesions are lined by cuboid-to-columnar epithelium and have a thin fibromuscular wall, type II lesions consisting of microscopic, adenomatoid cysts.

Bronchopulmonary sequestration is classified as intra- or extralobar sequestration. Extralobar sequestration is predominantly located on the left side between the lower lobe and the mediastinum and has its own pleural coating; it may occur extra-thoracic, i.e., intra-abdominal. The lesion is composed of non-functioning primitive pulmonary parenchymal tissue without connection to the tracheobronchial tree. Dilated bronchioles, alveolar ducts, and alveoli are found histologically. Intralobar sequestration, which is surrounded by normal lung and incorporated within the normal visceral pleura, is almost exclusively located in the lower lobes, most often on the left side (60%). A bilateral involvement is rarely seen. Intralobar sequestration is characterised by chronic inflammatory tissue replacing the normal pulmonary parenchyma, and multiple cysts filled with viscid fluid or gelatinous material. The pleura is thickened by adhesions to mediastinal and diaphragmatic parietal pleura.

Clinical Presentation

Patients with a tracheal bronchus are usually asymptomatic, but persistent or recurrent upper lobe pneumonia, atelectasis or air trapping, and chronic bronchitis may

occur. Infants with congenital lobar emphysema present with respiratory distress and the clinical examination reveals a hyperresonant thorax with absent breath sounds. A bronchogenic cyst usually causes symptoms due to tracheal or bronchial compression, such as cough, wheezing, stridor, dyspnea, cyanotic spells, and pneumonia (1). Most neonates with CCAM present with respiratory distress. In older infants cough, fever and recurrent pulmonary infections are common findings.

The clinical manifestation of bronchopulmonary sequestration depends on the two different forms of this malformation. Children with intralobar sequestration present more often with pulmonary infection compared to children suffering from extralobar sequestration. Extralobar sequestration is usually an incidental finding, when imaging studies are performed for the evaluation of associated congenital anomalies, such as cardiovascular malformations or diaphragmatic hernia. A communication to the gastrointestinal tract is possible, which can be the cause of feeding problems.

Imaging

Congenital lung malformations are increasingly diagnosed antenatally with use of prenatal ultrasound and foetal MR imaging. After birth, the diagnostic modalities include chest radiographs, ultrasound, scintigraphy, computed tomography (CT), magnetic resonance imaging (MRI), arteriography and bronchoscopy. In children with tracheobronchial malformations, such as tracheal stenosis or tracheal bronchus, bronchoscopy is usually the first method of choice, but recently multidetector spiral computed tomography (MDCT) with the capability of virtual tracheobronchoscopy and bronchography is sometimes used as an alternative.

The diagnosis of congenital lobar emphysema is based in most cases on the clinical examination and the findings of the plain radiographs. CT, and occasionally ventilation/perfusion scintigraphy, is helpful in confirming the diagnosis and in guiding management decisions.

Bronchogenic cysts are best studied with use of CT, but MRI may reveal additional information concerning the haemorrhage, protein or calcium content of the cysts. CCAM can be early identified by prenatal or perinatal ultrasound and MRI (3). Thereafter chest radiographs and CT examinations are the imaging modalities of choice.

Bronchopulmonary sequestration can be suspected on chest radiographs, when a persistent lower lobe opacity or mass is visible in children with recurrent respiratory tract infection. Ultrasound with colour-coded Doppler, CT and MRI provide most helpful information by identifying the anomalous arterial blood supply (4). Especially with the development of MDCT and high-resolution 3D reconstruction techniques, such as volume rendering techniques or maximum intensity projections, the visualisation and identification of the feeding arterial vessel and the venous drainage is accurately performed. Arteriography is only indicated for (pre-operative) embolisation of the systemic feeding artery.

Nuclear Medicine

Radionuclide scintigraphy has an ancillary role in assessing foregut anomalies. Many findings from scintigraphy are relatively non-specific. In infants with congenital lobar emphysema ventilation–perfusion scintigraphy demonstrates restricted ventilation in the affected lobe with ultimate isotope retention due to delayed emptying of alveoli, and a decreased perfusion caused by the markedly attenuated vascularity of the involved lobe.

Diagnosis

A tracheal bronchus is difficult to identify on plain radiographs, but a CT examination is most efficient in demonstrating the aberrant bronchus arising from the lateral tracheal wall (Fig. 1).

Congenital lobar emphysema presents in utero with a fluid-filled over-distended lobe, which may be identified by prenatal ultrasound. On postnatal chest radiographs an over-distended hyperlucent lobe, herniating across the midline, is characteristic. The mediastinum is shifted to

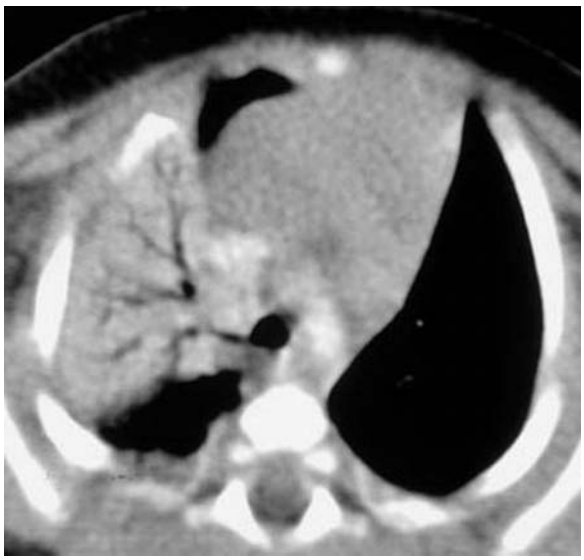

Congenital Malformations, Tracheobronchial Tree.
Figure 1 Chest-CT of a 6-week-old infant with persistent right upper lobe atelectasis demonstrates a tracheal

the contralateral side, the ipsilateral hemidiaphragm is flattened with no movement under fluoroscopy, and the extension of the lobe remains unchanged during exhalation. CT scans demonstrate the hyperlucent, hyperexpanded lobe with attenuated vessels, a midline substernal lobar herniation and compression of the remaining lung (Fig. 2).

A bronchogenic cyst may be identified on chest radiographs by a sharply delineated mass with close contact to the mediastinum, especially to the carina. CT reveals a well-defined round to oval mass with a smooth, thin wall, and a water- or soft-tissue attenuation (5) (Fig. 3). If the cyst is infected or contains secretions, the cyst may appear hyperdense. On T2-weighted MRI images, bronchogenic cysts show homogeneous and markedly high-signal intensity, whereas on T1-weighted MR images the signal intensity can vary between hypo-, iso- and hyperintense due to the fluid content of the cyst, which may consist of protein, blood or calcium (5).

CCAM appears on chest radiographs as a multiple air-filled cystic mass of varying size, which can rapidly expand a lobe due to air trapping with subsequent shift of the mediastinum to the contralateral side. In some patients a pneumothorax occurs. CT provides additional information with depiction of the exact size and extension of the multiple thin-walled, air-filled cysts (Fig. 4). Variable fluid contents in infected or haemorrhagic cysts can also be identified. As a differential diagnosis congenital diaphragmatic hernia, pulmonary sequestration, and bronchogenic cysts has to be considered.

Bronchopulmonary sequestration is visible on plain chest radiographs as a well defined homogeneous or sometimes cystic mass usually located in the posterior portion of the lower lobe. Intralobar sequestration may contain aerated areas due to collateral ventilation and air-trapping (4). Colour-coded Doppler sonography is an elegant method to identify the feeding arterial vessel and the venous drainage, but CT and MRI are often additionally performed, particularly pre-operatively or if

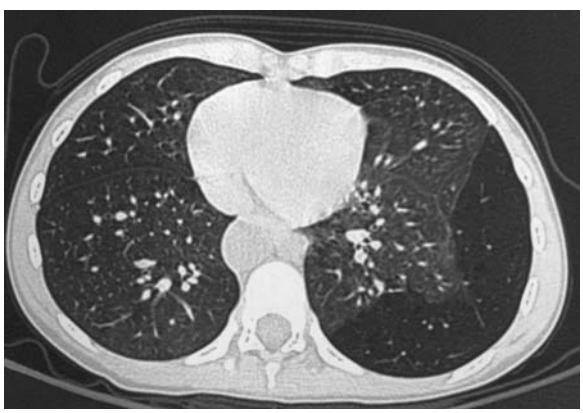

Congenital Malformations, Tracheobronchial Tree.
Figure 2 Congenital lobar emphysema of the left lower lobe. On the chest CT image an overdistended hyperlucent lower lobe on the left side is visible, which leads to a shift of

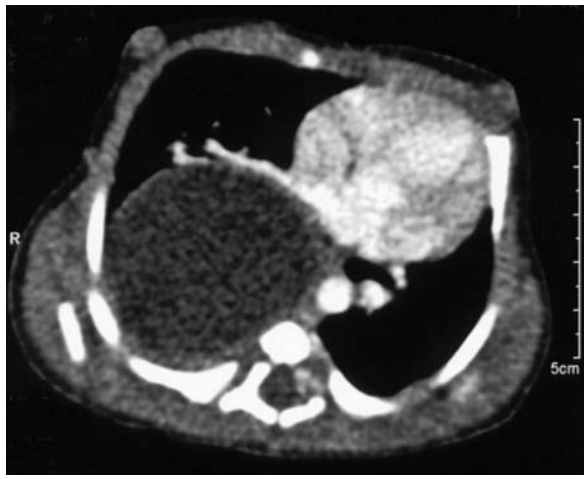

Congenital Malformations, Tracheobronchial Tree.
Figure 3 Contrast-enhanced CT of a newborn with a prenatally diagnosed intrathoracic cyst. A large oval-shaped cystic mass, with a sharply delineated smooth wall and close connection to the mediastinum is identified in the right lower lobe. The left-sided central pulmonary

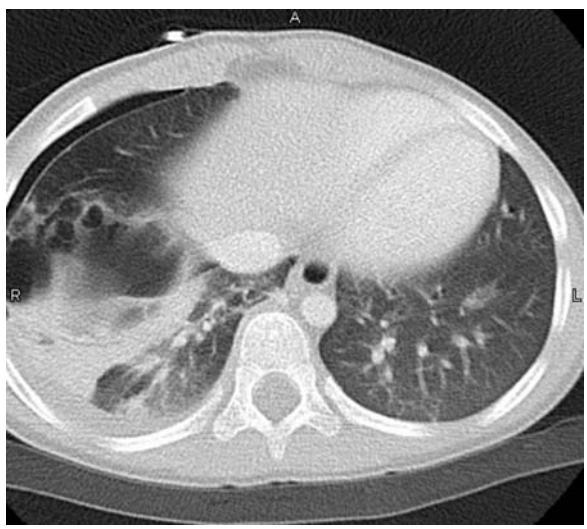

Congenital Malformations, Tracheobronchial Tree.
Figure 4 Chest CT of an adolescent with a CCAM located in the right lower lobe. Multiple air-filled cysts of various sizes are visible. Associated atelectasis in the posterior segments of the right lower lobe, pleural effusion, and a small pneumothorax are also present. (Image from Prof. R. Buchmann, Dept. of Pediatric Radiology, Arkansas

ultrasound cannot accurately delineate the anatomy or remains equivocal. On CT, the lesion enhances after intravenous contrast-material administration and CT-angiography (3D reconstruction) reveals exactly the course and configuration of the anomalous feeding vessel (Fig. 5). Typically the blood supply of bronchopulmonary sequestration arises from the aorta or its major branches such as subclavian, splenic, gastric and intercostal arteries. Venous drainage of extralobar bronchopulmonary sequestration occurs through the systemic circulation, usually via the azygos or hemiazygous veins or the IVC. Intralobar bronchopulmonary sequestration usually drains into pulmonary veins, but also alternative drainage routes via azygos, hemiazygos or IVC are possible. MR angiography is an excellent alternative to contrast-enhanced CT, and provides similar information for the diagnosis of bronchopulmonary sequestration without ionising radiation. For differential diagnosis various diseases have to be considered, such as pulmonary arterio-venous fistula, CCAM, hernias, some pneumonias or neoplasms.

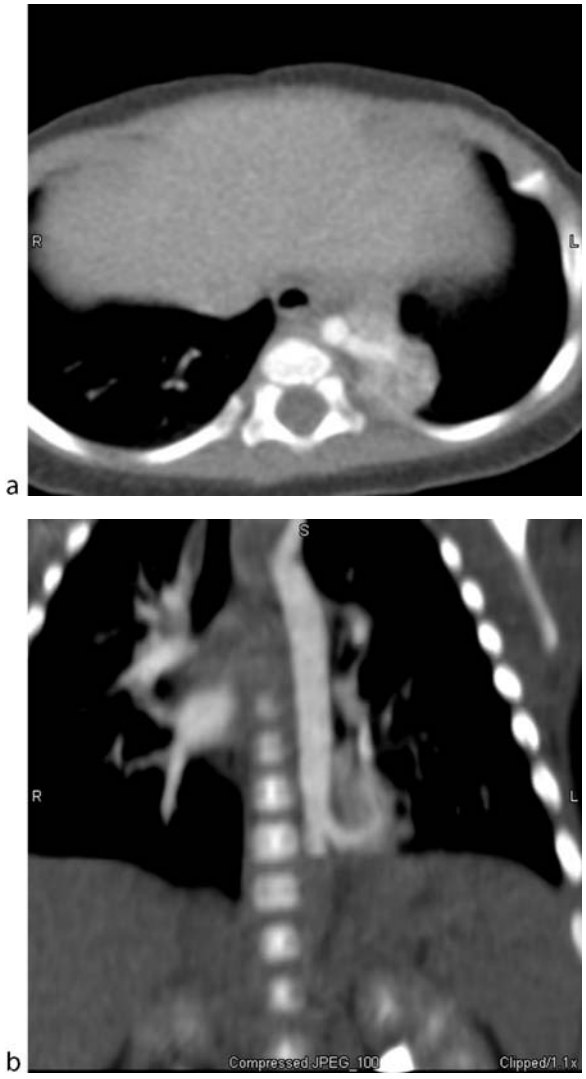

Congenital Malformations, Tracheobronchial Tree.
Figure 5 Arterial phase of contrast-enhanced, axial chest CT (a) and coronal multiplanar reformation (b) of intralobar lung sequestration. A well-defined homogeneously enhancing mass is visible in the posterior basal segment of left lower lobe. The arterial phase clearly depicts the anomalous feeding vessel, arising directly from the thoracic aorta. (Images from Prof. R. Buchmann, Dept. of Pediatric

Interventional Radiological Treatment

Interventional treatment is an interesting therapeutic option in bronchopulmonary sequestration. Transcatheter arterial embolisation (TAE) of the aberrant feeding artery has been performed as a curative therapy or as a pre-operative procedure to minimise the risk of vascular complications during resection.

Bibliography

1. Berrocal T, Madrid C, Novo S et al (2004) Congenital anomalies of the tracheobronchial tree, lung, and mediastinum: embryology, radiology, and pathology. Radiographics 24:e17 (Epub 2003 Nov 10)
2. Siegel MJ (1999) Lung, Pleura and chest wall. In: Pediatric Body CT. Lippincott Williams and Wilkins, Philadelphia, pp 101–140
3. Hubbard AM, Adzick NS, Crombleholme TM et al (1999) Congenital chest lesions: diagnosis and characterization with prenatal MR imaging. Radiology 212:43–48
4. Mata JM, Castellote A (2002) Pulmonary malformations beyond the neonatal period. In: Lucaya J, Strife JL (eds) Pediatric Chest Imaging, Chest Imaging in Infants and Children. Medical Radiology, Diagnostic Imaging (Baert Al, Sartor K (eds)). Springer, Berlin, Heidelberg, New York, pp 93–111
5. McAdams HP, Kirejczyk WM, Rosado-de-Christenson ML et al (2000) Bronchogenic cyst: imaging features with clinical and histopathologic correlation. Radiology 217:441–446

Congenital Malformations, Vascular, Brain

Massimo Gallucci, Nicola Limbucci
Department of Neuroradiology, University Of L'Aquila, L'Aquila, Italy
massimo.gallucci@cc.univaq.it

Synonyms

Arteriovenous malformation; Capillary angioma; Cavernous angioma; Cavernoma; Capillary telangiectasia; Cryptic/occult vascular malformations; Developmental venous malformation; Venous angioma

Definition

Intracranial congenital vascular malformations are classified as arteriovenous malformations (AVMs), cavernous angiomas (CAs), developmental venous anomalies (DVAs), and capillary telangiectasias (CTAs). Mixed lesions are often shown by imaging.

The definition of intracranial vascular malformation is univocal. Old terminology referred to these lesions as different patterns of occult vascular malformations (2); this terminology is based on angiographic features and should be considered obsolete.

CAs are vascular lesions formed by endothelial-lined sinusoidal vascular spaces, filled by slow-flow blood, with no intervening brain tissue.

AVMs can be pial or dural (the latter known as arteriovenous fistulas). Pial AVMs are collections of dysplastic plexiform vessels supplied by arterial feeders and drained by venous channels, with an intervening vascular network.

An arteriovenous dural fistula is a direct shunt without an intervening vascular network. For further details about AVMs please consult the relative chapter.

DVAs are composed of dilated, radially arranged veins draining into an enlarged vein with normal intervening brain. They are considered variations of normal venous drainage (1).

CTAs are small nests of dilated capillaries with normal intervening brain tissue.

Pathology/Histopathology

CAs appear as circumscribed, lobulated, berry-like masses, ranging from a few millimeters to some centimeters. They are composed of thin-walled endothelial-lined sinusoidal vascular channels, without the presence of tunica muscolaris or elastica. Calcifications are common. No intervening brain tissue is present among the channels. The vessels are filled by blood showing different stages of thrombosis. The lesion is surrounded by macrophages and astrocytes containing ferritin and hemosiderin; gliosis is sometimes present. In 23% of patients, CAs are associated with other malformations, usually DVA (3). CAs may occur in any location. About 80% of them are supratentorial and are frequently found at the corticomedullary junction; deep white matter and basal ganglia are also common locations.

DVAs are composed of tufts of dilated, radially arranged veins converging toward an enlarged collector vein that drains into the deep or superficial venous system. Venous walls and intervening brain are normal. DVAs are considered by most as extreme variations of normal venous drainage. In about 30% of cases, the lesions are associated with CAs. The most common location is cerebral or cerebellar deep white matter, often near the ventricles.

CTAs are formed by small nests of dilated capillaries. Vessels are thin-walled and lack muscolaris and elastica. The lesions are often multiple, and the most typical location is the pons.

AVMs usually consist of arterial feeders, collaterals, a nidus, and enlarged veins. In dual AVMs the nidus is absent.

Pathogenesis

Most CAs are congenital; however, *de novo* lesions have been described in familiar forms, in patients with an existing DVA, and after radiation therapy. The relationship among the various malformations is still debated. Some authors suggest that CA and CTA are different stages of the same process. Another theory is that small preexisting DVAs or CTAs induce flow and venous pressure alterations, leading to DVA formation (2). However, different gene mutations have been found in patients with CA and DVA, suggesting a distinct pathogenesis (4).

Pial AVMs are congenital, whereas dural AVMs often occur following recanalization of a venous sinus thrombosis.

Clinical Presentation

The prevalence of *CA* is estimated to be 4% (5–13% of all vascular malformations). CAs are multiple in at least 20–30% of patients, and in 10–15% of cases a familiar pattern is recognized. In familiar forms, the lesions are usually multiple. CAs are symptomatic in about 50–60% of cases, and their clinical course is more severe than for DVA and CTA. Symptoms include seizures, headache, and focal deficits, and they usually occur in young people (20–40 years). Seizures, often refractory, are the most common symptom (50–70%).

The most feared complication of CA is significant intraparenchymal hemorrhage (0.1–1% per year). Subclinical hemorrhage is more common and is responsible for the typical magnetic resonance imaging (MRI) features.

DVAs are considered the most common intracranial vascular malformation (63%) and are almost always clinically silent, representing an incidental finding. Seizures and focal deficits can occasionally be attributed to DVA, but surrounding brain and the venous drainage are normal. Hemorrhage has been described, but it should be considered exceptional. Most symptomatic patients have a mixed malformation, with a CA contiguous to the DVA, and the symptoms depend on the CA.

CTAs are very common and often multiple. They are usually incidentally detected at MRI or autopsy, and they are almost always clinically silent. Sometimes the lesion is part of a mixed malformation: in this case, it can, rarely, bleed.

AVMs present with hemorrhage in 50% of cases and with seizures in 25%.

Imaging

Cavernous Angioma

Digital subtraction angiography (*DSA*): CAs are typically defined as angiographically occult lesions. A faint contrast stain is rare.

Computed tomography (*CT*): CA appears as a small isodense or hyperdense mass, without edema or mass effect, usually with calcifications. After contrast administration the lesion often enhances. In bleeding lesions, CT shows the hematoma with mass effect, but the CA is not usually distinguished.

MRI: CAs have characteristic features. The typical lesion is a nodular mass with a popcorn-like shape and a central core containing areas with heterogeneous signal. The core mixed signal depends on blood clots with different stages of evolution, especially methemoglobin, which is hyperintense on T1. Fluid–fluid levels are sometimes seen in the biggest lesions. Typically, the lesion is surrounded by a complete ring, hypointense on all sequences, corresponding to ferritin and hemosiderin deposits (Fig. 1). The lesion "blooms" on gradient-echo (GE) sequences because of their high sensitivity to susceptibility artifacts. GE sequences should always be acquired because they allow identification of very small

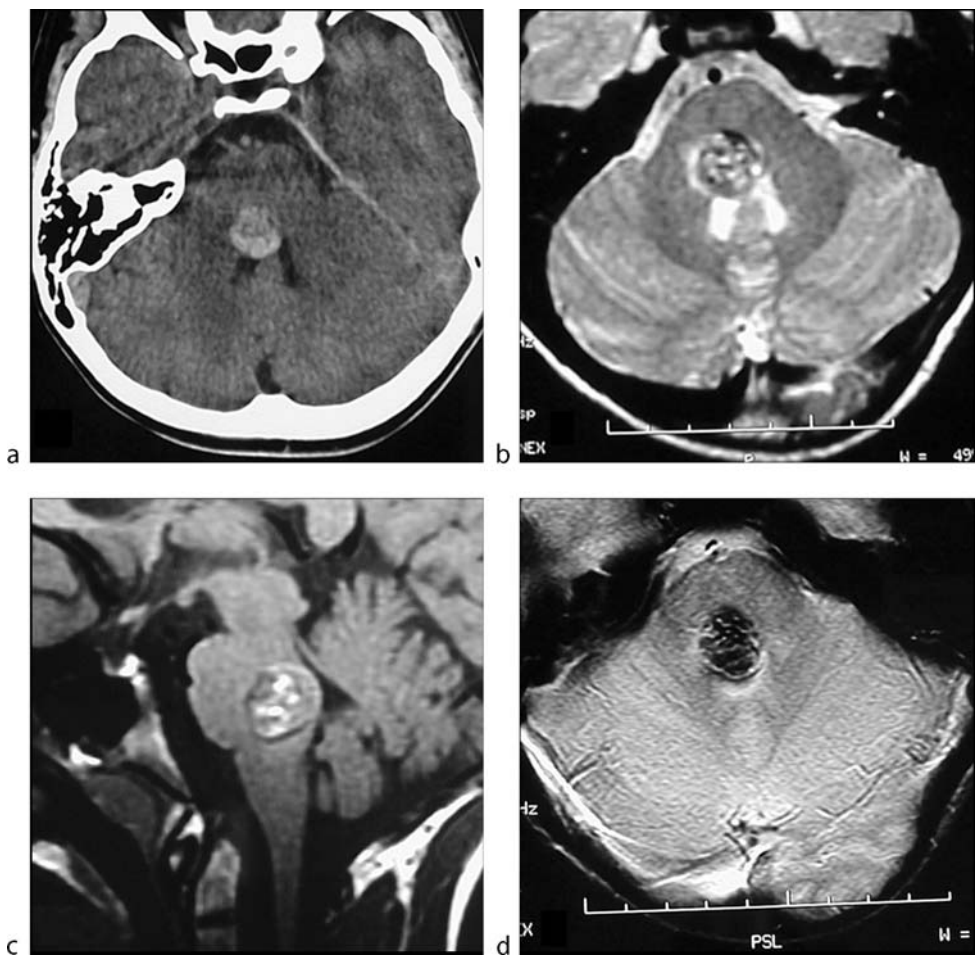

Congenital Malformations, Vascular, Brain. Figure 1 Giant ▶cavernous angioma of the pons. Computed tomography shows a well-defined hyperdense mass (a). On magnetic resonance imaging, the lesion exhibits the classic popcorn-like appearance, with nonhomogeneous aspects on fast-spin-echo T1-weighted (c) and T2-weighted (b) sequences. On gradient-echo sequences, (d) the lesion classically "blooms."

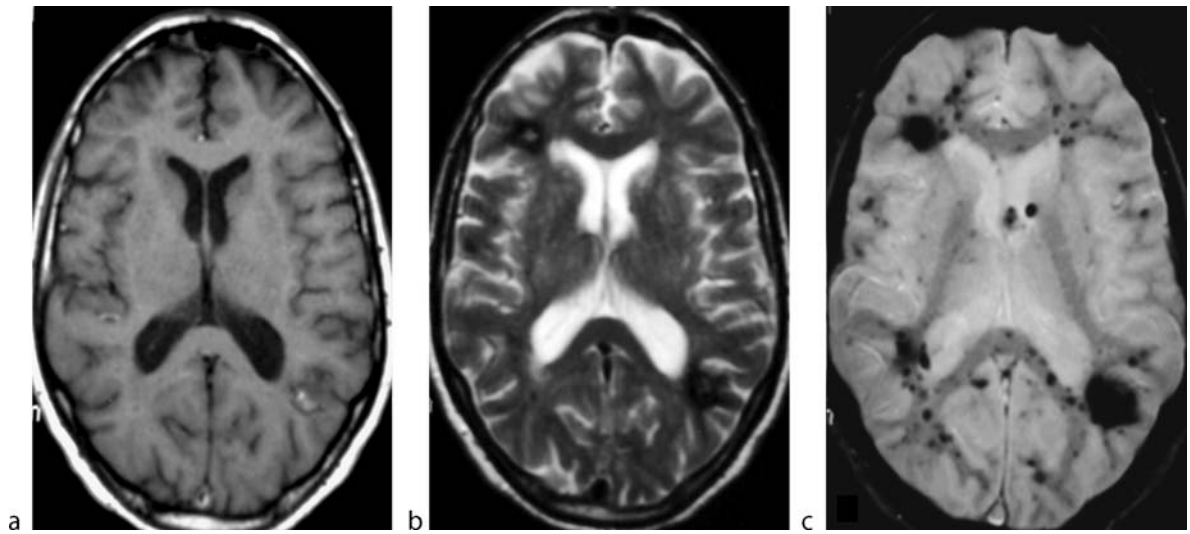

Congenital Malformations, Vascular, Brain. Figure 2 Multiple cavernous angiomas. Fast-spin-echo (FSE) T1-weighted sequence shows multiple round lesions with mixed signal (a). On FSE T2-weighted sequencing, most of the visible lesions are surrounded by a peripheral hypointense rim (b). On gradient-echo T2-weighted sequencing (c), the lesions are more clearly hypointense, and it is possible to detect many small lesions not visible on FSE sequences.

CAs as small hypointense spots that are otherwise not visible with other sequences, especially in multiple forms (Fig. 2).

CAs usually enhance after contrast administration. However, the characteristics of the lesion allow diagnosis without contrast. It is sometimes useful to detect possible associated DVA. Edema and mass effect are absent except in cases of acute bleeding. In this situation, it can often be difficult to identify the lesion within the hematoma.

Developmental Venous Anomaly

DSA: DVAs have a typical angiographic pattern. The arterial and capillary phases are normal, but in the venous phase the lesion becomes evident as a tuft of medullary veins converging toward an enlarged methemoglobin collector vein (caput medusae). The collector drains into a cortical vein, a sinus, or a subependymal vein. However, DSA is not required in the work-up of DVA.

CT: Unenhanced CT is usually normal, although a faint hyperdense area can be seen. After contrast injection, CT shows an intraparenchymal linear vessel corresponding to the collector vein, which can be followed until its entry in a sinus or cortical vein. Also, the venous nest converging toward the collector can usually be detected. Edema and mass effect are absent.

MRI: Unenhanced MRI is able to show the lesion in many cases. The large collector vein appears as a hypointense line on T1 and T2 because of flow void. Sometimes the vein is hyperintense on PD and T2 sequences because of flow-related enhancement due to flow misregistration artifact. Seldom, the radially converging veins can be seen. After contrast, caput medusae can be more easily detected as a tuft of hyperintense thin vessels converging toward a large vein (Fig. 3). On GE sequences an obvious hypointensity can be seen: this has been thought to be related to hemorrhage, but it could simply depend on deoxyhemoglobin in the venous blood. GE sequences are also useful for recognizing associated CA. A Magnetic resonance angiography (MRA) is not necessary but sometimes can show the converging veins. The adjacent parenchyma usually has normal intensity, although hyperintensity suggestive of gliosis has been described.

Capillary Telangiectasia

DSA and CT: Usually normal.

MRI: MRI occasionally shows a solitary hyperintense lesion on T2-weighted sequences, but the lesion is not visible on T1-weighted sequences. More commonly, CTA can be detected as a lacelike region of spotted contrast enhancement with no or minimal signal change on unenhanced images (Fig. 4). GE sequences show a hypointense spot and are more sensitive than unenhanced spin echo (SE) and fast spin echo (FSE) because the lesion often contains hemoglobin degradation products.

Arteriovenous Malformation

DSA: Both the enlarged feeding vessels as well as the nidus and the dilated draining veins can be visualized. Pial AVM

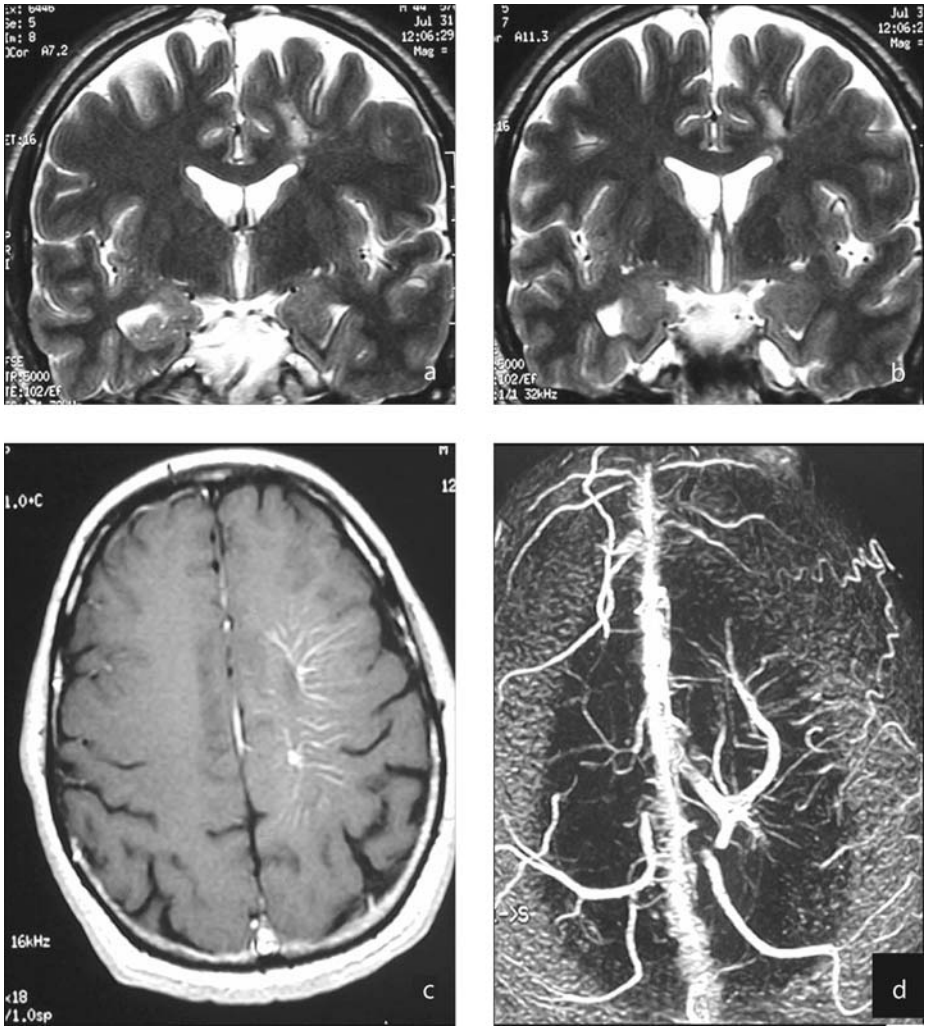

Congenital Malformations, Vascular, Brain. Figure 3 Developmental venous anomaly (DVA). FSE T2-weighted sequence (a, b) shows a left frontal hyperintense area contiguous with an enlarged cortical vein, recognized for the presence of flow void. After contrast administration (c), the DVA is evident by the classic medusae caput sign. MRA imaging (three-dimensional time-of-flight) offers a suggestive visualization of the enlarged veins converging toward a cortical vein (d).

often appears wedge-shaped with a broad cortical base. Dural AVM may have multiple dural feeders.

CT: Pial AVMs will appear slightly hyperdense on unenhanced CT with possible calcification. There is strong enhancement after contrast injection. CT often remains normal in dural AVM.

MRI: Pial AVMs will be visible on T2-weighted images, and different stages of associated hemorrhage can be assessed (Fig. 5). In dural AVM, dilated cortical veins can occasionally be detected.

Diagnosis

Classic CAs are easily diagnosed with MRI. An effort in determining anatomic location is important for surgical planning because eloquent areas could be damaged during surgery. Therefore, f-MRI is often performed to recognize eloquent areas, and MRI-based neuronavigation systems are used during surgery. Other important preoperative information is the presence of an associated DVA that should be spared by surgery.

In patients with acute hematoma, it is difficult to make out the CA, but it becomes obvious at follow-up. A bleeding CA must also be differentiated by hemorrhagic tumors: Useful tips are the complete peripheral ring and the absence of edema and tumoral tissue.

The differential diagnosis can be difficult for the smallest lesions appearing as focal hypointensity on T2-weighted FSE and GE sequences, as the same pattern could be related to residua of hemorrhage.

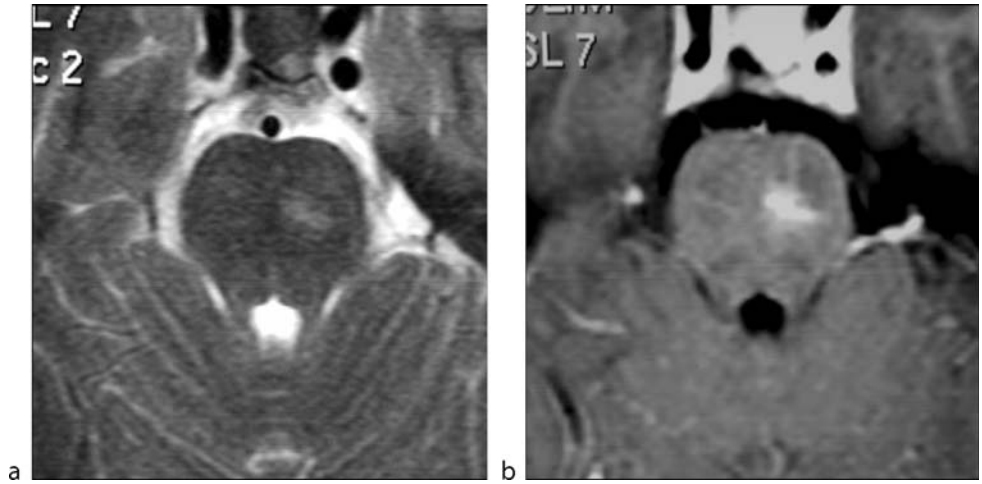

Congenital Malformations, Vascular, Brain. Figure 4 ►Capillary telangiectasia. The lesion appears as a smooth hyperintense area on T2-weighted image (a) that, after contrast administration (b), shows a faint contrast enhancement.

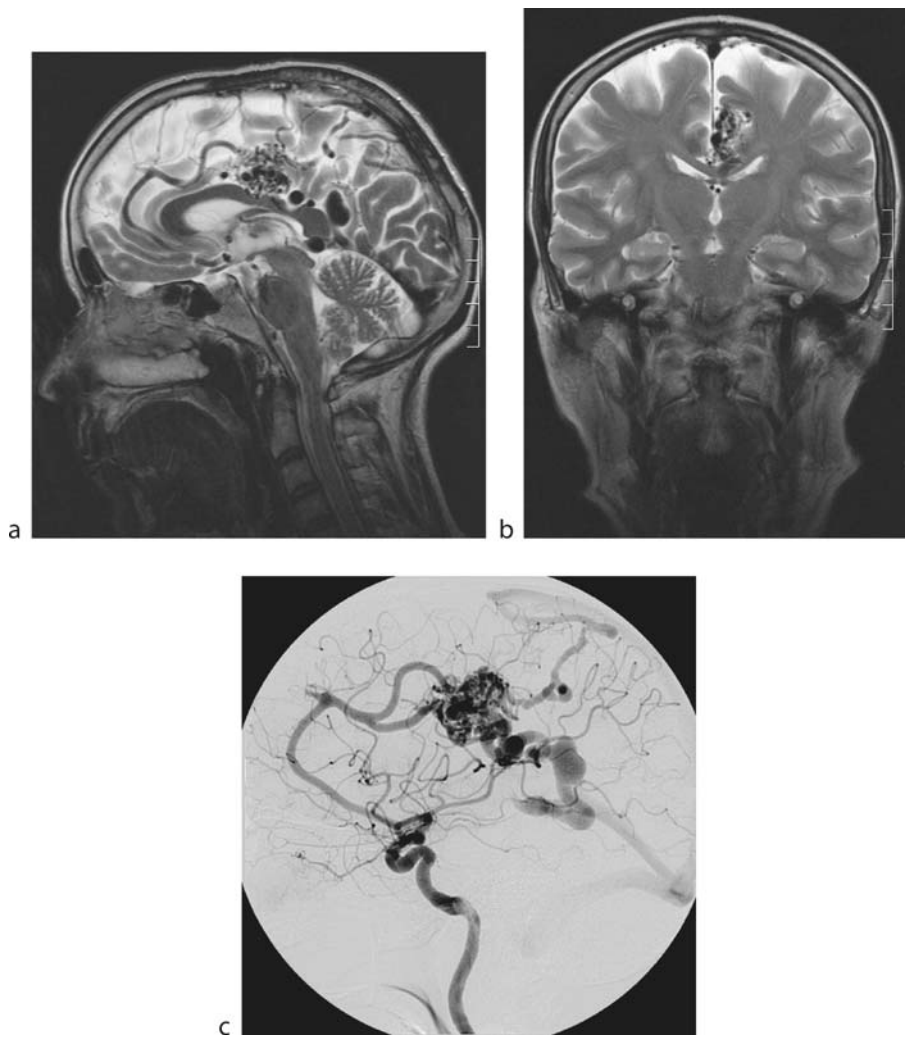

Congenital Malformations, Vascular, Brain. Figure 5 ►Arteriovenous malformation in the left cerebral hemisphere on magnetic resonance angiography (a). Dilated venous structures are seen on the axial (b) images as well as the nidus (c).

When multiple lesions are found, the diagnosis is easy if the lesions are typical for CA. However, if multiple hypointense foci are found and no typical lesion is recognized, the differential diagnosis with amyloid angiopathy, disseminated intravascular coagulation, and hypertensive angiopathy is difficult. In these cases, clinical information is essential.

Extraaxial CA can be difficult to differentiate from neurinoma or meningioma.

DVA imaging findings are very typical, so DVAs are rarely misdiagnosed. With perfusion MRI, an increased perfusion in the territory of the DVA can be evident; it is supposed to not correlate with symptoms and should not be interpreted as a complication.

The diagnostic work-up of AVMs includes DSA, MRI, and often fMRI to localize eloquent areas.

Bibliography

1. Lasjaunias P, Burrows P, Planet C (1986) Developmental venous anomalies (DVA): the so-called venous angioma. Neurosurg Rev 9:233–242
2. Dillon WP (1997) Cryptic Vascular malformations: controversies in terminology, diagnosis, pathophysiology, and treatment. Am J Neuroradiol 18:1839–1845
3. Guclu B, Ozturk AK, Pricola KL et al (2005) Cerebral venous malformations have distinct genetic origin from cerebral cavernous malformations. Stroke 36:2479–2480
4. Abe T, Singer RJ, Marks MP et al (1998) Coexistence of occult vascular malformations and developmental venous anomalies in the central nervous system: MR evaluation. Am J Neuroradiol 19:51–57

Congenital Metabolic Disorders

►Neurometabolic Disorders

Congenital Neonatal Pneumonia

►Chest, Neonatal

Congenital Scoliosis

Lateral curvature of the spine due to congenital vertebral anomalies.

►Congenital Malformations of the Musculoskeletal System

Congenitally Short Pancreas

►Congenital Anomalies of the Pancreas

Congential Malformations, Genitourinary Tract; Including Ureter and Urethra

M. Riccabona, R. Fotter
Department of Radiology
Division of Pediatric Radiology
University Hospital Graz, Graz, Austria
michael.riccabona@klinikum-graz.at
richard.fotter@meduni-graz.at

Synonyms

Congenital anomalies or malformations of the urinary tract

Definition

Urinary tract malformations include congenital anomalies that cause disease and potential sequelae. Differentiation of some anatomic variants from malformations is difficult and seen differently at different centres; in some conditions a clear differentiation of a 'variation' versus a 'malformation' can only be established retrospectively, with knowledge of the patient's history. Thus—in addition to 'real malformations'—a number of conditions and abnormalities have to be listed that may partially present as a non-symptomatic variants such as ►duplex kidneys (Table 1). These and rotational, positional as well as ►fusion anomalies of the kidneys have been addressed in the chapter ►Urinary Tract-anatomic variants, though some forms rather represent a malformation such as the rare 'cross fused ectopic duplex kidney'. Other variants may eventually cause disease and thus need to be mentioned here, such as an unusual course of the left renal vein (retroaortal left renal vein with nutcracker syndrome) or a prominent or accessory (segmental) renal artery obstructing the ureter, the uretero-pelvic junction or the calyceal neck causing a (disproportional) dilatation of the affected part. Malformations of the renal parenchyma include cysts (see entry ►Cystic Renal Disease, Childhood), ►dysplasia of various degrees as well as some syndromal or inherited

Congential Malformations, Genitourinary Tract; Including Ureter and Urethra. Table 1 List of common renal malformations

Duplex and triplex kidneys[a]
with orthotopic or ectopic ureteral insertion, duplex or triple ureter or ureter fissus
with or without partially dilated collecting system (refluxing or obstructive)
with or without (partial or segmental) dysplasia
bifid collecting system ('incomplete duplication')
Malrotation, malposition, and ectopia (abdominal, thoracic) and renal agenesis[a]
Fusion anomalies: horseshoe kidney (pre-aortal isthmus), crossed fused renal ectopia[a]
Persisting or unusual course of (accessory) renal vessels[a]
accessory renal arteries and/or veins, retro-aortal (left) renal vein
retro-/circumcaval ureter; compression of the ureter in a horseshoe kidney
Calyceal abnormalities: calyceal diverticulum, tertiary calyx, hydro- and megacalicosis[a]
(generalised or focally/isolated),
Dilatation of the renal pelvis:
laxity, non-symptomatic variation (extra-renal pelvis)[a]
secondary to
obstruction: megaureter, uretero-pelvic- and uretero-vesical junction obstruction
dilating VUR
Renal parenchymal malformations:
Cysts and cystic diseases (see also entry …)
Dysplasia, hypoplasia, nephronophthisis, nephroblastomatosis
Involvement in systemic or syndromal disease (Tyrosinosis, Alport syndrome …)

[a]These entities may be non-symptomatic, then considered a variant (see entry ▶Urinary tract, childhood, normal anatomy and variants) or may cause symptoms and sequelae and then considered a malformation.

conditions (Table 1). Furthermore, some variants may cause impaired urinary drainage and hydronephrosis such as an abnormal course and position of the ureter (i.e. in retro-caval ureter or compression of the ureter by a horseshoe kidney).

In the lower urinary tract, a number of conditions must be mentioned such as malformations of the uretero–vesical junction, an ureterocele, ectopic ureteral insertion, a persisting urachus, bladder diverticula, bladder septation and—in rare cases—duplication (Table 2). The most severe bladder malformation is ▶bladder exstrophy. The urethra as well has a number of malformations, the most common and most dreadful malformation being congenital posterior urethra valves (Table 2). Furthermore there are urethral diverticula as well as pathologic opening and fusion of the urethra leading to various degrees of hypospadia and epispadia. Other rare conditions which need to be mentioned are the prune belly syndrome, the megacystis–megaureter–hypoperistalsis syndrome and urinary tract malformations associated with other systemic or syndromal disease.

Embryology and pathogenesis: The embryology of the urinary tract is described in the entry ▶Urinary Tract, Normal Anatomy and Variations. The various malformations mostly are caused by disruption of the physiological development, and cannot be defined in detail for all these conditions. Due to the common development of the genital and the urinary tract, urinary tract malformations are frequently associated with genital anomalies, typically presenting on the same side as the urinary tract pathology (for more details see entry ▶Genital tract, Childhood). This association needs to be remembered and properly addressed by imaging, particularly as the female genitalia may be difficult to image after the initial months of life until late childhood. Typical anomalies are cystic seminal vesicles, vaginal and uterine duplications, uterine hypo- or aplasia, ovarian hypo- and dysplasia or agenesis and cystic remnants of the Wolffian and Müllerian duct. The most complex entity of these is the cloacal malformation, which usually involves not only the urinary, but also the genital and the anorectal tract, often associated with lower spinal malformations and neurological impairment, which are beyond the scope of this chapter to describe.

Imaging

Depending on the level and severity of the malformation, different modalities will become indicated. Ultrasound (US) in general constitutes the basic imaging tool that then helps to decide on further imaging needs. Depending on the underlying condition nearly all imaging modalities

Congential Malformations, Genitourinary Tract; Including Ureter and Urethra. Table 2 List of most important lower urinary tract malformations

Duplications of bladder, ureter, urethra, ureter fissus[a]
bladder septations[a]
Uretero-vesical junction pathology:
Megaureter (refluxing and/or dysplastic and/or obstructive)
ostial diverticula, atypical ostium (golf hole ostium …)
malpositioned or ectopic ureteric course and insertion[a]
draining into bladder neck, urethra, rectum and perineum genitalia (vagina)
Persisting urachus, urachus cyst/-diverticula[a]
Diverticulum and sacculation[a]
Megacystis[a]
Posterior urethral valve, urethral webs other urethral stenoses
hypo- and episadia, and strictures
Urethral, vesical and ureteral polyps, valves and folds
Complex cloacal malformations, urogenital sinus
Bladder extrophy
Agenesis of the bladder

Note: There may be numerous associated anomalies of the genital tract (see entry ▶genital tract, childhood).

[a]These entities may be non-symptomatic, then considered a variant (see entry ▶Urinary tract, childhood, normal anatomy and variants), or may cause symptoms and sequelae and then considered a malformation.

may become indicated and are used for complete—particularly pre-operative—workup of children with (complex) urinary tract malformations.

Imaging modalities: In mild forms and for pre-natal examinations imaging consists simply of US; post-natally this maybe complemented by voiding cystourethrography (VCUG) and scintigraphy. In more complex cases a more detailed renal imaging by intravenous urography (IVU) in former times and *MR-urography* (MRU) today commonly becomes necessary. *Renal scintigraphy* provides an excellent assessment of renal function and drainage and can be particularly useful for follow-up comparison. If associated skeletal anomalies need to be assessed and evaluated for planning surgical procedures like in complex bladder exstrophy, plain films (to look at the spine, pelvis) and a pelvic CT may become valuable, particularly using 3D reconstruction and viewing techniques of modern *multi-slice CT*. *Interventional radiology* may offer treatment options in severe obstruction—particularly as a bridging measure—till completion of diagnoses and definite surgery, or may serve as a tool for managing post-operative complications. While these interventional procedures were more frequently performed some decades ago, the change in paradigms based on modern insights in development and prognosis of urinary tract malformations has significantly reduced indication for these procedures, which today are considered helpful mostly for severe bilateral obstruction or intractable infection in an obstructed system. Today measures for remodelling the collecting system without impact on future renal development are deemed less important; the final goal of treatment is preservation of renal function. Therefore—in all these malformations—this final goal becomes the only evidence based driving force that indicates imaging and allows deciding on an individually adapted imaging algorithm.

Imaging algorithms: The task of imaging is often to confirm a pre-natally suspected condition and then to identify the entity. A thorough investigation of the entire genito-urinary tract for depiction of or ruling out associated malformations and dysfunctions needs to be performed in more severe findings such as severe dilatation (e.g. uretero-pelvic—and uretero-vesical junction obstruction, posterior urethral valve), cystic and dysplastic kidneys, duplex systems with disproportional widened moieties or focal dysplasia, ureteroceles, ▶ectopic kidneys and ureters, severe hypo-/epispadia and bladder exstrophy. Finally imaging must provide some grading, not only for initial estimation of the severity of the disease and consecutive implications on treatment, but also for comparison during follow-up, particularly in the increasing number of patients who are treated conservatively. And imaging should provide the pre-operative anatomic information as necessary for the surgeon.

Taking all these tasks into consideration imaging usually starts with a detailed US in a well hydrated child. US not only provides a basic information and overview, but very often is able to establish a definite diagnosis and —to a certain extent—rate the degree of disease. Further imaging is defined by these initial US findings: In a neonatal boy with significant urinary tract dilatation or bladder anomaly, an additional VCUG is recommended for assessment of urethral pathology. (Delayed) renal scintigraphy is usually performed for a baseline assessment of renal function and potential scarring. Diuretic renal scintigraphy and MRU are performed in obstructive and dilative uropathy that potentially need surgery. IVU is rarely used today, sometimes—if MR is unavailable—for pre-operative imaging (to provide basic anatomic information or to rule out a duplex system) and in the post-operative setting for diagnosing post-operative complications. Note, that these investigations should be tailored to the individual query with an adapted imaging protocol (contrast- and X-ray-dose, adapted timing of the individual exposures …). For follow-up, US supplemented by VCUG or contrast-enhanced cystosonography (for refluxing disease) or by diuretic renography

and functional semi-quantitative MRU (for obstructing uropathy) are generally recommended.

Diagnosis

Diagnosis is made by imaging as described above, using the criteria listed in the definition and imaging sections.

Bibliography

1. Barnewolt CE, Paltiel HL, Lebowitz RL et al (1998) The genito-urinary tract. In: Kirks DR (ed) Practical Pediatric Imaging. 3rd edn. Lippincot-Raven publishers, Philadelphia, pp 1005–1175
2. Berdon WE (1991) Contemporary approach to pediatric urologic problems. Radiol Clin North Am 29:605–618
3. Currarino G, Wood B, Majd M (1993) The genitourinary tract and retroperitoneum. congenital renal anomalies. In: Silverman FN, Kuhn JP (eds) Caffey's Pediatric X-Ray Diagnosis: An Integrated Imaging Approach. Vol. 2., 9th edn. Mosby St. Louis, Baltimore, Boston, Chicago, London, Philadelphia, Sydney, Toronto, pp 1223–1243
4. Daneman A, Alton DJ (1991). Radiographic manifestations of renal anomalies. Radiol Clin North Am 29: 351–363
5. Ritchey M (1992) Anomalies of the kidney. In: Kelalis PP, King LR, Belman AB (eds) Clinical Pediatric Urology. Vol. 1, 3rd edn. WB Sounders Company Philadelphia, London, Toronto, Montreal, Sydney, Tokyo, pp 500–528

Congential Malformations, Mullerian Duct

Justus E. Roos
Department of Radiology
Stanford University Medical Center, Stanford, USA
justus.roos@stanford.edu

Synonyms

Congenital anomalies of the uterus

Definition

The female reproductive system develops from the two paired müllerian ducts (synonym: paramesonephric duct) that originate in the embryonal mesoderm lateral to each wolffian duct (synonym: mesonephric duct). The paired müllerian ducts grow in medial and caudal directions, and at 9 weeks of gestation, the cranial part remains nonfused and forms the fallopian tubes. The caudal part fuses to a single canal forming the uterus and the upper two-thirds of the vagina. This is called lateral fusion. In a process called vertical fusion, the intervening midline septum undergoes regression. The caudal part of the vagina arises from the sinovaginal bulb and fuses with the lower fused müllerian ducts. The ovaries originate from the gonadal ridge, a completely different tissue than the mesoderm forming both the urinary and genital systems. Pathogenesis of müllerian duct anomalies (MDA) can be basically classified into the presence of agenesis, hypoplasia, and defects in vertical and lateral fusion of the paired ducts. In 1988, the American Fertility Society (AFS) (1) presented a consensus in classification of uterovaginal anomalies and published a schematization system that is widely accepted among specialists. Most MDA are considered to occur sporadically and some reports give descriptions of the patterns of inheritance. The most well-known anomalies are those induced by exposure to teratogenic agents such as di-ethyl-stilbestrol (DES) and thalidomide (2).

Pathology

According to the classification of the AFS (1), MDA can be classified into seven different classes of uterine anomalies (Fig. 1). Because of the wide variability and overlap of associated cervical and vaginal anomalies, the classification primarily describes uterine defects, whereas cervicovaginal defects must be added separately in the form of a subset. The diagnosis of MDA is based on the clinical presentation and physical examination. This examination consists mainly of the work-up with different imaging methods (3, 4), in which magnetic resonance imaging (MRI) takes a leading role, especially in complex uterine malformation. The different types of MDA and their definition based on their presentations are described in the diagnosis section.

Clinical Presentation

To state the real prevalence, incidence, and distribution of MDA is difficult because of the use of nonstandardized classification systems, different datasets, and varying patient populations examined in clinical studies. The overall data suggest that the prevalence of uterovaginal anomalies approximates 1% in the general population among women with normal and abnormal fertility (3, 4). While the majority of women with MDA have little problem conceiving, they run the risk of spontaneous abortion, premature delivery, abnormal fetal position, and difficulties during delivery. The prevalence of MDA among women with repeated pregnancy loss is around 3% (3–5).

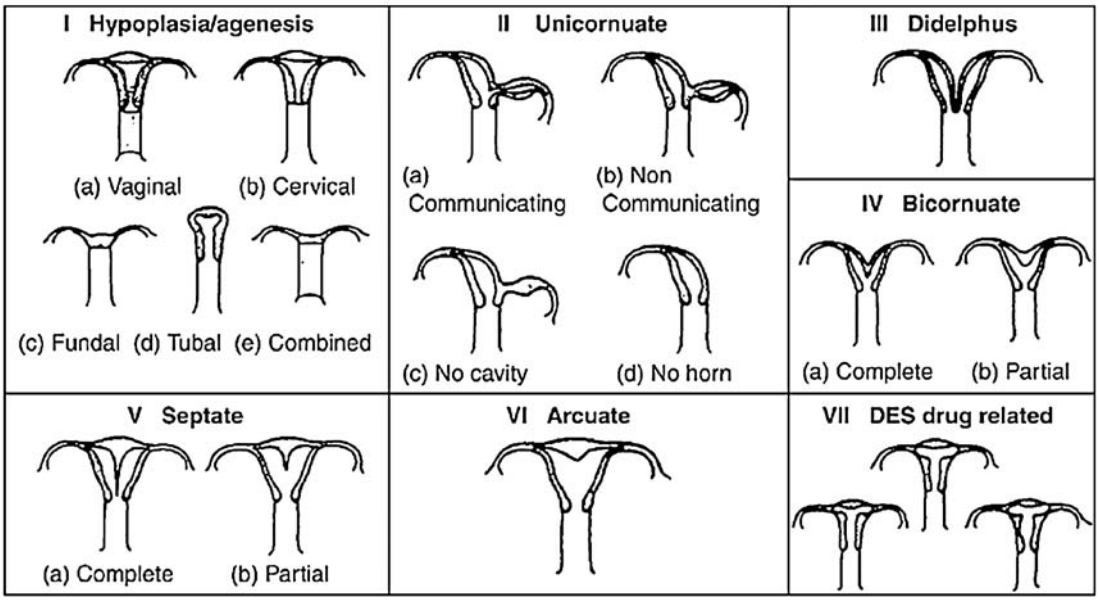

Congential Malformations, Mullerian Duct. Figure 1 Classification system of müllerian duct anomalies (American Fertility Society) (Anonymous, 1998 The American Fertility Society classifications of adnexal adhesions, distal tubal occlusion, tubal occlusion secondary to tubal ligation, tubal pregnancies, müllerian anomalies and intrauterine adhesions. Fertil Steril 49:944–955).

Imaging

The three imaging pillars of MDA are ultrasonography (US), conventional hysterosalpingography (HSG), and MRI.

US imaging should be performed during the secretory phase for the best evaluation of the endometrium cavity, external uterine contour, and surrounding tissue. Transabdominal US (performed with a 2.5.–5-MHz probe) provides information about the entire abdomen, especially of the kidney and the genital organs. Transvaginal US (performed with a 5–8-MHz endovaginal transducer) has the advantage of increased spatial resolution, although at the expense of a decreased field of view. Hysterosonography, which consists of endovaginal US with prior infusion of saline or ultrasound contrast agent into the endometrial canal, allows a better delineation of the endometrial cavity and is performed only for selected indications, that is, in patients with a history of infertility. It is approximately 92% accurate for the detection of MDA. Newer techniques, such as three-dimensional US, further improve the imaging diagnostics by giving better information about the external contour of the uterus and its volume.

HSG provides a morphological assessment of the endometrium cavity and supplies information regarding tubal patency. Because only the internal contour of the uterus can be assessed and the outer contour remains unclear, the characterization of uterine anomalies is somehow difficult, especially in the common case of differentiation between bicornuate and septate uterus.

MRI has the best accuracy in the evaluation of uterine anomalies among the three major imaging methods. Accuracy of up to 100% has been reported. MRI allows an excellent delineation of the entire uterus anatomy including the internal and external uterine contour as well as the diagnosis of secondary findings, that is, endometriosis.

The MRI parameter for a complete evaluation of uterine malformations should include the use of: (i) phased array MR surface coil; (ii) acquisition of oblique T2-weighted (T2-W) and T1-weighted (T1-W) fast spin-echo (FSE) images parallel to the long axis of the uterus; (iii) transverse T1-W and T2-W images of the entire pelvis; and (iv) coronal single shot FSE (SSFSE T2-W) or spoiled gradient-echo images (FSPGR) with the kidney in the field of view (3, 4).

Diagnosis

Class I Anomalies

Class I anomalies are characterized by *dysgenesis* (segmental agenesis and variable hypoplasia) of the müllerian ducts (uterus and upper two-thirds of the vagina). Mayer–Rokitansky–Küster–Hauser syndrome is the most common form of Class I anomaly and includes agenesis of the uterus and vagina.

Class II Anomalies

Unicornuate uterus is a result of partial or complete hypoplasia of one müllerian duct (Fig. 2).

Variants: Unicornuate uterus may be isolated (35%) or associated with a contralateral rudimentary horn. The rudimentary horns present with or without communication to the endometrial cavity and may be associated with or without endometrium, which is also called no cavity rudimentary horn. The variable forms of the rudimentary horns determine the surgical procedure.

Class III Anomalies

Uterus didelphys is a result of complete nonfusion of the müllerian ducts forming a complete uterine duplication (Fig. 3).

Variants: Uterus didelphys may be associated with a longitudinal (75%) or, more rarely, with a transverse vaginal septum, the latter causing obstructive hematometrocolpos. A nonobstructive uterus didelphys is usually asymptomatic.

Class IV Anomalies

Bicornuate uterus is the result of incomplete fusion of the cranial parts of the müllerian ducts (Fig. 4).

Variants: Bicornuate uterus occurs with a wide variability. Extension of the intervening fundal cleft to the internal cervical os characterizes the complete bicornuate uterus with a single cervix (bicornuate, unicollis uterus), whereas variants of partial bicornuate uterus exist if the cleft is of variable length. Bicornuate uterus may be associated with a duplicated cervix (bicornuate bicollis uterus) as well as with a longitudinal vaginal septum, which coexists in up to 25% of cases of bicornuate uterus.

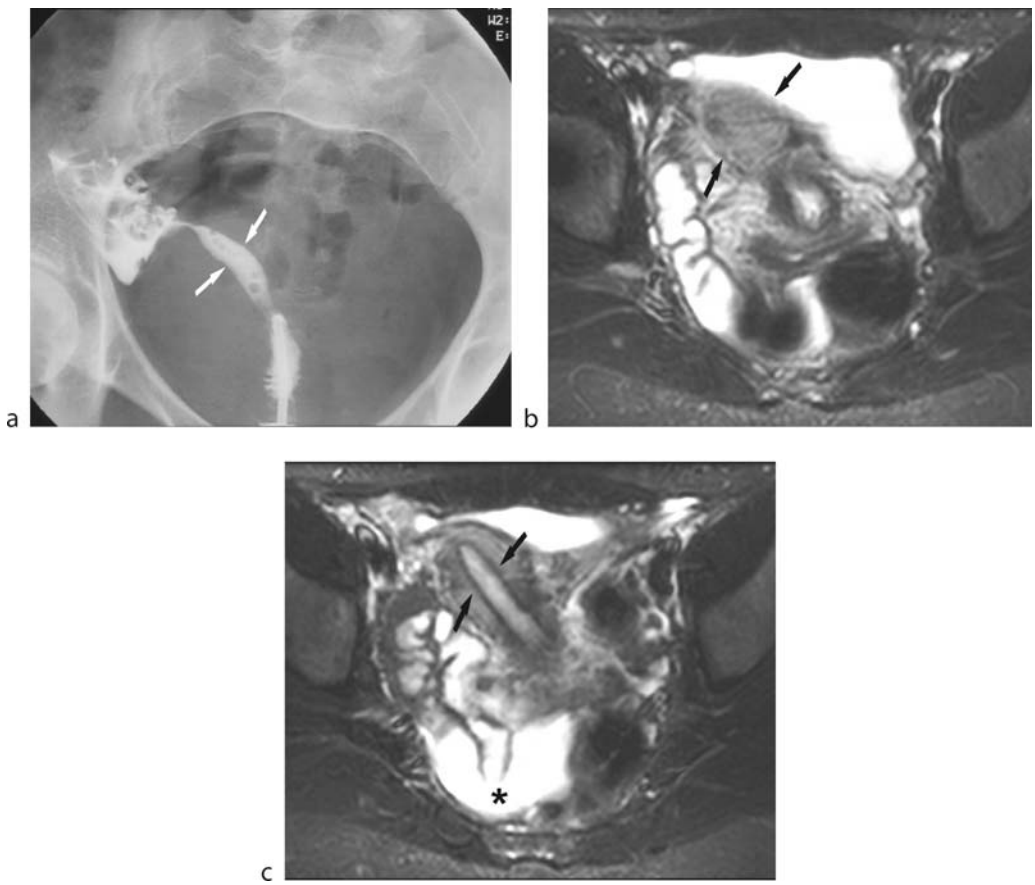

Congential Malformations, Mullerian Duct. Figure 2 A 28-year-old female patient with infertility. HSG (a) shows a fusiform configuration of one endometrial cavity (*arrow*) draining into one fallopian tube. Note the small uterus, which is deviated to one side suggesting the diagnosis. Iatrogenic filling defects in the uterine cavity by air bubbles. Oblique T2-W MR images (b, c) confirm the diagnosis of a unicornuate uterus with presence of a small but elongated uterus that shows normal zonal anatomy (*arrows*). No rudimentary horn is present in this case. Some fluid is present in the pouch of Douglas (*asterisk*).

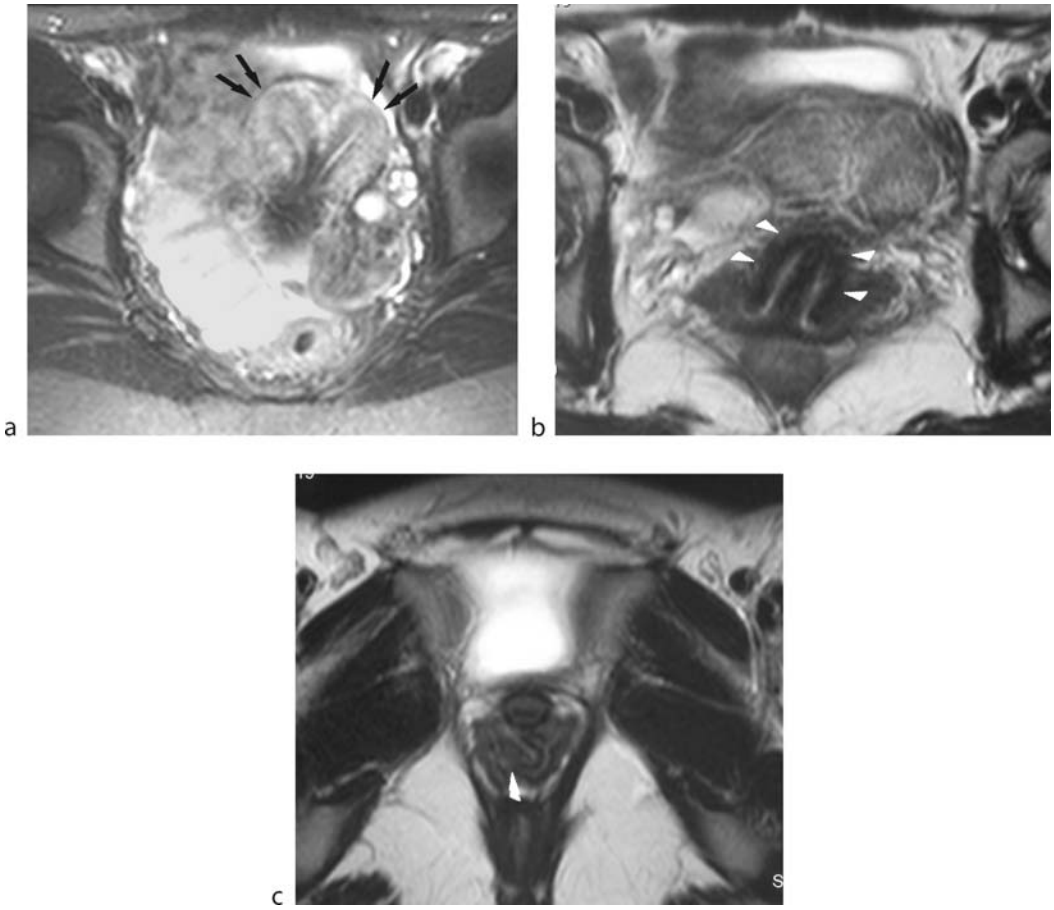

Congential Malformations, Mullerian Duct. Figure 3 **A 33-year-old female patient with history of partially resected longitudinal vaginal septum. Transverse oblique T2-W MR images (a, b) show complete duplication of the uterine horns (*arrows*) as well as two duplicated cervices (*arrowheads*). No communication between the two endometrial cavities is present; the cavities show their normal zonal anatomy. Note the longitudinal vaginal septum (c) which appears in 75% of uterus didelphys (*double arrowhead*).**

Class V Anomalies

Septate uterus is the result of partial or complete nonregression of the midline uterovaginal septum. According to its definition, the external contour of the uterine fundus may be either convex or mildly concave (<1 cm). This distinction determines whether it is a septate uterus or a bicornuate or didelphic uterus (Fig. 5).

Variants: Septate uterus is the most common MDA and is unfortunately associated with the poorest reproductive outcome (Table 1). Because of different treatment options, septate uterus must be differentiated from bicornuate and didelphic uterus. A widely accepted definition therefore—empirically invented during laparoscopy procedures—states that a uterus is septate if the outer contour of the uterine fundus is only mildly concave in the presence of a septum. The cutoff of concavity is 1 cm; deeper concavity is associated with bicornuate uterus and uterus didelphys. In a complete septate uterus, the septum extends to the external cervical os. In 25% of septate uteri, the septum extends even further into the upper part of the vagina.

Class VI Anomalies

Arcuate uterus is the result of a near complete regression of the uterovaginal septum forming a mild and broad saddle-shaped indentation of the fundal endometrium. Differentiation from bicornuate uterus is based on the complete fundal unification; however, a broad-based septate uterus is difficult to distinguish from an arcuate uterus. There is much controversy as to whether an arcuate uterus should be considered a real anomaly or an anatomic variant.

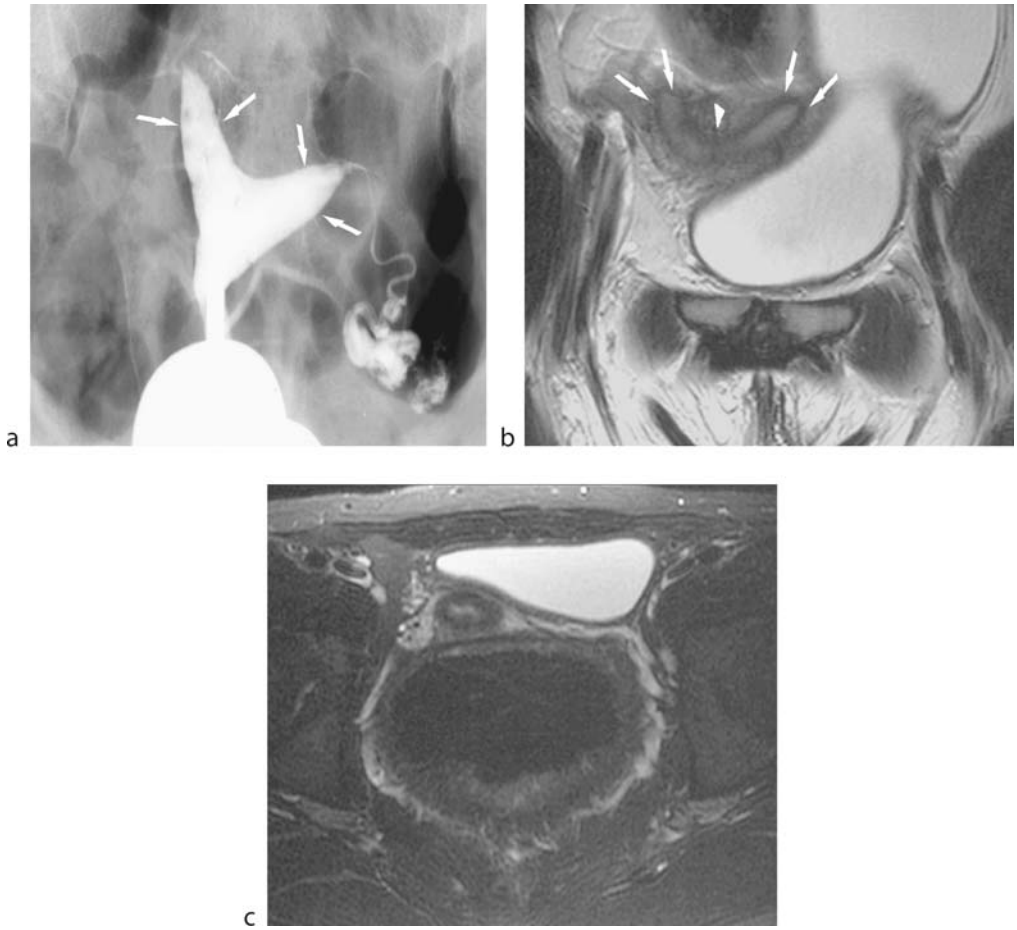

Congential Malformations, Mullerian Duct. Figure 4 A 17-year-old female patient with chronic obstipation and a history of anal surgery as a neonate. HSG (a) shows one cervix, but two separated endometrial cavities (*arrows*), (b) T2-W MR image shows the two separated uterine horns (*arrows*) with communication of their endometrial horns in the mid to lower portion of the uterus. Note the deep (>1 cm) external fundal cleft (*arrowhead*) between the endometrial cavities (*arrows*), a specific characteristic allowing differentiation from a uterus septus. Transverse T2-W MR image at the level of the cervix demonstrates a single cervix, called the bicornuate unicollis uterus.

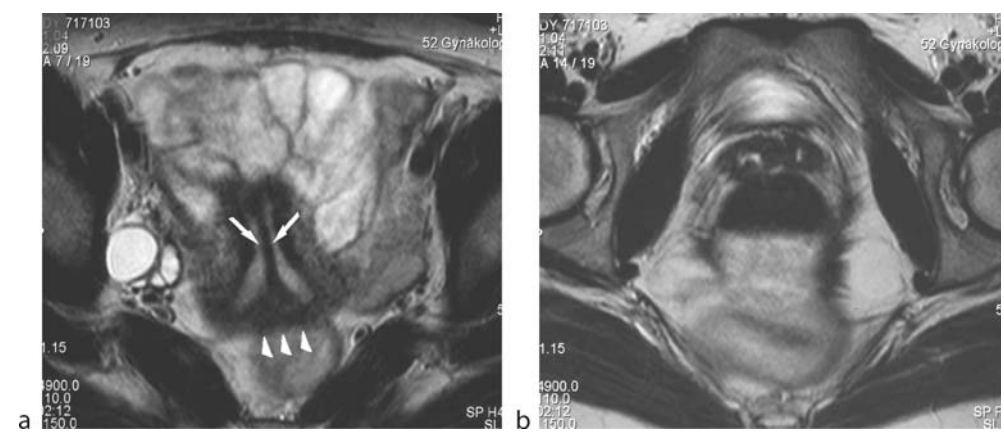

Congential Malformations, Mullerian Duct. Figure 5 A 29-year-old female patient with infertility. Transverse oblique T2-W MR image (a) demonstrates a retroverted uterus with convex uterine fundal contour (*arrowheads*) and a hypointense thin septum dividing the endometrial cavity (*arrows*). The se•ptum extends to the external cervical os (b).

Congential Malformations, Mullerian Duct. Table 1

Müllerian duct anomalies (MDA)	Influence on reproductive/obstetric outcome			Other major associations
	Spontaneous abortion	Premature delivery	Fetal survival rate	
Class I: Dysplasia (4–10%)	No potential for reproduction			Mayer–Rokitansky–Küster–Hauser syndrome
Class II: Unicornuate uterus (5%–20%)	50% (41–62%)	15% (10–20%)	40% (38–57%)	Renal agenesis 67%
Class III: Uterus didelphys (5–11%)	45% (32–52%)	38% (20–45%)	55% (41–61%)	Longitudinal vaginal septum 75%
Class IV: Bicornuate uterus (10–39%)	30% (28–35%)	20% (14–23%)	60% (57–63%)	High cervical incompetence 38%
Class V: Septate uterus (34–55%)	65% (26–94%)	20% (9–33%)	30% (10–75%)	Vaginal septum 25%
Class VI: Arcuate uterus (7%)	Mostly compatible with normal-term gestation			
Class VII: DES-exposed uterus	Increased	Increased	Decreased	Cervical anomalies 44%

Note: All percentages data are pooled from the current literature (4, 5), values in brackets represent percentages ranges (4, 5).

Class VII Anomalies

DES-exposed uterus. DES (synthetic estrogen, 1948–1971) may induce abnormal myometrial hypertrophy in the fetal uterus forming small T-shaped endometrial cavities as well as increase the risk of developing a clear cell carcinoma of the vagina (2). The characteristic uterine abnormalities must be categorized in the group of complex uterine anomalies and may occur with or without exposure to DES.

Bibliography

1. Anonymous (1998) The American Fertility Society classifications of adnexal adhesions, distal tubal occlusion, tubal occlusion secondary to tubal ligation, tubal pregnancies, müllerian anomalies and intrauterine adhesions. Fertil Steril 49:944–955
2. Kaufman RH, Adam E, Hatch EE et al (2000) Continued follow-up of pregnancy outcomes in diethylstilbestrol-exposed offspring. Obstet Gynecol 96:483–489
3. Saleem SN (2003) MR imaging diagnosis of uterovaginal anomalies: current state of the art. Radiographics 23:e13
4. Troiano RN, McCarthy SM (2004) Müllerian duct anomalies: imaging and clinical issues. Radiology 233:19–34
5. Nahum GG (1998) Uterine anomalies. How common are they, and what is their distribution among subtypes? J Reprod Med 43:877–887

Congestive Cardiac Cirrhosis

Cardiac cirrhosis includes a spectrum of hepatic derangements that occur in the setting of right-sided heart failure. Clinically, the signs and symptoms of congestive heart failure (CHF) dominate the disorder. Cardiomegaly, pulmonary venous hypertension, pulmonary edema, or pleural effusion may be observed on chest radiography, while hepatomegaly, splenomegaly, and ascites are usually shown at abdominal US, CT, or MR examination.

▶Vascular Disorders, Hepatic

Connective Tissue Disorders, Gastrointestinal Tract

Frank Pilleul
Gastro-intestinal and Emergency Imaging Department, Hôpital Universitaire Edouard Herriot, Lyon-France
frank.pilleul@chu-lyon.fr

Definition

A family of more than 200 disorders affects the connective tissues. These disorders can result either from alterations in genes responsible for building tissues, known as heritable connective tissue disorders (HCTD), or from chronic degenerative and/or inflammatory conditions that result from abnormal immune reactions to compounds absorbed from the environment, known as connective tissue diseases (CTD) or autoimmune diseases (AID).

In cases of HCTD, the structure and development of skin, bones, joints, heart, blood vessels, lungs, bowel wall, eyes, and ears may change directly related to mutations in genes. Ehlers–Danlos syndrome and Marfan syndrome, which affect large blood vessels including the splanchnic arterial system, are two common HCTD indirectly involving the gastrointestinal (GI) tract by ischemia, hemorrhage, or both.

CTD affect approximately 8% of the population, 78% of whom are women (1). The reasons for the high prevalence in women are unknown. AID can affect virtually every site in the body, including the endocrine system, connective tissue, GI tract, heart, skin, and kidneys. At least 15 diseases are known to be the direct result of an autoimmune response, while circumstantial evidence

implicates more than 80 conditions involving autoimmunity. Some of these CTD can involved the GI tract, such as systemic lupus erythematosus (SLE), vasculitis (Behçet's disease, polyarteritis nodosa, microscopic polyangiitis, rheumatoid vasculitis, Buerger's disease, Takayasu arteritis), and scleroderma.

Pathology/Histopathology

The pathogenesis of AID or CTD is not completely known. AID tend to cluster in families and in individuals, which indicates that common mechanisms are involved in disease susceptibility. Studies of the prevalence of AID in monozygotic twins show that genetic as well as environmental factors (such as infection) are necessary for the disease to develop (2).

Because infections generally occur well before the onset of symptoms of AID, clinically linking a specific causative agent to a particular AID is difficult. AID occurs when a response against one or more self-antigens involving T cells, B cells, or autoantibodies induces injury systemically or against a particular organ (2).

In most animal models of autoimmunity, disease has been transferred to naïve animals with autoimmune cells (splenocytes or T cells), autoantibodies, or both, which provides compelling evidence that infections induce AID by immunomediated mechanisms.

Furthermore, some hypotheses suggest that individuals who express specific human leukocyte antigens (HLA) such as HLA-DR4 or HLA-DQB1 are genetically predisposed. The frequency of HLA-DR4 in patients with CTD is estimated to be 52%. The specific nature of the HLA associations that occur in patients with CTD may vary depending on the ethnicity of the population studied.

Clinical Presentation

GI tract involvement is nonspecific in connective tissue disorders and includes dysphagia, abdominal pain, nausea, vomiting, constipation, diarrhea, and malabsorption. Some complications such as ischemia, infarction, occlusion, perforation, and bowel hemorrhage have been described in the literature as being due to focal or diffuse necrotizing vasculitis in the systemic vasculature.

In cases of HCTD such as type IV Ehlers–Danlos syndrome, GI complications include diverticula, rectal prolapse, GI bleeding, and spontaneous perforation of the bowel. Spontaneous bowel perforation is a rare, but particularly troublesome complication because of its tendency to recur despite aggressive surgical management. Bowel rupture typically occurs in young adults and is usually situated in the sigmoid colon (3).

In SLE, inflammation of the small blood vessels of the gut produces a variety of complications including intestinal ischemia, hemorrhage, ileus, ulceration, infarction, and perforation (4). SLE may involve any part of the GI tract from the esophagus to the rectum. However, the territory of the superior mesenteric artery is most commonly affected.

In general, in CTD with necrotizing vasculitis, the vasa recta and intramural arteries can affect all sizes of blood vessels. The clinical course of disease depends on the size and location of the affected vessel and may be indistinguishable from signs of mesenteric ischemia, GI or intraabdominal hemorrhage, ulceration, or stricture formation.

Digestive involvement in systemic sclerosis is frequent and serious. Esophageal disorder is common with the occurrence of gastroesophageal reflux disease. Gastric involvement is rarely recognized, nor is small intestinal involvement, which may lead to malabsorption, pseudo-obstruction, and bacterial overgrowth. Anorectal involvement is frequent and leads to fecal incontinence and rectal prolapse.

Imaging

Barium Examination

In cases of systemic sclerosis or SLE, a double-contrast examination of the upper GI tract can demonstrate signs of esophagitis, showing "smudged" or "cobblestone" mucosa with thickened and distorted longitudinal folds and sometimes stenosis (Fig. 1).

In cases of CTD with necrotizing vasculitis and SLE, small bowel follow-through can demonstrate irregular thickening and spiculation in the folds of the multiple segments of the duodenum to the terminal ileum, thumbprinting suggestive of ischemic change, and multiple submucosal nodules. Furthermore, in some cases large ovoid or irregular ulcers with marked thickening or multiple small, discrete, "punched-out" ulcers can be identified.

Computed Tomography

Computed tomography (CT) has recently proved to be effective not only for detecting primary lesions, but also for excluding extraluminal complications. Ischemia due to SLE or CTD produces various morphologic changes, including homogeneous or heterogeneous hypoattenuating or hyperattenuating wall thickening, dilatation, abnormal wall enhancement (Fig. 2), mesenteric stranding, vascular engorgement, ascites, pneumatosis, and portal venous gas, particularly in the distribution of the superior mesenteric artery. The bowel wall thickening

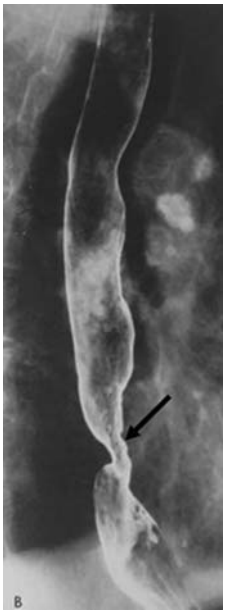

Connective Tissue Disorders, Gastrointestinal Tract. Figure 1 Esophageal stenosis (*black arrow*) postesophagitis in a case of systemic lupus erythematosus identified on upper gastrointestinal follow-through.

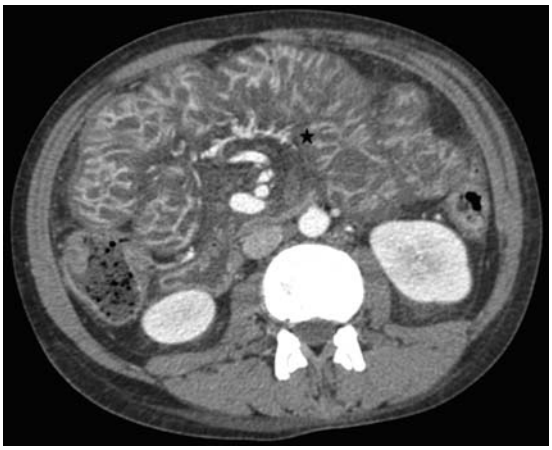

Connective Tissue Disorders, Gastrointestinal Tract. Figure 2 Contrast-enhanced computed tomography scan shows diffuse small bowel wall thickening (*black star*) in a patient with systemic lupus erythematosus.

detected on CT is due to mural edema, hemorrhage, and/or superinfection of the ischemic bowel wall (5). The greatest incidence of bowel wall thickening is observed in cases of reversible mesenteric ischemia (80%).

Furthermore, CT is very sensitive for detecting abdominal complications such as perforation, occlusion, GI hemorrhage, visceral arterial aneurysm (Fig. 3), and

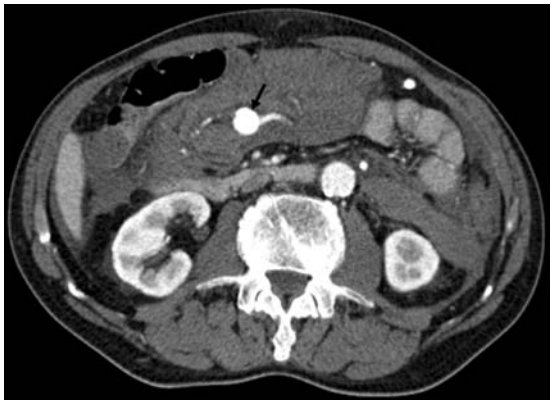

Connective Tissue Disorders, Gastrointestinal Tract. Figure 3 Contrast-enhanced computed tomography scan demonstrates aneurysms of the superior mesenteric artery complicated by mesenteric hematoma in a patient with Behçet's disease.

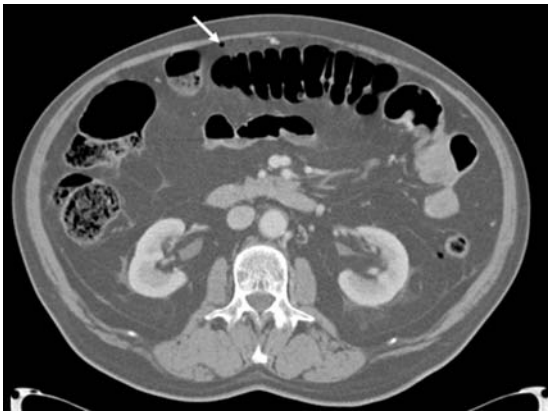

Connective Tissue Disorders, Gastrointestinal Tract. Figure 4 Contrast-enhanced computed tomography scan identifies free air within the peritoneum in a case of systemic lupus erythematosus with small bowel involvement.

peritonitis; CT can easily demonstrate a small amount of intraperitoneal air (Fig. 4), extravasation of contrast within the abdomen, and evident signs of small bowel obstruction.

Diagnosis

The diagnosis and classification of the vasculitis subgroup of CTD relies on a combination of clinical, serological, hematological, radiological, and histological findings. The

Chapel Hill International Consensus Conference classified 10 selected vasculitides depending on the type of vessel predominantly affected.

A diagnosis of SLE can be made with 98% specificity and 97% sensitivity if at least four of the 1982 revised criteria for the classification of SLE are present (7).

Diagnosis of HCTD is often difficult due to the complexity of symptoms and the lack of specific genetic tests. In adulthood, four main clinical findings—a striking facial appearance; easy bruising; translucent skin with visible veins; and ruptured vessels, gravid uterus, or intestines—contribute to the diagnosis, which can be confirmed by the identification of a mutation in the COL3A1 gene coding for type III procollagen.

Bibliography

1. Jacobson DL, Gange SJ, Rose NR et al (1997) Epidemiology and estimated population burden of selected autoimmune disease in the United States. Clin Immunol Immunopathol 84:223–243
2. Rose NR (2002) Mechanisms of autoimmunity. Semin Liver Dis 22:387–394
3. Stillman AE, Painter and R, Hollister W (1991) Ehlers–Danlos syndrome type IV: diagnosis and therapy of associated bowel perforation. Am J Gastroenterol 86:360–362
4. Kistin MG, Kaplan and MM, Harrington JT (1978) Diffuse ischemic colitis associated with systemic lupus erythematosus: response to subtotal colectomy. Gastroenterology 75:1147–1151
5. Ha HK, Lee SH, Rha SE et al (2000) Radiologic features of vasculitis involving the gastrointestinal tract. Radiographics 20:779–794
6. Tan EM, Cohen AS, and Fries JF (1982) The 1982 revised criteria for the classification of systemic lupus erythematosus. Arthritis Rheum 25:1271–1277

Connective Tissue Disorders, Musculoskeletal System

G M Lingg, C Schorn
Department of Radiology
Sana Rheumazentrum Rheinland Pfalz
Bad Kreuznach, Germany
dr.lingg@sana-rheumazentrum-rlp.de

Synonyms

Connectivitis

Definition

Connective tissue diseases (CTDs) consist of the following entities: Systemic lupus erythematosus (SLE), panarteritis nodosa (PAN), systemic scleroderma (SSc), dermatomyositis/polymyositis (DM/PM), and mixed connective tissue disease (MCTD, Sharp's disease). In a more general sense, Sjögren's syndrome and vasculitis (Wegener's granulomatosis, Churg–Strauss syndrome) also belong to this group. The common histologic finding of all these diseases is fibrinoid necrosis and immunocomplex deposition.

Pathology/Histopathology

Immunocomplex deposition in the basal membranes, vascular walls, and interstitial tissue leads to inflammatory and necrotic foci in different organs. Thus multiple organ manifestations are possible among which musculoskeletal disease is seen with various degrees of severity.

Systemic Lupus Erythematosus

Clinical Presentation

The general clinical course is characterized by periods of severe illness and remission. Disease onset is often acute with skin rash after a sun bath indicating photosensibility. Typically, the rash is found on the face in the form of the so-called butterfly erythema. Scalp involvement leads to alopecia. ▶Raynaud's phenomenon may occur. Temperature rise, weakness, weight loss, and polyarthralgia are common. Gastrointestinal involvement is frequent. Neurologic dysfunctions such as mental disorders, seizures, cerebral nerve palsies, or cerebral infarction are facultative but not uncommon symptoms. Lupus nephritis can cause nephrotic syndrome and glomerulonephritis with proteinuria and erythrocyturia and may indicate a serious disease course. Interstitial pneumonitis with dyspnea and cough is a typical feature. Some patients suffer from relapsing pleuritis with pleural pain. Heart manifestations consist of myocarditis, pericarditis, and endocarditis. Hematological disorders include hemolytic anemia and thrombocytopenia.

Reasons for death are mainly cardiovascular diseases, thromboembolic events, and infections. The patients with unfavorable prognosis show rapid development of severe prognostic signs in relation to the mean duration of the disease and frequent and severe complications. Risk factors at disease onset are male sex, nephritis, heart disease, and central nervous system disease.

Laboratory findings are positive LE cells, anti-DNA antibodies, and anticardiolipin antibodies.

Imaging

In the case of polyarthralgia, X-ray imaging is used in order to exclude arthritis. However, in SLE findings are

unspecific. For myalgia/►myositis, magnetic resonance (MR) imaging may be employed.

Signs and Patterns in SLE

Typically, there are rarely objective radiological findings. In fact, in the setting of no or few radiologic signs despite massive clinical symptoms, SLE should be considered as the differential diagnosis. ►*Regional osteoporosis* is unspecific but not uncommon and may progress to general osteoporosis. It may be the only finding. Rarely, *small subchondral cysts* in the metacarpal and metatarsal heads as well as in the carpal and tarsal bones occur and are thought to be micronecrotic foci. Periosteal ossification, tiny soft tissue calcifications, and acroosteolysis are rare findings. Capsular and muscular contractions are the cause of severe sub-/luxations of the finger joints resembling the "*Jaccoud hand*," which was originally described in rheumatic fever after streptococcal infection. Typically, the grave deformities contrast the absence of destructive arthritis (Fig. 1). Pressure erosion following the deformity may occur and should be distinguished from destructive arthritis. Destructive arthritis is a sign of an overlap syndrome with rheumatoid arthritis and is seen in approx. 10% of cases. Epiphyseal necrosis with or without steroid therapy is a relatively common feature and does not differ from its usual aspect in patients with different conditions.

In cases with polyarthralgia, MR imaging shows synovial hyperplasia and joint capsule edema or mild joint effusions, but no specific findings. Epiphyseal necrosis

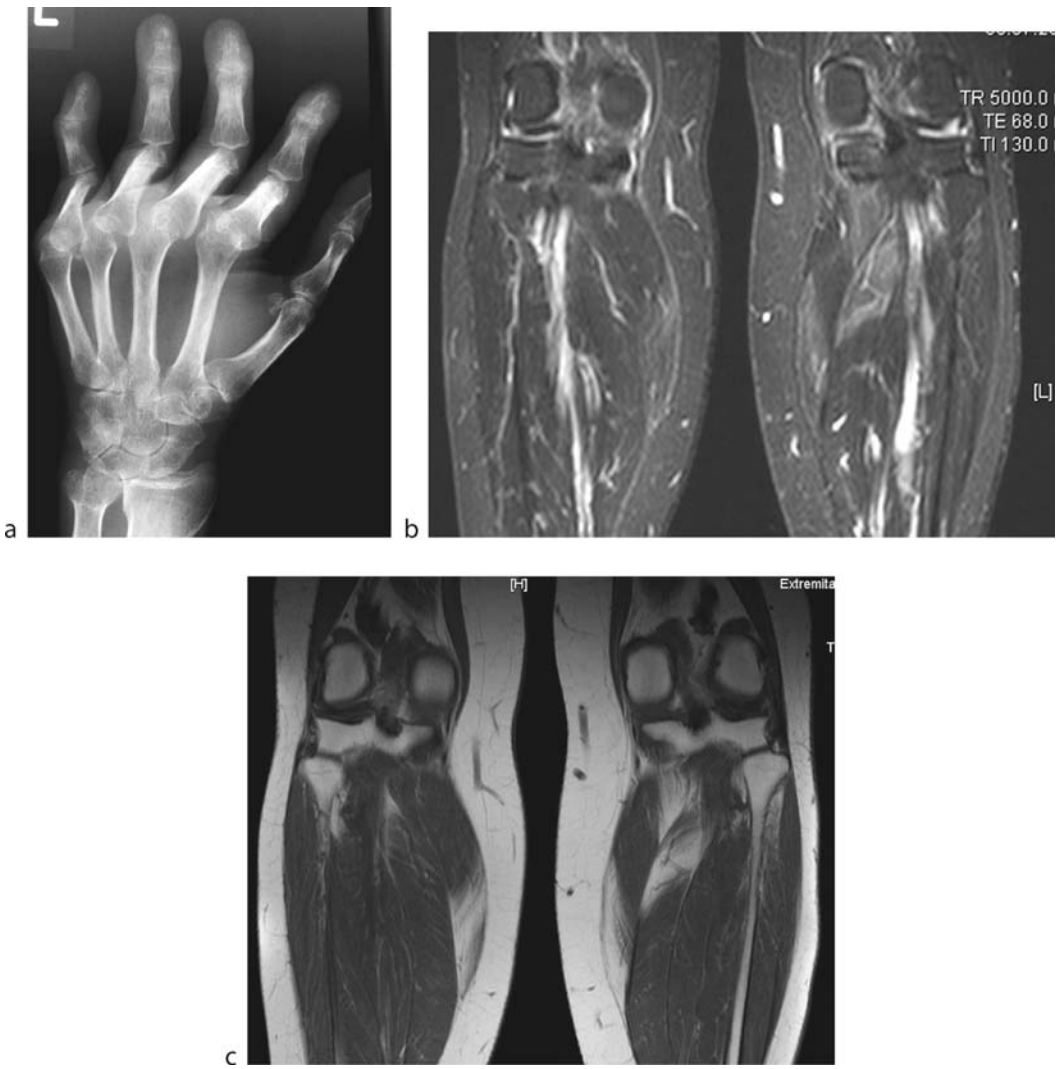

Connective Tissue Disorders, Musculoskeletal System. Figure 1 SLE. (a) "Jaccoud hand" with irregular deformities but without arthritic destructions. (b) Mild myositis of the lower leg with faint edema in the triceps surae and medial head of m. gastrocnemius, STIR image. (c) Short TE TR images show already fatty atrophy of the involved muscles.

can be diagnosed earlier and with more conspicuity in comparison to plain X-ray imaging. Polymyalgia and *myositis* most often affect muscles of the thigh with sparing of the m. sartorius. The lower leg is the second most frequent location (Fig. 1). STIR and T1-weighted images in the coronary and the transverse plane should be acquired. Application of contrast material is not necessary. The most prominent finding in the acute phase of disease is muscle edema and contrast material enhancement if it is applied. Long-standing myositis leads to fatty atrophy. Hemorrhages may occur.

Diagnosis

The clinical picture is most variable and often unspecific. It depends on the organ systems that are affected. Some patients show only mild symptoms at disease onset, others suffer severely and early diagnosis is mandatory. Schematic diagnosis criteria are therefore employed (Table 1) with reasonable sensitivity and specificity. Laboratory findings are important for classification and are included in the classification set.

Systemic Scleroderma

Clinical Presentation

SSc is characterized by an insidious onset mostly in the fourth to fifth decade. There is a twofold female predominance. *Raynaud's phenomenon* is frequently present months or years before actual disease onset. Edema and skin thickening of the hands and feet, the face, or the trunk are often one of the first symptoms. Polyarthralgia is frequent. Within months or years the skin hardens and shrinks leading to joint contractures and trophic deterioration with acral cutaneous necrosis. Teleangiectasias appear, and sweat glands and hair follicles become atrophic. ▶*Calcinosis cutis* can be felt as hard subcutaneous nodules. Dysphagia is a result of esophageal sclerosis with loss of peristalsis and stasis and gastroesophageal reflux. Abdominal distension may be a sign of small bowel involvement. Dyspnea and cough occur in patients with pulmonary fibrosis. Cardiomyopathy (myocardial fibrosis) is possible. Proteinuria or microhematuria is a sign of renal manifestation.

Limited cutaneous and diffuse cutaneous SSc with different severity and survival have been recognized as distinct subsets (Table 2). The features of ▶CREST syndrome (calcinosis, Raynaud's, esophagus dysmotility, sclerodactyly, teleangiectasias) are not confined to the limited subsets of SSc.

Connective Tissue Disorders, Musculoskeletal System.
Table 1 ARA criteria (1982) for the diagnosis of SLE

Skin and mucosal manifestations	Butterfly erythema
	Discoid lupus
	Photosensibility
	Oral ulcerations/aphthae
Lung, abdominal manifestation	Serositis, pleuritis, pneumonitis
Renal manifestation	Nephrotic syndrome, nephritis
	Polyarthralgia, nonerosive arthritis
Cerebral manifestation	Seizures, cerebral nerve palsy, mental disorders
Hematological manifestation	Hemolytic anemia, thrombo-/leukopenia
Immunologic findings	Anti-ds-DNS, Anti-sm, LE-cell-phenomenon, Phospholipid antibodies
	Antinuclear antibodies (ANA)

Definite diagnosis requires 4 of 11 criteria.

Imaging

Patients with scleroderma exhibit marked osteoporosis. Specific findings are fading of the acral soft tissue. Conical deformation of the finger tips and extension deficit lead to the aspect of "*prayer's hand*." ▶*Acral osteolysis* (unguicular process) and ▶*cutaneous necrosis at the finger tips like rat bites* occur later in the disease course. Osteolytic changes can manifest at the distal interphalangeal joints. *Calcinosis cutis* is found especially at mechanically exposed locations, for example, the finger tips or osseous prominences (Fig. 2). However, a peri- or intraarticular location is not uncommon. The calcification is speckled and grouped. It is a characteristic feature of CREST syndrome but can also be seen without CREST. Nondestructive joint deformities with flexion contracture due to skin shrinking are late findings. Erosive arthritis resembling rheumatoid arthritis is possible.

MR imaging shows skin thickening and edema in the early stages, shrinking and atrophy in late stages. Synovial and capsule edema as well as tenosynovitis may be present in symptomatic joints. A rare finding is epimysial edema. In patients with destructive arthritis, joint effusion, synovial thickening, and pannus as well as erosion are found.

Diagnosis

The following set of criteria for the classification of SSc was proposed: (i) autoantibodies to centromere proteins, Scl-70 (topo I), fibrillarin; (ii) symmetric basilar pulmonary fibrosis; (iii) contractures of the digital joints or prayer sign; (iv) dermal thickening proximal to the wrists; (v) calcinosis cutis; (vi) Raynaud's phenomenon; (vii) esophageal distal hypomotility or reflux-esophagitis;

Connective Tissue Disorders, Musculoskeletal System. Table 2 Scleroderma: limited and diffuse disease subsets

Clinical symptom	Limited disease	Diffuse disease
Raynaud's phenomenon	Long standing	Acute onset
Nailfold capillaroscopy	Tortuous, widened	Widened, microinfarction
Skin	Facial and acral skin thickening, dactylitis, teleangiectasia, calcinosis	Hands, forearms, face, feet, corps:
		Skin thickening, dactylitis, teleangiectasia, acral necrosis
Joints	Arthralgia, deformity	Arthralgia, deformity
Muscles	Myositis	Myositis
Lungs	Interstitial pneumopathy, primary pulmonary hypertonia	Interstitial pneumopathy, Secondary pulmonary hypertonia
Gastrointestinal tract	Esophageal dysfunction, dilatation	Esophageal and intestinal dysfunction, dilatation, ulceration
Heart	Pericarditis	Pericarditis, myocarditis, myocardial fibrosis
Autoantibodies	Anticentromere antibodies	Anti-scl-70-antibodies

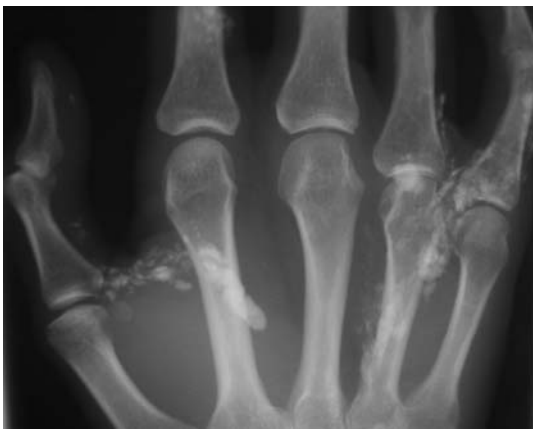

Connective Tissue Disorders, Musculoskeletal System. Figure 2 Scleroderma. Typical calcinosis subcutaneously, peritendinously, periarticularly in a patient with CREST syndrome.

(viii) sclerodactyly or nonpitting digital edema; (ix) teleangiectasias. The diagnosis of definite systemic sclerosis requires at least three of the above criteria.

Microvascular lesions (enlarged and giant capillaries together with hemorrhages, loss of capillaries, and ramified capillaries and vascular architectural disorganization) are a predominant feature in systemic sclerosis and are detected and graded by means of nailfold capillaroscopy.

Overlap Syndromes, Mixed Connective Tissue Disease

Definition

Many patients presenting with symptoms suggestive of a CTD do not fulfill criteria for a specific diagnosis at the initial presentation. Such patients have been designated as having undifferentiated CTD. In time, some of them will develop a specific CTD, whereas others will have a stable clinical course or show overlapping features of two or more CTDs. MCTD is the prototype of a rheumatic diseases overlap syndrome characterized by overlapping features of SLE, scleroderma, polymyositis, and rheumatoid arthritis in the presence of antibodies to U1-ribonucleoprotein (anti-U1-RNP). There is evidence that the clinical and serological features of MCTD represent a distinctive subset of CTD; however, this subject has not been settled yet.

Clinical Presentation

Common features are: Raynaud's phenomenon, sclerodactyly, isolated keratoconjunctivitis sicca, swollen hands, unexplained polyarthritis, myalgia, myositis, rash, pleuritis, pericarditis, central nervous system symptoms, pulmonary symptoms, peripheral neuropathy, raised erythrocyte sedimentation rate. In addition to clinical overlap, serological overlap has also been recognized in patients with CTDs.

Imaging

X-ray imaging is required for the differential diagnosis of synovitis and arthralgia. In cases of MCTD, however, no specific radiologic sign is found. The soft tissue swelling is not necessarily in a synovitic pattern. Calcifications like those found in SSc are possible. MR imaging can assist in the assessment and localization of myositis. Muscle edema is present in the acute phase; later, fatty muscle atrophy develops.

Diagnosis

Multiple sets of criteria for the diagnosis of MCTD have been proposed, indicating how difficult it is to give a precise definition. The presence of anti-U1-RNP antibodies is indispensable but not in itself sufficient. However, its specificity is moderate, accounting for the fact that there may be high titers in SLE, SSc, and RA, too. Reasonable sensitivity and specificity are provided with the Alarcon-Segovia Criteria, when in addition to high titers of anti-U1-RNP, three of five clinical manifestations (edema of the hands, synovitis, myositis (myalgia), Raynaud's phenomenon, and acrosclerosis) are present.

Idiopathic Inflammatory Myopathies

Definition

The idiopathic inflammatory myopathies are characterized by chronic muscle inflammation and involvement of internal organs, which contribute considerably to the morbidity and mortality of the disease. Seven types are described. Type 1: Polymyositis; Type 2: Dermatomyositis; Type 3: Polymyositis or dermatomyositis associated with cancer; Type 4: Childhood polymyositis or dermatomyositis; Type 5: Polymyositis or dermatomyositis in CTD; Type 6: Inclusion body myositis; Type 7: Unspecified myositis: nodular, eosinophilic, granulomatous myositis.

Clinical Presentation

Proximal muscle weakness and also pain which increases with exercise most often affecting the thigh are the clue symptoms. Muscle atrophy, fibrosis, and contracture are late-stage features. Arthralgia and arthritis are relatively common, especially in polymyositis with CTD. Erosion and cartilage destruction, however, are rarely seen. Pericarditis and myocarditis may occur and cause arrhythmia. Skin involvement predominates dorsally at the metacarpophalangeal and proximal interphalangeal joints with papules and livid erythemas. Raynaud's phenomenon and teleangiectasia of the nailfold are similar to scleroderma. Calcinosis is mainly seen in children.

Pulmonary complications (i.e., aspiration pneumonia due to myositis-related esophageal dysfunction and ventilatory insufficiency) and cardiac complications are the most frequent causes of death. Variables associated with poor outcome are older age, pulmonary and esophageal involvement, and cancer.

Imaging

In plain X-ray imaging, indistinct soft tissue findings predominate. The favorite sites of edema are the subcutis and muscles, with swelling, slight attenuation, and fat line disappearance. Fibrosis and contractures lead to atypical projections. In the late stage, muscle volume is decreased as a result of atrophy. The most characteristic finding is ►*soft tissue calcification* mainly muscular or epifascial, sometimes intratendinously or in fat. Subcutaneous linear calcifications are common at the knee, elbow, and fingertips. Blane and coworkers described four distinct patterns of calcification in childhood dermatomyositis: deep calcareal masses, superficial calcareal masses, deep linear deposits, and a lacy, reticular, subcutaneous deposition of calcium encasing the torso. Soft-tissue calcification was identified in 40–60% of cases.

Arthralgia in polymyositis and dermatomyositis does not result in erosion and cartilage destruction. Periarticular osteoporosis and soft tissue swelling, however, may occur.

MR imaging is employed for localization of inflammatory affected muscles in order to find a promising biopsy location. In the acute stage, excessive edema and contrast material enhancement of the affected muscles are seen. Fasciitis in the neighborhood is common. In dermatomyositis, subcutaneous edema and contrast material enhancement of reticular pattern are present. In the chronic phase, edema in muscles, epifascially and subcutaneously resolves. Muscle atrophy with fat interposition and fascial undulation develops.

Diagnosis

According to the widely used criteria (Bohan and Peter criteria 1975), DM is differentiated from PM only by skin changes. Following new diagnostic criteria including histopathological characteristics, dermatomyositis is a microangiopathy affecting skin and muscle; activation and deposition of complement cause lysis of endomysial capillaries and muscle ischemia. In polymyositis and inclusion body myositis, cytotoxic T cells invade muscle fibers that express MHC class I antigens, which leads to fiber necrosis. In inclusion body myositis, vacuolar formation with amyloid deposits coexists with the immunological features.

Diagnosis is definite in the presence of the following criteria: proximal muscle weakness, elevated muscle enzymes (CK, LDH, aspartatransferase, alanine aminotransferase, aldolase), electromyography findings, myositis in muscle biopsy, typical skin manifestation.

Bibliography

1. Fernando MM, Isenberg DA (2005) How to monitor SLE in routine clinical practice. Ann Rheum Dis 64:524–527
2. Masi AT, Rodnan GP, Medsger TA (1980) Preliminary criteria for the classification of systemic sclerosis (scleroderma). Arthritis Rheum 23:581–590

3. Alarcón-Segovia D, Villareal M (1987) Classification and diagnostic criteria for mixed connective tissue disease. In: Kasukawa R, Sharp GC (eds) Mixed Connective Tissue Diseases and Antinuclear Antibodies. Elsevier, Amsterdam, pp 33–40
4. Bohan A, Peter JB, Bowman RL (1977) A computer assisted analysis of 153 patients with polymyositis and dermatomyositis. Medicine (Baltimore) 56:255–261
5. Mastaglia FL, Phillips BA (2002) Idiopathic inflammatory myopathies: epidemiology, classification and diagnostic criteria. Rheum Dis Clin North Am 28:723–741
6. Bohan A, Peter JB (1975) Polymyositis and Dermatomyositis. N Engl J Med 292:344–347, 403–407

Connectivitis

▶Connective Tissue Disorders, Musculoskeletal System

Conservative Breast Surgery

▶Breast Conserving Therapy

Conservative Surgical Therapy

▶Breast Conserving Therapy

Contrast Media, Ultrasound, Phase Modulation

Robert Eckersley
Imaging Sciences Department, Imperial College London, London, UK
r.eckersley@imperial.ac.uk

The compromise of sensitivity against spatial resolution in harmonic mode imaging led to the development of phase modulation imaging (1). This mode is now widespread and available on many commercial clinical systems. The form of phase modulation imaging which has now become standard, and is often referred to as pulse

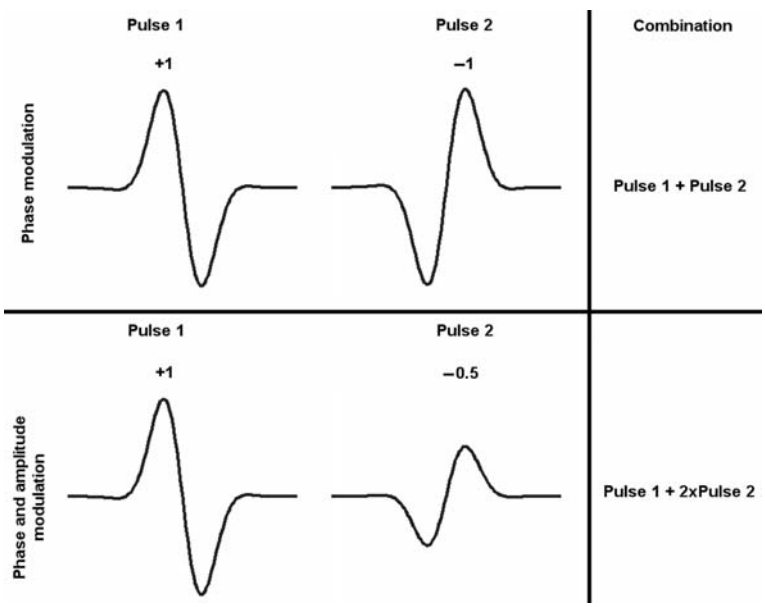

Contrast Media, Ultrasound, Phase Modulation. Figure 1 This figure shows (upper panel) a simple two pulse phase modulation sequence. When the echoes of pulse 1 and pulse 2 are summed, any linear signals will be canceled. The second harmonic signals in the echoes from microbubbles are preserved by this approach. Also presented (lower panel) is a two pulse sequence with combined phase and amplitude modulation. Linear signals can again be removed by appropriate combination of the echoes. This approach can detect nonlinear signals at the fundamental frequency as well as the second harmonic.

inversion imaging is based on alternating the polarity between successive pulses, that is, +1,−1 and so on. (see Fig. 1). When these pulses are scattered linearly from tissues, the echoes of subsequent pulses will cancel when combined. The response of the microbubbles to the +1 and −1 pulse is significantly different, and when the echoes are combined, a residual signal arising from the nonlinearity of the bubbles remains. The nonlinear signal detected by phase modulation imaging comes from the second harmonic signals in the echoes. Broadband imaging pulses can be used, and, unlike harmonic imaging, this multipulse approach does not suffer from the same compromise in specificity and sensitivity to microbubbles against resolution. This approach can be extended (by using more than two pulses) to allow detection target motion using Doppler processing. Successful phase modulation imaging requires precise pulse shaping within the ultrasound equipment to ensure good cancellation of the linear echoes. The specificity of this approach is limited by the generation of harmonic signals during the propagation of the sound through tissues especially at higher MI.

Bibliography

1. Hope Simpson D, CT Chin, Burns PN (1999) Pulse inversion Doppler: a new method for detecting nonlinear echoes from microbubble contrast agents. IEEE Trans Ultrason Ferroelectr Freq Control 46(2):372–382

Continuous Diaphragm Sign

In pneumomediastinum, mediastinal air may also track extrapleurally along the upper surface of the diaphragm and air beneath the heart combines the margins of the bilateral diaphragms.

▶Pneumomediastinum

Contour Wall Alteration

▶Compression, Extrinsic, Esophagus
▶Compression, Extrinsic, Stomach and Duodenum

Contrast Echo

▶Contrast Media, Ultrasound, Applications in Echocardiography

Contrast Echocardiography

This technique consists in injecting 5–10 cc of agitated saline into a peripheral vein while simultaneously imaging the right and left atria using echocardiography. In patients without right-to-left shunting, the contrast is visualized in the right atrium as a cloud of echoes and gradually dissipates as the bubbles become trapped in the pulmonary circulation. In patients with intracardiac or intrapulmonary shunting, the contrast is visible in the left atrium within one cardiac cycle or 3–8 cardiac cycles, respectively.

▶Fistula, Arteriovenous, Pulmonary
▶Contrast Media, Ultrasound, Applications in Echocardiography

Contrast Enhancement

After intravenous injection of contrast medium there is an increased density on CT and increased signal intensity on T1-weighted sequences in MRI. Contrast-enhanced structures appear bright on these images.

▶Neoplasms, Oral Cavity

Contrast Induced Nephrotoxicity

Contrast induced nephrotoxicity is defined as a temporary or permanent reduction in renal function caused by the administration of an imaging contrast medium. In most scientific investigations, this is determined on the basis of laboratory, rather than clinical, grounds. The lower border of what constitutes clinically significant nephrotoxicity is poorly defined.

▶Adverse Reactions, Iodinated Contrast Media, Acute Renal

Contrast Induced Renal Dysfunction

▶Adverse Reactions, Iodinated Contrast Media, Acute Renal

Contrast Induced Renal Failure

▶Adverse Reactions, Iodinated Contrast Media, Acute Renal

Contrast Media MR, Organ Specific

Peter Reimer
Deaprtment of Radiology, Klinikum Karlsruhe, Academic Teaching Hospital of the University of Freiburgh, D-76133 Karlsruhe
Peter.Reimer@klinik.um-karlsruhe.com

Synonyms

Currently, three organ-specific contrast agents with uptake into hepatocytes followed by variable biliary excretion represent the only clinically approved organ-specific contrast agents besides iron oxides:

- Mangafodipir trisodium (Teslascan, GE-Amersham Health, Oslo, Norway)
- Gadobenate dimeglumine (MultiHance, Bracco Imaging S.p.A., Milan, Italy)
- Gadoxetic acid (Primovist, Schering AG, Berlin, Germany).

Enhancement during the distribution phase of contrast agents mainly depends on tumor vascularity (hypovascular vs. hypervascular) and its blood supply while enhancement on delayed images is characterized by the cell specificity of magnetic resonance (MR) contrast agents (extracellular vs. intracellular). Therefore, enhancement characteristics of hepatobiliary contrast agents are applicable to the diagnosis of primary benign and malignant hepatocellular liver tumors (1).

Definition

Mangafodipir Trisodium "Teslascan"

Mangafodipir trisodium is a manganese (Mn) chelate [manganese(II)-*N*,*N*′-dipyridoxylethylenediamine-*N*,*N*′-diacetate-5,5′-bis(phosphate)sodium salt]. Mangafodipir has two components: fodipir and a manganese(II) ion. When mangafodipir is labeled with the ^{14}C-label residing in the fodipir, after a single intravenous dose of 5 μmol/kg of ^{14}C-mangafodipir, the mean ± SD area under the radioactivity plasma concentration curve (AUC) is 22.7 ± 3.2 μg h/mL. Generally, the total body store of manganese in adults is 20 mg. Most of this is from dietary intake (2–5 mg/day). Mangafodipir contains 2.75 mg/mL of chelated manganese. In a 70 kg adult, 5 μmol/kg of mangafodipir injection contains 19.2 mg of chelated manganese. Therefore, single injections will approximately double the total body store of manganese before excretion occurs. Manganese is an essential trace metal in humans with a normal whole body content of 12–20 mg.

Mangafodipir trisodium is a paramagnetic complex and following IV administration, mangafodipir is metabolized by dephosphorylation to Mn-DPMP and Mn-PLED and transmetallated by zinc (Zn) to the corresponding compounds. Mn^{2+} ions released from mangafodipir trisodium are most probably bound by alpha2-macroglobulin and transported to the liver. Its T1 relaxivity in aqueous solution is similar to gadolinium, however, due to the intracellular uptake of Mn^{2+}, its T1 relaxivity in liver tissue is three times greater than that of gadolinium (21.7 mmol/L^{-1}sec^{-1} vs. 6.7 mmol/L^{-1}sec^{-1}). In humans, the manganese(II) ion of mangafodipir is eliminated in the urine by 15% within 24 h and by 59% in the feces in 5 days (2).

Gadobenate Dimeglumine "MultiHance"

Gadobenate dimeglumine [(Gd) benzyloxy-propionic tetraacetic acid (Gd-BOPTA)] is an octadentate chelate of the paramagnetic ion gadolinium. Its kinetic properties resemble those of conventional iodinated contrast media and can be described by a biexponential function comprising a distribution phase and an elimination phase. This agent differs from other available gadolinium-chelates in that it distributes not only to the extracellular fluid space (ECF), but is selectively taken up by functioning hepatocytes and excreted into the bile. The biliary excretion rate is only 3–5% in humans (renal 78 to 96% and feces 0.6 to 4%). The uptake of gadobenate dimeglumine by hepatocytes and excretion into the bile is accomplished *via* the adenosine triphosphate (ATP)-dependent bile-canalicular multispecific organic anion transporter (cMOAT), which is shared by bilirubin and inhibited by bromosulfophthalein (BSP). Gadobenate dimeglumine has a higher relaxivity than equimolar formulations of other approved extracellular contrast agents due to its more lipophilic structure and its capacity for weak and transient interaction with serum albumin. In the liver, the estimated relaxivity is about 30 mmol^{-1}sec^{-1}, compared with calculated values of 16.6 mmol^{-1}sec^{-1} for gadoxetic acid and 21.7 mmol^{-1}sec^{-1} for mangafodipir trisodium. Gadobenate dimeglumine is not metabolized with an elimination half-life of 1.17 to 2.02 h (3).

Gadoxetic Acid

Gadolinium-ethoxybenzyl-diethylenetriamine-pentaacetic-acid is a paramagnetic contrast agent with hepatocellular uptake *via* the anionic-transporter protein and a molecular weight of 725.71 Da ($C_{23}H_{28}GdN_3Na_2O_{11}$). Gadoxetic acid is a highly water-soluble, hydrophilic compound with a lipophilic moiety due to the ethoxybenzyl group. T1-relaxivity as measured in water at 0.47 T of 4.9 $mM^{-1}sec^{-1}$ is comparable to gadopentetate dimeglumine with 3.7 $mM^{-1}sec^{-1}$. The T1-relaxivity in human plasma ($R1$ 8.7 $mM^{-1}sec^{-1}$) is higher than for gadopentetate dimeglumine ($R1$ 5.0 $mM^{-1}sec^{-1}$) and displays only slight dependency on the strength of the magnetic field. This may be explained by the greater degree in protein binding (10.7±3.4%) compared to gadopentetate dimeglumine (1.6±4.2%). At 37°C, the solution has an osmolality of 0.89 osmol/kg H_2O and a viscosity of 1.22 mPasec. Gd-EOB-DTPA is an aqueous formulation with a concentration of 0.25 mol/L and a high thermodynamic stability (log KGdl = −23.46). Gd-EOB-DTPA is equally eliminated *via* the renal and hepatobiliary routes with a half-life of approximately 60 min. The pharmacokinetics is dose-linear up to the dose of 0.4 mL/kg (100 µmol/kg). A total serum clearance (Cltot) of about 250 mL/min was recorded, whereas the renal clearance (Clr) corresponds to about 120 mL/min. Gadoxetic acid is not metabolized and may be bolus-injected at a flow rate of 2 mL/sec (4).

Indication

All three contrast agents are approved for MR imaging of suspected liver tumors. In addition, gadobenate dimeglumine has also been approved for magnetic resonance imaging (MRI) of the central nervous system (CNS) and mangafodipir for pancreatic MRI.

Contraindication

Safety and effectiveness have not been established in pediatric patients for any of the contrast agents. Specific contraindications and precautions for the three contrast agents are as follows.

Mangafodipir

Mangafodipir is contraindicated in patients with known allergic or hypersensitivity reactions to manganese, fodipir or any of the inert ingredients. The dialysability of mangafodipir and its metabolites has not been studied. Pharmacokinetic differences due to drug interactions or race after intravenous of mangafodipir were not studied. Patients with a history of drug reactions to contrast media, other allergies, or immune system disorders should be observed for several hours after drug administration. Caution should be exercised before administering to patients who have or cannot tolerate nausea or vomiting. The possibility of complications from nausea and vomiting should be considered when administering mangafodipir to patients who cannot tolerate vomiting, who have reflux esophagitis or who cannot roll over to prevent aspiration.

Mangafodipir is cleared from the body partially by glomerular filtration and partially by hepatobiliary excretion. Dose adjustments in renal or hepatic impairment have not been studied. The safety of repeated doses has not been studied. If the physician determines those imaging needs to be repeated, repeat images could be obtained up to 24 h after the original injection without reinjection. Safety, effectiveness, or pharmacokinetics of mangafodipir injection in pediatric patients below the age of 12 years has not been established.

Gadobenate Dimeglumine

A known allergic or hypersensitivity reactions to gadolinium or any other ingredients, including benzyl alcohol represents a contraindication. Further contraindications are sickle cell anemia or other hemoglobinopathies and hemolytic anemias. Precautions should be taken to avoid local extravasation during administration. Gadobenate should not be administered to patients who may be using medications or who may have underlying metabolic, cardiac, or other abnormalities that may predispose them to cardiac arrhythmias.

Gadobenate is not recommended in patients with severely impaired renal function (creatinine clearance <30 mL/min). Small quantities of benzyl alcohol (<0.2%) may be released during storage. Therefore, gadobenate should not be used in patients with history of sensitivity to benzyl alcohol.

Gadoxetic Acid

Hypersensitivity to the active substance or to any of the excipients represents a clear contraindication. Caution should be exercised in patients with severe renal impairment due to reduced elimination capacity of gadoxetic acid. Caution should also be exercised when gadoxetic acid is administered to patients with severe cardiovascular problems because only limited data are available so far. It cannot be excluded that of gadoxetic acid may cause torsade de points arrhythmias in an individual patient.

Intramuscular administration may cause local intolerance reactions including focal necrosis and should therefore be strictly avoided.

Pregnancy/Lactation

It is recommended that breastfeeding be discontinued before administration of any of the contrast agents and not reinitiated until 24 h after administration. Use is recommended only if potential benefit to the pregnant woman outweighs the potential risks to the fetus. However, it is recommended not to use mangafodipir since this may cause harm to the fetus when administered to a pregnant woman. Manganese has caused embryo toxicity and fetal toxicity in various animals. Animal studies have shown that 54Mn manganese crosses the placenta and locates in the fetus. At least 24 h after injection, radioactivity is detected in liver and bones of the fetus. It has been reported that manganese enters nerve terminals, accumulates in nervous tissue, and could be associated with neurotoxicity in fetuses. Adequate and well-controlled studies were not conducted in pregnant women. If mangafodipir is used during pregnancy, or if the patient becomes pregnant while taking this drug, the patient should be told of the potential hazard to the fetus.

Use and Dosage

Mangafodipir is administered at a dose of 5 μmol Mn/kg as a short IV infusion over 10–20 min. Near maximal enhancement is achieved at 20 min after the start of the infusion, and persists for several hours. Postcontrast imaging may start as soon as 20 min after the start of the infusion, but longer time intervals are possible because of a plateau-like enhancement up to and several hours.

Gadobenate dimeglumine is administered as a bolus injection at a dose of 0.05 mmol Gd/kg body weight and can be used for rapid dynamic imaging of the liver following bolus injection in the same way in which nonliver-specific contrast materials are used. This approach exploits the differences in blood flow between lesions and normal liver parenchyma. The fraction of gadobenate dimeglumine taken up into the hepatocytes manifests itself as a strong enhancement of the liver parenchyma signal intensity in T1-weighted images between 40 and 120 min postinjection.

Gadoxetic acid is administered as a bolus injection at a dose of 25 μmol Gd/kg body weight (Fig. 1). Near maximal enhancement is achieved at 20 min after the start of the injection, and persists for several hours. Thus, postcontrast imaging may start as soon as 20 min after the start of the infusion, but longer time intervals are possible because of a plateau-like enhancement (5).

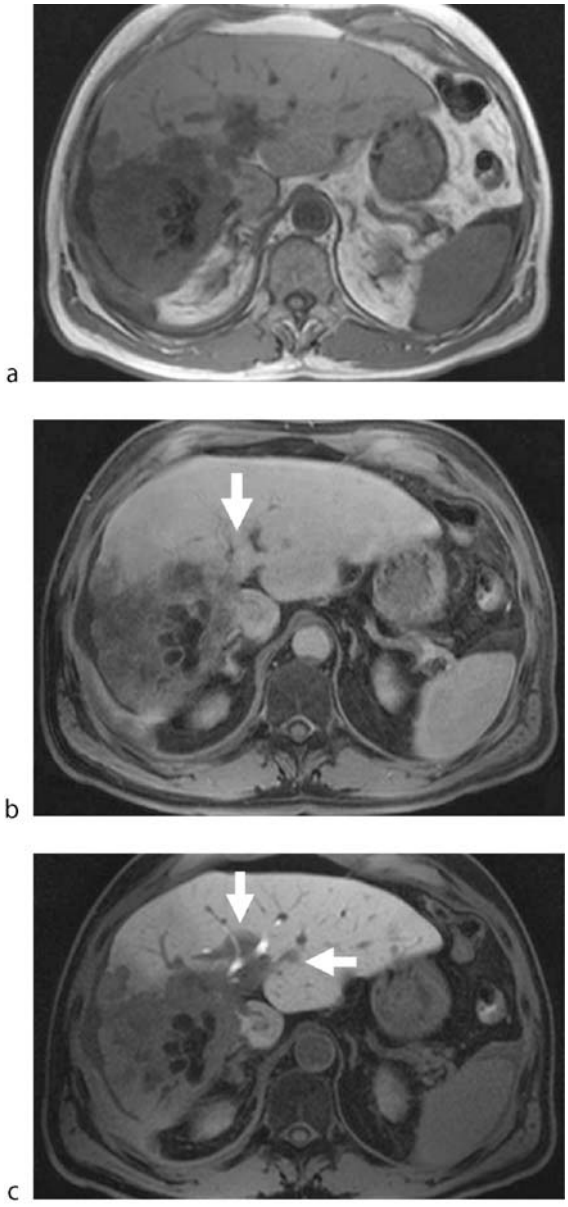

Contrast Media MR, Organ Specific. Figure 1 Patient with Cholangiocarcinoma. The portalvenous system (b) shows weak enhancement following Primovist compared to plain T1 (a). Tumor extension is much better visualized images in the hepatocellular phase (c).

Adverse Reactions

The possibility of a reaction, including serious, life-threatening, or fatal, anaphylactic, or cardiovascular

reactions, or other idiosyncratic reactions, should always be considered, especially in those patients with a history of known clinical hypersensitivity or a history of asthma or allergic respiratory disorders. Caution should be exercised in patients with deoxygenated sickle erythrocytes in all paramagnetic contrast agents.

Mangafodipir showed warmth or flush, nausea, heart pounding (increase in blood pressure and heart rate), and dizziness as the most frequent side effects in clinical studies with facial flushing in 55% of patients. Mild to moderate nausea was observed in 9%. The majority (93%) of adverse events were of mild to moderate intensity: chest pain, dizziness, hot flushes, hypersensitivity, hypertension, palpitation, pruritus, rash, taste perversion, urticaria. A transient increase in blood pressure and heart rate occurred immediately after injection, but returned to baseline after 5 min in all patients. Facial flushing was more often reported after rapid IV bolus injection than after IV infusion. No dosage adjustment is recommended in patients with mild to moderate renal impairment or hepatic impairment.

Gadobenate dimeglumine shows various side effects, which redocumented according to the organ system. Specifically, anemia has occurred in 0.5% of patients. Hypertension (up to 0.7%) and tachycardia (up to 0.5%) have been observed in the cardiovascular system, whereas vital signs remained essentially stable in other studies. The overall incidence of tachycardia in phase II studies ($n = 360$) was less than 1% (doses up to 0.2 mmol/kg). Other rarely reported cardiovascular effects have included acute pulmonary edema, cardiac arrhythmias, electrocardiogram (ECG) abnormalities, hypotension, and syncope. In the CNS, headache (5.8%) and dizziness (3.6%) have been reported following injection. One patient experienced seizures approximately 17 min after administration of gadobenate dimeglumine. The patient had a reported history of seizures. Other rarely reported central nervous system effects have included hemiplegia, hyperonia, paralysis, tremor, and aphasia. Most frequent events in the GI system were nausea, vomiting, and dry mouth in less than 2% of patients. No alteration of renal or liver function has been observed in available studies. Most frequent reactions at the injection site were pain, discomfort, and cold or tingling. Less frequent reactions include pruritus and other allergic-type cutaneous reactions. During postmarketing use of gadobenate dimeglumine, there were reports of anaphylactoid reactions, anaphylactic shock, and loss of consciousness. The observed spectrum is similar to approved extracellular gadolinium chelates.

During the clinical development phase of gadoxetic acid the overall incidence of adverse reactions, which were classified as drug, related was below 5%. Most of the undesirable effects were transient and of mild to moderate intensity. Laboratory changes as elevated serum iron, elevated bilirubin, increases in liver transaminases, decrease of hemoglobin, elevation of amylase, leukocyturia, hyperglycemia, elevated urine albumin, hyponatremia, elevated inorganic phosphate, decrease of serum proteins, leukocytosis, hypokalemia, elevated LDH were reported in clinical trials. ECGs were regularly monitored during clinical studies and transient QT prolongation was observed in some patients without any associated adverse clinical events. In very rare cases, anaphylactoid reactions leading to shock may occur. In the event of excessive inadvertent overdose, the patient should be carefully observed including cardiac monitoring. In this case, induction of QT prolongations is possible.

The most frequent reported definitely, possibly, or probably related AEs were nausea, vasodilatation, headache, taste perversion, and injection site pain. In patients with mild and moderate hepatic impairment, a slight to moderate increase in plasma concentration, half-life, and urinary excretion, as well as decrease in hepatobiliary excretion have been observed in comparison to subjects with normal liver function. However, no clinically relevant differences in hepatic signal enhancement were observed. In patients with severe hepatic impairment, especially in patients with abnormally high (>3 mg/dL) serum bilirubin levels, plasma concentration and half-life are increased with pronounced decrease in hepatobiliary excretion and reduced hepatic signal enhancement. In patients with end-stage renal failure, the half-life is markedly prolonged. Hemodialysis increased the clearance of Gd-EOB-DTPA. In an average dialysis session of about 3 h duration, about 30% of the Gd-EOB-DTPA dose was removed by hemodialysis (6).

Interactions

Transmetallation of manganese may occur. The extent to which this might affect laboratory assays of ferritin, iron, bilirubin, and zinc is not known. Specific interaction studies of mangafodipir, gadobenate dimeglumine, or gadoxetic acid with other medical products have not been carried out during the clinical development. In general, anionic drugs primarily excreted into the bile (such as rifampicin) may compete with the hepatic contrast enhancement and the biliary excretion of hepatobiliary contrast media. Animal studies demonstrated that compounds belonging to the class of rifamycins block the hepatic uptake of hepatobiliary contrast media, thus reducing the hepatic contrast effect. In this case, the expected benefit of an injection of hepatobiliary contrast media might be limited.

Elevated levels of bilirubin or ferritin can reduce the hepatic contrast effect of hepatobiliary contrast media.

Serum iron determination using complexometric methods (e.g., Ferrocine complexation method) may result in false values for up to 24 h after the examination with gadoxetic acid because of the free-complexing agent contained in the contrast medium solution. This has not been studied for gadobenate dimeglumine.

Bibliography

1. Earls JP and Bluemke DA (1999) New MR imaging contrast agents. Magn Reson Imaging Clin N An 7(2):255–273
2. Giovagnoni A and Paci E (1996) Liver. III: Gadolinium-based hepatobiliary contrast agents (Gd-EOB-DTPA and Gd-BOPTA/Dimeg). Magn Reson Imaging Clin N Am 4(1):61–72
3. Huppertz A et al (2004) Improved detection of focal liver lesion at MR imaging: multicenter comparison of gadoxetic acid-enhanced MR images with intraoperative findings. Radiology 230(1):266–275
4. Reimer P, Schneider G, and Schima W (2004) Hepatobiliary contrast agents for contrast-enhanced MRI of the liver: properties, clinical development and applications. Eur Radiol 14(4):559–578
5. Rofsky NM and Earls JP (1996) Mangafodipir trisodium injection (Mn-DPDP). A contrast agent for abdominal MR imaging. Magn Reson Imaging Clin N Am 4(1):73–85
6. Schima W et al (1997) Contrast-enhanced MR imaging of the liver: comparison between Gd-BOPTA and Mangafodipir. J Magn Reson Imaging 7(1):130–135

Contrast Media, Barium

Jean-Philippe Barraud
Guerbet, Roissy,
France
barraudj@guerbet-group.com

Introduction

Barium sulphate contrast media are nearly exclusively used for gastrointestinal tract imaging with conventional X-ray, computed tomography (CT) or less frequently magnetic resonance imaging (MRI) modalities.

The gastrointestinal tract is a succession of hollow organs. Its investigation by means of X-rays requires, in most cases, the use of contrast media, introduced orally or *via* the rectum, because of the small differentiation of soft-tissue permeability to X-rays. The first studies involved various substances, including bismuth sub-nitrate or sub-carbonate, sometimes mixed with bread or gruel, to prepare a meal. Bismuth was sometimes associated with the production of toxic metabolites. In 1910, Bachem and Günther proposed the routine use of barium sulphate, which replaced all other products because of its higher purity and absence of toxicity.

There are two types of contrast media for gastrointestinal tract imaging:

- 'Clarifying' media which are less radio-opaque (to X-rays) than the surrounding tissues: air, gas, e.g. carbon dioxide, water, aqueous solution of methylcellulose.
- 'Opacifying media' which are more radio-opaque than the surrounding tissues.

The opacifying contrast media contain heavy metals with a high atomic number (Z) to increase their radio-opacity: iodine ($Z = 53$) and barium ($Z = 56$) are presently used.

Definitions

Barium and Barium Salts

Barium is normally present in nature as barium carbonate $BaCO_3$ (whiterite) or barium sulphate $BaSO_4$ (barytine).

Barium is a toxic element. Therefore, only those barium salts which are completely insoluble in water, acids and fluids present in the gastrointestinal tract, are devoid of toxicity.

Soluble barium salts are barium chloride, nitrate and carbonate, which are slightly soluble in acids, and barium sulphides and oxides, which are soluble in acids. These salts are heavily toxic: when transported directly to the central nervous system (CNS), they increase CNS excitability and paralyse it.

Non-toxic insoluble barium salts are those salts which are insoluble in water, and remain insoluble after contact with hydrochloric acid in the stomach.

Barium sulphate ($BaSO_4$) is the sole barium salt, which is insoluble in various gastrointestinal tract media and which is therefore not absorbed by the mucosa.

Barium sulphate is obtained from two different pathways:

1. Natural barium sulphate which is extracted from mines and treated by physical (grinding, washing) and chemical processes to reach the specifications of the relevant pharmacopoeia.
2. Precipitated barium sulphate which is obtained by precipitation of other barium salts with sulphuric acid, and thoroughly washed to ensure its purity.

Barium sulphate as a raw material has the following advantages:

- Insolubility in water and acids
- Stability
- High atomic number, generating a good radiological contrast
- Relatively low cost.

The main risks concern the possible passage of barium sulphate into the circulation *via* a breach of the

gastrointestinal tract following trauma or a perforated ulcer, or into the respiratory tract via an oesophageal-bronchial fistula, for example.

Barium sulphate is listed in the European Pharmacopeia and in the US Pharmacopeia, which describe its purity and some physical characteristics, for example its sedimentation rate. Barium contrast media available on most markets are prepared with PE or USP grade barium sulphate.

General Information on Barium Sulphate Contrast Media

Barium sulphate is nearly insoluble in water (2.4 mg/L at 25°C).

Barium sulphate is therefore used as a suspension of two phases:

1. A dispersed phase of barium sulphate particles and excipients used to produce the suspension.
2. A dispersant phase and water-soluble excipients.

The stability and properties of these suspensions, which are usually less stable than solutions are obtained by optimising the parameters of the barium sulphate particles and the formulation of the excipients.

Parameters and Characteristics of the Dispersed Phase

1. The grain size, that is particle size, influences the sedimentation rate, the particulate surface and the viscosity of the suspension.

Grain Size and Sedimentation Rate

The smaller the grain size, the lower the rate of sedimentation will be. Particles of 1 m diameter will have a sedimentation speed of circa 1 cm/h. The sedimentation speed follows approximately Stokes law, which states that the speed of a sphere in a liquid is a function of gravity, the difference of densities of the sphere (d_1) and of the surrounding suspending solution (d_2), the square of radius of the sphere (a) and the viscosity of the solution (η):

$$V = \frac{2ga^2(d_1 - d_2)}{9\eta}$$

Stokes law does not strictly apply because the particles are not perfectly spherical and have different diameters. Nevertheless, the influences of the various parameters are similar: the sedimentation rate decreases if the grain size decreases and if the viscosity increases.

The influence of the grain size is very strong since its square value is implied.

Grain Size and Particle Surface

For a given weight of barium sulphate, a smaller grain size will induce a comparatively larger particulate surface.

For instance, 1 g of $BaSO_4$ will show a particulate surface of

- 1,500 cm^2, if it is divided into particles of 10
- 15,000 cm^2, if it is divided into particles of 1 .

The particle surface is the contact zone between particles and the dispersant phase (water).

This zone is concerned by physical adsorption phenomenon with the water molecules and some ions present in the dispersant phase. The particle size is therefore increased and tends to stick to each other and build some clumps. The homogeneity of the suspension is therefore decreased. Stabilisers are added to prevent the formation of $BaSO_4$ aggregates.

Grain Size and Viscosity

The use of small grain sizes in barium sulphate contrast media induces a high viscosity. Inversely, the use of large grain sizes allows the preparation of lower viscosity barium sulphate contrast media. This is used for preparation of high density (HD) products, which contain particles of up to 30 , and still have a low viscosity for optimal and quick coverage of the stomach mucosa.

2. The electric charge of the particles in suspension and the stabilising excipients.

All solid particles immersed in a liquid have an electric charge which arises from the absorption of certain ions or by the loss of electrons or ions from the particle surface.

This electric charge attracts molecules and ions (sometimes called counter-ions), which are present in the liquid phase. They build a diffuse layer which extends from the fixed layer which sticks to the particle itself to the electrically neutral zone where the electrostatic field has disappeared.

The electrical difference of potential between the fixed layer and the neutral zone is called zeta potential. The zeta potential measures the apparent charge of the particles. It is correlated to the suspension aggregation phenomenon and to the viscosity of the suspension. These electrical phenomena are more important with small size particles. They become negligible for large particles.

Stabilisers are products which are absorbed by $BaSO_4$ particles and which modify their electric charge.

They induce an increase in the apparent negative electric charge of the particles, which consequently creates repulsive forces between particles and thus avoid particulate aggregation and increase the stability of the suspension. One can observe a drop of the value of the zeta potential.

Typology of Commercially Available Barium Sulphate Contrast Media

1. *Powders* contain barium sulphate and excipients, to which water must be added to prepare a suspension of barium sulphate adapted to the concerned radiological examination. The user must adapt the volume of water to the final concentration and derived radioopacity of the contrast media. Thorough mixing is usually necessary. Filtration of the suspension is sometimes recommended.
2. *Suspensions* or gels of a given concentration, to which water might be added within some limits to obtain a different and lower concentration of barium sulphate.
3. *Pastes* mainly designed for studies of the oesophagus and of the rectum, which can be mixed with barium sulphate suspensions to reduce its concentration or viscosity.

Main Features of Barium Sulphate Contrast Media

1. Concentration
   The concentration is expressed in
   - Per cent weight of $BaSO_4$/volume for suspensions and gels
   - Per cent weight of $BaSO_4$/weight for powders and pastes.

   The concentration selected depends on the type of radiological examination performed:
   - Repletion technique of the stomach, small bowel or colon for which the concentration should not exceed 100% w/v.
   - Double-contrast techniques of the stomach for which the concentration can be as high as 250 w/v.
   - Double-contrast technique of the small bowel and of the colon for which concentrations as high as 100% are used.
   - Gastrointestinal tract delineation during CT examinations, for which low concentrations (0.5 to 1.5 w/v) of $BaSO_4$ are used.
2. Fluidity or viscosity
   The required viscosity depends on the concerned examination:
   - Examination of the pharynx and oesophagus require the use of a highly viscous paste which will not fall quickly into the stomach.
   - Double-contrast examination of the stomach requires the use of low-viscosity suspensions to visualise all details of the mucosa, and possibly of high density (in weight and to X-rays) in order to obtain a better contrast.

   Barium sulphate suspensions are non-Newtonian and thixotropic: the relation between shear rate and stress is non-linear and the curves displaying the correspondence between stress and shear rate form a hysteresis loop when shear rates are increased and subsequently decreased. Measurements of viscosity are directly related to the type of apparatus used.

   Viscosity is sometimes measured in seconds needed to empty a standardised cup through a hole.

   Viscosity of the barium sulphate suspension is related to its coating and mucosal adherence performance. The bowel preparation agents prior to double-contrast barium enemas can influence it.
3. Stability
   Stability is usually measured by the sedimentation rate of the suspension, which is expressed by the depth of the supernatant lying over the suspension–supernatant interface after a given period of time.
   Stability of $BaSO_4$ suspension is needed to obtain films free from sedimentation artefacts. The necessary stability will therefore depend on the technique used:
   - Small grain size $BaSO_4$ suspensions (1 m) are mainly used for repletion techniques and double-contrast examinations of the small bowel and of the colon. Their sedimentation rate is usually very low.
   - High density (HD) $BaSO_4$ (1 to 30 and more micrograms grain sizes) are mainly used for double-contrast examinations of the stomach.
4. Hydrophilicity of the $BaSO_4$ suspension is necessary for double-contrast examinations of the colon, because of the very high water adsorption capacity of the colon. The $BaSO_4$ film is therefore subjected to severe dehydration. Hydrophilic resins are used in some products in order to trap the water and avoid drying out of the $BaSO_4$ film. The derived loss of elasticity and uniformity would induce difficulties in image interpretation.
5. Palatability is related to the flavouring agents added in the $BaSO_4$ contrast media for oral use. This is of particular importance for CT barium contrast media used for delineation of the GI tract, which are sometimes self-administered by the patient, outside a strictly medical environment. Pleasant taste and odours lead to an optimal patient compliance to the ingestion of the appropriate dose of $BaSO_4$ contrast media.

Conclusion

Availability of Barium Contrast Media

It is estimated that around 9,000 t of barium sulphate have been used for medical imaging worldwide in 2003.

Barium sulphate contrast media have been made available from more than 20 manufacturers worldwide in forms varying from bulk material to ready-to-use presentations in sophisticated packaging.

Use of Barium Contrast Media

The above-mentioned amount of barium sulphate has been mainly used in conventional fluoroscopic imaging studies in both repletion and double-contrast techniques and in CT studies for GI tract delineation purposes.

Dynamic studies of deglutition and defecation functions are also often based on the use of barium contrast media.

A new and promising field of development concerns CT and MR colonography (also called virtual coloscopy), which are sometimes involving faecal tagging techniques. Barium contrast media absorbed orally have been used for tagging of the faeces in CT (2) and MR (3) colonography.

Bibliography

1. Swanson DP, Chilton HM, Thrall JH (1990) Pharmaceuticals in medical imaging Macmillan Publishing Company
2. Lefère PA, Grypspeerdt SS, Dewyspelaere J, Baekelandt M, Van Holsbeeck BG (2002) Dietary fecal tagging as a cleansing method prior to computed tomographic colonography: Initial results-polyp detection and patient acceptance. Radiology 224:393–403
3. Lauenstein TC, Goehde SC, Ruehm SG, Holtmann G, Debatin JF (2002) MR colonography with barium-based fecal tagging: Initial clinical experience. Radiology 223:248–254
4. Miller RE, Skucas J (1989) Radiographic contrast agents. University Park Press
5. Gallot D. (1983) Le sulfate de baryum: aspects galéniques et formulation, J Pharm Clin
6. Conry BG, Jones S, Bartram CI (1987) The effect of oral magnesium-containing bowel preparation agents on mucosal coating by barium sulphate suspensions. Brit J Radiol 60:1215–1219
7. Bachem C, Gunther H (1910) Bariumsulfat als schattenbildendes Kontrantmittel bei Röntgenuntersuchungen. Z Röntgenk Rad Forschr, 12:369–376

Contrast Media, Extravasation

Marie-France Bellin[1], Jarl Å. Jakobsen[2], Henrik S. Thomsen[3], Sameh K. Morcos[4]
[1]Department of Radiology, University Hospital Paul Brousse, AP-HP. University Paris-Sud 11, Villejuif, France
[2]Department of Radiology, Rikshospitalet, Oslo, Norway
[3]Department of Diagnostic Radiology, Copenhagen University Hospital at Herlev, Herlev, Denmark
[4]Department of Diagnostic Imaging, Northern General Hospital, Sheffield Teaching Hospitals NHS Trust, Sheffield, UK
marie-france.bellin@pbr.ap-hop-paris.fr

Definition

Subcutaneous extravasation is a well-recognized complication of intravenous administration of iodinated and magnetic resonance (MR) contrast media. Most extravasations involve small volumes of contrast material and induce minimal swelling or localized erythema, which rapidly diminish. Extensive tissue necrosis and severe skin and subcutaneous ulceration are rare and usually follow high-volume extravasations. The Contrast Media Safety Committee of the European Society of Urogenital Radiology has produced guidelines for preventing and managing extravasation of contrast media (Table 1) (1).

Contrast Media, Extravasation. Table 1 Contrast Media Safety Committee of the European Society of Urogenital Radiology guidelines for preventing and managing extravasation of contrast media

Risk factors are related to	• The technique
	• Use of a power injector
	• Less optimal intravenous sites, including lower limb and small distal veins
	• Large volume of contrast medium
	• High-osmolar contrast medium
	• The patient is
	• Unable to communicate
	• With fragile or damaged veins
	• With arterial insufficiency
	• With compromised lymphatic and venous drainage
To reduce the risk	• Always use careful intravenous technique, preferably with plastic catheters
	• Use low-osmolar contrast medium
Type of severe injuries	• Most injuries are minor. Severe injuries include skin ulcerations, necrosis of soft tissue, and compartment syndrome
Treatment	• Conservative management is adequate in most cases
	• Limb elevation
	• Application of ice packs
	• Careful monitoring
	• If a serious injury is suspected, seek the advice of a surgeon

Characteristics

Risk Factors

Patient Factors

High-risk patients include noncommunicative patients (infants, small children, and unconscious patients) and patients receiving chemotherapy, because chemotherapy may induce fragility of the vein wall (1, 2). Extravasation injuries are more severe in patients with low muscular mass

and atrophic subcutaneous tissue. In addition, patients with arterial insufficiency (such as atherosclerosis, diabetes mellitus, or connective tissue diseases) or compromised venous drainage (such as thrombosis) or lymphatic drainage (such as radiation therapy, surgery, or regional node dissection) are less able to tolerate extravasation than those with unimpaired circulation (1–5).

Contrast Media Type and Volume

Extravasation of low-osmolar contrast media is better tolerated than extravasation of high-osmolar media. The vast majority of extravasations involve small volumes of contrast material, and symptoms resolve completely within 24 h. Rarely, severe skin ulceration and necrosis can follow extravasation of volumes as small as 10 mL. Large-volume extravasation may lead to severe damage to extravascular tissue and is most likely to occur when contrast medium is injected with an automated power injector and the injection site is not closely monitored.

Factors Due to Injection Technique

Extravasations are more frequent with metallic needles than with plastic cannulae and when indwelling intravenous catheters are used (3). The site of injection also appears to be important: injections into the dorsum of the hand, foot, or ankle are frequently associated with extravasation injury. The frequency of extravasation of contrast medium after mechanical bolus injection is higher than that reported for hand-injection or drip infusion techniques (4) and varies from 0.2 to 0.4%, with power injection rates between 1 and 2 mL. In a study by Jacobs et al (5), the incidence of extravasation (0.6%) did not differ significantly between groups of patients receiving different injection rates of contrast media. In addition, no correlation was noted between the extravasation rate and catheter location, catheter size, or catheter type.

Mechanism

Multiple factors are involved in extravasations. The first factor is osmolality above 1.025–1.420 mOsm/kg water. Both iodinated radiographic and MR contrast agents of low osmolality are better tolerated than high-osmolar iodinated contrast agents. The second factor is the cytotoxicity of contrast media. While Cohan et al (6) found that ionic contrast media were more toxic than nonionic agents, no difference was found by Jacobs et al (5). The presence of meglumine as a cation may also play a role in the cytotoxicity of ionic contrast media (7). The third factor is the volume of extravasated contrast medium. Although severe skin lesions have been described following an extravasation of less than 15 mL, the majority have occurred with large-volume extravasations (8). The fourth factor is the mechanical compression caused by large-volume extravasations that may lead to compartment syndromes. Infection of the extravasated site may increase the severity of local lesions. Extravasation from indwelling intravenous lines is often due to phlebitis that develops in the cannulated veins. Other mechanisms include inadequate placement of the catheter in the vein, multiple punctures of the same vein, and high injection pressure, which can break the vessel wall (1, 2).

Presentation

Symptoms of extravasation are quite variable, and patients may be asymptomatic or complain of stinging or burning pain. At physical examination, the extravasation site appears edematous, erythematous, and tender; swelling may be due to tissue necrosis associated with progressive edema and skin ulceration. Most extravasation injuries resolve spontaneously in 2–4 days; rarely, they lead to long-term sequelae including hypoesthesia, marked weakness, and pain (1, 2, 4). The initial examination does not allow one to predict whether the extravasation injury will resolve or result in ulceration, necrosis, or damage to soft tissue. A number of clinical findings suggest severe injury and justify the advice of a surgeon. These include skin blistering, altered tissue perfusion, paresthesias, and increasing or persistent pain after 4 h (2). Extravasation may also result in acute compartmental syndromes, producing tense and dusky forearms with swelling and diminished arterial pulses. Compartmental syndromes may necessitate emergency fasciotomy to relieve neurovascular compromise (9).

Extravasation injuries must be distinguished from other local reactions to injected fluid, including hypersensitivity reactions and local irritative effects of iodinated contrast agents on the vessel wall. In these reactions, edema and erythema are absent, and the catheter is well positioned in the vein. Extravasated gadolinium is better tolerated than conventional ionic radiographic contrast media and produces a zone of signal void on short relaxation time MR images because of its high local concentration (10). New devices for detecting extravasation are currently under evaluation (11).

Treatment

Elevation of the affected limb: Elevation is often useful to reduce the edema by decreasing the hydrostatic pressure in capillaries.

Topical application of heat or cold: Heat produces vasodilatation and thus resorption of extravasated fluid and edema (12), whereas cold produces vasoconstriction and limits inflammation (13). Cooling can be produced

with ice packs placed at the injection site for 15–60 min three times a day for 1–3 days or until symptoms resolve.
Prevention of secondary infection: Application of silver sulfadiazine ointment is recommended by many plastic surgeons whenever blistering is evident (14).
Hyaluronidase, dimethylsulfoxide (*DMSO*), *corticosteroids, and vasodilators*: Most studies have failed to demonstrate any value of these agents or did not evaluate extravasations of contrast media.
Surgery: Most plastic surgeons believe that the majority of extravasation injuries heal without surgery and that a conservative policy is therefore recommended (15). Surgical drainage or emergency suction applied within 6 h can be effective (16), and the use of emergency suction alone or combined with saline flushing have also been helpful (17, 18).
Aspiration of fluid from the extravasated site: This treatment is controversial, as it usually removes only a small amount of extravasated fluid and carries a risk of infection.

Conclusions

Extravasation of contrast material is a relatively common complication of enhanced imaging studies, but large-volume extravasation may result in severe damage. Early identification is important, and conservative management is effective in most cases. Radiologists should be aware of ways to prevent, recognize, treat, and document extravasation injuries.

Bibliography

1. Bellin MF, Jacobsen JA, Tomassin I et al and members of Contrast Media Safety Committee of European Society of Urogenital Radiology (ESUR) (2002) Contrast medium extravasation injury: guidelines for prevention and management. Eur Radiol 12:2807–2812
2. Cohan RH, Ellis JH, Garner WL (1996) Extravasation of radiographic contrast material: recognition, prevention, and treatment. Radiology 200:593–604
3. Sistrom CL, Gay SB, Peffley L (1991) Extravasation of iopamidol and iohexol during contrast-enhanced CT: report of 28 cases. Radiology 176:65–67
4. Federle MP, Chang PJ, Confer S et al (1998) Frequency and effects of extravasation of ionic and nonionic CT contrast media during rapid bolus injection. Radiology 206:637–640
5. Jacobs JE, Birnbaum BA, Langlotz CP (1998) Contrast media reactions and extravasation: relationship to intravenous injection rates. Radiology 209:411–416
6. Cohan RH, Leder RA, Bolick D et al (1990) Extravascular extravasation of radiographic contrast media: effects of conventional and low-osmolar contrast agents in the rat thigh. Invest Radiol 25:504–510
7. Kim SH, Park JH, Kim YI et al (1990) Experimental tissue damage after subcutaneous injection of water-soluble contrast media. Invest Radiol 25:678–685
8. Upton J, Mulliken JB, Murray JE (1979) Major intravenous extravasation injuries. Am J Surg 137:497–506
9. Benson LS, Sathy MJ, Port RB (1996) Forearm compartment syndrome due to automated injection of computed tomography contrast material. J Orthop Trauma 10:433–436
10. Carrier DA, Ford JJ, Hayman LA (1993) MR appearance of extravasated gadolinium contrast medium. Am J Neuroradiol 14:363–364
11. Birnbaum BA, Nelson RC, Chezmar JL et al (1999) Extravasation detection accessory: clinical evaluation in 500 patients. Radiology 212:431–438
12. Hastings-Tolsma TM, Yucha CB, Tompkins J et al (1993) Effect of warm and cold applications on the resolution of IV infiltrations. Res Nurs Health 16:171–178
13. Elam EA, Dorr RT, Lagel KE et al (1991) Cutaneous ulceration due to contrast extravasation: experimental assessment of injury and potential antidotes. Invest Radiol 26:13–16
14. Heckler FR (1989) Current thoughts on extravasation injuries. Clin Plast Surg 16:557–563
15. Cohan RH, Dunnick NR, Leder RA et al (1990) Extravasation of nonionic contrast media: efficacy of conservative treatment. Radiology 174:65–67
16. Loth TS, Jones DEC (1988) Extravasations of radiographic contrast material in the upper extremity. J Hand Surg 13:395–398
17. Gault DT (1993) Extravasation injuries. Br J Plast Surg 46:91–96
18. Vandeweyer E, Heymans O, Deraemaecker R (2000) Extravasation injuries and emergency suction as treatment. Plast Reconstr Surg 105:109–110

Contrast Media, Iodinated

Henrik S. Thomsen
Department of Diagnostic Radiology, Copenhagen, Denmark, University Hospital, Herlev, Denmark
hentho01@heh.regionh.dk

Iodinated contrast agents are essential in all modern radiographic imaging. The ideal contrast agent should be totally inert, causing no interactions with the organism at any level. Furthermore, it should be excreted rapidly and completely. In reality, none of the current contrast agents is totally inert, but the newer classes of agents are much closer to this state than the old ones.

Iodinated contrast media may be divided into water-soluble and oily contrast media. Oily contrast media include Lipiodol, a stable compound of 40% iodine in poppy seed oil, introduced in the 1920s and later replaced by Lipiodol ultra and Ethiodol, ethyl esters of iodinated fatty acids of poppy seed oil containing 48 and 37% iodine, respectively. These oils are still, to some extent, used for lymphography, hysterosalpingography, and dacryocystography.

Water-soluble contrast agents for use in radiographic techniques are iodinated benzoic acid derivates. They are by

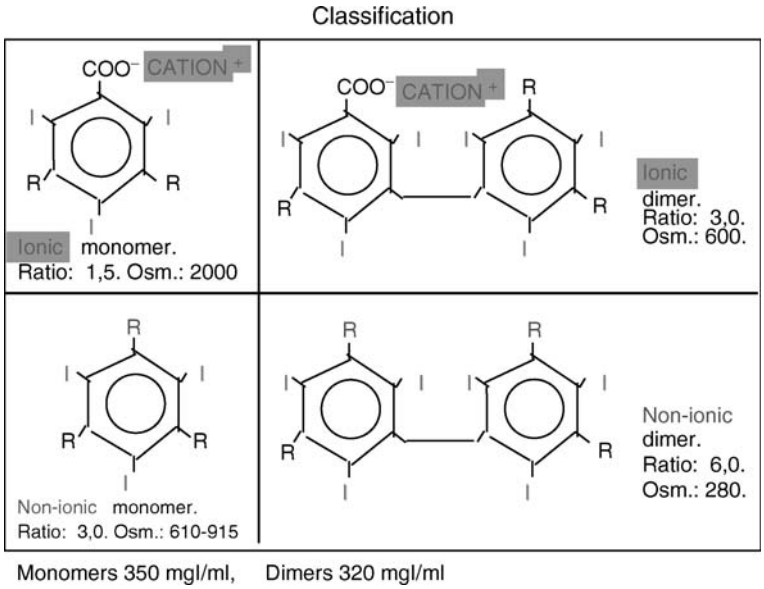

Contrast Media, Iodinated. Figure 1 Classification of water-soluble iodinated contrast media.

far the most used agents for radiography. The current iodinated contrast agents can be divided into four classes (Fig. 1): (a) high-osmolar ionic monomeric agents, (b) low-osmolar nonionic monomeric agents, (c) low-osmolar ionic dimeric agents, and (d) iso-osmolar nonionic dimeric agents. They all are distributed in the extracellular phase, none penetrate an intact blood–brain barrier, and all are excreted *via* glomerular filtration. The high-osmolar ionic monomeric media which are sodium and meglumine salts of tri-iodinated benzoic acid have been available since the 1950s. They are very hyperosmolar, being 5–8 times the osmolality of the blood. The hyperosmolality greatly increases the hemodynamic and toxic effects of these agents. In the 1970s, low-osmolar contrast media became available. This was achieved through converting tri-iodinated benzoic acid into a nonionic molecule by replacing the COOH radical with an amide ($CONH_2$). This molecule in solution will not dissociate, allowing the availability of three atoms of iodine with only one active particle [a ratio of 3:1]. Another development was the introduction of the mono-acid dimer in which two tri-iodinated benzoic rings are linked together with a bridge and the COOH of one ring is converted into an amide. This gives the same iodine: particle ratio of 3:1 in solution, since there are six iodine atoms and two active particles in one molecule. The osmolality of the ionic dimeric contrast media is almost the same as the nonionic monomeric agents and is about two times that of the blood at an iodine concentration of 300 mgI/mL. In the late 1980s the nonionic dimeric contrast media were introduced. This was possible through attaching two nonionic tri-iodinated benzoic rings. These dimers give an iodine:particle ratio of 6:1 since there are six iodine atoms and only one active particle in the molecule. The osmolality of the nonionic dimers at the concentration of 300 mgI/mL is equal to that of the blood. In the 1990s there was a worldwide introduction of nonionic monomeric contrast agents stimulating the conversion. At the turn of the century, both the nonionic monomeric and dimeric agents have firmly established themselves as the agents of choice since they are exceptionally well tolerated by the great majority of patients and are associated with a markedly reduced incidence of life-threatening anaphylactoid reactions as well as moderate and minor adverse reactions. Today more than 90% of all intravascular injections of an iodinated contrast medium in Western Europe and North America are done with a nonionic agent. By far, computed tomography (CT) and cardiac angiography are the examinations where the largest amounts are currently being used.

The benzene ring is, as mentioned earlier, the basis for all iodinated water-soluble contrast agents. One of the purposes of the side chains is to protect the body from the toxic benzene ring with three iodine atoms. The side chains do this well considering the low toxicity of the current iodinated contrast media. The minor variation within one class is mainly for patent protection. The variation in the number of hydroxyl groups may affect the hydrophilicity slightly, but the difference is of minor importance, as several small and large clinical studies have not been able to show any significant difference between

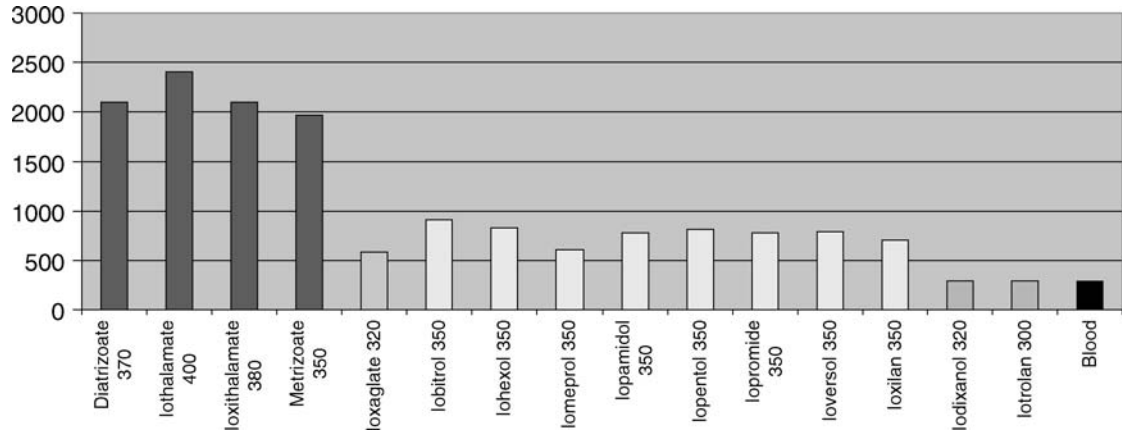

Contrast Media, Iodinated. Figure 2 Osmolality (m Osm/kg water) at 37°C of currently available iodinated contrast media.

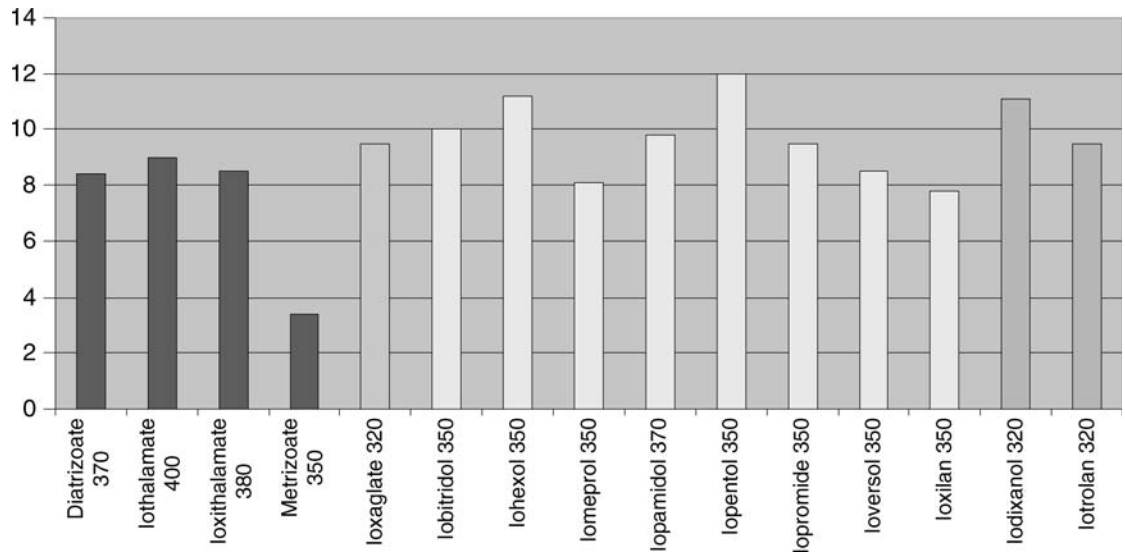

Contrast Media, Iodinated. Figure 3 Viscosity (cP) of current available iodinated contrast media at 37°C.

the various nonionic low-osmolar agents with regard to pharmacokinetics, pharmacodynamics, general safety, renal tolerance, induction of thrombosis, diagnostic effect, and so on. Today many contrast agents are available with various osmolality (Fig. 2) and viscosity (Fig. 3). A decrease in osmolality increases to some extent the viscosity, but there is no linear relationship between osmolality and viscosity. The main disadvantage of increased viscosity is the difficulty it may cause during the intravascular administration of contrast media particularly if a high-flow injection is required or a catheter with very small inner diameter is used.

Attenuation

Iodine has the atomic number 53 and an atomic weight of 127. Attenuation increases with the atomic number of the atom but decreases with the energy (keV) of the X-ray photons, except at the K-edges. The K-edge of iodine is 33 keV. Below 33 keV only very few photons will pass through the body. For CT, the maximal X-ray photon energy is between 120 and 140 keV and the most common photon energies in the spectrum are between 60 and 70 keV. For common radiographic examinations, the maximal X-ray photon energy is

between 70 and 90 keV. Thus, the common photon energies in the spectrum are above the K-edge of iodine (33 keV). The attenuation by the iodinated contrast agent molecule is enhanced by the fact that it contains three iodine atoms.

Administration—Dose

More contrast medium than necessary to confirm the presence or absence of a suspected abnormality or to perform a therapeutic procedure should not be used in any patient. The dose necessary differs from examination to examination. For example, for a dacryocystography a few milliliters of a 350-mgI/mL solution may be needed, for CT of the urinary tract (CT urography) 100 mL of a 300-mgI/mL solution given a split bolus may be more optimal than a single bolus injection of 150 mL, and for coronary angiography it may be diagnostically better to use 250 mL of a 350-mgI/mL solution than 300 mL of a 300-mgI/mL solution. Thus, the dose of contrast medium should be tailored to the actual problem that is being examined. Proper documentation of the intravascular use of contrast media should be included in the patient's records.

Administration—Extravasation

Infants, young children, and unconscious and debilitated patients are particularly at risk of extravasation during contrast media injection. Automated power injection may result in extravasation of large volumes and can lead to severe tissue damage. Fortunately, most extravasations result in minimal swelling or erythema, with no long-term sequelae. However, severe skin necrosis and ulceration may occur. Large volumes of high-osmolar contrast media are known to induce significant tissue damage. Compartment syndrome may be seen associated with extravasation of large volumes. The intravenous technique should always be performed carefully, preferably using plastic catheters for power injection. Conservative management is often adequate, but in serious cases the advice of a plastic surgeon is recommended.

Adverse Reactions

Radiation Versus Contrast Media

For pregnant women, the radiation exposure to the fetus may be a bigger risk than the exposure to contrast media. The same applies to newborns, children, and young adults. For patients over 40 years of age the opposite is the case, as the long-term effects of radiation (e.g., development of solid cancers) diminishes with age and the risk of an adverse reaction to a contrast agent in general increases with age (e.g., nephrotoxicity).

Adverse Reactions to Water-Soluble Contrast Agents

Adverse reactions to intravascular contrast media are nowadays infrequent and generally classified as either idiosyncratic or chemotoxic. Idiosyncratic (i.e., anaphylaxis-like, anaphylactoid) reactions occur unpredictably and independently of the dose or concentration of the agent. Most anaphylaxis-like reactions relate to the release of active mediators. Conversely, chemotoxic-type effects relate to dose, the molecular toxicity of each agent, and the physiological characteristics of the contrast agents (i.e., osmolality, viscosity, hydrophilicity, calcium-binding properties, and sodium content). Some reactions to injection of contrast media (e.g., sudden cardiopulmonary arrest) are difficult to categorize into either of the two major reaction types.

Chemotoxic effects of contrast media are more likely in patients who are debilitated or medically unstable. Hence, patients should be screened for conditions such as renal dysfunction, renovascular disease, severe cardiovascular disease, or recent seizures.

Adverse reactions to intravascular administration of iodinated contrast media are classified into renal and nonrenal. The latter is subdivided into acute (<1 h) and delayed (>1 h) reactions.

Acute Nonrenal Adverse Reactions

An acute reaction to contrast media can be divided into minor, intermediate, and severe life-threatening reactions. The minor reactions include flushing, nausea, arm pain, pruritus, vomiting, headache, and mild urticaria. They are usually mild in severity, of short duration, self-limiting, and generally require no specific treatment. The incidence of these reactions to high-osmolar contrast media is probably between 5 and 15%. Intermediate reactions, more serious degrees of the above symptoms, include moderate degrees of hypotension and bronchospasm. They usually respond readily to appropriate therapy. The incidence of these reactions to high-osmolar contrast media is about 1–2%. Severe life-threatening reactions include severe manifestation of all of the symptoms included under minor and intermediate reactions, convulsions, unconsciousness, laryngeal edema, severe bronchospasm, pulmonary edema, severe cardiac dysrhythmias and arrest, cardiovascular and pulmonary collapse. The incidence of serious reactions with high-osmolar contrast media is around 0.06–0.04%. The prevalence of contrast reactions with low-osmolar

contrast media is lower in comparison to high-osmolar contrast media by a factor of 5. It is mandatory that one is always prepared to treat a reaction.

There are several predisposing factors to contrast reactions. The incidence of severe adverse reactions increases in the presence of these risk factors, particularly allergy or bronchial asthma. A previous reaction to a contrast medium is also an important predisposing factor. For the time being, no medical prevention is recommended; steroid prophylaxis can be administered, but it does not avoid occurrence of adverse reactions in all patients.

Delayed Nonrenal Adverse Reactions to Contrast Media

Most delayed reactions are not serious or life-threatening and include flu-like illness, parotitis, nausea and vomiting, abdominal pain, and headache. Delayed allergy-like reactions with skin manifestation are the most frequent type. Thyrotoxicosis may occur up to 3 months after the injection.

Renal Adverse Reactions to Contrast Media

Contrast medium-induced nephrotoxicity is defined as an impairment in renal function (an increase in serum creatinine by more than 25 or 0.5 mg/dL (44 μmol/L) occurring within 3 days after the intravascular administration of contrast media and the absence of alternative etiology. It is considered an important cause of hospital-acquired renal failure. Diagnostic and interventional procedures using contrast media are performed with increasing frequency. In addition, the patient population subjected to these procedures is progressively older with more comorbid conditions. Prevention of this iatrogenic condition is important to avoid the substantial morbidity and even mortality that can sometimes be associated with contrast medium-induced nephrotoxicity. Even a small decrease in renal function may greatly exacerbate the morbidity and mortality caused by coexisting conditions such as acquired sepsis, bleeding, coma, and respiratory failure, which are more frequent in patients with acute renal failure. Therefore, several measures have been tested to reduce the frequency of contrast medium-induced nephropathy. No measure has yet resulted in avoidance of its occurrence in all patients, but adequate hydration reduces the incidence. When it has occurred, no specific treatment is possible.

Interactions

Several of the *in vitro* studies on the hematologic effects of contrast media have not been confirmed by *in vivo* and clinical studies. Clinical studies indicate that all contrast media possess an anticoagulant effect and that this effect is stronger with ionic contrast media. A meticulous angiographic technique is the most important factor for reducing the thrombotic complications associated with angiographic procedures.

Contrast media may interact with other drugs and may interfere with isotope studies and biochemical measurements. Awareness of the patient's drug history is important to avoid potential hazards.

Contrast Media, Iodinated, Applications in Conventional Radiography and CT

Henrik S. Thomsen, Marie-France Bellin
Université Paris 11, AP-HP, Service de Radiologie, Hôpital Paul Brousse, Villejuif, France
Department of Diagnostic Radiology, Copenhagen, Denmark, University Hospital at Herlev, Herlev, Denmark
hentho01.@heh.regionh.dk

Synonyms

Radiocontrast media; Radiographic contrast media

Definition

Contrast media are drugs that enhance the differences seen on the images between the body tissues. The ideal contrast agent should be totally inert, causing no interactions with the organism at any level. Furthermore, it should be excreted rapidly and completely.

They can be divided into water-soluble iodinated contrast media and non-water-soluble barium agents. The water-soluble iodinated contrast media can be further subdivided according to the number of benzene-rings: monomers (one ring), dimers (two rings). Both types are available as ionic and non-ionic. Thus iodinated contrast agents can be divided into four classes: (i) High-osmolar ionic monomeric agents, (ii) Low-osmolar non-ionic monomeric agents, (iii) Low-osmolar ionic dimeric agents, and (iv) Iso-osmolar non-ionic dimeric agents. Low-osmolar non-ionic monomeric agents are today the most used agents.

Indication

Water-soluble iodinated contrast media, which diffuse throughout the extracellular space after intravascular

administration, are principally used for angiography, during computed tomography (CT) and conventional radiography, notably intravenous urography (IVU). They can also be administered directly into the gastrointestinal tract and urinary tract, or into body cavities to opacify fistulas for example.

Barium sulphate preparations used to visualize the gastrointestinal tract consist of a suspension of insoluble barium sulphate particles which are not absorbed from the gut.

Contraindications

Iodinated Contrast Media

Absolute:

All contrast media: manifest hyperthyroidism

Ionic contrast media: subarachnoidal injection.

Relative:

Reduced renal function, asthma, history of allergy, previous reaction to a iodinated contrast medium

Pregnancy/Lactation

If the examination has been found to be indicated based on a thoroughly analysis of the history, symptoms and signs, one should go ahead and use the contrast media whenever it is necessary in order to confirm the presence or absence of a lesion. In early pregnancy, mutagenic and teratogenic effects may occur but they have never been shown to occur after administration of iodinated contrast media. In late pregnancy, potential harmful effects on fetal thyroid owing to the presence of free iodine are of concern. Therefore, neonates of mothers exposed to iodinated contrast media in the late pregnancy must be checked for thyroid dysfunction within 7 days after birth. In many countries it is already a routine.

It is been recommended to stop lactation for a day or two after administration of iodinated contrast media. However, the neonate will receive between 0.3–0.5% of the maternal dose and again only 1% of those tiny amounts may enter the extracellular fluid of the neonate. Thus, breast feeding may be continued normally when iodinated contrast agents are given to the mother. The baby may notice that the milk has a different taste.

Use and Dosage

The overwhelming majority of iodinated contrast media is used for CT-scanning, cardiac angiography, and interventional radiology. Only a minority is used for the remaining indications. Contrast media are available in various concentrations (140, 150, 180, 200, 240, 250, 300, 350, 370, 400mg/mL). For CT-scanning most radiologists use a contrast medium in a 300mgI/mL solution (monomer) or 270mgI/mL (dimer), whereas for cardiac and coronary angiography most cardiologists prefer concentrations of 350–400mgI/mL of a monomer whereas the dimers are mainly used in concentrations of 320mgI/mL.

The amount of contrast media used depends on the type of examination. For CT fixed doses in mL or in mL/kg body weight are used. The dose varies from country to country for example in some countries only 50mL of a 300mgI/mL solution is used for brain CT studies whereas others give 100mL of the same solution. There is no consensus about the optimal dosage. Regarding the latter not only the total mg of iodine is important, but also speed of injection, size of the bolus, kilovoltage, mAs, pitch affect the resulting image. When it comes to conventional arteriography like coronary angiography and direct injection into body cavities as the renal pelvis, dose depends on many factors including type of the lesion, the skills of the physician, kilovoltage, mAs, body weight, and so on. For an examination like CT urography many protocols have been proposed ranging from 50 to 200mL of 300mgI/mL contrast medium. A split bolus is now advocated by some radiologists, whereas others still recommend the old single injection including a bolus and a much slower follow-up during the first minutes. Optimal dosage is a sensitive area and a consensus has not yet been reached.

For barium studies of the gastrointestinal tract, 300–800mL of barium sulphate preparations are used.

Adverse Reactions

Adverse reactions to iodinated contrast media are more likely to develop in patients with reduced renal function, with asthma, a history of allergy or contrast reaction and in those who are debilitated or medically unstable. These reactions can be divided into renal and non-renal and the later are subdivided into acute and delayed. Acute non-renal adverse reactions can be minor, intermediate or severe. Fatal reactions are rare. The introduction of low-osmolar agents has caused an overall reduction in the number of non-fatal contrast reactions. See the sections: Adverse reactions, contrast media, iodinated, acute, non-renal; Adverse reactions, contrast media, iodinated, delayed; Adverse reactions, iodinated contrast media, acute, renal.

Interactions

See Contrast Media, Iodinated, Interactions with Drugs.

Bibliography

1. Thomsen HS (2006) (ed) Contrast Media: Safety Issues and ESUR Guidelines. Springer Verlag, Heidelberg

Contrast Media, Iodinated, Dose, and Administration

Robert P. Hartman, Bernard King
Department of Diagnostic Radiology, Mayo Clinic, Rochester MN, USA
hartman.robert@mayo.edu

Definition

Computed tomography (CT) utilizing multidetector scanners has introduced many new challenges regarding doses and rates of administration for iodinated contrast to obtain the best quality images of a wide variety of organs and vascular systems in the body. Routine CT of parenchymal organs in many instances requires more volume of contrast material injected at lower rates than CT angiography, which often requires less volume at a higher rate. The exact dose of contrast for any given vascular bed or organ system is becoming standardized but may still vary from institution to institution. In this section, some general principles of contrast administration and dosing will be discussed.

Characteristics

Administration

Whatever exam one wishes to perform the route of contrast material administration is similar. For most multidetector CT protocols, a bolus injection *via* power injectors is superior to IV drip infusion. These power injectors, however, can lead to potential complications including large volume extravasation and/or air embolism. Proper preparation of the injector and IV site as well as communication with the patient is important to limit these potential events. Pain or swelling at the IV site during the injection can be early signs of extravasation and the patient should be monitored for these signs. Whenever possible a nurse or technologist should monitor the site with direct palpation as the injection occurs for signs of extravasation. If detected the injection should be aborted immediately.

The best site for the IV access is an antecubital or forearm vein. Flexible venous cannulas should be used for the access site. Although 22-gauge cannulas can theoretically handle injection rates of 5 cc/sec it is recommended that a 20-gauge or larger IV is used for rates of 3 cc/sec or greater. The more peripheral the IV site the lower the rate of injection. Hand or wrist venipuncture sites may be limited to rates in the 1.5 cc/sec range.

Central venous catheters can be used safely if necessary when peripheral IV access cannot be obtained. The exact specifications and recommendations for any central catheter to be injected should be followed. Often large-bore (9.5 to 10 F) central venous catheters will be able to handle 2.5 cc/sec injection rates without exceeding the manufacturers' specified limitations.

Use and Dosage

Uses

At this time, CT enhanced with iodinated contrast is a wonderful tool for imaging a wide variety of body parts. Imaging of primary tumors of the brain, lung and abdominal organs as well as metastatic disease is a common everyday occurrence. CT angiography is now being routinely performed to detect abnormalities ranging from pulmonary emboli to vascular malformations, arterial stenoses, or acute hemorrhage. Anatomic CT angiography is widely accepted for pretransplant Kidney evaluation as well as pretreatment for peripheral vascular disease. Changes from ischemia, inflammation, and infection in the GI tract can also be readily identified on arterial and venous phase CT imaging. New techniques such as CT perfusion are emerging and will provide even more capabilities in the future.

When determining the dose and timing of the contrast bolus one should first identify the specific body part to be examined. Parenchymal organs are often scanned when the tissue is homogeneously enhancing providing an enhanced background for detecting any abnormalities. However, certain organs including the liver, pancreas, and kidneys, may require multiple phases (arterial, venous, and excretory) imaging to fully evaluate. CT angiography is best performed at the peak of the first pass of the contrast material bolus through the specific vascular bed. Given the wide variety of exams available, it is easy to see that a "one size fits all" dose is not possible but some general dose sizes and timing can be suggested.

Dosing

As mentioned, proper dosing requires a preprocedural determination of the organ system or vascular bed to be studied. Routine examination of the head requires a different dose and rate of injection than a thoracic aorta CT angiogram. In general, routine CT exams for parenchymal organs in the head, chest, abdomen, or pelvis require more volume of contrast injected at a slower rate than CT angiography. The maximal dose of iodinated contrast, in general, is limited to a total of 45 g of iodine. The concentration of the contrast material also may vary. For most examinations, a concentration of 300 mg/mL

Contrast Media, Iodinated, Dose, and Administration. Table 2 Contrast bolus volume, rate of injection, and timing of scan

Area of Interest	Timing (sec)	Bolus Dose (mL) 300 mg/mL concentration [b]350 mg/mL concentration	Injection Rate (mL/sec)
Head and neck			
Carotid/circle of Willis CTA	15[a]	100[b]	4
Routine neck and chest	20	80	3
Routine head	240	100	1
Chest			
Pulmonary arteries (PE study)	15[a]	120	4
Routine chest	20	80	3
Thoracic aorta CTA	20–25[a]	125[b]	4
Abdomen and pelvis			
Abdominal aorta CTA	25–30[a]	125[b]	4
Pancreas arterial phase	40	140	4
Pancreas parenchymal phase	65	140	4
Urogram corticomedullary renal phase	45	100	3
Liver arterial phase	40	140	4
Liver portovenous phase	60	140	4
Urogram nephrographic renal phase	90	100	3
Renal artery CTA	20–25[a]	125[b]	5
Mesenteric CTA	25–30[a]	125[b]	4
Enterography arterial phase	25	150	4
Enterography mucosal phase	60	150	4
Routine abdomen and pelvis	70	140	3
Lower extremity run off CTA	30–35[a]	140[b]	3
Routine chest, abdomen and pelvis	65	140	3

[a]CTA should be performed with bolus timing sequences when available. Times listed are an estimation based on an average individual.
[b]Contrast concentration of 350 mg/mL.

Contrast Media, Iodinated, Dose, and Administration. Table 1 Contrast media volume should be based on patient weight and renal function and can be standardize as in the example below

Volume of Contrast Medium in mL						
	No Diabetes			Diabetes		
Weight	<140 lbs <64 kg	140–240 lbs 64–109 kg	>240 lbs >109 kg	<140 lbs <64 kg	140–240 lbs 64–109 kg	>240 lbs >109 kg
Serum creatinine <1.5 mg/dL	100 mL	140 mL	200 mL	80 mL	120 mL	140 mL
Serum creatinine 1.5–1.9 mg/dL	80 mL	100 mL	140 mL	Consult with Radiologist		
Serum creatinine >1.9 mg/dL	Consult with Radiologist			Consult with Radiologist		

Iodine is sufficient. CT angiography will often be performed with 350–375 mg/mL Iodine.

Contrast volume administered may range from 80–150 cc in the average adult depending on the exam. Certain patient populations however may require adjustment of the overall dose such as diabetics and patients with renal insufficiency. Weight can also be a factor requiring volume adjustments. Table 1 shows one possible method of adjustment in these patients. (Based on a CT exam for an average size healthy patient receiving 1,400 cc of 300 mg/mL). The adjustments are made not only for consideration of image quality but also with the risk of contrast induced nephropathy in mind. As shown, certain situations require consideration of a different modality

Contrast Media, Iodinated, Dose, and Administration.

Table 3 Suggested contrast media dosing rate and volume for bariatric patients

Bariatric Patient (>300 lbs 137 kg)			
Creatinine <1.4 mg/dL			
225 mL of Iodixanol 320 with 50 mL Saline flush			
Injection rate	5 mL/sec	4 mL/sec	3 mL/sec
Scan delay	80	90	100
IV infusion following exam	250–500 mL 0.9 normal saline		

exam or noncontrast exam if it is felt iodinated contrast should not be administered. Alternatively, IV hydration reduced dose of contrast or use of iso-osmolar contrast can be utilized.

As previously mentioned different body, parts require different doses. Although, the type of scanner used and patient health and size play integral roles in the exact dose, some general guidelines for some of the more common exams are provided in Table 2. The volume, rate of injection and timing of the exam are given for contrast material concentration of 300 mg/mL unless otherwise noted.

Pediatric patients are best served by dosing specifically based on weight. In general, 1 mL/2.2 kg (1 mL/lbs) of contrast material up to 100 mL is an excepted dose. Newer scanners allow for examinations on markedly obese patient populations. In these bariatric patients, dosing can be difficult. Some general guidelines for these patients are included in Table 3.

Bibliography

1. Bush WH (ed) (1999) Radiology Life Support. Oxford University Press Inc., New York, NY
2. Katzberg R (ed) (1992) The Contrast Media Manual. Williams and Wilkins, Baltimore, MD
3. King B (ed) (2004) Manual on Contrast Media. American College of Radiology, Reston, VA
4. Thomsen HS (ed) (2004) Guidelines on contrast media, European Society of Urogenital Radiology, Am J Roentgenol 2003; 181: 1463–1471

Contrast Media, Iodinated, Interactions with Drugs

Sameh K. Morcos
Department of Diagnostic Imaging, Northern General Hospital, Sheffield Teaching Hospitals NHS Foundation Trust, Sheffield, UK

Many patients with multiple medical problems who are receiving a variety of drugs are investigated with imaging techniques that require intravascular contrast media. This involves possible interactions between contrast media with other drugs including interference with isotope studies and biochemical measurements.

Drugs that will be Retained in the Body Because of Reduction in Renal Function Induced by Contrast Media

One of the potential adverse effects of iodinated contrast media is reduction of renal function. This leads to retention of drugs that are excreted exclusively through the kidneys. A good example is the indirect interaction between contrast media and metformin. Significant reduction of renal function can be induced by contrast agents in the presence of pre-existing kidney disease particularly diabetic nephropathy. The reduction in renal function induced by contrast media causes retention of metformin potentially leading to the serious complication of lactic acidosis.

Drugs that cause diuresis and natriuresis can be hazardous and should be avoided in patients receiving lithium. Although contrast media especially those of high osmolality can induce significant diuresis and natriuresis, their role of in increasing lithium toxicity is not widely studied.

Drugs that Enhance the Renal Effects of Contrast Media

Nephrotoxic drugs such as non-steroidal anti-inflammatory drugs (NSAIDs) have the potential to increase the renal effects of contrast media. This class of drugs inhibits the intrarenal synthesis of vasodilatory prostaglandins augmenting the renal vasoconstrictor effect of iodinated contrast media and may facilitate the development of contrast media nephrotoxicity. Other nephrotoxic drugs such as gentamicin, cyclosporine and cisplatin may also augment the nephrotoxic effects of contrast media.

Diuretics such as acetazolamide, furosemide, spironolactone, may augment the diuretic effect of contrast media particularly those of high osmolality, leading to dehydration, increased risk of contrast medium nephropathy, electrolyte imbalance and hypotension.

Drugs that Enhance Allergy Like Reactions to Contrast Media

β-Blockers

Patients on β-blockers including the ophthalmic preparations who are given iodinated contrast media are three

times more likely to have an anaphylactoid reaction than matched controls. There is also increased risk of contrast media induced bronchospasm particularly in asthmatics. Anaphylaxis like reaction in these patients is more refractory to conventional treatment because of low reactivity to emergency medication. Adrenaline may be ineffective or promote undesired alpha-adrenergic or vagal effects.

Interleukin-2

In a prospective study of patients undergoing CT who had received Interleukin-2 (IL-2) and intravenous non-ionic low-osmolar or oral-ionic high-osmolar contrast media, or both, there were immediate urticarial reactions in 1.8% of the patients within an hour of contrast administration. No acute reactions were observed in a control group who received contrast media but had not been treated with IL-2. Delayed reactions (erythema, rash, fever, flushing, pruritis and flu-like symptoms) developed in 12% of IL-2 patients and only in 4% of the control group. Two of the IL-2 patients required admission to hospital. The mean onset of symptoms was 4.5 h after injection of contrast media and the mean duration of reaction was 16.4 h. The patients had no risk factor for delayed reactions other than IL-2 therapy and all had previous uneventful exposure to contrast media. None of the patients with immediate reactions developed delayed reactions. The average time since IL-2 therapy was 6 months (range 24 days to 2.4 years). Previous contrast media reaction in an IL-2 patient should be considered a relative contraindication to further contrast media administration. An increased risk of contrast reactions may remain for two years after stopping IL-2 treatment.

The administration of contrast media may also precipitate IL-2 toxicity. Fever, diarrhea, nausea and vomiting have been observed 2–4 h after enhanced CT scanning with non-ionic low-osmolar contrast media. The exact mechanism is not clear but contrast media may generate the release of endogenous IL-2 or reactivate the IL-2 receptors. Patients who develop these reactions should avoid further exposure to contrast media and imaging techniques such as MRI or CT without contrast media injection should be considered for monitoring response to treatment.

Hydralazine

Patients on hydralazine treatment, which can induce systemic lupus erythematosus (SLE) like syndrome may develop cutaneous vasculitis several hours after intravascular administration of non-ionic iodinated contrast medium. Hypersensitivity reactions to iodine-containing compounds have also been described in patients with systemic lupus erythematosus. It was suggested that injection of iodinated contrast media should be avoided in patients receiving hydralazine therapy as they may provoke severe reactions.

Drugs that Interfere with the Hematological Effects of Contrast Media

Effects of Contrast Media on Coagulation

It is well established that contrast media interact with the coagulation mechanism, platelet activation and degranulation and with thrombolytic drugs. Ionic contrast media are more effective than non-ionic agents at increasing the clotting time and give a fourfold increase in the whole blood clotting time when compared to non-ionic agents. Non-ionic contrast media cause less significant alteration of clothing by inhibiting the coagulation cascade after the generation of thrombin at the step of fibrin monomer polymerization. Thus, both ionic and non-ionic contrast media can prolong clotting time and may exaggerate the effects of anticoagulant and antiplatelet drugs.

Effects of Contrast Media on Fibrinolysis

Contrast media impede fibrinolysis and delay the onset of lysis by recombinant tissue-type plasminogen activator (rt-PA), urokinase and streptokinase. This effect is reduced by increasing the concentration of the lysis agent. Contrast media cause fibrin to form in long/thin fibrils, which have a lower mass/length ratio and are more resistant to fibrinolysis. In clinical practice, if coronary angiography is performed before starting thrombolysis the recent administration of contrast media may reduce therapeutic success.

Contrast Media and Drugs Acting on the Central Nervous System

Cerebral angiography with high osmolar contrast media may lower the fit threshold in patients receiving antipsychotics, tricyclic antidepressants, or analeptics. However, this concern does not seem to be important with the routine use of non-ionic low-osmolar contrast media for cerebral angiography.

Drugs that Enhance the Effects of Contrast Media on the Heart

Patients receiving calcium channel blockers may develop hypotension after left ventriculography with high-osmolar

ionic agents. This effect is not significant with low-osmolar non-ionic contrast media, which are less vasoactive and have minimal negative inotropic effect on the myocardium.

Effects of Contrast Media on Isotope Studies

The administration of iodinated contrast media interferes with both diagnostic scintigraphy and radioiodine treatment. The reduced uptake of the radioactive tracer is caused by the free iodide in the contrast medium solution. A delay before undertaking scintigraphy of 4–6 weeks for water soluble and 12 weeks for cholangiographic contrast media is advocated.

Intravascular administration of contrast media shortly after injection of isotope material (Tc-pyrophosphate) for bone imaging can interfere with the body distribution of the Tc-pyrophosphate. Increase uptake of the isotope material in kidneys and liver with low uptake in bones was observed. The diuretic effect of contrast media may increase the elimination of the isotope material in urine so less is available for deposition in skeleton. The increased uptake in the liver is not fully explained.

Intravascular administration of contrast media may also interfere with red blood cell labeling with isotope material. Tc-99m labeling of red blood cells should be performed before contrast media injection. How contrast media interfere with red blood cells labeling is not fully understood.

Mixing Contrast Media with Other Drugs

Contrast media should not be mixed with other drugs before intravascular use. It is also advisable not to inject other drugs through the same venous access used for contrast media injection. If the same venous access is used, there should be adequate flushing with normal saline first.

Effects of Contrast Media on Biochemical Assays

Measurements of clotting time and other coagulation factors can be falsely increased after the intravascular administration of contrast media. Therefore, clotting tests should be avoided for 6 h or more after injection of contrast media.

Iodinated contrast media in the urine may also interfere with some of the protein assay techniques leading to false positive results. Care must be exercised in interpreting tests for proteinuria for 24 h postcontrast media injection.

Gadodiamide and gadoversetamide may cause spurious hypocalcemia particularly at doses of 0.2 mmol/kg or higher in patients with renal insufficiency. These contrast media interfere with calcium measurements obtained by assay using the ortho-cresolphthalein complexone (OOC) method but not with the assays using the Arsenazo III method. The false measurements of serum calcium did not occur with gadopentetate dimeglumine (Gd-DTPA) or gadoteridol. In very high concentrations, Gd-DTPA may interfere with calcium determination when methylthymolblue is used. Awareness of this effect on calcium measurements by some MRI contrast agents is important to avoid incorrect and potentially hazardous treatment.

Iodinated contrast media may interfere with determination of bilirubin, cubber, iron, phosphate and proteins in blood. Caution should be exercised when using colorimetric assays for angiotensin-converting enzyme, calcium, iron, magnesium, total iron binding capacity and zinc in serum samples who have recently received gadolinium based contrast media. Biochemical assays are better performed before contrast media injection or delayed for at least 24 h afterwards or longer in patients with renal impairment. Urgent laboratory tests performed on specimens collected shortly after contrast media injection should be carefully assessed. Accuracy of unexpected abnormal results should be questioned and discussed with colleagues from the hospital laboratories.

Conclusion

Contrast media have the potential for interaction with other drugs and may interfere with biochemical assays. Awareness of these interactions is important to avoid misinterpretation of biochemical data and causing harm to the patient following imaging and interventional procedures. Proper documentation of intravascular use of contrast media should be included in the patient's records.

Bibliography

1. Morcos SK, Thomsen HS, Exley CM et al (2005) Contrast media: interactions with other drugs and clinical tests. Eur Radiol 15:1463–1468

Contrast Media, Iodinated, Oily

Finn Rasmussen
Aarhus University Hospital, Denmark
frasm@as.aaa.dk

Synonyms

Ethiodol; Lipiodol

Definition

Sicard and Forrestier in 1923 first reported the use of iodized poppy seed oil as contrast medium. They injected Lipiodol into an antecubital vein to observe blood flow through the heart and pulmonary arteries.

Oily contrast media include Lipiodol, a stable compound of 40% iodine in poppy seed oil. Lipiodol ultra fluid and *Ethiodol*, ethyl esters of iodinated fatty acids of poppy seed and containing 48 and 37% iodine, respectively, later replaced Lipiodol.

The oily contrast material is phagocytized by polymorphonuclear cells and metabolized to sodium iodide by esterase. After elimination of the oily substance, the foreign-body reaction subsides. Excretion of sodium iodine occurs mainly *via* the kidneys, but the pancreas, liver, and salivary glands take part in its elimination.

Sensitivity reactions occur with an incidence of approximately 0.1%.

After its introduction, iodized oil has been used as a contrast medium in lymphography, bronchoscopy, hysterosalpingography, myelography, and sialography.

Indications

Sialography

Catheterization of the parotid and submaxillary duct using a catheter can be performed after preliminary dilatation of the duct orifice. Injection of 1–2 cc oily contrast media is usually sufficient to outline the main duct and all its branches. Over-distension is avoided by completing the injection when the patient notes a feeling of fullness. Oily contrast media have been replaced by nonionic, low-osmolar, water-soluble contrast media.

Myelography

In 1944, iodophenylundecylic acid (Myodil, Pantopaque) was introduced for myelography. A major drawback of the oily contrast media is the lack of resorption. Complete removal through aspiration is usually not possible after a procedure and the remaining droplets may lead to chronic irritation and arachnoiditis. Low-osmolar, nonionic, water-soluble contrast media for myelography have replaced oily contrast material.

Hysterosalpingography

The injected contrast medium outlines the uterine cavity and fallopian tubes, and spill of contrast medium to the peritoneum can be ascertained. The contrast material is injected through a cannula, a balloon catheter, or a suction device. The contrast medium is injected under image intensifier control. The contrast medium can accidentally be injected through the endometrium and taken up by the interstitial lymph or veins, which outline the uterine wall (Fig. 1).

Oily contrast materials have been used for hysterosalpingography for decades and a low complication rate has been found. In fact, a therapeutic effect of the hysterosalpingography with the use of oily contrast has been observed and pregnancy rates of up to 30% have been reported in infertile couples after the use of oily contrast media. There is still debate on the most superior contrast medium for hysterosalpingography (1, 2).

Lymphangiography

Lymphangiography is performed to visualize lymph vessels in the upper and lower extremities, the thoracic duct, and regional lymph nodes.

The main indication for lymphangiography using oily contrast material is the detection of lymph nodes

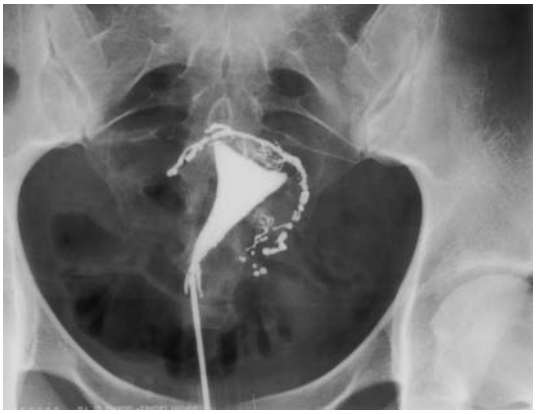

Contrast Media, Iodinated, Oily. Figure 1 Hysterosalpingography demonstrates bilateral tubal occlusion and intravasation.

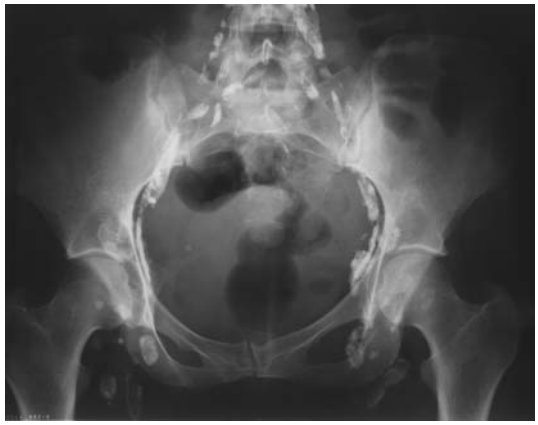

Contrast Media, Iodinated, Oily. Figure 2 Lymphangiography in the nodal phase.

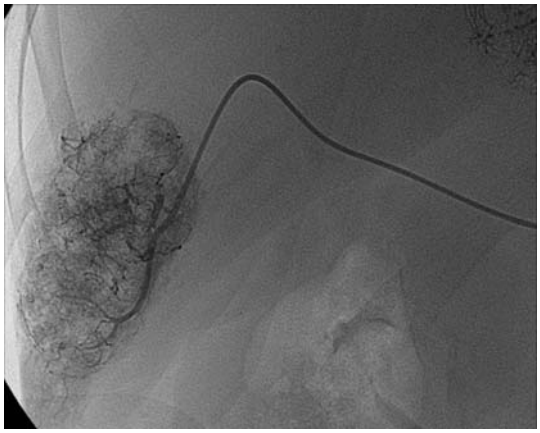

Contrast Media, Iodinated, Oily. Figure 3 The uptake of Lipiodol in a hepatocellular carcinoma after selective catherization and embolization.

metastases in cases of malignant disease, e.g., malignant lymphoma and malignant testicular tumors.

Lymphangiography is performed by demonstrating a lymphatic vessel, dissecting it, and then cannulating it. When the vessel is cannulated, the oily contrast medium is injected slowly with a maximum of 7 mL/h. No more than 10 mL of oily contrast medium should be injected. Images may be obtained in the vascular phase and in the nodular phase (Fig. 2). Contrast medium in excess of that retained in the nodes enters the systemic veins *via* the thoracic duct or lymphatic venous communications. From the veins, it passes into the lung capillaries. The contrast material remains in the lymph nodes for 6 months to 2 years in pathological cases.

Apart from local complications related to the placement of the needle in the lymphatic vessel, the most common complication is embolization to the lung.

Because of the invasiveness of the procedure, the complication rate, and the rather poor imaging impact compared with ultrasound (US), computed tomography (CT), magnetic resonance imaging (MRI), and positron emission tomography (PET)/CT, lymphangiography is no longer performed on a large scale.

Liver Imaging

Oily contrast medium injected into the hepatic artery is taken up by tumors. Normal hepatic parenchyma also takes up the contrast material, but this is cleared from normal liver within a week, whereas it is retained in tumors. Two theories for this phenomenon exist: (1) contrast material is taken up by tumors due to some abnormality of tumor vasculature, making the leakage of contrast into the tumor possible, (2) contrast material is cleaned by the Kupffer cells in normal liver parenchyma, but because such cells do not exist in tumor tissue, contrast material is retained. Usually, 10 mL contrast emulsion is injected into the hepatic artery and a CT scan is performed 7–10 days later. False-negative interpretations of Lipiodol CT may occur in cases of avascular, necrotic, or fibrotic tumors that have not taken up the agent. Focal nodular hyperplasia, hemangioma, cirrhosis, and metastatic lesions may cause false-positive interpretations. However, the pattern of Lipiodol uptake within the lesion is most often characteristic for hepatocellular carcinoma (HCC).

Multirow detector CT and functional MRI with the use of liver-specific contrast agents will probably replace this invasive way of imaging the liver, without the pulmonary side effects seen after injection of oily contrast material.

Liver Chemoembolization

A number of embolic agents have been used to treat liver tumors; one of them is oily contrast material (Fig. 3). With the angiogenesis and parasitization of flow that accompanies hepatic malignancies, no agent is truly permanent. Lipiodol alone has no antitumor effect and must be combined with a cytostatic substance or radioisotope to achieve therapeutic results.

It has been observed that oily contrast material is shunted from arterioles to portal venules before entering the tumor bed. Additional occlusion devices such as coils, Gelfoam, or microspheres can be used. A synergistic effect between embolization and chemotherapy exists. Hypoxia will cause an increased effect of the chemotherapeutic drug. A higher extraction of the drug occurs when passage through the liver is reduced.

Chemoembolization should not be performed if most of the liver is involved by tumor, in the presence of

insufficiency of the liver, significant portal hypertension, occlusion of the portal vein, hepatorenal syndrome, or in significant reduced pulmonary insufficiency.

Randomized studies have shown increased survival in patients with HCC (3). In hormone-producing liver tumors, a reduction in hormone activity has been found after chemoembolization. With regard to colorectal liver metastases, the results are more controversial.

Adverse Reactions

Oily-iodinated contrast materials induce a foreign-body reaction and this can be seen in the form of arachnoiditis in myelography, localized peritoneal fibrosis in hysterosalpingography, localized fibrosis in salivary glands in sialography, and fibrosis and scar reactions in the marginal sinuses and fibrous encapsulation of oil droplets in lymph nodes in lymphangiography. This will also happen in a lymph node that has accidentally been exposed to oily contrast medium in other examinations.

The most important side effect is pulmonary oil embolism. When the iodized oil enters the pulmonary capillaries, lung embolism will appear. Miliary or reticular deposits of oily substance in the lungs are then visible even on a conventional chest image within 24 h after injection. Most of the patients have neither clinical symptoms nor respiratory impairment, but lung scintigraphy reveals that lung embolization has occurred. Twenty-four hours after the oily contrast is injected, it is not found exclusively in the capillary bed of the lung but is scattered in the interstitial tissue of the lung.

The macrophages in the alveolar spaces phagocytize parts of the agent, which is later removed by the sputum. With an increase in the administered dose, the lung becomes a less efficient filter for the oily particles, and the amount reaching other organs such as the liver, spleen, kidneys, and bone marrow is greater. Reactive granulation tissue within the alveolar walls and areas of focal atelectases due to small infarctions are frequently encountered.

Cerebral oil embolism, iodine sialitis and thyroiditis, and hypersensitivity reactions have been reported.

Bibliography

1. Rasmussen F, Lindequist S, Larsen C et al (1991) Therapeutic effect of hysterosalpingography: oil-versus water—soluble contrast media—a randomized study. Radiology 179:75–78
2. Lindequist S, Justesen P, Larsen C et al (1991) Diagnostic quality and complications of hysterosalpingography: oil-versus water—soluble contrast media—a randomized prospective study. Radiology 179:69–74
3. Takayasu K, Arii S, Ikay I et al (2006) Prospective cohort study of transaretrial chemoembolization for unresectable hepatocellular carcinoma in 8510 patients. Gastroenterology 131:461–469

Contrast Media, Iodinated, Water Soluble

Richard H. Cohan, James H. Ellis
University of Michigan, Michigan, USA
rcohan@umich.edu

C

Synonyms

Chemical composition of contrast media; Classification of contrast media; Iodinated contrast media; Pharmacokinetics of contrast media

Definition

Iodinated radiographic contrast media are well tolerated, with large doses routinely administered without significant adverse effects in the vast majority of patients. They are used at higher doses than any other intravascular drug (1). For example, the amount of contrast material administered to a patient for a CT scan and the iodine that the contrast material contains are routinely as high as 90 and 45 g, respectively.

Characteristics

Chemical Composition and Classification

Ionic Monomers: All currently utilized iodinated contrast material is derived from a benzene ring to which have been added three iodine atoms, at the 2-, 4-, and 6-positions.

The earliest of these contrast agents were acids; containing a carboxyl group at the 1-position (required to make the molecule water soluble). These contrast molecules dissociated into two ions in solution: an anion consisting of the carboxylated tri-iodinated benzene ring, and the cation usually consisting of sodium or methylglucamine (or meglumine) or a combination of both (2). Various side chains have been attached to the 3- and 5-positions of these benzene molecules (to further facilitate their water solubility and to minimize toxicity), with variations in these side chains found in the different manufactured agents.

These contrast agents are now termed high-osmolality agents, because at standard concentrations used for CT and angiography, their osmolality is many times that of blood. They are also called ionic monomers, ionic because of the previously discussed dissociation in solution into

Contrast Media, Iodinated, Water Soluble. Table 1 Properties of iodinated contrast media

Type	Ratio (I to particles)	Range in osmolality* (mOsm/kg)	Viscosity* at 37°C (cps)
Ionic monomers	3:2	1,400–1,515	2.3–4.3
Nonionic monomers	3:1	585–672	4.7–6.3
Ionic dimer	6:2	600	7.5
Nonionic dimers	6:1	290	11.8

*Values are given for commercially available iodine concentrations at or closest to 300 mg/mL. These are the concentrations most commonly utilized for excretory urography and CT (but not for angiography)

ions, and monomers because each contrast molecule includes only *one* tri-iodinated benzene ring (3).

One way to compare the properties of various contrast media is to consider the relationship of their X-ray attenuation characteristics to their osmolality. This is done by calculating the ratio of the number of iodine atoms in a contrast molecule to the number of particles that molecule forms in solution. For high-osmolality contrast agents, this ratio is 3:2. For every three iodine atoms in solution, two different particles must be present, the benzene ring analog anion and the cation with which it is conjugated (Table 1).

Nonionic Monomers: Nonionic contrast agents were created using an alternate way to make tri-iodinated benzene ring molecules water soluble: removing the ionizing carboxyl group at the 1-position and replacing it and the side chains at 3-, and 5-positions with much larger components each of which contained several hydrophilic hydroxyl groups. The resulting nonionic monomers are all similar to one another, with mild differences in side-chain composition again accounting for the different brands that are available. Although side-chain modifications can be expected to produce subtle differences in the properties of various nonionic monomers, no significant differences in tolerability or safety among these agents have been identified (1, 3).

Each nonionic monomeric molecule does not dissociate in solution. Hence, one, rather than two, particles are present for each molecule in solution. Thus, the ratio of iodine atoms to particles is 3:1, rather than 3:2. For this reason, the osmolality is halved for a given iodine concentration (Table 1). In fact, the reduction in osmolality is reduced by even more than a factor of two because of the tendency of some of the contrast molecules to associate with one another in solution. Since nonionic monomers have dramatically reduced osmolality compared to ionic monomers, they are referred to as low-osmolality contrast agents. They produce considerably fewer adverse reactions than do ionic monomers.

Ionic Dimers: Another way to reduce the osmolality of contrast media is to replace one of the side chains in an ionic monomer with a side chain containing a second tri-iodinated benzene ring; the result is an ionic dimer. Only one such contrast agent is currently available: ioxaglate. Each ioxaglate molecule contains a cation, and an anion consisting of two tri-iodinated benzene rings, connected to one another by side chains at the 3-position of one molecule and the 5-position of the other. One of these benzene rings still contains an ionizing carboxyl group at the 1-position; however, the other does not (instead containing a nonionizing organic side chain). Ionic dimers contain 6 iodine atoms for every 2 particles in solution. Therefore, they have approximately half the osmolality (at a similar iodine concentration) as do ionic monomers (3) and they are also classified as low-osmolality contrast agents.

The penalty for reducing contrast medium osmolality in this way is that the contrast molecule is still ionic. If ionicity is responsible for some adverse events after contrast media injection, the number of reactions might not be decreased as much when an ionic dimer is injected, compared to a nonionic monomer. Indeed, some adverse reactions, particularly nausea and vomiting, have been observed more frequently after administration of ioxaglate than after administration of nonionic monomers.

Additionally, larger molecules containing more atoms tend to be more viscous. Increased viscosity makes contrast material harder to inject (particularly through long and/or thin catheters), especially when the vessels are small (2).

Nonionic dimers: More recently, nonionic dimers have been produced, in which the lone carboxyl group of an ionic dimer has been replaced with a nonionizing hydrophilic side chain, while the other side chains have also been made increasingly hydrophilic. One nonionic dimer molecule contains 6 iodine atoms for every 1 particle in solution. As a result, at a given iodine concentration, nonionic dimers have the lowest osmolality of all iodinated contrast agents. At traditional concentrations of 250–300 mg I/mL, nonionic dimers have an osmolality nearly equal to that of human blood (290 mOsm/kg). Nonionic dimers are, therefore, termed iso-osmolality contrast agents (Fig.1) (Table 1).

Again, the unwanted result of creating such a large contrast molecule (with two benzene rings and many long side chains) is increased viscosity, a feature which may be responsible for the observation that delayed adverse reactions (reactions beginning at least 1 h after injection), particularly delayed dermatologic reactions, have been reported more frequently in some series when these agents are injected (3).

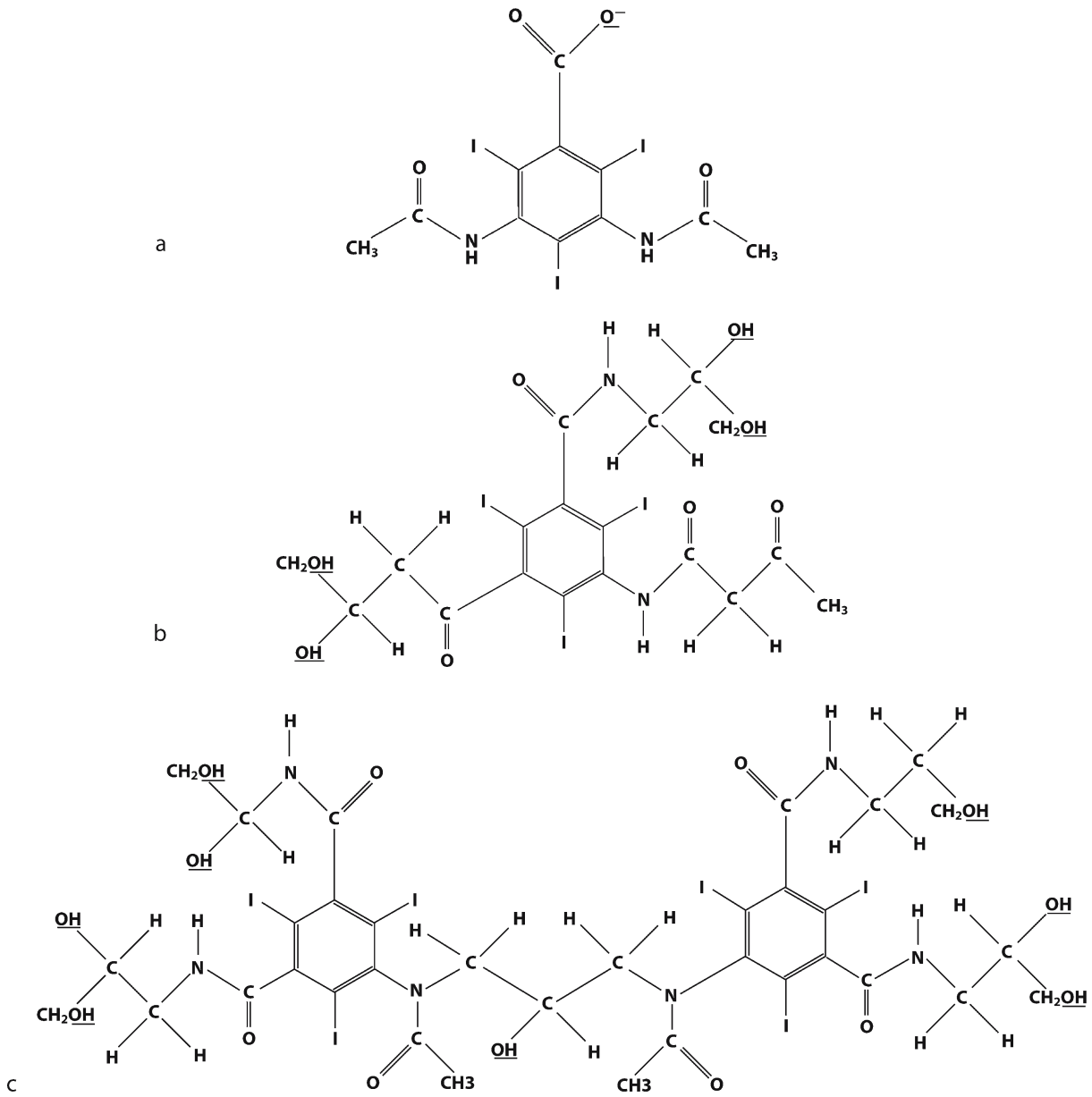

Contrast Media, Iodinated, Water Soluble. Figure 1 **Chemical formulae of several contrast media: (a) Ionic monomer: diatrizoate, (b) Nonionic monomer: iopromide—note that there are many hydroxyl groups (*underlined)* in the side chains, to make this nonionizing molecule water soluble, (c) Nonionic dimer: iodixanol—note again that a large number of hydroxyl groups (*underlined*) have been added to make the molecule water soluble.**

Other Contents in Administered Contrast Material

Free iodide: Although water-soluble iodinated contrast media contain only tiny amounts of free iodide, the amount of administered free iodide still greatly exceeds the recommended daily dose (of 0.15 mg) (4). The maximal amount of free iodide in a bottle of contrast material produced at a concentration of 300 mg I/mL is only 0.05 mg/mL immediately after manufacture (although it rises as shelf-life lengthens) (4). Thus, a 150 mL dose of this agent (as is often administered for CT) would expose a patient to up to 7.5 mg of free iodide. Some additional iodide may also accumulate due to deiodination of contrast material molecules *in vivo* (4).

Additives and Contaminants: Chemical additives are present in all bottles of contrast media. The pH of contrast agents is often adjusted by adding hydrochloric acid or sodium hydroxide. Other additives include tromethamine

(a buffer) and edetate calcium disodium (a "stabilizer"). In addition, calcium chloride dihydrate and sodium chloride are added to iodixanol to provide a sodium/calcium ratio equal to that of blood.

Contaminants may leach into contrast material stored in either vials or prefilled syringes, from chemicals originally located within rubber stoppers or silicone coating (the latter used in prefilled syringes).

Pharmacodynamics

At similar iodine concentrations, all iodinated contrast media produce the same degree of arterial opacification on imaging studies. Venous opacification is slightly diminished, although not to a clinically significant extent, when higher osmolality agents are used, due to a dilutional effect, because high-osmolality agents draw more water into the vascular system.

Postinjection: Following injection of intravenous contrast material, there is gradual equilibrium between extracellular/interstitial and intravascular spaces (3, 5). Contrast molecules are very small, exhibit no significant protein binding, and easily pass outside of the vascular spaces, although they do not enter cells to any significant extent (1).

Vascular enhancement increases with the concentration of injected contrast material and the rate and duration of administration (6). Physiologic parameters that affect the degree of vascular enhancement are cardiac output (directly related) and central blood volume (inversely related). The dynamics of parenchymal organ enhancement are different. The liver, in particular, enhances in a different fashion due to its dual blood supply. Liver enhancement is delayed and its intensity related primarily to the total dose of contrast material injected (6).

Excretion: More than 90% of iodinated contrast media is cleared by renal glomerular filtration and excreted by the kidneys (2, 3, 5). The remainder is eliminated by the liver, bowel, and salivary glands. The normal half-life of contrast material varies between 30 min and 1–2 h in healthy patients (with excretion prolonged in the elderly) (3).

Physiologic Effects of Contrast Media

Aside from their effects on X-ray opacification, iodinated contrast media have a number of normal physiological side effects when injected into patients. Many of these are likely due to hyperosmolality. Thus, many effects are most pronounced when high-osmolality contrast media are used, less so when low-osmolality agents are injected, and absent when iso-osmolality agents are employed.

Cardiac effects: Coronary artery injection with ionic monomers transiently decreases left ventricular contractility (3). In comparison, nonionic monomers produce increased left ventricular contractility and left ventricular systolic shortening (3). Intravenous contrast material injections can lower the threshold for cardiac dysrhythmias, including ventricular fibrillation (3).

Renal effects: Iodinated contrast media produce a brief transient increase (about 1 min long) followed by a longer decrease in renal blood flow (3). The latter is associated with decreased glomerular filtration (3). Potential nephrotoxic effects of high- and low-osmolality agents due to these and/or other factors are usually of little consequence in patients without preexisting renal disease. While small clinical studies found that nonionic dimers produce less nephrotoxicity in patients with underlying renal disease, an *in vitro* study recently demonstrated that they are equally toxic to renal tubule cells at comparable iodine concentrations (7).

Pulmonary effects: Iodinated contrast media produces at least subclinical bronchospasm in all patients (3). Pulmonary vascular resistance may also increase, particularly after injection of high-osmolality agents (3).

Neurologic effects: The most commonly encountered neurologic effects are nausea and vomiting (more often seen with ionic monomers and ionic dimers). In some patients, particularly those in whom the blood brain barrier is disrupted, seizures may be induced (3, 5).

Peripheral vascular effects: Any contrast material with osmolality exceeding that of blood increases circulating blood volume, as it draws in water from the extravascular tissue (3). Vasodilatation also occurs after contrast media injection, resulting in decreased peripheral vascular resistance. These changes may be sensed by the patient as warmth or flushing (5). Blood pressure may transiently decrease, with compensatory increases in cardiac output.

Effects on the thyroid gland: Administered free iodide accumulates in the thyroid gland and can interfere with uptake of any other administered iodide. For this reason, it is often recommended that radioisotope imaging of the thyroid or radioactive iodine treatment for thyroid cancer not be performed within two months of iodinated contrast material injection (4). Clinically apparent adverse affects of contrast media on thyroid function are rare in euthyroid patients, although they are occasionally encountered, most often in the elderly (likely because some older patients have incidental undiagnosed thyroid disease) (4). Exacerbation of hyperthyroidism may be encountered in patients with preexisting thyroid dysfunction (Grave's disease, multinodular goiter, or thyroid autonomy) (4).

Thrombogenic effects: All iodinated contrast media have an inhibitory effect on thrombogenesis. These effects are more pronounced with high-osmolality agents (3, 5).

Local effects: Iodinated contrast media rarely produce local arm pain and erythema even when properly injected into an artery or vein. Local irritation of vascular

endothelium may be responsible (due to chemotoxicity and hyperosmolality). In rare instances, venous thrombosis can occur (3).

Bibliography

1. Christianson C (2005) X-ray contrast media-an overview. Toxicology 209:185–187
2. Morris TW, Fischer HW (1986) The pharmacology of intravascular radiocontrast media. Ann Rev Pharmacol Toxicol 26:143–160
3. Stacul F (2001) Current iodinated contrast media. Eur Radiol 11:690–697
4. Van der Molen A, Thomsen HS, and Morcos SK (2004) Effect of iodinated contrast media on thyroid function in adults. Eur Radiol 14:902–907
5. King BF (1999) Intravascular contrast media and premedication. In: Bush WH, Krecke KN, and King BF (eds) Radiology Life Support. Oxford University Press, New York, pp 10–12
6. Fleischmann D (2003) Use of high-concentration contrast media in multiple-detector-row CT: principles and rationale. Eur Radiol 13: M14–M20
7. Heinrich MC, Kuhlmann KL, Grgic A, et al (2005) Cytotoxic effects of ionic high-osmolar, nonionic monomeric, and nonionic isoosmolar dimeric iodinated contrast media on renal tubular cells *in vitro*. Radiology 235:843–849

Contrast Media, MRI, Blood Pool Agents

Jens Bremerich
Department of Radiology, University Hospital Basel, Basel, Switzerland
jens.bremerich@unibas.ch

Synonyms

Intravascular contrast media

Definition

Biodistribution: Blood pool agents (BPA) are defined by their biodistribution. After intravenous administration, such contrast media extravasate less than standard extravascular agents do. Therefore, BPA are also referred to as intravascular contrast media.

Characteristics and Classification: BPA are retained within the intravascular fluid compartment because of their larger molecular weight, their particle size, or their binding to large intravascular molecules impeding their extravasation, such as albumin. BPA may also be classified with respect to their magnetic properties. Gadolinium (Gd)-based BPA have a predominant T1 effect. Ultrasmall particles of iron oxide (USPIO), on the other hand, are very small coated iron particles with a diameter of ~20 nm. USPIO have a strong T1 effect and a considerable T2 effect. BPA are also classified according to their terminal half-life. While low-molecular agents are eliminated even faster than the extravascular agents (rapid-clearance BPA), high-molecular agents may circulate for several days in the vascular space (slow-clearance BPA).

Gadolinium-Based BPA: The prototype of a large molecular weight BPA is albumin loaded with Gd-DTPA, resulting in a large molecule of 92 kDa with strong T1/T2 relaxivities of 13.7/18.4 $mM^{-1}sec^{-1}$ and an intravascular half-life of 90 min. This compound, however, has unfavorable allergenic properties and clearance pathways and thus cannot be used in humans. Medium molecular weight BPA such as gadomelitol (6.4 kDa; r1/r2 = 27.1/56 L mM^{-1} sec^{-1}; Vistarem) and SHL643A (35 kDa; 13 L $mmol^{-1}$ sec^{-1} gadomer-17) are currently under investigation for use in humans. Reduction of molecular weight not only improves the allergenic properties but also allows renal elimination.

Small molecular weight BPA such as Gadovosfeset trisodium (Vasovist®) reside predominantly in the blood pool because they bind reversibly to various proteins such as albumin and other components of blood plasma. Such binding modifies biodistribution and slows down rotation of the molecule, thus enhancing T1 and T2 relaxivity. Gadobenate dimeglumine (Multihance® Gd-BOPTA) shows some weak protein binding with an *in vivo* blood relaxivity approaching twice the aqueous solution. In 2007 Gadovosfeset trisodium (Vasovist®) gadobenate dimeglumine (Multihance® Gd-BOPTA) is the only intravascular media with intravascular properties approved for use in patients.

Iron oxide BPA: Iron-based BPA are coated USPIO with a strong T1 and T2 shortening effect. Such compounds have a prolonged residence in the intravascular space because of their large particle size of approximately 20 nm and reduced reticuloendothelial system (RES) uptake compared with the larger superparamagnetic particles (SPIO) used for liver imaging (ferumoxides in Endorem®/Feridex® or ferucarbotran in Resovist®). Examples for USPIO are NC100150 injection (Clariscan®), ferumoxtran-10 (Combidex®, Sinerem®), ferumoxytol (Advanced Magnetics), SHU-555C (Supravist®), and very small superparamagnetic iron oxide particles (VSOP). SPIO with a predominant T2 shortening effect have also been referred to as BPA, but they have very short vascular half-lives of less than 10 min due to endocytosis in the liver, spleen, and other RES tissues.

On T1-weighted pulse sequences, USPIO-enhanced angiography vessels appear bright. Sequences with short echo times are required to minimize sensitivity to susceptibility effects.

Indication

General Aspects

Motivation for development of BPA includes the following:

1. BPA with high molecular weight or binding to large molecules provides strong T1 relaxivity because large molecules have a low tumbling rate, resulting in more efficient interaction with water protons.
2. The prolonged intravascular phase of BPA allows for longer acquisition times, which may be useful for angiography with high resolution or in various positions (Fig. 1), double (cardiac and respiratory)-gated coronary angiography, and perfusion imaging at rest and during pharmacologic stimulation.
3. BPA may allow for perfusion quantification because of their well-defined distribution in organ tissue.
4. BPA are used to probe microvascular integrity after myocardial ischemia and infarction; to assess permeability of vessels in tumors, allowing for an estimation of their dignity; and to detect occult bleeding in the gastrointestinal tract.

Angiography

BPA with prolonged vascular enhancement are of particular interest for coronary artery imaging. Debiao et al (1) used SH L 643 A-enhanced magnetic resonance (MR) for free-breathing coronary angiography. The acquisition time of this sequence with prospective cardiac and retrospective respiratory gating was 6–8 min, thus requiring strong and prolonged vascular enhancement. Outside the heart, however, angiography during the equilibrium phase of such BPA is limited by confounding enhancement of both arteries and veins. Wyttenbach et al (2) compared peripheral angiography during the first pass of standard extracellular contrast material versus GdBOPTA. These authors found a comparable diagnostic performance of both compounds in the aortoiliac region. In the distal run-off vessels, however, GdBOPTA yielded higher specificity and a significantly smaller number of nonassessable segments than extracellular contrast media did (2).

Perfusion

BPA enhance normal myocardium to a lesser degree than extracellular agents because the fractional distribution volume of BPA (~5%) is substantially smaller than that of extracellular compounds (~20%). Thus, BPA enhance normal myocardium to a lesser extent than extracellular agents. This might indicate reduced utility of BPA for evaluating myocardial perfusion. An advantage of BPA might be the longer temporal window, which might be used for perfusion imaging during the equilibrium phase. Another advantage might be the improved quantification of perfusion as the first-pass curves return almost to baseline, whereas extravascular agents present an overlap of perfusion and extravasation. Thus, intravascular contrast agents should allow improved qualitative perfusion studies outside the brain. Another potential advantage may be the prolonged acquisition window for imaging at various physiologic conditions. However, the sensitivity of BPA for infarction and the potential for the assessment of myocardial viability is unknown. Bjerner et al (3) assessed myocardial perfusion with first-pass USPIO-enhanced T2-weighted imaging and found a significant signal loss in normally perfused myocardium. Reimer et al (4) used T1-weighted USPIO-enhanced MR for qualitative perfusion imaging. These authors found susceptibility-induced signal loss in the right ventricle,

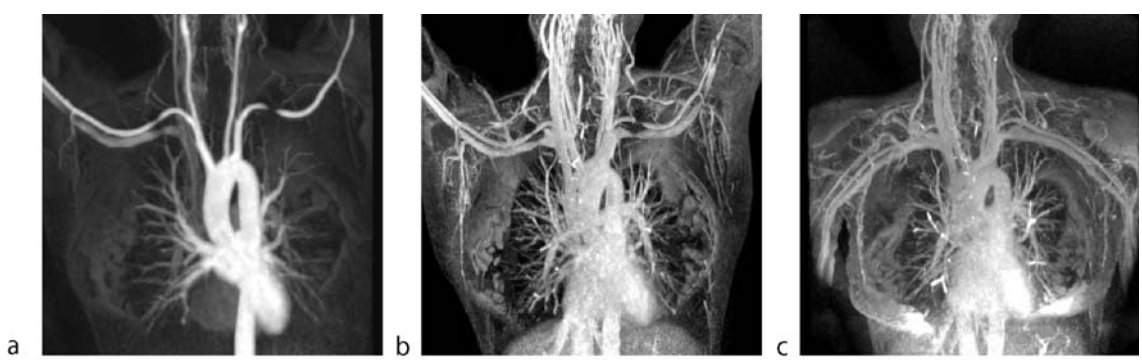

Contrast Media, MRI, Blood Pool Agents. Figure 1 A 42-year-old female with thoracic outlet syndrome. 3D MR Angiograms enhanced with single injection of (Gadovosfeset trisodium, Vasovist©, 0.03 mmol/kg @ 0.8 mL/sec) are shown. Angiograms were acquired with (a) arms-up in arterial phase, (b) arms-up in equilibrium phase, and (c) arms-down in equilibrium phase. With arms-up significant stenoses are present in left subclavian artery (*arrow*) and vein (*arrowhead*), with arm-down stenoses resolve. (Courtesy of Dr. Heyder, Grabs, Switzerland)

which can be explained by a high USPIO concentration, an important limitation of USPIO-based perfusion imaging. Susceptibility effects are most pronounced at high regional concentrations and heterogeneous distribution of USPIO, making quantification difficult.

Tumor Imaging

For grading of breast tumors, Gd-based slow- and rapid-clearance BPA have been used to probe transendothelial permeability of blood vessels, microvascular density, and fractional blood volume using dynamic MR data-fitted to a bidirectional two-compartment model. Transepithelial permeability and microvascular density correlate with tumor grade when using slow-clearance albumin-$(GdDTPA)_{30}$ but not when using rapid-clearance BPA. In a human breast tumor model in mice, a delayed accumulation of gadomelitol after 30 min and 3 h suggests a potential to improve characterization of benign and malignant tumors. On the other hand, USPIO-derived microvascular permeability has been shown to correlate strongly with histopathologic tumor grade in an animal model of breast cancer (5). Thus, BPA may allow tumor grading in the future.

Gastrointestinal Hemorrhage

Attempts to detect and localize intestinal or peritoneal bleedings with BPA have been performed as well, but they lack specificity and do not fulfill all clinical requirements.

Plaque Imaging

After prolonged vascular circulation of USPIO, these are partially taken up by intravascular monocytes or endothelial macrophages, thereby potentially extending pure angiographic imaging to vessel wall imaging and plaque characterization.

Contraindication

The vendors of gadovosfeset trisodium (Vasovist®) and gadobenate dimeglumine (Multihance Gd-BOPTA) mention allergy against Gd chelates as a contraindication. Disturbances of iron metabolism, however, can be expected to be relative contraindications for iron oxide particles.

Pregnancy/Lactation

Gadovosfeset trisodium (Vasovist®) and gadobenate dimeglumine (Multihance Gd-BOPTA) are not recommended in pregnant or lactating women. During lactation, the vendor recommends interrupting lactation for 24 h after contrast administration. In animal experiments, less than 0.5% of the administered dose was transferred to the newborn. This information can be found on the drug information sheet and seems to imply that GdBOPTA may also be administered during lactation. But, the physician is responsible for such administration.

Use and Dosage

Gadobenate dimeglumine (Multihance Gd-BOPTA) can be administered as infusion or bolus injection. The vendor recommends a dose of 0.05 mmol/kg for liver imaging and 0.1 mmol/kg for the central nervous system. Gadovosfeset trisodium (Vasovist®) is approved and has been introduced clinically. Bolus administration or infusion is allowed at a dose of 0.03 mmol/kg. Iron oxide particles such as SHU-555C (Supravist) may be infused or injected as a bolus; a dose of 40 mol Fe/kg seems to be appropriate for first-pass MR angiography and cardiac perfusion.

Adverse Reactions

As with all contrast media, there is a risk of potentially live-threatening adverse reactions. First experiences in controlled studies, however, indicate that the safety profile of such BPA is similar to that for standard extracellular contrast media. In phase III studies with gadovosfeset trisodium (Vasovist®), the incidence of serious or severe adverse events was low.

Interactions

The vendor of gadobenate dimeglumine (Multihance Gd-BOPTA) indicates that no interactions are known for this specific agent. There is a potential risk of drugs competing with gadovosfeset trisodium (Vasovist®) at albumin-binding sites. Caution is required with measurements of iron metabolism with iron oxide particles. Such measurements should not be performed within 15 days after USPIO administration. Moreover, USPIO administration is not recommended in hemosiderosis, when body iron content is already elevated. USPIO has also been reported to interfere with factor XI activity, resulting in changes in thromboplastin time.

Bibliography

1. Debiao L, Zheng J, Weinmann HJ (2001) Contrast-enhanced MR imaging of coronary arteries: comparison of intra- and extravascular contrast agents in swine. Radiology 219:670–678

2. Wyttenbach R, Gianella S, Alerci M et al (2003) Prospective blinded evaluation of Gd-DOTA versus Gd-BOPTA enhanced peripheral MR angiography, as compared with digital subtraction angiography. Radiology 227:261–269
3. Bjerner T, Johansson L, Ercsson A et al (2001) First-pass myocardial perfusion MR imaging with outer-volume suppression and the intravascular contrast agent NC100150 injection: preliminary results in eight patients. Radiology 221:822–826
4. Reimer P, Bremer C, Allkemper T et al (2004) Myocardial perfusion and MR angiography of chest with SH U 555 C: results of placebo-controlled clinical phase I study. Radiology 231:474–481
5. Turetschek K, Huber S, Floyd E et al (2001) MR imaging characterisation of microvessels in experimental breast tumors by using a particulate contrast agent with histopathologic correlation. Radiology 218:562–569

Contrast Media, MRI, Gadolinium Derivates

Bernd Tombach[1], Rolf Vosshenrich[2]
[1]Department of Clinical Radiology, University of Münster (Germany), Institut für Klinische Radiologie, Universitätsklinikum Münster, Münster, Germany
[2]Radiologen-Gemeinschaftspraxis, MRT im Friederikenstift Hannover, Germany, Radiologen-Gemeinschaftspraxis MRT im Friederikenstift, Hannover, Germany
tombach@uni-muenster.de
vosshenrich@t-online.de

Synonyms

Chemical formulas, trade names, and manufacturers of commercially available open chain and cyclic gadolinium (Gd) complexes as magnetic resonance (MR) contrast agents: Gadopentetate dimeglumine (Gd-DTPA, Magnevist, Schering AG, Germany); Gadodiamide (Gd-DTPA-BMA, Omniscan, GE Amersham Health, UK); Gadobenate (Gd-BOPTA, MultiHance, Altana Pharma, Germany); Gadoteridol (Gd-HP-DO3A, Pro Hance, Altana Pharma, Germany); Gadoterate meglumine (Gd-DOTA, Dotarem, Guerbet, France); Gadobutrol (Gd-DO3A-butrol, Gadovist, Schering AG, Germany)

Definition

Water-soluble paramagnetic compounds for magnetic resonance imaging (MRI) signal enhancement detoxified by chelation resulted in a first patent in 1981 covering the composition of paramagnetic complexes (1). The preclinical investigations of Gries, Rosenberg, and Weinmann from Schering AG (Berlin, Germany) included the preparation of the highly soluble T1-MR contrast agent gadopentetate dimeglumine (Gd-DTPA) providing good relaxation properties and an excellent safety profile in animals. In 1983, the clinical development started with the first intravenous injection in humans (phase I clinical trial) resulting in an approval from the health authorities as the first extracellular MR contrast agent (Magnevist) in 1988 (2).

Generally, the image contrast in MRI reflects a complex interaction of intrinsic tissue properties (T1 and T2 relaxation time, proton density, and flow velocity) and extrinsic factors (field strength, gradients, and pulse sequences). Due to the overlap in relaxation times of normal and abnormal tissues, para- or superparamagnetic MR contrast agents specifically altering tissue relaxation times might be beneficial. The paramagnetic gadolinium derivates containing the "magnetic active" ion of Gd^{3+} with seven unpaired electrons shorten both T1 and T2 relaxation times, but predominantly, the longitudinal relaxation of protons (T1) at diagnostically approved doses resulting in a bright signal on T1-weighted images (3, 4). The power of MR contrast agents depend on their concentration in the respective tissue and the resulting intrinsic relaxation times and is called relaxivity R1 and R2 (defined as 1/T1 and 1/T2). For paramagnetic Gd chelates a typical R2/R1 ratio of 1.3 is found, resulting in a decrease of the relaxation time of biological fluids by 50% at a dose of 0.1 mmol/kg body weight.

To reduce the high toxicity for clinical applications, the magnetically active gadolinium ions have to be bound either to open chain (linear) or to cyclic chelators, resulting in highly hydrophilic and stable Gd-chelate complexes with a low molecular weight (MW) of <1 kDa (Fig. 1). Presently, six different compounds with slight differences in their physicochemical properties are approved for clinical use in different countries (Table 1). The similarities of these agents include a strong chelation of the gadolinium ion, comparable effects on tissue signal intensities, and an excellent safety profile in humans. The main differences of these gadolinium chelates are the electrical charge of the chelates, the chemical structure of the ligands, the prepared concentration, and the potential of temporary plasma protein binding (5).

Ionic gadopentetate dimeglumine, nonionic gadodiamide, and ionic gadobenate are open chain Gd complexes. Gadobenate, originally designated as a liver-specific agent with a hepatobiliary excretion rate of approx. 50% in rabbits, is even classified predominantly as an extracellular agent due to the rather low hepatobiliary excretion rate of 2%–4% in humans. This compound offers a temporary serum protein binding resulting in an increased R1 with potential advantages for contrast-enhanced MR angiography (CE-MRA). Nonionic gadoteridol, ionic gadoterate meglumine, and nonionic gadobutrol are macrocyclic

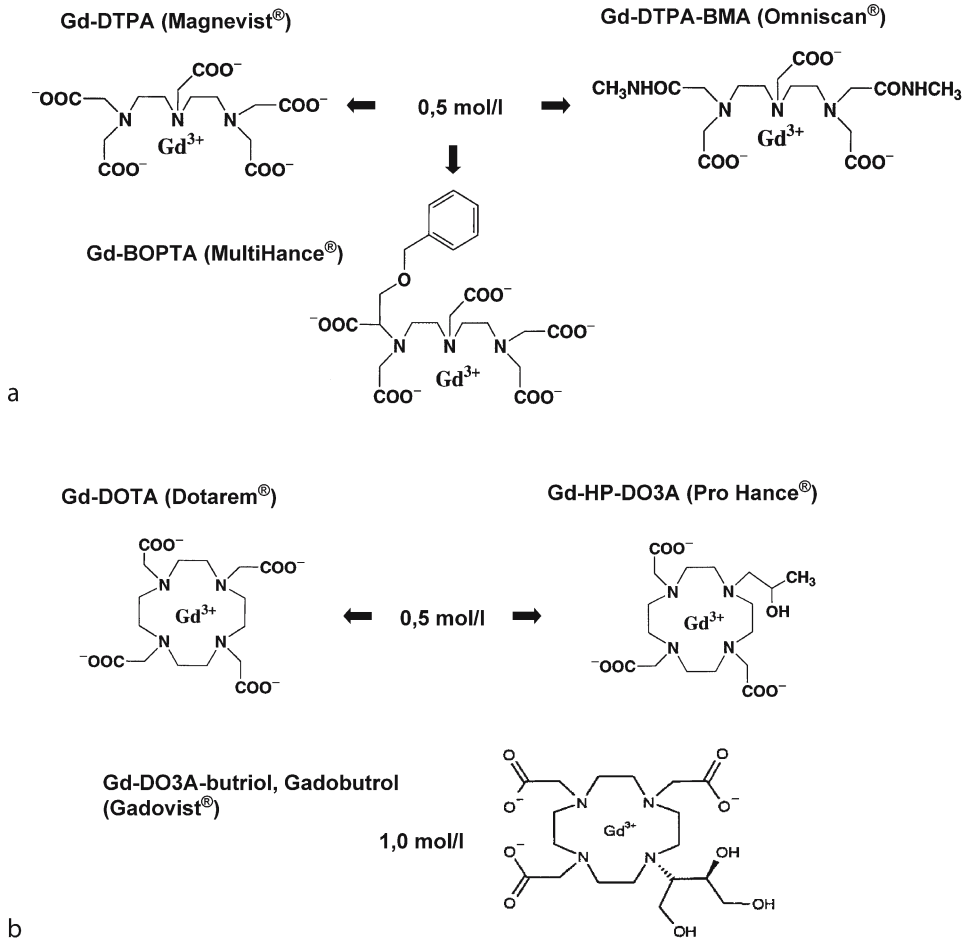

Contrast Media, MRI, Gadolinium Derivates. Figure 1 Chemical structures of gadolinium chelates . Chemical structure of the (a) linear extracellular Gd chelates gadopentetate dimeglumine (Gd-DTPA, Magnevist, Schering AG, Germany) and gadodiamide (Gd-DTPA-BMA, Omniscan, GE-Amersham Health, England), and (b) cyclic extracellular gadoteridol (Gd-HP-DO3A, Pro Hance, Bracco), gadoterate meglumine (Gd-DOTA, Dotarem, Guerbet, France), and gadobutrol (Gadovist, Schering AG, Germany).

complexes with slightly higher complex stabilities of up to 10^{-23} compared with linear chelators with complex stabilities of up to 10^{-18}. Compared to all other commercially available extracellular Gd chelates (0.5 M), gadobutrol is prepared at a 1-M concentration. At the same injection dose, gadobutrol can therefore be applied with half the injection volume and time, which can be advantageous for first-pass imaging like CE-MRA and perfusion studies.

While gadolinium is responsible for the paramagnetic effect of these complexes, the ligand determines the pharmacokinetic behavior. In healthy volunteers, the pharmacokinetic profile of extracellular MR contrast agents is similar to iodinated x-ray contrast agents, indicating a rapid distribution in the extracellular fluid space and a short intravascular phase due to the high hydrophilicity and the low MW. Glomerular filtration is the predominant elimination pathway with a plasma half-life of about 90 min for the unmetabolized Gd chelates. Even in patients with impaired renal function, extracellular Gd chelates can safely be applied without changes of the safety profile. However, the elimination half-life may be prolonged up to more than 20 h in patients with severe renal impairment. In patients requiring hemodialysis treatment, no change in dialysis schedule is required, because low-MW Gd chelates are effectively removable within three dialysis sessions (97–98%) (6, 7).

Indication

The diagnostic power of MRI has been significantly improved since the first intravenously injectable MR

Contrast Media, MRI, Gadolinium Derivates. Table 1 Physicochemical properties of extracellular contrast agents

	Gadobutrol [1 mol/L]	Gadoteridol [0,5 mol/L]	Gadoterate meglumine [0.5 mol/L]	Gadopentetate dimeglumine [0.5 mol/L]	Gadodiamide [0.5 mol/L]	Gadobenate dimeglumine [0.5 mol/L]
Thermodynamic complex stability (log K_{eq})	21.8	23.8	25.8	22.1	16.9	22.6
Osmolality [osmol/kg]	1.60	0.63	1.35	1.96	0.65	1.97
Viscosity [mPa s]	4.96	1.30	2.0	2.9	1.4	5.3
T1 relaxivity [l/mmol s] 0.47 T, plasma	5.6	4.6	4.3	4.9	4.8	9.7

contrast agent came on the market. Worldwide, more than 25% of all MR examinations are performed with contrast agents (8). Typical indications are the detection of tumors and inflammatory processes, whereas degenerative diseases are mostly investigated without contrast agents. Intracranially, contrast-enhanced MRI allows the early detection of a damaged blood–brain barrier. Since high-performance MR scanners are more and more available, newer applications like CE-MRA and organ perfusion studies with extracellular Gd chelates are part of daily clinical routine MR investigations.

Pregnancy/lactation

Since there are only a few safety data available in the literature, the Contrast Media Safety Committee of the ESUR (European Society of Urogenital Radiology) has reviewed the literature and drawn up the following guidelines (9):

Pregnancy: Following the injection of gadolinium agents to the mother, no neonatal tests are necessary.

Lactation: Breast-feeding may be continued normally when gadolinium agents are given to the mother.

Pregnant or lactating women with renal impairment: No additional precautions are necessary for the fetus or neonate. Follow ESUR guidelines for contrast media administration when renal function is impaired.

Use and dosage

The recommended application doses depend on the clinical question and type of MR investigation on the one hand, and the approval status regarding the patient's age and the approved MR indications on the other hand, which are currently extended. However, the approved doses for extracellular contrast agents are in the range of 0.1–0.3 mmol/kg body weight with an accepted standard dose of 0.1 mmol/kg body weight. Compared with low osmolar nonionic x-ray contrast agents, the total osmotic load is much lower and without any effect on safety or tolerability for the extracellular contrast agents used in the approved dose range in MRI.

Adverse Reactions

Controlled clinical trials regarding safety aspects and pre- or postmarketing surveillance studies document an overall incidence of adverse reactions of 1–2% (e.g., nausea, vomiting, local warmth and pain, headache, dizziness), which may be increased by a factor of 2–3 in patients with a history of allergic reactions. However, the incidence of anaphylactic reactions is about six times lower compared to nonionic x-ray contrast agents. Overall, extracellular contrast agents provide by far the safest profile compared to all other contrast agents without any relation to the injected dose up to 0.3 mmol/kg body weight.

Interactions

Gadodiamide and gadoversetamide may cause spurious hypocalcemia, particularly at doses over 0.2 mmol/kg body weight in patients suffering from renal impairment. These contrast agents interfere with calcium measurements using the ortho-cresolphthalein complexone (OOC) method. No false measurements of serum calcium have occurred with gadopentetate dimeglumine or gadoteridol (10). Awareness of this effect is important in order to avoid incorrect and potentially hazardous treatment.

In a study comparing a standard dose gadoteridol and gadodiamide and searching for Gd in human bone tissue by inductively coupled plasma mass spectroscopy gadodiamide left approximately 4 times more Gd behind in bone than did gadotridol (11).Recently, it has been reported that a serious adverse reaction called nephrogenic systemic fibrosis (NSF) may occur after exposure of Gd. Development of NSF was strongly associated with gadodiamide administration in the setting of either acute

hepatorenal syndrome or dialysis-dependent chronic renal insufficiency (12,13). These gadolinium chelates should not be administered in patients with reduced renal function and in general renal function may be considered more closely. Only those gadolinium chelates shall be administered which have been tested and licensed for use in patients with decreased renal function.

References

1. Gries H, Rosenberg D, Weinmann H-J (Schering AG Berlin) (1981). *Paramagnetische Komplexsalze, deren Herstellung und Mittel zur Verwendung bei der NMR Diagnostik.* Patent DE 3129906 (Publication Date of Offenlegungsschrift, February 10, 1983), publication date May 17, 1990; priority date July 24
2. Laniado M, Weinmann HJ, Schorner W et al (1984) Physiol Chem Phys Med NMR 16:157
3. Knopp MV, von Tengg-Kobligk H, Floemer F et al (1999) J Magn Reson Imaging 10:314
4. Bellin MF, Vasile M, Morel-Precetti S (2003) Eur Radiol 13:2688
5. Robert R. Edelman, John R. Hesselink, Michael B. Zlatkin (1996) Clinical Magnetic Resonance Imaging. 2nd edn. W.B. Saunders Company
6. Tombach B, Bremer C, Reimer P et al (2001) Radiology 218:651
7. Tombach B, Bremer C, Reimer P et al (2002) AJR Am J Roentgenol 178:105
8. de Haen C (2001) Top Magn Reson Imag 12, 221
9. Webb JA, Thomson HS, Morcos SK (2005) Eur Radiol 15:1234
10. Morcos SK, Thomson HS, Exley CM (2005) Eur Radiol 15:1463
11. White GW, Gibby WA, Tweedle MF (2006) Invest Radiol 41:272
12. Thomsen HS (2006) Eur Radiol 16:2619
13. Broome DR, Girguis RS, Paron PW et al. (2007) Amer J Roentgenol 188:586

Contrast Media, MRI, Oral Agents

Thomas C. Lauenstein
Department of Radiology, The Emory Clinic
Atlanta, USA
tlauens@emory.edu

Definition

Due to the excellent soft-tissue contrast coupled with the lack of ionizing radiation, magnetic resonance imaging (MRI) of the bowel has emerged as the primary radiological examination tool in many departments. Similar to experiences from computed tomography (CT), the presence of intraluminal contrast facilitates the evaluation of bowel segments.

Contrast agents should fulfill different requirements for oral applications in the clinical routine (1). A homogeneous bowel distension as well as uniform opacification of the lumen should be provided. As for image quality, high contrast between the bowel wall and lumen is necessary, and the presence of intraluminal contrast must not lead to artifact formation. Furthermore, the agents should not be absorbed, or reabsorption must at least be kept to a minimum. Eventually, different aspects should be considered, including high safety (concerning side effects or allergic reactions), sufficient patient acceptance (regarding taste and volume of the agents), and cost-effectiveness.

Similar to all other tissues displayed on MR images, the signal intensity of oral contrast agents mainly depends on the ▶*longitudinal relaxation time* (T1), the ▶*transverse relaxation time* (T2), and the ▶*proton spin density*. Signal intensity can be enhanced as T1 increases, T2 decreases, and/or proton spin density increases. Hence, contrast compounds may modify signal characteristics according to three mechanisms:

1. Agents affecting T1 relaxation times (e.g., paramagnetic chelates).
2. Agents changing T2 relaxation times by disturbing the local magnetic field (e.g., superparamagnetic particles).
3. Agents replacing protons and hydrogen molecules.

Consecutively, substances may be categorized as *positive*, *negative*, or ▶*biphasic agents* (2). A *positive oral contrast compound* produces high signal intensities on both T1-weighted and T2-weighted images, whereas ▶*negative contrast agents* lead to low signal on both T1-weighted and T2-weighted sequences. The term *biphasic* relates to agents with different signal characteristics on different sequence types, such as low signal on T1-weighted images and high signal on T2-weighted images, or vice versa. However, this classification may be confusing because most agents simultaneously influence T1 and T2 relaxation times as well as proton density. Thus, the actual signal intensity may eventually depend on the agents' concentration and the weighting of the image sequence employed (3).

The following substances are clinically used as oral MRI contrast agents:

1. Gadolinium
   Gadolinium-containing agents reduce the T1 relaxation times of all surrounding water molecules. In clinically used concentrations (1 mmol/L), signal intensity of the bowel lumen is rendered bright both on T1- and T2-weighted images due to an only moderate T2-shortening effect. Thus, gadolinium chelates can be considered ▶positive contrast agents. However, in higher concentrations an early T2-shortening effect will be predominant, leading to a signal loss on T2-weighted images. One commercially available oral gadolinium compound is gadopenatetate dimeglumine (Magnevist Enteral,

Schering, Berlin). This agent contains gadolinium at a dosage of 1 mmol/L plus mannitol (15 g/L). Mannitol increases the osmolarity of the formula and thus reduces reabsorption in the gastrointestinal tract.

2. Barium

Barium compounds provide low signal intensities on T1-weighted images. However, signal characteristics on T2-weighted images strongly depend on the concentration of barium. Used in high concentrations (e.g., 1g $BaSO_4$/mL), these formulas lead to low signal of the bowel lumen on T2-weighted images. However, in lower concentrations barium compounds may act like water, providing a higher signal on T2-weighted images. Barium is cheap and commercially available worldwide. A minor drawback might be the relatively long bowel transit times.

3. Superparamagnetic particles

Superparamagnetic iron-based particles may be considered as typical negative contrast agents. They induce local field inhomogeneities, which results in shortening both T1 and T2 relaxation times. However, T2-weighted effects are predominant. Thus, superparamagnetic particles lead to decreasing signal intensity on T2-weighted sequences and on most T1-weighted sequences. This can be considered helpful, especially for labeling bowel fluid and for diminishing the signal of the bowel lumen for MR cholangiopancreatography (MRCP) studies. One commercially available agent (Abdoscan, GE Healthcare) consists of ferrite crystals bound to monodisperse polymer particles. The mean particle diameter is 3.5 m, and the iron contents amount to 20%. This compound is well tolerated when administered orally. Another commercially available formula is Lumirem (Guerbet, Anulay sur Bois, France). It contains iron oxide crystals (Fe_2O_3 and Fe_3O_4) that are coated with silicone, which prevents absorption of the iron. The mean iron content is 175 mg/L, and the average particle diameter is 300 nm (Fig. 1).

4. Manganese-containing agents

Manganese-containing substances are usually biphasic contrast agents. Due to a paramagnetic effect, signal

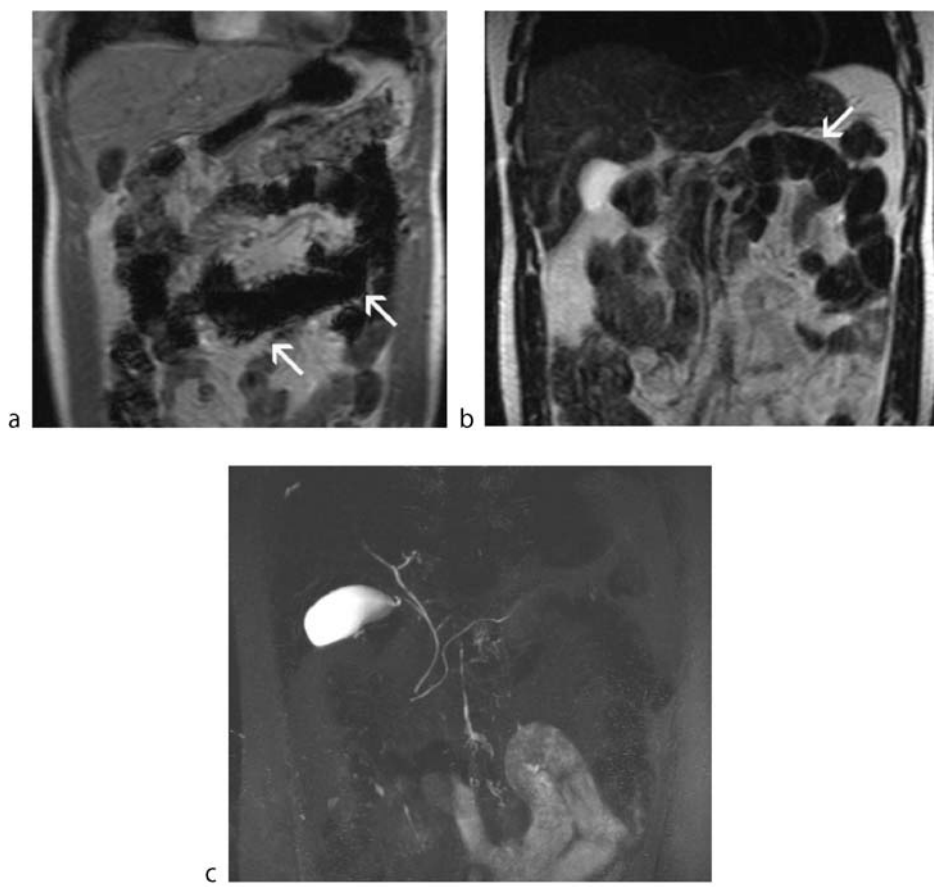

Contrast Media, MRI, Oral Agents. Figure 1 Magnetic resonance (MR) images after the oral ingestion of an agent containing superparamagnetic particles. Signal intensity is rendered dark both on (a) T1-weighted images and (b) T2-weighted images. Therefore, this kind of agent is used to suppress the signal intensity of the duodenum in MR cholangiopancreatography studies (c).

intensity of the bowel lumen is enhanced on T1-weighted images. Furthermore, manganese has a considerable T2-shortening effect, leading to low signal intensity on heavily T2-weighted images. Manganese-containing compounds are commercially available (Lumenhance, Bracco, Milan, Italy). Furthermore, some fruit juices such as pineapple juice and blueberry juice contain a high manganese concentration and therefore may be used as biphasic contrast agents as well (Fig. 2).

5. Water
   Water causes signal increase on T2-weighted images, whereas signal intensities on T1-weighted images are intermediate to low. This biphasic agent is the safest and least expensive oral contrast compound. However, it provides only fair bowel distension, especially in distal bowel segments, because of the fast reabsorption in the small bowel. Thus, it may be used mainly to label the stomach and duodenum and has only a moderate potential to support imaging of the jejunum and ileum.
6. Hydro solutions
   These agents provide signal properties similar to those of water. However, in contrast to pure water, they are not (or only slightly) reabsorbed in the gastrointestinal tract. This is mainly due to additives increasing the agents' osmolarity and/or viscosity. Thus, bowel distension, especially of the jejunum and ileum, is significantly increased. Mannitol, a widely used carbohydrate, mixes well with water, and in concentrations between 1.5 and 2.5%, it has been shown to provide good bowel distension. Sorbitol, another sugar alcohol, has been reported to have similar effects. Another substance is polyethylene glycol 4000 (PEG 4000), a strong hydrophilic molecule, which has no intestinal absorption. PEG 4000 has been shown to provide high luminal distension of small bowel loops.

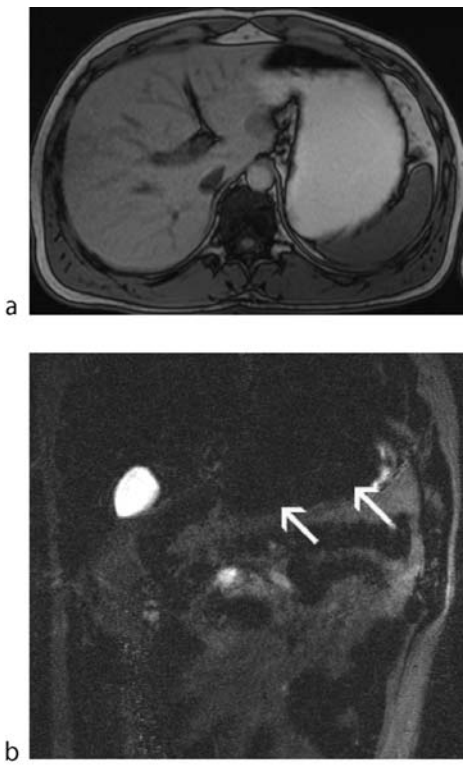

Contrast Media, MRI, Oral Agents. Figure 2
Manganese-containing oral contrast agents are biphasic: while the signal intensity is high on T1-weighted images (a, stomach), signal is reduced on heavily T2-weighted sequences (b, *arrow*).

Indication

Indications to use oral contrast agents for MRI can be divided into three groups.

(1) For the morphological assessment of the stomach or bowel, a high and uniform bowel distension is absolutely mandatory. Collapsed bowel segments may lead to false-positive or false-negative findings; even relatively large lesions may be hidden, or nondistended bowel segments may mimic bowel wall thickening. Therefore, the use of oral MRI contrast agents is obligatory.
(2) Similar to the morphological assessment, functional MRI analysis of the gastrointestinal tract also requires the use of oral contrast. This is especially true for motility studies of the esophagus and stomach. By marking and distending the lumen of these organs, assessment of motility is possible.
(3) Labeling the lumen of stomach and small bowel may be extremely helpful for depicting and analyzing adjacent abdominal organs. This is especially important to image the pancreas, to suppress high bowel signal for MRCP studies, and to facilitate the perceptibility of retroperitoneal and mesenteric lymph nodes.

Contraindication

The consideration of contraindications must be tailored to the specific contrast compounds:

(1) Gadolinium-containing agents must not be used in patients with suspected ileus. Furthermore, their use in dehydrated patients represents a relative contraindication.
(2) Barium-containing agents must not be administered in cases of suspected bowel perforation or before bowel surgery. After endoscopic polypectomy, a

minimal time delay of 7 days should be fulfilled before using barium-containing oral contrast agents.
(3) No contraindications are known for the oral administration of superparamagnetic particles, manganese-containing agents, or hydro solutions.

Pregnancy/Lactation

There are no restrictions on the oral use of barium or water during pregnancy or lactation. As for the administration of all other groups of oral contrast compounds, no definite recommendations are given. However, animal studies have not shown these agents to imply any embryotoxic or teratogenic potential.

Use and Dosage

For labeling of the stomach or the duodenum, relatively low doses of contrast agents (300–600 mL) are sufficient. However, data acquisition should be performed directly after administration of the substances to avoid insufficient marking in patients with fast bowel transit times.

For assessing the small bowel itself, there are technically two different methods for the application of oral contrast agents. To assure high distension of small bowel loops, the MR Sellink technique was developed: A hydro solution (1,000 mL and 2,000 mL) is administered *via* a fluoroscopically placed nasoduodenal or nasojejunal tube at a flow rate of approximately 100 mL/min. Image sets then can be collected following rapid filling of the entire small bowel. This technique provides excellent image quality. However, some patients may perceive the intubation as unpleasant.

The sole oral ingestion of some hydro solutions may also provide high small bowel distension without the need for duodenal intubation. Doses between 1,000 mL (for PEG) and 1,500 mL (for mannitol- or sorbitol-containing agents) should be ingested over 45–60 min before the MR examination.

Adverse Reactions

If applied in recommended doses, there are only mild side effects for all oral MRI contrast compounds. Thus, ingestion of mannitol-containing agents as well as of superparamagnetic particles may lead to flatulence or diarrhea. Regarding the use of barium, cases of constipation have been reported. Barium-containing products have a well-documented safety profile, and allergic reactions or severe side effects are not known.

Interactions

Ingestion of mannitol-containing agents may lead to byproducts such as explosive gases. Therefore, diathermia treatment should not be performed 48 h after the MR examination. Furthermore, bowel surgery in conjunction with electrocautery may not be performed. Interactions with other oral MR contrast compounds are not known.

Bibliography

1. Laghi A, Paolantonio P, Iafrate F et al (2002) Oral contrast agents for magnetic resonance imaging of the bowel. Top Magn Reson Imaging Dec; 13(6):389–396
2. Debatin JF, Patak MA (1999) MRI of the small and large bowel. Eur Radiol 9(8):1523–1534
3. Giovagnoni A, Fabbri A, Maccioni F (2002) Oral contrast agents in MRI of the gastrointestinal tract. Abdom Imaging Jul–Aug; 27 (4):367–375

Contrast Media, MRI, Organ Specific

Peter Reimer
Department of Radiology, Klinikum Karlsruhe, Academic Teaching Hospital of the University of Freiburg, D-76133 Karlsruhe
peter.reimer@klinik.um-karlsruhe.com

A variety of MR contrast agents has been developed to improve the sensitivity and specificity of MR imaging for the diagnosis of disease. Readers will become familiar and understand the indication, contraindication, interactions, and limitations of approved MR contrast agents. Furthermore, candidates, likely to get approval within the near future will be covered.

Contrast agents are administered either orally or intravenously. Oral contrast agents play a minor role and the text will focus on intravenous contrast agents. The mechanism of action is either to increase predominantly (Mn, Gd, or Fe) or to decrease (Fe) signal intensity. Upon intravenous administration, contrast agents leave the intravascular space (unspecific) into the interstitium, are taken up into cells (cell specific), or stay in the intravascular space (blood pool) for some time.

The use of low molecular extracellular nonspecific gadolinium chelates in MRI is well established and quite a number of different contrast agents are clinically approved. These nonspecific contrast agents enhance both normal and diseased tissues. Therefore, contrast agents with tissue specificity to improving the detection and

characterization of disease were developed. Contrast agents may either be directed to normal tissue or to diseased tissue. It turned out that directing contrast agents to normal tissue or to normal structures is much easier than specifically directing contrast agents to diseased tissue such as inflammation, degeneration, tumor, or gene expression. At present, attempts to achieve receptor, optical, or gene specificity propelled the development of a new field called molecular imaging and optical imaging, which is described elsewhere.

The principle of tissue specificity means direction of a contrast agent toward a certain tissue-like liver tissue, splenic tissue, pancreatic tissue, lymph nodes, bone marrow, blood, or inflammation. Contrast agents with this specificity are either superparamagnetic iron oxides (SPIOs) or paramagnetic agents with gadolinium or manganese as magnetic components. As for imaging reticulo-endothelial system (RES) containing organs such as the liver, spleen, lymph nodes, or bone marrow iron oxides of different sizes are used. The larger the iron oxides the higher and faster the uptake in liver and spleen and the lower and slower the uptake in lymph nodes and bone marrow. In addition, ultrasmall iron oxides may also be utilized for vascular imaging based upon their prolonged circulating time and T1-effects as compared to larger iron oxides. Furthermore, by binding specific markers to the magnetic components, further tissue specificity may be achieved. This also applies to paramagnetic-based contrast agents, which are directed to different tissues by means of a modification of the chemical structure resulting in specific attachment to specific tissue.

The most thoroughly investigated and approved tissue specific contrast agents relate to hepatic MRI. A variety of liver contrast agents has been developed for contrast-enhanced MRI of the liver, which is designed to overcome the limitations of unspecific tissue uptake by extracellular low molecular gadolinium chelates. The two main classes of liver-specific contrast agents are SPIO with uptake *via* the RES mainly into the liver and spleen and hepatobiliary contrast agents with uptake into hepatocytes followed by variable biliary excretion. Two hepatobiliary contrast agents, mangafodipir trisodium (Teslascan, 6E, USA) and gadobenate dimeglumine (MultiHance, Bracco Imaging S.p.A., Milan, Italy), are already clinically approved in many Countires. A third hepatobiliary contrast agent, gadoxeficacid, Gd-EOB-DTPA (Primovist, Schering AG, Berlin, Germany), has already been approved in Europe and several other countires. These agents exhibit different features for the detection and characterization of liver tumors. Enhancement during the distribution phase of contrast agents mainly depends on tumor vascularity (hypovascular vs. hypervascular) and its blood supply, while enhancement on delayed images is characterized by the cellular specificity of MR contrast agents (extracellular vs. intracellular—hepatocyte phase or accumulation phase). Therefore, enhancement characteristics of hepatobiliary contrast agents are applicable to the diagnosis of primary hepatocellular liver tumors.

With the advent of rapid three-dimensional imaging sequences combined with existing extracellular gadolinium-based contrast agents, MRA has shown promising signs of becoming a time-efficient and cost-effective tool for the complete assessment of many vascular regions or clinical referrals like peripheral vascular. The use of intravenous low and high molecular gadolinium chelates for contrast-enhanced MRA is limited by the rapid equilibration of these agents between the intravascular and extravascular–extracellular compartments. Alternative paramagnetic and superparamagnetic agents for enhancing MR angiographic images, known as blood-pool agents, are currently being studied. Several blood-pool contrast agents have been designed and some are under clinical investigation. MR contrast agents confined to the intravascular space, so-called blood-pool agents, could change the way vessels are currently imaged by means of MRA. Furthermore, if these agents also exhibited a prolonged plasma half-life, new avenues could be opened to additional applications within the field of MRA but also beyond MRA. Blood-pool agents are particularly promising in contrasting smaller vessel, vessels with slow flow, and vessels with complex flow. In addition, blood-pool agents may be used for perfusion imaging, functional imaging, or imaging of angiogenesis. Two classes of blood-pool agents are under development: paramagnetic gadolinium-based molecules of different size and some ultrasmall iron oxides. Whereas the design of iron oxides suited for blood-pool imaging is well understood and developed, a variety of gadolinium-based agents with different pharmacological profiles is under development.

In the relevant entries we review those concepts of contrast agents which are clinically approved or are in advanced clinical trials. Each of these agents has unique properties that offer advantages for contrast-enhanced MR imaging. Use of these agents, however, requires an understanding of their current and potential clinical indications and inherent limitations. Our purpose is to provide information on the properties, the clinical development, and clinical applications of MR contrast agents which have been approved or are likely to get approval within the near future. Furthermore, since approval is rarely a general approval for whole body MRI and MRA, the approved applications will be explained.

Bibliography

1. Allkemper T et al (2002) Contrast-enhanced blood-pool MR angiography with optimized iron oxides: effect of size and dose on vascular contrast enhancement in rabbits. Radiology 223(2):432–438

2. Balzer JO et al (2003) Safety of contrast-enhanced MR angiography employing gadobutrol 1.0 M as contrast material. Eur Radiol 13 (9):2067–2074
3. Bellin MF, Vasile M, Morel-Precetti S (2003) Currently used non-specific extracellular MR contrast media. Eur Radiol 13 (12):2688–2698
4. Brasch RC (1992) New directions in the development of MR imaging contrast media. Radiology 183(1):1–11
5. Dawson P (1996) Contrast agents in magnetic resonance imaging. Eur J Radiol 23(3):201–204
6. Giovagnoni A, Fabbri A, Maccioni F (2002) Oral contrast agents in MRI of the gastrointestinal tract. Abdom Imaging 27 (4):367–375
7. Hentsch A et al (2003) Gadobutrol-enhanced moving-table magnetic resonance angiography in patients with peripheral vascular disease: a prospective, multi-centre blinded comparison with digital subtraction angiography. Eur Radiol 13(9):2103–2114
8. Laghi A et al (2002) Oral contrast agents for magnetic resonance imaging of the bowel. Top Magn Reson Imaging 13(6):389–396
9. Mitchell DG (1997) MR imaging contrast agents—what's in a name? J Magn Reson Imaging 7(1):1–4
10. Nyman U et al (2002) Are gadolinium-based contrast media really safer than iodinated media for digital subtraction angiography in patients with azotemia? Radiology 223(2):311–318; discussion 328–329
11. Paley MR, Ros PR (1997) MRI of the gastrointestinal tract. Eur Radiol 7(9):1387–1397
12. Reimer P, Tombach B (1998) Hepatic MRI with SPIO: detection and characterization of focal liver lesions. Eur Radiol 8(7):1198–1204
13. Reimer P, Balzer T (2003) Ferucarbotran (Resovist): a new clinically approved RES-specific contrast agent for contrast-enhanced MRI of the liver: properties, clinical development, and applications. Eur Radiol 13(6):1266–1276
14. Reimer P, Schneider G, Schima W (2004) Hepatobiliary contrast agents for contrast-enhanced MRI of the liver: properties, clinical development and applications. Eur Radiol 14(4):559–578
15. Runge VM (2000) Safety of approved MR contrast media for intravenous injection. J Magn Reson Imaging 12(2):205–213
16. Runge VM (2001) Safety of magnetic resonance contrast media. Top Magn Reson Imaging 12(4):309–314
17. Runge VM, Muroff LR, Jinkins JR (2001) Central nervous system: review of clinical use of contrast media. Top Magn Reson Imaging 12(4):231–263
18. Semelka RC, Helmberger TK (2001) Contrast agents for MR imaging of the liver. Radiology 218(1):27–38
19. Spinosa DJ, Kaufmann JA, Hartwell GD (2002) Gadolinium chelates in angiography and interventional radiology: a useful alternative to iodinated contrast media for angiography. Radiology 223(2):319–325; discussion 326–327
20. Tombach B et al (2002) Using highly concentrated gadobutrol as an MR contrast agent in patients also requiring hemodialysis: safety and dialysability. Am J Roentgenol 178(1):105–109
21. Tombach B et al (2002) First-pass and equilibrium phase MRA following intravenous bolus injection of SH U 555 C: phase I clinical trial in elderly volunteers with risk factors for arterial vascular disease. Acad Radiol 9 Suppl 2:S425–427
22. Tombach B, Heindel W (2002) Value of 1.0- M gadolinium chelates: review of preclinical and clinical data on gadobutrol. Eur Radiol 12(6):1550–1556
23. Tombach B et al (2003) Do highly concentrated gadolinium chelates improve MR brain perfusion imaging? Intraindividually controlled randomized crossover concentration comparison study of 0.5 versus 1.0 mol/L gadobutrol. Radiology 226(3):880–888
24. Wang YX, Hussain SM, Krestin GP (2001) Superparamagnetic iron oxide contrast agents: physicochemical characteristics and applications in MR imaging. Eur Radiol 11(11):2319–2331
25. HJ Weinmann et al (2003) Tissue-specific MR contrast agents. Eur J Radiol 46(1):33–44

Contrast Media, MRI, RES Specific Iron Oxide Particles

Peter Reimer
Department of Radiology, Klinikum Karlsruhe, Academic Teaching Hospital of the University of Freiburg, D-76133 Karlsruhe
Peter.Reimer@klinik.um-karlsruhe.com

Definition

Iron oxides possess a large magnetic moment when brought into a magnetic field. A distinguishing feature of superparamagnetic iron oxides (SPIO/USPIO) is that they do not show residual magnetization after removal from the field. Magnetic susceptibility describes the ratio of such induced magnetization to the strength of the applied magnetic field. Typical for all SPIO/USPIO is a non-linear behaviour between induced magnetization and applied field, contrary to paramagnetic agent's which demonstrate a linear behaviour. The effect of superparamagnetic iron oxides (SPIO) on proton relaxation times is best explained by two mechanisms. The large magnetic moment of SPIO generates local field inhomogeneities and promotes dephasing of proton spins and acceleration of transverse relaxation. Second, the large susceptibility difference between particles and the surrounding medium creates magnetic field gradients at microscopic levels. Diffusion in these field gradients leads to an irreversible loss of phase coherence and thus decreases transverse relaxation times of protons.

The iron crystals clustered within phagolysosomes cause a significant superparamagnetic disturbance of the local magnetic field resulting in a pronounced shortening of both T2 and also T1 relaxivity. Therefore, the fundamental principle contrast enhancement after administration of iron oxide particles goes along with the presence or relative absence of Kupffer cells within the normal parenchyma and specific lesions. A significant decrease of the signal in tissue containing Kupffer cells such as normal tissue can be appreciated after SPIO administration, resulting in a relative signal increase in

tissues with a lack of Kupffer cells. Hypovascular liver metastases and cystic lesions are the typical examples for this contrast pattern. Nevertheless, the persistence of Kupffer cells in some hepatocellular tumours can be beneficial in differential diagnostic considerations. These contrast patterns apply to the accumulation phase of SPIO imaged >10 min following injection. Ferucarbotran may be used imaging the perfusion phase of lesions providing additional information especially for lesions characterization especially in hypervascular lesions. However, also due to the much lower dose the contrast yield is lower than observed for low molecular gadolinium chelates.

After intravenous administration, iron oxides circulate in the blood stream for a variable length of time depending on particle size and surface characteristics. Typically, particles accumulate in macrophages of the reticuloendothelial systems (RES; e.g. liver, spleen, lymph nodes, bone marrow etc.). Tissue localization also depends on organ blood flow, opsonisation of iron oxides by plasma proteins, receptor or target cell affinity and relative concentration of binding sites.

Biodegradation of iron oxides is assumed to occur in phagolysosomes within macrophages. Elemental iron from the iron oxide core is incorporated into the body iron pool and can be demonstrated in haemoglobin. In cases of severe hepatic cirrhosis, the splenic signal loss after iron oxide administration is surpassing the signal loss in the liver by far due to the loss of functioning hepatic Kupffer cells. This phenomenon is known as 'colloid shift' from nuclear medicine studies. After ultrasmall iron oxides (USPIO) administration the spleen presents the highest uptake (7.1%/g after 24 h) in comparison to liver (6.3%/g), lymph nodes (3.6%/g) and bone marrow (2.9%/g).

Two different classes of iron oxides are currently clinically approved or have completed phase three trials:

1. SPIO with a high R2/R1 relaxivity ratio and short blood half-life (<10 min). There are currently two clinically approved SPIO ferumoxides (Guerbet, Paris, France) and ferucarbotran (Schering, Berlin, Germany). A high R2/R1 ratio of 5 to 15 is characteristic for superparamagnetic colloids of the SPIO type (Reimer 1998, Reimer 2003, Ros 1995, and Wang 2001).
2. USPIO with a lower R2/R1 relaxivity ratio and longer blood half-life (<3 h) (Harisinghani 2003 and Weissleder 1990). Clinical approval of Ferumoxtran-10 is pending (Guerbet, Paris, France).

Ferumoxides (Feridex, Guerbet, France) consists of crystalline superparamagnetic iron oxide microparticles stabilized as a colloid with low-molecular weight coated with dextran. Ferucarbotran (SH U 555 A, Schering AG, Germany) consists of superparamagnetic iron oxide microparticles coated with carboxydextran. The R1 relaxivity of SPIO varies considerably within the range of diagnostically applied field strengths while the R2 relaxivity is relatively stable within the range of diagnostically applied field strength. Thus, at lower imaging field the T1 effect of these materials is better used. Both contrast agents are approved for hepatic MRI (Reimer 1998, Reimer 2003, Ros 1995 and Wang 2001).

Ferumoxtran-10 [BMS 180549, Sinerem^{TM}], consists of iron-oxide particles coated with dextran (Harisinghani 2003 and Weissleder 1990). It is an ultrasmall superparamagnetic contrast agent that is awaiting registration with Guerbet in Europe. The US FDA has issued an 'approvable letter' for use of Combidex (with Advanced Magnetics in the USA) in the diagnosis of lymph node disease, and the detection, diagnosis and characterisation of benign versus malignant lesions of the liver and spleen. Since, the US FDA has made comments about some data and indications an additional clinical trial may be required to settle the issues. Ferumoxtran-10 has been licensed to Guerbet for Western Europe and Brazil. It is awaiting registration (as Sinerem^{TM}) for imaging cancer in the pelois (uterus, prostal and rectum). Guerbet is also conducting additional clinical trials with ferumoxtran-10 for imaging of multiple sclerosis plaques and breast cancer. Advanced Magnetics has granted exclusive marketing and distribution rights for Combidex for oncology applications in the USA to Cytogen Corporation.

Indication

SPIO and USPIO have been developed for contrast-enhanced MR imaging of the liver, spleen, lymph nodes, bone marrow and other indications. The larger SPIO agents efficiently accumulate in liver with approximately 80% of the injected dose and spleen with 5–10% of the injected dose within minutes after intravenous administration. The smaller USPIO exhibit a longer blood-half life and higher accumulation in the RES within spleen, lymph nodes, bone marrow or vascular plaques.

Both SPIO are approved for imaging of liver tumours (Fig. 1). Benign hepatic lesions derived from hepatocytes such as focal nodular hyperplasia, hepatocellular adenomas, regenerative nodules and dysplastic nodules may embody various amounts of Kupffer cells. Therefore, the relative signal loss after SPIO administration in these lesions may parallel the signal loss in normal hepatic parenchyma indicating a most likely Kupffer cell containing benign lesion. Hemangiomas also show signal changes, which are believed to be based upon the blood pool of hemangiomas and uptake into sinusoidal cells within hemangiomas. Therefore, the relative signal loss after SPIO administration in these lesions may parallel the signal loss in normal hepatic parenchyma indicating a most likely

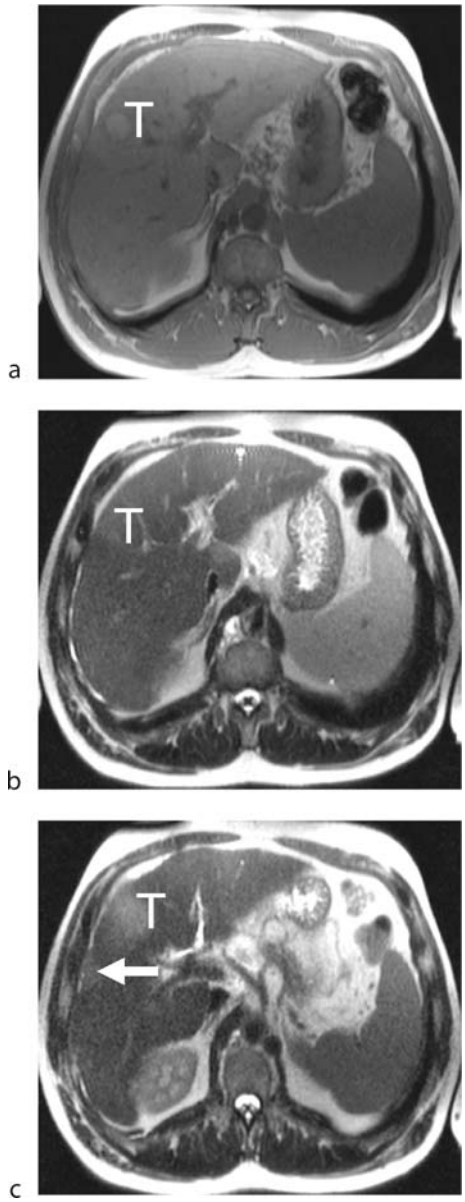

Contrast Media, MRI, RES Specific Iron Oxide Particles. Figure 1 Patient with Hepatocellular Carcinoma. Precontrast imaging (a and b) show a single tumor in the right liver lobe (t). An additional tumor (*arrow*) is visualized following ferucarbotran (c).

Kupffer cell containing benign lesion. On mild to heavily T2-w, images hemangiomas exhibit decreased signal intensity. T1-w sequences may show a signal increase.

The contrast pattern in malignant liver tumours also depends on the hepatocyte content of the lesions. All metastases are devoid of RES cells and thus hypovascular metastases show stable signal and thus increased conspicuity. Hypervascular metastases may exhibit perfusion changes and pooling during the accumulation phase resulting in a temporary signal decrease or increase dependent on T1-effects. Hepatocyte derived malignant lesions reveal more complex patterns. Poorly or moderately differentiated hepatocellular carcinomas are nearly completely devoid of Kupffer cells. Therefore, they exhibit a contrast pattern comparable to metastases going along with their vascularity (hypovascular vs. hypervascular). Well-differentiated hepatocellular carcinomas and hyperplastic regenerative nodules may also contain Kupffer cells. Subsequently, these tumours may show uptake into Kupffer cells and thus proportional to the content and activity a signal decrease on accumulation phase images. This may cause a decreased conspicuity during the accumulation phase compared to plain images. Furthermore, the perfusion phase may be imaged with additional information regarding lesion vascularity.

Ferumoxtran-10 is awaiting registration for imaging cancer in the lymphatic system, perfusion imaging of the brain, heart, liver and spleen, in the delineation of reduced blood flow in damaged tissues following heart attack or stroke, and as an adjunct to magnetic resonance angiography.

Contraindication

Safety and effectiveness have not been established in paediatric patients for any of the contrast agents. Specific contraindications and precautions for the three contrast agents are a prior hypersensitivity to the compounds, dextran or carboxydextran. A known allergic or hypersensitivity reactions to iron-containing products or disorders associated with iron overload represent a contraindication.

An injection should not be considered to patients with asthma, allergies and history of allergic responses to medications, cardiovascular disease or other abnormalities that may predispose them to cardiac arrhythmias or cardiovascular effects.

Iron oxides were not investigated in patients with severe renal or hepatic insufficiency and are thus not recommended in these patients.

Pregnancy/Lactation

The application during pregnancy or lactation is not approved or recommended.

Use and Dosage

Prior to contrast injection T1- and T2-weighted sequences at least in the transverse plane should be obtained. Specific parameters and strategies (breathheld vs. triggered) are somewhat vendor, scanner type and software release dependent. In order to use the information provided by looking at lesion perfusion the weak perfusion effect of Ferucarbotran may be studied by either T1- or T2*-weighted sequences. For T2*-weighting, it appears advantageous not to maximize for T2* in order maintain sufficient signal-to-noise. Initial timing may follow the usual time-points of the arterial-phase and portal-venous-phase followed by delayed acquisitions up to 10 min. Accumulation phase imaging may start as early as 10 min post injection with T2-weighted sequences including a GRE sequence with proton-density characteristics for detection. Mild and heavily T2-weighted TSE-sequences also provide useful information on the signal decrease within RES-containing tumours.

The two SPIO are approved for liver imaging in adult patients. Malignant liver tumours are typically devoid of a substantial number of phagocytic cells so they appear as hyperintense/bright lesions contrasted against the hypointense/dark liver on T2-w sequences. Tumours with a substantial number of phagocytic cells such as focal nodular hyperplasia, hepatocellular adenoma, well-differentiated hepatocellular carcinoma and/or a significant blood-pool (hemangioma or hypervascular lesions) may show sufficient uptake of SPIO with decreasing signal intensity on T2-w sequences. The signal decrease is related to the Kupffer cell activity or tumour vascularity. Furthermore, SPIO show signal changes in T1-w sequences, both during the perfusion phase (ferucarbotran) and accumulation phase (ferumoxides and ferucarbotran) providing additional information.

Ferumoxides is diluted in 100 mL of 5% dextrose solution and drip infused over 30 min, Ferucarbotran may be bolused for dynamic imaging during the vascular phase, however, providing less signal than gadolinium chelates approved at a higher dose. Post-contrast MRI with ferumoxides may start after completion of infusion up to a couple of hours later. For ferucarbotran post-contrast MRI may start as early as 10 min following injection. The post-contrast time window for both agents is probably up to 24–36 h.

Different dosages are approved for use in the USA, Europe and Japan. For ferumoxides, a dosage of 15 µmol Fe/kg is approved in Europe and Japan in contrast to 10 µmol Fe/kg in USA. The different dosages result in considerably varying T1- and T2*-effects especially when gradient-echo sequences are applied. This phenomenon might be even more striking in ferucarbotran, in which dosages up to 16 µmol Fe/kg bodyweight produce maximum contrast effects. Clinically, to simplify contrast injections it was hypothesized that the conventional bodyweight-based injection of iron per kg may be replaced by fixed volumes coming in pre-filled syringes (≤60 kg–0.9 mL and >60 kg 1.4 mL). The effective dose administered per kg bodyweight varies between about 7 and 11 µmol Fe/kg bodyweight.

Ferumoxtran-10 has been given at a dose 0.8 to 1.7 mg Fe/kg bodyweight for suspected hepatic lesions. MRI may be performed as early as after completion of infusion. A dose of 1.7 mg Fe/kg bodyweight was effective for detection of lymph node imaging of patients with prostate cancer, pelvic cancer and head and neck cancer. For the detection of metastases in patients with non-small-cell lung cancer, 2.6 mg Fe/kg bodyweight has been administered. Post-contrast MRI may be performed as early as 24 or 36 h after completion of infusion. An infusion time of 25 to 30 min is required to minimize hypotension or acute lumbar pain.

Adverse Reactions

Adverse reactions vary among the different iron oxides. The two dextran-stabilized compounds show a characteristic reaction when infused rapidly with hypotension, headache, nausea, abdominal pain or lumbar pain (5–30%). Clinical trials with intravenously administered Ferumoxides have been initiated as early as 1987. Early studies were performed with bolus injections of relatively high doses (≤50 µmol Fe/kg bodyweight) of an initial formulation of AMI-25 causing significant hypotension. Subsequently, the agent was reformulated to achieve iso-osmolarity and is currently administered by drip infusion over a period of 30 min since side effects (facial flash, dyspnea, rash, lumbar pain) depend on the dose rate. However, in most cases the administration can be reinitiated after reduction of the injection rate. Dermatologic allergic reactions like urticaria, erythema, pruritus, rash, pain at the infusion site, a sensation or warmth during infusion, or dermatographism have been reported. Non-significant effects are an increase in monocyte counts and mild eosinophilia.

During the clinical development of ferucarbotran, a dose dependent (5–40 µmol Fe/kg bodyweight) increase in PTT was observed, however, the normal range was not exceeded. These minor changes in PTT were attributed to a transient decrease in clotting factor XI activity. The transient decrease of clotting factor XI did not cause any clinical side effects in phases I–III. Previous studies assessing other SPIO or USPIO contrast agents did not report detailed information on clotting parameters. Safety data were obtained during the entire clinical

development. A total of 162 adverse events were documented within 1053 patients, of whom 75 were classified as possibly, probably or definitely drug related. The majority occurred within the first 3 h (73/75) and was of mild intensity. The frequency of adverse events was within the range of other approved MR contrast agents such as gadolinium chelates or placebo medication and no specific pattern was observed, although no direct comparative studies are available so far. Ferucarbotran proved to be a safe contrast agent since no significant cardiovascular changes during close monitoring of blood pressure and heart rate within the magnet bore. Blood tests evaluated revealed minor changes with the increase in iron and ferritin as well as the decrease in total iron binding capacity as a result of the iron injection.

Interactions

The administered free iron is incorporated into the normal iron metabolism, however, the administered dosage of SPIO is not significantly affecting the body's iron pool (e.g. 15 μmol Fe/kg ~840 ng Fe/body weight). Till the degradation of the clustered iron particles the superparamagnetic effects last for several days providing an imaging window of several hours up to several days after administration. Human tissues contain iron in the form of hemosiderin, ferritin and transferrin. Normal liver contains approximately 0.2 mg Fe/g wet weight of liver and total iron stores amount to approximately 3.5 g. The amount of iron oxides that is required for clinical MR imaging (1–2 mg Fe/kg bodyweight; for a 70 kg subject 70–140 mg) is small compared to normal iron stores.

Bibliography

1. Harisinghani MG et al (2003) Noninvasive detection of clinically occult lymph-node metastases in prostate cancer. N Engl J Med 348 (25):2491–2499
2. Reimer P and Tombach B (1998) Hepatic MRI with SPIO: detection and characterization of focal liver lesions. Eur Radiol 8(7): 1198–1204
3. Reimer P and Balzer T (2003) Ferucarbotran (Resovist): a new clinically approved RES-specific contrast agent for contrast-enhanced MRI of the liver: properties, clinical development, and applications. Eur Radiol 13(6):1266–1276
4. Ros PR et al (1995) Hepatic MR imaging with ferumoxides: a multicenter clinical trial of the safety and efficacy in the detection of focal hepatic lesions. Radiology 196(2):481–488
5. Wang YX, Hussain SM, and Krestin GP (2001) Superparamagnetic iron oxide contrast agents: physicochemical characteristics and applications in MR imaging. Eur Radiol 11(11):2319–2331
6. Weissleder R et al (1990) Ultrasmall superparamagnetic iron oxide: an intravenous contrast agent for assessing lymph nodes with MR imaging. Radiology 175(2):494–498
7. Weissleder R et al (1990) Ultrasmall superparamagnetic iron oxide: characterization of a new class of contrast agents for MR imaging. Radiology 175(2):489–493

Contrast Media, Ultrasound, Amplitude Modulation

Robert Eckersley
Imaging Sciences Department, Imperial College London, London, UK
r.eckersley@imperial.ac.uk

Amplitude modulation imaging is a bubble-specific mode which uses alternating pulse amplitudes, that is, +1, +1/2 and so on. (see Fig. 1). This approach works in a similar manner to phase modulation in which appropriate combination of the echoes will result in a complete cancellation for linear scatterers, while non-linear microbubble echoes will show residual signals. These residual signals arise because the microbubbles respond non-linearly to the different amplitude pulses, that is, the double amplitude pulse does not elicit an echo with twice the amplitude, whereas for tissue this would be the case. An advantage of amplitude modulation over phase modulation is that it is able to detect non-linear signals at the fundamental frequency and not just the second harmonic. However, the use of alternating lower power pulses does reduce the sensitivity of this approach. A combination of pulse inversion and amplitude modulation has been shown to improve the sensitivity to microbubbles over tissues still further (1). As with phase modulation, this sequence can be extended to more that two pulses to improve the sensitivity and to enable the use of Doppler processing for motion detection.

Bibliography

1. Eckersley RJ, Chin CT, Burns PN (2005) Optimising phase and amplitude modulation schemes for imaging microbubble contrast agents at low acoustic power. Ultrasound Med Biol 31(2):213–219

Contrast Media, Ultrasound, Applications in Blunt Abdominal Trauma

David Cosgrove
Imaging Sciences Department, Imperial College, Hammersmith Hospital, London, UK
d.cosgrove@csc.mrc.ac.uk

Synonyms

Contrast-enhanced sonography in abdominal trauma; Contrast-enhanced ultrasound in abdominal trauma

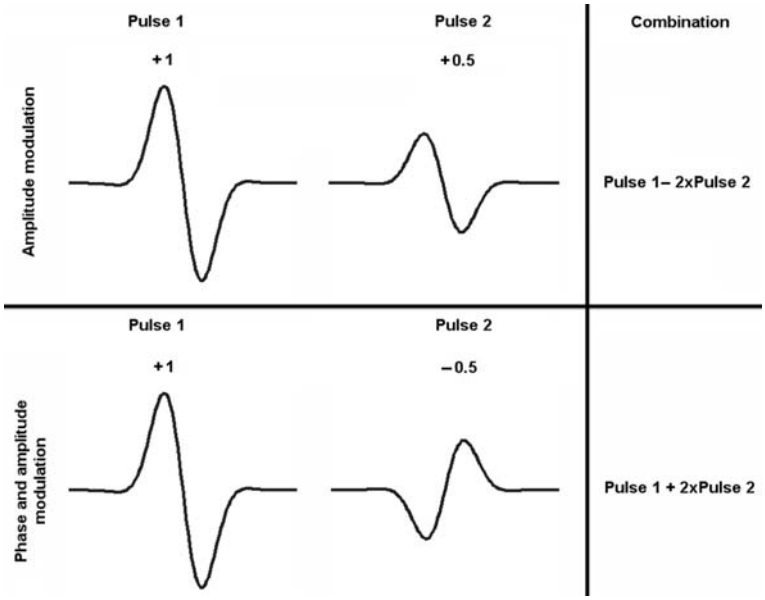

Contrast Media, Ultrasound, Amplitude Modulation. Figure 1 This figure shows (upper panel) a simple two-pulse amplitude modulation sequence. When the echoes of pulse 1 and pulse 2 are combined by doubling pulse 2 and subtracting the result from pulse 1 any linear signals will be cancelled. Both non-linear signals at the fundamental and second harmonic signals in the echoes from microbubbles are preserved by this approach. Also presented (lower panel) is a two-pulse sequence with combined phase and amplitude modulation. Linear signals can again be removed by appropriate combination of the echoes. Combing the two modulation approaches can improve the sensitivity to microbubbles.

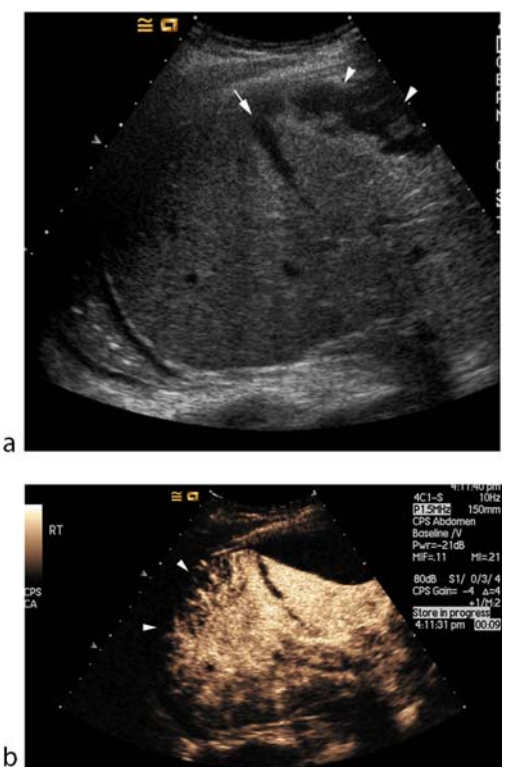

Contrast Media, Ultrasound, Applications in Blunt Abdominal Trauma. Figure 1 Abdominal trauma in a road crash. This patient presented with upper abdominal pain following a car crash. The B-mode ultrasound scan showed a wedge-shaped defect in the right liver (*arrow* in a), suggestive of a tear, as well as an echopoor region (*arrowheads*) that could not confidently be assigned to liver or peritoneum. Following i.v. SonoVue and working in the CPS mode (Sequoia, Siemens), this could be seen to lie outside the liver, which was compressed by it. The liver tear was confirmed, but in addition, there was extensive devascularised liver tissue superiorly (*arrowheads* in b). In this case, the contrast-enhanced scan revealed the full extent of the liver injury as well as the presence of intra-peritoneal bleeding. (Images courtesy of Dr Paul Sidhu, King's College Hospital,

Definition

The use of ultrasound (US) microbubble contrast agents combined with contrast-specific imaging techniques for the detection of traumatic lesions of the abdomen (mainly spleen, liver and kidney)

Introduction

Conventional ultrasound is poor at detecting trauma to abdominal organs because freshly cut tissue has the same appearances as viable tissue on grey scale imaging (1). Large haematomas can be detected, but the extent of tissue damage is under-estimated (2). Colour Doppler might be expected to offer an improvement by depicting non-perfused tissue but, though it does improve sensitivity somewhat overall it has proved disappointing in trauma (3). The critical limitation of Doppler is its inability to detect flow in small vessels where flow is slow, because Doppler cannot distinguish tissue movement from blood flow.

Thus, the role of ultrasound as a means to triage patients according to the severity of their injury is mostly restricted to detecting free fluid in the peritoneum, which in the context of abdominal trauma, is assumed to represent blood, though fresh blood cannot be distinguished form serous fluid using ultrasound. The method, known as focused assessment with sonography in trauma (FAST), examines the right and left upper quadrants and the pelvis for free fluid as a measure of intra-abdominal bleeding and forms a baseline for comparison with subsequent scans to detect deterioration. However, FAST has major limitations, including its inability to pinpoint the source of bleeding and the fact that up to 10% of parenchymal trauma does not result in bleeding into the peritoneum (4). Therefore, in general, contrast-enhanced CT is the preferred technique and it also has the important advantage of being able to assess the head thorax and spine, and so all stable trauma patients are referred for CT unless the injury seems to be trivial.

While an improved ultrasound approach, such as the use of contrast enhancement would have many advantages (performed at the bedside, repeatable, no risk form ionising radiation), CT would always be required to detect head, chest and skeletal injuries.

Contrast Agents and Parenchymal Trauma

Almost all instances of soft tissue injury produce non-perfused regions of tissue, often together with haematomas. Detecting unperfused tissue requires demonstration of the integrity of the microvasculature and this is now possible with microbubble contrast agents (5, 6). Multi-pulse methods with software designed to detect their resonance signals, display the contrast image separately from the grey-scale image, either as a side-by-side display or as a colour-coded overlay. The ability to detect contrast in the microcirculation sets contrast ultrasound apart from Doppler, which can only detect flow in vessels down to arteriolar calibre.

Operation at a low transmit power (using a mechanical index of less than about 0.4) allows real time scanning after administration of contrast. In the kidney, for example, the high perfusion of the cortex is shown as a rapidly developing enhancement that intensifies to a complete colour fill, usually commencing after 15–30 sec, depending on the patient's cardiac output, before washing out over the next few minutes. In the liver and spleen, the microbubbles arrive in the arteries in the same way but less strikingly because of their lower overall blood flow; in the liver the portal supply dominates the wash-in phase and in both, the microbubbles linger within the capacious

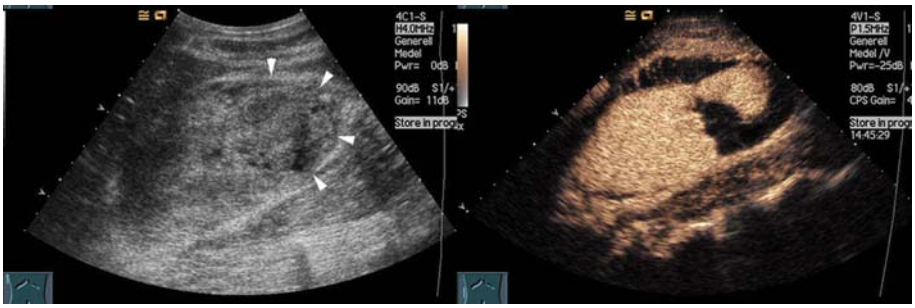

Contrast Media, Ultrasound, Applications in Blunt Abdominal Trauma. Figure 2 Blunt trauma to the right upper abdomen. Following a road traffic crash, this patient was admitted with right flank pain. The grey-scale ultrasound did not reveal any free fluid but an ill-defined irregularity of the texture of the lower pole of the right kidney was noted (arrowheads in A). Following i.v. SonoVue and using the CPS mode (Sequoia, Siemens) complete enhancement in the renal cortex revealed a large defect in the posterior portion of the kidney. A laceration was confirmed on contrast-enhanced CT scanning. (Images courtesy of Dr Anders Knutsson and Dr Lars Thorelius, University Hospital, Linköping, Sweden)

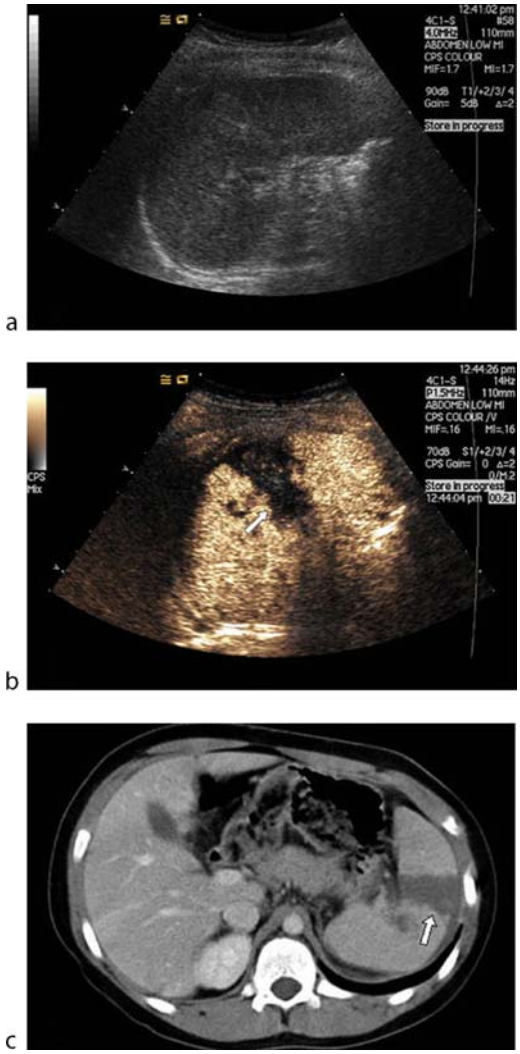

Contrast Media, Ultrasound, Applications in Blunt Abdominal Trauma. Figure 3 Twelve-year old boy with blunt abdominal trauma. (a) Unenhanced oblique intercostal B-mode US 1 day after blunt abdominal trauma. The spleen shows homogeneous parenchyma and regular contour with no focal abnormality. (b) Contrast-enhanced coherent pulse sequencing (CPS) scan in oblique intercostal section 1 day after BAT. Contrast enhancement in normal perfused parenchyma is represented by the gold-coloured overlay, whereas the haematoma appears as a wedge-shaped enhancement defect (*arrow*). (c) Axial contrast-enhanced CT in the portal-venous phase confirming the splenic parenchymal laceration seen on CEUS (*arrow*). (Images courtesy of Dr Thomas Albrecht, Charité—Campus Benjamin Franklin, Berlin, Germany).

microcirculation where they persist for several minutes in the so-called 'sinusoidal' or 'late' phase.

Thus, the arterial phase is critical for demonstrating renal trauma (and other renal abnormalities). The cortical enhancement washes out after around a minute and this allows time for a sweep through the entire renal volume. A second injection is required for the contralateral kidney and usually these can both be drawn from the same ampoule of contrast agent. For the liver and spleen, the sinusoidal phase is the most useful time to scan. It begins at around 30 sec after injection and develops fully over the next 30–60 sec. This leads to a natural protocol for scanning these four organs in which the kidneys are studied first using separate injections, after which the liver and spleen are interrogated with no further injection required in most cases. Thus, the examination can be completed in less than 5 min. Since the microbubble contrast agents used are not cardio- or nephrotoxic, there are generally no contra-indications even in unstable patients and they can be repeated as often as needed, dictated by changes in the patient's vital signs.

Large prospective studies of the potential for contrast-enhanced ultrasound in trauma are underway. Pending completion and publication of the results, only anecdotal reports and pilot studies are available on which to form impressions of the potential role of contrast-enhanced ultrasound in trauma. Several case reports have been presented (7, 8). They often show dramatic images of arterial and sinusoidal phase defects in the kidneys, liver or spleen that were impossible to demonstrate using conventional modes. One report of results in abdominal trauma presented several cases, mostly following road traffic incidents, and demonstrated that lesions could be clearly seen with good correspondence with CT (9) (Fig. 1). A study of 25 patients with presumed splenic trauma using a recently introduced contrast agent and non-linear imaging showed good correlation with CT, only one of 18 lesions being missed, and this was a minor lesion (10). However, only patients with ultrasonographic abnormalities were recruited and this probably biased the results in favour of ultrasound; nevertheless, it is an encouraging result (Figs. 2 and 3).

Active Bleeding

Animal studies have shown that active bleeding from the kidney following experimental injury can be detected as extra-parenchymal enhancement. No systematic human studies have been reported but incidental demonstration of active bleeding from a recently biopsied kidney (Correas J-M, 2002, personal communication) have been reported.

Clinical Role

Clearly, the clinical role of contrast-enhanced ultrasound for the detection of abdominal trauma has not yet been defined but, in many trauma units in countries where

these agents are licensed, the method is acquiring respectability as a means for demonstrating injury to the liver, spleen and kidneys following both blunt and penetrating injuries. However, thus far it has found most use as a means to follow trauma for example, to check for stability before a patient is discharged. It is also useful in children where there is a strong reason to minimise the dose of ionising radiation that is inevitable with CT.

Because ultrasound cannot examine the brain and thorax, or the skeleton, whole-body CT will remain the definitive imaging test in polytrauma. Contrast-enhanced ultrasound may well find a role in follow-up and where trauma is considered to be limited to the abdomen (especially in children).

Bibliography

1. Stengel D, Bauwens K, Sehouli J et al (2001) Systematic review and meta-analysis of emergency ultrasonography for blunt abdominal trauma. Br J Surg 88(7):901–912
2. Brooks A (2001) The role of ultrasound in trauma. J R Army Med Corps 147(3):268–273
3. Nilsson A, Lorén I, Nirhov N et al (1999) Power Doppler ultrasonography: alternative to computed tomography in abdominal trauma patients. J Ultrasound Med 18:669–672
4. Miller M, Pasquale M, WJ B et al (2003) Not so fast. Trauma 1:52–60
5. Cosgrove D (ed) (2004) Advances in Contrast Agent Imaging Using Cadence Contrast Pulse Sequencing Technology (CPS) and Sono-Vue, vol 14, Springer Verlag, Heidelberg, Germany p 124
6. Quaia EE (2005) Contrast Media in Ultrasonography. Springer Verlag, Heidleberg
7. Kraemer N, Cosgrove D, and Blomley M (2004) Microbubble ultrasound demonstrates liver trauma. J Trauma 56(4):913–914
8. Oldenburg A et al (2004) Imaging of paediatric splenic injury with contrast-enhanced ultrasonography. Pediatr Radiol 34(4):351–354
9. Thorelius L (2004) Contrast enhanced ultrasound in trauma. Eur Radiol 14(S8):P43–P52
10. Catalano O, Lobianco R, Sandomenico F et al (2003) Splenic trauma: evaluation with contrast-specific sonography and a second-generation contrast medium. J Ultrasound Med 22:467–477

Contrast Media, Ultrasound, Applications in Echocardiography

Harald Becher[1,*], Robert Olszewski[2]
[1]Oxford University, John Radcliffe Hospital, Oxford, UK
*Cardiac Investigation Annexe, John Radcliffe Hospital, Oxford, UK
[2]Department of Cardiology, Military Medical Institute, Warsaw, Poland
harald.becher@orh.nhs.uk

Synonyms

Contrast echo; Contrast echocardiography; Contrast-enhanced echocardiography

Definition

Contrast in echocardiography is used mainly for three purposes: detection of intracardiac and intrapulmonary shunting, left ventricular opacification and myocardial perfusion. The contrast effect is based on the use of gas microbubbles as blood tracers exploiting their acoustic behaviour during exposure to ultrasound.

Characteristics

The first agents to be used for echocardiography were hand-agitated saline or glucose. These are still used to detect intracardiac shunts. The more recent second generation contrast agents consists of different types of perfluorocarbon gases encapsulated by modified phospholipids, albumin or galactose crystals. These agents are used for left ventricular opacification and myocardial perfusion imaging.

The agitated contrast media used for shunt detection provide intensive opacification of the right heart after intravenous injection. However, agitated agents are unable to cross the pulmonary vasculature. Only, if there is a right to left shunt contrast agent can be displayed in the left heart chambers. The most frequent application of agitated saline is the detection of right to left shunting in atrial septal defects and patent foramen ovale (1) (Fig. 1).

The second generation of contrast agents provide intensive opacification of the right and left heart chambers when administered intravenously. Two techniques for contrast applications are introduced: infusions are preferential for assessment of myocardial perfusion and bolus injections of agents may be satisfactory for left ventricular

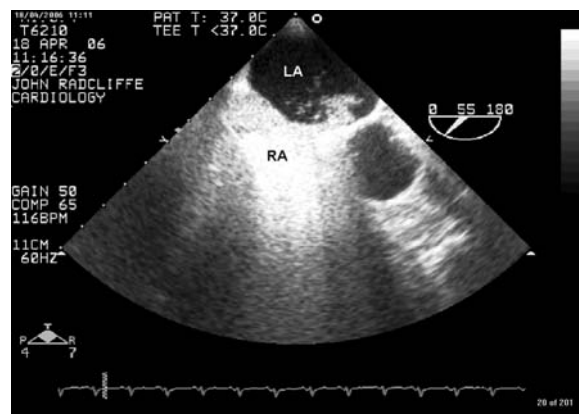

Contrast Media, Ultrasound, Applications in Echocardiography. Figure 1 Contrast transesophageal echocardiography. Contrast is seen mostly in right atrium (RA) and entering to left atrium (LA) via patent foramen ovale.

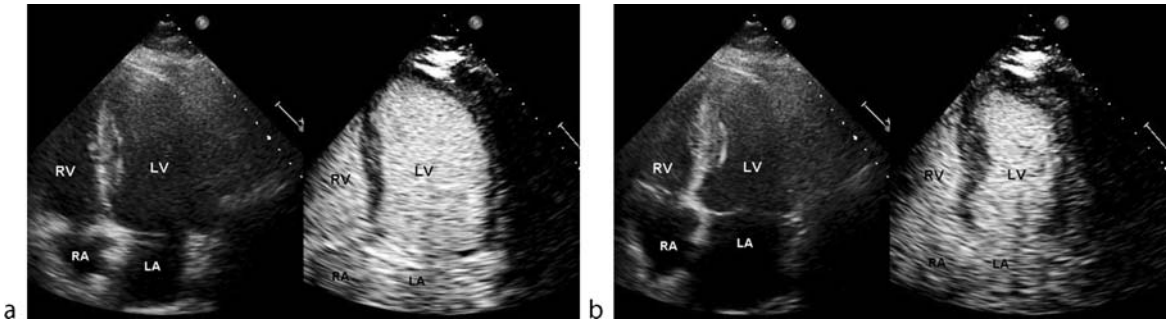

Contrast Media, Ultrasound, Applications in Echocardiography. Figure 2 Transthoracic echocardiographic images of the apical four-chamber view obtained from a patient before (*left*) and after (*right*) the administration of contrast agent. (a) enddiastolic, (b) endsystolic frames. The endocardial border is not well seen at baseline but becomes readily apparent with contrast enhancement. LV—left venticle, RV—right ventricle, LA—left atrium, RA—right atrium.

opacification in many cases. The dosages of contrast needed for LV opacification are minimal—0.1–0.3 ml—compared to those in other imaging modalities like X-ray. These small dosages are possible because of very sensitive contrast specific imaging technologies, which have been implemented in all state of the art ultrasound systems (2).

The major indication for the second generation contrast agents is left ventricular opacification and endocardial border definition. Although image quality has been improved with the introduction of harmonic imaging, there are still a number of studies remaining of inadequate quality, and it is here that the use of contrast agents comes into its own. Even with high-end ultrasound equipment, without contrast, the percentage of suboptimal images ranges from 10 to 15% (Fig. 2). The recent guidelines of the European Association of Echocardiography (EAE) and the American Society of Echocardiography (ASE) suggest to use the delineation of the endocardium as a selection criterion (3). Contrast agents should be considered when less the 80% of the circumference of the LV endocardium is not clearly seen. This is of major importance in stress echocardiography where there is always the need for optimal image quality. Clinical studies have shown the benefit of contrast in improving image quality, percentage of wall segments visualized, and confidence of interpretation of regional and global function both at rest and at peak stress (4).

Less frequently contrast agents are needed for better delineation of thrombi and masses.

In tandem with the development of contrast agents there have been advances in imaging modalities. The first contrast specific modality was harmonic imaging.

Second harmonic imaging enhances contrast effect compared to fundamental imaging and has been used for border definition using real-time imaging. However, it also leads to bubble destruction and artefacts. Latest developments such as power modulation and power pulse inversion, use less transmitting power than harmonic imaging and are almost non-destructive for bubbles and can be performed real-time imaging without the limitations of harmonic imaging and with less contrast. As tissue returns are not displayed, unlike with harmonic imaging, they are ideal for accurately delineating the left ventricular borders and assessing myocardial perfusion.

Harmonic Power Doppler is another method for perfusion imaging. It takes advantage of the signals obtained from bubble destructions during exposure to ultrasound. Power Doppler provides the highest signal to noise ratio for detecting contrast media, but has to be used with trigged mode. That means intermitted power of scanning to replenish the contrast in the myocardium.

Myocardial contrast echocardiography (MCE) is an imaging tool for the assessment of the myocardial microcirculation. Myocardial perfusion is defined as tissue blood flow at the capillary level. The two components of tissue blood flow—capillary blood volume and blood velocity—can be assessed by MCE.

Contrast perfusion imaging can be used to assess inducible myocardial ischemia and viability. The advantage of using perfusion imaging in stress echocardiography is higher accuracy in detecting coronary stenoses. In addition shorter and simple stress protocols can be used.

MCE can be used to determine the spatial extent of viable tissue post-infarction. It has been shown to be superior for detection of acute coronary syndromes in the emergency department compared with routine evaluation. MCE, a rapid bedside method, can be used to define the extent of collateral perfusion during coronary occlusion and hence to predict the ultimate infarct size. It has been performed safely in several thousand patients (5) (Fig. 3).

Current research focuses on using the microbubbles of ultrasound contrast media as drug and gene carriers and applying targeted ultrasound for local drug delivery. Another promising application is the use of the microbubbles to target arteriosclerotic vascular lesions.

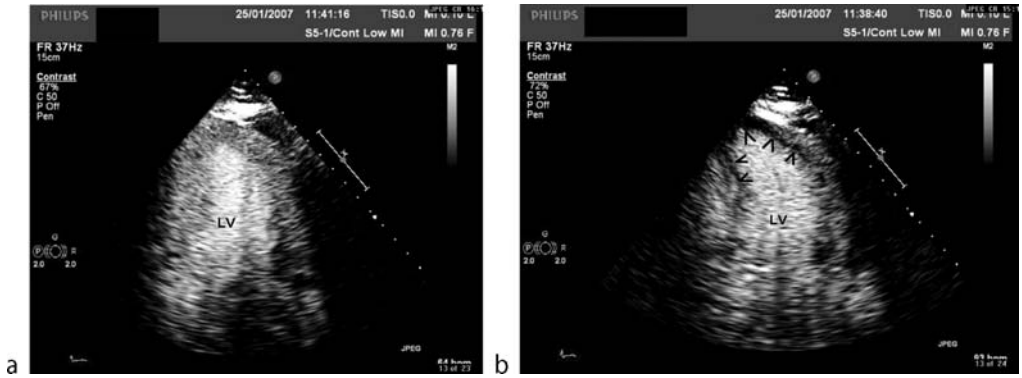

Contrast Media, Ultrasound, Applications in Echocardiography. Figure 3 Contrast study with adenosine. (a) Apical two chamber view in systole at rest showing normal perfusion. (b) After adenosine injection a perfusion defect is displayed in apical anterior and inferior wall (*arrows*) LV—left venticle.

Bibliography

1. Woods TD, Patel A (2006) A critical review of patent foramen ovale detection using saline contrast echocardiography: when bubbles lie. J Am Soc Echocardiogr 19(2):215–222
2. Becher H, Burns P (2000) Handbook of Contrast echocardiography. Springer Verlag. Free download ▶//www.sunnybrook.utoronto.ca/EchoHandbook
3. Lang RM, Bierig M, Devereux RB et al (2006) Recommendations for chamber quantification. Eur J Echocardiogr 7:79–108
4. Olszewski R, Timperley J, Szmigielski C et al (2007) The clinical applications of contrast echocardiography. Eur J Echocardiogr in press
5. Lepper W, Belcik T, Wei K et al (2004) Myocardial contrast echocardiography. Circulation 109(29):3132–3135

Contrast Media, Ultrasound, Applications in Focal Splenic Lesions

Christopher J. Harvey, Adrian K. P. Lim, Martin J. K. Blomley, David O. Cosgrove
Hammersmith and Charing Cross Hospital NHS Trust & Imperial College, London, UK
charvey_99@yahoo.com

Synonyms

Contrast-enhanced ultrasound of the spleen; Microbubble-enhanced ultrasound of the spleen

Definition

The use of microbubble agents and contrast-specific ultrasound (US) imaging modes for detecting splenic pathology. This technique also allows the further evaluation and characterisation of ▶focal splenic lesions, ranging from malignant tumours to benign entities such as splenic infarcts, haemangiomata or abscesses based on patterns of perfusion and splenic parenchymal contrast uptake.

Characteristics

Introduction

The advent of ▶microbubbles has allowed more accurate ultrasonic characterisation of focal splenic lesions to rival that of computed tomography (CT), magnetic resonance imaging (MRI) and nuclear medicine techniques.

Microbubbles were initially thought to be purely vascular agents. However, three agents demonstrate hepatosplenic-specific uptake after their disappearance from the blood-pool phase. They are Levovist, Sonavist (both Schering AG, Germany) and Sonazoid (NC100100; GE Amersham, Norway), of which only Levovist is currently in clinical use. Interestingly, the most widely used microbubble in Europe, SonoVue (Bracco, Italy), demonstrates splenic specificity only (1–3).

In the arterial phase, the spleen demonstrates heterogeneous and patchy ▶enhancement from 0 to 20 sec with the spleen then becoming homogeneous throughout within 50 sec. These enhancement characteristics are similar to those reported with iodinated contrast agents within the spleen on CT and MR imaging and are thought to be due to variable flow rates through the cords and sinuses of the red pulp. Therefore, it is recommended that lesion detection and assessment of the spleen with microbubbles should include the late phase, at least 60 sec post-intravenous injection.

Technological advances combined with the availability of more stable microbubbles (e.g. SonoVue) have facilitated the development of real-time non-destructive (low mechanical index (MI)) ▶microbubble-specific imaging modes that are widely used for focal splenic lesion assessment. Contrast-enhanced imaging of focal splenic lesions may be divided into arterial (20–25 sec) and portal (45–90 sec) phases and sinusoidal (>90 sec). Real-time imaging allows these phases to be followed successively, so that the dynamic enhancement pattern and vascular morphology may be assessed (1–3). The low MI means that continuous imaging can be performed for as long as the agent persists (5–10 min after a full dose of SonoVue). The fundamental and enhancement characteristics of splenic lesions are described later.

Focal Splenic Lesions

Congenital Lesions

A splenunculus is accessory splenic tissue, which is present in 10–30% of the population. They may be single or multiple and most commonly occur at the splenic hilum (75%). They typically have a round contour and their echogenicity is identical to that of the parent spleen. Splenunculi have identical enhancement patterns with ultrasound microbubbles to the adjacent spleen. Splenunculi and the parent spleen enhance simultaneously in the arterial phase and exhibit a heterogeneous sinusoidal phase. Some agents (Levovist, Sonovue) have a delayed splenic-specific parenchymal phase, which is useful in differentiating splenunculi from lymph nodes or pancreatic masses.

Cystic Lesions

Cystic splenic lesions may be subdivided into primary cysts, which are either non-parasitic (epithelial) or parasitic (echinococcosis infection), or secondary cysts, which are thought to be traumatic in aetiology. They contain blood, debris and may exhibit mural calcification.

Non-parasitic cysts show the classic ultrasound features of anechoic contents with posterior acoustic enhancement and smooth walls. Microbubble contrast agents may be helpful in defining the thin wall of the cyst and demonstrating the absence of central enhancement to differentiate benign simple cysts from infective or neoplastic cystic lesions.

Hydatid cysts are rare in the spleen (less than 5% of echinococcus infections). They may be anechoic or have heterogeneous echogenecity. The 'water-lily sign' is characteristic of the condition and is caused by separation of the membranes of the cyst. With intravenous (IV) microbubbles, hydatid cysts show peripheral but not internal enhancement.

Haemangiomas

Haemangiomas are the commonest benign primary splenic neoplasm with a prevalence of 0.3–14% at autopsy. They are tumours of the epithelium of the vascular sinuses and are more commonly cavernous than capillary in pattern. Cavernous haemangiomas are usually small (<2 cm) and are incidental findings on imaging. They are slow growing. Occasionally, haemangiomas may be large and may present as a mass or with rupture and bleeding.

Multiple splenic haemangiomas occur in Klippel–Trenaunay syndrome and may be complicated by rupture, hypersplenism and malignant change.

On ultrasound, haemangiomas typically appear as well-defined avascular echogenic lesions. Atypical features, which are more commonly present in large cavernous haemangiomas, include cystic change and calcification. Small haemangiomas uniformly enhance with microbubbles whereas larger lesions exhibit centripetal filling in on delayed imaging (Fig. 1). However, larger lesions with cystic/necrotic/thrombotic components may show heterogeneous enhancement rather than the centripetal pattern (4). This is due to the fact that cystic spaces (often central) do not possess blood-filled vascular spaces.

Hamartomas

Splenic hamartomas, also known as splenomas, splenadenomas and nodular hyperplasia of the spleen are rare benign tumours occurring with an incidence of 0.024–0.13% in autopsies.

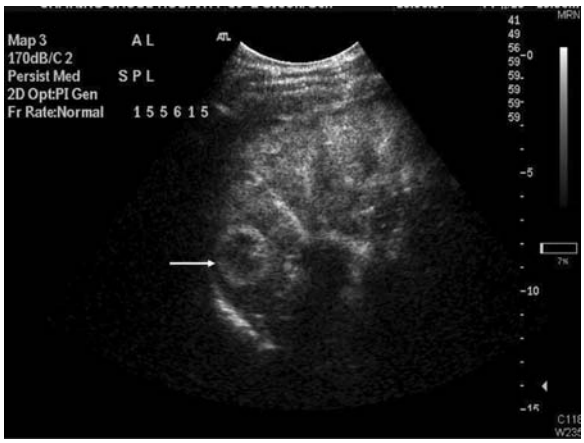

Contrast Media, Ultrasound, Applications in Focal Splenic Lesions. Figure 1 Splenic haemangioma: imaging in the late splenic-specific phase with SonoVue (Bracco, Milan, Italy) using phase inversion mode (HDI 5000, Phillips, USA) shows partial centripetal filling-in of the lesion (arrow) at 3 min post-injection.

Splenic hamartomas are usually found incidentally, although rupture has been described.

On ultrasound, splenic hamartomas are usually solid homogeneous masses and hyperechoic relative to the adjacent splenic parenchyma. However, some may be heterogeneous with cystic changes and areas of calcification secondary to ischaemia or haemorrhage. They are usually hypervascular on colour Doppler. This is thought to reflect the hypervascularity of the red pulp in the hamartoma. Variable enhancement is seen following the intravenous microbubble injection (4, 5).

Lymphangioma

Splenic lymphangioma is a rare slow growing benign tumour. It is characterised by splenic cysts of varying sizes from a few millimeters to several centimeters in size. Splenic lymphangiomas may occur in isolation or with multisystem organ involvement. Complications are associated with the more extensive or larger lymphangiomas and include bleeding, hypersplenism, consumptive coagulopathy and portal hypertension. Malignant transformation is rare but has been described in one case.

On ultrasound, splenic lymphangiomas appear as cystic lesions with septation, echogenic debris and calcification. Lymphangiomas are avascular on colour Doppler and do not enhance with microbubbles.

Lymphoma

Malignant lymphoma is the most common cause of splenic infiltration. The typical ultrasound appearances are of echopoor focal lesions that may be difficult to distinguish from cysts. The borders of the lesions may be poorly defined. 'Target sign' lesions and echogenic lesions have been described. Typically, Hodgkin's and low-grade non-Hodgkin's lymphoma result in diffuse infiltration or focal lesions, which are lesser than 3 cm in size. By comparison, high-grade non-Hodgkin's lymphoma causes focal lesions of greater than 3 cm in size. With microbubbles, irregular peripheral enhancement is seen with the lesions appearing as defects in the late phase (4).

Metastases

Splenic metastases are rare; 7% of post-mortems in patients with metastatic carcinomas and 8% of all splenic lesions were shown to be metastases in one series. The spleen may be involved by direct tumour invasion in pancreatic tail, colon, stomach, bronchus and diaphragmatic carcinomas. The ultrasound appearances are variable with echopoor metastases, being the most common. Echogenic metastases are the least common (5) and target lesions are less common than in the liver. Serosal metastases from ovarian carcinoma result in scalloping of the splenic margin. On Doppler, metastases are usually avascular. Imaging with microbubbles may show variable enhancement in the arterial phase but essentially, all lesions appear as defects surrounded by normally enhancing splenic parenchyma in the late phase (Fig. 2). Metastases may be revealed that are not seen on baseline B-mode/fundamental scanning by increasing their conspicuity. This improves the detection and facilitates the detection of subcentimetre metastases that would otherwise remain occult (4).

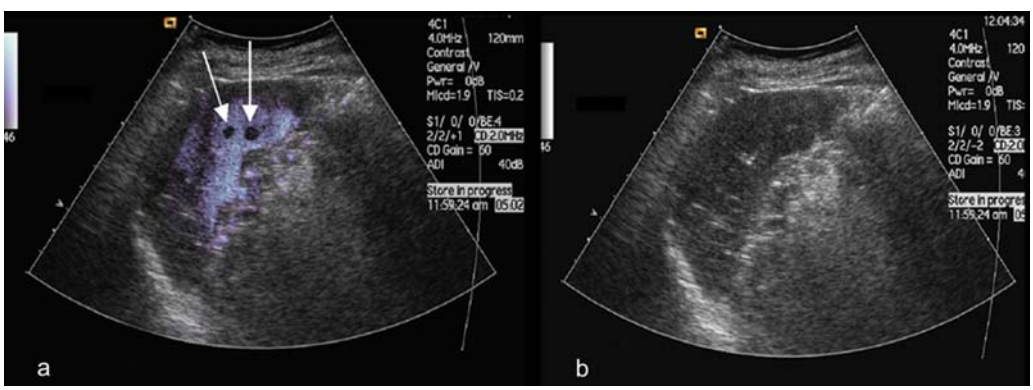

Contrast Media, Ultrasound, Applications in Focal Splenic Lesions. Figure 2 Splenic metastases from melanoma. (a) A duration of 3 min after Levovist (Schering), imaging using a late phase destructive mode (Agent Detection Imaging (ADI), Siemens, USA) demonstrates two metastases as defects (arrows) surrounded by normal splenic microbubble uptake. (b) When the colour overlay is removed, no corresponding B-mode lesions could be identified. This case demonstrates the imaging of the late splenic-specific phase of Levovist that improves the detection of occult metastases by increasing their conspicuity.

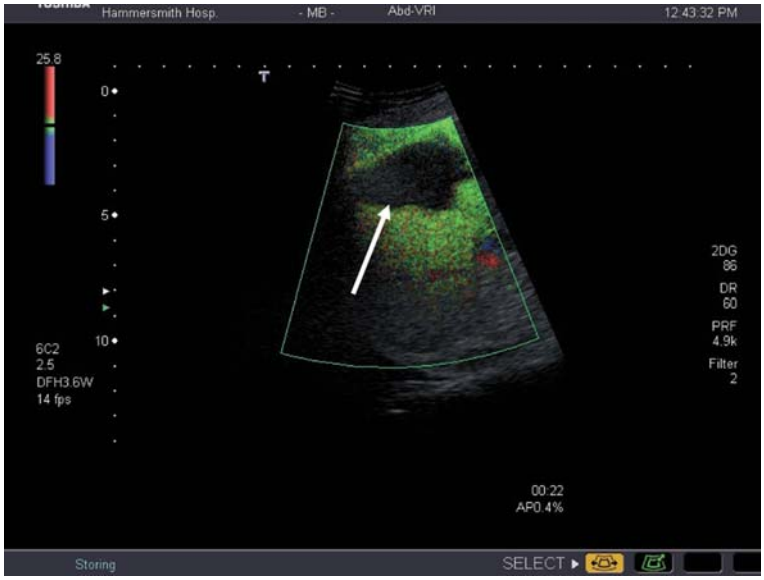

Contrast Media, Ultrasound, Applications in Focal Splenic Lesions. Figure 3 Imaging using Vascular Recognition Imaging (VRI, Aplio, Toshiba, Tokyo, Japan). A duration of 3 min after SonoVue administration shows a wedge-shaped non-enhancing defect consistent with an infarct (arrow) with normal enhancement of the surrounding spleen depicted by stationary microbubbles in green.

Splenic Infarction

Splenic infarction may result from emboli (endocarditis), hyperviscosity syndromes, sickle cell disease and myeloproliferative disorders. On B-mode, acute infarction is ill-defined, characteristically peripheral, wedge-shaped and echopoor. On colour Doppler absent signals confirm the diagnosis. Chronic infarction is seen as an echogenic area due to fibrotic change or calcification with overlying cortical retraction secondary to scarring. Microbubbles improve the ultrasound confidence of diagnosing early infarction (Fig. 3) by delineating an angular geographical hypo-enhancing area in all phases (4).

Splenic Abscesses

Splenic abscesses on ultrasound may be echopoor, septated, irregular walled containing debris and gas. They may have variable peripheral vascularity. Microbubbles may show the vascular rim of the abscesses. Common organisms include *Mycobacterium tuberculosis*, *Pneumocystis carinii* and *Candidiasis*. The latter have been described as showing a characteristic 'bull's eye' appearance with multifocal small lesion (0.5–2 cm in size) consisting of echogenic centres surrounded by echopoor rims. The detection of these lesions is improved by using a high-frequency linear probe. US contrast improves the detection of microabscesses by improving their conspicuity against the normal splenic parenchyma (4).

Heterogeneous Splenic Echotexture

This is seen as multiple tiny (2–3 mm) echogenic foci or just a heterogeneous echopattern on B-mode ultrasound. It is a non-specific finding typically in previous granulomatous infection such as tuberculosis, fungi as well as sarcoidosis, Wegener's granulomatosis, amyloidosis and Crohn's disease. These foci are generally defects in the late phase after microbubble administration.

Summary

Ultrasound is a reliable method of imaging splenic abnormalities. The introduction of microbubbles has further improved the diagnostic capabilities of ultrasound, allowing the investigation of splenic enhancement patterns and characterisation of focal lesions. US imaging in contrast is useful in distinguishing splenunculi from lymph nodes, demonstrating the characteristic enhancement patterns in haemangiomas, improving the visualisation of splenic infarction as well as improving the detection of microabscesses and focal malignancies.

Bibliography

1. Harvey CJ, Blomley MJ, Eckersley RJ et al (2001) Developments in ultrasound contrast media. Eur Radiol 11:675–689

2. Correas JM, Bridal L, Lesavre A et al (2001) Ultrasound contrast agents: properties, principles of action, tolerance, and artifacts. Eur Radiol 11:1316–1328
3. Lim AKP, Patel N, Eckersley RJ et al (2004) Evidence for spleen-specific uptake of a microbubble contrast agent: a quantitative study in healthy volunteers. Radiology 231:785–788
4. Peddu P, Shah M, Sidhu PS (2004) Splenic abnormalities: a comparative review of ultrasound, microbubble-enhanced ultrasound and computed tomography. Clin Rad 59:777–792
5. Abbott RM, Levy AD, Aguilera NS et al (2004) Primary vascular neoplasms of the spleen: radiologic–pathologic correlation. Radiographics 24:1137–1163

Contrast Media, Ultrasound, Applications in Kidney Tumor

Anders Nilsson
Department of Radiology, Ultrasound University, Uppsala University Hospital, Uppsala
anders.nilsson@akademiska.se

Synonyms

CEUS; Contrast-enhanced ultrasound of the kidneys

Definition

Contrast-enhanced ultrasound (CEUS) of the kidneys is mainly dependent on two things: (1) the availability of a contrast agent that will give off strong echoes, by reflection and resonance, and that can be injected intravenously and insonated without significant destruction of the contrast itself, and (2) ultrasound machine software that allows specific recognition of a signal/echo emanating from the contrast agent at an ultrasound output level that will not destroy the agent.

When these requirements are met, we can produce images where the echogenicity is dependent on the contrast agent concentration rather than on the reflectivity and absorption of the insonated tissue. Most contrast agents in clinical use today consist of stabilized gas bubbles, the resonance of which can be distinguished from tissue echoes by dedicated software implemented in the ultrasound machines. Ultrasound contrast agents are so-called ►*blood pool agents*; that is, they do not, in contrast to X-ray contrast media, leave the blood vessels.

Characteristics

Pathology

It is important to understand that the established phases of ultrasound contrast enhancement in the liver (1, 2) do not apply in the kidney because they are dependent on contrast accumulation in normal liver tissue. However, circulation in a capillary bed such as in the kidney is, of course, considerably slower than arterial flow. Because tumor tissue contain pathological vessels with ►*arteriovenous shunting*, it stands to reason that differences in the contrast uptake over time will be different in renal tumors than in normal renal tissue. Preliminary work suggests that the perfusion differences between tissues with a normal capillary bed and the ►*neovascularization* of tumors can be detected if the pattern of contrast enhancement is followed over time, either subjectively or with the aid of analyses programs, preferably built into the ultrasound machine itself (3).

Furthermore, areas completely without blood perfusion will remain dark in a contrast-based image, as no contrast agent will reach these areas. Therefore, images based on contrast concentration can help in the detection of nonperfused focal lesions like cysts, abscesses, infarctions, and post radio-frequency ablation necroses and in their differentiation from tumor tissue. Normal variants, like a ►*column of Bertin*, will have the same enhancement pattern as other normal parts of the renal parenchyma, which may help to make a more confident diagnosis.

Imaging

Normal Kidney

Different stages of renal enhancement exist but are not the same as those described in the liver due to both lack of contrast accumulation and the perfusion differences between the renal cortex and the medulla. The contrast phases must be understood in order to avoid misdiagnosis. The arteries enhance shortly after a bolus injection of contrast agent and are followed closely by a complete fill-in of the cortex. The pyramids, having less vascularity, then gradually enhance over the next 30–40 sec to become isoechoic or almost isoechoic with the cortex. The enhancement then decreases slowly as the contrast concentration in the general circulation falls off (Fig. 1). When this happens, a difference may again appear between the cortex and pyramids, the latter becoming once more hypoechoic. This reappearance of hypoechoic areas corresponding to the pyramids must be remembered because it has a likeness to the enhancement pattern seen in most malignant tumors (see below).

Cysts, Abscesses, and Infarctions

Because structures without perfusion will have no contrast uptake, they will have no brightness in the ultrasound contrast image; they will remain dark with an excellent delineation against surrounding tissues. Simple cysts will thus be unechoic during all the contrast phases even if they

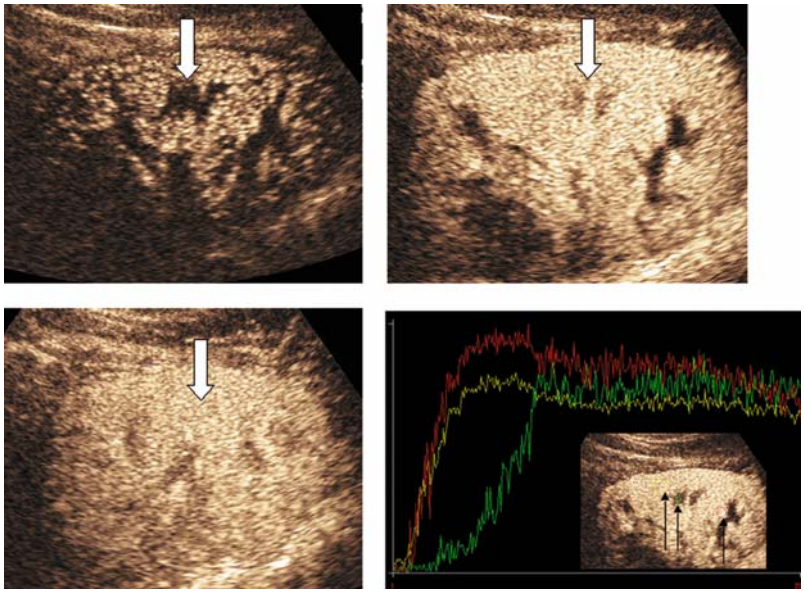

Contrast Media, Ultrasound, Applications in Kidney Tumor. Figure 1 Normal renal enhancement after an intravenous bolus of ultrasound contrast agent. The pyramids (*arrows*) enhance slower but show a complete fill-in after about 60 sec. This is also shown by the quantification graph where regions-of-interest have been placed in a segmental artery, cortex and a pyramid.

are echoic on native ultrasound. In this manner, smaller cysts can be detected and, more importantly, cysts containing echoes (e.g., after a bleeding) can be seen completely without perfusion. The spatial resolution of ultrasound can therefore be used for characterizing indeterminate focal lesions detected on computed tomography (CT), for example (4). New software programs have an excellent sensitivity for detecting even tiny amounts of contrast agents, which makes it possible to detect thin but perfused septae indicative of malignancy rather than simple cysts (Fig. 2).

Similarly, focal lesions that on native ultrasound contain echoes but have no perfusion, such as abscesses and cortical infarctions, can be detected and distinguished from perfused, possibly malignant lesions.

Tumors, Malignant

The contrast enhancement of small hypovascular tumors may be hard to detect on CT, making confident diagnosis of a renal cell carcinoma difficult. It is, of course, an important distinction that can often be made by CEUS, due to the high sensitivity to the presence of contrast agents, even in small quantities. Thus, tumoral vessels can be detected, possibly with the aid of quantification software that can prove an increase in image brightness, assisting the subjective assessment. In addition, small vessels may be depicted in mural nodules, septae, or thickened cyst walls even when they are too small to be detected by Doppler (5) (Fig. 2). Thus, CEUS may be used for evaluating unequivocal CT or magnetic resonance (MR) findings, atypical cysts, or cyst-like lesions with echogenic contents, the existence of contrast within the suspected areas being equivalent to the existence of vessels (i.e., perfused viable tissue).

In the same way, biopsies can be guided to viable areas of a suspected lesion, avoiding necrosis and thus improving the diagnostic yield (6).

Renal tumors often have a contrast enhancement pattern similar to the normal renal parenchyma in the early stages. There may be a rim enhancement in a pseudocapsule (7), but as there is no real accumulation of contrast in the kidneys, the detection rate of small tumors is unlikely to be as much improved by CEUS as is seen with focal liver lesions. However, the vasculature of malignant tumors differs from that of normal tissues, and early experiences indicate that contrast will be washed out of the neovasculature faster than from the renal capillaries, creating a similar but weaker equivalent to the situation in the liver, possibly helping characterization if not detection (8). Thus, malignant tumors tend to be hypoechoic compared with normal parenchyma in the later phases (Fig. 3). This could be helpful in evaluating normal variants, such as a prominent column of Bertin (see above). The suspected area must then be followed to the later stages of the contrast enhancement, at least for 1 min. Most often, a clear difference can be detected by

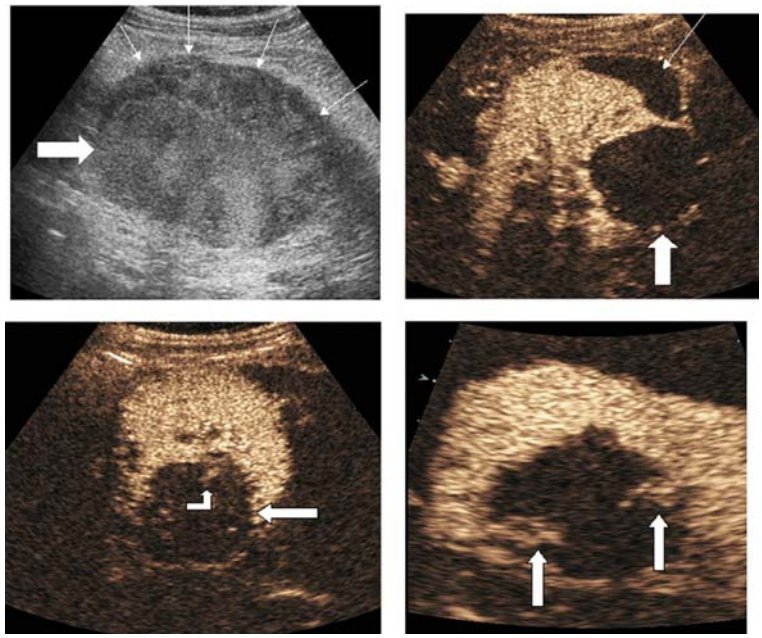

Contrast Media, Ultrasound, Applications in Kidney Tumor. Figure 2 Patient with sudden onset of pain in the right flank. Native ultrasound shows the kidney (*fat arrow*) surrounded by a hematoma (a). On CEUS the hematoma is better delineated (*thin arrow*) and a cyst is seen, probably haemorrhagic as it was not detected on B-mode (b). CEUS also detects small contrast enhancing nodules (*arrows*) within the cyst (c, d). A cystic renal cell carcinoma was later removed.

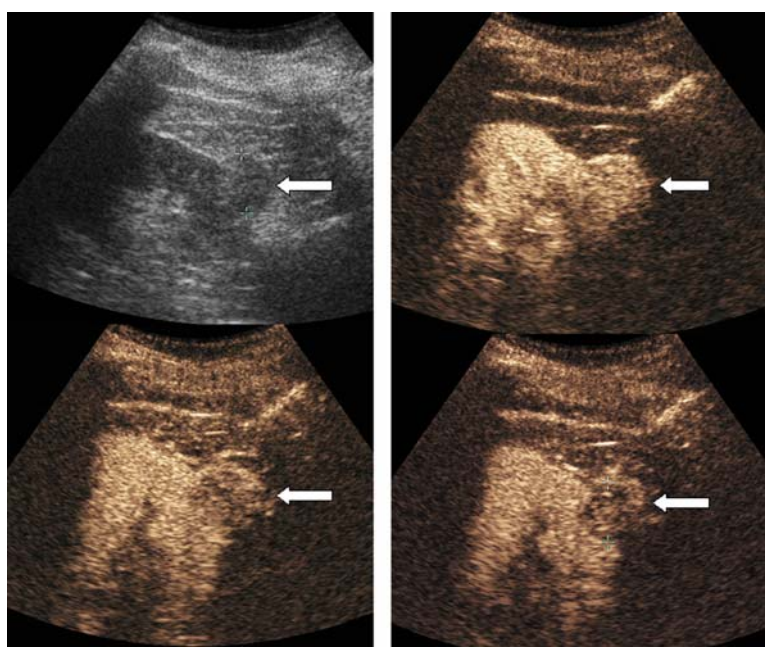

Contrast Media, Ultrasound, Applications in Kidney Tumor. Figure 3 Small renal cell carcinoma seen both on B-mode (a) and CEUS with a contrast enhancement typical of most malignant lesions, i.e. almost isoechoic with the normal parenchyma in the early stages (b = 15 sec) and then increasingly hypoechoic compared to the kidney (c = 30 sec, d = 60 sec).

analysis software at that stage and seen subjectively shortly thereafter. Necrotic areas of the tumor will remain dark, but because partially necrotic tumors tend to be large, they are easily diagnosed on native ultrasound. The detection of necroses is, therefore, of limited importance except as guidance for biopsies.

Tumors, Benign

Vessel anatomy may eventually help distinguish malignancies from benign oncocytomas, but at present, there is not enough scientific evidence to allow us to make that distinction. Lesions such as angiomyolipomas have been shown to enhance less than renal cell carcinomas in the arterial phase (9) and tend to retain the contrast better than a malignant tumor in the later phases, presumably due to vessel anatomy. However, knowledge about how a small, highly differentiated malignant tumor would behave is limited, and differentiation in the individual patient remains difficult.

Diagnosis

It is important to remember that even though the accumulated experience so far indicates that malignant tumors are hypoechoic in the later contrast stages, it cannot be inferred that a lesion that retains contrast is benign. There are as yet no scientific data proving an ability to differentiate between benign and malignant focal lesions, but with improved knowledge of contrast enhancement patterns, this ability may be only a matter of time.

Even though the detection rate of small renal cell carcinomas is unlikely to be improved, CEUS can play an important role in characterizing atypical lesions, detecting small nodules in cystic tumors, and differentiating them from normal variants.

Bibliography

1. Wilson SR, Burns PN, Muradali D et al (2000) Harmonic hepatic US with microbubble contrast agent: initial experience showing improved characterisation of haemangioma, hepatocellular carcinoma and metastasis. Radiology 215:153–161
2. Albrecht T, Hoffmann CW, Schmitz SA et al (2001) Phase inversion sonography during the liver specific late phase of contrast enhancement: improved detection of liver metastases. Am J Roentgenol 176:1191–1198
3. Cosgrove D, Eckersley R, Blomley M et al (2002) Quantification of Blood Flow. Ultrasound. ECR Categorical Course Syllabus. Springer, Berlin Heidelberg New York, pp 84–90
4. Correas JM, Claudon M, Tranquart F et al (2003) Contrast-enhanced ultrasonography: renal applications. J Radiol 84:2041–2054
5. Ascenti G, Zimbaro G, Mazziotti S et al (2001) Usefulness of power Doppler and contrast-enhanced sonography in the differentiation of hyperechoic renal masses. Abdom Imaging 26:654–660
6. Krause J, Nilsson A (2003) Targeted tumor biopsy under contrast-enhanced ultrasound guidance. Eur Radiol 13(Suppl 4):L239–L240
7. Ascenti G, Gaeta M, Magno C et al (2004) Contrast-enhanced second-harmonic sonography in the detection of pseudocapsule in renal cell carcinoma. Am J Roentgenol 182(6):1525–1530
8. Quaia E, Siracusano S, Bertolotto M et al (2003) Characterization of renal tumours with pulse inversion harmonic imaging by intermittent high mechanical index technique: initial results. Eur Radiol 13(6):1402–1412
9. Siracusano S, Quaia E, Bertolotto M et al (2004) The application of ultrasound contrast agents in the characterization of renal tumors. World J Uro 22(5):316–322

C

Contrast Media, Ultrasound, Applications in Transcranial and Intra-Operative Brain Ultrasound

Thilo Hoelscher
Department of Radiology
University of California, San Diego, USA
thoelscher@ucsd.edu

Synonym

Contrast-enhanced ultrasound imaging of the brain

Definition

Transcranial Doppler describes the assessment of flow velocities of intracranial vessels by interpretation of flow spectra while insonating through the intact skull. Other than Doppler flow measurements alone, duplex sonography enables one to combine the visualization of morphological structures with flow velocity assessment using Doppler. Transcranial duplex sonography of the adult brain was introduced in the early 1990s and has been used since then mainly to visualize and assess the circle of Willis. Signal absorption and phase aberration due to insonation through the bone limit the applicability. The introduction of ultrasound contrast agents (UCA) and the development of contrast-specific imaging techniques have improved vascular imaging of the brain significantly. To date, contrast-enhanced ultrasound of the brain includes transcranial macro- and microvascular imaging and assessment as well as intraoperative and therapeutic applications. In this context, the term transcranial Doppler is established and commonly used, whereas new technologies and applications broaden the spectrum of brain ultrasound, exceeding the definition of transcranial Doppler.

Imaging

Macrovascular Imaging

The visualization and assessment of intracranial arteries (circle of Willis) are the domain of transcranial color-coded duplex sonography (TCCS). The main difference compared with conventional transcranial Doppler (TCD) is the color-coded representation of arterial blood flow to allow the unequivocal identification of the circle of Willis within the anatomic grayscale (B-mode) image of the brain parenchyma. Using the Doppler mode, the blood flow can be analyzed semiquantitatively, as in conventional TCD, but with the added advantage of visual control by tracking the target vessel using the color flow map. The major limitation of all transcranial ultrasound techniques has been the massive acoustic signal absorption while insonating through the intact skull. The introduction of UCA improved transcranial vascular imaging significantly, and the diagnostic benefits have been proven in multiple studies (1, 2). Besides the unequivocal advantages of UCA for transcranial ultrasound imaging, contrast-specific artifacts such as "blooming" may limit the diagnostic impact. Strong acoustic signals, encoded as color pixels on the screen, may appear "outside" the anatomical delineation of the vessel, especially in the early phase after UCA injection. The enhancement appears as an overamplification of the color or power Doppler signals on the screen of the ultrasound equipment (Fig. 1). Due to the rapidly increasing knowledge of the acoustic properties of UCA, contrast-specific modalities have been developed to improve transcranial image quality. To date, UCA-specific imaging enables one to visualize intracranial arteries in an angiography-like pattern with higher spatial resolution, fewer artifacts, and lower acoustic output power (Fig. 2) (3). Clinically, contrast-enhanced transcranial ultrasound has the highest impact on stroke diagnosis. The fast and unequivocal assessment of vessel occlusion/patency in the emergency room, or even in the ambulance, may help to optimize the therapeutic strategy for the individual stroke patient.

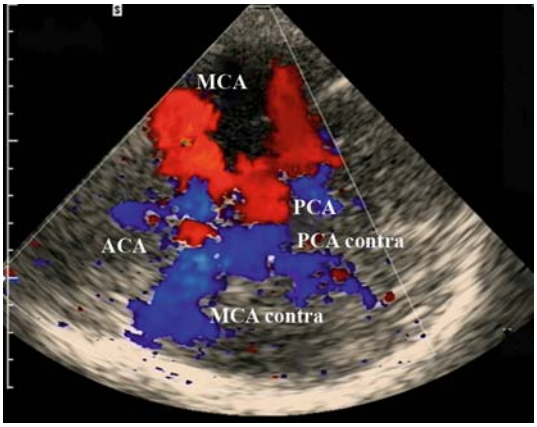

Contrast Media, Ultrasound, Applications in Transcranial and Intra-Operative Brain Ultrasound. Figure 1 "Blooming" artifact contrast-enhanced transcranial ultrasound of the circle of Willis (axial scanning plane *via* the temporal bone window). Vessel delineation is diminished because of the strong contrast signal ("blooming") after intravenous bolus injection of the UCA. *Lighter area* coding represents flow toward the transducer, *darker area* coding flow away from it. MCA: middle cerebral artery, MCA contra: middle cerebral artery contralateral, PCA: posterior cerebral artery, PCA contra: posterior cerebral artery contralateral, ACA: anterior cerebral artery.

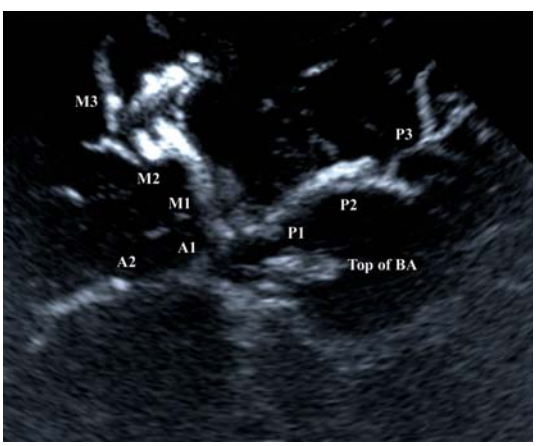

Contrast Media, Ultrasound, Applications in Transcranial and Intra-Operative Brain Ultrasound. Figure 2 Transcranial ultrasound angiography (tUSA) tUSA image of the circle of Willis and its branches after UCA injection. M1, M2, M3: middle cerebral artery segments, A1, A2: anterior cerebral artery segments, P1, P2, P3: posterior cerebral artery segments, BS: brain stem, Top of BA: hyperechogenic distal part of the basilar artery.

Microvascular Imaging

Contrast-specific transcranial ultrasound imaging modalities to assess the parenchymal brain perfusion are mainly based on UCA destruction, due to the high acoustic power used for insonation through the intact skull. Most perfusion techniques applied in brain ultrasound are based on the fact that UCA microbubbles undergo destruction, splitting, and fusion at higher acoustic pressures. These broadband noises partially pass the wall filter used in color and power Doppler and, due to the Doppler shift are interpreted as flow signals, independent of the movement of microbubbles. Three main principles of destructive imaging techniques to assess parenchymal perfusion can be described: (a) bolus kinetic, (b) depletion, and (c) replenishment methods.

Most commonly, the bolus kinetic technique is used to describe the wash-in/wash-out behavior of the UCA after intravenous bolus injection. After data acquisition over time in a predefined scanning plane and using a low frame rate, regions of interests (ROI) are placed in dedicated anatomical areas (Fig. 3). The interpretation of parameters such as signal peak intensity or time to peak intensity is used to semiquantify perfusion patterns and to differentiate between normal (4) or disturbed perfusion (5). Contrast-enhanced brain perfusion

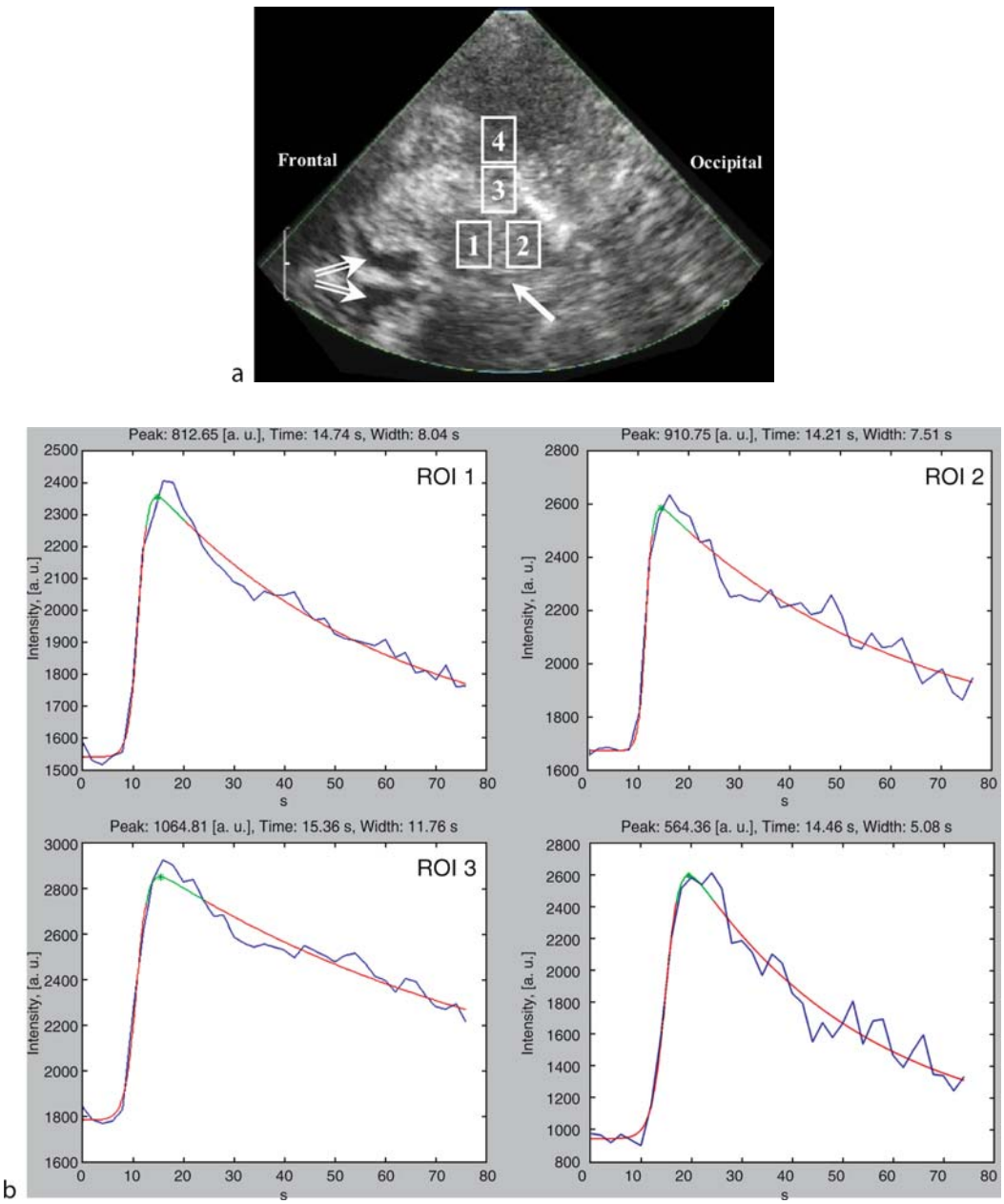

Contrast Media, Ultrasound, Applications in Transcranial and Intra-Operative Brain Ultrasound. Figure 3 Time intensity curves of certain ROIs (a) Axial B-mode image of the diencephalic scanning plane. Visualization of the third (*white arrow*) and the lateral (*dashed white arrows*) ventricles. Projection of the parenchymal ROIs: anterior parts of the thalamus (1), posterior parts of the thalamus (2), lentiform nucleus (3), white matter (4). (b) Corresponding time intensity curves displaying the wash-in/wash-out behavior of the UCA over time in certain ROIs.

imaging achieves clinical importance predominantly in the acute stroke setting and for monitoring the therapeutic effect of thrombolysis (6). Early as well as subsequent information about the microvascular status in the presence or absence of intracranial vessel occlusion may help to optimize the individual therapeutic strategy and extend the therapeutic window for thrombolysis.

Intraoperative Applications

The intraoperative application of ultrasound during neurosurgical interventions has been shown in several studies (7). Although intraoperative magnetic resonance imaging (MRI) and computed tomography (CT) have undoubted benefits, the techniques are costly and therefore not commonly available. In comparison, ultrasound is cost-effective, easy to use, and the only true real-time imaging method. The main goals of intraoperative imaging with ultrasound are the localization of and the navigation to lesions (i.e., tumor, aneurysm, arteriovenous malformation), the assessment of the vascular supply of these pathologies, and the ability to immediately monitor the success of the neurosurgical intervention. The intraoperative use of UCA is of interest, especially in the context of advanced transducer technologies and contrast-specific imaging modalities. To date, vascular structures in the submillimeter range (~100 μm) can be displayed. Single UCA microbubbles can be visualized and tracked, enabling the study of real-time flow dynamics in intracranial aneurysms (Fig. 4). The use of UCA facilitates intraoperative real-time navigation and assessment of the intra- and peritumoral vasculature (8) as well as of aneurysms or arteriovenous malformations. Moreover, the immediate monitoring of the surgical intervention helps to optimize the neurosurgical case management in the operating room.

Interventional Radiological Treatment

Therapeutic Applications

Ultrasound therapy is currently a challenging research field. Therapeutic approaches are mainly based on the well-known physics of ultrasound such as heating or cavitation. Less well known are the biomechanical effects of ultrasound, such as sonothrombolysis or sonoporation.

Sonothrombolysis

Recent studies have demonstrated that ultrasound enables temporary disaggregation of the fibrin structure of thrombotic blood clots and improvement of the enzyme activation of plasminogen in the presence of tissue plasminogen activator (9, 10). Enhanced clot lysis is the key factor for successful stroke therapy. Recombinant tissue plasminogen activator (rt-PA) is currently the only Food and Drug Administration (FDA)-approved drug for acute stroke therapy. To enhance the therapeutic effect of rt-PA in stroke patients with transcranial ultrasound is challenging and the first clinical studies are promising (11). Besides the increasing knowledge of the acoustic properties of UCA microbubbles for diagnostic purposes, their potential as targeted drug carriers for therapeutic applications is of special interest. Specific targeting of thrombotic emboli with UCA as well as rt-PA binding to microbubbles is feasible and the *in vivo* applicability has

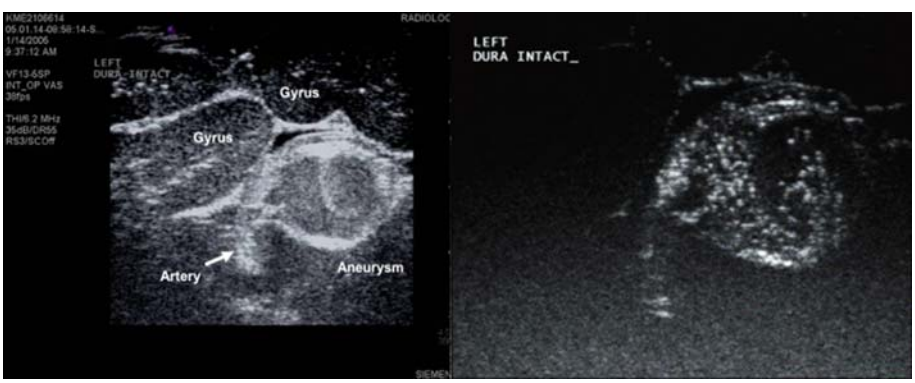

Contrast Media, Ultrasound, Applications in Transcranial and Intra-Operative Brain Ultrasound. Figure 4 Intraoperative aneurysm On the left: Precontrast, the morphology of the aneurysm is visualized in an oblique view through the intact dura mater, posterior to two gyri. The feeding artery can be seen on the left of the aneurysm as a hyperechogenic band (*arrow*). On the right: After contrast injection, acoustic signals from single microbubbles can be visualized as white spots, entering the aneurysm sac in an early systolic phase.

been proven (12). The future goal of transcranial ultrasound in stroke patients is to use clot-targeted rt-PA carrying microbubbles and to enhance thrombolysis with ultrasound while monitoring the therapeutic effect, using the same device.

Sonoporation

Besides sonothrombolysis, ultrasound-mediated gene transfection has opened a new therapeutic avenue. Although the mechanisms are poorly understood, it is evident that ultrasound has the ability to produce nondestructive, transient pores into cell membranes (13), thus enabling the uptake of higher-molecular-weight substances like oligonucleotides. Ultrasound-mediated local gene delivery in tumors (i.e., antisense TGF-β) or tumor-associated neovascularization (i.e., antisense VEGF) is the focus of research (12). Further potential applications are neointimal hyperplasia after arterial balloon injury and gene delivery to infarcted myocardial tissue. The impact of UCA microbubbles in these scenarios is defined by the feasibility of tissue targeting, their use as carriers of genetic sequences, and the positive effect on sonoporation. The future outlook of local drug and gene delivery to treat brain tumors or to enhance neuronal stem cell activity (unpublished data) in neurodegenerative diseases or stroke using acoustically active carriers in combination with brain ultrasound is challenging and remains experimental to date.

Bibliography

1. Bogdahn U, Frohlich T, Becker G et al (1994) Vascularization of primary central nervous system tumors: detection with contrast-enhanced transcranial color-coded real-time sonography. Radiology 192:141–148
2. Gerriets T, Goertler M, Stolz E et al (2002) Feasibility and validity of transcranial duplex sonography in patients with acute stroke. J Neurol Neurosurg Psychiatry 73:17–20
3. Hölscher T, Wilkening WG, Lyden PD et al (2005) Transcranial ultrasound angiography (tUSA): A new approach for contrast specific imaging of intracranial arteries. Ultrasound Med Biol 31:1001–1006
4. Hölscher T, Wilkening W, Draganski B et al (2005) Transcranial ultrasound brain perfusion assessment with a contrast agent-specific imaging mode. Results of a 2-center trial. Stroke 36:2283–2285
5. Postert T, Federlein J, Weber S et al (1999) Second harmonic imaging in acute middle cerebral artery infarction. Preliminary results. Stroke 30:1702–1706
6. Eyding J, Krogias C, Schollhammer M et al (2006) Contrast-enhanced ultrasonic parametric perfusion imaging detects dysfunctional tissue at risk in acute MCA stroke. J Cereb Blood Flow Metab;26(4):572–82
7. Woydt M, Vince GH, Krauss J et al (2001) New ultrasound techniques and their application in neurosurgical intra-operative sonography. Neurol Res 23:697–705
8. Kanno H, Ozawa Y, Sakata K et al (2005) Intraoperative power Doppler ultrasonography with a contrast-enhancing agent for intracranial tumors. J Neurosurg 102:295–301
9. Braaten JV, Goss RA, Francis CW (1997) Ultrasound reversibly disaggregates fibrin fibers. Thromb Haemost 78:1063–1068
10. Devcic-Kuhar B, Pfaffenberger S, Gherardini L et al (2004) Ultrasound affects distribution of plasminogen and tissue-type plasminogen activator in whole blood clots *in vitro*. Thromb Haemost 92:980–985
11. Alexandrov AV, Molina CA, Grotta JC et al (2004) Ultrasound-enhanced systemic thrombolysis for acute ischemic stroke. N Engl J Med 351:2170–2178
12. Unger EC, Matsunaga TO, McCreery T et al (2002) Therapeutic applications of microbubbles. Eur J Radiol 42:160–168
13. Tachibana K, Uchida T, Ogawa K et al (1999) Induction of cell-membrane porosity by ultrasound [letter]. Lancet 353:1409

C

Contrast Media, Ultrasound, Applications in Vesico-ureteral Reflux

Kassa Darge
Department of Pediatric Radiology, Institute of Radiodiagnostic, Bavarian Julius-Maximilians-University Wuerzburg, Wuerzburg, Germany
darge@roentgen.uni-wuerzburg.de

Synonyms

Contrast-enhanced voiding urosonography (VUS); Contrast-enhanced reflux sonography

Definition

►Voiding urosonography (VUS) is an ultrasound (US) examination of the bladder, ureters, and kidneys (± urethra) utilizing intravesically administered US contrast media with the primary purpose to exclude or diagnose reflux into the ureters and pelvi-calyces. ►Vesicoureteral reflux (VUR) a common pediatric problem can, particularly in the presence of urinary tract infection (UTI), result in renal damage and consequently renal function impairment and hypertension. Three different imaging modalities are currently employed for the diagnosis of VUR. The two radiologic modalities, ►voiding cystourethrography (VCUG) and ►radionuclide cystography (RNC) have been in use for several decades. Since the mid-90s the modality without radiation exposure, VUS, has become available as a further diagnostic option for VUR (1).

Indication

Evolvement of US for Diagnosis of VUR

In 1976, the first report appeared on the use of US for the diagnosis of VUR. Further attempts to implement US for reflux diagnosis in children have been underway in two directions (1). The indirect methods were based on the US of the urinary tract, without administration of any kind of substance into the bladder. These included depicting various sonomorphologic changes of the urinary tract as a result of VUR, detecting newly appearing or an increase in existing ureteral or pelvicalyceal dilatation and assessing ureteric jet changes with duplex and color Doppler. The direct means used to diagnose VUR involved instilling various substances intravesically. The most frequently administered fluid was physiological saline solution. The ballooning of the renal pelvis during the filling of the bladder represented the criterion for diagnosis of VUR. Application of air bubbles, by shaking the normal saline before administration or adding carbon dioxide, had also been tried. US studies were also carried out, in which the empty bladder was solely filled with air. In addition to low diagnostic accuracy, all the above methods have major limitations making them impractical for use in routine imaging.

Diagnosis of VUR Using US Contrast Media

The use of an US contrast agent consisting of sonicated albumin (Albunex; Molecular Biosystems, San Diego, USA) for the diagnosis of VUR in a child was reported in 1994 from Japan (1). Utilizing the same US contrast medium, another study compared VUS with both VCUG and RNC in a small group of patients. The sensitivity was found to be 64% and 86% in comparison to VCUG and RNC, respectively. In both cases, the specificity was 100% (1). A further US contrast medium used in the past was a galactose-based microbubbles-containing agent (Echovist, Schering, Berlin, Germany). The comparison of VCUG with VUS using this US contrast medium showed high diagnostic concordance. However, its very short imaging window of approximately 5 min hindered its routine use (1). The "breakthrough" in the US diagnosis of reflux in children came about in the mid-90s with the availability of US contrast agents containing stabilized microbubbles. The US contrast medium Levovist (Schering, Berlin, Germany) was the first of such contrast agents that became available for clinical use in Europe. It is a galactose-based contrast agent that contains microbubbles stabilized with a layer of palmitic acid. The inherent properties of the US contrast medium, resulting in long echo enhancement duration of more than half-an-hour and relatively dense and homogeneous echoes make the search and detection of VUR much easier. In a large number of studies incorporating hundreds of children, the diagnostic accuracy of VUS with the use of Levovist has been compared with that of VCUG (1–4). There is a significant correlation between the two imaging modalities with the concordance rate ranging from 89–97% and more refluxes being detected in the VUS (approximately 10%) (4). Moreover, up to 90% of grade I refluxes in the VCUG are found to be grade II or higher in the VUS (3).

Selection Criteria for VUS

There are mainly two indications for performing a reflux examination in a child: (1) UTI (pyelonephritis) and (2) dilatation of a ureter or renal pelvis. It should be noted that there is a wide variation in practice among all those involved in the diagnosis and management of children with VUR. Consequently, the criteria for the selection of an imaging modality for reflux entail the adaptation to local practices. Currently, the most common criteria applied for performing a VUS or a VCUG as the primary diagnostic modality area are as follows: (a) VUS selection criteria: (i) follow-up examinations, (ii) first examination for VUR in girls, (iii) screening high-risk patients; (b) VCUG selection criteria: (i) first examination for VUR in boys, (ii) specific request for urethral and/or bladder imaging, (iii) inadequate visualization of the bladder or one of the kidneys on US. The selection criteria for RNC are usually as those for VUS.

Contraindication

There are no absolute contraindications for administering the US contrast medium, Levovist, intravesically. Galactosemia, a contraindication for the intravenous administration, is only a relative contraindication. The inability to visualize, for whatever reason, the bladder or one of the kidneys on US excludes the performance of a VUS.

Pregnancy/Lactation

There are no reports regarding the intravesical administration of US contrast media for reflux examination during pregnancy or lactation.

Use and Dosage

VUS Procedure

The VUS examination incorporates four basic steps (2, 3):

1. Precontrast examination: standard US of the urinary tract in supine (±prone) positions.

2. Catheterization or suprapubic puncture of the bladder under sterile condition and administration of normal saline and the US contrast medium.
3. Postcontrast examination: a repeat of the standard US of the urinary tract.
4. Postcontrast voiding examination: US of the renal pelves and terminal ureters (±urethra) during and after micturition.

The necessity and extent of the precontrast examination is determined by the availability of a current US examination of the urinary tract and the type of US imaging modality being used. It is crucial that the normal saline instilled into the bladder is not from a container sealed under vacuum. All plastic containers are not sealed under vacuum but almost all glass containers. The normal saline in the latter is desaturated and the air in the microbubbles diffuses very rapidly in the solution with the consequence of fast decrease of echo-enhancement. The contrast medium is administered slowly into the bladder under sonographic monitoring. Reflux is diagnosed when echogenic microbubbles are detected in the ureters or pelvi-calyces. During the postcontrast examinations, the right and left renal pelves are scanned alternatively. The scan during voiding can be carried out when the patient is lying or sitting on a pan or standing and voiding into a urine bottle. The severity of reflux is graded in a similar manner as the international reflux grading system in VCUG from grade I to V. Comparative studies have shown the high concordance rate of over 85% between the reflux grading system in VCUG and VUS (1, 3).

VUS Imaging Modalities

Depending on the availability, different US imaging modalities are employed in VUS to depict the refluxing microbubbles. These imaging options not only affect the conspicuity of the microbubbles but also the overall diagnostic accuracy of the examination. The most widely employed modality for VUS is conventional (=fundamental) US. This can be combined with color Doppler to enhance the detection of reflux. A recent innovation in US and one with major impact on the application of US contrast media is harmonic imaging. When using harmonic imaging for VUS not only do the microbubbles become strikingly conspicuous compared to fundamental mode but also the sensitivity is significantly increased (Fig. 1) (5). Furthermore, it is possible to visualize intrarenal reflux. Advanced contrast-specific imaging modalities tuned for individual contrast medium, e.g., agent detection imaging (Sequoia, Siemens, Issaquah, USA) have brought about a profound improvement in detecting refluxing microbubbles. The microbubbles are not only enhanced and color-coded but it is also possible to visualize only the refluxing microbubbles blocking out the background gray-scale image (Figs. 2, 3).

Dosage of US Contrast Media for VUS

Currently, the US contrast medium Levovist is the most widely used and the one approved for use in VUS. The concentration of Levovist used for VUS is 300 mg/mL. The dose administered depends on the imaging modality being employed. For fundamental US, the volume of Levovist administered is 5–10% of the filling volume of the bladder (1–3). In case of harmonic imaging or advanced contrast-specific imaging modalities 3–5% of the filling volume of the bladder suffices, i.e., for one cycle of examination just one 2.5-g flask of Levovist will be adequate (5). Recently, a second-generation US contrast agent, SonoVue (Bracco, Milan, Italy), has become

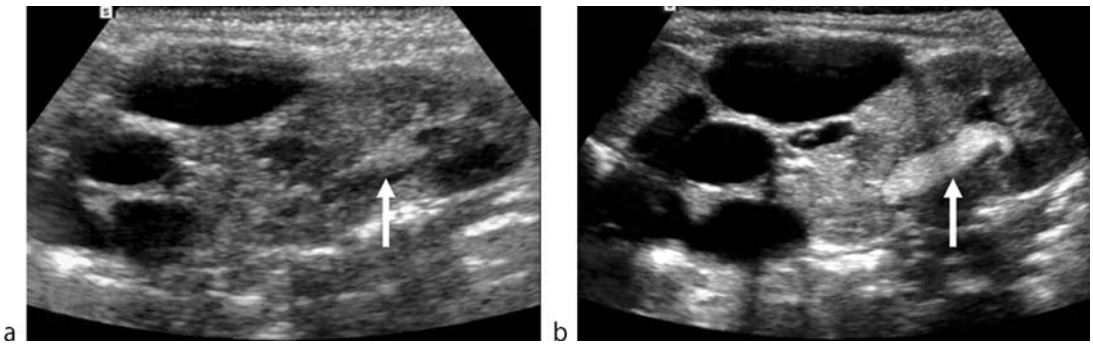

Contrast Media, Ultrasound, Applications in Vesico-ureteral Reflux. Figure 1 Longitudinal scan of a duplex kidney with a multicystic dysplastic upper moiety from ventral after intravesical administration of the US contrast medium Levovist in (a) fundamental and (b) harmonic imaging modalities. The refluxing microbubbles in the lower moiety (arrow) are more conspicuous in the harmonic imaging modality (b).

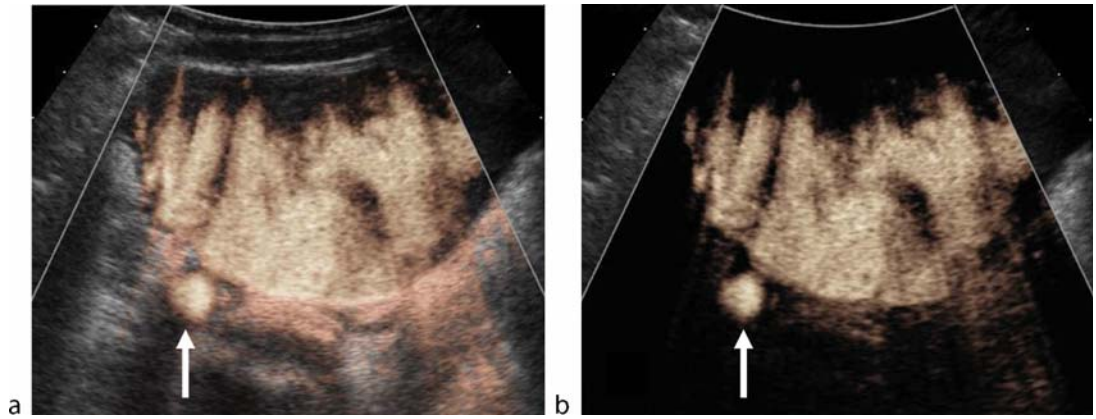

Contrast Media, Ultrasound, Applications in Vesico-ureteral Reflux. Figure 2 Transverse section of the bladder and dilated right terminal ureter (arrow) after intravesical administration of the US contrast medium Levovist using an advanced contrast-specific imaging modality (agent detection imaging). Note the reflux in the right terminal ureter without (a) and after (b) blocking the background gray-scale image.

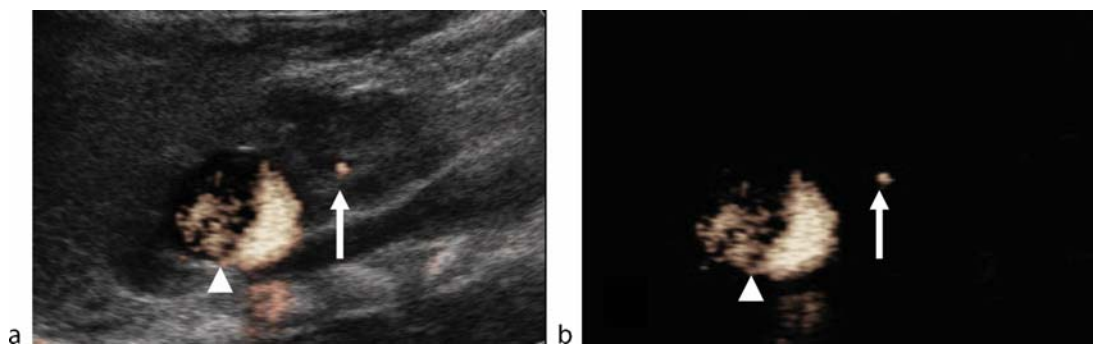

Contrast Media, Ultrasound, Applications in Vesico-ureteral Reflux. Figure 3 Longitudinal section of a duplex kidney from ventral after intravesical administration of the US contrast medium Levovist using an advanced contrast-specific imaging modality (agent detection imaging). Note the reflux in both moieties (arrowhead—upper, arrow—lower) without (a) and after (b) blocking the background gray-scale image.

available in Europe. Preliminary comparative studies have revealed that the dose of this contrast medium for intravesical use is less than 1% of the bladder filling (1). This has a huge potential in the future not only in reducing the amount of contrast medium necessary for an examination but also in markedly lowering the cost for a VUS.

Adverse Reactions

There are no reports of adverse reactions with regard to intravesical instillation of US contrast media, in particular of Levovist.

Interactions

No interactions of intravesically administered US contrast media have been reported.

References

1. Darge K, Riedmiller H (2004) Current status of vesicoureteral reflux diagnosis. World J Urol 22:88–95
2. Darge K, Troeger J, Duetting T et al (2001) Reflux in young patients: comparison of voiding US of the bladder and retrovesical space with echo enhancement versus voiding cystourethrography for diagnosis. Radiology 210:201–207
3. Berrocal T, Gaya F, Arjonilla A et al (2001) Vesicoureteral reflux: diagnosis and grading with echo-enhanced cystosonography versus voiding cystourethrography. Radiology 221:359–365

4. Valentini AL, De Gaetano AM, Destito C et al (2002) The accuracy of voiding urosonography in detecting vesico-ureteral reflux: a summary of existing data. Eur J Pediatr 161:380–384
5. Darge K, Zieger B, Rohrschneider W et al (2001) Contrast-enhanced harmonic imaging for the diagnosis of vesicoureteral reflux. AJR 177:1411–1415

Contrast Media, Ultrasound, Commercial Products

Christian Greis
Bracco ALTANA Pharma GmbH, Clinical Development Ultrasound Contrast Agents, Konstanz, Germany
christian.greis@altanapharma.com

Synonyms

Echo enhancers; Sonographic contrast agent; Sonographic signal enhancers; Ultrasound contrast agents; Ultrasound contrast media; Ultrasound signal enhancers

Definition

An ultrasound contrast medium is a compound that increases the contrast of an ultrasound image. This is obtained by increasing (or decreasing) the echogenicity of a particular compartment within the body. Usually, an ultrasound contrast agent is injected into a blood vessel resulting in an increased echogenicity of the blood and thus in an increased *contrast between blood and tissue*. The currently commercially available ultrasound contrast agents contain ►micro-bubbles with a diameter of a few µm, which consist of an echogenic gas surrounded by a shell for stabilisation. Due to the size of the micro-bubbles, such ultrasound contrast agents are ►blood pool agents not leaving the vascular system. Ultrasound contrast agents of the first generation contain air inside, whereas agents of the second generation contain a gas with low solubility in water (or blood) giving the micro-bubbles a higher stability and longer persistence.

Indication

Currently, there are three major indications described for ultrasound contrast agents:

1. Echocardiography including *left ventricular opacification* (LVO) with the aim to improve *endocardial border delineation* (EBD) and *myocardial contrast echocardiography* (MCE) with the aim to demonstrate and quantify myocardial perfusion,
2. Vascular *Doppler* ►*enhancement* with the aim to overcome insufficient signal-to-noise ratio, especially to obtain higher accuracy in low-flow, no-flow and/or slow-flow conditions,
3. *Sonography of parenchymatous organs* with the aim to detect abnormal vascularity and perfusion.

Not all agents on the market have regulatory approval for all the three indications. To obtain regulatory approval, a significant clinical benefit has to be demonstrated in addition to the sole existence of a contrast effect. In other words, the contrast enhancement should result in diagnostic confidence and not in confusion.

There is a significant difference in the perception of the clinical benefit of contrast enhancement between Europe and the United States. In the United States, the clinical value of contrast enhancement is only recognised for echocardiography and accordingly this is the only indication for ultrasound contrast agents approved by the FDA. In Europe, both echocardiography and vascular/extra-cardiac sonography are accepted indications for contrast enhancement and there are agents with regulatory approval for all the three indications mentioned earlier.

Echocardiography

The improvement of the endocardial border delineation of the heart cavities was the first indication for ultrasound contrast agents. Due to a limited signal-to-noise ratio of the non-digital ultrasound scanners in the early 1990s, the cardiac cavities often appeared not well delineated but obscured by noise signals and signal dropouts in the cardiac wall. Opacification of the blood in the heart cavities resulted in a marked improvement of the endocardial border delineation, allowing a much more reliable determination of *cardiac volumes* and *wall motion*. Even with up-to-date high-end scanners, this clinical advantage is evident (due to the elimination of obscuring echoes from the trabecular structures), as shown in recent controlled multicenter studies (1).

Using recent generations of ultrasound scanners with ►*contrast-specific imaging* modalities (2), the blood distribution can be demonstrated not only in the cavities but also in the micro-vasculature of the myocardium. For this indication called myocardial contrast echocardiography, it is necessary to separate the signals coming from the blood (contrast agent) and those coming from the tissue. This is done by the contrast mode software of the scanner. The visibility and distribution of the contrast enhancement in the myocardium is obvious. However, the evidence for the clinical value of this information has still to be

established and is evaluated in numerous clinical research programs currently ongoing. Up to now, none of the agents available has obtained regulatory approval for the myocardial perfusion indication.

Vascular Imaging

The most sensitive method for vascular imaging is *Doppler sonography*. The demonstration of blood with Doppler sonography is based on the movement of blood cells with a certain velocity (higher than the wall motion velocity) towards or away from the transducer. In some cases, only an insufficient Doppler signal can be obtained, mainly when the blood volume is very small (e.g. in high-grade stenoses) or the vessels are behind highly echogenic structures (e.g. in transcranial Doppler sonography). In such cases, the enhancement of the echogenicity of the blood by an ultrasound contrast agent allows in nearly all cases the demonstration of an adequate flow signal (3).

Parenchymal Vascularity and Perfusion

There is a general limitation for Doppler sonography: it does not work in case of nearly stationary blood (e.g. in capillaries) or indeterminate flow direction (e.g. in complex vascular structures), as found in parenchymal structures or focal lesions. The adequate demonstration of blood in the *micro-vasculature* requires a velocity-independent separation of signals from blood and tissue, which can be obtained during contrast enhancement by the contrast-specific elements in the signal. Using this principle, the micro-vascular distribution and geometry can be demonstrated in B-mode with high spatial resolution and without any movement artefacts. Furthermore, when injected as bolus injection the contrast agent can be used as *tracer* to evaluate the dynamic wash-in and wash-out in the tissue, allowing the assessment of parenchymal *perfusion*. For detection and characterisation of focal liver lesions, the clinical benefit of micro-vascular perfusion assessment has already been demonstrated (4) and the use of contrast enhancement is recommended in respective guidelines (5, 6). Fore some other organs, clinical research programs are still ongoing to establish the clinical value of perfusion assessment for diagnosis or therapeutic monitoring. In Europe, some of the agents available obtained already regulatory approval for micro-vascular imaging.

Commercial Products

Echovist is a 'right heart' contrast agent, i.e. an agent which is not stable enough to survive the pulmonary passage after intravenous injection. The active ingredient of Echovist is Galactose micro-particles containing air. The agent is available in two concentrations with 200 and 300 mg/mL micro-particles in the final suspension. Echovist has been approved in 1991 for the examination of the right heart and venous system and for hysterosalpingo-contrast-sonography after transcervical injection. Echovist is marketed by Schering in Germany and UK.

Levovist is an improved formulation of Echovist, also containing Galactose micro-particles with air but coated with palmitic acid, making the micro-particles more stable. Levovist micro-particles survive the pulmonary circulation and allow the enhancement of the whole circulation. The agent can be prepared in different concentrations (200, 300 and 400 mg/mL micro-particles in the final suspension). In 1995, Levovist has been approved in Germany and until now in more than 40 countries including most European countries, Canada, China and Japan. Levovist obtained regulatory approval for Doppler enhancement including diagnosis of cardiac, vascular and tumour diseases and for diagnosis of vesiculo-ureteral reflux after transurethral injection. Levovist is marketed by Schering.

Albunex has been the first transpulmonary agent on the market, approved 1993 in Japan and 1994 in the United States. It consists of human albumin coated micro-bubbles containing air. In the meantime, Albunex has been replaced by Optison.

Optison contains also human albumin coated micro-bubbles, but containing octafluoropropane gas (perflutren), making the micro-bubbles more stable. The gas concentration is 0.19 mg/mL solution. Optison is the first 'second-generation' contrast agent using gas with low solubility in water to increase stability and persistence. Like Albunex, Optison has been developed only for echocardiography (left ventricular opacification) and obtained first approval in 1998 in the United States and later also in most European countries. Developed by Molecular Biosystems, Optison is marketed now after several transitions by GE Healthcare.

SonoVue consists of sulphurhexafluoride micro-bubbles surrounded by a flexible phospholipid shell. The final solution contains 8 μL/mL SF_6 gas, which is enough to obtain an enhancement of several minutes in the whole vascular system. SonoVue has been approved by the EU medical agency in 2001 for a broad range of indications, including echocardiography (left ventricular opacification), (macro-)vascular Doppler enhancement and assessment of vascularity in focal lesions in liver and breast (micro-vascular enhancement). SonoVue is marketed by Bracco in cooperation with several partners in Europe and China.

Definity consists of octafluoropropane (perflutren) micro-bubbles, surrounded by a phospholipid shell. The final solution contains 150 μL/mL C_3F_8 gas. Definity has been approved by the FDA in 2001 for echocardiography (left ventricular opacification) and in Canada also for liver and kidney imaging. In Europe, a submission for regulatory

approval has been filed. Definity has been developed by ImaRx and is marketed now by Bristol-Myers Squibb.

Imagent consists of tetradecafluorohexane (perflexane) micro-bubbles, surrounded by a phospholipid shell. The final solution contains 92 µg/mL C_6F_{14} gas. Imagent has been developed and approved in the United States in 2003 for echocardiography (left ventricular opacification). Developed by Alliance Pharmaceuticals, Imagent is now marketed by IMCOR Pharmaceutical in the United States.

Contraindication

In general, ultrasound contrast agents are pharmacologically inactive and, with the exception of known hypersensitivity to any of the ingredients, no absolute contraindications exist. They contain no toxic molecules and there are no toxic effects on organs (e.g. the kidneys). However, there may be side effects after the injection of any contrast agent, which require a benefit/risk assessment to assure the best possible safety for the patient. The only significant adverse effects reported are hypersensitivity reactions following the injection of the contrast agent. Such reactions are rare (in about 0.01%) but can be life-threatening. Considering this potential risk (even if the incidence is very low), contraindications were defined for patients having an increased risk in case of a hypersensitivity reaction which is not balanced by a special benefit for this particular patient group (e.g. patients during acute coronary syndrome not having an immediate clinical need for a contrast examination). For the detailed contraindications of the different agents see the respective SPCs approved by the regulatory authorities.

Pregnancy/Lactation

Since the micro-bubbles are not leaving the vascular compartment, there should be no transition into the foetal blood circulation or breast milk. From pharmacological and toxicological studies no special risks are known. However, as for other contrast agents no special clinical studies were performed in pregnant women. Therefore, the experience in this patient group is limited and special care should be taken.

Use and Dosage

Ultrasound contrast agents are usually administered by intravenous *bolus injection*. Due to the low injection volume, a saline injection for flushing directly after the contrast injection is recommended. To avoid high mechanical forces impairing the stability of the micro-bubbles, injection with strong pressure should be avoided and the needle diameter should not be too small (at least 20G).

Recommended doses for one injection are given in the following list:

- Echovist: 3.0–10.0 mL
- Levovist: 6.5–19.5 mL (2.5 or 4.0 g micro-particles)
- Optison: 0.5–3.0 mL
- SonoVue: 2.0/2.4 mL
- Definity: 10 µL/kg BW
- Imagent: 6.25 µL/kg BW

The injection can be repeated, if required. If a longer, continuous contrast enhancement is useful (e.g. for prolonged left ventricular opacification or vascular enhancement), a continuous *infusion* of the contrast agent is possible. In that case, an infusion pump with a rotating syringe holder is preferable, to avoid rising of the micro-bubbles to the superficial layer due to buoyancy.

Adverse Reactions

The most common side-effects reported after the injection of ultrasound contrast agents are mild and resolved within a short time without sequelae. They include local reactions at the injection site, headache, nausea, flush and sensations of heat, coldness or altered taste. In rare cases (about 0.01%), hypersensitivity reactions were reported as known from other colloidal suspensions and contrast agents. Such hypersensitivity reactions (anaphylactoid reactions) can be life-threatening and require immediate treatment. Adequately trained staff and emergency equipment should be available for that reason.

Interactions

Since ultrasound contrast agents are administered only for a short time during the diagnostic examination and the *elimination* from the blood circulation is quite fast (within a few minutes), possible interaction with other medication is limited. Usually, no special interaction studies are performed with contrast agents. From a theoretical point of view, there may be an influence on the bioavailability of drugs given at the same time point, especially if these drugs are able to adhere to albumin or lipid surfaces (depending on the shell of the micro-bubbles). Therefore, it is recommended to use separate intravenous lines if the contrast agent has to be administered simultaneously with another drug (e.g. in case of pharmacological stress echo).

Bibliography

1. Hoffmann R, von Bardeleben S, ten Cate F et al (2005) Assessment of systolic left ventricular function: a multi-centre comparison of cineventriculography, cardiac magnetic resonance imaging, unenhanced and contrast-enhanced echocardiography. Eur Heart J 26:607–616
2. Greis C (2004) Technology overview: SonoVue. Eur Radiol 14(Suppl 8):P11–P15
3. Martegani A, Aiani L, Borghi C (2004) The use of contrast-enhanced ultrasound in large vessels. Eur Radiol 14(Suppl 8):P73–P86
4. Albrecht T, Hohmann J, Oldenburg A et al (2004) Detection and characterisation of liver metastases. Eur Radiol 14(Suppl 8):P25–P33
5. Albrecht T, Blomley M, Bolondi L et al (2004) Guidelines for the use of contrast agents in ultrasound. Ultraschall Med 25:249–256
6. Bruix J, Sherman M (2005) Management of hepatocellular carcinoma. Hepatology 42:1208–1236

Contrast Media, Ultrasound, Hepatic

Thomas Albrecht
Department of Radiology and Nuclear Medicine, Campus Benjamin Franklin, Charité - Universitätsmedizin Berlin, Berlin, Germany
thomas.albrecht@charite.de

Synonyms

Contrast-enhanced sonography of the liver; Contrast-enhanced ultrasound (US) of the liver

Definition

The use of ultrasound (US) microbubble contrast agents combined with contrast-specific imaging techniques for the detection and characterization of liver disease (mainly tumors).

Introduction

Although often the first-line modality for liver imaging, conventional US without the use of contrast agents has a limited role in the diagnosis of liver tumors. Its ability to detect and characterize focal liver lesions is generally inferior to that of other cross sectional imaging modalities [computed tomography (CT) and magnetic resonance imaging (MRI)].

The advent of microbubble contrast agents has greatly enhanced the role of US in liver imaging. Both detection and characterization of liver lesions can be considerably improved by the use of US contrast agents.

US Contrast Agents for Liver Imaging

US contrast agents consist of microbubbles (cross reference) which are less than 10 μm in diameter. They are safe and effective echo enhancers. When given intravenously, microbubbles produce marked augmentation of the US signal for several minutes with up to 25 dB (greater than 100-fold increase) enhancement in echo strength. The signal enhancement is primarily caused by nonlinear bubble behavior (cross reference). Contrast-specific nonlinear imaging modalities (cross reference) such as phase modulation (cross reference) or amplitude modulation (cross reference) or a combination of the two exploiting the nonlinear bubble behavior (cross reference) must be used for contrast-enhanced US of the liver, since the signal enhancement is insufficiently visualized with conventional fundamental US imaging.

With real-time low ▶ *mechanical index* (MI) imaging, the dynamic enhancement pattern and the vascular

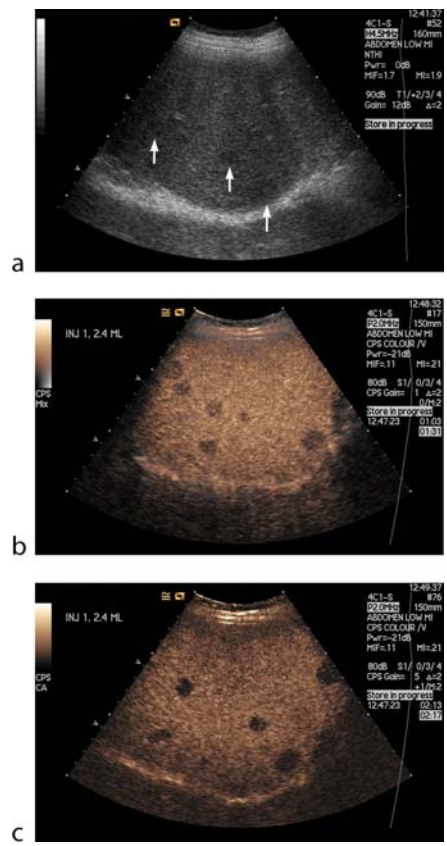

Contrast Media, Ultrasound, Hepatic. Figure 1 Patient with multiple small metastases. (a) Baseline US shows three ill-defined hypoechoic lesions in a slightly heterogeneous liver. (b, c) In the portal venous and delayed phase after SonoVue, multiple lesions are revealed throughout the liver, some of them only a few millimeters in diameter.

morphology of a lesion are assessed during the arterial (starting 10–20 sec and ending 25–53 sec after injection) and portal venous (starting 30–45 sec and ending 120 sec after injection) phases. The delayed phase (>2 min after injection) is particularly useful for detection of metastases because they appear as nonenhancing defects. Characterization is also aided by delayed-phase imaging.

Some agents have a liver-specific late phase where the bubbles accumulate in normal liver parenchyma starting 2–5 min after injection when the vascular enhancement has faded and persisting there for many minutes to hours, analogous to liver-specific contrast agents used in MRI. This late phase is particularly useful for lesion detection and differentiation of benign and malignant tumors. Microbubbles known to exhibit liver-specific behavior are ▶*Levovist*, *Sonavist* (both Schering AG, Germany), ▶*Sonazoid* (NC100100; General Electric, USA), and ▶*BR14* (Bracco SPA, Italy). In the late phase, the bubbles are stationary or extremely slow moving. The mechanism of hepatic accumulation is not completely understood. Possible explanations are mediation by the reticuloendothelial system or pooling and endothelial adherence in the liver sinusoids. For some agents (Sonavist and Sonazoid), Kupffer cell uptake has been demonstrated.

Two contrast agents are currently licensed for liver imaging in Europe: Levovist (Schering AG, Berlin, Germany) and ▶*SonoVue* (Bracco SPA, Milan, Italy). The imaging techniques with these two contrast agents vary considerably. Contrast-specific imaging modes exploiting nonlinear bubble behavior (cross reference) must be used with both agents to achieve clinically useful signal enhancement. Such imaging modes are now available on most medium- and high-end US systems.

Levovist, which was the first agent to be commercially available has liver-specific properties during its late phase; this is advantageous for detection of metastases. High MI imaging (MI>0.7) must be applied when using Levovist. It provides signal enhancement due to strong nonlinear signals from disrupting microbubbles. The disadvantage of this technique is the highly transient nature of the signals, which persist only for a few frames after insonation of an individual area until the bubbles in the imaging plane are destroyed. To exploit the enhancement for clinical use, special scanning techniques such as rapid

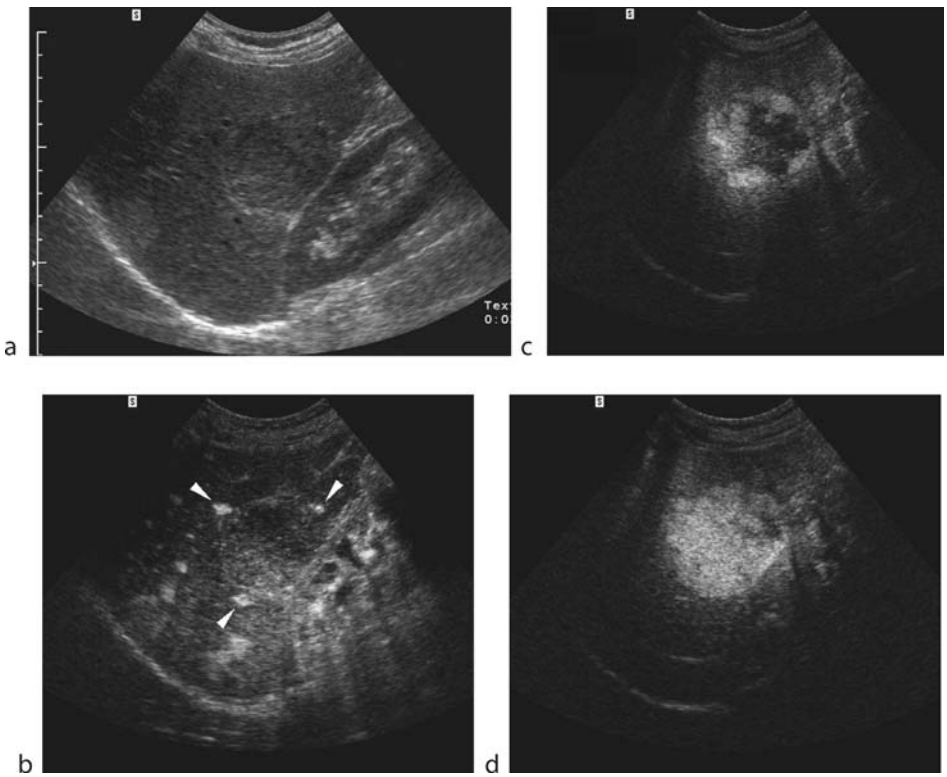

Contrast Media, Ultrasound, Hepatic. Figure 2 Typical dynamic enhancement of a hemangioma using Sonazoid. (a) Atypical baseline appearances: isoechoic lesion (*arrow*) suggestive of metastases in a patient with colon carcinoma. (b) Arterial phase with peripheral nodular enhancement (*arrowheads*). (c) Partial centripetal fill-in in the portal venous phase (45 sec p.i.). (d) Complete filling of the hemangioma in the delayed phase (3, 5 min p.i.).

sweeping through the liver to image intact bubbles with each new frame or intermittent imaging have to be employed. Such scanning techniques are somewhat cumbersome and multiple sweeps through the liver are only possible with repeated injections. For these reasons, Levovist is no longer used on a large scale despite some very good results in the detection and characterization of focal liver lesions.

SonoVue, a more recent agent, provides strong and persistent signal enhancement due to its strong harmonic resonance at low (≤0.2) and very low (<0.1) MI, where minimal or no bubble destruction occurs. This allows for continuous real-time imaging of a lesion during its vascular phase as well as comprehensive surveying of the liver in multiple planes during the delayed phase. Low MI imaging with SonoVue is now preferred in most instances, although it has weaker liver-specific properties than Levovist.

Several experimental agents such as Sonazoid or BR14 combine the advantages of good enhancement at low MI with strong liver-specific properties. Early clinical studies have demonstrated the potential of such agents for detection of metastases. Unfortunately, manufacturers are currently hesitant to continue the clinical development of such agents for commercial reasons.

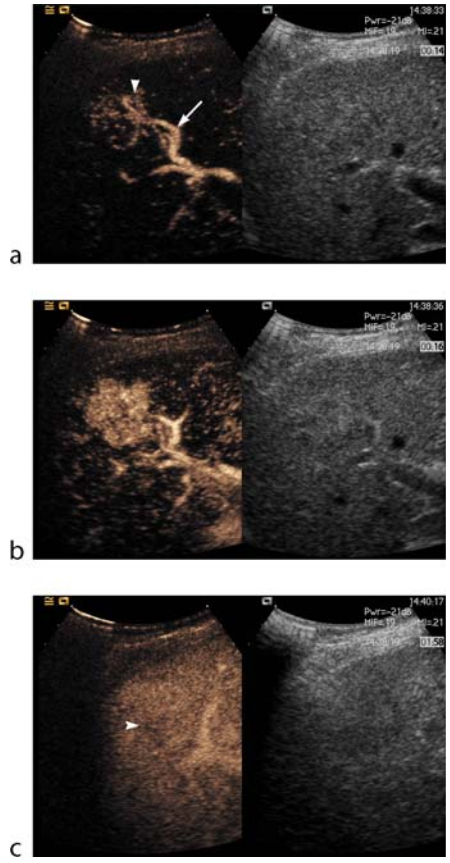

Contrast Media, Ultrasound, Hepatic. Figure 3 Typical focal nodular hyperplasia after SonoVue. (a) Large feeding artery (*arrow*) and spoke-wheel vascular pattern in the lesion (*arrow heads*) during the early arterial phase (14 sec after injection). (b) Two seconds later the lesion is completely filled with contrast and appears hyperenhancing to normal liver. (c) In the portal venous/delayed phase (2 min post injection) the lesion is isoenhancing to normal liver with the exception of a small hypoenhancing central scar (*arrow*).

Indications and Clinical Use

According to the guidelines of the European Federation of Societies for Ultrasound in Medicine and Biology (EFSUMB), the use of contrast agents is indicated in the following clinical situations:

- Detection of focal liver lesions (especially metastases)
- Characterization of focal liver lesions
- Monitoring of liver tumor ablation.

Detection: As with other imaging modalities, the use of contrast agents improves the ability of US to detect liver metastases substantially. As described earlier, metastases are seen as nonenhancing defects in an otherwise homogeneously enhancing liver in the portal venous and particularly in the delayed phase after contrast injection (Fig. 1). The impact on detection is most marked for lesions smaller than 1 cm in diameter and for lesions that are isoechoic on baseline US. Contrast-enhanced US has a sensitivity of approximately 80% in detecting hepatic metastases, which is similar to contrast-enhanced CT. The detection of primary hepatic malignancies such as hepatocellular carcinoma and cholangiocarcinoma is also improved with the use of US contrast agents in comparison to unenhanced US.

Characterization: All common solid liver lesions have rather characteristic dynamic imaging features on contrast-enhanced US (Figs. 2 and 3). Most of these features are analogous to those on dynamic CT and MRI scans. In addition to the vascular phases, the delayed phase is of particular value for differentiating malignant and benign lesions: the great majority of benign lesions show contrast uptake similar to normal liver in this phase, whereas most malignant lesions (especially metastases) appear as enhancement defects. Contrast-enhanced US is an effective tool for liver lesion characterization: approximately 85–90% of liver lesions can accurately be diagnosed as a specific lesion type, and classification of

benign and malignant lesions can be achieved in over 90% of the cases.

Monitoring of liver ablation: Treatment monitoring during or after liver ablation (radiofrequency ablation, laser ablation, percutaneous ethanol injection) is based on the assessment of vascularization and tissue perfusion in the target area to differentiate necrosis from residual viable tumor. Unenhanced US, even when combined with color/power Doppler, does not provide any reliable information about the outcome of ablation treatments, which was an important limitation of US-guided ablative procedures before the advent of US contrast agents. Conversely, with the use of US contrast agents, tissue perfusion can be visualized and crucial information about the extent of the thermal necrosis is thus obtained. Complete ablation is indicated by the disappearance of any previously visualized intralesional enhancement on contrast-enhanced images. Residual viable tumor tissue is suspected when a portion of the original lesion shows persistent enhancement in the arterial or portal venous phase.

Bibliography

1. Albrecht T, Blomley M, Bolondi L et al (2004) Guidelines for the use of contrast agents in ultrasound. Ultraschall Med Jan 2004 25: 249–256
2. Albrecht T, Blomley MJ, Burns PN et al (2003) Improved detection of hepatic metastases with pulse-inversion US during the liver-specific phase of SHU 508A: multicenter study. Radiology 227: 361–370
3. Konopke R, Kersting S, Saeger HD et al (2005) Detection of liver lesions by contrast-enhanced ultrasound—comparison to intraoperative findings. Ultraschall Med 26:107–113
4. Quaia E, Calliada F, Bertolotto M et al (2004) Characterization of focal liver lesions with contrast-specific US modes and a sulfur hexafluoride-filled microbubble contrast agent: diagnostic performance and confidence. Radiology 232:420–430

C

Contrast Media, Ultrasound, High Solubility Gas

N. DE JONG
Erasmus MC, Rotterdam, The Netherlands
n.dejong@erasmusmc.nl

Synonyms

Air agents; First (second) generation contrast agent

Definitions

An agent containing gas bubbles, of which the gas in the bubble easily dissolved in the surrounding liquid (typically water/plasma).

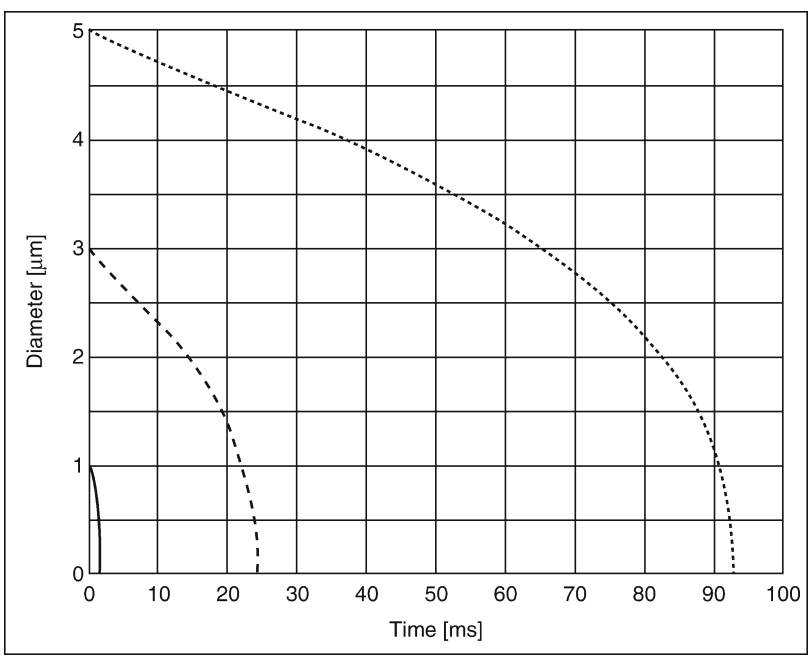

Contrast Media, Ultrasound, High Solubility Gas. Figure 1 Diameter's change versus time for three different sizes; 1, 3, and 5 μm.

Characteristics

Maintaining a gas bubble at a constant size is a technical challenge and many fluctuations in size occur with local environment. Indeed, bubbles suspended in a liquid can coalesce, grow or shrink in response to changes in the environment. Outward diffusion of gases due to surface tension, higher hydrostatic pressures or acoustic pressures induce consequent alterations in bubble size, which can occur very rapidly, within seconds to minutes. Smaller bubbles are more susceptible to these influences. The kinetics of the dissolution of a gas microbubbles is given by the equation of Epstein and Plesset (1):

$$\frac{dR}{dt} = DL\left(\frac{\frac{C_i}{C_0} - 1\frac{2\sigma}{RP_0} - \frac{p_{ov}}{P_0}}{1 + \frac{4\sigma}{3RP_0}}\right)\left(\frac{1}{R} + \frac{1}{\sqrt{\pi Dt}}\right),$$

where, R is the radius of the bubbles, t is the time, D is the diffusion constant, C_i/C_o is the ratio of the dissolved gas concentration to the saturation concentration, σ is the surface tension, P_0 is the ambient pressure, L is the Ostwald coefficient, p_{ov} is the overpressure.

The equation was numerically solved to extract the size variation of a gas bubble. (Fig. 1) shows the change in bubble size as a function of time at three different sizes: 1, 3, and 5 μm diameter. The gas contained in the bubble is air. We can appreciate that the smallest bubble (1 μm) disappears in less than 2 msec, whereas the predicted lifetime of a 5μm air bubble is ∼93 msec. The disappearance of these microbubbles is caused mainly by the diffusion of the contained gas, which dissolves in the surrounding medium.

Bibliography

1. de Jong N, Ten Cate FJ, Lancee CT et al (1991) Principles and recent developments in ultrasound contrast agents. Ultrasonics 29(4):324–330

Contrast Media, Ultrasound, Influence of Shell on Pharmacology and Acoustic Properties

Volkmar Uhlendorf
ETH Zürich, Institut für Pharmazeutische Wissenschaften, Zürich, Switzerland
volkmar.uhlendorf@pharma.ethz.ch

Synonyms

Capsule of ultrasound contrast media; Coating of ultrasound contrast media

Definition

When microbubbles are used as ultrasound contrast media, they usually need some coating—a shell. The shell surrounds the microbubble, stabilises it and thus provides transpulmonary stability. The shell influences both the pharmacological and acoustic properties of the microbubble.

Characteristics

When coated by a protective shell, microbubbles are at least nearly spherical, but as free microbubbles (after removal of the shell) they have an exactly spherical shape. Furthermore the shell has one or several of the following basic functions:

1.1 Reduction of gas exchange (outwards or inwards, depending on type of gases involved),
1.2 Stabilisation against aggregation and fusion of microbubbles (during storage or after administration),
1.3 Control of the surface characteristics on a molecular level (important for immune response, or for targeting),
1.4 Control of elastic and acoustic properties (threshold for acoustic disruption of bubble shell).

A further function might be seen in the encapsulation of drug substances within the bubble or within the shell, but this shall not be considered here in detail.

1.1 together with 1.2 allows providing a sufficiently stable population of small microbubbles. 1.3 is very important for the pharmacology of the bubbles. Finally, 1.4 is important for the acoustic behaviour during ultrasound imaging. These points are discussed in more detail.

The shell material typically belongs to the following classes:

- Fatty acids or lipids,
- Proteins—often denatured,
- Bio-degradable synthetic polymers,
- Combinations of the above,
- Surface-active components of the surrounding body fluid may play some role after administration.

In addition, there may be important functional groups or targeting molecules on the shell surface.

The total mass of shell material differs from agent to agent and also depends on the imaging procedure. For two reasons it usually is very low. First, in nearly all cases the shell is relatively thin when compared to the bubble diameter. Second, the injected amount of contrast agent is typically very low, as bubbles are easily detectable.

1.1 Reduction of Gas Exchange

A small, uncoated microbubble of soluble gas (like air) is not stable, even in a gas-saturated liquid. The surface tension is creating an enhanced pressure within the bubble (up to some atmospheres) which will enforce microbubble dissolution, typically within milliseconds. In a closed vial of contrast media and in a very concentrated bolus there may be a local overpressure or oversaturation, respectively, which temporarily can help to stabilise a microbubble population. But, at least after injection these stabilizing factors no longer exist. A shell can slow down the dissolution process, thus providing sufficient time for contrast imaging.

Several ultrasound contrast media contain hydrophobic (often perfluorated) gases of very low solubility in water. Due to their higher molecular weight compared to air, they also have a reduced diffusivity. In this case, diffusion of soluble low molecular weight gas may lead to a net inflow of gas and some growth of the mean diameter of bubbles without shell. One contrast agent claims to use about the steady-state mixture to prevent such a growth. But, even when insoluble gases or mixtures are used, there remain other reasons for having microbubbles coated.

1.2 Preventing Aggregation and Fusion of Microbubbles

For several reasons, aggregation (coagulation) of microbubbles has to be prevented, both during storage of suspensions and after injection. First, aggregates might become too large for unimpeded passage of capillaries and —in severe cases—would even create a safety risk. Aggregates also could lead to bubble growth by fusion of microbubbles, in particular for hydrophobic gases. Finally, any bubble aggregate is likely to respond acoustically similar to one large bubble and would thus reduce the efficiency. A shell of suitable composition helps to prevent these undesired processes. For this purpose, the shell may contain some (usually negatively) charged groups that lead to repulsion of microbubbles. In addition, there may be molecules preventing fusion for sterical reasons.

During development of a particular contrast agent, the effects should have been studied in detail and an adequate formulation found which guarantees stability during shelf life and *in vivo*. It is therefore not advisable to mix an agent with any other substance (unless allowed by the manufacturer) as this may lead to reduced stability.

1.3 Shell Surface and Microbubble Targeting

There are two relatively simple cases. One is the case of unspecific contrast agents, which remain in the blood pool and do not show uptake in certain organs or attachment to any targets. In the early years of ultrasound contrast agents, this was the intended mode of action. The second 'simple' case is just the opposite, namely purposeful targeting using one of the several techniques, which may not be limited to ultrasound contrast agents. It typically means to provide a bubble shell with a suitable number of targeting molecules, often attached to a linker on the shell surface. In recent years, in several cases the principle could be shown to work as intended.

Unspecific uptake of coated microbubbles in liver and spleen has been observed for several agents. It is expected as a normal response of the immune system, which tends to remove the coated bubbles as foreign particles. The surface properties of the bubble shell are determining the uptake rate, which can be controlled to some degree. This can be important when a long duration of contrast in the blood pool is intended, but also when rapid clearance is desired to get a low background signal for detection of targeted bubbles.

Delayed liver enhancement is a special case of unspecific uptake, mainly observed for Levovist. Its diagnostic applications in tumour imaging are described in a separate entry. The phenomenon is not completely understood and is still subject to research.

1.4 Influence of Shell on Elastic and Acoustic Properties

The acoustic properties of scatterers are determined by their density, elastic properties, shape and size. A bubble shell may have influence on all of these factors.

In nearly all cases, the shells of contrast agent microbubbles are very thin compared to their total diameters. The density of the shell material is very similar to the density of water, plasma or tissue. Therefore, a coated microbubble is essentially a gaseous inclusion in a medium with the density of water, with a size given by the inner diameter of the shell. While density and size are not much affected by the shell, the shell material has a very important influence on the effective elastic—and thus acoustic—properties.

A rigid, inelastic shell will prevent oscillations like those of a 'free' bubble. Therefore, scattering will be weak and about linear. On the other hand, a thin rubber-like, highly elastic shell will allow a bubble response almost like a 'free' bubble, preserving most of their highly desirable nonlinear acoustic behaviour. The same would apply to a shell consisting of smaller, loosely assembled pieces, which do not impede bubble motion.

Actually, most shells have properties between these extreme cases. Some types of thin, but almost rigid shells can be ruptured by sufficiently strong excitation in a

diagnostic ultrasound pulse. This allows controllable switching from weak, linear scattering to much stronger and non-linear scattering. A broken shell also leads to rapid dissolution of microbubbles consisting of air or other soluble gases (see 1.1). Disappearing bubbles can be detected with very high sensitivity in colour Doppler mode, even a single microbubble can be detected with a normal diagnostic ultrasound scanner.

Contrast Media, Ultrasound, Low Solubility Gas

N. DE JONG
ErasmusMC, Rotterdam,
The Netherlands
n.dejong@erasmusmc.nl

Synonyms

Perfluorocarbon gas agents; Second (third) generation contrast media

Definitions

An agent containing gas bubbles of which the gas in the bubble hardly dissolved in the surrounding liquid (typical water/plasma).

Characteristics

The first generation of ultrasound contrast agents were based on air core, whereas the new generations are composed of gases with higher molecular weights. For the kinetics of the dissolution of a gas, microbubble see—High solubility gas ultrasound contrast media. In that equation, the Ostwald coefficient (L) represents the ratio of the gas solubility in liquid to the gas density (1). From the equation, it is clear that microbubbles containing gases with lower Ostwald coefficients persist longer than bubbles containing gases with higher values. (Fig. 1) displays the dissolution in time of a 3 μm diameter bubble containing two different gases: air and sulfur hexafluoride SF_6. The air gas bubble disappears in less than 25 msec whereas the predicted lifetime of an SF_6 gas bubble with the same size is more than 100 msec. Second-generation contrast agents designed with improved lifetime to enable opacification of LV and myocardial microcirculation are composed of less-diffusable gases such as perfluorocarbons, perfluoropropane (optison), or sulfur hexafluoride (sonovue). These types of inert gases have a high molecular weight. Since the diffusion of a gas is inversely proportional to the square root of its molecular weight (2), the higher the molecular weight, the slower the solubility or diffusion of the gas. Table 1 summarizes, for different gases, the Ostwald coefficient and the predicted lifetime of a bubble of 3-m diameter. The gases chosen here are used in commercially available contrast agents or in those under clinical investigations. Clearly, gases with lower solubility provide the bubbles longer persistence. As a matter of fact, not only the Ostwald coefficient plays an important role in the choice of the type of gas for improved stability, but also the saturated vapor pressure at body temperature. Lower vapor pressures will make the bubble to condense into liquid losing therefore the contrast.

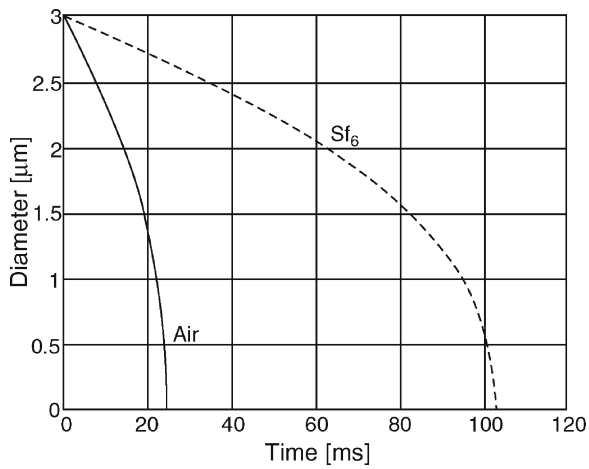

Contrast Media, Ultrasound, Low Solubility Gas. Figure 1 Diameter's change versus time for a bubble of 3 mm diameter; solid: air bubble, dashed: SF_6 gas bubble.

Contrast Media, Ultrasound, Low Solubility Gas. Table 1 Ostwald coefficient and disappearance time for 3-μm diameter bubbles containing different gases

	Ostwald Coefficient ($\times 10^6$)	Disappearance Time (msec)
Air	23,168	24.4
Sulfur hexafluoride (SF_6)	5,950	102.9
Perfluoropropane (C_3F_8)	583	1,110
Perfluorohexane (C_6H_{14})	24	2,000

Bibliography

1. Kabalnov A, Bradley J, Flaim S et al (1998) Dissolution of multicomponent microbubbles in the bloodstream: 2. Experiment. Ultrasound Med Biol 24(5):751–760
2. Porter EA (1995) Effect of blood and microbubble oxygen and nitrogen content on perfluorocarbon-filled dextrose albumin microbubble size and efficacy. J Am Soc Echocardiogr 11:421–425

Contrast Media, Ultrasound, Multipulse Techniques

Multi-pulse techniques are used in microbubble specific imaging for two key purposes. Firstly, a phase and/or amplitude modulated pulse train can be used to preferentially detect the non-linear response of the microbubbles to differing acoustic stimuli against the linear tissue background. Secondly, multiple pulses can be used to provide information on the motion of the microbubbles within the circulation, in the same way that multiple pulses are processed for color or power Doppler imaging.

See under Contrast Media, Ultrasound, Specific Imaging Techniques. ►Contrast Media, Ultrasound, Phase Modulation, for further details.

Contrast Media, Ultrasound, New Clinical Development

Christian Greis
Bracco ALTANA Pharma GmbH, Klinische Entwicklung Ultraschallkontrastmittel, Konstanz, Germany
christian.greis@altanapharma.com

Synonyms

Drug-delivery systems; Microbubbles; Target-specific microbubbles; Ultrasound contrast agents; Ultrasound contrast media

Definition

A classic ultrasound contrast medium consists of echogenic microbubbles, which, after intravenous injection, are distributed freely within the blood compartment. Several of these agents are already in the market and more are under clinical development. These agents differ in the composition of the shell and the encapsulated gas, which has an impact on the stability and the behavior in the sound field. However, microbubble contrast agents can also be used in a broader sense.

One approach is to modify the shell of the microbubbles to obtain an affinity to structures or tissues in the body. Such *target-specific microbubbles* can adhere to cells or specific molecular structures in the body, thereby allowing the imaging of these targets. Since the sensitivity of recent contrast-specific ultrasound technologies is so high that single microbubbles can be detected, such an agent can be used to image individual target molecules on the surface of cells or structures *in vivo* (*molecular imaging*).

Another approach is to incorporate drugs, genes, or other active substances in microbubbles, with the aim of releasing them at a specific location in the body. Such an agent can be used as a *drug-delivery system* allowing local therapy after intravenous administration of the agent. The local release of the active substance can be obtained either with target-specific microbubbles (distributing the encapsulated compound over time) or by local destruction of free circulating microbubbles using local insonation of the target region with high insonation power.

Indication

Standard ultrasound contrast media are used as markers for blood distribution and perfusion. They can help to delineate vascular structures, demonstrate the vascular geometry separated from the tissue background, and act as tracers for the assessment of blood distribution and perfusion.

For some of the existing agents, a certain affinity to endothelial structures has been described, even if they have not been developed for that purpose. Albumin-based contrast agents can attach to activated endothelial cells (1) and the attached microbubbles can be detected there after wash-out of the freely circulating agent. Other agents are captured by the reticuloendothelial system in the liver and spleen (2) or the microbubbles can even be phagocytosed by cells (3), allowing the imaging of phagocytotic active tissue. The attachment and/or phagocytosis of microbubbles in the liver is facilitated by the fenestration of the endothelium in the liver sinusoids, permitting the close contact of microbubbles and perivascular cells. An intracellular uptake of ultrasound contrast agents can also be obtained by using much smaller echogenic nanoparticles, e.g., consisting of biodegradable polymers (4). Such nanoparticles usually have a very high stability and are stored in the tissue for days and weeks.

Usually, ultrasound contrast agents are delivered, after intravenous injection, *via* the vascular system. However, alternative delivery pathways are possible too. For imaging of lymph nodes, the intravenous administration results in the demonstration of lymph node vascularity and perfusion. However, after subcutaneous injection, the agent is delivered *via* the lymphatic pathway to the lymph nodes (5). This allows the demarcation of sentinel nodes without using a radiotracer. Conventional microbubble agents as well as smaller nanoparticle agents can be used for lymphatic delivery.

A more specific attachment of microbubbles to tissues or structures can be achieved by coupling microbubbles to antibodies, binding to specific molecules on the surface of target cells/structures (6). Such agents can be used for targeted imaging down to a molecular level. Possible indications for targeted imaging include the detection of thrombotic material in the vascular system, the demonstration and quantification of neoangiogenesis in tumors, and the imaging of inflammation.

Beyond the diagnostic use, microbubble agents can also be used as therapeutic agents, e.g., to initiate or enhance local therapy. One capability of microbubbles is the local intensification of mechanical forces induced by the ultrasound wave. In combination with high insonation power, this can increase the endogenous or exogenous thrombolytic activity (*accelerated thrombolysis*) or can result in the transient formation of micropores in the capillary vessels (*sonoporation*), facilitating the transport of substances into the target tissue. Furthermore, the microbubble itself can be used simultaneously for the transport and delivery of active substances, acting as a ►drug-delivery system. Using such a system, the local concentration and activity of a drug can substantially be increased, allowing local therapy with reduced systemic effects.

For some pathologies, constant treatment over a long period (or lifelong treatment) is required, creating the need for continuous administration of a drug. In such cases, gene therapy may be preferable, resulting in the repair of pathological functions or induction of protective mechanisms. The first preclinical studies have demonstrated that lipid-coated microbubbles can be used as vectors for the transportation of *genes* or *antisense molecules* instead of using viral vectors. The combination of ►target-specific imaging and local therapy is a very promising opportunity for microbubble contrast agents, and an increasing number of research groups around the world are currently elaborating indications for the diagnostic and therapeutic use of such products. Many positive and encouraging results have already been published, coming from in vitro and animal studies. However, before the first product can be used in clinical studies in humans, extensive pharmacological and toxicological studies have to be performed.

Use and Dosage

Microbubble contrast agents are usually administered intravenously. The shell of the microbubbles ensures stability and integrity until the target region is reached and/or the microbubbles are destructed by a high-power ultrasound pulse. For target-specific imaging, normal doses of the contrast agent can be used. Due to the high sensitivity of contrast-specific imaging modalities, single microbubbles can be detected, so that the current doses used for blood-pool imaging are sufficient. For therapeutic purposes, the dose is mainly dependent on the efficacy of the incorporated drug. However, the lumen in the microbubbles is quite large, and for several drugs as well as oligodendronucleotides (used for gene therapy) it has been shown that effective doses can be obtained.

Adverse Reactions

Since the microbubbles do not contain any toxic substances, no substantial side effects caused by the microbubble carrier are known or expected. As for the current blood-pool imaging agents, allergic reactions can occur due to the colloidal character of the microbubbles. However, such reactions are rare and do not seem to be increased by labeling or loading of the microbubbles. Also for biopolymer nanoparticles, which are accumulated and stored for a long time in the target tissue, no particular side effects have been observed. However, the data available are limited and long-term effects need to be investigated.

Adverse effects of drug-delivery systems seem to be acceptable and are mainly related to the side effects of the encapsulated drug. Due to the local accumulation of the active substance, the side effects of the drug seem to be fewer compared to the systemic administration of the same drug. Therefore, it is expected that higher doses of the drug can be used to increase the local therapeutic effect.

References

1. Villanueva FS, Jankowski RJ, Manaugh C et al (1997) Albumin microbubble adherence to human coronary endothelium: implications for assessment of endothelial function using myocardial contrast echocardiography. J Am Coll Cardiol 30:689–693
2. Blomley MJK, Albrecht T, Cosgrove DO et al (1999) Stimulated acoustic emission to image late liver and spleen-specific phase of Levovist in normal volunteers and patients with and without liver disease. Ultrasound Med Biol 25:1341–1352
3. Takeuchi H, Ohmori K, Kondo I et al (2004) Interaction with leukocytes: phospholipid-stabilised versus albumin-shell microbubbles. Radiology 230:735–742
4. Bauer A, Blomley M, Leen E et al (1999) Liver-specific imaging with SHU 563A: diagnostic potential of a new class of ultrasound contrast media. Eur Radiol 9 [Suppl 3]:S349–352

5. Goldberg BB, Merton DA, Liu JB et al (2004) Sentinel lymph nodes in a swine model with melanoma: contrast-enhanced lymphatic US. Radiology 230:727–734
6. Ellegala DB, Leong-Poi H, Carpenter JE et al (2003) Imaging tumor angiogenesis with contrast ultrasound and microbubbles targeted to $\alpha_v\beta_3$. Circulation 108:336–341

image based on contrast agent concentration rather than basic tissue echogenicity.

Many applications have been developed for this type of imaging, most notably to date the detection and characterisation of the liver and other organs. The ability to differentiate perfused from non-perfused tissue also has many applications in several organ systems.

Contrast Media, Ultrasound, Safety and Adverse Reactions

Anders Nilsson
Department of Radiology
Ultrasound University, Uppsala University Hospital, Uppsala, Sweden
anders.nilsson@akademiska.se

Synonym

Adverse events to ultrasound contrast media

Definition

All existing ultrasound contrast agents consist of gas bubbles slightly below the size of red blood cells and are stabilised by a shell. This is to ensure their survival in the blood circulation long enough for an ultrasound examination to be made and, in the case of the newer agents, to enable an examination with a reduced ►mechanical index (MI) to be made without significant destruction of the bubbles. They pass through capillary beds and thus can be injected intravenously. As they can be seen as particles, they do not leave the circulation, i.e. they are so-called blood pool agents. The contrast effect is caused, with increasing ultrasound intensity, by reflection, asymmetrical oscillation and finally bursting. Ultrasound contrast media are generally extremely well tolerated. Like with all drugs, adverse reactions to these agents may occur, but are very rare and seldom clinically relevant.

Indication

Ultrasound contrast media increase the reflectivity of blood. This can be used to enhance Doppler signals, both in spectral and colour Doppler. The asymmetrical oscillation, without significant bubble destruction, is the basis for so-called non-linear imaging techniques where dedicated ultrasound machine software can recognise the non-linear signal from a microbubble and produce an

Contraindications

Ultrasound contrast agents should not be used in patients with previous allergic reactions to the same compounds. Caution should be exercised when microbubbles are used in patients with ischaemic heart disease. Right-to-left ventricular shunts and pulmonary hypertension are also stated as contraindications, see below.

Pregnancy/Lactation

There is no evidence that compounds from ultrasound contrast agents would cause harm in pregnancy or when breastfeeding but as their use in pregnancy and paediatrics is contrary to the product information in most of the contrast agents, experience is limited and contrast used with caution.

Dosage

As different contrast agents have different physical properties and vary in the number of microbubbles per volume unit the dosage varies and must be adjusted with regards to the agent used, the ultrasound machine software and the indication for use.

Adverse Reactions

First, it should be pointed out that both ultrasound within recommended MIs and microbubbles as contrast agents seem to be extremely safe (1). Second, that as ultrasound contrast agents have physical rather than chemical properties in common (stabilised gas bubbles) the adverse reactions may vary more between different agents than is the norm for X-ray contrast media.

The most commonly reported adverse reactions are the same as with other types of contrast media, i.e. headache, a feeling of warmth and flushing. Less often reported are nausea, dizziness, chills, altered taste and dyspnoea. Similar findings were, however, also seen in the placebo groups.

Allergic reactions seem to be very infrequent and mild with general flush and erythema (2). Recently, a small

number of more severe anaphylactic reactions to the agent SonoVue (Bracco SPA, Milano, Italy) have been reported, though, suggesting that repeated exposure over a short period of time should be considered with some care.

As microbubbles are particles they carry a risk of embolisation if they aggregate (individual bubbles are smaller than capillaries and therefore have no embolic potential). This, however, seems extremely unlikely given their extremely low concentration in the blood pool. Contrast injections are given intravenously and thus any such emboli should be filtered out by the capillary beds of the lungs but the existence of right-to-left shunts is usually a contra-indication for the use of microbubble-based contrast agents.

At higher ultrasound intensities a cavitation phenomenon occurs, i.e. the growth and collapse by implosion of microbubbles. This causes significant changes in pressure and temperature and *in vitro*/animal studies have shown local haemolysis, platelet aggregation and damage to endothelial cells (3). Even though these unwanted side effects have not been seen in clinical practise (4), it would be prudent to perform ultrasound contrast examinations with as low an acoustic output as possible. This is not a problem since most modern contrast-specific software use a low MI in order to minimise bubble disrupture.

It should be pointed out that as ultrasound contrast agents are relatively new products, it will take many more years of surveillance to accurately assess the possible existence of other rare adverse reactions.

Bibliography

1. EFSUMB Study Group (2004) Guidelines for the use of contrast agents in ultrasound. Ultraschall Med 25:249–256
2. Correas J-M, Bridal L, Lesavre A et al (2001) Ultrasound Contrast agents: properties, principles of action, tolerance and artefacts. Eur Radiol 11:1316–1328
3. Miller DL, Gies RA (1998) Enhancement of ultrasonically induced hemolysis by perfluorocarbon-based compared to air-based echocontrast agents. Ultrasound Med Biol 24:285–292
4. ter Haar GR (2002) Ultrasonic contrast agents: safety considerations reviewed. Eur J Radiol 41:217–221

Contrast Microbubbles

▶Microbubbles

Contrast Reactions

▶Adverse Reactions, Iodinated Contrast Media, Acute, Non renal

Contrast Reversal

Finding of computed tomography about hepatic steatosis gives a clear evidence of hepatic vessels on unenhanced scans which appear relatively hyperdense compared to the fatty liver, simulating the images obtained after contrast administration.

▶Steatosis, Hepatic

Contrast Specific Imaging Techniques

▶Specific Imaging Techniques, Contrast Media, Ultrasound

Contrast-Enhanced Echocardiography

▶Contrast Media, Ultrasound, Applications in Echocardiography

Contrast-Enhanced Reflux Sonography

▶Contrast Media, Ultrasound, Applications in Vesicoureteral Reflux

Contrast-Enhanced Sonography in Abdominal Trauma

▶Contrast Media, Ultrasound, Applications in Blunt Abdominal Trauma

Contrast-Enhanced Ultrasound (US) of the Liver

▶Contrast Media, Ultrasound, Hepatic

Contrast-Enhanced Ultrasound Imaging of the Brain

▶Contrast Media, Ultrasound, Applications in Transcranial and Intra-Operative Brain Ultrasound

Contrast-Enhanced Ultrasound in Abdominal Trauma

▶Contrast Media, Ultrasound, Applications in Blunt Abdominal Trauma

Contrast-Enhanced Ultrasound of the Spleen

▶Contrast Media, Ultrasound, Applications in Focal Splenic Lesions

Contrast-Enhanced Voiding Urosonography (VUS)

▶Contrast Media, Ultrasound, Applications in Vesicoureteral Reflux

Contrast-Specific Imaging

An imaging modality that allows the selective detection and demonstration of the contrast agent in the body. This requires a separation of signals coming from the contrast agent from those coming from the tissue. The separation of both signals is based on specific characteristics in the contrast agent signal, which are not present in the tissue signal.

▶Contrast Media, Ultrasound, Commercial Products

Contrast-enhanced CT or MRI in ACKD

The gold standard in the diagnosis of acquired cystic kidney disease (ACKD) as well as in the characterization of renal masses (hemorrhagic cysts or solid renal tumors). Can be performed in patients undergoing dialysis but should be replaced by MRI in patients with contraindications to iodinated contrast agents (alteration of renal function or previous allergic reaction).

▶Cystic Renal Disease, Acquired

Contusion, Breast

Reversible infiltration of the breast parenchyma by extravasated blood and edema following trauma.

▶Trauma, Breast

Contusion, Hepatic

Hepatic contusion appears as a hypodense area due to interstitial bleeding, with irregular margins, and is usually associated with major hepatic injuries such as lacerations and hematomas.

▶Trauma Hepatobiliary

Conventional Defecography - Evacuation Proctography

▶Pelvic Floor Dysfunction, Anorectal Manifestations

Conventional Renal Carcinoma

▶Carcinoma, Renal Cell

Core Needle Biopsy

Biopsy in which a histologic specimen is taken, usually with a 14-gauge needle (in contrast to vacuum-assisted biopsy or fine needle aspiration biopsy, FNAB).

▶Carcinoma, Lobular, *In situ*, Breast

Coronary Angiography

Diagnostic modality based on X-rays able to obtain angiographic images of the Coronary arteries by means of a Catheter positioned through the femoral artery.
▶Ischemic Heart Disease, CT

Coronary Angioplasty

Interventional procedure based on transcutaneous placement of a Catheter inside the lumen of a Coronary artery by which it is possible to dilate a stenosis.
▶Ischemic Heart Disease, CT

Coronary Artery Bypass Surgery

Surgical procedure used to revascularize obstructed Coronary arteries.
▶Ischemic Heart Disease, CT

Coronary Artery Disease

Atherosclerotic disease involving the Coronary arteries.
▶Ischemic Heart Disease, CT
▶Ischemic Heart Disease, Ultrasound

Coronary Artery Steal

In patients with internal mammary artery to coronary artery by-pass graft, the presence of a proximal subclavian occlusion may cause coronary artery steal syndrome presenting as angina during arm exercise.
▶Steal Syndrome Vertebral

Coronary Artery Stenosis

Obstruction of a Coronary artery usually determined by atherosclerosis.
▶Ischemic Heart Disease, CT

Coronary Stent

Device used after Coronary artery dilatation to keep the lumen of the Coronary arteries open.
▶Ischemic Heart Disease, CT

Corpus Cavernosum, Thrombosis

Räto T. Strebel[1], Hubert John[2]
[1]Department of Urology, University Hospital Zurich, Zurich, Switzerland
[2]Klinik Hirslanden, Leiter Zentrum für Urologie, Zurich, Switzerland
raeto.strebel@usz.ch

Synonym

Segmental/partial priapism

Definition

A partial priapism of the corpus cavernosum is an exceedingly rare condition. Most frequently, it is characterized by thrombosis within a proximal segment of one corpus cavernosum.

Corpus Cavernosum, Thrombosis. Figure 1 Peyronie's disease with typical penile deformity on erect penis.

Clinical Presentation

Patients complain usually a painful perineal mass some days before seeking medical attention. On physical examination, a tender and painful mass is palpable perineally near the base of the penis.

Imaging

Magnetic resonance imaging of the pelvis should be the imaging modality of choice and reveals the underlying pathology. Frequently, an ultrasound of the perineal region or even a transanal ultrasound is performed beforehand to rule out any perianal abscess. Alternatively, a CT scan may be performed (Fig. 1).

Corpus Luteum Cysts

Corpus luteum cysts have thicker, better vascularized walls than follicular cysts. Similar to follicular cysts, the content varies from watery to proteinaceous to hemorrhagic.

▶Cyst, Follicular, Ovarium

Coxa Valga

Increased angle between the femoral neck and shaft (normal 150° at birth, then gradually decreasing up to 120–130° in adults).

▶Congenital Malformations of the Musculoskeletal System

Coxa Vara

Decreased angle between the femoral neck and shaft (<120°).

▶Congenital Malformations of the Musculoskeletal System

CPPD

Lynne S. Steinbach
Department of Radiology, University of California, San Francisco, USA
lynne.steinbach@radiology.ucsf.edu

Synonyms

Calcium pyrophosphate deposition disease; Chondrocalcinosis; Pseudogout

Definitions

One of the most confusing aspects of calcium pyrophosphate dihydrate (CPPD) arthropathy is the associated nomenclature. A variety of terms have been used. *Chondrocalcinosis* is a more general term that is reserved for pathologically or radiologically evident cartilage calcification. It can include CPPD, dicalcium phosphate dihydrate, or calcium hydroxyapatite crystals, or combinations of the three. CPPD *crystal deposition disease* is a specific term for a disorder characterized by the exclusive presence CPPD crystals in or around joints. The term "*pseudogout*" is not a radiological diagnosis; rather it is reserved for a gout-like clinical syndrome produced by CPPD crystal deposition disease that is characterized by intermittent acute attacks of arthritis. *Pyrophosphate arthropathy* is a term that describes a particular pattern of structural joint damage that occurs in CPPD crystal deposition disease. This arthropathy is similar to osteoarthritis but has some separate distinct features. *Articular and periarticular calcification* can occur with CPPD crystal deposition disease; however, calcium deposits other than CPPD crystal accumulation also may produce this type of calcification.

Pathology/Histopathology

The deposition of various crystals within the articular tissues can cause an acute inflammatory response and acute synovitis and lead to chronic destructive arthritis. First, deposition of CPPD crystals is observed in the articular cartilage, around the chondrocyte lacunae. This may alter biochemistry of cartilage, e.g., proteoglycan concentrations. The acute synovitis of CPPD is probably due to the rupture of preformed deposits of calcium pyrophosphate dihydrate from cartilage into the adjacent synovial cavity.

Clinical Presentation

The clinical presentations of CPPD crystal deposition disease are highly variable, ranging from asymptomatic disease to severe pain associated with a destructive arthropathy. Indeed, this disease has been called a "great mimicker" of other arthritides. Furthermore, occasionally, several of these clinical patterns present at different times during the course of the arthritis.

The *asymptomatic* form of this arthropathy is probably the most common; however, it is difficult to document this because many asymptomatic patients are never seen by a physician. Absence of symptoms occurs in at least 10 to 20% of documented cases of CPPD crystal deposition disease.

Many patients with CPPD crystal deposition disease present with an arthropathy that simulates *osteoarthritis*. An occasional acute inflammatory component is seen in 35 to 60% of such patients. This osteoarthritic form is a chronic and progressive arthritis that is frequently bilateral and symmetric, presenting in the knee, hip metacarpophalangeal, elbow, ankle, wrist, and glenohumeral joints. Flexion contractures are common, especially in the knee and elbow.

Patients with CPPD crystal deposition disease also may have inflammatory symptoms and signs. For example, attacks of *pseudogout* occur in 10 to 20% of symptomatic patients. The pseudogout syndrome is caused by shedding of pyrophosphate crystals into the joint fluid. Although most cases of pseudogout develop spontaneously, situations that trigger acute pseudogout include direct joint trauma, concomitant medical illness such as stroke and myocardial infarction, surgery (especially parathyroidectomy), blood transfusion, parenteral fluid administration, institution of thyroxine replacement therapy, and joint lavage. Hypocalcemia is present in many of these situations and is believed to provoke some attacks of pseudogout. This produces pain, erythema, and tenderness, which can be mistaken for other disorders such as gout or septic joint. The attacks are self-limited and can last from one day to several weeks. They generally are less painful than those of gout and are most common in the knee, but other sites including the hip, glenohumeral, elbow, ankle, wrist, acromioclavicular, talocalcaneal, and metatarsophalangeal joints also are affected. Fever and elevation of the erythrocyte sedimentation rate may accompany pseudogout attacks.

Two to six percent of patients with CPPD crystal deposition disease present with an arthritis that simulates *rheumatoid arthritis*. These attacks are characterized by morning stiffness, fatigue, synovial thickening, restricted joint motion, and an elevated erythrocyte sedimentation rate, and they persist from 4 weeks to several months.

CPPD crystal deposition disease also can have a *pseudoneurotrophic* presentation in as many as 2% of patients. Indeed, CPPD crystalline arthropathy should be considered in the differential diagnosis of rapidly progressive destruction of large joints.

Imaging

Conventional Radiography

Radiographically, chondrocalcinosis usually is apparent in CPPD crystal deposition disease, but the arthropathy can also precede radiographically detectable cartilage calcification, the calcification may not always be dense enough to be visualized on conventional radiographs, or it may be difficult to identify such calcification if the joint is severely deranged. In one study of 3228 patients undergoing knee arthroscopy, a radiographic diagnosis of chondrocalcinosis was made in only 39.2% of patients with pathologically proven CPPD crystal deposition (1).

Computed Tomography and Magnetic Resonance Imaging

Computed tomography (CT) can accurately demonstrate chondrocalcinosis due to the high soft tissue contrast and tomographic nature of this imaging method. However, CT is rarely used to evaluate the painful joint. Magnetic resonance imaging (MRI) is often the cross-sectional imaging procedure performed for painful joints. It is therefore common to encounter CPPD crystal deposition disease in older patients who are being studied with routine MRI. Calcification can be difficult to detect on MRI. Correlation with conventional radiographs is often necessary. Despite this problem, CPPD crystal deposition disease in hyaline cartilage is occasionally detected with standard MRI techniques. Prominent linear or punctate hypointense areas frequently are demonstrated. A small halo of hyperintense signal intensity surrounding the hypointense areas is occasionally seen, probably related to magnetic susceptibility artifact.

Although the low signal intensity calcification can be detected in routine spin echo, fast spin echo, and short tau inversion recovery (STIR) images, the hyaline cartilage calcification is better seen on gradient echo images in which the difference between the magnetic susceptibility of hyaline cartilage and CPPD crystals is enough to create local magnetic field inhomogeneity resulting in signal distortion. In these types of images, foci of cartilage calcification become larger, the so-called "blooming" effect.

Low signal intensity in the hyaline cartilage may be overlooked on MRI if the reader does not include it in a search pattern for chondrocalcinosis. There is also a differential diagnosis for this pattern, which includes hemosiderin from trauma, pigmented villonodular synovitis, and hemophilia; gas related to vacuum phenomenon;

and magnetic susceptibility artifact around postsurgical intra-articular material such as micrometallic debris.

There are also documented cases of CPPD crystal deposition in which the calcification in the hyaline cartilage or menisci was not seen on MRI. This is more common in cases of meniscal calcification in which the short T2 relaxation times of the meniscus and calcification are similar. Occasionally, with MRI, CPPD crystal deposition disease in a meniscus can mimic a meniscal tear. This has important implications and can lead to inappropriate treatment including unnecessary surgery. Gale et al reported areas of high signal intensity in regions of meniscal chondrocalcinosis with T2-weighted spin echo MR sequences (2). This finding may be attributed to the hyperintense halo artifact seen adjacent to calcification of low signal intensity. No reports have described high signal intensity in areas of chondrocalcinosis in T1-weighted images. Such a finding which would potentially simulate a meniscal tear, is theoretically possible given that increased signal intensity of calcium deposits has been found in the discs of the lumbar spine.

Nuclear Medicine

Skeletal scintigraphy may show increased radiotracer uptake in the joints, but these findings are nonspecific.

Diagnosis

CPPD crystal deposition disease is characterized by calcification in and around joints and structural joint changes termed pyrophosphate arthropathy. This arthropathy resembles osteoarthritis; however, it occurs in articulations not usually affected by osteoarthritis, often affecting non-weight-bearing regions such as the radiocarpal, metacarpophalangeal joints, glenohumeral joints, and elbow. It usually is bilateral and symmetric and is most common in the knee, wrist, and metacarpophalangeal joints. Furthermore, CPPD crystal deposition disease has an unusual intra-articular distribution in certain joints such as the knee and wrist where patellofemoral and radiocarpal joint space narrowing may be seen (3).

CPPD crystal deposition disease frequently presents on routine radiography with normal mineralization, narrowing of various articulations, and subchondral sclerosis. Osteophytes are common, but occur with a frequency less than that of osteoarthritis. Subchondral cysts are one of the hallmarks of this arthropathy. The cysts usually are larger, more numerous and widespread than in osteoarthritis. Cysts may form before cartilage loss is evident. Osseous fragmentation and collapse may be related to fracture of these cystic lesions. Intra-articular osteochondral bodies commonly are associated with CPPD crystal deposition disease. These may be free in the joint cavity or embedded in cartilage or synovium.

Cartilage

Chondrocalcinosis is usually caused by CPPD crystal deposition. In 5% of cases, however, it can be related to other crystals such as dicalcium phosphate dihydrate and calcium hydroxyapatite (4). Both hyaline cartilage and fibrocartilage can contain CPPD crystals. The CPPD crystal tends to be deposited in the middle layer of degenerated hyaline cartilage. These deposits are thin and linear and parallel the subjacent subchondral bone (Fig. 1). CPPD crystals are also deposited on the surface of the hyaline cartilage, especially when there is superficial chondral erosion. Hyaline cartilage calcification is most common in the wrist, knee, elbow, and hip.

CPPD crystal deposition in fibrocartilage is most commonly observed in the menisci of the knee, triangular fibrocartilage of the wrist, labra of the acetabulum, symphysis pubis, and annulus fibrosus of the intervertebral disc. Other less common sites of CPPD crystal deposition in cartilage include the articular discs of the sternoclavicular and acromioclavicular joints and glenoid labra.

Synovium and Capsule

Synovial calcification is common in CPPD crystal deposition disease. Synovial calcification can be so widespread that it appears to fill the entire joint cavity,

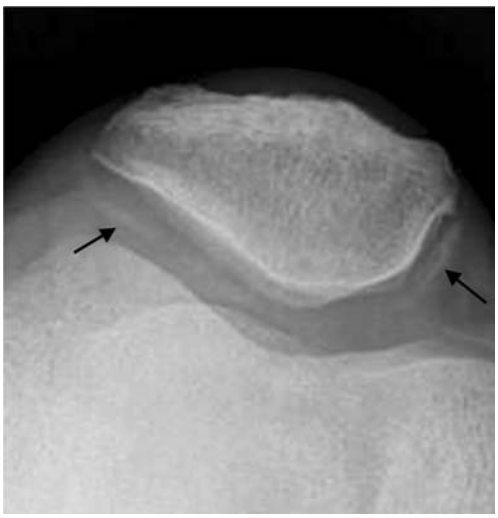

CPPD. Figure 1 Linear calcification is seen along the hyaline cartilage of the medial and lateral facets of the patella (*arrows*) on this Merchant view of the patellofemoral joint.

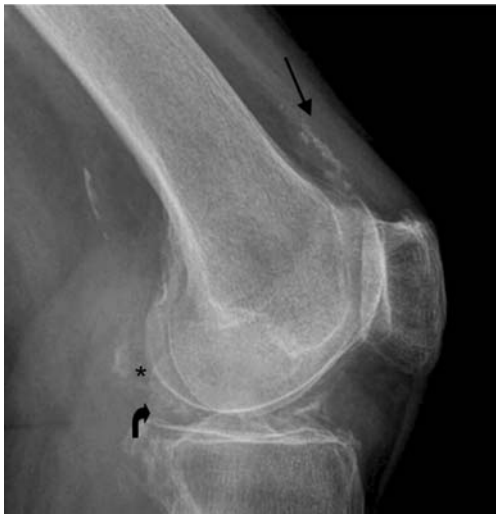

CPPD. Figure 2 Synovial calcification is appreciated along the suprapatellar bursa on this lateral knee radiograph (*arrow*). Hyaline and meniscal calcification is also identified (*curved arrow*). Osteochondral bodies lie posteriorly (*).

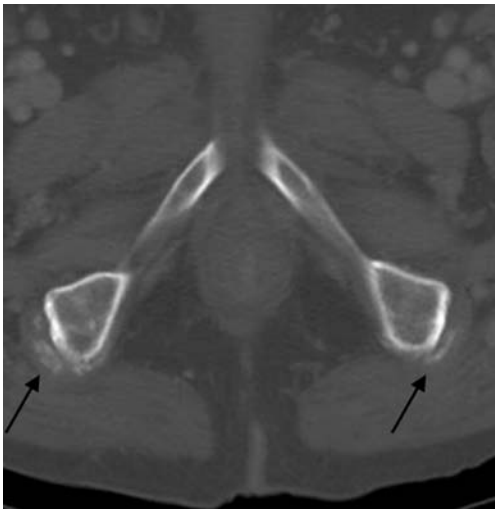

CPPD. Figure 3 Calcium pyrophosphate dihydrate (CPPD) crystal deposition is present in the hamstring tendon origins bilaterally on this CT image (*arrows*).

mimicking synovial osteochondromatosis. Synovial deposits are more common in the wrist, knee (Fig. 2), metacarpophalangeal, and metatarsophalangeal joints. The synovial membrane may demonstrate acute and chronic inflammatory changes in association with CPPD crystal deposition disease. It is not known if the crystals migrate into the synovium from the adjacent cartilage or are deposited directly within the synovium. Capsular calcification may appear as a linear peripheral density and may be difficult to distinguish from early synovial calcification. It is most commonly observed in the elbow, glenohumeral, metatarsophalangeal, and metacarpophalangeal joints.

Tendons, Ligaments, and Bursae

Tendon calcifications are observed with high frequency in patients with CPPD crystal deposition disease. An incidence of 13.5% was reported in such patients in one study (5). Those tendons more frequently involved include the supraspinatus, triceps, quadriceps, gastrocnemius, and Achilles tendons. Hip adductor, rectus femoris, and hamstring tendon calcification may also be seen (Fig. 3). Tendon calcifications commonly are linear or punctate and usually can be distinguished from the more homogeneous, discrete, and nodular calcifications of calcium hydroxyapatite crystal deposition. Calcification often extends far from the tendon attachment. There is a high correlation between the existence of these tendon calcifications and the extent and intensity of calcific deposits in other joints. Direct translocation of CPPD crystals from the articular or bursal surfaces may be responsible for some of the tendinous calcification.

Ligaments can also calcify. Sometimes, the calcification is not dense enough to be visualized on conventional radiographs. The ligamentum flavum and dura mater can contain calcific deposits. Bursal calcification is most common in the olecranon and subacromial bursae.

Other Extra-Articular Soft Tissues

Soft tissue and vascular calcification may be seen in CPPD crystal deposition disease. In particular, tumor-like masses of CPPD crystals can be seen in the extra-articular soft tissues. This manifestation of CPPD crystal deposition disease, known as "tophaceous pseudogout," is rare. In one study, 7 cases of massive focal CPPD crystal deposition disease were identified in atypical locations (6). The patients ranged in age from 31 to 86 years and 6 of them were women. These crystalline masses have been seen near the elbow, finger, jaw, acromioclavicular joint, and hip. Lesions are solitary and usually occur in areas of chondroid metaplasia without predisposing metabolic abnormality. Although the mechanism for development of these masses is not known, it has been postulated that hypertrophic metaplastic chondrocytes accumulating proteoglycans intracellularly provide a seeding site for crystal formation. These calcified masses may initially be mistaken for benign or malignant chondroid or other soft-tissue tumors, tophaceous gout, and tumoral calcinosis. Misdiagnosis sometimes leads to unnecessary surgery. The patterns of calcification usually can be differentiated from the lobular pattern of calcification in tumoral

calcinosis by their granular and more delicate appearance. Calcified soft tissue masses related to CPPD crystal deposition are of intermediate to low signal intensity on MR imaging examinations. They can present as the only manifestation of CPPD crystal deposition disease. Pressure erosion of adjacent osseous structures may be seen. It is important to identify the CPPD crystals, as these masses have also been mistaken for malignant cartilaginous tumors on histologic evaluation because of the presence of chondroid metaplasia.

Bibliography

1. Fisseler-Eckhoff A, Muller KM (1992) Arthroscopy and chondrocalcinosis. Arthroscopy 8:98–104
2. Bencardino JT, Hassankhani A (2003) Calcium pyrophosphate dihydrate crystal deposition disease. Semin Musculoskelet Radiol 7:175–185
3. Steinbach LS, Resnick D (1996) Calcium pyrophosphate dihydrate crystal deposition disease revisited. Radiology 200:1–9
4. McCarty DJ, Hogan JM, Gatter RA et al (1966) Studies on pathological calcifications in human cartilage. I. Prevalence and types of crystal deposits in the menisci of two hundred-fifteen cadavers. J Bone Joint Surg 48A:309
5. Foldes K, Lenchik L, Jaovisidha S et al (1996) Association of gastrocnemius tendon calcification with chondrocalcinosis of the knee. Skeletal Radiol 25:621–624
6. Kaushik S, Erickson JK, Palmer WE et al (2001) Effect of chondrocalcinosis on the MR imaging of knee menisci. Am J Roentgenol 177:905–909

CR

▶Computed Radiography

Cranial Nerves

The cranial nerves (CN) consist of 12 pairs of which the CN III–XII are genuine peripheral nerves.

▶Nerves, Cranial

Cranial Settling

Cranial settling is a characteristic deformity of the occiput-C2 region in rheumatoid arthritis. It is also known as vertical atlantoaxial subluxation or pseudobasilar invagination. Two conditions should be met: (i) the superior aspect of the odontoid process should be even or above the foramen magnum line of McRae and (ii) the anterior arch of C1 should assume an abnormally low position in relation to C2. Cranial settling is a high risk factor for development of myelopathy.

▶Rheumatoid Arthritis

Craniopharyngioma

A tumor located inside the sella turcica, outside in the suprasellar region, or with a sellar and suprasellar component, but always arising from remnants of Rathke's pouch. The tumor often appears cystic, with calcification and irregular peripheral enhancement.

▶Pituitary Gland

Crazy Paving

The superimposition of ground glass opacity and reticular pattern often having the appearance of interlobular septal thickening is described by the term crazy paving. The term was described as being pathognomonic for alveolar proteinosis, in fact it shows a 100% prevalence in patients with alveolar proteinosis. However, it is not specific, because it is also observed in diseases characterized by filling in of the alveolar spaces with liquid or semiliquid and cellular material combined with thickening of the intra- and interlobular septa such as edema, ARDS, hemorrhage, acute interstitial pneumonitis (AIP), or pneumonia.

▶Pulmonary Opacity, Extensive Pattern

CREST

CREST (calcinosis, Raynaud's phenomenon, esophageal dysfunction, scleroderma, teleangiectasia)is a subset of systemic scleroderma. It is not identical to the limited form of systemic scleroderma, but it is thought to show a slightly better prognosis than systemic scleroderma.

▶Connective Tissue Disorders, Musculoskeletal System

Cretinism

▶Congenital Malformations, Thyroid, and Functional Disorders

CRM

▶Circumferential Resection Margin

CRMO

Chronic recurrent multifocal osteomyelitis, usually not associated with organisms and thus not true osteomyelitis. May be a feature of SAPHO (synovitis, acne, pustulosis, hyperostosis [CRMO], and osteitis [CRMO]).
▶Osteomyelitis, Neonates, Infants, Childhood: Including Septic Arthritis and Other Important Soft Tissue Infections/Abscesses

Crohn Disease

Francesca Maccioni[1], Sara Parlanti, Francesca Siliquini, Federica Carrozzo[1]
Department of Radiological Sciences, Policlinico Umberto I-University of Rome La Sapienza, Rome, Italy
francesca.maccioni@uniroma1.it

Synonyms

Crohn disease; Granulomatous enteritis; Granulomatous enterocolitis; Regional ileitis

Definition

Crohn disease is a chronic inflammatory disorder of the alimentary tract of unknown etiology. It is most common in northern Europe, North America, and Japan. The disease most frequently affects the wall of the distal ileum and the right colon, but it may involve any gastrointestinal segment, from mouth to anus, with a typical segmental spreading and a chronic course of relapse and remission.

Generally, the disease has an early onset, around the second to third decade of life, but is not rare in the pediatric age group; a second peak of incidence is observed in an older age group. It can present at virtually any age and lasts for the patient's entire life, with a typical relapsing–remitting course.

Although the pathogenesis of Crohn disease remains unknown, there is an emerging consensus that it results from the complex interaction of multiple genetic, immunologic, and environmental factors. It starts as a breach of the mucosal barrier by a specific infectious agent or environmental toxin, causing inflammation perpetuated by exposure of luminal microflora to the mucosal immune system, and it becomes chronic as a result of a genetically determined failure of immunologic downregulation. Uncontrolled fibrogenesis may lead to stricture formation, and microbial antigens across the mucosa determine the extraintestinal localizations of disease.

Although unpredictable, three main Crohn disease phenotypes (or courses) have been recently identified according to the Vienna classification of Crohn disease (International Working Party for the World Congress of Gastroenterology, 1998): inflammatory (nonfibrostenosing and nonperforating), perforating, and fibrostenosing, with the perforating phenotype being more aggressive and frequently associated with severe complications (1, 2).

Pathology/Histopathology

The disease may involve any part of the gastrointestinal tract, but preferentially the distal ileum, with the majority of patients having an ileitis or ileocolitis.

The small bowel is affected in approximately 80% of cases, particularly the distal ileum, either alone (in 25–35% of cases) or associated with colon localization (in about 30–55% of cases); in only 15–25% of patients is the colon involved alone, frequently at multiple sites.

Involvement of the esophagus, stomach, duodenum, or jejunum in isolation or in association with other common sites is rare. Perianal disease is usually associated with rectal involvement.

Macroscopically, the disease is characterized by a thickened bowel wall and frequently also by a narrowed bowel lumen, which is associated with edematous and thickened mesenteric fat tissue and enlarged local lymph nodes. On the mucosal surface, longitudinal and irregular

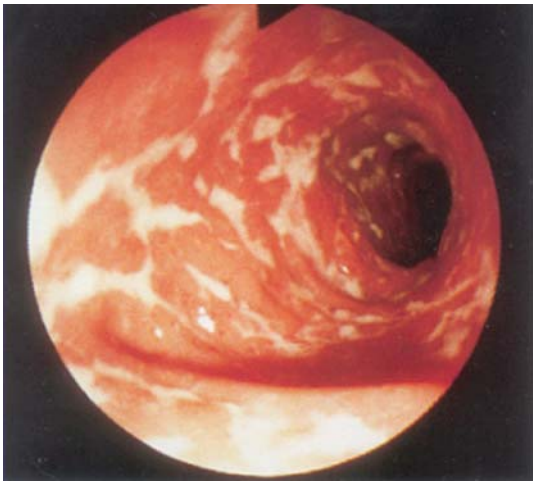

Crohn Disease. Figure 1 Active Crohn disease of the distal ileum. Endoscopic image shows hyperemic mucosa with multiple serpiginous ulcerations, covered by fibrin exudate, at the level of the distal ileum. (Courtesy of Dr. V. D'Ovidio, Department of Gastroenterology, University of Rome La Sapienza.)

ulcerations may be present. At endoscopy, in active disease the mucosal surface is usually hyperemic and is associated with aphthoid or more severe ulcerations—linear, irregular, or serpiginous—usually arising on the mesenteric border (Fig. 1).

Microscopically, the main characteristic of Crohn disease is transmural inflammation, with inflammatory cell infiltrates involving all wall layers. The inflammatory process typically starts in the submucosa layer, consisting of lymphocytes, macrophages, and plasma cells and producing lymphoid hyperplasia and mucosal aphthoid ulcers in the early phases. Aphthoid ulcers develop into linear ulcers and fissures to produce an ulceronodular, so-called cobblestone appearance. In more advanced phases, chronic inflammatory cell infiltrates spread to all wall layers, occasionally producing noncaseating submucosal granulomas consisting of macrophages within the lamina propria in relation to cryptic disruption.

In advanced disease, fibrosis, deep mucosal ulcerations, and transmural fissures are common findings. There is a tendency to involve the serosal surface, which is usually inflamed and hyperemic, associated with involvement of mesenteric fat and adjacent tissues. Typically, the inflammatory process progressively extends outside the intestinal wall, involving first the perivisceral fat tissue (thus producing fibrofatty proliferation and mesenteric adenopathies), and then the adjacent bowel loops, muscles, and genitourinary structures, producing adhesions and enteroenteric, enterocutaneous, and enterovesical fistulas, abscesses, and phlegmons. Toxic megacolon and neoplasms such as lymphoma and carcinoma may also occur.

Clinical Presentation

Crohn disease is characterized by cardinal symptoms, including diarrhea (85%) with variable daily and nocturnal evacuation frequency (three to six times per day), caused by bile salt malabsorption and bacterial overgrowth; bloody diarrhea; abdominal pain (55%); weight loss (65%); and bowel distension, reflecting the typical ileocecal disease localization.

Clinical findings may include a fullness in the right iliac fossa, low-grade fever, tachycardia, and elevated laboratory inflammation findings, such as erythrocyte sedimentation rate, C-reactive protein, and white blood cell count. Other blood tests may be helpful in detecting Crohn disease, such as the antiendomysial antibody test, which is related to the differential diagnosis at initial presentation; the anti-*Saccharomyces cerevisiae* antibody (ASCA) test; and the antiperinuclear neutrophil cytoplasmic antibody (pANCA) test. The ASCA test is thought to be relatively specific to Crohn disease, probably reflecting leakage of the yeast antigen across the mucosal barrier. Conversely, the pANCA test has shown a higher specificity for ulcerative colitis. However, neither of the tests is as specific as originally thought, but they can provide useful discriminatory information when used in combination (ASCA positive, pANCA negative in Crohn disease, and vice versa in ulcerative colitis).

In some cases, the disease can be nonspecific in its presentation, with little more than malaise and weight loss; these cases are a major diagnostic challenge.

Lactose intolerance is common, with milk, cream, and rich cheese foods particularly troublesome. Constipation can reflect an intestinal stricture with subacute obstruction or inflammation confined to the distal colon. Abdominal pain is often localized to the right iliac fossa and suprapubic region, is mild to moderate in intensity and cramping, and is exacerbated by spasm, particularly before passing stool. In the majority of patients, the physical signs of Crohn disease may be evident, represented by anemia, glossitis, aphthous ulceration in the oral cavity, and dehydration requiring prompt medical intervention (1, 2).

The presence of a positive family history of ►inflammatory bowel disease markedly increases the probability of a diagnosis of Crohn disease: 10–20% of Crohn disease patients have an affected first or second-degree relative, compared with less than 1% of the general population. There is also a significant

association of Crohn disease with ankylosing spondylitis, resulting from a shared genetic susceptibility. Major histocompatibility complex associations observed in the subgroup of Crohn disease patients include ankylosing spondylitis (HLA-B27) and primary sclerosing cholangitis (haplotype A1-B8-DR3).

Imaging

Several imaging modalities are used to detect and assess Crohn disease, including barium studies (conventional enteroclysis, small bowel follow-through, and barium enema studies), colonoscopy, ultrasonography, computed tomography (CT), and magnetic resonance imaging (MRI). These modalities can help localize lesions, confirm the clinical diagnosis, assess the extent of disease, and establish inflammatory activity.

Endoscopy and barium studies are widely considered the principal tools for diagnosing and evaluating Crohn disease in the small and large bowel; however, they have a limited capability to demonstrate the transmural extent of disease or extraintestinal complications.

After more than 50 years from their clinical introduction, barium studies of the small bowel are still considered the gold standard for evaluating the small bowel. The contrast agent can be orally administered and its passage followed through the entire small bowel, or it can be administered through a nasojejunal tube. Such administration allows the use of a double-contrast technique, which is otherwise not possible, by adding air or methylcellulose to the barium contrast agent. Barium studies can detect the site and length of lesions, the severity of strictures, and the presence of enteroenteric fistulas with high accuracy. At barium studies, the pathologic segment is usually well separated from the adjacent bowel loops by the fibrofatty proliferation and by bowel wall thickening. However, extraintestinal abscesses, phlegmons, and nonenteric fistulas can be underestimated (Figs 2 and 3).

Colonoscopy allows evaluation of the involvement of colonic mucosa, and in most cases it can be extended to the distal ileum (ileocolonoscopy). Moreover, at endoscopy multiple biopsies are routinely obtained, which is considered extremely important for confirming the diagnosis of Crohn disease.

Cross-sectional imaging, offering three-dimensional visualization and vascular information, has the advantage of identifying the presence of intraperitoneal or extraintestinal complications, such as abscesses and enterocutaneous and extraintestinal fistulas that may require surgical planning. On the other hand, cross-sectional imaging does not allow detection of subtle or advanced mucosal lesions.

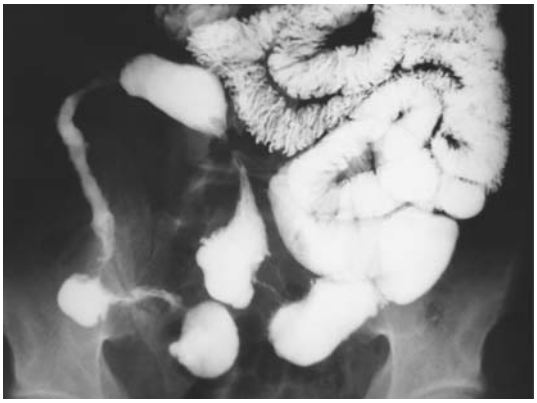

Crohn Disease. Figure 2 Active Crohn disease lesions of the distal ileum. Follow-through barium study shows a long segment of the distal ileum characterized by multiple stenoses and sacculated prestenotic dilations due to the typical segmentary spreading of disease. At the level of the stenotic segments, a cobblestone pattern is also observed.

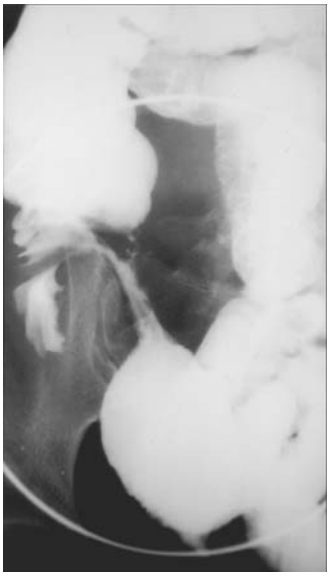

Crohn Disease. Figure 3 Enterocolic fistula. At the barium study, a tight stricture of the distal ileum and irregularity of the cecal fundus are observed, suggestive of ileocecal Crohn disease. A spot view demonstrates a tiny fistulous tract between the terminal ileum and the right colon adjacent to the ileocecal valve, a common extramural bowel complication.

Ultrasound (US), thanks to its noninvasiveness, low cost, and ready availability, is increasingly used as the initial screening modality and as an alternative examination in patients with atypical abdominal symptoms, either

acute or chronic. With modern US equipment, it is possible to make a confident US diagnosis of Crohn disease in most cases.

US can suggest ileocecal Crohn disease quite reliably. The sonographic hallmark is bowel wall thickening that involves all layers of the affected intestinal tract, ranging from 5 to 20 mm. Next to the terminal ileum, the cecum and appendix are not infrequently involved. The layer architecture of the bowel wall is often locally disturbed. In most chronic lesions, the submucosal layer is typically thickened and hyperechoic, likely due to increased submucosal fat either in active or nonactive disease; such submucosal increased thickening and echogenicity produces the typical layered pattern of Crohn disease. The affected bowel shows decreased peristalsis and a narrowed lumen, and it is often surrounded by noncompressible swollen fatty tissue. Mesenteric lymph nodes may be markedly enlarged, and in many cases an abscess, fistula formation, or prestenotic dilatation can be diagnosed as well.

With severe inflammation, the wall may appear diffusely hypoechoic with partial or total loss of layering due to transmural edema, with a central hyperechoic line that corresponds to the narrowed lumen. Peristalsis is reduced or absent, and the diseased segment is noncompressible and rigid, with a loss of haustra. However, the same finding of layering loss may be observed in the presence of diffuse wall fibrosis with nonactive disease.

The accuracy of US is further improved by the use of color Doppler imaging, which is helpful in detecting hyperemia of an inflamed bowel wall and adjacent fat during active disease (Fig. 4).

In conclusion, the liberal use of US in patients with abdominal symptoms constitutes a powerful and reliable tool for the early detection of ileocecal Crohn disease. It decreases the diagnostic delay and prevents unnecessary surgical interventions.

CT is a well-established imaging modality for detecting Crohn disease lesions and is preferred for evaluating the transmural extent of the disease and for diagnosing extraintestinal and intraperitoneal complications. In contrast to US, CT is generally not performed as an initial screening procedure in patients with atypical and protracted and abdominal symptoms. However, because CT is increasingly used as an emergency imaging modality in patients with acute abdominal symptoms, it may undoubtedly help detect clinically unsuspected cases of Crohn disease.

The CT scan is usually obtained in the supine position from the dome of the liver to the level of the perineum to get a panoramic visualization of the entire intestine, with a 5-mm thickness. High-quality multiplanar reformatted images, particularly coronal planes, obtained with multidetector CT equipment can be extremely useful for localizing Crohn disease lesions.

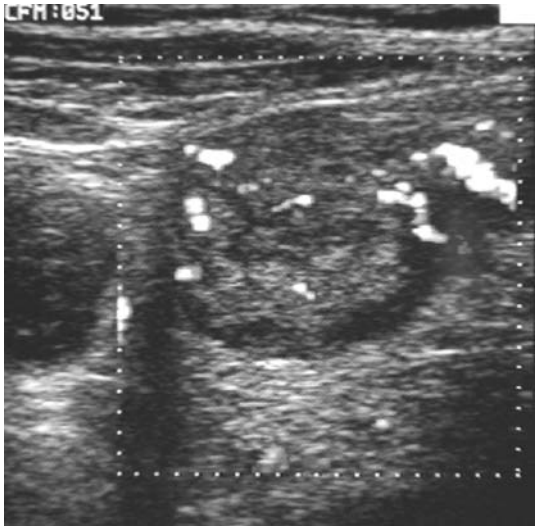

Crohn Disease. Figure 4 Active Crohn disease of the distal ileum. Ultrasound image shows a marked concentric thickening of the bowel wall and a narrowed lumen of the terminal ileum. Increased color Doppler signal suggests a high degree of inflammation of the bowel wall, as well as initial inflammatory involvement of the adjacent mesenteric fat.

To obtain diagnostic CT abdominal images or to provide positive or negative lumen contrast and dilation, various types of intraluminal contrast agents should be administered. Such contrast agents can be administered either orally (about 1–1.5 L given 90 min before the examination) or through a nasojejunal tube (CT-enteroclysis). The contrast agent should provide a homogeneous luminal enhancement, high contrast between the lumen and the bowel wall, and minimal mucosal absorption, and lead to no artifact formation or significant adverse effects.

Positive contrast agents at CT (iodinate or barium solutions) can be helpful for distinguishing bowel loops from enlarged lymph nodes or extramural fluid collections. However, using intraluminal positive contrast agents for bowel wall enhancement after intravenous administration of contrast material may obscure submucosal lesions.

Negative intraluminal contrast agents (methylcellulose or water iso-osmolar solutions) can similarly help detect normal or pathologic bowel wall segments, with the advantage of better visualization of the wall contrast enhancement and submucosal lesions (Fig. 5).

The use of an intravenous contrast agent is extremely important for better visualization of the normal and inflamed bowel wall (3, 4).

MRI is currently considered an emerging cross-sectional modality for evaluating abdominal and intestinal diseases, and is the modality of choice for evaluating

Crohn disease lesions at some institutions. In fact, recent technological advances (increased gradient strength, phased array coils, fast sequences, and so on) have greatly improved the quality of abdominal MR images, allowing acquisition of high-resolution images of the intestine during a single breath-hold, with significant increases in temporal and spatial resolution. In the next years, MRI could become the modality of choice for Crohn disease patients, first because it provides a diagnostic capability similar to CT but without radiation exposure, a fact that is particularly important for younger patients and children, who will have multiple studies during their lives. Moreover, it has an intrinsic higher tissue contrast than CT, allowing better assessment of inflammation in Crohn disease lesions. Finally, the multiplanar panoramic capability of MRI allows, differently from US, evaluation of the entire bowel using multiple planes, similar to multidetector CT images, allowing better identification of Crohn disease lesions and their complications. The lack of radiation exposure justifies and allows the use of MRI for the periodic assessment of Crohn disease activity, for clinical trials, and for follow-up studies.

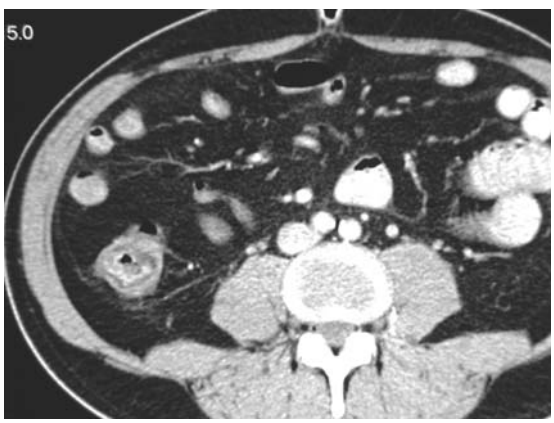

Crohn Disease. Figure 5 Recurrent Crohn disease in a patient who underwent ileocecal resection. The computed tomographic image, on axial plane, shows a marked thickening of the wall of the ileal anastomotic loop, with a narrowed lumen and proliferation of perivisceral fat tissue.

The MRI examination is preferably performed using a high magnetic field (1.5 T) and phased array coil for increased signal-to-noise ratio. The diagnostic imaging protocol should include both T1 and T2-weighted sequences to detect and characterize intestinal lesions, with the acquisition of axial and coronal thin, contiguous images. Acquisition of coronal and axial images is obtained with a 4–6-mm section thickness and a field of view of at least 350350 mm to cover all the bowel loops, adding sagittal plane images if necessary for a complete evaluation of disease.

Various kinds of intraluminal MRI contrast agents have been clinically tested: positive (gadolinium solutions), negative (superparamagnetic), and biphasic (water-like). Negative or biphasic contrast agents are more commonly used for evaluating small bowel diseases. Biphasic intraluminal contrast agents may produce either high or low signal, depending on the pulse sequence used; the more widely used have a water-like behavior, demonstrating low signal intensity on T1-weighted sequences and high signal intensity on T2-weighted sequences.

To assess inflammatory lesion activity, T1-weighted spoiled gradient imaging, after intravenous administration of a gadolinium chelate, and T2-weighted fat-suppressed imaging are used (Fig. 6) (3, 5). On the other hand, to obtain morphologic information, fast T2-weighted sequences (fast half-Fourier acquired single-shot fast spin-echo) and fast T1 and T2-weighted sequences with a steady precession (true-FISP or FIESTA) are preferred. True fast imaging with a steady precession (FISP) sequence provides high-resolution images of the intestine, mesenteric lymph nodes, and vessels. However, this kind of

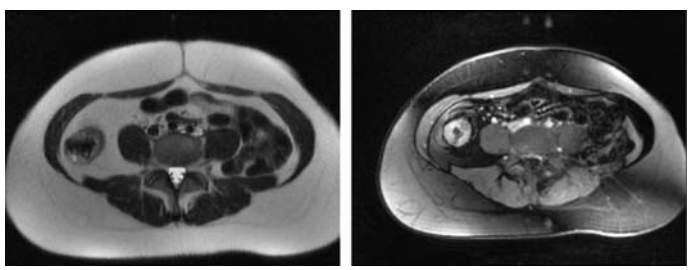

Crohn Disease. Figure 6 Crohn disease of the right colon. T1-weighted magnetic resonance images on axial plane obtained after intravenous administration of gadolinium chelate contrast agent and with suppression of the fat tissue, showing marked bowel wall enhancement with concentric bowel wall thickening at the level of the right colon. The T2-weighted image, obtained at the same level, shows bright bowel wall signal, and wall thickening can be observed as well.

sequence is susceptible to artifacts from intraluminal air due to chemical shift phenomenon, obscuring subtle bowel wall thickening.

The T2-weighted turbo spin-echo sequence provides excellent soft-tissue contrast and is not susceptible to black luminal artifacts; when used with fat suppression, bowel wall edema and mesenteric inflammation can be highlighted, which is useful for assessing the degree of disease activity.

The gadolinium-enhanced fat-suppressed T1-weighted sequences provide excellent visualization of hypervascular inflamed bowel wall, being extremely useful to localize active and complicated intestinal lesions, as well as assess the degree of disease activity (3–5).

Usually, a variable combination of true FISP, T2-weighted turbo spin-echo, and gadolinium-enhanced echo sequences, with or without fat suppression, is used to evaluate the extramural extent of Crohn disease lesions and complications.

Nuclear Medicine

Nuclear medicine plays little role in the initial characterization of Crohn disease. Leukocytes labeled with either technetium-99m-hexamethyl-propylene-amine-oxime (HMPAO) or indium-111 can be used to assess active bowel inflammation in any inflammatory bowel disease.

Once the histological diagnosis of Crohn disease has been established, technetium-99m-HMPAO-labeled white blood cells, with single photon emission CT imaging, may be used to assess disease activity and disease length.

Compared with the indium-111 label, the Tc-99m HMPAO label is preferred due to the better radionuclide availability and better imaging characteristics; moreover, it allows imaging sooner after injection. However, imaging must be done within an hour after injection of Tc-99m-HMPAO-labeled leukocytes because there is normal excretion into the bowel after this time, unlike indium-111-labeled leukocytes, not having bowel excretion.

Advantages over barium studies include the contemporary examination of both large and small bowel, lower radiation exposure (particularly important in younger patients), and higher patient tolerance.

False-positive bowel activity can be found with gastrointestinal bleeding, swallowed leukocytes, or activity related to in-dwelling enteric tubes. In addition, leukocyte uptake is not specific for Crohn disease and will be seen in most infectious or inflammatory bowel processes. As mentioned earlier, there is often normal bowel excretion of Tc-99m-HMPAO leukocytes if imaging is done more than an hour after injection.

Diagnosis

Complete evaluation of Crohn disease is usually difficult because it should include the characterization of the disease, differentiation from other inflammatory bowel diseases, localization within the small and large bowel, the extent of disease, disease severity and possible complications, and the degree of inflammatory activity.

The early phase of the disease is commonly suspected and assessed based on clinical and laboratory findings. Colonoscopy and barium study are the most commonly used imaging modalities in early phases, being able to appreciate enlarged lymphoid follicles, erosions, and aphthoid ulcers. Because of its noninvasiveness, low cost, and ready availability, US should be performed as a primary imaging modality in the clinical evaluation of Crohn disease in association with conventional imaging and laboratory findings.

CT and MRI are preferred when evaluating more advanced phases to assess the transmural extent of the disease and any intraperitoneal complications. Extraintestinal complications are largely detected on cross-sectional imaging. CT and MRI are also useful for characterizing the different disease courses, thus helping with the planning of medical treatment in cases of active inflammatory disease and of ▶surgical treatment in fistulating, fibrostenosing, or perforating disease with abscesses.

Panoramic views and multiplanar images associated with high soft-tissue contrast, static and dynamic imaging capabilities, and the absence of ionizing radiation exposure represent the advantages of the MR modality over CT. On the other hand, CT offers other advantages over MRI, such as shorter examination times, higher availability, higher spatial resolution, and the possibility to choose thickness slices and planes after data acquisition.

Treatment

The ▶medical treatment of Crohn disease varies according to the different disease phases, in particular the acute and the remission phases. During acute exacerbation, the main medical management consists of intravenous administration of glucocorticoids (hydrocortisone or methylprednisolone) in addition to metronidazole. Steroid therapy should be limited because of its various adverse effects, including osteonecrosis, myopathy, osteoporosis, and growth retardation. Intravenous cyclosporine may be used to inhibit cell-mediated immunity for further immune modulation and to increase the corticosteroid response.

The target of chronic therapy is remission of bowel inflammation. Local aminosalicylates have been the main therapeutic agents because of their anti-inflammatory

activity, each one having a different carrier molecule directed to a specific region of the bowel. Sulfasalazine and balsalazide are primarily released in the colon. Dipentum and Asacol are formulations for targeted release in the distal ileum and colon. Pentasa is released in the duodenum to the distal colon, whereas Rowasa is specific for the rectum and distal colon.

Azathioprine, 6-mercaptopurine, and methotrexate are other nonsteroidal immune modulators that are used as alternatives to glucocorticoids for inducing remission. Adverse effects of azathioprine and 6-mercaptopurine are uncommon (incidence of pancreatitis, allergic reactions, infection). The main disadvantage to the use of azathioprine and 6-mercaptopurine is their slow onset of action; response to therapy is usually noted after 3–6 months of treatment. Methotrexate, the long-standing folic acid antagonist, is effective in many patients with disease refractory to azathioprine and 6-mercaptopurine. Nevertheless, it has well-known adverse effects, mainly leukopenia and gastrointestinal upset.

New therapies are targeting tumor necrosis factor-alpha. Biological agents such as infliximab, a monoclonal chimeric antitumor necrosis factor-alpha antibody, are becoming available and showing promising results, with an increased remission rate. Other agents such as mycophenolate have been developed to inhibit guanine nucleotide synthesis and thereby inhibit B and T lymphocytes.

Most patients with Crohn disease undergo surgery within 20 years of diagnosis. Surgical treatment is required in cases of stricture, intractable or fulminant disease, anorectal disease, and intraabdominal abscess. Commonly, half of the patients who have had one surgical treatment will require further surgery for recurrent disease within 10 years. Recurrence occurs more frequently in cases of younger age of onset, enterocutaneous fistulas, multiple sites of disease, and a perianastomotic site of recurrence in stricturoplasty. Recurrence is often defined as detectable active disease associated with reactivation of symptoms (1, 2).

The basic tendency in surgery for Crohn disease is to limit small bowel resection of the involved segments. Stricturoplasty, performed by incising a stricture longitudinally and then suturing it transversely to widen the lumen, is often done when a severe stricture is present to preserve the small bowel and prevent short-bowel syndrome. In the majority of cases, the lack of perioperative deaths with stricturoplasty is a favorable feature compared with surgical resection.

Finally, CT-guided percutaneous abscess drainage may obviate surgery in selected cases. Recently, this has shown great success both as a temporizing measure and as definitive therapy, with a decreased rate of recurrence compared with that of surgery.

Key Points

Crohn disease is a chronic inflammatory bowel disease that commonly involves the distal ileum and the cecum and right colon, characterized by clinical, radiological, and histological features.

Infectious agents or environmental toxins associated with immunological downregulation cause inflammation of the mucosal layer that becomes chronic, until there is uncontrolled fibrogenesis, strictures, lesions, and extramural complications.

Several imaging modalities can detect and assess Crohn disease. Each has distinct advantages and disadvantages, and the decision of which one to use depends on the patient's condition and the phase of the disease.

Medical management is used in the acute or chronic/relapsing phases of the disease. Glucocorticoids (hydrocortisone or methylprednisolone) in addition to metronidazole represent the main acute therapy. Aminosalicylates, methotrexate, azathioprine, and 6-mercaptopurine are used in the chronic phases. Infliximab (a monoclonal antibody) is a new therapy that targets tumor necrosis factor-alpha.

Surgical treatment is indicated in cases of strictures, bleeding, abscesses, perforation, and carcinoma, which are complications not amenable to medical treatment. There is actually a tendency to conservative surgical management; nevertheless, recurrences are common.

Bibliography

1. Derek PJ, Miles P, Neil M (1999) Gastroenterology and Hepatology. McGraw-Hill, New York, Clinical Medicine Series, chapter 42, pp 395–415
2. Thoeni RF (1994) Idiopathic inflammatory disease of the large and small bowel. In: Freeny PC, Stevenson GW (eds) Margulis and Burhenne's Alimentary Tract Radiology. 5th edn. Mosby, St Louis, pp 585–601
3. Furukawa A, Saotome T, Yamasaki M et al (2004) Cross-sectional imaging in Crohn disease. Radiographics 24:689–702
4. Maccioni F, Viscido A, Marini M et al (2002) MRI evaluation of Crohn disease of the small and large bowel with the use of negative superparamagnetic oral contrast agents. Abdom Imaging 27:384–393
5. Maccioni F (2004) MRI of colitis. In: Chapman AH (ed) Radiology and Imaging of the Colon. Diagnostic Imaging. Springer, New York, chapter 20, pp 201–213

Cross-sectional Imaging

Include ultrasonography (US), computed tomography (CT) and magnetic resonance imaging (MRI).

▶Colitis, Ulcerative

Crossing Artery

Accessory renal arteries are frequent at the lower pole of the kidney and may have a close relationship to the ureteropelvic junction.

▶Ureteropelvic Junction Syndrome

Crouzon Syndrome

Crouzon syndrome (acrocephalosyndactyly type II), the most frequent craniofacial dysostosis, is characterised by bilateral coronal synostosis with brachycephalic or oxycephalic vault, maxillary hypoplasia, shallow orbits with proptosis, hypertelorism, cleft palate. Concurrent intracranial anomalies (anomalous venous drainage, hydrocephalus, Chiari I malformation) are common. Other non-obligatory features include calcification of the stylohyoid ligament, cervical spine abnormalities, elbow malformations, minor hand deformities, visceral anomalies, musculoskeletal deformities and skin lesions. Limb anomalies are non-specific.

▶Congenital Malformations, Nose and Paranasal Sinus

Cryotherapy, Hepatic Tumours

Technique for treatment of hepatic neoplasm based on local tumour destruction *in situ* by freezing. The resulting freeze process causes irreversible cellular damage and tissue necrosis is obtained.

▶Interventional Hepatic Procedures

Cryptococcosis

Cryptococcosis is an infection caused by the saprophytic yeast-like fungus Cryptococcus neoformans.

▶Infection, Opportunistic, Brain

Cryptorchidism

Cryptorchidism is the absence of the testis in the ipsilateral hemiscrotum. About 90% of undescended testes are located in the inguinal canal, with the remaining 10% located in the abdomen. Very rarely, the missing testis is ectopic and can be found in the perineum, in the contralateral hemiscrotum, or at the base of the penis.

▶Genital Tract

CSF

Cerebro-spinal fluid.

▶Tumors, Spine, Intradural, Extramedullary

CT

▶Computed Tomography

CT Angiogram Sign

The CT angiogram sign refers to the presence of contrast-enhanced, well-visible vascular structures surrounded by consolidated lung parenchyma with a much lower contrast uptake. Originally it was described as being pathognomonic for bronchioloalveolar carcinoma, but it is also seen in pneumonia and lymphoma. It is not seen in an atelectatic lung (due to the strong enhancement of the atelectatic lung parenchyma) and always indicates a pulmonary process.

▶Atelectasis

CT Dentascan

The CT Dentascan is a special computerized reformatting program that has been developed to obtain true cross section of the mandible and maxilla from CT scan.

▶Neoplasms, Odontogenic

CTA

Computed tomography angiography is based on helical or spiral CT and provides the exploration of one volume with each tube rotation.

Ultra rapid, non-invasive X-ray technique for visualisation of the vascular tree.

▶Cerebral Aneurysms

CTAP

Computed tomography (CT) arterioportography. This technique CT allows a higher level of intrahepatic enhancement to be obtained by means of catheter injection of the contrast medium directly into the celiac axis or hepatic artery. It was introduced to increase the detection rate of CT for small hepatic lesions. The use of CTAP has been largely replaced by multiphase helical scanning and tissue-specific enhanced magnetic resonance imaging.

▶Metastases, Hepatic

CTC

▶Computed Tomographic Colonography

Cubital Tunnel Syndrome

Compression of ulnar nerve in cubital tunnel of elbow region, may be due to sports or occupational injury or tumor.

▶Neoplasms, Soft Tissues, Benign

Cup-and-Saucer Deformity

Cup-and-saucer deformity is a characteristic aspect of inflammatory joint mutilation in the late stage of rheumatic arthritis or psoriatic arthritis, with typical pointed residual bone of the proximal phalanx and grooved destruction of the distal phalanx articulating with each other.

▶Spondyloarthropathies, Seronegative

Cushing's Syndrome

Corresponds to the presence of an adrenocorticotropic hormone (ACTH)-producing tumor. Up to 70% of the pituitary tumors will be visible on magnetic resonance imaging (MRI). To find the source of ACTH overproduction in false-negative MRI cases, bilateral inferior petrosal sinus sampling is recommended to measure the ratio of central to peripheral plasma ACTH levels.

▶Pituitary Gland

Cutaneous Lesions, Breast

Geert M. Villeirs
Division of Genitourinary Radiology
Ghent University Hospital
Ghent, Belgium
geert.villeirs@ugent.be

Definition

The skin of the breast can harbour a number of dermatologic pathologies (e.g. eczema, erythema, keratinization disorders, pigmentation disorders, etc.) and manifestations of systemic disease (e.g. scleroderma, dermatomyositis, polyarteritis nodosa, sarcoidosis, lupus erythematosus, etc.). These abnormalities usually do not significantly differ from similar involvement at other sites in the body.

The breast skin may also be involved in a generalized or focal non-skin disease process. A thickened oedematous skin may be seen especially in the dependent parts of one or both breasts due to cardiac decompensation, renal insufficiency, hypoalbuminaemia and fluid overload. Unilateral skin thickening can also be the result of venous or lymphatic stasis caused by venous thrombosis or lymphatic interruption (e.g. axillary dissection, nodal metastases, radiation therapy, etc.). Skin changes such as thickening, erythema and increased temperature, or thickening, dimpling and retraction may be ancillary findings in an underlying inflammatory (mastitis, abscess), post-traumatic (fat necrosis, scar formation) or malignant disease process. Special types of such reactions are Mondor's disease (band-like skin thickening and erythema due to thrombosis of a superficial vein) and ▶Paget's disease (eczematous involvement of the nipple–areolar complex due to ductal carcinoma *in situ*, see elsewhere in this Encyclopaedia).

Both benign (naevi, warts, sebaceous cysts, keloids, fibromas, haemangiomas, lymphangiomas, etc.) and malignant tumours (melanomas, sarcomas, metastases and cutaneous infiltration by haematologic malignancies) may be encountered as nodular or diffuse lesions of the skin.

Pathology/Histopathology

The skin can react to primary or secondary irritation with only a limited number of symptoms, such as erythema, oedema, diffuse or focal thickening, desquamation, ulceration, etc. Because of its superficial location, it is obvious that most reactions are readily diagnosed clinically and that imaging techniques only play a secondary role. On the other hand, some skin manifestations may trouble the mammographic assessment, because they obscure the underlying tissue due to oedema, or cause nodular densities or (pseudo) calcifications that can be mistaken for intramammary lesions.

Clinical Presentation

Inspection, clinical examination and patient history are of utmost importance for correct diagnosis of dermatologic pathologies, skin tumours and cutaneous manifestations of systemic disease. A detailed description of these pathologies is beyond the scope of this text.

In unilateral or bilateral skin oedema, in which the skin gets swollen and dimpled, the clinical history, general physical examination and lab results are also important to correctly attribute cutaneous thickening to systemic diseases such as cardiac decompensation, renal or hepatic insufficiency. Focal inflammatory disease, post-traumatic status and tumoral lesions underneath the skin of the breast may elicit secondary skin reactions that are readily explainable when the underlying disease is identified, either clinically or with imaging techniques. In ►Mondor's disease, for example, thrombosis of a subcutaneous vein may cause a painful erythematous cord-like skin thickening, often associated with preceding trauma or surgery to the breast. In inflammatory carcinoma, obstruction of the cutaneous lymphatics by tumour deposits causes skin thickening with accentuated pores, resembling the skin of an orange, frequently referred to as ►'peau d'orange'.

Mammography

Except for digital mammography, correctly exposed mammograms do not usually show the skin, especially in high-density breasts. The normal breast skin may measure up to 3 mm in thickness and is usually symmetric, but varies individually and thins with ageing.

Dermatologic pathologies and manifestations of systemic disease may not be visible on the mammogram, except when they are large enough to cause nodular or ill-defined densities, or when they become calcified or pseudocalcified (due to ointments, creams or balms containing X-ray attenuating powders). In both cases, tangential views (with or without a marker on the cutaneous lesion) may be necessary to confirm their dermal origin.

Pathologic skin thickening due to oedema or fibrosis is usually associated with accentuation of the oedematous subcutaneous trabecular framework and may be bilateral, or localized and asymmetric. In the latter case, it can only be well visualized in tangent.

When nodular masses of the skin are visible on the mammogram, they can be distinguished from intramammary lesions by their cutaneous location (on tangential views) and by their characteristic radiolucent rim or fissures caused by soft tissue to air interfaces when the breast is compressed (Fig. 1).

Skin calcifications usually originate in sebaceous glands of the skin. They are characteristically spherical (Fig. 2) and have a lucent centre, but occasionally may be more polygonal or punctate. They are peripherally located (sometimes requiring tangential views) and

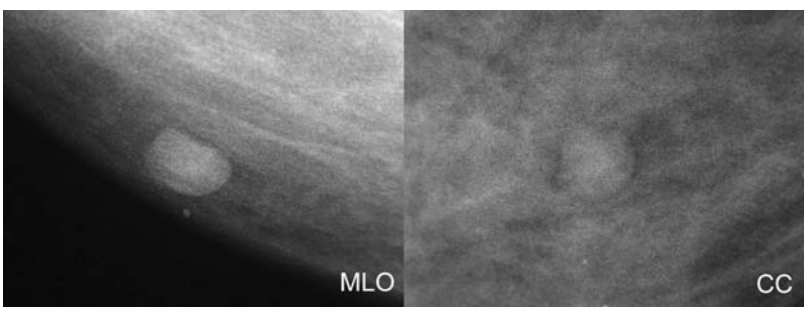

Cutaneous Lesions, Breast. Figure 1 Cutaneous nodule with a radiolucent rim along the boundaries of the lesion in both mammographic projections.

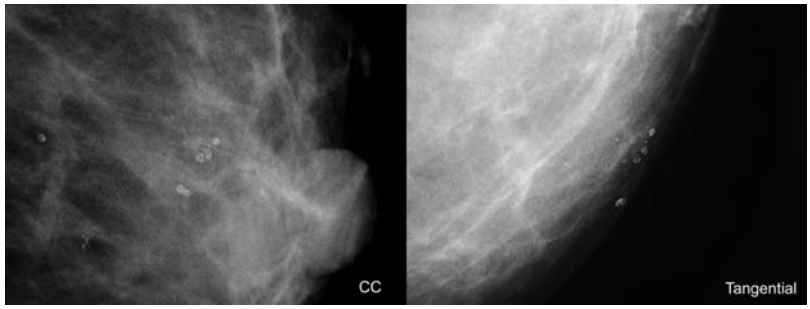

Cutaneous Lesions, Breast. Figure 2 Round lucent-centered calcifications. Their cutaneous origin can be demonstrated on tangential views.

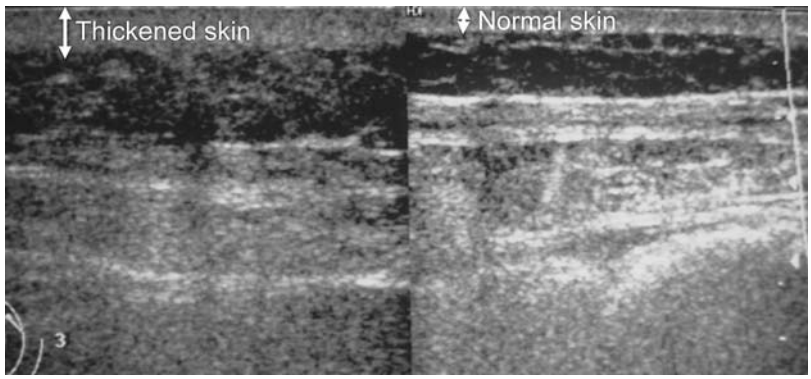

Cutaneous Lesions, Breast. Figure 3 Skin thickening after radiotherapy for breast carcinoma, with indistinct deep margin. Note difference with untreated side.

may be scattered or clustered, but typically maintain a fixed position to one another on different projections or on similar projections at different times ('tattoo sign').

Sonography

The thickened skin is visualized as a broadened hyperechoic rim indistinctly marginated from the underlying isoechoic subcutaneous fat (Fig. 3). The visibility of this area may be improved by using an ▶acoustic standoff pad.

Although sonography can readily demonstrate skin thickening, its role in the diagnostic work-up of cutaneous lesions is limited, except when performed to detect a subcutaneous lesion as the cause of a secondary skin reaction, or to confirm a ▶sebaceous cysts, especially when the latter becomes inflamed. Sebaceous cysts are usually round or oval cutaneous or subcutaneous lesions with varying echogenicity, depending on their relative amount of fluid and echogenic material. Inflamed sebaceous cysts may cause additional skin thickening and increased echogenicity of the surrounding fat.

Magnetic Resonance Mammography

Similar to sonography, MR only plays a minor role in the diagnosis of cutaneous lesions. However, it may be useful for detection or exclusion of underlying disease, especially in mammographically dense breast tissue that could obscure a lesion, or in the post-treatment follow-up to differentiate cutaneous recurrence from post-treatment changes.

Percutaneous Biopsy

Cutaneous lesions that remain indeterminate after inspection, clinical examination, laboratory tests, patient history or even imaging examination(s), may require shave, punch or excisional biopsy for histological

diagnosis. These are usually performed under clinical guidance, although imaging may occasionally be used for selection of the most appropriate biopsy site.

Bibliography

1. Britton CA (1994) Mammographic abnormalities of the skin and subcutaneous tissues. Crit Rev Diagn Imaging 35:61–83
2. Ralleigh G, Walker AE, Hall-Craggs MA et al (2001) MR imaging of the skin and nipple of the breast: differentiation between tumour recurrence and post-treatment change. Eur Radiol 11:1651–1658
3. Sener SF, Milos S, Feldman JL et al (2001) The spectrum of vascular lesions in the mammary skin, including angiosarcoma, after breast conservation treatment for breast cancer. J Am Coll Surg 193:22–28
4. Loffman Felman RL (2002) The tattoo sign. Radiology 223:481–482
5. Ulger H, Erdogan N, Kumanlioglu S et al (2003) Effect of age, breast size, menopausal and hormonal status on mammographic skin thickness. Skin Res Technol 9:284–289

Cutaneous Necrosis at the Finger Tips Like Rat Bites

Cutaneous necrosis at the finger tips like rat bites is a complication of long-standing Raynaud's phenomenon with consecutive ischemia and is relatively common in scleroderma.

"Jaccoud hand" was originally described in rheumatic fever after streptococcal infection. Typically the grave deformities contrast the absence of destructive arthritis. Nowadays, thanks to the rigorous antibiotic treatment of streptococcal infection, it is more often seen in systemic lupus erythematosus.

▶Connective Tissue Disorders, Musculoskeletal System

Cyclopia And Synophthalmia

▶Congenital Malformations, Orbit

Cyst, Breast

Luis Pina
Department of Radiology,
Clínica Universitaria de Navarra, Spain
ljpina@unav.es

Definition

Cysts are local dilatations of terminal duct lobular units filled with fluid (1, 2).

Pathology

Cysts are lined by an epithelium that consists of two layers: an inner epithelial layer and an outer myoepithelial layer. Occasionally they have no epithelial lining (1, 2). The fluid shows a variety of colors, such as clear, green, gray, brown, or almost black, and chemical substances, including pigmented secretions, lipofuscin, hemoglobin-derived products, and even secretory substances related to the diet. Some cysts show apocrine metaplasia, with low proportion of sodium and high proportion of potassium in the fluid, indicating a more active cellular secretion and more frequent recurrence. Other cysts have a transudate-like fluid, with high concentration of sodium and low concentration of potassium. Papillary tumors in the wall of a cyst are rare. Both papilloma and ▶papillary carcinoma may be found.

Clinical Findings

Cysts are very frequent lesions, affecting more than half of the female perimenopausal population, although they may be found in women under the age of 30 and also in postmenopausal women. Most cysts are multiple and bilateral and tend to disappear in older women, but hormonal replacement therapy may induce cyst formation.

Usually cysts are asymptomatic lesions detected on routine imaging techniques. However, cysts may be palpable and discovered by the patient, who may be concerned about a lump in her breast. Usually these cysts are mobile, smooth-contoured masses, although they may be hard and indistinguishable from breast cancer. Palpation may suggest the presence of a cyst, but ultrasound is required because some carcinomas can simulate benign lesions as cysts.

▶Simple cysts are benign lesions with no significative risk to develop into breast cancer. Whether the concurrence of family breast cancer history and cysts increases that risk is debatable.

Imaging

Mammography

Cysts present as round to oval well-circumscribed masses if they are surrounded by fat. If cysts are surrounded by fibroglandular tissue, they show obscured margins or may not even be detected on mammography (Fig.1). Curvilinear calcifications in the cyst wall or calcifications inside the cyst cavity (milk of calcium) may be found (3, 4). Cysts usually are multiple and bilateral, but they may also be single.

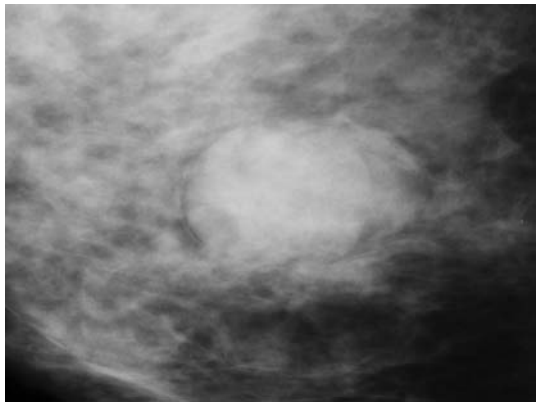

Cyst, Breast. Figure 1 Mammographic appearance of a breast cyst. An oval mass with circumscribed and obscured margins is seen.

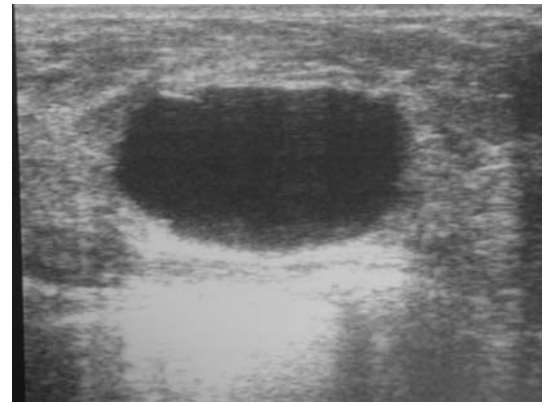

Cyst, Breast. Figure 2 Simple cyst on ultrasonography. An oval, anechoic lesion with posterior acoustic enhancement is seen. A few reverberation echoes are visible peripherally.

In some cases, a cyst is aspirated and filled with air to evaluate the cyst wall on mammography (pneumocystography). This technique allows a good evaluation of the cyst wall, especially for detecting intracystic masses. Nevertheless, the high accuracy of ultrasonography has largely eliminated the use of pneumocystography.

Ultrasound

Simple cysts are thin-walled, anechoic, round to oval lesions with posterior enhancement (Fig. 2). Acoustic shadows are seen at the margins. Sometimes a reverberation artifact may produce internal echoes (3–5). These lesions are soft and may be compressed with the transducer, changing their shape. If the lesions are too deep or small (<5 mm), the acoustic enhancement may not be seen. New ultrasonographic techniques, such as spatial compound imaging or tissue harmonic imaging, may be useful for characterizing a lesion as a cyst (5). Simple cysts are classified as BI-RADS category 2 (benign finding). Occasionally thin septa are seen inside the cyst. Clusters of small cysts may also be observed (Fig. 2).

►Complicated cysts have many of the features of simple cysts but show diffuse and mobile internal echoes (5). These cysts may contain proteinaceous material, blood, cellular debris, infection, or cholesterol crystals. The positive predictive value for carcinoma in these cysts is 0.3%, and therefore they are classified as BI-RADS category 3 (probably benign finding).

►Complex cysts include cysts with internal masses, thick septations, or thick or irregular wall (5). These lesions are suspicious and should be classified as BI-RADS category 4 (suspicious finding). Papilloma, papillary carcinoma, necrotic tumors, abscesses, and hematomas may correlate with these findings (Fig. 3).

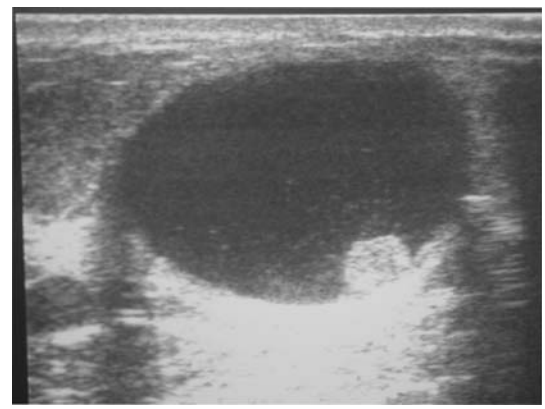

Cyst, Breast. Figure 3 Complex cyst. Ultrasonography reveals a solid lesion within the cyst. Biopsy revealed ►intracystic papilloma.

Magnetic Resonance Imaging

Cysts are smooth-contoured hypointense lesions on T1-weighted sequences and hyperintense on T2-weighted sequences. Typically, cysts do not enhance after contrast medium administration, except if there is wall inflammation or an intracystic mass (3).

Nuclear Medicine

Cysts are not an indication for a nuclear medicine study.

Diagnosis

Ultrasonography is the technique of choice for diagnosing breast cysts (5).

Asymptomatic simple cysts detected on ultrasonography do not need further diagnostic procedures. A 6-month follow-up may be proposed for asymptomatic complicated cysts showing diffuse and mobile internal echoes, as an alternative to fine-needle aspiration.

Symptomatic cysts (palpable, painful) may be aspirated after an ultrasound examination. If the fluid is green or yellow, there is no need for cytologic examination. However, if the fluid is hemorrhagic or if the cyst is complicated, a cytologic study is recommended.

Complex cysts are suspicious lesions that need to be carefully studied. If a negative cytology result is obtained after aspiration of a complex cyst, a biopsy should be performed. Cytology, and even core needle biopsy, may be unable to differentiate between benign papilloma and papillary carcinoma. Sometimes the cytologic examination result of the fluid of a cyst with a carcinoma may be negative (3).

Bibliography

1. Hughes LE (2000) Cysts of the breast. In: Hughes LE, Mansel RE, Webster DJT (eds) Benign Disorders and Diseases of the Breast. Concepts and Clinical Management, Saunders, London, pp 123–135
2. Schnitt S, Connolly JL (2004) Pathology of benign breast disorders. In: Harris JR, Lippman ME, Morrow M et al (eds) Diseases of the Breast. Lippincott Williams & Wilkins, Philadelphia, pp 77–99
3. Heywang-Köbrunner SH, Schreer I, Dershaw DD (1997) Cysts. In: Heywang-Köbrunner SH, Schreer I, Dershaw DD (eds) Diagnostic Breast Imaging. Thieme, Stuttgart, pp 156–165
4. Cardeñosa G (2001) Lobules. In: Cardeñosa G (ed) Breast Imaging Companion. Lippincott Williams & Wilkins, Philadelphia, pp 272–279
5. Mehta TS (2003) Current uses of ultrasound in the evaluation of the breast. Radiol Clin North Am 41:841–856

Cysts, Cerebral and Cervical, Childhood

Huisman T. A.
Johns Hopkins University, Baltimore, USA
thierry.huisman@kispi.unizh.ch

Synonyms

Arachnoid cyst; Cystic hygroma; Branchial cleft cyst; Leptomeningeal cyst; Lymphangioma; Neuroepithelial cyst; Thyroglossal duct cyst

Definition

Epithelial-lined, fluid-filled, well-circumscribed, nonneoplastic benign lesions.

Pathology and Histopathology

Most cerebral and cervical cysts are benign disorders of development. Cysts can also develop as complications of surgery or trauma. Next to esthetic concerns, head and neck cysts can be symptomatic due to compression of vital structures. Intracranial cysts may be incidental findings on imaging or the leading cause of focal neurological deficits. Cysts within the neck may compress neurovascular structures as well as the upper airways. Hemorrhages within these cysts may result in a rapid increase in size, aggravating displacement, and compression of adjacent structures. Finally, secondary infection may complicate the spontaneous course of head and neck cysts (1, 2).

Arachnoid cysts are benign, fluid-filled lesions that are lined by a thin layer of arachnoidea. Arachnoid cysts are believed to result from a duplication or splitting of the arachnoidea. They are located in the space between the dura and pia mater. These cysts are filled with a clear fluid that resembles cerebro-spinal fluid (CSF). The protein content may be elevated compared to CSF. Intralesional hemorrhages are frequently complicated by the development of fibrous membranes dividing the cyst in multiple compartments. Cysts are isolated from and consequently do not communicate with the subarachnoid space or ventricular system. Arachnoid cysts may remodel the adjacent skull (thinning and scalloping) by chronic compression.

Leptomeningeal cysts are complications of skull fractures due to an entrapment of lacerated meninges within the fracture. Chronic CSF-pulsations may prevent fracture consolidation, the fracture may even be widened (growing fracture). Meninges and underlying brain tissue can protrude through the growing skull defect into the subcutaneous tissues. Surgical repair with a dural patch covering the skull defect may be necessary (3).

Neuroepithelial cysts are benign, nonneoplastic malformative fluid-filled cysts lined by a single layer of ependymal like cells. The exact etiology is not yet fully understood. These cysts occur at multiple locations and are named accordingly: intraventricular ependymal cysts, choroid plexus cysts, and choroid fissure cysts. Large cysts may compress adjacent structures. Intraventricular cysts may lead to an entrapment of parts of the ventricular system depending on their location.

Lymphangioma or cystic hygroma is a congenital malformation of the lymphatic channels within the neck.

Lymphangiomas can show multiple small cystic components (capillary lymphangioma), multiple medium-sized cysts (cavernous lymphangioma), or large fluid-filled compartments (cystic lymphangioma or hygroma). They can occur in combination with hemangiomas (lymphhemangioma). Lymphangiomas may involve multiple anatomical spaces within the neck simultaneously. Cysts are lined by a thin endothelial cell layer. Connective tissue stroma may be intermixed.

Branchial cleft anomalies include cysts, sinus tracts, and fistula that result from an anomalous development of the branchial apparatus. Depending on the involved branchial component, different locations of the branchial cleft anomalies are encountered. Anomalies of the first and especially the second branchial apparatus are most frequent. Anomalies of the third and fourth branchial apparatus are rare. Because the branchial apparatus is ectodermal in origin, the branchial cleft anomalies are lined by stratified squamous epithelium. Occasionally, respiratory epithelium is incorporated. Cysts result from a failure to obliterate parts of the branchial apparatus. In sinuses, a residual opening exists into the deep cervical spaces or skin while in fistulas two openings are seen connecting the skin with the deep cervical compartments. Secondary infection may complicate branchial cleft anomalies.

Thyroglossal duct cysts are developmental anomalies that result from a failure of a segment of the thyroglossal duct to obliterate. The thyroglossal duct is the "path" that the thyroid gland follows during its descent from the foramen cecum at the tongue base to its final position in the infrahyoid neck. Cysts may occur at any location along the thyroglossal duct and are lined by squamous or respiratory epithelium. Cysts are usually filled with a serous/mucinous fluid. Small, "lost" thyroid gland components may accompany the cysts.

Clinical Presentation

Arachnoid, leptomeningeal and neuroepithelial cysts are symptomatic due to compression or displacement of functional center of the central nervous system (CNS). Depending on the location, focal neurological deficits, seizures or CSF-circulation disturbances (hydrocephalus) are observed. In many instances however, these cysts are clinically silent and only found incidentally on imaging that is performed for other reasons.

Lymphangioma or cystic hygroma are primarily symptomatic due to a displacement and/or compression of adjacent neuro-vascular structures or upper respiratory tract. In addition, large lesions may interfere with the normal development of the viscerocranium. This may require a more aggressive treatment. On the occasion of viral infections, lymphangiomas may show an intermittent increase in size. Accompanying hemangiomas with involvement of the skin are easily identified on visual inspection.

Branchial cleft and thyroglossal duct cysts usually present as a soft, compressible, painless mass in the neck. Depending on the embryological origin, lesions are in the median or lateral neck. Cysts may enlarge during viral infections. In rare cases, bacterial infection complicates

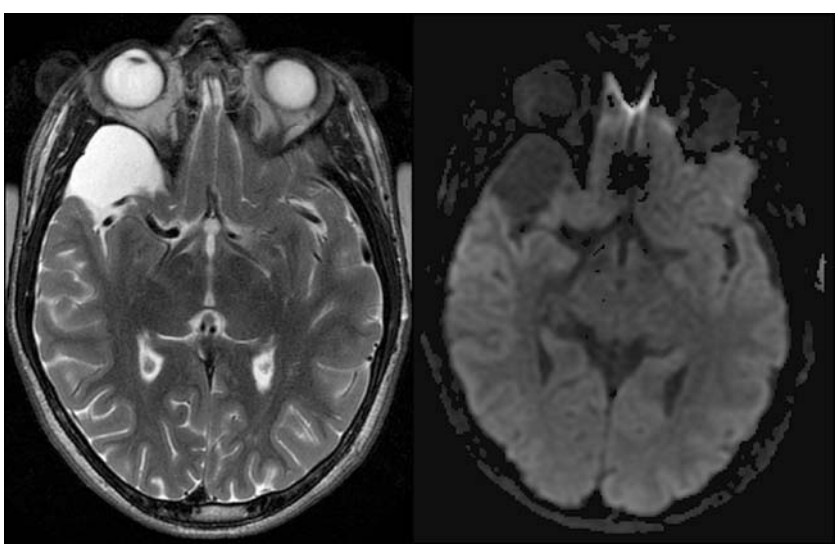

Cysts, Cerebral and Cervical, Childhood. Figure 1 Axial T2-FSE and DWI of a middle cranial fossa arachnoid cyst. The arachnoid cyst is CSF isointense on both sequences. The adjacent temporal lobe is hypoplastic. The dorsal border of the orbit is displaced anteriorly.

the cyst requiring incision or resection of the cyst including fistula and/or sinus tract. Life-threatening compression or displacement of vital structures is rare.

Imaging

Ultrasound is the first line imaging modality in the evaluation of cystic head and neck lesions. Ultrasound usually allows to differentiate between cystic and solid lesions/tumors. Cystic lesions are hypoechoic on ultrasound and may display an accompanying dorsal signal enhancement. Calcifications are equally well delineated with a dorsal signal loss or shadowing. Compared to CT and MRI, ultrasound is more sensitive in identifying intracystic membranes or septae (e.g., in lymphangioma). The real time imaging technique is also very helpful to delineate the exact boundaries of lesions and their relation to neighboring structures. This may be especially helpful in e.g., complex branchial cleft cysts. Duplex sonography allows to evaluate the vascularity of the lesions as well as the relation to adjacent vascular structures. CT and MRI may be used as second line imaging tool. The high spatial resolution and the high tissue contrast as well as the large field-of-view are especially helpful in complex anatomical malformations or lesions. Intracranial cystic lesions can also be examined by ultrasound as long as the fontanelles are not yet closed and may serve as an acoustic window. Transcranial sonography is usually limited because the spatial resolution does not allow to identify accompanying smaller intracerebral lesions.

Arachnoid cysts are sharply marginated extraaxial fluid collections (Fig. 1). On computer tomography (CT) the fluid is isodense with the CSF, on magnetic resonance imaging (MRI) isointense with CSF on all sequences. Acute intralesional hemorrhages increase the density on CT and intensity on T1-weighted imaging. Fluid-sedimentation levels may be identified. Increased protein contents may alter the density and signal intensity of arachnoid cysts. This is especially obvious on FLAIR-imaging. The cyst wall should not enhance. Adjacent brain tissue will be compressed and displaced. The interface between cyst and brain tissue is smooth. Occasionally, an intraparenchymal FLAIR and T2-hyperintense gliosis may be observed. There is no direct communication between the arachnoid cyst and subarachnoid space or ventricular system. The overlying skull or adjacent skull base can be remodeled with outpouching of the skull away from the arachnoid cyst. The internal tabula may be thinned but remains intact. On diffusion weighted imaging (DWI) signal intensity parallels CSF (no restricted diffusion). DWI is especially helpful in differentiating arachnoid cysts from subarachnoidal epidermoids (restricted diffusion). Cisternography can be used to study the exact location and possible communication with additional lesions. This is especially helpful in complex postoperative cases in which recurrent arachnoid cysts developed. Ultrasonography can be helpful in neonates. Uncomplicated arachnoid cysts rarely increase in size. Arachnoid cysts may increase in size after an intralesional hemorrhage or postoperative due to adhesions.

Leptomeningeal cysts may be located next to a skull fracture or extend through a widened fracture into the subcutaneous tissues. Fracture margins are usually smooth. The chronic pulsations may enlarge the fracture (growing fracture) preventing consolidation (Fig. 2). The adjacent subarachnoid space may be widened, brain tissue may protrude through the fracture. On ultrasonography

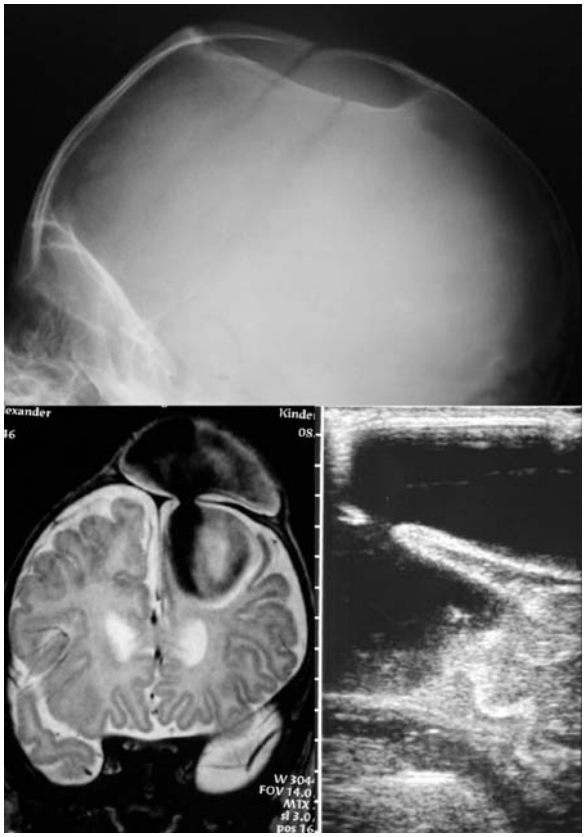

Cysts, Cerebral and Cervical, Childhood. Figure 2 Lateral skull X-ray shows a widened anterior fontanel with smooth osseous borders. Coronal T2-FSE (second row, first image) reveals a large cystic defect within the superior frontal gyrus that communicates across a dural tear with an extracranial cystic component. A T2-hypointense CSF-flow void is seen across the dural tear and within both cystic components. High resolution ultrasonography (second row, second image) confirms MRI findings.

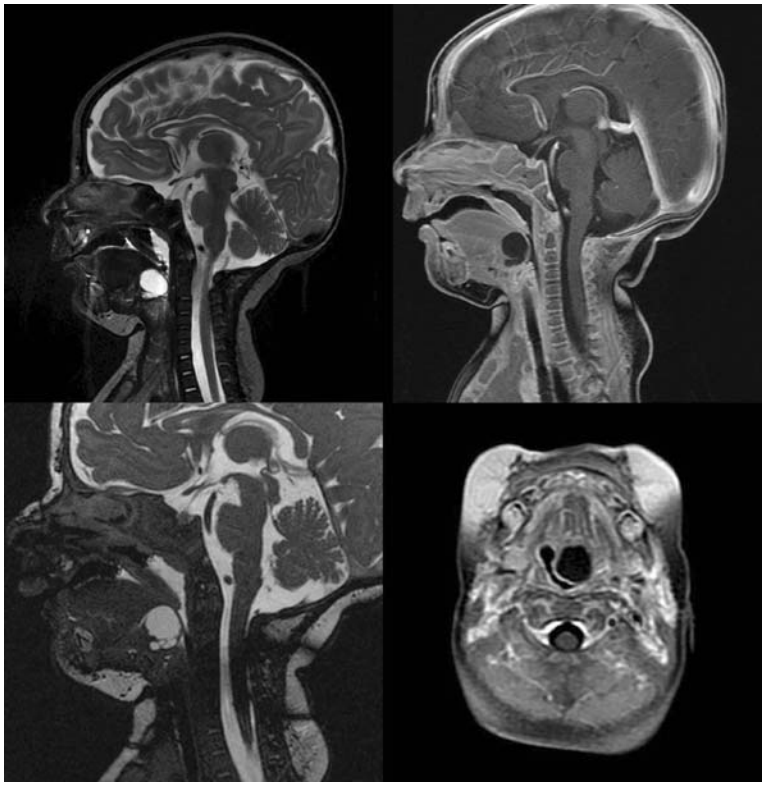

Cysts, Cerebral and Cervical, Childhood. Figure 3 Sagittal T2-FSE, contrast enhanced T1-SE (upper row), sagittal thin slice strongly T2-weighted and contrast enhanced axial T1-SE MR image. A large T2-hyperintense, nonenhancing thyroglossal duct cyst is seen within the floor of the posterior tongue, caudally to the foramen cecum. Several smaller, additional cysts are seen along the lower border of the large cyst.

and MRI, CSF-flow and pulsation artifacts may be seen across the fracture (3). T2*-weighted sequences can be helpful to identify hemorrhagic lacerations within the adjacent cortex. CT is especially helpful to examine the margins of the fracture line. Leptomeningeal cysts can also occur within the skull base after skull base fractures.

Neuroepithelial cysts have similar imaging characteristics as arachnoid cysts. *Lymphangioma or cystic hygroma* appear as hypodense cystic masses on CT. On MRI the cysts are strongly T2-hyperintense and moderately T1-hypointense. Depending on the category of lymphangioma, the lesion may be uniloculated or multiloculated. Cyst walls are usually thin and do not enhance after contrast medium injection unless there is associated infection or hemorrhage. Lymphangiomas often cross the borders of the neck compartments and may displace or wrap neuro-vascular bundles. Fluid–fluid levels may occur spontaneously but are more frequently seen after trauma or punctures. Intralesional hemorrhage changes the density (CT) and intensity (MRI) of the cyst contents. Similar to intracranial arachnoid cysts, elevated protein contents increase density/signal intensity on imaging. Frequently, lymphangiomas show additional contrast enhancing hemangiomatous components. Ultrasonography is the primary imaging modality. The high sensitivity for intralesional septa is especially helpful. In large lymphangiomas the limited field-of-view and penetration depth of ultrasound waves are however disadvantageous to determine the exact extent of large lesions. CT and MRI are used for preoperative planning.

All *branchial cleft (1st to 4th branchial apparatus) and thyroglossal duct cysts* have similar imaging appearances. The cysts are fluid-filled (CT-hypodense, T1-hypointense, T2-hyperintense), well-marginated round or ovoid structures lined by thin walls. Calcifications are rare. The wall of the cysts may show an enhancement if there has been associated recurrent infection. The location and relation to adjacent neck structures allow differentiation between the different cysts. First branchial cleft cysts are located in the area between the external auditory canal and submandibular triangle or in the parotid area. Second branchial cleft cysts are along the anterior border of the sternocleidomastoid muscle, lateral to the carotid arteries and posterior to the submandibular gland. Third branchial cleft cysts are posterior to the carotid arteries and superior to the superior laryngeal nerve while the fourth branchial

cleft cysts are located between the left pyriform sinus apex and thyroid gland, inferior to the superior laryngeal nerve. Thyroglossal duct cysts are midline cysts located somewhere between the foramen cecum and the pyramidal lobe of the thyroid gland (Fig. 3).

Nuclear Medicine

Nuclear medicine studies are used to identify ectopic thyroid gland components.

Diagnosis

Diagnosis relies on the combination of a good clinical examination and high resolution imaging. The differentiation between the different cystic neck masses is based on the proper identification of the anatomical landmarks. Ultrasonography can be especially valuable to differentiate between a uniloculated and multiloculated cystic neck lesion. Thin septa can be missed on CT or MRI. Finally, necrotic neoplastic lesions may mimic cystic lesions and should be considered and consequently be out ruled.

Bibliography

1. Osborn AG (2005) Diagnostic Imaging: Brain. Amirsys, Inc, Salt Lake City, Utah, pp I-7-4-41
2. Harnsberger HR Diagnostic Imaging: Head and Neck. Amirsys, Inc, Salt Lake City, Utah, pp I-7-4-41
3. Huisman TA, Fischer J, Willi UV et al (1999) "Growing fontanelle": a serious complication of difficult vacuum extraction. Neuroradiology 41(5):381–383

Cyst, Posttraumatic

Intramedullary cavity normally of one vertebral segment extension, well marginated. On MRI images cyst shows isointensity with the CSF in all pulse sequence and does not grow.

▶Spinal Trauma

Cystadenoma

Cystadenoma is the most common type of cystic benign ovarian tumor. It accounts for up to 50% of benign ovarian tumors in the reproductive age, and for up to 80% in the postmenopausal age. Cystadenomas are thin-walled unilocular or multilocular cystic lesions filled with serous, mucinous, and sometimes hemorrhagic contents.

▶Masses, ovarian

Cystic Dilatation of the Renal Tubules (1–3)

▶Medullary Sponge Kidney

Cystic Disease of the Renal Pyramids

▶Medullary Sponge Kidney

Cystic Disease, Renal Childhood (MCDK, PCKD)

M. Riccabona[1], R. Fotter[2]
[1]Division of Pediatric Radiology, University Hospital Medical University of Graz, Austria
michael.riccabona@meduni-graz.at
[2]Division of Pediatric Radiology, University Hospital Medical University of Graz, Austria
richard.fotter@meduni-graz.at

Synonyms

Cystic kidney disease; Renal cysts

Definition

Fluid- or urine-filled compartments/cysts replacing a varying amount of renal parenchyma. There are a variety of renal cystic diseases that need to be considered and often can be classified on imaging based on their position, size and appearance: besides the simple renal cyst and rare acquired cystic renal diseases (e.g., in renal failure, posttraumatic), the polycystic kidney disease (PKD, i.e., autosomal recessive or autosomal dominant PKD, medullary cystic disease complex and juvenile nephronophthisis, and glomerulocystic kidney disease), syndromal cystic

kidney disease (hereditary and non-hereditary), ►multicystic dysplastic kidney (MCDK) and dysplastic cysts, ►medullary sponge kidney, as well as complicated renal cysts (haemorrhaged or infected cysts, multiloculated cysts including segmental MCD and ►cystic nephroma), as well as cystic renal tumours have to be considered.

Embryology and Pathogenesis

Cystic renal disease is far less common in childhood than in adults. Inherited diseases as well as a disturbed renal embryogenesis and renal development create a wide spectrum of manifestations that spans from diffuse severe bilateral congenital disease to simple single renal cysts. One of the main mechanism is a disturbance at the junction between metanephrogenic tissue and the ureteral bud, other mechanism in differentiation of the renal parenchyma/genetic origin are also discussed, furthermore degenerative and hyperproliferative changes as well as neoplasms and injuries to the renal parenchyma can lead to cyst formation. Depending on its pathogenesis and the individual entity more or less regular imaging is indicated. Secondary cysts develop after trauma, after infections, in tumours, in chronic renal insufficiency and in inherited cystic kidney disorders.

Clinical Presentation

Presentation and symptoms vary with the underlying condition, from completely asymptomatic in incidental findings to haematuria, hypertension, palpable mass and pain in cystic tumours.

Imaging

Imaging usually relies on ultrasound (US), sometimes (for differentiation of complex cysts, e.g. suspected caliceal diverticula, differential diagnosis against abscesses or tumours, post-traumatic cysts) sectional imaging (usually magnetic resonance imaging (MRI), if unavailable contrast-enhanced computed tomography (CT)) and for rare indications intravenous urography (IVU, e.g. medullary sponge kidney) may be become indicated.

Imaging Strategy

Renal cysts in paediatric patients are generally detected by US. As simple renal cysts are far less common in children than in adults, at least follow-up exams and a detailed family history with nephrourological workup should be considered. If these are just simple cysts, US is sufficient as the single imaging modality. If these cysts grow and cause symptoms, an image-guided drainage and sclerotherapy may become a therapeutic option. If there is a congenital or hereditary (poly-)cystic kidney disease, additional scintigraphy may be valuable for the assessment of (split) renal function during the course of the disease. If the cysts appear to be complicated and do not match any congenital PKD, they should be studied by IVU (for DD against calyceal cysts or detection of a medullary sponge

Cystic Disease, Renal Childhood (MCDK, PCKD).
Figure 1 Schematic drawing of renal cyst and cystic renal diseases. Typical cyst forms and locations in various cystic kidney diseases, with typical features. (Adapted from Riccabona M, Ring E (2001) In: Fotter R (ed) Pediatric Uroradiology. Springer, Berlin-Heidelberg, p 236.) ARPKD, multiple small cysts, situated mostly cortical or at the cortico-medullary border, ADPKD, some big cysts, in all parenchymal areas, GCKD (glomerulocystic kidney disease), predominantly small cortical or subcapsular cysts, MCD medullary cystic disease complex is the medullary microcysts, centered close to the cortico-medullary junction, MSK (medullary sponge kidney) medullary cystic changes, in a radial pattern, centered towards the papilla. Dysplastic cysts may resemble renal cysts, acquired cysts, cysts in ADPKD and MCDK, or complicated cysts.

kidney) and/or MRI or contrast-enhanced CT. If there are still equivocal findings, they should be monitored or—particularly when showing growth or atypically shaped and vascularised areas—should undergo biopsy or surgery.

Diagnosis

Diagnosis is made by imaging, with sometimes only histology revealing the final entity (Fig. 1). Imaging criteria for the simple *uncomplicated renal cysts* on US are small, echo-free, fluid-filled defects, with a regular border and without regional parenchymal abnormalities or solid components. *Dysplastic cysts* look similar and may occur in any form of either primary or secondary dysplastic kidneys, the latter potentially due to a congenital urinary tract malformation such as high-degree vesicoureteral reflux (VUR, reflux nephropathy) or high-grade obstruction (Fig. 2a). The cysts usually are small, may be situated in all renal compartments, and on US the kidneys exhibit some degree of other parenchymal changes such as reduced cortico-medullary differentiation or increased parenchymal echogenicity. In some cases, one can also find a diffuse vascular rarefaction on (amplitude-coded) colour Doppler sonography. As dysplastic cysts may not only grow in size and number, but potentially may undergo malignant transformation (e.g., during renal

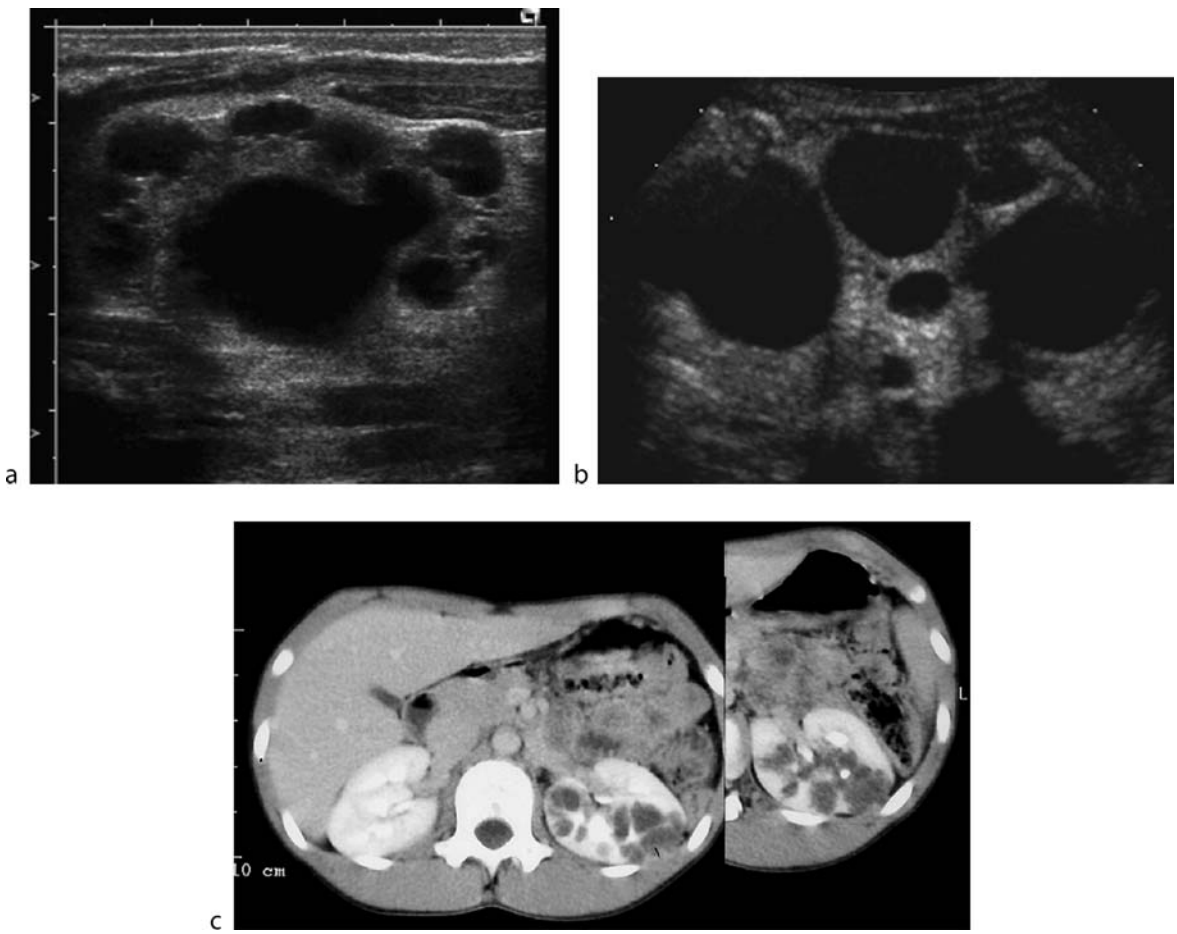

Cystic Disease, Renal Childhood (MCDK, PCKD). Figure 2 DD of renal cysts—imaging examples. (a) Cystic renal dysplasia. US of a hydronephrotic and dysplastic kidney with echogenic and undifferentiated parenchyma and multiple dysplastic cortical cysts. (b) Longitudinal US view of a multicystic dysplastic kidney. Note the missing connection between the cysts of varying size that have no parenchymal outer rim, the lack of a normal collecting system, but some central echogenic-dysplastic residual renal parenchyma, enabling a clear sonographic differentiation from a severe ureteropelvic junction obstruction (UPJO). (c) Contrast-enhanced CT (late phase) of a segmental cystic nephroma. (Adapted from Riccabona M, Ring E (2001) In: Fotter R (ed) Pediatric Uroradiology. Springer, Berlin-Heidelberg, p 246.)

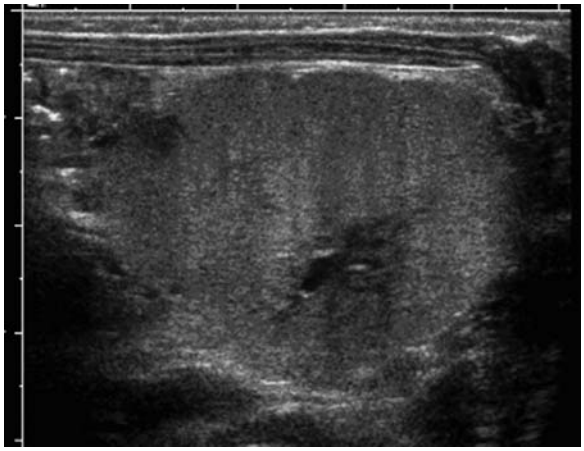

Cystic Disease, Renal Childhood (MCDK, PCKD).
Figure 3 Axial view of a neonate with ARPKD. Not the increased echogenicity, the tiny hyperechic parenchymal dots with some shadowing causing the 'salt and pepper' appearance, and that the microcysts may not or hardly be visible in spit of high-resolution US.

insufficiency), a regular follow-up—not only of the cysts, but also of the entire urinary tract for following the primary condition—is recommended. For this, US is substituted by static renal scintigraphy (Tc99m dimercaptosuccinic acid, DMSA) for the assessment of split renal function, which in future may be replaced by MR-urography.

The most severe form of cystic dysplasia is the *MCDK* (bilateral MCDK is called ▶Potter syndrome or Potter sequence, incompatible with extra-uterine life due to complete renal insufficiency and pulmonary hypoplasia), where the renal parenchyma is nearly entirely replaced by huge cysts, that can more or less resemble a collecting system (Fig. 2b). There may be some (central) residual parenchyma, usually echogenic and undifferentiated on US; sometimes residual perfusion may be depicted on Doppler sonography. Usually there is no renal function. As MCDK has a tendency to regress and vanish spontaneously, nephrectomy is usually postponed and only indicated in those kidneys that cause compression of adjacent structures or grow monstrously, or cause clinical symptoms such as hypertension, infection or malignant transformation. For initial diagnosis US is used, then voiding cystourethrogram (VCUG), MR-urography or DMSA-scintigraphy are performed additionally for the confirmation of the diagnosis and complete work-up which includes assessment of potential residual renal function (i.e. duplex system or segmental MCDK, severe ureteropelvic junction obstruction) and differentiation from severe reflux-nephropathy. Further more, a thorough work-up of the entire genitourinary tract is advocated, as a higher incidence of other urinary tract malformations and ipsilateral genital malformations is reported. Regular US follow-ups are recommended after establishing the initial diagnosis.

The so-called *multicystic nephroma* or multilocular nephroma or multiloculated renal cyst is another rare entity that is a cystic 'malformation' of (parts of) the kidney. On US (as well as on CT or MRI), it is characterised by a conglomeration of small cysts of similar size, with thin membranes and straight borders, without renal tissue involved in the tumour-like formation; usually no or only minimal contrast enhancement or perfusion is seen in the walls of the cysts (Fig. 2c). It is basically a benign tumour that may grow, but usually does not cause destruction or metastasis. Therefore, once imaging (and biopsy, as metanephric tissue making it a potential tumour can only be detected on histology) has established the diagnosis, a conservative approach can be considered. However, in cases with abnormal growth or other indecisive features such as irregular borders of the cysts, destructive behaviour or atypical parenchyma these need to be resected.

Polycystic kidney disease is an inherited familial condition of either autosomal dominant (ADPKD) or autosomal recessive promotion (ARPKD). Different types are established and the age of manifestation varies. On US, the recessive form usually manifests with diffuse parenchymal changes in a diffusely enlarged kidney due to microcysts not depictable by imaging. It may present already neonatally with renal insufficiency (infantile form), or in any other age (juvenile and adult forms). The cysts can be seen unilateral or bilateral, and often they initially are too small to be detected, creating a bilaterally speckled appearance of the kidneys with increased echogenicity of the renal tissue, with inhomogeneously reduced tissue differentiation, also called the 'pepper-salt kidney' (Fig. 3). During the course of the disease, the cysts constantly increase mainly in number, but also in size, eventually leading to an end-stage kidney and chronic renal insufficiency. Additional imaging of the other parenchymal abdominal organs for extra-renal manifestation such as liver fibrosis or pancreatic cysts is recommended. ADPKD is one of the most common inherited diseases that may be detected during childhood, but usually manifests only in adulthood (adult PKD) and exhibits some isolated, uncomplicated (macro-)cysts that tend to grow in size and number, then gradually replacing renal parenchyma—in childhood, this rarely needs treatment and usually is only followed up by US, once the diagnosis is established by family history and US

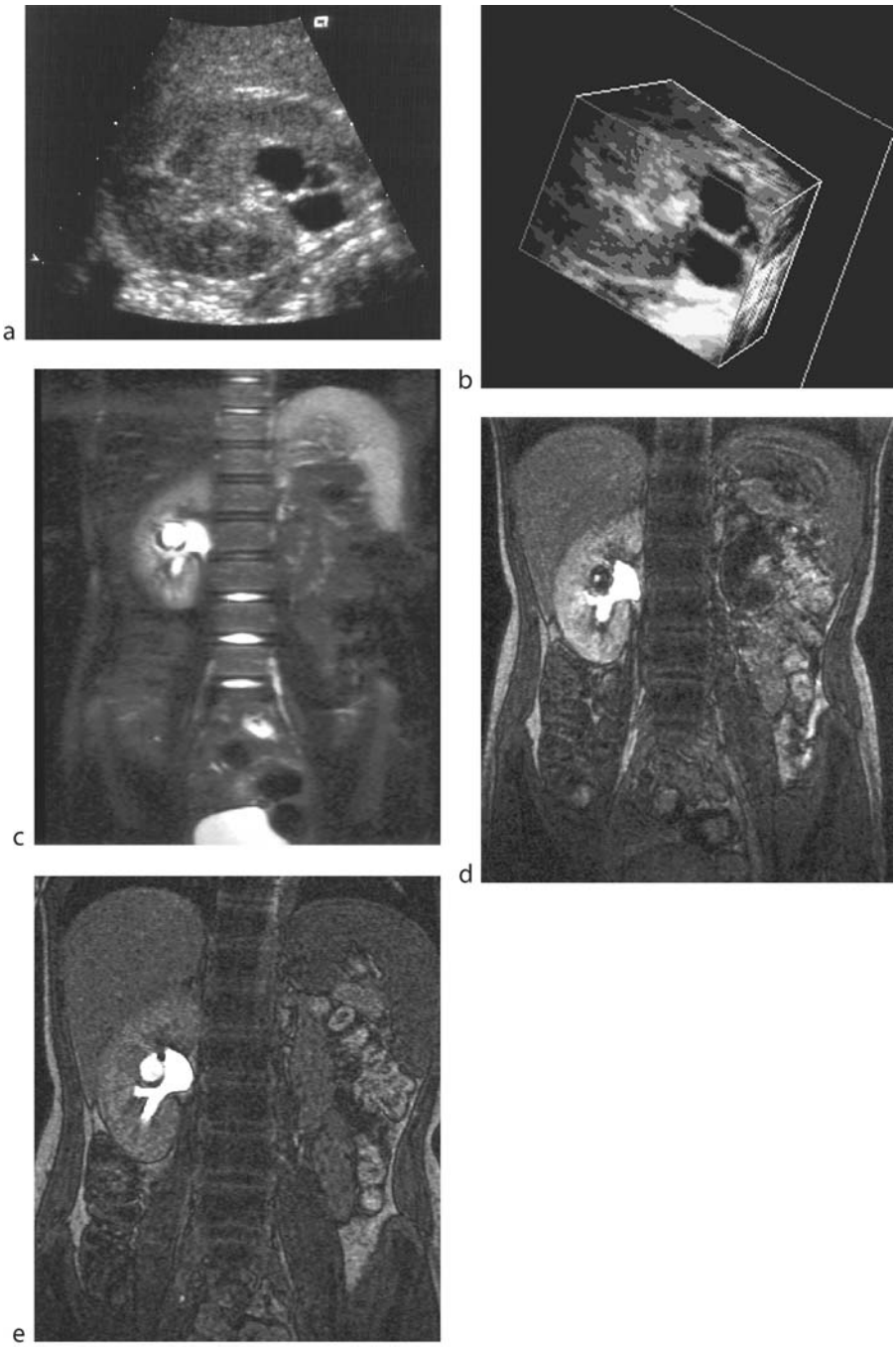

Cystic Disease, Renal Childhood (MCDK, PCKD). Figure 4 Imaging and diagnostic criterial in caliceal diverticulum A: axial conventional to the ultrasound image, demonstrating a cystic lesion located centrally in the kidney close to the renal pelvis. B: 3D-US of the same cyst, suggesting a connection of the cyst to the urinary collecting system (diverticula neck, see arrows and description). C–E: dynamic MR-urography images demonstrate initially the topographic anatomic situation of the "cyst" in a T2-weighted coronal unenhanced image (D), then the contrast enhancement dynamics with a well contrasted collecting system and no contrast within the "cyst" (arrow) in the early phase (E), and the filling of the "cyst" (arrow) in the delayed phase of a gadolinium enhanced T1-weighted 3D-gradient echo sequence proving the connection of the cyst with the collecting system, enabling the diagnoses of a caliceal diverticula.

assessment of the family. Note that ADPKD has a high coincidence with cerebral vessel malformations (particularly cerebral artery aneurysm), thus potentially indicating an active search for them. As PKD has typical US appearances, no other imaging is needed in childhood usually; rarely cysts may haemorrhage or get infected, needing contrast-enhanced CT or MRI for establishing the diagnosis. As we must consider coexisting conditions of the spleen, the liver and the pancreas, all other abdominal parenchymal organs should be included in the regular US follow-up studies.

Glomerulocystic kidney disease is a rare congenital condition with small cystic degeneration of the glomeruli. These tiny cysts are often situated subcapsularly in the renal cortex and—particularly in neonates—may be missed or only be depicted by high-resolution imaging. The kidneys usually are large, with an increased echogenicity of a widened cortex. As diagnosis is made by histology and family history, only US is performed.

Medullary cystic disease (complex) is an autosomal dominant inherited disease with a late onset of chronic renal failure. Histology shows glomerular cysts with thickening of the multilayered membrane, accompanied by some tubular cysts. Depending on the disease state, a growing amount of interstitial fibrosis, chronic inflammation and tubular atrophy with consecutive chronic sclerosing tubulo-interstitial nephropathy is observed. No specific imaging or US features are known.

Medullary sponge kidneys usually exhibit a cyst-like dilatation of the tubules with congestive sludge and calcification in the ectatic tubuli, which easily may be missed during early stages on US. The imaging modality of choice particularly in early stages of a suspected medullary sponge kidney still is IVU.

There are a number of hereditary and non-hereditary *syndromal cysts* as well as cysts in aneuploidies, with partially autosomal recessive, partially autosomal dominant transmission. They usually are part of a complex systemic disease with disturbance of nephrogenesis, combined with dysplastic features. They can present as multiple renal cysts as GCKD, MCDC or ►ARPKD and ADPKD. The pediatric radiologist needs to consider these entities for differential diagnosis and further diagnostic imaging of associated malformations or abnormalities, otherwise the presentation and imaging of syndromal renal cysts does not differ from the imaging of the other cystic renal entities.

(Post-)traumatic, post-surgery and (post-)inflammatory cysts may be tricky. Particularly if infected or after haemorrhage, sedimentations may be present, with a more or less distinguished wall and local parenchymal structural abnormalities. The may also be difficult to differentiate from an urinoma (particularly on US). When the suspicion is raised clinically or sonographically, MR-urography or contrast-enhanced CT may help to distinguish these entities or rare malformations such as a *tertiary calix* or a *calyceal diverticula*, with delayed excretory phase acquisition of either CT- or MR-images being mandatory to differentiate these entities. Note that post-infectious cysts should be considered particularly after uncommon infections such as tuberculosis or after renal abscesses.

Most renal tumours can exhibit cysts, either as part of their entity (e.g. multicystic nephroma) or as regressive or necrotic parts of the tumour (e.g. renal cell carcinoma). Even Wilm's tumour may present in a rare cystic form. Therefore all unusual cysts should be monitored by US and—at least when they grow, develop other signs, or present with a 'complicated' unusual appearance—additional sectional imaging with MRI (or—if unavailable—contrast-enhanced CT) should be considered. Surgery or biopsy with histology remains the ultimate possibility to define the entity in an unclear or equivocal cystic lesion.

Bibliography

1. Babut JM, Bawab F, Jouan H et al (1993) Cystic renal tumours in children—a diagnostic challenge. Europ J Pediatr Surg 3:157–160
2. Kaplan BS, Kaplan P, Rosenberg HK et al (1989) Polycystic kidney diseases in childhood. J Pediatr 115:867–880
3. Kissane JM (1990) Renal cysts in pediatric patients: a classification and overview. Pediatr Nephrol 4:69–70
4. Riccabona M, Ring E (2001) Renal agenesis, dysplasia, hypoplasia and cystic diseases of the kidney. In Fotter R (ed) Pediatric Uroradiology. Springer, Berlin-Heidelberg, pp 229–252
5. Wood BP (1992) Renal cystic disease in infants and children. Urol Radiol 14:284–295

Cystic Duct Anomalies

These anomalies include the congenital variations in the course and site of the cystic duct.

►Congenital Malformations, Liver and Biliary Tract

Cystic Duct Cyst

Saccular cystic dilatation of the cystic duct.

►Congenital Malformations, Liver and Biliary Tract

Cystic Fibrosis

Gundula Staatz
Department of Radiology, Division of Pediatric Radiology, University of Erlangen-Nürnberg, Erlangen
gu.stz.uni-erlangen@t-online.de

Synonym

Mucoviscidosis

Definitions

►Cystic fibrosis is an autosomal recessive inherited disease, caused by a defect in the gene for cystic fibrosis transmembrane conductance regulator (CFTR) on chromosome 7. The incidence in Europe is approximately 1:2500. The disease is characterised by viscous mucous production of exocrine glands resulting in airway plugging and obstruction, bronchiectasis and bacterial infection.

Pathology/Histopathology

The lungs of patients with cystic fibrosis show a variety of abnormalities such as atelectasis, ►mucoid impactions, acute and chronic inflammation, ►bronchiectasis, cyst formation, and fibrosis. Airway mucosal oedema and inflammation, respiratory muscle weakness and fatigue, contribute to the development of respiratory failure.

Histologically luminal neutrophils, neutrophilic and lymphocytic mural inflammation of the bronchial walls, squamous metaplasia of large and small airways, peribronchial and peribronchiolar fibrosis, obliterating fibroproliferative bronchiolitis and prominent hypertrophy of peribronchiolar smooth muscle are found (1). The alveoli adjacent to the bronchi show collapse and epithelialisation, the adjacent intra-alveolar septa are cellular infiltrated. The terminal bronchiole is often completely destroyed due to peripheral abscesses.

Clinical Presentation

Infants with cystic fibrosis have normal lungs at birth and present often initially with gastrointestinal problems like meconium ileus. With the onset of recurrent pulmonary infection, coughing (chronic), wheezing, dyspnoea on exertion, respiratory distress with retractions, chest pain, pneumothorax and haemoptysis occur. The sputum may be purulent, and on physical examination, clubbing, cyanosis and crackles during auscultation are found. Pulmonary infections are predominantly caused by *Staphylococcus aureus*, *Pseudomonas*, *Haemophilus influenza* and fungi. Other symptoms are caused by the involvement of the nose and sinuses, the gastrointestinal system, liver, pancreas, hepatobiliary system, urogenital tract, skin and skeletal system. Severe intra-abdominal manifestations of cystic fibrosis include neonatal meconium ileus, distal intestinal obstruction syndrome (DIOS), biliary cirrhosis, pancreatic cysts, pancreatic fibrosis and atrophy. Cor pulmonale and pulmonary hypertension are late-stage complications, but death is predominantly caused by chronic respiratory failure at a mean age of 33 years (2).

Imaging

Plain chest radiography is performed routinely in almost all patients. Several scoring tests have been established for the assessment of the disease severity, but image findings on chest X-rays may be subtle especially in mild disease and in early stages. High-resolution CT (HRCT) reflects most accurately the morphologic changes in patients with cystic fibrosis with excellent spatial resolution. CT-scoring systems provide a sensitive method for monitoring disease status and progression. MRI is useful for the assessment of mediastinal and vascular anatomy. In recent times, new MRI techniques for functional ventilation imaging with use of inhaled contrast aerosols, oxygen, hyper-polarised noble gases (Helium-3, Xenon-129) and fluorinated gases (sulphur-hexafluoride) have been developed (3). A higher sensitivity in the detection of ventilation defects compared to ventilation scintigraphy, CT or standard pulmonary function tests with lack of radiation is expected for this new MRI technique (3).

The abdominal manifestations of cystic fibrosis are efficiently imaged by ultrasound. Routine sonographic follow-up examinations of the liver, the biliary system, the pancreas and the bowel tract should be performed in each patient. In case of severe abdominal disease, such as liver cirrhosis with ascites or DIOS, CT may be necessary for further evaluation.

Nuclear Medicine

Ventilation perfusion scintigraphy may provide useful information in demonstrating marked functional impairment and abnormal matched ventilation and perfusion defects (1).

Diagnosis

In most children the diagnosis is based on clinical findings, positive newborn screening tests and sweat tests with measurement of sweat chloride concentrations. The chest radiographs of newborns are normal. Early findings on chest radiographs are hyperinflation of the lungs with flattening of the diaphragm and bronchial wall thickening (1). In later stages, peribronchial interstitial thickening, mucoid impactions, bronchiectasis, ring shadows (empty cavities of bronchiectasis), atelectasis, bulla, interstitial emphysema, pneumothorax, hilar lymphadenopathy and cor pulmonale occur (Fig. 1). The disease has a predilection for the upper and middle lung zones.

In HRCT bronchiectasis, peribronchial wall thickening, mosaic perfusion pattern and mucous plugging are the most frequently observed morphologic CT abnormalities in patients with cystic fibrosis. Less frequent are emphysema, collapse, sacculations and bullae observed (4) (Fig. 2). The disease is often accompanied by hilar and mediastinal lymph node enlargement (Fig. 3). The most common morphologic CT abnormalities increase in extent and severity with increasing patient age and correlate significantly with worsening of non-morphologic parameters of pulmonary status (4).

There are only a few studies using ►functional ventilation imaging with MRI in children with cystic fibrosis. Donelly et al. examined 4 children with cystic fibrosis using H-1 and ^{3}He MRI. In all subjects, areas of absent lung ventilation were depicted on the hyperpolarised ^{3}He MR images. These areas of absent ventilation ranged from wedge-shaped peripheral defects to signal voids in entire lung zones. Ventilation was most severely impaired in the upper posterior lung zones, and normal in the lower lung zones (3, 5).

Interventional Radiological Treatment

In patients with long-standing cystic fibrosis, haemoptysis may occur as a complication. Abnormal thin walled and tortuous bronchial arteries, commonly found in areas of bronchiectasis, are eroded secondary to chronic infection. In case of severe haemoptysis, arteriography of the bronchial arteries with subsequent embolisation may be

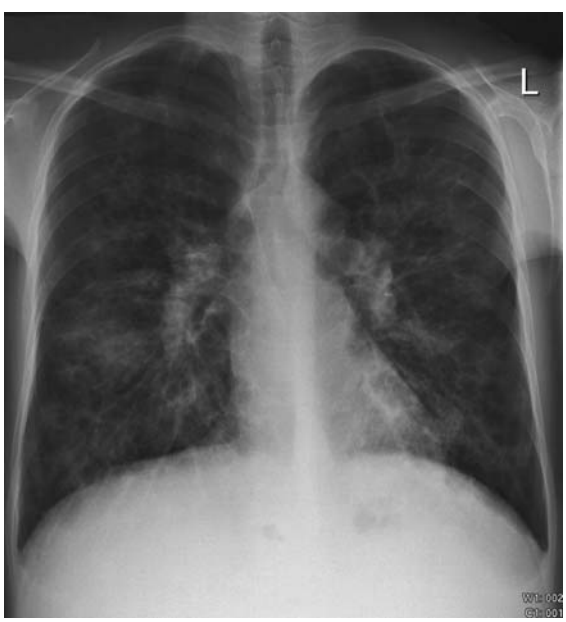

Cystic Fibrosis. Figure 1 A 17-year-old boy with cystic fibrosis. The chest radiograph demonstrates marked hyper-aerated lungs, bronchial wall thickening, bronchiectasis, peribronchial fibrosis, mucoid impactions and bilateral hilar lymphadenopathy.

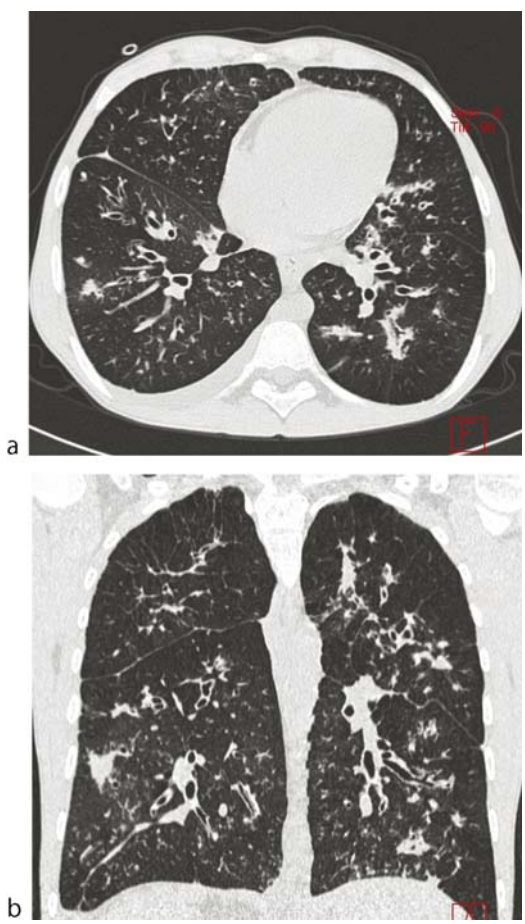

Cystic Fibrosis. Figure 2 Axial HRCT image (a) of cystic fibrosis in a 17-year-old boy and coronal multiplanar reconstruction (b) show emphysema, bronchiectasis, peribronchial wall thickening, mucous plugging and peribronchial fibrosis.

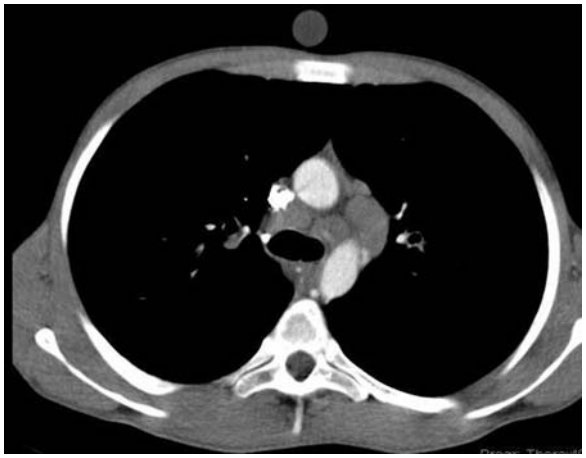

Cystic Fibrosis. Figure 3 Contrast-enhanced CT in a 21-year-old patient with cystic fibrosis. Bilateral hilar and mediastinal lymphadenopathy are identified.

necessary. As embolic materials, polyvinyl alcohol particles, gelatine sponge particles or coils are usually used. Bronchial artery embolisation has shown good results in controlling acute and chronic haemoptysis but in up to 50% of cases repeated embolisation procedures have to be performed due to a high incidence of bleeding from non-bronchial systemic collateral vessels. As major complications of bronchial artery embolisation transverse myelitis, bronchial infarction, oesophago-bronchial fistula, ischaemic colitis and—most feared—spinal infarction and paraplegia due to embolisation of a spinal artery have been described.

Bibliography

1. Rossi UG, Owens CM (2005) The radiology of chronic lung disease in children. Arch Dis Child 90:601–607
2. Moskowitz SM, Gibson RL, Effmann EL (2005) Cystic fibrosis lung disease: genetic influences, microbial interactions, and radiological assessment. Pediatr Radiol 35:739–757. Epub 2005 May 3
3. Kauczor HU, Chen XJ, van Beek EJ et al (2001) Pulmonary ventilation imaged by magnetic resonance: at the doorstep of clinical application. Eur Respir J 17:1008–1823
4. Helbich TH, Heinz- Peer G, Eichler I et al (1999) Cystic fibrosis: CT assessment of lung involvement in children and adults. Radiology 213:537–544
5. Donnelly LF, Mac Fall JR, McAdams HP et al (1999) Cystic fibrosis: combined hyperpolarized ^{3}He-enhanced and conventional proton MR imaging in the lung: preliminary observations. Radiology 212:885–889

Cystic Fibrosis

▶Meconium Ileus

Cystic Hygroma

Multiple cystic structures in neck region, showing lack ofcommunication between cervical lymphatics and venous system.

▶Lymphangioma

Cystic Hygroma, Branchial Cleft Cyst

▶Cysts, Cerebral and Cervical, Childhood

Cystic Hyperplasia

▶Fibrocystic Disease, Breast

Cystic Kidney Disease

▶Cystic Renal Disease, Childhood (MCDK, PCKD)

Cystic-Like Lesions, Hepatic

Chiara Franchini, Riccardo Lencioni
Department of Diagnostic and Interventional Radiology, University of Pisa, Italy
lencioni@med.unipi.it

Definition

Cysts and cystic-like lesions are any focal lesions that contain fluid (liquid or semisolid) material.

True cysts are closed cavities lined by epithelium, while cystic-like lesions do not have necessarily an epithelium and are not necessarily closed cavities.

Pathology and Histopathology

Cysts and cystic-like lesions of the liver in the adult can be classified as developmental, inflammatory, neoplastic, and miscellaneous. Developmental cystic lesions include simple cyst, autosomal dominant polycystic liver disease, ►biliary hamartoma, ►Caroli's disease. Inflammatory cystic lesions include pyogenic, amoebic and tubercular abscesses, and intrahepatic hydatid cyst. Neoplastic cystic lesions include biliary cystadenoma and cystadenocarcinoma, cystic subtypes of primary liver neoplasms, and cystic metastases. Other cystic lesions are intrahepatic haematoma and biloma (1).

Simple Cysts (Bile Duct Cysts)

Simple or true hepatic cysts are very common benign congenital lesions that do not communicate with the biliary tree (1, 2). They result from the obstruction of congenitally aberrant bile ducts, with subsequent stasis and retention of bile. They can be solitary or multiple and their size is very variable, even though frequently is inferior to 5 cm. They tend to increase in number and size with age. They are more common in women. Cysts are cavities lined by epithelium, with a thin wall and a serous content. Rarely they may present as "complicated" cysts due to the presence of hemorrhage or inflammation (1, 2).

Polycystic Liver Disease

►Polycystic liver disease is an autosomal dominant disorder characterized by the presence of multiple, sometimes innumerable cysts in the liver. In some cases, polycystic liver disease appears to occur sporadically. It is characterized by the presence of cysts ranging in size from less than 1 cm to more than 10–15 cm; the cysts are lined by cuboidal or flattened biliary epithelium and contain straw-colored fluid. They do not contain pigmented bile and appear to be detached from the biliary tree (1, 2–5). Polycystic liver disease is thought to be due to a ductal plate malformation of the small intrahepatic bile ducts, which lose communication with the biliary tree. Spontaneous intracystic hemorrhage, infection, and rupture may occur. Polycystic liver disease is often found in association with adult renal polycystic disease (1). Hepatic cysts are found in 40% of cases of autosomal dominant polycystic disease involving the kidneys; nevertheless, they may be seen without identifiable renal involvement at imaging.

Biliary Hamartoma

Bile duct hamartomas, also called von Meyenburg complexes, originate from a failure in involution of embryonic bile ducts (1, 3). They are small clusters of slightly dilated bile ducts embedded in a fibrous, sometimes hyalinized stroma, close to or within the portal tracts. These bile duct microhamartomas contain bile concrements. At pathologic analysis, they appear as grayish-white nodular lesions 0.1–1.5 cm in diameter scattered throughout the liver parenchyma. The nodules may coalesce into larger masses. They do not communicate with the biliary tree (3).

Caroli's Disease

Caroli's disease was described by Jacques Caroli in 1958 as a congenital communicating cavernous ectasia of the biliary tree. It is a rare, autosomal recessive condition characterized by segmental, nonobstructive saccular, or fusiform dilatation of the intrahepatic bile ducts. Other typical pathologic features are the presence of intraluminal bulbar protrusions, bridges across the dilated lumina, and portal radicles partially or completely surrounded by dilated bile ducts. The abnormality may be segmental or diffuse. The pure form of the disease is quite rare, while a various degree of congenital hepatic fibrosis is usually associated. ►Caroli's syndrome is the condition in which features of both congenital hepatic fibrosis and Caroli's disease are simultaneously present (1, 4).

Both varieties may be associated with cystic renal disease, more often autosomal recessive polycystic kidney disease, but also autosomal dominant polycystic kidney disease, medullary sponge kidney, nephronophtisis. There is also an association with cystic dilatation of extrahepatic bile ducts (1, 4). Caroli's disease is supposed to be due to an insufficient resorption of ductal plates, resulting in large dilated segments of the primitive bile duct surrounding a portal vessel (4). If the large intrahepatic bile ducts are affected, the result is the pure form of Caroli's disease, while abnormal development of the small interlobular bile ducts leads to congenital hepatic fibrosis.

Clinical Presentation

Simple Cysts

Hepatic cysts are a common finding, being found in 1% to 3% of the liver routine examinations. They are more often discovered in women and are usually asymptomatic (1, 2); rarely they may cause symptoms like pain, palpable abdominal mass, hepatomegaly, jaundice. Complications occur rarely and are mainly represented by intracystic hemorrhage, infection, compression of adjacent structures, occasionally torsion of the cyst, and rupture.

Polycystic Liver Disease

Usually, patients with polycystic liver disease are asymptomatic and liver dysfunction is quite unlikely to occur (5). However, advanced disease may cause hepatomegaly, which may results in abdominal discomfort and dyspnea. Symptoms may arise in relation to complications, such as intracystic bleeding, infection, or rupture of a cyst, which are quite frequent due to the great number of cysts (1, 5).

Biliary Hamartoma

Bile duct hamartomas are rather common and usually represent an incidental finding at imaging or laparotomy in asymptomatic patients, or at autopsy. The estimated incidence in autopsy series is 0.69–2.8% (1, 3). Complications such as superinfection with formation of microabscesses and degeneration into cholangiocarcinoma are extremely rare (3).

Caroli's Disease

The clinical onset of Caroli's disease usually occurs during childhood. In the pure form it is related to complications including stone formation, cholangitis, and hepatic abscesses. Clinical symptoms are recurrent attacks of right upper quadrant pain, fever, and, more rarely, jaundice. In Caroli's syndrome the clinical scenario is dominated by hepatic fibrosis and portal hypertension, with splenomegaly, oesophageal varices, hemorrhage of the gastrointestinal tract.

Cholangiocarcinoma complicates Caroli's disease in 7% of cases (5).

Imaging

Simple Cysts

At ultrasound (US) a cyst has the typical appearance of an anechoic, round or ellipsoid structure, with posterior acoustic enhancement, and sharply delineated margins, without an own wall. The solid–liquid interfaces appear as highly hyperechoic lines. Sometimes, subtle lateral acoustic shadows can be seen. Rarely, septa or calcifications may be present. Cysts may behave sometimes as occupying-space masses, displacing intrahepatic vessels or biliary branches, or causing swelling of the hepatic margin. A complicated cyst (intracystic bleeding or infection) presents internal echoes (1). At CT scans an hepatic cyst appears as a round or ovoid well-defined lesion, with no evident wall. The content is homogeneous and hypodense with attenuation values similar to the water (<20 HU). Both the wall and their content do not show any enhancement after contrast media administration. In small lesions, attenuation values can be higher due to partial volume effect; in these cases a thin section thickness should be used in order to avoid misdiagnosis of solid nodule; the absence of contrast enhancement will confirm the cystic nature of the lesion. Any enhancement in the periphery or thickening of the wall suggests an inflammatory or neoplastic nature, rather than a simple cyst. Internal inhomogeneity and higher attenuation values (>20 HU) are present in complicated cysts, in which the differential diagnosis from metastases arising from cystic carcinomas (as pancreatic or ovarian ones) can be difficult (1). The ipointensity on T1-weighted images and homogeneous very high signal intensity on T2-weighted images is due to their high water content. On heavily T2-weighted images an increase in signal intensity is seen. This behavior allows differentiation of these lesions from metastatic disease. The wall is never seen and no enhancement is present at the dynamic study. Intracystic bleeding determines high signal intensity, sometimes with a fluid–fluid level, on both T1- and T2-weighted images; the hemorrhage may be dated on the basis of the different appearance of the different phases of degradation of hemoglobin. Fat-saturation sequences may be helpful in confirming the blood content (1).

Polycystic Liver Disease

At ultrasound polycystic liver disease is characterized by the presence of multiple anechoic lesions of various size, often clustered, which causes a diffuse dishomogeneity of the liver parenchyma. The appearance of cystic lesions does not differ from that of simple cysts (1, 2). At CT the typical finding is the presence of multiple homogeneous water-density lesions with regular borders, without a detectable wall. The lesions do not show peripheral neither internal enhancement after contrast media administration. Hemorrhagic cysts, more frequently encountered than in cases of simple hepatic cysts due to the great number of lesions, have attenuation values higher than water at unenhanced CT scans; calcification of the cyst walls, due to previous hemorrhage, may also be detected (1). At MR, hepatic cysts in polycystic liver disease have a homogenous signal intensity and appear markedly hypointense on T1-weighted images and markedly hyperintense on T2-weighted images. Because of their serous content they become even brighter on heavily T2-weighted images. They do not enhance after administration of gadolinium chelates. The intracystic hemorrhage is characterized by signal intensity inhomogeneity (1). Although the diagnosis of polycystic liver disease is easily made with both CT and MR imaging, MR imaging is more sensitive for the detection of complicated cysts.

Biliary Hamartoma

At ultrasound biliary hamartomas have been described as either hypoechoic or anechoic small nodules with posterior acoustic enhancement. Hyperechoic biliary hamartomas or a combination of hypo- and hyperechoic lesions, however, has also been reported (3). In almost all described cases, unenhanced CT showed hypodense small hepatic nodules, scattered throughout the liver and typically measuring between 0.5 and 1.0 cm in diameter. The latter feature is the most essential one in the differential diagnosis from multiple simple cysts. Furthermore, simple cysts are typically regularly outlined, whereas bile duct hamartomas have a more irregular outline. Although homogeneous enhancement of these lesions has been noted in some cases, in most reports no enhancement was seen after contrast media administration (1, 3). The MR appearance of bile duct hamartomas has been reported sporadically. All lesions were hypointense compared with liver parenchyma on T1-weighted images and markedly hyperintense on T2-weighted images. On heavily T2-weighted images, the signal intensity increases further, nearly reaching the signal intensity of fluid. Biliary hamartomas do not exhibit a characteristic pattern of enhancement after administration of gadolinium chelates; some authors observed homogeneous enhancement of these lesions, some others a thin rim enhancement, whereas others did not find any enhancement. At MR cholangiography, bile duct hamartomas appear as multiple tiny cystic lesions that do not communicate with the biliary tree, helping in the differential diagnosis with Caroli's disease (1, 3).

Caroli's Disease

US reveals localized saccular dilatations of intrahepatic bile ducts which appear as multiple cystic lesions. Besides these findings, peculiar features may be demonstrated such as intraluminal bulbar protrusions, complete or incomplete bridging across the dilated ducts, and small portal branches within the cystic structures. The Doppler mode should be used in order to demonstrate this typical aspect. Inside the dilated segments stones or debris may be present, appearing as hyperechoic deposits with or without shadowing. CT typically shows hypoattenuating water-density structures which communicate with the biliary tree (Fig. 1). The presence of small dots showing strong contrast enhancement during the portal-venous phase within the dilated lumina, also known as "central dot sign," is considered very suggestive of Caroli's disease. Bulbar protrusions and bridge formation may also be depicted. Intraluminal biliary calculi may be demonstrated (Fig. 2) (1, 4).

At MR imaging, the cystic dilatations of the biliary tree appear hypointense on T1-weighted images and strongly hyperintense on T2-weighted images. The intraluminal portal radicles present clear enhancement in the portal phase at the dynamic study. MR can demonstrate internal septa and protrusions inside the dilated lumina. MR cholangiography can be extremely useful in diagnosis of Caroli's disease by demonstrating the communication between the saccular or fusiform dilatations of the intrahepatic bile ducts and the biliary tree (Fig. 3). Furthermore, stones, when present, are evident as signal voids within ducts and cystic spaces. Sludge or debris may be also evident. The use of a hepatobiliary contrast medium by imaging the liver in the biliary phase can more confidently demonstrate the biliary nature of the cystic dilatations, which show contrast enhancement. The cholangiographic features of Caroli's disease are well established as saccular or fusiform

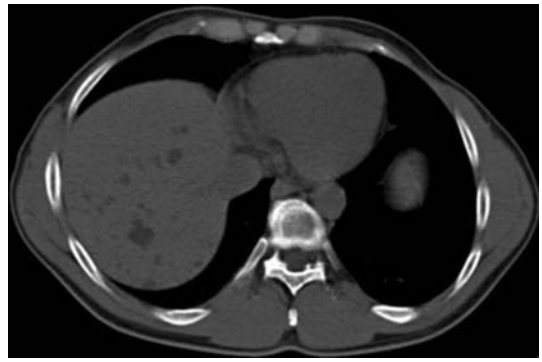

Cystic-Like Lesions, Hepatic. Figure 1 Caroli's disease. Unenhanced CT shows multiple hypoattenuating water-density areas.

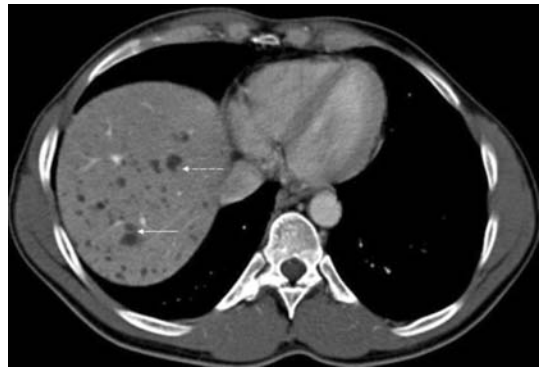

Cystic-Like Lesions, Hepatic. Figure 2 Caroli's disease. Bridging septa within the cystic dilatations may be depicted (*arrow*). The presence of small dots showing strong contrast enhancement during the portal-venous phase within the dilated lumina, also known as "central dot sign," is considered very suggestive of Caroli's disease (*dashed arrow*).

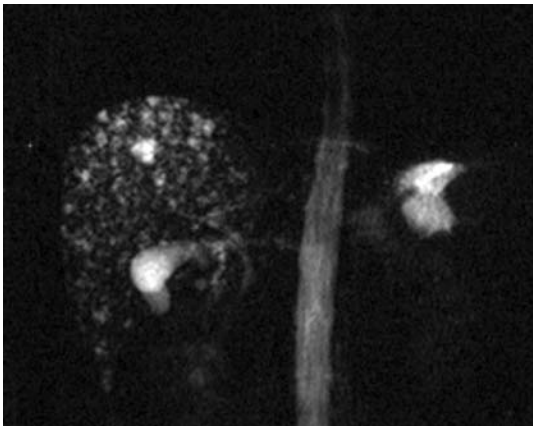

Cystic-Like Lesions, Hepatic. Figure 3 Caroli's disease. MR cholangiography demonstrates the communication between the saccular or fusiform dilatations of the intrahepatic bile ducts and the biliary tree.

dilatation of the intrahepatic bile ducts. Alternating areas of stricture and dilatation are a common observation with cholangiograms (1, 4).

Nuclear Medicine

Hepatobiliary scintigraphy with ^{99m}Tc (IDA iminodiacetic acid) agents reveals large, irregular, multifocal collections of the radiotracer in the liver. These collections correspond to the segmental dilatations, and no extrahepatic obstruction is present, although bile stasis and stone formation may result in atypical obstruction. On early images, if the ducts are dilated enough, they appear as photopenic branching areas within the liver. Overall, scintigraphy is not helpful compared with cross-sectional imaging techniques. Cholangitis can impair hepatic uptake of radiotracers. Obstruction related to stones or debris from the ducts may cause misdiagnosis.

Diagnosis

The diagnosis of a hepatic cystic lesion is based on US, which is the most accurate technique for establishing its cystic nature compared to solid lesions in the liver. At contrast CT or MR, any enhancement in the periphery or thickening of the wall suggests an inflammatory or neoplastic nature, rather than a simple cyst. MR is indicated when cystic lesions have atypical appearance on US. MR allows the distinction between complicated hepatic cysts presenting with hemorrhage inside and other cystic lesions such as underlying metastatic disease with target or halo sign. In the majority of cases, imaging findings in combination with critical clinical information allow an adequate lesion characterization.

Bibliography

1. Mortelé Koenraad J, Ros Pablo R (2001) Cystic focal liver lesions in the adult: differential CT and MR imaging features. Radiographics 21:895–910
2. vanSonnenberg E, Wroblicka JT, D'Agostino HB et al (1994) Symptomatic hepatic cysts: percutaneous drainage and sclerosis. Radiology 190:387–392
3. Wohlgemuth WA, Böttger J, Bohndorf K (1998) MRI, CT, US and ERCP in the evaluation of bile duct hamartomas (von Meyenburg complex): a case report. Eur Radiol 8:1623–1626
4. Choi BI, Yeon KM, Kim SH et al (1990) Caroli disease: central dot sign in CT. Radiology 174:161–163
5. Singh Y, Winick AB, Tabbara SO (1997) Multiloculated cystic liver lesions: radiologic-pathologic differential diagnosis. Radiographics 17:219–224

Cystic Mastopathy

▶ Fibrocystic Disease, Breast

Cystic Neoplasms, Pancreatic

Laura Crocetti[1], Carlo Bartolozzi[1], Piero Boraschi[2], Carla Cappelli[1]
[1]Department of Diagnostic and Interventional Radiology, University of Pisa, Italy
[2]2nd Department of Radiology, University Hospital, Pisa, Italy
l.crocetti@med.unipi.it

Synonyms

Cystic pancreatic tumors; Exocrine cystic neoplasms of the pancreas

Definitions

Cystic tumors of the pancreas are relatively uncommon, accounting for about 10% of cystic lesions of the pancreas and for 1% to 5% of primary pancreatic neoplasms. The incidence is increased in patients with von Hippel–Lindau disease.

According to the AFIP (Armed Forces Institute of Pathology) system, the pancreatic cystic tumors represent primary exocrine lesions and they are distinct into benign,

borderline (with an uncertain malignant potential) and malignant. Serous cystic tumors, mucinous cystic neoplasms and intraductal papillary-mucinous tumors/neoplasms (IPMTs/IMPNs) represent the majority of the cases encountered in practice, accounting for more than 90% of the primary cystic neoplasms of the pancreas; solid pseudopapillary neoplasms represent less than 10%; other cystic neoplasms are represented by other tumors with cystic appearance (e.g. cystic neuroendocrine tumor, acinar cystadenocarcinoma, ►lymphangioma, cystic teratoma) (1).

Pathology and Histopathology

Serous cystic tumors were also known as microcystic adenomas or glycogen-rich cystadenomas. They have an extremely low potential for malignant disease: malignant serous cystadenocarcinomas have been reported, but they are exceedingly rare, accounting for less than 1% of cases. Serous cystadenomas are generally well circumscribed, lobulated tumors, consisting of single (macrocystic or oligocystic adenoma) or multiple (microcystic adenoma) cysts, separated by delicate fibrous septae. The cysts are filled with clear, watery fluid and are often arranged around a central stellate scar, which may be calcified and that lacks in oligocystic adenomas. Cysts are lined by a simple, glycogen-rich cuboidal epithelium. When the cyst is large, it can be difficult to differentiate them from mucinous cystic neoplasms.

The histopathological features of mucinous cystic neoplasms and IPMNs are similar except for a dense mesenchymal ovarian-like stroma which is a requisite feature of mucinous cystic tumors. Moreover characteristically mucinous cystic neoplasms lack a communication with the pancreatic ductal system, whereas a communication is a key feature of IPMN (1).

Mucinous cystic tumors of the pancreas are multiloculated tumors. The inner surface is smooth, but sometimes, especially in large malignant tumors, papillary excrescences and solid nodules can be observed. Microscopically 3 distinct layers can be recognized: the inner epithelial layer producing mucin; the middle layer, which is the densely cellular ovarian-like mesenchymal stroma; the outermost layer, which is the hyalinized connective tissue. The epithelial cells lining the cysts produce abundant mucoid secretion; therefore the cysts contain viscous material, which can also be hemorrhagic. These tumors are classified on the basis of histology as benign, borderline or malignant based on degree of dysplastic changes of the epithelium. According to the model of neoplastic progression, mucinous cystic neoplasms progress through stages of increasing dysplasia from mucinous cystadenoma to borderline mucinous cystic neoplasm to mucinous cystic neoplasm with in situ carcinoma, finally to reach the stage of invasive carcinoma. Cystadenomas contain a single layer of epithelium without significant atypia. In borderline neoplasms the epithelium may form papillae; an in situ carcinoma or invasive carcinoma can arise focally within a mucinous cystic lesion. All these lesions are different from IPMNs, because they are grossly visibile neoplasms that do not involve the duct system of the pancreas (1).

IPMNs are papillary, villous neoplasm that arises within the main pancreatic duct or its branches. They are usually classified into 3 types: main duct, branch duct and mixed, according to the site and extent of involvement. The tumors hypersecrete mucin, which often leads to duct dilatation and/or chronic obstructive pancreatitis. Histologically the involved duct is lined by mucin-producing columnar epithelium which forms papillary proliferations; the tumor can shows varying degrees of atypia and can progress from adenomas without atypia to IPMN borderline with a moderate amount of atypia, to IPMN with carcinoma in situ and finally to infiltrating carcinoma. The tumors generally show intraluminal growth, but they can invade periductal tissues (1).

Clinical Presentation

Many patients with a pancreatic cystic tumor present with no relevant signs or symptoms and such tumors may be discovered incidentally at abdominal ultrasound (US) or computed tomography (CT). Most of the remaining patients present with a variety of non-specific symptoms such as abdominal pain, anorexia, nausea, vomiting, also related to recurrent pancreatitis. If the tumor is large enough, symptoms related to mass effects may predominate, such as a palpable abdominal mass and biliary obstruction. Patients with malignant changes may have a history of weight loss and jaundice.

Imaging

Classically, serous cystic lesions have a lobulated external contour and are composed of a grapelike cluster of cysts. A central stellate scar with calcification is pathognomonic and small septae and internal debris may be seen in individual cysts. Approximately 10% of all serous cystadenomas have cystic components larger than 2 cm and can't be distinguished from mucinous cystic neoplasms. Because the capsule of these tumors is poorly developed, poor distinction of the tumor from the surrounding pancreatic parenchyma is often observed. However, when the cysts are small, it can be difficult to

identify the cystic nature of the neoplasm. The central scar and calcifications may be demonstrated on CT scans, but are not well depicted on US. Endoscopic ultrasonography (EUS) allows better resolution of the honeycomb structure (2). Magnetic resonance (MR) is the modality of choice for the depiction and characterization of cystic pancreatic masses. Serous cystadenomas are usually hyperintense on T2-weighted images and hypointense on T1-weighted images. Occasionally, debris and hemorrhage in the cysts can alter this signal intensity pattern. The septae are well depicted on T2-weighted images, but the central scar is not. Magnetic resonance cholangiopancreatography (MRCP) is helpful in demonstrating the relationship of the mass to the main pancreatic duct. Usually no communication occurs with the pancreatic duct. The main duct is almost never obstructed, but the duct and its branches may be displaced (3,4) (Fig. 1).

Mucinous cystic neoplasms are often larger than 5 cm. US reveals a large, cystic mass sometimes with internal septa, excrescences, mural nodules and debris. The tumor usually has sharply marginated walls and smooth borders. CT shows a well-defined, unilocular or multilocular mass with fluid attenuation. Compared with serous cystic tumors, the cysts are larger (>20 mm in diameter) and less numerous (usually <6). Larger cysts may demonstrate small daughter cysts along their internal surface. Thick internal septae separating the different cystic cavities are typical. Visualization of nodular or papillary excrescences with irregular borders of the septae is possible. If present, calcifications are curvilinear or punctate and confined to the wall or septa. After the contrast medium administration, enhancement of the cyst wall, internal septations, mural nodules and other intracavitary projections is present. The presence of papillary excrescences, mural nodules and other intracavitary projections suggests the differentiation between benign mucinous cystadenoma and cystadenocarcinomas; however, the absence does not indicate that the tumor is benign. At MR, mucinous cystadenoma and cystadenocarcinoma are hypointense or hyperintense on T1-weighted images depending on protein content. T2-weighted images show multiple hyperintense cysts separated by multiple hypointense septa. Intracystic excrescences and mural nodules also have low signal intensity, but they enhance significantly after gadolinium-based contrast agents administration (3,4) (Fig. 2).

Main ductal type of IPMN may be focal or diffuse, the findings of which are reflected on imaging. When there is diffuse involvement of the pancreatic duct, dilatation is present along its whole length. This dilatation is often associated with diffuse and generally uniform pancreatic atrophy. In the early stages of focal or segmental involvement, the features may be difficult to differentiate from focal chronic obstructive pancreatitis. Branch IPMT is most frequently encountered in the region of the uncinate process. It may be microcystic or macrocystic. The microcystic variety may mimic serous cystadenomas on imaging, but communication with the main pancreatic duct (which is frequently dilated) is characteristic. The macrocystic variety may mimic a peripheral mucinous cystic tumor. IPMN can be more confidently diagnosed when imaging reveals a filling defect in the main duct or a branch pancreatic duct. The filling defects are hyperechoic on US (but extremely difficult to visualize), hyperdense on CT and hypointense on T2-weighted MR images. The thickness of the cyst wall and septa is variable with benign tumors; they tend to be thin and regular. In malignant

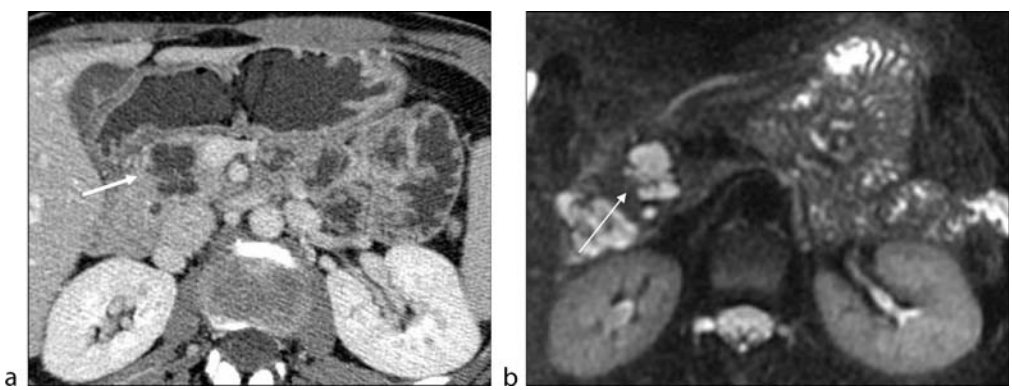

Cystic Neoplasms, Pancreatic. Figure 1 Serous cystoadenoma of the head of the pancreas (arrows). Multidetector CT study (a) and MR study (b). At CT is possible to appreciate a well circumscribed lesion, presenting lobulated borders, constituted by few microcysts. The borders are poorly defined from the normal pancreatic parenchyma and the lesion does not show evidence of contrast enhancement; a thin stellate central scar is also visible but there are no signs of calcifications (a). In an axial fat-suppressed fast spin-echo T2-w, it is possible to appreciate the same lesion as a lobulated hyperintense area with no relationship with pancreatic ducts (b).

tumors, the walls and septa appear irregular and thick, with solid nodules. MRCP study represents the technique of choice for visualizing the typical communication between the IPMN and the ductal system and to evaluate the extent of the tumor. A main pancreatic duct with a maximum diameter of greater than 15 mm, and diffuse dilatation of the duct are suggestive of malignancy in main duct type tumors. Among branch duct-type tumors, malignant tumors tend to be larger than benign tumors (Fig. 3). The intravenous administration of secretin allows the improvement of the pancreatic ducts delineation and therefore the depiction of typical findings of IPMN (5,6).

Because of the anatomical location of the pancreas near to the gastric and duodenal loop, EUS appears to be reliable in distinguishing between solid and cystic lesions. However the features that can be visualized often do not appear to be sufficiently accurate to allow a differentiation between benign and malignant tumors.

Endoscopic retrograde cholangiopancreatography (ERCP) may depict ductal changes in cystic tumors of the pancreas in approximately 80% of patients, allowing also tissue sampling and therapeutic intervention. In particular, in IPMN the communication with the pancreatic duct and an anomalous ampulla of Vater with discharging mucus may be visualized.

Nuclear Medicine

Positron emission tomography (PET) imaging can depict cystic malignant tumors, because it is sensitive to

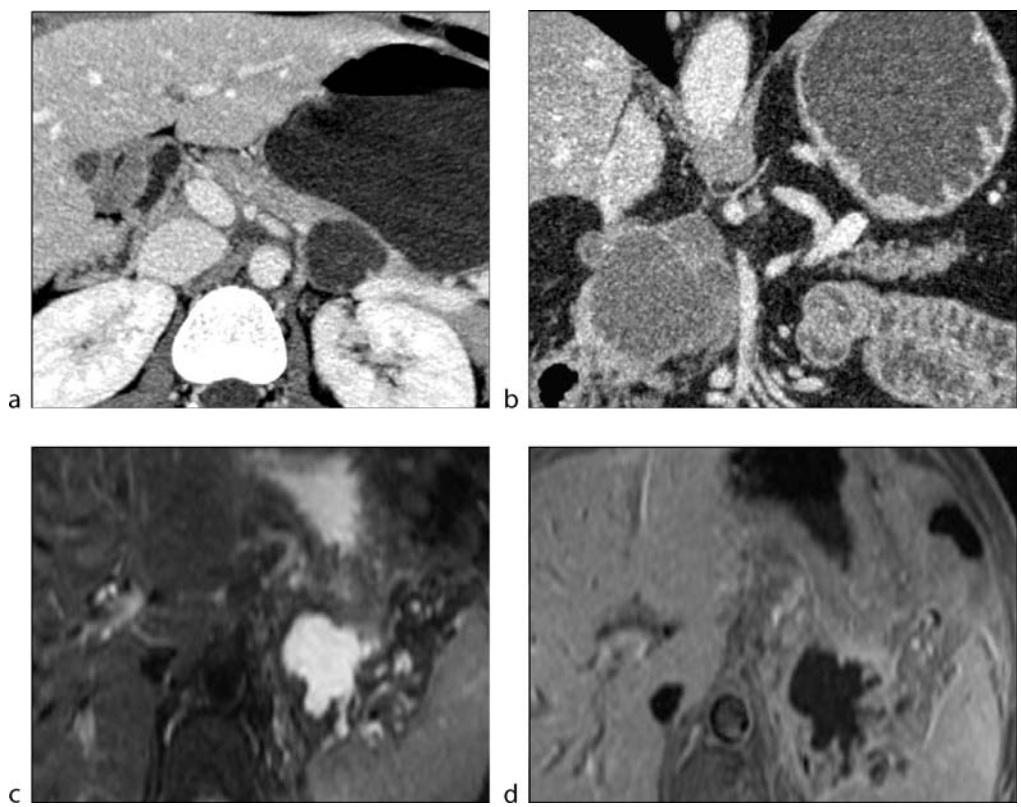

Cystic Neoplasms, Pancreatic. Figure 2 Mucinous tumors of the pancreas at multidetector CT (a,b) and MR (c,d). In (a) a uniloculated, well defined benign mucinous tumor of pancreatic body/tail is depicted. It is possible to appreciate the smooth borders of the lesion, the absence of internal septa and the smooth inner surface. Multiplanar reconstruction (b) on the coronal plane shows a multiloculated malignant mucinous tumor of the pancreatic head: the irregular profile and the thickness of the borders as well as the presence of contrast enhancement are depicted. There is no presence of internal septa or intracavitary projections. The neoplasm infiltrates the fat tissue around the pancreatic head and it is contiguous to the superior mesenteric artery wall, without certain signs of vascular compression. In (c) and (d) a mucinous cystadenocarcinoma of the pancreatic tail is shown by MR images. Axial fat-suppressed fast spin-echo T2-w (c) and gadolinium-enhanced fat-suppressed SPGR T1-w (d) images well exhibit a prevalently cystic lesion at the level of the pancreatic tail. The lesion shows irregularly lobulated, thickened internal walls presenting marked contrast enhancement.

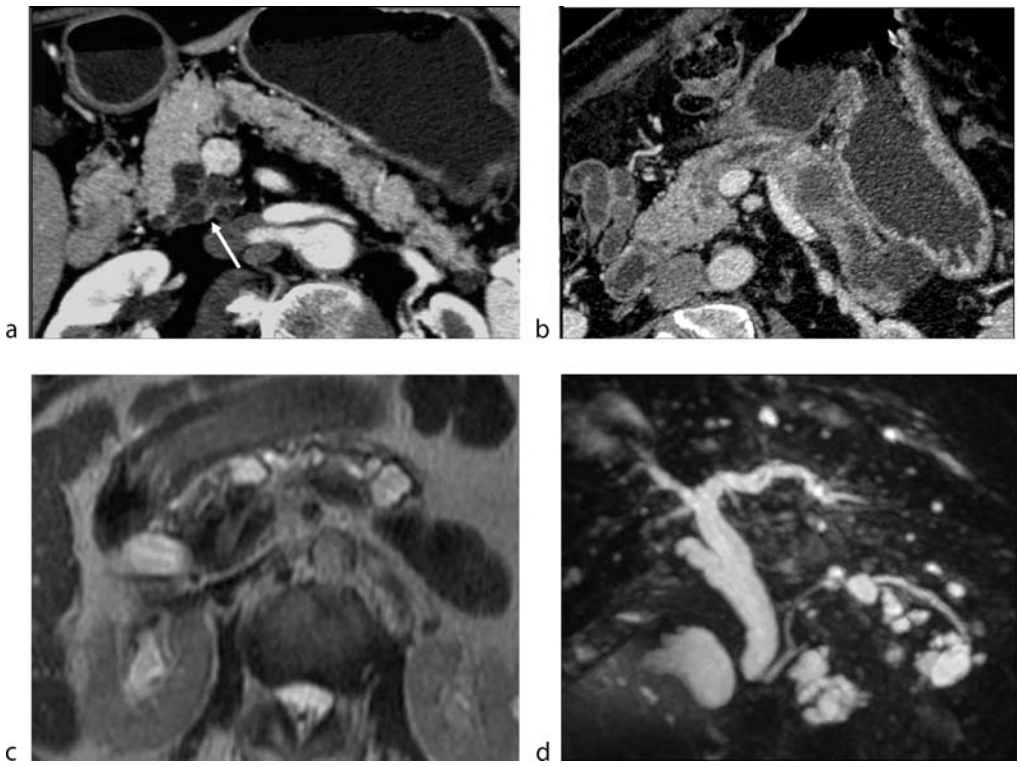

Cystic Neoplasms, Pancreatic. Figure 3 IPMN of the pancreas at multidetector CT (a,b) and MR (c,d). In (a) a IPMN "branch duct-type": a multilobulated lesion constituted by a grape-like cluster of microcysts originating from secondary pancreatic ducts is shown in the uncinate process (a); these microcystic lesions, differently from the serous ones, do not present a central scar. The lesion also shows thin margins and there are no internal septae. The main pancreatic duct is not dilated. In (b) a IPMN "main duct-type": two uniloculated macrocystic lesions, localized in the tail and in the body of the pancreas and originating from the Wirsung duct can be appreciated; the cystic lesions appear filled with an ovarian like stroma fluid and their growth has determined the Wirsung dilatation and the consequent glandular atrophy, due to compression. In (c) and (d) a branch duct-type IPMN can be appreciated at MR. Axial single-shot fast spin-echo T2-w image (c) and coronal oblique MIP reconstruction of MRCP (d) show multiple, diffuse cystic dilatations of secondary pancreatic ducts. The main pancreatic duct appears slightly dilated at the level of the pancreatic tail. Extraepatic biliary tree is also dilated.

hypermetabolic processes. FDG PET is more accurate than CT in identifying malignant lesions and could be used, in combination with CT and tumor markers, in the preoperative evaluation of patients with pancreatic cystic lesions. A positive result on FDG PET strongly suggests malignancy and, therefore, a need for resection. A negative result shows a benign tumor that may be treated with limited resection or follow-up. However, PET is not yet approved for use in the workup of pancreatic lesions.

Diagnosis

With the widespread use of advanced imaging techniques, cystic lesions of the pancreas are now diagnosed relatively frequently. US may aid in the differentiation of solid and cystic lesions, but a complete evaluation of the pancreas is often difficult. CT is excellent not only for the initial detection of the lesion but also for the characterization (by visualization of calcifications, septa, mural nodules) and the staging of malignant lesions (by assessing vascular invasion, infiltration of the adjacent structures and the presence of lymph node metastases, distant metastases or peritoneal carcinosis). MR has the added advantage of providing better characterization of the features of a cyst and its relationship with the pancreatic duct by means of MRCP sequences. Despite advances in imaging, often the differential diagnosis of pancreatic cystic lesion remains difficult; however an accurate diagnosis is imperative for appropriate patient management because the most

important determinant of the prognosis is the identification of malignant or premalignant cysts that require resection. Serous cystadenoma is usually benign, whereas some serous cystadenomas show progressive growth; therefore, surgery is indicated, because complications, such as obstructive jaundice, can result. Surgical removal of the mucinous cystic neoplasms and IPMNs is recommended because of the potential malignant behaviour of these lesions. Therefore obtaining fluid cyst or tissue for histologic confirmation may be essential. A variety of tumor markers that may be present in cyst fluid have been proposed for use in the differentiation among the major types of cystic lesions. Ca 19.9 concentration in cyst fluid has not been confirmed as a useful indicator for discriminating between mucinous and non-mucinous cystic lesions but serum levels of Ca 19.9 are slightly elevated in some patients who have malignant cystic lesions. Levels of cystic carcinoembryonic antigen (CEA) can be increased in the mucin content of the cysts, and they proportionally rises with the degree of malignancy of the tumor. Although amylase is not a tumor marker, its presence in cyst fluid is often used as an indicator of a communication between a cystic lesion and the ductal system, as in cysts that are associated with IPMNs.

The differential diagnosis includes other tumors with cystic appearance and pancreatic lesions with a cystic presentation (including pancreatic pseudocysts or pancreatic fluid collections, ▶congenital pancreatic cysts, retention pancreatic cysts, ▶parasitic cysts, ▶lymphoepithelial cysts).

References

1. Buetow PC, Rao P, Thompson LDR (1998) From the archives of the AFIP. Mucinous cystic neoplasms of the pancreas: radiologic-pathologic correlation. Radiographics 18:433–449
2. Sahani DV, Kadavigere R, Saokar A et al (2005) Cystic Pancreatic Lesions: a simple imaging-based classification system for guiding management. Radiographics 25:1471–1484
3. Demos TC, Posniak HV, Harmath C et al (2002) Cystic lesions of the pancreas. Am J Roentgenol 179:1375–1387
4. Suzuki Y, Atomi Y, Sugiyama M et al (2004) Cystic neoplasm of the pancreas. A Japanese multiinstitutional study of intraductal papillary mucinous tumor and mucinous cystic tumor. Pancreas 28(3):241–246
5. Tanaka M (2004) Intraductal papillary mucinous neoplasm of the pancreas: diagnosis and treatment. Pancreas 28(3):282–288
6. Silas AM, Morrin MM, Raptopoulos V et al (2001) Intraductal papillary mucinous tumors of the pancreas. Am J Roentgenol 176:179–185

Cystic Nephroma

A basically benign, sometimes semi-malignant multicystic renal lesion, usually comprised of multiple small, similar sized cysts that may include some areas of nephroblastomatosous cells (potential malignant transformation), that may replace the entire or parts of the kidney.

▶Cystic Renal Disease, Childhood

Cystic Pancreatic Tumors

▶Cystic Neoplasms, Pancreatic

Cystic Renal Disease, Acquired

JM Correas, O Hélénon
University of Paris V,
Paris, France
jean-michel.correas@nck.ap-hop-paris.fr

Definition

Acquired cystic kidney disease (ACKD) is defined as the development of multiple renal cysts (at least three per kidney) in patients with end-stage renal disease, before or after starting dialysis, without hereditary cystic disease. It can affect the native kidneys in renal transplanted patients, whatever the renal function and the renal graft during chronic rejection.

Pathology/Histopathology

Pathology reveals multiple renal cysts in both atrophic kidneys from the cortex and the medulla. They are typically small, ranging in size from a few millimeters to 30 mm. The presence of hemorrhagic cysts or oxalate crystal deposition in cystic walls and septations as well as within the cysts is common. Atypical cystic walls exhibit multilayered epithelial lining, and papillary proliferations are not unusual (1). Multiple renal tumors are associated with ACKD, including adenomas and carcinomas of various types, with a strong increase in papillary tumor incidence compared with the general population (1). Renal cancer can be detected in approximately 5% of ACKD patients. Tumors are typically multifocal, bilateral, and aggressive, with a rate of metastases of 15% (2). The mean duration of dialysis before development of renal cancer is about 12 ± 7.9 years (2).

Clinical Presentation

The incidence of ACKD increases with the duration of end-stage renal failure. Before patients start dialysis, ACKD is found in about 10% of them. This number increases to 10–20% within the first 3 years of dialysis and can reach 90% after 10 years of dialysis (3), whatever the cause of renal failure. The kidneys regularly increase in size because of the development of cysts in patients undergoing dialysis, whereas they remain small in transplanted patients.

In most cases, ACKD is detected incidentally because the disease is asymptomatic. The recovery of normal renal function after transplantation has no demonstrated impact on the development of ACKD.

Cyst complications, including bleeding and infection, can also appear and reveal the disease. The presence of hemorrhagic cysts is frequent at imaging procedures. Rarely, the hemorrhage is symptomatic and provokes back pain. Severe cyst bleeding can extend to the retroperitoneum or the collecting system and result in reduced hemoglobin serum level, hypotension, and even shock.

Renal tumors are rarely symptomatic and are detected in most cases by incidental imaging studies or systematic follow-up in hemodialyzed or transplanted patients. The incidence of renal cell carcinomas is significantly increased up to seven times in patients undergoing dialysis (2). Seven percent of dialyzed patients can develop small solid renal tumors. In transplanted patients, the prevalence of renal cell carcinoma discovered incidentally is 1.6%.

Imaging

Ultrasonography and Color Doppler Ultrasound

At ▶ultrasound (US), the cysts are detected as sonolucent round lesions with increased posterior acoustical energy. They are typically bilateral, localized within the parenchyma in small kidneys with reduced corticomedullary differentiation. Harmonic tissue imaging is helpful to detect and characterize small hypoechoic lesions (Fig. 1). Almost 50% of hemorrhagic cysts can exhibit a pseudosolid echoic pattern on US. ▶Contrast-enhanced computed tomography (CT) or magnetic resonance imaging (MRI) is then required. Hemorrhagic cysts can remain anechoic, and US can be useful to characterize hyperattenuating cysts at CT in the case of absence of iodinated contrast agent administration or when the enhancement remains equivocal. On color Doppler US (CDUS), typical cysts do not exhibit any signals. Contrast-enhanced US might be useful for diagnosing pseudotumors and to detect vascularity within echoic renal lesions to confirm the presence of a solid renal mass (Fig. 2).

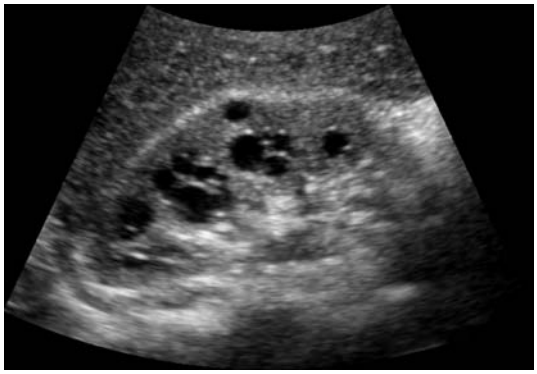

Cystic Renal Disease, Acquired. Figure 1 Harmonic compounding imaging of the native kidney in a renal transplanted patient. Many typical cysts are detected within the cortex and the medulla.

However, US examination in ACKD is difficult due to the reduced size of the kidneys and the hyperechoic parenchyma, making identification of the kidney difficult within the retroperitoneal fat.

CT and MRI

Contrast-enhanced CT remains the gold standard in the diagnosis of ACKD as well as in the characterization of renal masses. Baseline CT is mandatory to detect hyperattenuating cysts and to provide baseline attenuating values. Contrast-enhanced CT improves the detection of numerous small cysts located in both kidneys, predominantly in the cortex (Fig. 3). CT can also detect calcifications in cystic walls or septations.

Hemorrhagic cysts are very common (up to 50% of ACKD patients). They typically exhibit increased attenuation values at baseline (above 50 HU) and no enhancement after iodinated contrast agent administration. Delayed acquisitions during nephrographic and excretory phases are necessary to differentiate these lesions from solid renal tumors. In the case of acute back pain revealing renal bleeding, CT can detect an enlarged hemorrhagic cyst and/or a subcapsular hematoma. The hematoma can extend to the retroperitoneal space. The disappearance of the hematoma should be monitored until disappearance to avoid the misdiagnosis of a bleeding cystic carcinoma.

Solid renal masses are seen as round lesions significantly enhanced after iodinated contrast agent injection. The threshold varies from 15 to 20 HU. In the case of hemorrhagic mass, the enhancement is typically poor and remains below the threshold value. The change in the shape of the lesion that becomes heterogeneous

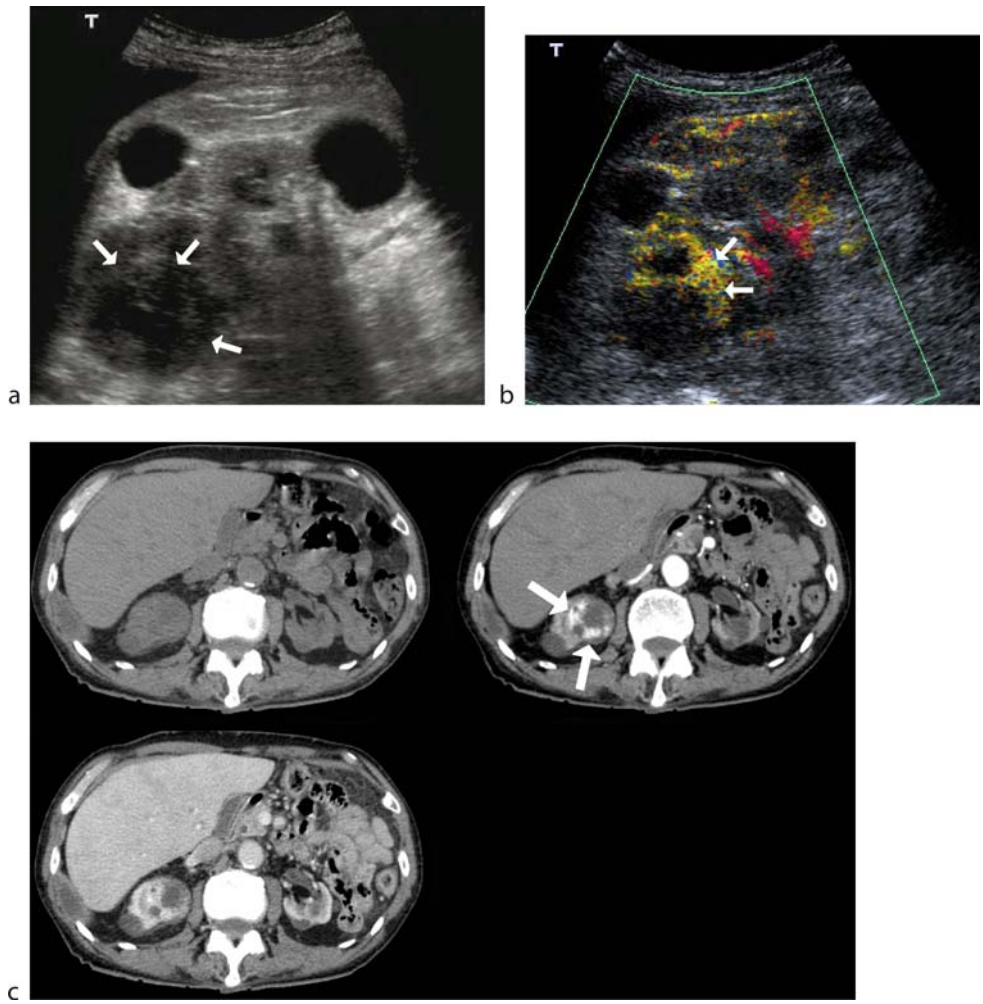

Cystic Renal Disease, Acquired. Figure 2 Ultrasound (US) follow-up of a patient under hemodialysis. (a) At tissue harmonic imaging, a heterogeneous and echogenic mass was detected at the upper pole of the right kidney (*arrows*). (b) Contrast-enhanced US following the administration of SonoVue confirmed the presence of vascularity within the mass, strongly enhancing during arterial phase (*arrows*). (c) Contrast-enhanced computed tomography (CT) with baseline (*top left*), arterial (*top right*), and nephrographic (*bottom left*) acquisitions. CT confirmed the presence of a partially necrotic mass with strong peripheral enhancement. At pathology, the lesion corresponded to a renal cell carcinoma.

indicates the presence of vascularity, and thus is highly suspicious for solid tumors. Solid renal masses should be differentiated from focal renal parenchyma hypertrophy. These pseudotumors exhibit a similar enhancement compared with the normal atrophic parenchyma at all phases of the transit of the iodinated contrast agent, and they remain homogeneous. In the case of equivocal diagnosis, MRI can be useful to confirm the diagnosis of pseudomass.

The staging of a solid renal mass primarily relies on contrast-enhanced CT to detect venous and lymph node extension.

If contrast-enhanced CT can be performed in patients undergoing dialysis, CT cannot be used in patients with persistent renal function. In this case, contrast-enhanced MRI becomes the modality of choice for the diagnosis of ACKD and the characterization of renal masses.

MRI examination should include at least T2-weighted spin-echo sequences with fat suppression and dynamic breath-hold T1-weighted gradient-echo sequences with fat suppression, before and after bolus administration of gadolinium chelate contrast agent. Typical cysts are easily characterized as round lesions of high signal intensity on T2-weighted sequences, of low signal intensity on

T1-weighted sequences at baseline, and with no enhancement after injection of contrast agent (Fig. 4). Hemorrhagic cysts are typically hyperintense on both T1- and T2-weighted sequences and do not exhibit any enhancement. The presence of a fluid iron level indicates the presence of a hemorrhagic cyst.

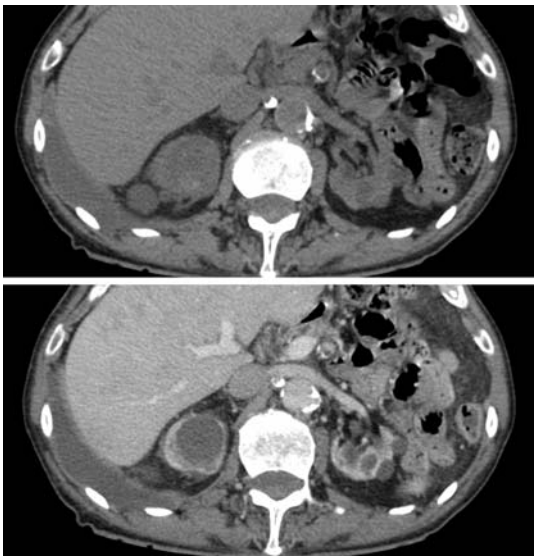

Cystic Renal Disease, Acquired. Figure 3 Computed tomography in ▶acquired cystic kidney disease (*top*: baseline scan; *bottom*: nephrographic phase). Multiple bilateral small cysts are detected within the atrophic parenchyma.

In hemorrhagic cystic tumors, the enhancement can be masked by the baseline hypersignal of the lesion. Follow-up is then necessary to confirm the absence of enhancement when the signal of the lesion will be changed due to metabolism of methemoglobin.

Solid renal masses are typically slightly hyperintense on T2-weighted sequences, and they significantly enhance after contrast agent injection. MRI participates in the staging of renal masses when the administration of iodinated contrast agents is contraindicated or when CT and sonographic findings are inconclusive, particularly regarding tumor extension to the inferior vena cava, the spleen, and the liver.

Angiography

Renal angiography is not done for ACKD diagnosis but for selective embolization in patients with severe active bleeding. To avoid the misdiagnosis of a bleeding tumor, CT needs to be performed until the hematoma disappears.

Nuclear Medicine

Scintigraphy has no value in the diagnosis of ACKD.

Diagnosis

The most difficult ▶differential diagnosis of ACKD is the presence of multiple simple cysts. The size of the cysts and

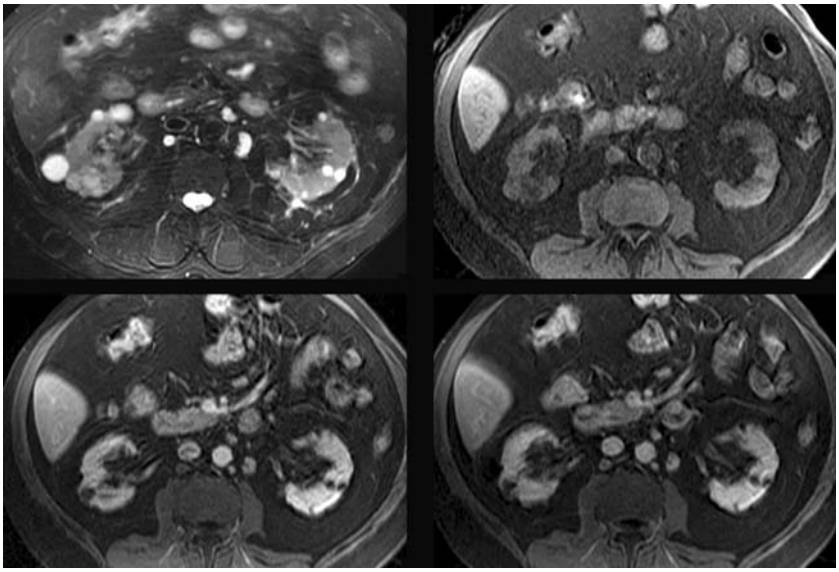

Cystic Renal Disease, Acquired. Figure 4 Typical magnetic resonance imaging (MRI) aspects in acquired cystic kidney disease. *Top left*: T2-weighted acquisition; *top right*: T1-weighted baseline dynamic acquisition; *bottom left*: T1-weighted dynamic acquisition during nephrographic phase; *bottom right*: T1-weighted dynamic acquisition during excretory phase.

their location are not helpful for differentiating the two diseases. When renal function is preserved, the diagnosis is likely to be ACKD, but multiple renal cysts can be found in patients with chronic renal failure.

In medullary cystic disease, the cysts are small and strictly located within the medulla.

At the moment of diagnosis of ACKD, the size of the kidneys is normal or reduced, in contrast to autosomal dominant polycystic kidney disease (ADPKD). In ADPKD, the renal cysts are much bigger than in ACKD, as they typically exceed 5 cm. Cysts can be detected in other locations such as the liver, the spleen, and the pancreas.

Other diseases such as von Hippel Lindau and tuberous sclerosis are easily ruled out with the context (family cases), the presence of associated tumors (hemangioblastoma of the central nervous system, pheochromocytoma, pancreatic cysts, or angiomyolipoma).

There is no definite imaging modality recommended for screening ACKD patients. US offers a clear advantage in terms of cost (Fig. 2). However, the examination is often difficult due to the size and echogenicity of the kidney. CT has the disadvantage of higher cost and secondary effects of iodinated contrast agents (renal toxicity and allergic reactions). However, it is an effective imaging technique and allows comparison when repeated examinations are performed over the years. MRI is probably the most effective modality because it does not have the limitations of iodinated contrast agents. However, its use is limited by restricted access to the machine, the cost of the examination, and some contraindications. The screening test should be repeated once a year, even after successful transplantation.

Still under debate is the efficacy of a screening program for elderly patients undergoing dialysis due to numerous comorbidity factors that reduce the impact of early treatment of renal cancer on the survival rate (4). Minimally invasive treatment of renal tumors such as radio frequency ablation might improve the tolerance of treatment compared with radical nephrectomy in this population at risk for cardiovascular complications. The screening program can be directed at patients at high risk of cancer (male, prolonged dialysis, enlarged kidneys) with good clinical status after 3 years of dialysis (5, 6). The incidence of renal tumors may have been underestimated by imaging techniques. The screening program can also include patients undergoing peritoneal dialysis.

In patients awaiting renal transplantation, the native kidneys should be scanned by either US or CT before the surgical procedure.

After renal transplantation, the native kidneys can be studied by US at the same time as the examination of the renal graft. Despite the lack of published data, transplanted patients, including children, might represent the best population to benefit from a renal tumor screening protocol (7). The decrease in ACKD after successful transplantation should be balanced against the increased aggressive behavior of renal cancers. When an echoic renal mass is detected, contrast-enhanced CT or MRI should be performed, depending on renal function.

Bibliography

1. Ishikawa I, Kovacs G (1993) High incidence of papillary renal cell tumours in patients on chronic haemodialysis. Histopathology 22:135–139
2. Ishikawa I (2004) Present status of renal cell carcinoma in dialysis patients in Japan: questionnaire study in 2002. Nephron Clin Pract 97:c11–c16
3. Levine E (1996) Acquired cystic kidney disease. Radiol Clin North Am 34:947–964
4. Sarasin FP, Wong JB, Levey AS et al (1995) Screening for acquired cystic kidney disease: a decision analytic perspective. Kidney Int 48:207–219
5. Choyke PL (2000) Acquired cystic kidney disease. Eur Radiol 10:1716–1721
6. Peces R, Martinez-Ara J, Miguel JL et al (2004) Renal cell carcinoma co-existent with other renal disease: clinico-pathological features in pre-dialysis patients and those receiving dialysis or renal transplantation. Nephrol Dial Transplant 19:2789–2796
7. Querfeld U, Schneble F, Wradzidlo W et al (1992) Acquired cystic kidney disease before and after renal transplantation. J Pediatr 121:61–64

Cystic Teratoma

▶Teratoma, Ovaries, Mature, Ovalar

Cystitis

Lorenzo E. Derchi, Pietro Pavlica
University of Genova, Largo R. Benzi, 8,
I-16122 Genova, Italy
derchi@unige.it

Definition

The term cystitis indicates the presence of an inflammatory disease of the urinary bladder. Such diseases are a common clinical problem, with more than half of the population experiencing an episode of cystitis during life. They can have a large variety of causes and can be divided, according to their etiology, into two broad categories:

those due to infectious causes, and those of noninfectious origin. In the first group, bacterial lesions are the most frequent, but viral, fungal, and parasitic diseases can also be encountered. Noninfectious inflammations can be congenital, such as the chronic irritative changes of the bladder mucosa in exstrophy of the urinary bladder, or acquired such as lupus erithematosus cystitis, eosinophilic cystitis, pelvic lipomatosis, involvement of the bladder from inflammatory diseases of adjacent organs, and iatrogenic lesions (1, 2).

Pathology/Histopathology

Pathological changes can be limited to the mucosal surface of the bladder or extend to the deep layers of the wall, and vary according to the etiology of the disease process.

Infectious Cystitis

In patients with bacterial cystitis, the main finding is edema of the mucosa, with thickening of the mucosal folds. When severe, edema can cause decreased capacity of the bladder. Bullous edema, that is fluid-filled cystic areas in the lamina propria of the mucosa, can develop, and is often more prominent at the level of the bladder base. The inflammatory process can be focal, and presenting as inflammatory polypoid lesions. In emphysematous cystitis, a condition that is most commonly encountered in patients with poorly controlled diabetes mellitus, bacterial fermentation of excessive glucose causes development of carbon dioxide within the bladder wall. Gas can extend also into the bladder lumen (3). Immunocompromised or debilitated patients can develop, after urologic procedures, infection from urease-producing microorganisms, able to transform urea into ammonia. This causes modification of pH in urine, which becomes alkaline, leading to formation of struvite and calcium phosphate that form stones and encrustations on the bladder wall. The disease, called alkaline-encrustation cystitis may also extend to the ureters and the kidneys. Encrustations are usually thin and regular, covering the urothelial surface, but may be irregular and thick; thickening of the bladder wall and perivesical soft-tissue edema can be associated (4). Mycotic infections of the bladder can cause formation of "fungus balls" within the bladder lumen; these are clusters of pseudomicelia, usually mobile according to patient's decubitus. In diabetic patients with Candida infection, gas can be present in the bladder given the capability of Candida to ferment sugar. If a fungus ball is in the bladder, gas can remain trapped within it. In patients with infestation from schistosomiasis, the disease process is caused by eggs deposited by the female parasite in the small veins of the submucosal layer of the bladder wall, around which a granulomatous reaction and embolic vasculitis develop. The deposited eggs calcify, and this is a macroscopic hallmark of the disease (5). Involvement of the urinary bladder occurs in about one third of patients with urinary tract tuberculosis, usually late in the course of the disease. The mucosa is edematous, with tubercles that coalesce and undergo ulceration. Calcifications can develop.

Noninfectious Cystitis

A large variety of noninfectious conditions can cause inflammatory changes of the bladder mucosa. In lupus erithematosus cystitis, a marked vasculitis of the bladder develops, with immune-complex deposition along small vessels and smooth muscle in the lamina propria of the bladder. Biopsy of the bladder wall in cases of eosinophilic cystitis shows pancystitis, with eosinophils, mast cells, and lymphocytes within the mucosa and tunica propria. Muscle necrosis and fibrosis can be found. Interstial cystitis is a pancystitis of unknown cause, often associated with systemic diseases. Biopsy shows transmural inflammation and fibrosis, submucosal edema and vasodilatation, and presence of mast cells in the submucosa and muscular layers. Cystitis can develop in most patients with pelvic lipomatosis, a condition characterized by benign overgrowth of pelvic fat. The pathogenetic relationship between cystitis and pelvic lipomatosis is not clear; however up to 80% of these patients develop cystitis glandularis. When the bladder is involved by neoplastic or inflammatory disorders arising within surrounding pelvic organs, histology shows an infiltrating inflammatory process, most marked in the outer part of the bladder wall. Perforation into the bladder may occur. Iatrogenic inflammation from foreign bodies, drugs, or radiation can develop in the bladder. The most common one is due to indwelling urethral catheters, in which histology shows vascular dilatation on the mucosa and lamina propria, with bullous edema visible on the surface of the mucosa, especially at the point where the tip of the catheter is in contact with the wall. Such changes can regress very quickly after catheter removal. Drug-induced cystitis may be related to either to direct toxic effect of drug metabolites on the urothelium or to an allergic-type of reaction of the bladder mucosa. Cyclophosphamide cystitis is the typical example of the first type of reaction. Biopsy reveals fibroblastic proliferation with associated atypia; wall fibrosis may develop after several months of therapy. Infiltration of the tunica propria with eosinophils and lymphoreticular cells develops in patients with the allergic-type of induced cystitis. Inflammatory changes of the bladder following pelvic radiotherapy are characterized, in the acute phase, by mucosal ulcerations and

panvesical fibrosis; later effects produce vasculitis and fibrosis with reduced bladder capacity.

Chronic Cystitis

Patients with chronic inflammation of the urinary bladder undergo changes that follow a predictable pathway. Bladder lesions start from Brunn's nests, solid nests of urothelial cells lying in the lamina propria of the wall. Degeneration of the central part of these nests leads to the development of fluid-filled cysts (cystitis cystica). Further chronic irritation leads to the development of these lesions into glandular structures (cystitis glandularis). At last, squamous metaplasia may occur.

Clinical Presentation

Symptoms of cystitis include urgency, frequency, incontinence and suprapubic pain, or discomfort. Hematuria may be the prominent symptom, and in these cases, the term hemorrhagic cystitis is frequently used. Such symptoms, however, are nonspecific, and do not allow to differentiate among the different forms of the disease. Taking into account clinical history can help in the differential.

In bacterial cystitis symptoms vary according to the age of the patient: in neonates, failure to thrive may be observed as a result of poor feeding, vomiting, and diarrhea. In the older child, fever becomes a more prominent symptom. In the adult, the classic symptoms are present. A history of diabetes is commonly found in patients with emphysematous cystitis or in those with mycotic infections. Patients with alkaline encrusting cystitis are usually immunocompromised, with previous urologic procedures. Schistosomiasis is encountered in subtropical Africa, Middle East and in part of southern Europe. A history of tuberculous infection of the upper tract is commonly found in patients with tuberculous cystitis.

For patients with *noninfectious cystitis*, a history of radiation exposure or chemotherapy, or presence of an indwelling catheter allow to address the diagnosis when urinary symptoms develop. Patients with eosinophilic cystitis have predisposing factors such as asthma, bladder trauma, food allergies, and a history of eosinophilic gastroenteritis. Eosinophilia is associated in 50% of cases. When a pelvic inflammatory process extends to the bladder, symptoms are those of the primary process, with the addition of irritative voiding complaints. If a fistula develops, fecaluria and/or pneumaturia are associated.

Interstitial cystitis is a chronic inflammatory disease of the urinary bladder of unknown cause, often associated with systemic diseases such as rheumatoid arthritis, polyarteritis and lupus erithematosus, and/or an allergic condition, predominantly affecting middle-aged women. The diagnosis can be made on presence of chronic unexplained irritative bladder symptoms, sterile urine, and cystoscopic demonstration of urothelial lesions (Hunner's ulcers).

Imaging

Usually, imaging is not needed for the diagnosis of cystitis, which is commonly suspected on clinical grounds and confirmed by urinary cultures. When requested, radiologic studies are chiefly aimed at identifying underlying pathology that may predispose to the development of infection, such as reflux and urinary outlet obstruction. This is especially needed in patients with recurrent episodes of cystitis. Furthermore, it must be remembered that changes affecting the mucosa of the urinary bladder are better analyzed by cystoscopy, and this technique has the capabilities to provide clues for the differential diagnosis of the different forms of the disease and, most important, to allow for biopsy (1, 2).

Imaging is pointed at detecting changes of the wall and content of the bladder. Plain films can show calcifications and gas within the bladder wall, while urography can show irregularities of the mucosal surface. Such findings can be better evaluated when the bladder is not completely full. CT, ultrasonography and MRI can show thickening of the wall, as well as focal lesions. Calcifications are easily seen at CT, but can be appreciated also by ultrasonography.

Nuclear Medicine

Nuclear medicine studies do not offer clues for demonstration of cystitis. Radionuclide retrograde cystography can be used in the pediatric age group to show reflux in children who present with recurrent urinary infections.

Diagnosis

The imaging diagnosis of cystitis is based on demonstration of changes of the bladder wall and content. At urography, thickening and irregularity of the mucosa can be seen, together with decreased capacity of the inflamed, irritated bladder. Such findings are often more prominent at the level of the bladder base, and can be better demonstrated when the bladder is only partially filled in with contrast or in the postvoiding films. Ultrasonography and CT can show diffuse thickening of the wall of the bladder. In patients who develop bullous edema, focal filling defects of rounded shape may be seen, especially near the bladder base. On ultrasonography, bullous edema has been described to cause hypoechoic regions

of wall thickening with smooth transition to normal bladder wall (Fig. 1). Focal forms of cystitis can also present with polypoid lesions that can be difficult to differentiate from malignancies (1).

The diagnosis of emphysematous cystitis is based on demonstration of gas within the bladder wall. Gas within the bladder lumen can be associated. On a plain abdominal film, this can be difficult to distinguish from bowel gas or an adjacent abscess, but can be easily recognized at urography, CT, or ultrasound (Fig. 2). The bladder wall can be thickened, with an irregular outline. Presence of gas in the bladder lumen and not within the bladder wall is usually described as a separate entity (pneumocystis); intraluminal gas has to be differentiated from gas entering from an enteric fistula or following catheterization maneuvers (3).

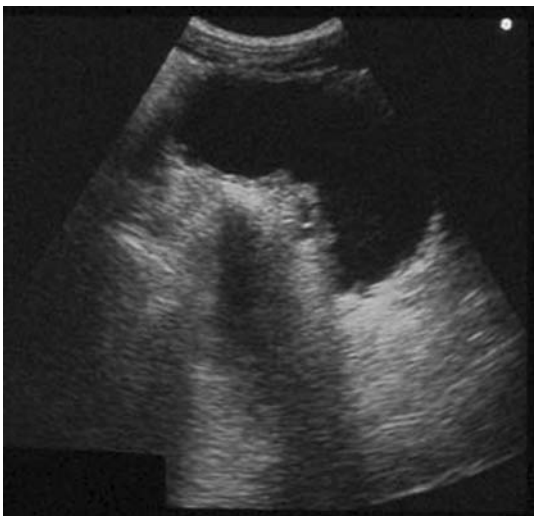

Cystitis. Figure 1 Bullous edema of the posterior wall of the urinary bladder demonstrated by ultrasonography. There is focal thickening of the wall, with smooth transition toward the normal portions; areas of hypoechogenicity are visible within the thickened region.

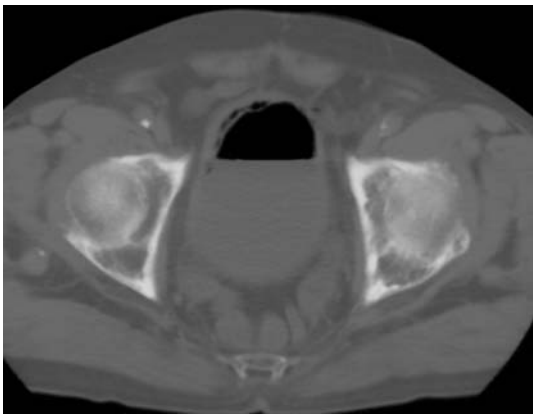

Cystitis. Figure 2 Emphysematous cystitis. CT obtained without i.v. contrast medium shows presence of gas both within the wall and within the bladder lumen.

In patients with alkaline encrusting cystitis, the bladder wall is characterized by presence of encrustations; the disease may also involve the ureters and the kidneys, and calcifications and stones can be seen also at these levels. Detection of wall calcifications in the proper clinical setting on conventional radiographic studies is diagnostic; however, calcifications may be thin, and impossible to recognize. Ultrasonography can detect the encrustations as a linear hyperechogenicities on the mucosal surface of the bladder. Nonenhanced CT is regarded as the best technique to diagnose encrustations. Lesions are usually thin and regular, covering the urothelial surface, but may be irregular and thick; there is also thickening of the bladder wall, and perivesical soft tissue stranding can be associated (4). In mycotic infections, imaging can be normal or show only nonspecific inflammatory changes of the bladder wall; on sonography, echogenic urine can be shown, A "fungus ball," that is a cluster of pseudomicelia, can develop within the bladder, presenting as a nonopaque mass. Such balls are usually mobile within the bladder: on ultrasonography, it is easy to demonstrate changes of position of the fungus ball according to changes in patient decubitus. In diabetic patients with Candida infection, gas can be present in the bladder given the capability of Candida to ferment sugar. In some cases, gas can be seen within the "fungus ball" (1). Schistosomiasis infestation can be imaged at urography as edema of the bladder wall in the early stages. When eggs calcify, they can be seen on plain films or urography; the pattern of calcifications may vary, from thin and regular to thick and irregular, involving the bladder wall completely or only focally (Fig. 3). In the early stages of the disease, contraction capability of the calcified bladder is preserved. Both ultrasonography and CT can detect easily the calcifications in the bladder wall. Involvement of the ureter is the rule, and is early during the disease process. Urography can detect filling defects and stenoses of the distal portions of the ureters, while ultrasound can show thickening of the ureteric walls (5). In patients with tuberculosis of the bladder, diffuse wall thickening, ulcerations of the mucosal surface, fibrous bands, and mural nodules have been described at urography and ultrasound. Calcifications may develop in the wall, and can be seen radiographically.

Patients with pelvic lipomatosis have a typical pear-like appearance of the urinary bladder; when cystitis is associated, imaging can show irregularities of the bladder mucosa. In case of bladder involvement from an adjacent inflammatory process, focal inflammatory changes such as edema, nodularity, or thickening of the wall may be

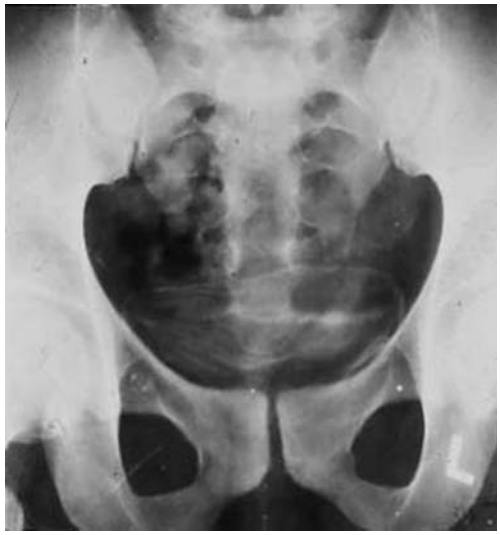

Cystitis. Figure 3 Schistosomiasis of the bladder. Plain radiograph of pelvis shows linear calcifications involving the whole bladder wall.

observed on intravenous urography. CT and ultrasound can show both the primary disease and bladder changes. Fistulous tract may be difficult to demonstrate directly, and can be inferred by presence of air in the bladder. Nonspecific thickening of the bladder mucosa can be detected by urography. Patients with drug-induced and radiation cystitis present with bladder wall edema in the early phases, but late effect of these diseases may cause wall fibrosis and reduction of bladder capacity (1).

Bibliography

1. Saluja S, Lazzarini KM, and Smith RC (2000) Inflammation of the urinary bladder In: Pollak HM and McClennan BM (eds) Clinical Urography. 2nd edn. Philadelphia, WB Saunders, pp 1019–1039
2. Schaeffer AJ (1998) Infections of the urinary tract. In: Walsh PC, Retik AB, Vaughan ED, et al (eds) Campbell's Urology. 7th edn. Philadelphia, WB Saunders, pp 533–614
3. Grayson DE, Abbott RM, Levy AD, et al (2002) Emphysematous infection of the abdomen and pelvis: a pictorial review. Radiographics 22:543–561
4. Thoumas D, Darmallaicq C, Pfister C, et al (2002) Imaging characteristics of alkaline-encrusted cystitis and pyelitis. Am J Roentgenol 178:389–392
5. Palmer PES and Reeder MM (2000) Parasitic diseases involving the urinary tract. In: Pollak HM and McClennan BM (eds) Clinical Urography. 2nd edn. Philadelphia, WB Saunders, pp 1167–1192

Cystocele

Descent of the posterior bladder wall during Valsalva maneuver below the level of the vesico-urethral junction of more than 1 cm is called a cystocele. A cystocele impresses the anterior vaginal wall (grade II) and may evert it to outside the introitus (grade III). A cystocele may persist after relaxation and need manual reposition. ►Pelvic Floor Dysfunction, Genitourinary

Cystosarcoma Phyllodes

►Neoplasms, Phyllodes, Breast

Cyst, Follicular, Ovarium

Rosemarie Forstner
Department of Radiology, Paracelsus Private Medical University, Salzburger Landeskliniken, Salzburg
r.forstner@salk.at

Synonyms

Corpus luteum cysts; Follicle cysts; Follicular cysts; Luteal cysts; Physiologic ovarian cysts; Simple ovarian cysts

Definitions

Physiologic cysts including follicular and luteal cysts constitute the vast majority of cystic ovarian lesions. They typically result from failure during folliculogenesis, most often from rupture or regression of the ovarian follicles. They may also result from continued hemorrhage in a corpus luteum. Follicle cysts are usually larger than the mature ►graafian follicle and range from 3 to 5 cm in size; however, they may attain a diameter of 8–12 cm. ►Physiologic ovarian cysts are an extremely common incidental finding during the reproductive ages. However, they may be found in all age groups, particularly in adolescents and in the early postmenopausal period. Functional ovarian cysts may also develop due to irregularities of pituitary gonadotropin hormone release or due to external hormonal replacement therapy.

Pathology/Histopathology

In women who do not take birth control pills, numerous small, thin-walled cystic follicles and a dominant follicle

are seen within the ovarian peripheral stroma. At midcycle the latter attains a size of 15–25 mm and can be identified partially protruding from the ovarian surface (1). After ovulation the rupture stigma is sealed by a mass of coagulated follicular fluid, fibrin, and connective tissue (1). The normal corpus luteum demonstrates a convoluted yellow lining and usually measures 1.5–2 cm in diameter. If it is larger than 3 cm, it is defined as a corpus luteum cyst (1).

Microscopically, follicle cysts are lined by an inner layer of granulosa cells and an outer layer of theca interna cells (1). They may be luteinized in both layers. ►Corpus luteum cysts demonstrate a convoluted inner lining consisting of large luteinized granulosa cells and an outer lining of luteinized theca interna cells (1). Capillaries from the theca interna penetrate the granulosa layer to reach the central cavity (1). The contents of follicle and luteal cysts vary from serous to serosanguinous to clotted blood.

Follicles may persist for several years after menopause and give rise to sporadic ovulations or cyst development. Solitary ►follicular cysts are a different entity from follicular cysts that occur during the reproductive age (1). They tend to be larger and are most commonly found during menarche and menopause, but may also be seen in the fetus. Cysts related to anomalies in the release of anterior pituitary hormones tend to recur and manifest as multiple large cysts in both ovaries (1).

Clinical Presentation

Most functional cysts are asymptomatic and not hormonally active. Vague abdominal or pelvic pain, pelvic pressure, and lower back pain may be caused by larger functional cysts. Corpus luteum cysts may be hormonally active and become clinically apparent by menstrual disorders and prolonged hemorrhage. Complications of functional cysts include rupture, hemorrhage, and torsion. Intraperitoneal hemorrhage following rupture is characterized by an acute onset of pelvic pain. Similarly, patients with ovarian torsion most commonly experience abrupt onset of severe lower abdominal pain. Follicle cysts in precocious puberty are manifestation of McCune–Albright syndrome (1).

Imaging

Ovarian cysts are a common incidental finding in ovarian imaging.

Transabdominal in combination with *endovaginal sonography* is the primary imaging modality in assessing the ovaries. If physiological cysts do not exceed a size of more than 3 cm they cannot be differentiated from normal follicular derivates in women of reproductive age.

Other imaging modalities for assessing cystic ovarian lesions include *computed tomography (CT) and magnetic resonance imaging (MRI)*. They are infrequently used for further characterization of sonographically detected cystic lesions. More often, functional cysts are incidental findings in pelvic imaging studies for other indications.

Due to partial volume average and proteinaceous contents, follicles are often missed in CT. Furthermore, CT usually does not allow differentiation between ►hemorrhagic functional cysts and hemorrhagic cysts in endometriosis. Hemorrhagic cysts may also mimic solid ovarian lesions in CT. This problem can be overcome by performing a noncontrast series before application of intravenous contrast media. This technique and thin-slice multispiral CT also improve the detection of smaller ovarian cysts. In cystic ovarian lesions, contrast-enhanced images provide better detail of the internal morphology of cystic lesions. They also assist in the differential diagnosis between simple ovarian cysts and other cystic ovarian lesions, for example, cystadenomas, hydrosalpinx, and cystic ovarian cancer.

In MRI imaging, sequences for assessing cystic ovarian lesions include T1-weighted imaging (WI), T2-WI, and contrast-enhanced imaging. If lesions display high signal intensity (SI) on T1-WI, fat saturation techniques are useful to differentiate between proteinaceous or hemorrhagic contents and fat that is pathognomonic for dermoid cysts.

Nuclear Medicine

Nuclear medicine usually does not contribute to the diagnosis of functional ovarian cysts.

Diagnosis

Sonography, particularly endovaginal sonography, is the modality of choice in monitoring follicles and ovarian follicle cysts (Fig. 1).

Ovarian cysts larger than 3 cm in diameter are regarded as follicular cysts (2). Follicle cysts are thin-walled ovarian lesions most commonly filled with watery contents. Compared with follicle cysts, corpus luteum cysts have thicker, well-vascularized walls. The internal echoes depend on the quality of the contents. Bleeding in an unruptured cyst causes a spectrum of sonographic findings related to the temporal sequence of clot formation (3). Corpus luteum cysts often display mildly echogenic echoes, most likely presenting partially solid

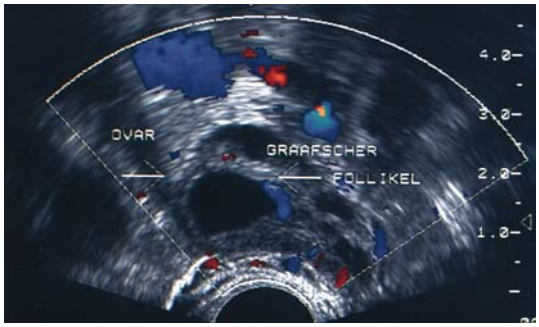

Cyst, Follicular, Ovarium. Figure 1 Color Doppler sonography of a normal ovary at midcycle in a 25-year-old female patient. Transvaginal sonography demonstrates a normal ovary which is located medial of the iliac vessels. Within the ovarian parenchyma, ovarian vessels and small follicles are demonstrated. The graafian follicle presents the largest cystic lesion and measures 15 mm in diameter. (Courtesy of R. Gruber, Salzburg)

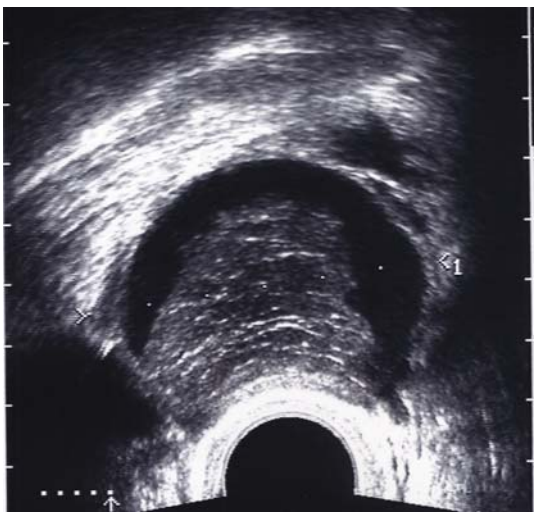

Cyst, Follicular, Ovarium. Figure 2 Hemorrhage in a physiologic cyst. In a 29-year-old female patient with acute pain, a 6-cm right ovarian lesion is demonstrated. It is well delineated and is composed of a solid area with irregular borders surrounded by liquid. The sonographic follow-up showed continuous decrease in size and change in morphology of the internal clot. (Courtesy of R. Gruber, Salzburg)

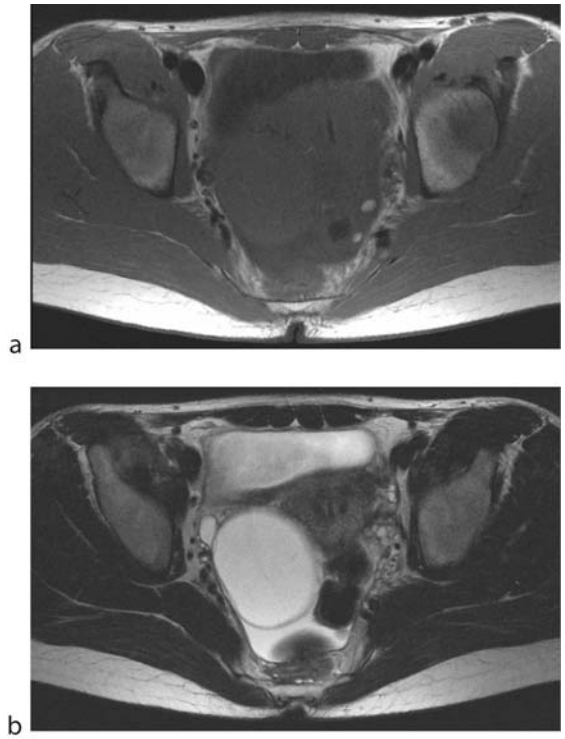

Cyst, Follicular, Ovarium. Figure 3 Follicle cyst in a 31-year-old female patient. Transaxial T1-weighted imaging (WI) (a) and T2-WI (b) show a 6-cm right adnexal lesion. It is cystic and displays higher signal than water on T1-WI (a) due to proteinaceous contents. Thin walls and no evidence of mural thickening or solid areas are demonstrated on T2-WI. Small amounts of ascites in the cul-de-sac are a physiologic finding in this age. The differential diagnosis from unilocular cystoma was only possible by a follow-up.

clots (3). They may also present as cystic lesions with irregular walls due to an adherent clot or may contain internal debris that is not vascularized. Recent hemorrhage frequently appears as an irregular echogenic mass (3) (Fig. 2). A complex mass with internal echoes enhanced through transmission is also a common finding of hemorrhagic functional cysts (3).

Echogenic free fluid in the cul-de-sac is a typical finding of cyst rupture into the peritoneal cavity. However, in women of reproductive age, a pregnancy test is mandatory for differentiation of hemorrhagic functional cysts and ▶ectopic pregnancy.

The clue for establishing the diagnosis of functional cysts with watery contents or hemorrhage and for their differentiation from cystadenomas is the decrease in size and change of the internal architecture during a sonographic follow-up. The vast majority of functional cysts will regress within a 2-month observation period (2).

MRI is usually performed complementary to sonography in indeterminate cases. It is particularly helpful for differentiating functional cysts with a complex pattern from hemorrhagic ovarian lesions of other etiologies and teratomas.

Simple ovarian cysts display well-defined, thin walls (<3 mm). Most ovarian cysts have a low to intermediate signal on T1-WI and very high SI on T2-WI due to the presence of simple fluid (2). Cyst walls are usually clearly identified on T2-WI, they display low SI, and enhance mildly following contrast media application. Hemorrhagic and corpus luteum cysts display high to intermediate signal on T1-WI and intermediate to high SI on T2-WI (2). Their appearance varies according to the quantity and age of their hemorrhagic and proteinaceous contents (Fig. 3). Corpus luteum cysts tend to have thicker walls that display smooth distinct contrast enhancement (2). Internal debris is often present, but does not enhance. Enhancement is a sign of solid internal contents, and is highly suggestive of malignancy. Low-signal intensity on T2-WI presenting shading is due to repetitive hemorrhage and allows the diagnosis of endometriomas (2). The diagnostic feature of benign teratomas is demonstration of intralesional fat, which can be diagnosed by fat-suppression techniques.

If an ovarian cyst does not decrease in size, unilocular cystoma, which can present with the same imaging features as functional cysts, is the most important differential diagnosis (2). ►Mesothelial and tubal inclusion cysts occur in the same age group and can also display similar imaging findings to simple ovarian cysts. They can only be differentiated from physiologic ovarian cysts when they are visualized separate from the ipsilateral ovary.

Bibliography

1. Clement PB (2002) Anatomy and histology of the ovary. In: Kurman RJ (ed) Blaustein's Pathology of the Female Genital Tract. Springer, New York, pp 649–674
2. Sala EJS, Atri M (2003) MRI of benign adnexal disease. TMRI 14:305–28
3. Baltarowich OH, Kurtz AB, Pasto ME et al (1987) The spectrum of sonographic findings in hemorrhagic ovarian cysts. Am J Roentgenol 148:901

Cytochrome *c*

A major caspase activation pathway is the cytochrome *c*-initiated pathway. In this pathway, a variety of stimuli cause cytochrome *c* release from mitochondria, which in turn induces a series of biochemical reactions that result in caspase activation and subsequent cell death.
►Apoptosis